Biofunctionalization of Silsesquioxane Nanoparticles

TECHNISCHE UNIVERSITÄT DARMSTADT

Vom Fachbereich Chemie
der Technischen Universität Darmstadt

zur Erlangung des akademischen Grades eines

Doktor-Ingenieurs (Dr.-Ing.)

genehmigte kumulative Dissertation

vorgelegt von

Dipl.-Ing. Sebastian Hörner
aus Viernheim

Referent: Prof. Dr. Harald Kolmar
Korreferent: Prof. Dr. Siegfried Neumann

Tag der Einreichung: 06. Februar 2017
Tag der mündlichen Prüfung: 27. März 2017

Darmstadt 2017

Die vorliegende Arbeit wurde unter der Leitung von Herrn Prof. Dr. Harald Kolmar am Clemens Schöpf-Institut für Organische Chemie und Biochemie der Technischen Universität Darmstadt seit Februar 2011 angefertigt.

1. Index

2. Publications

The results of the present research work were published in peer-reviewed journals, patents, or presented as follows:

Lead author:

[1] Sebastian Fabritz,[‡] **Sebastian Hörner**,[‡] Martin Empting, Doreen Könning, Michael Reinwarth, Christian Dietz, Bernhard Glotzbach, Holm Frauendorf, Harald Kolmar[*] and Olga Avrutina[*]. From Pico to Nano: Biofunctionalization of Cube-octameric Silsesquioxanes by Peptides and Miniproteins. *Org. Biomol. Chem*., **2012**, *10*, 6287-6293.

[2] **Sebastian Hörner**,[‡] Sebastian Fabritz,[‡] Henry D. Herce,[*] Olga Avrutina, Christian Dietz, Robert W. Stark, M. Cristina Cardoso and Harald Kolmar[*]. Cube-octameric silsesquioxane-mediated cargo peptide delivery into living cancer cells. *Org. Biomol. Chem*., **2013**, *11*, 2258-2265.

[3] Sebastian Fabritz,[‡*] **Sebastian Hörner**,[‡] Olga Avrutina and Harald Kolmar, Bioconjugation on Cube-octameric Silsesquioxanes. *Org. Biomol. Chem*., **2013**, *11*, 2224-2236.

[4] **Sebastian Hörner**,[‡] Christina Uth,[‡] Olga Avrutina, Holm Frauendorf, Manfred Wiessler, Harald Kolmar[*]. Combination of inverse electron-demand Diels–Alder reaction with highly efficient oxime ligation expands the toolbox of site-selective peptide conjugations. *Chem. Commun*., **2015**, *51*, 11130-11133.

[5] **Sebastian Hörner**,[‡] Sascha Knauer,[‡] Christina Uth,[‡] Marina Jöst, Volker Schmidts, Holm Frauendorf, Christina M. Thiele, Olga Avrutina, and Harald Kolmar[*]. Nanoscale biodegradable organic-inorganic hybrids for efficient cell penetration and drug delivery. *Angew. Chem. Int. Ed*., **2016**, *55*, 14842-14846.

[6] **Sebastian Hörner**,[‡] Sascha Knauer,[‡] Christina Uth,[‡] Marina Jöst, Volker Schmidts, Holm Frauendorf, Christina MarieThiele, Olga Avrutina, and Harald Kolmar[*]. Nanoskalige, biologisch abbaubare organisch-anorganische Hybride für effiziente Zellaufnahme und Wirkstofftransport. *Angew. Chem*., **2016**, *128*, 47, 15063–15068.

Co-author:

[7] Christina Uth, Stefan Zielonka, **Sebastian Hörner**, Nicolas Rasche, Andreas Plog, Hannes Orelma, Olga Avrutina, Kai Zhang, Harald Kolmar. A Chemoenzymatic Approach to Protein Immobilization onto Crystalline Cellulose Nanoscaffolds. *Angew. Chem. Int. Ed*., **2014**, *53*, 12618–12623.

[8] Christina Uth, Stefan Zielonka, **Sebastian Hörner**, Nicolas Rasche, Andreas Plog, Hannes Orelma, Olga Avrutina, Kai Zhang, Harald Kolmar. Eine chemoenzymatische Kupplungsstrategie zur Immobilisierung von Proteinen auf kristalliner Nanocellulose. *Angew. Chem*., **2014**, *126*, 12826–12832.

[9] Stephan Dickgießer, Nicolas Rasche, Daichi Nasu, Stephen Middel, **Sebastian Hörner**, Olga Avrutina, Ulf Diederichsen, Harald Kolmar. Self-Assembled Hybrid Aptamer-Fc Conjugates for Targeted Delivery: A Modular Chemoenzymatic Approach. *ACS Chem. Biol*., **2015**, *10 (9), 2158-2165.*

‡ shared lead author

[10] Sascha Knauer, Tobias M. L. Roese, Olga Avrutina, Harald Kolmar, **Sebastian Hörner**. Method for peptide synthesis and apparatus for carrying out a method for solid phase synthesis of peptides. European patent number 14186879.4 – 1453. Submitted September 29th **2014**.

[11] Olga Avrutina, **Sebastian Hörner**, Sascha Knauer, Harald Kolmar, Christina Uth. Neuer hocheffizienter Wirkstofftransporter für biomedizinische/zellbiologische Anwendungen. National patent submitted May **2016**.

Presentations:

Sebastian Hörner. Cube-octameric silsesquioxanes (COSS): Nanoscaffolds for tumor imaging and drug delivery. 11. deutsches Peptidsymposium, München, 18.-21.3.2013.

Posters:

Sebastian Hörner, Sebastian Fabritz, Olga Avrutina, Henry D. Herce, Christian Dietz, Robert W. Stark, M. Cristina Cardoso and Harald Kolmar. Cube-octameric Silsesquioxanes: Nanoscaffolds for Tumor Imaging and Drug Delivery. 11. deutsches Peptidsymposium, München, 18.-21.3.2013.

Sebastian Hörner, Sebastian Fabritz, Olga Avrutina, Henry D. Herce, Christian Dietz, Robert W. Stark, M. Cristina Cardoso and Harald Kolmar. Cube-octameric Silsesquioxanes: Nanoscaffolds for Tumor Imaging and Drug Delivery. Chemical Biology 2012, EMBL Heidelberg, 26.-29.9.2012.

Volker Schmidts, Sascha Knauer, **Sebastian Hörner**, Olga Avrutina, Harald Kolmar, Christina M. Thiele, NMR spectroscopic Characterization of Unsymmetrical Cube-Octameric Silsesquioxanes (COSS), GDCh FGMR 35th Annual Discussion Meeting, Frauenchiemsee, September 2013.

Volker Schmidts, Sascha Knauer, **Sebastian Hörner**, Olga Avrutina, Harald Kolmar, Christina M. Thiele, NMR spectroscopic Characterization of Unsymmetrical Cube-Octameric Silsesquioxanes (COSS), SMASH 2013, Santiago de Compostela/Spain, September 2013.

3. Preface

Peptide drugs: prospects and challenges

Molecular recognition of the effector molecule is the determining step in any biological signal transduction. Many effector molecules that trigger cellular biochemical events are peptides with the recognition site representing either a part of a larger protein or a stand-alone, functionally complete moiety. With the average size of eleven amino acids (from few to about 40 residues), a recognition sequence required for a receptor-ligand interaction is rather short,[1] implying that in principle all receptors could be regulated by artificial peptides.[2] Today, more than 7000 naturally occurring peptidic molecules have been identified that act as hormones, neurotransmitters and growth factors or are involved into defence against pathogens.[1a, 3]

The variety of side-chain functional groups endows peptides with the ability to form numerous interactions with their targets. As a consequence, the high selectivity of peptidic drugs provides an option to reduce side effects, thus enabling good tolerance. Due to their structural diversity, peptides are suitable for the (almost unlimited) application in the fields of oncology, endocrinology, immunology, and for the control of infectious diseases. Currently, more than 100 peptidic drugs have been approved, the majority of them possessing less than 20 amino acids.[4] Approximately 200 peptides have been to date investigated in clinical trials and another 400 are in early preclinical development.[4-5] Simple synthetic manufacturing combined with good predictability of metabolism[5b] makes peptidic drugs particularly attractive.

However, peptide drugs often suffer from limited bioavailability and metabolic instability mainly caused by hydrolysis and oxidation reactions.[6] Additionally, their bioavailability can be compromised upon opsonisation, agglutination, and non-covalent association with serum components.[7] To date, a number of approaches has been developed aimed on the improvement of systemic availability and site-selective delivery of peptide drug candidates. Thus, the stability of such architectures can be increased upon substitution of certain amino acids or modification/removal of potential protease binding sites. Aggregation can be reduced by avoiding hydrophobic regions or by modulating isoelectric point using amino acid exchange.[6] Stability towards proteolytic degradation can be enhanced by cyclization and/or incorporation of non-canonic amino acids or backbone elements.[3a, 8] Furthermore, the pharmacokinetics of peptides has been significantly improved upon PEGylation and fusion with vitamin B12, as well as by conjugation with fatty acids.[9]

Oligomerization represents another important strategy towards the improvement of peptidic drugs. Indeed, linkage of monomeric counterparts leading to higher-ordered constructs provides a number of advantages in terms of stability. One possibility to improve the half-life of peptidic molecules in the bloodstream is to increase their size. Upon intravenous application, compounds with a molecular mass lower than 5500 Dalton are quickly renal secreted as their size enables the passage through the pores of the nephron in the kidney. Larger molecules possess longer half-lives in the bloodstream.[10] Conjugation of multiple peptides could therefore lead to increased plasma circulation time. Furthermore, being involved in numerous biological processes, oligomeric protein structures are ubiquitous structural motives in nature. Molecular architectures comprising $n>1$ copies of identical biomolecules could enable modulation of certain regulatory processes inside the cell as e.g. the growth factor thrombopoietin does. This dimeric cytokine controls proliferation, cell maturation, as well as the production of thrombocytes by inducing the formation of a homodimer of the respective receptor on the cell surface.[11] Obviously, such intracellular events could be regulated applying structurally similar oligomers of synthetic peptides (scheme 1a).

Oligomerization of functional peptidic monomers can improve their binding to the desired extracellular targets. It is obvious that if the local concentration of the ligand in spatial proximity to a binding site increases, the probability of additional interactions is increased as well. Thereby, spatial

separation of the oligomeric binder and the binding site can be prevented. Due to this effect called avidity, strong binding strength can be achieved also for low-affinity peptide monomers (scheme 1b).[12] This approach can find application in e.g. diagnostics of tumour disease via medical imaging technique, as oligomerization can simultaneously improve both pharmacokinetics and binding strength. As the stability of the oligomeric construct can be tailored, the retention time inside the body can be precisely adjusted, thus allowing for e.g. reduced exposure to radionuclides.

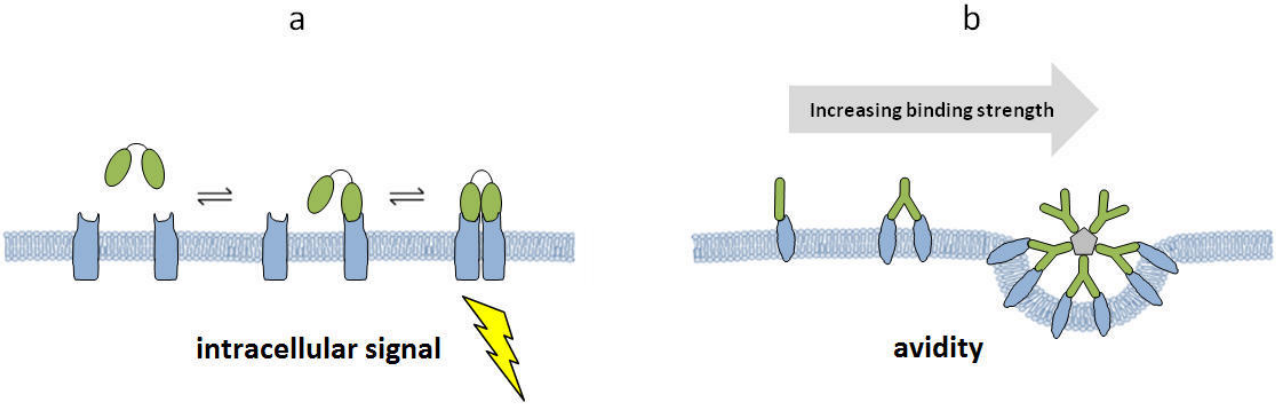

Scheme 1: Modulation of intracellular processes by using n>1 copies of identical biomolecules. a) Induction of homodimer-formation of cell-surface receptors. b) Increasing binding strength upon formation of multiple interactions.

In addition to the mentioned extracellular applications, peptides are suited for the control of signal transduction inside the cell, too. However, due to the relatively high molecular mass and particularly charged functional groups, intracellular bioavailability of these molecules is fundamentally restricted. They are not able to cross epithelial barriers and cellular membranes.[13] The membrane translocation of peptides can be improved by decreasing their polarity via the introduction of hydrophobic amino acids or lipophilic building blocks. Cellular uptake of functional peptidic molecules can be enabled upon their co-administration/fusion with the so-called cell-penetrating peptides (CPPs) or via the attachment of ligands possessing affinity to surface receptors (e. g. carbohydrate or lipoprotein receptors).[4, 14]

Though being promising drug candidates, the majority of peptides are poor orally available. Indeed, due to the degradation in the gastrointestinal tract and limited tissue absorption, the current administration is predominantly intravenous or subcutaneous.[15] Realization of oral availability of peptidic drugs via e.g. their chemical stabilization or co-administration with absorption enhancers and enzyme inhibitors would be a significant improvement from the standpoint of the patient.

Drug delivery as a cornerstone for future-oriented therapeutic approaches

Despite significant achievements in recent years, the transport of peptides remains the major handicap limiting their therapeutic application. This extends to all modern therapeutic approaches based on the application of biomacromolecules, especially those composed of amino and nucleic acids. Indeed, by import of nucleic acids, living cells can be manipulated in different ways. To date, a variety of highly innovative technologies based on tailor-made DNA and RNA constructs has been developed, which carry an impressive potential for ground-breaking improvements in medical treatments. However, these novel approaches often require efficient intracellular transporters. Thus, genome editing requires delivery of respective programmable nucleases into the cells of interest.[16] Also for siRNA which enables gene silencing by tagging the corresponding mRNA, thereby initiating its degradation, efficient import is currently the biggest challenge.[17] Development of viable approaches aimed on the induction of biosynthesis of therapeutic proteins in the organism of the patient is another future-oriented research field. To launch protein synthesis, the required genetic information must be either transiently (mRNA) or permanently (DNA) available inside the cell. Therefore, as soon as the desired nucleotide-comprising constructs have reached the cell interior, the production of e.g. monoclonal antibodies in

the patient's body is ensured. This methodology could obviate the need for side-effect-afflicted high-dose injections and would significantly contribute to a reduction of the treatment costs.[18]

In order to translate the above-mentioned innovative approaches into clinical practice, efficient transport and site-specific release in the desired cellular compartments is essential. As a consequence, the development of a viable carrier system becomes as important as the ability of the drug to address its target. A proper delivery platform should enable efficient and safe cellular import of the desired cargo. Thus, to protect biomacromolecules from degradation upon transport, they can be deposited into polymers, nano-emulsions, hydrogels, or particles of nano-dimension.[19] To date, a variety of nanoparticle formulations has been applied to the delivery of proteins (antibodies, enzymes, etc.) and nucleotide-based constructs (plasmid-DNA, siRNA, mRNA, etc.). In contrast to the majority of proteins or peptides often addressing surface-bound targets, nucleic acids need to be delivered into the cytoplasm or the nucleus. Current transport systems for these compounds are composed of positively charged polymers, cationic lipids, as well as viral vectors.[17] Following cellular uptake, nanoparticles are commonly processed to the early and late endosomes and, as a rule, the cargo is degraded in the Golgi network. Strategies to bypass this degradation pathway are based on hampering the acidification in the late endosomes via the so-called proton sponge effect caused by basic functional groups, usually amines or imines within the used polymeric delivery module. As an alternative, application of lipid nanoparticles can enable release of the cargo upon its fusion with the endosomal membrane or pH-dependet changes of the conformation of certain peptides can lead to pore formation (scheme 2).[20]

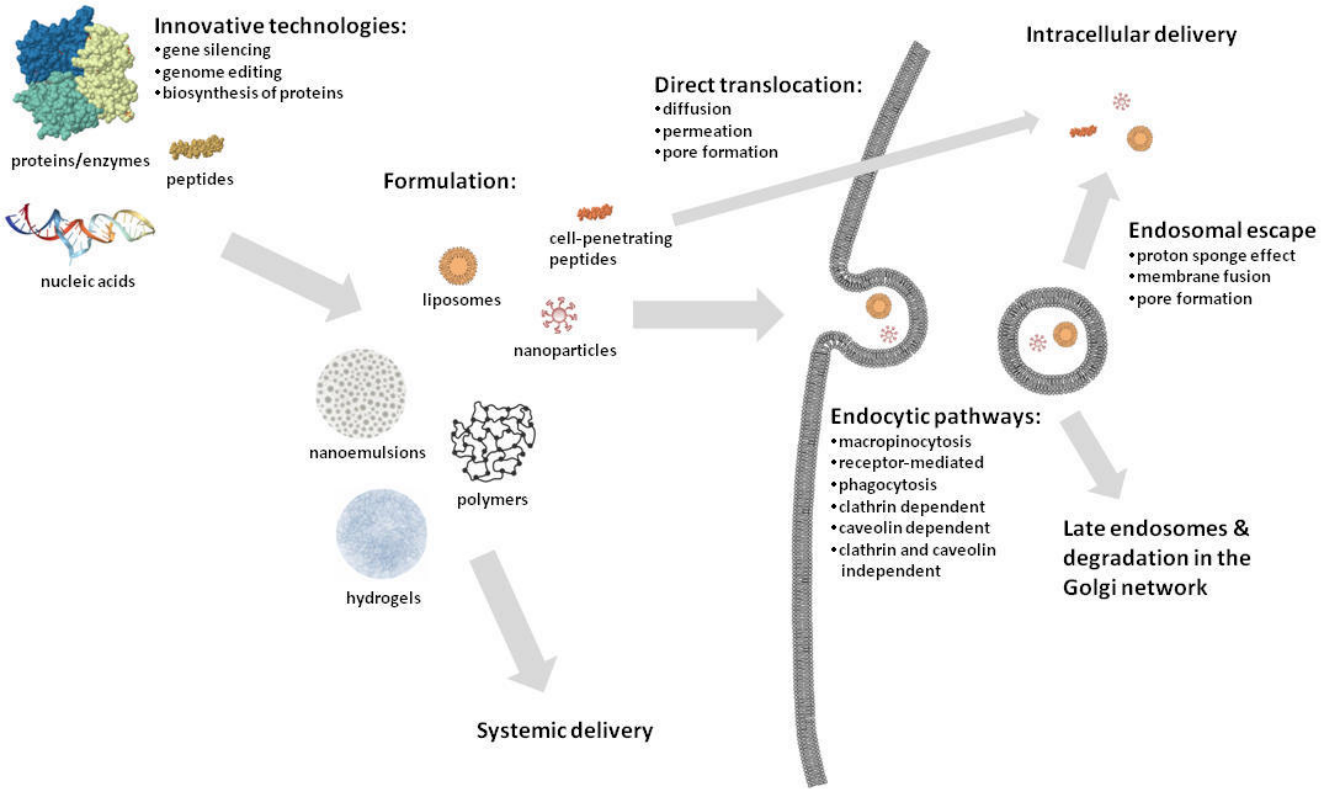

Scheme 2: Current drug delivery strategies allowing either for systemic or intracellular delivery of complex biomolecules enabeling future-oriented technologies as e. g. gene silencing, genome editing, and biosynthesis of proteins.[21]

In addition to nanoparticle-based transport systems, cell-penetrating peptides (CPPs) are in research focus since almost two decades.[22] Following different mechanisms, cationic peptides enable highly efficient membrane transduction. It has been shown that conjugation of numerous cargoes, e.g. small molecules, antibodies, peptides, proteins, nucleic acids, as well as transport systems like liposomes or nanoparticles, with CPPs is able to improve their membrane translocation.[23] The applicability of cell-

penetrating peptides for drug delivery is currently in early clinical trials.[23] However, despite these impressive achievements, CPPs still possess significant drawbacks and need to be optimized with respect to stability, toxicity and uptake efficacy. Additionally, large-scale synthesis of cell-penetrating peptides is time-consuming and expensive; moreover, the peptidic structure limits the possibilities for optimization. These intrinsic handicaps can be omitted by using inert scaffold molecules lacking needless, in terms of function, structural moieties e. g. peptide backbone. Being potentially labile, these elements can in fact compromise the overall stability of the carrier. In general, exclusively the number and the spatial arrangement of the functional groups endowing the carrier with the ability to penetrate cells is crucial for the efficacy of such molecular transporters.[24] In order to maximize cellular uptake, compact and rigid assembly of functional groups is beneficial.

Molecular scaffolds that almost perfectly meet these requirements are polyhedral silsesquioxanes. They compose a particular class of silicon oxide nanoparticles comprising an inert inorganic core of mutually alternating Si and O atoms. Similar to silicone polymers, Si atoms can bear organic groups carrying a variety of addressable functional moieties. Due to their biocompatibility, silicones are used in many medical fields, and silsesquioxanes have found their application in medical engineering (for e.g. structuring of silicon resins), too.[25] Some silsesquioxane derivatives are hydrolysed under physiological conditions resulting in a mixture of primary and secondary siloxanes.[26] The duration of such processes strongly depends on the functional groups attached to the inorganic core and can therefore be tuned by appropriate selection of the organic residues.[27] The smallest representatives of this class of organic-inorganic hybrid molecules are cube-octameric silsesquioxanes (COSS). Its inorganic core is arranged in a cage-like structure and comprises a size of less than 1 nm.[28] Up to eight organic residues can be attached to the silicon atoms (scheme 3). Such high valency in combination with the small size and the highly defined structure makes COSS an attractive scaffold for medical applications. Today, COSS are manufactured on a large scale and a variety of inexpensive derivatives is commercially available.[29]

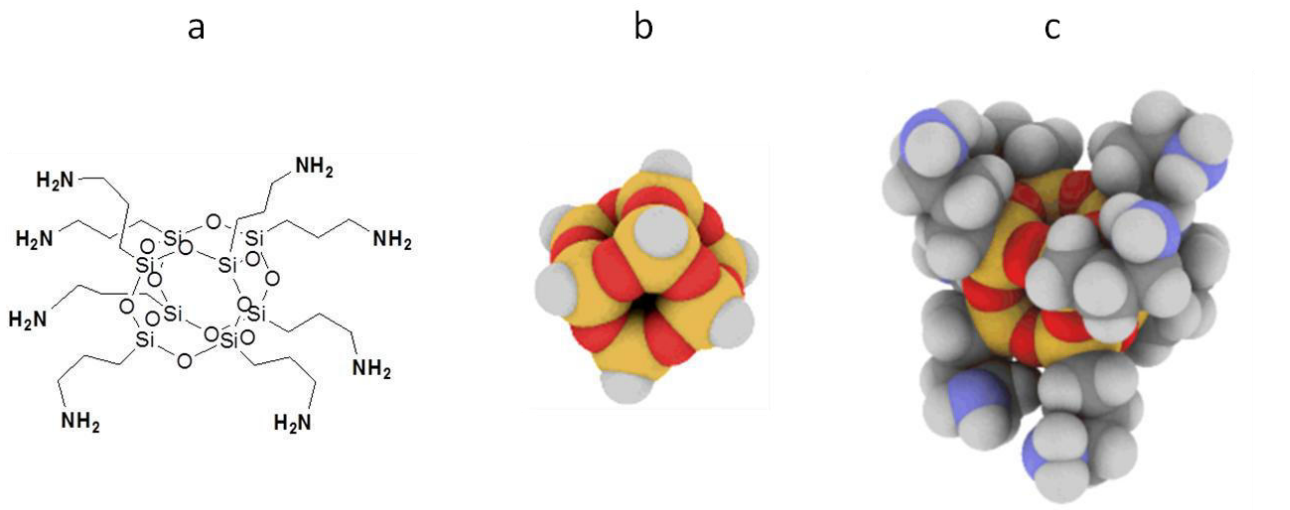

Scheme 3: a) Molecular structure of octakis(3-aminopropyl)octasilsesquioxane. b) Space-filling model of the inorganic core of COSS composed of Si (yellow) and O (red). For clarity, hydrogen (white) substituted COSS is shown. c) Space-filling model of octakis(3-aminopropyl)octasilsesquioxane composed of Si (yellow), O (red), C (grey), H (white), and N (blue).[30]

Objectives

1. The present cumulative dissertation is focused on the investigation of silsesquioxane nanoparticles as modular multifunctional platforms for the application in biomedical engineering and associated research areas. To itemize, COSS modules were considered as molecular frameworks for the intracellular delivery of bioactive cargoes. Indeed, the unique architecture of cube-octameric silsesquioxanes allows to tailor their pendant groups in such a way that efficient cell penetration could be achieved. On the other hand, each cargo of interest could be covalently attached to the COSS scaffold at the desired (up to eight monomers) oligomerization degree. To achieve these goals, several issues have to be addressed.

2. A simple and efficient method for the biofunctionalization of COSS scaffolds must be elaborated, providing compatibility with multifunctional biomolecules and support integrity of the siloxane core. To this end, the focus was set on site-selective covalent attachment of bioactive peptides of different size and molecular complexity.

3. Taking into consideration the limited stability of COSS system in the presence of certain nucleophiles, a viable functionalization strategy must be developed that is based on efficient biorthogonal transformations. This synthetic scheme must allow for the controlled, single-corner COSS derivatization with the molecules of peptidic nature.

4. The suitability of COSS as a drug delivery vehicle should be evaluated upon import of an engineered peptidic cargo targeting a particular cellular compartment in living mammalian cells. The effects of the carrier on biological systems must be studied *in vitro*.

5. Engineering of COSS scaffold to improve its cell-penetrating efficiency must be conducted. Thus, based on the knowledge on permeation mechanisms and chemical moieties required, the pendant groups must be suitably manipulated. The required chemistry must be established, and the properties of novel compounds have to be studied in detail. In order to assess the potency of novel COSS derivatives in cell experiments, the proper reporter and chemistry for its covalent attachment must be considered as well.

6. The biological effects of the novel cell-penetrating COSS modules must be carefully investigated with respect to their potential medical applications. This includes studies on uptake mechanisms, toxicity, and degradation in living cells.

Conclusions

For functionalization with peptides and miniproteins, COSS bearing eight aminopropyl groups was selected as starting material (discussed in section 8.1). Although pendant amine groups allowed to apply a vast arsenal of nucleophile-comprising chemical modifications, the synthetic procedure had to be carefully designed. Indeed, an intramolecular attack of the amino groups on the inorganic core leads to degradation of the siloxane cage following the so-called “back-bite” mechanism.[27] To avoid this uncontrolled degradation, all synthesis requiring basic reaction conditions were performed in dry solvents. Due to high polarity of octakis COSS derivative, only *N,N*’-dimethylsulfoxide (DMSO) was suited as a solvent for the introduction of functional groups at ambient temperature. In order to avoid thermal stress, the solvent was removed by lyophilisation.

In the present work, the amino groups were either transformed into different functional groups in order to modify the biological features of COSS, or were used for the introduction of functional groups allowing for the coupling of complex biomolecules. Functional groups allowing for the attachment of peptides and miniproteins were designed according to the repertoire of conjugation methods that can be applied to both peptidic and COSS counterparts. In general, besides high coupling efficacy the method must be biorthogonal and has to ensure the integrity of the inorganic core. Depending on the desired application, different coupling strategies have been selected and diverse ligation methods were established (Table 1). Thus, the well-established base-promoted conjugation via activated carboxylic acid was found inadequate due to the lack of selectivity. On the other hand, formation of a thioether between maleimide-bearing COSS and thiol-decorated peptides (i.e. those containing an additional cysteine residue) proceeded smoothly and was found suitable for the peptides lacking disulfide bonds. However, this method could not be applied to the cystine-rich molecules as e.g. knotted miniproteins. For the same reason, the promising thiazolidine ligation between an aldehyde and an aminoterminal cysteine had to be withdrawn.[31] The copper-catalyzed azide-alkyne cycloaddition that shows its maximal efficiency under alkaline aqueous conditions did not demonstrate its benefits in dry solvents.[32] Due to steric hindrance caused by the bulky and hydrophobic alkyne-bearing moieties, the copper-free version of this reaction was discarded as well.

Finally, the oxime ligation between aminooxy and aldehydic groups was identified as a viable coupling strategy.[33] Indeed, reactive carbonyls can be easily installed into biomolecules enzymatically[34] or upon periodate- or pyridoxal phosphate-mediated oxidation of certain N-terminal amino acids.[35] As the oxime ligation is carried out under acidic conditions, the integrity of the inorganic core of COSS is ensured in aqueous reaction media as well. Because aldehydes can be easily introduced into (oligo)saccharides by oxidation of their hydroxyls by sodium periodate, this ligation strategy can be considered as a versatile and highly efficient way towards biofunctionalization of COSS. Being applied to COSS functionalization with peptides of different length and architecture, this reaction enabled coupling of up to eight (in the case of peptides comprising 9-35 amino acids) and up to three (in the case of miniproteins with about 30 amino acids and three disulfide bonds) copies within few hours at ambient temperature. Oligomerization on the COSS scaffold did not compromise bioactivity of matriptase-1 inhibitors, as confirmed in an enzymatic assay.[36]

Table 1: Coupling strategies for biofunctionalization of COSS.

Coupling strategy	**Functional groups involved**	**Applicability**
Amide coupling	Activated carboxylic acid and amine	Not applicable due to lack of selectivity
Thioether formation	Maleimide and sulfhydryl	Suitable for peptides lacking disufide bonds; not applicable to cystine-rich molecules
Thiazolidine formation	*N*-termially installed cysteine and aldehyde	Suitable for peptides lacking disufide bonds. Not applicable to cystine-rich molecules
Copper-catalyzed azide-alkyne cycloaddition	Azide and alkyne	Not applicable to complex peptides due to compromized efficacy in dry solvents
Strain-promoted azide-alkyne cycloaddition	Azide and alkyne-bearing moiety	Not applicable due to bulky and hydrophobic alkyne-bearing moieties
Oxime ligation	Aminooxy and aldehyde	Applicable for conjugation of peptides of different length and architecture

Synthesized compounds were fully characterized by the appropriate analytical methods. The stability of COSS-oligomerised peptides was investigated under physiological conditions by size-exclusion chromatography. Whereas the inorganic core of fully-loaded peptide-COSS conjugates was found to be stable for at least 12 hours, degradation of partially functionalized cages occurred within few hours resulting in breakdown of the COSS oligomers. These observations indicate that the stability of the system can be customized to the individual needs by proper selection of the COSS pendant groups, conjugated ligands, and degree of oligomerization. In the case of binding peptides, COSS-based oligomers could contribute to tumour diagnostics by medical imaging as application of these constructs could improve both pharmacodynamics and binding strength. As the hydrolysis rate can be tuned, the patient exposure time to e. g. radioactive nuclides can be reduced.

Besides the establishment of an efficient method for oligomerization of peptides, the catalyst-free inverse electron demand Diels-Alder reaction (DAR_{INV}) (section 8.2) and disulfide-bond formation were successfully applied to single-corner modification of COSS scaffold. The applicability of both methods, which allow for the introduction of at least two different sorts of addressable moieties, was experimentally confirmed. Due to the reductive milieu of the cytoplasm, conjugation via disulfide bond enables fast release of the cargo after cellular uptake and is therefore particularly of interest for drug delivery.

In the frame of the present cumulative dissertation different COSS-based synthetic molecular transporters were developed with respect to cellular uptake and suitability for cargo transport. In the year 2005, COSS bearing seven aminopropyl groups has been found to be the smallest cell-penetrating nanoparticle to date.[37] To investigate whether polyhedral silsesquioxanes could serve as drug delivery modules, this heptaammonium COSS derivative was studied in detail (section 8.3). This study was aimed on functional transport of a peptide with low intrinsic membrane permeation ability in a cell culture experiment. By live-cell confocal imaging, efficient translocation of fluorescently labelled COSS in the nucleus was observed. In order to investigate suitability as a carrier molecule, a 17-residue peptide possessing high affinity towards the Proliferating Cell Nuclear Antigen (PCNA) was attached via a disulfide bond. PCNA is a DNA camp involved in DNA replication and repair. By live-cell confocal imaging, activity of the peptide after cellular uptake was proven by co-localization of the fluorescein-labelled PCNA-binding peptide with its target PCNA, genetically fused to the red fluorescent protein. Hereby, for the first time selective labelling of an enzyme inside living cells was achieved by using a rather short oligopeptide. Furthermore, the COSS transport system was investigated by flow cytometry to quantify cellular uptake in mammalian cells. Its efficacy was found to be in the same order of magnitude as that for the cell-penetrating peptide Tat.[38] In case of this well-known transporter, six arginine and two lysine residues define its cell-penetrating behaviour. In contrast to Tat, the investigated COSS derivative bears seven aminopropyl groups only. Therefore, its surprisingly high cellular uptake can be attributed to the rigid and dense assembly of the functional groups surrounding the inorganic core. Indeed, a significant increase in cellular import was achieved by reduction of conformal freedom upon cyclization of cell-penetrating peptides.[24a] Furthermore, the cubic structure of COSS presumably associated with the formation of ordered structures, as well as the exceptional arrangement of the functional groups could contribute to the observed increase in activity.[39] Indeed, evidence for spontaneous formation of ordered structures was also found upon atomic force microscopy (AFM) investigations.[40]

Since principle applicability of COSS for drug delivery was proven, the investigated COSS derivative was used as the starting point for the synthesis of improved transport systems. By chemical modification of the functional groups surrounding the COSS scaffold, the efficacy of cellular uptake was significantly improved. To this end, amine, guanidine, and trimethylammonium groups were installed at different remoteness from the inorganic core (section 8.4). Employing live-cell confocal imaging, intracellular localization of the fluorescently labelled COSS derivatives was verified in human cancer cell line HeLa. Thereby, more efficient cellular uptake and pronounced accumulation inside the nucleus was found for the compounds comprising shorter linkage between the siloxane core and the

charged counterparts. Less compact structure of COSS transporters (longer linkers) was associated with lower efficacy and cytoplasmic accumulation.
By using flow cytometry, these delivery modules were compared to well-established cell-penetrating peptides as Tat, Penetratin, and polyarginines.[22] Compared to the starting heptaammonium COSS, installation of permanently positively charged tetrasubstituted ammonium groups improved cellular uptake. However, the most efficient transport in all investigated cell lines (HeLa, HEK-293, and CHO) was demonstrated by the derivative bearing seven densely arranged guanidinium groups (GuCOSS). In HeLa cells, this carrier was found to be more efficient than both Tat (approximately 157 times) and decaarginine. Interestingly, cellular uptake of GuCOSS was 35-fold higher compared to that of cell-penetrating peptide heptaarginine, notwithstanding that both carriers bear the same number of identical guanidine groups. Thus, this gain in the efficacy can be attributed the unique, compact structure of the COSS scaffold. Additionally, fluorescence microscopy revealed indications for cellular uptake of the GuCOSS system in bacteria, yeasts and archaea. With regard to possible applications of GuCOSS as a molecular transporter for antibiotics, cellular uptake was in detail investigated in *E. coli*. To this end, bacteria were incubated with fluorescently labelled GuCOSS and solitary fluorescent dye tetramethylrhodamine (TAMRA), respectively. Whereas solitary TAMRA did not provide staining of bacteria, a strong fluorescence signal revealing for more than 36 hours was found when using labelled GuCOSS. As under physiological conditions the inorganic core of COSS degrades within this period and no staining of cells was observed with TAMRA alone, it could be concluded that the dye has been entrapped inside the cells.

In order to characterize the transporter with respect to potential *in vitro* and *in vivo* applications, toxicity studies were performed in HeLa cells. Thus, the toxicity of GuCOSS was found to be comparable to that of the derivative investigated in section 8.3, as well as to common cell-penetrating peptides.[38] Since the hydrolytic degradation of the inorganic core of COSS was described in detail, the GuCOSS transport system was characterized with respect to its stability.[26] To that end, degradation was quantitatively investigated at different pH values in time-resolved HPLC analysis. Thereby, direct correlation between pH value and half-life of the carrier was found. Whereas the transporter was stable under acidic conditions, elevated concentrations of nucleophilic hydroxyl ions present already at neutral pH promoted decomposition of the inorganic core. The degradation mechanism of COSS was investigated using mass spectrometry. It was found that the cubic architecture of the core is initially disrupted upon nucleophilic attack of hydroxyl ions at the silicon atoms. Further incorporation of hydroxyl ions ultimately leads to separation of silicon atoms bearing functional groups, thus the ability to translocate cellular membranes is lost. Complete hydrolysis of the inorganic core results in the formation of monomeric and dimeric hydroxyorganosilanes.[26] By using an assay based on a Förster resonance energy transfer (FRET), degradation of the GuCOSS system was found after about 11 hours in human blood serum and inside living HeLa cells. As low-molecular-mass fragments can be easily secreted, no intracellular accumulation of GuCOSS is expected.

Suitability of GuCOSS as a drug delivery vehicle was proven by transport of a model drug. For this experiment cytotoxic anti-cancer drug Doxorubicin was selected. By DNA intercalation, it interferes with DNA and RNA synthesis and inhibits Topoisomerase II, which results in the induction of cell death.[41] In cell culture experiments, COSS-conjugated Doxorubicin was significantly more effective than the solitary drug. As GuCOSS possesses good water solubility, it could serve as molecular transporter and solubility enhancer at the same time. Depending on the coupling strategy, either sustained release or immediate cleavage of the cargo inside the cell can be achieved. By control of the release rate, the intracellular localization of the cargo can be tailored as well. Due to rapid accumulation of the carrier in the nucleus, irreversible attachment using the DAR_{INV} described in section 8.2 can lead to sustained release upon hydrolytic degradation of the inorganic core. Thereby, a constant supply of this cellular compartment with the cargo of interest can be achieved. In recent years, bioorthogonality of the DAR_{INV} reaction has been demonstrated in numerous *in vitro* and *in vivo* studies. In the frame of the present research, it was proven that this coupling method is suited for

peptide conjugation due to its good to quantitative turnover rates.[42] This ligation approach was applied to the conjugation of peptides with silsesquioxane nanoparticles, too.
In order to achieve rapid release inside the cytoplasm, additionally a covalent ligation strategy based on a redox-controlled disulfide bond was established. Disulfide bond was formed either under oxidation with hydrogen peroxide, or applying activation of one thiols by Aldrithiol. As the second procedure allows for selective coupling under mild reaction conditions, this synthesis route should be concerned as the method of choice.

To summarize, different generally applicable and highly efficient conjugation methods were established for biofunctionalization of COSS with peptides and small molecules. Thereby, this unique scaffold molecule was made accessible for a vast number of scientific approaches based on oligomerization of biomolecules. Furthermore, a novel molecular transporter allowing for efficient cellular delivery of drugs and superior to common cell-penetrating peptides was developed. With its simple synthesis and the defined half-life under physiological conditions, GuCOSS could serve as a platform enabling future-oriented scientific and clinical approaches.

[1] a) N. A. Khazanov, H. A. Carlson, *PLoS Comput Biol* **2013**, *9*, e1003321; b) H. C. J. Ertl, B. Dietzschold, L. Otvos, *European Journal of Immunology* **1991**, *21*, 1-10.
[2] L. Otvos, J. D. Wade, *Frontiers in Chemistry* **2014**, *2*.
[3] a) K. Fosgerau, T. Hoffmann, *Drug Discovery Today* **2015**, *20*, 122-128; b) A. Padhi, M. Sengupta, S. Sengupta, K. H. Roehm, A. Sonawane, *Tuberculosis*, *94*, 363-373.
[4] D. J. Craik, D. P. Fairlie, S. Liras, D. Price, *Chemical Biology & Drug Design* **2013**, *81*, 136-147.
[5] a) D. W. Swistok, J. Khan, *Peptides for Youth. The Proceedings of the 20th American Peptide Symposium* **2009**, 467-468; b) P. Vlieghe, V. Lisowski, J. Martinez, M. Khrestchatisky, *Drug Discovery Today* **2010**, *15*, 40-56.
[6] B. J. Bruno, G. D. Miller, C. S. Lim, *Therapeutic delivery* **2013**, *4*, 1443-1467.
[7] V. Torchilin, *Drug Discovery Today: Technologies* **2008**, *5*, e95-e103.
[8] H. Brückner, A. D'Aniello, G. H. Fisher, N. Fujii, H. Homma, *Nova Biomedica Books* **2007**, 415-430.
[9] R. Webster, V. Elliot, B. Park, D. Walker, M. Hankin, P. Taupin, *PEGylated Protein Drugs: Basic Science and Clinical Applications* **2009**, *Basel, Switzerland*, 127-146.
[10] M. Gekle, E. Wischmeyer, S. Gründer, M. Petersen, A. Schwab, F. Markwardt, N. Klöckner, R. Baumann, H. Marti, *Taschenlehrbuch Physiologie* Thieme Verlag Stuttgart, **2010**.
[11] K. Kaushansky, *Trends in Endocrinology & Metabolism*, *8*, 45-50.
[12] a) S. Liu, *Bioconjugate Chemistry* **2009**, *20*, 2199-2213; b) L. Röglin, E. H. M. Lempens, E. W. Meijer, *Angewandte Chemie International Edition* **2011**, *50*, 102-112.
[13] G. M. Pauletti, S. Gangwar, T. J. Siahaan, A. Jeffrey, R. T. Borchardt, *Advanced Drug Delivery Reviews* **1997**, *27*, 235-256.
[14] a) A. K. Petrus, T. J. Fairchild, R. P. Doyle, *Angewandte Chemie International Edition* **2009**, *48*, 1022-1028; b) J. Wang, D. Wu, W.-C. Shen, *Pharmaceutical Research* **2002**, *19*, 609-614; c) J. Wang, D. Chow, H. Heiati, W.-C. Shen, *Journal of Controlled Release* **2003**, *88*, 369-380; d) T. Teesalu, K. N. Sugahara, V. R. Kotamraju, E. Ruoslahti, *Proceedings of the National Academy of Sciences* **2009**, *106*, 16157-16162.
[15] B. J. Aungst, H. Saitoh, D. L. Burcham, S.-M. Huang, S. A. Mousa, M. A. Hussain, *Journal of Controlled Release* **1996**, *41*, 19-31.
[16] D. B. T. Cox, R. J. Platt, F. Zhang, *Nat Med* **2015**, *21*, 121-131.
[17] K. Tiemann, J. J. Rossi, *EMBO Molecular Medicine* **2009**, *1*, 142-151.
[18] H. Samaranayake, T. Wirth, D. Schenkwein, J. K. Räty, S. Ylä-Herttuala, *Annals of Medicine* **2009**, *41*, 322-331.
[19] a) K. Y. Lee, S. H. Yuk, *Progress in Polymer Science* **2007**, *32*, 669-697; b) P. Shah, D. Bhalodia, P. Shelat, *System. Rev. Pharm.* **2010**, *1*, 24-32; c) A. Kumari, S. K. Yadav, S. C. Yadav, *Colloids and Surfaces B: Biointerfaces* **2010**, *75*, 1-18.
[20] C. A. Lackey, O. W. Press, A. S. Hoffman, P. S. Stayton, *Bioconjugate Chemistry* **2002**, *13*, 996-1001.

[21] a) M. Babu, N. Beloglazova, R. Flick, C. Graham, T. Skarina, B. Nocek, A. Gagarinova, O. Pogoutse, G. Brown, A. Binkowski, S. Phanse, A. Joachimiak, E. V. Koonin, A. Savchenko, A. Emili, J. Greenblatt, A. M. Edwards, A. F. Yakunin, *Molecular Microbiology* **2011**, *79*, 484-502; b) Talafous J., Marcinowski K. J., Klopman G., Z. M. G., *Biochemistry* **1994**, *33*, 7788-7796; c) S. Bourbigot, A. C. Dock-Bregeon, J. Coutant, B. Kieffer, I. Lebars, *Solution structure of the 5'-terminal hairpin of the 7SK small nuclear RNA*, DOI: 10.2210/pdb5iem/pdb, **2016**.

[22] a) D. Derossi, S. Calvet, A. Trembleau, A. Brunissen, G. Chassaing, A. Prochiantz, *Journal of Biological Chemistry* **1996**, *271*, 18188-18193; b) S. Futaki, T. Suzuki, W. Ohashi, T. Yagami, S. Tanaka, K. Ueda, Y. Sugiura, *Journal of Biological Chemistry* **2001**, *276*, 5836-5840; c) E. Vivès, P. Brodin, B. Lebleu, *Journal of Biological Chemistry* **1997**, *272*, 16010-16017.

[23] M. Rizzuti, M. Nizzardo, C. Zanetta, A. Ramirez, S. Corti, *Drug Discovery Today* **2015**, *20*, 76-85.

[24] a) G. Lättig-Tünnemann, M. Prinz, D. Hoffmann, J. Behlke, C. Palm-Apergi, I. Morano, H. D. Herce, M. C. Cardoso, *Nat Commun* **2011**, *2*, 453; b) R. M. Martin, G. Ter-Avetisyan, H. D. Herce, A. K. Ludwig, G. Lättig-Tünnemann, M. C. Cardoso, *Nucleus* **2015**, *6*, 314-325.

[25] H. P. P. Release, *Hybrid Plastics, Hattlesburg, MS, USA* **August 11 2011**.

[26] a) B. Trastoy, D. A. Bonsor, M. E. Pérez-Ojeda, M. L. Jimeno, A. Méndez-Ardoy, J. M. García Fernández, E. J. Sundberg, J. L. Chiara, *Advanced Functional Materials* **2012**, *22*, 3191-3201; b) J. Henig, É. Tóth, J. Engelmann, S. Gottschalk, H. A. Mayer, *Inorganic Chemistry* **2010**, *49*, 6124-6138.

[27] F. J. Feher, K. D. Wyndham, D. Soulivong, F. Nguyen, *Journal of the Chemical Society, Dalton Transactions* **1999**, 1491-1498.

[28] H. Mori, Y. Miyamura, T. Endo, *Langmuir* **2007**, *23*, 9014-9023.

[29] D. B. Cordes, P. D. Lickiss, F. Rataboul, *Chemical Reviews* **2010**, *110*, 2081-2173.

[30] Tarini M., Cignoni P., M. C., *IEEE Transactions on Visualization and Computer Graphics* **2006**, *12*, 1237-1244.

[31] D. Forget, D. Boturyn, O. Renaudet, E. Defrancq, P. Dumy, *Nucleosides, Nucleotides and Nucleic Acids* **2003**, *22*, 1427-1429.

[32] a) H. C. Kolb, M. G. Finn, K. B. Sharpless, *Angewandte Chemie International Edition* **2001**, *40*, 2004-2021; b) A. J. Dirks, S. S. van Berkel, N. S. Hatzakis, J. A. Opsteen, F. L. van Delft, J. J. L. M. Cornelissen, A. E. Rowan, J. C. M. van Hest, F. P. J. T. Rutjes, R. J. M. Nolte, *Chemical Communications* **2005**, 4172-4174; c) J.-F. Lutz, *Angewandte Chemie International Edition* **2007**, *46*, 1018-1025.

[33] a) A. Dirksen, T. M. Hackeng, P. E. Dawson, *Angewandte Chemie International Edition* **2006**, *45*, 7581-7584; b) O. Renaudet, D. Boturyn, P. Dumy, *Bioorg Med Chem Lett* **2009**, *19*, 3880-3883.

[34] D. Rabuka, J. S. Rush, G. W. deHart, P. Wu, C. R. Bertozzi, *Nat. Protocols* **2012**, *7*, 1052-1067.

[35] K. F. Geoghegan, J. G. Stroh, *Bioconjugate Chemistry* **1992**, *3*, 138-146.

[36] S. Fabritz, S. Horner, D. Konning, M. Empting, M. Reinwarth, C. Dietz, B. Glotzbach, H. Frauendorf, H. Kolmar, O. Avrutina, *Organic & Biomolecular Chemistry* **2012**, *10*, 6287-6293.

[37] C. McCusker, J. B. Carroll, V. M. Rotello, *Chemical Communications* **2005**, 996-998.

[38] S. Hörner, K. Sascha, C. Uth, M. Jöst, V. Schmidts, H. Frauendorf, M. C. Thiele, O. Avrutina, H. Kolmar, *Accepted Manuscript Angew. Chem. Int. Ed.* **2016**.

[39] S. Fabritz, S. Horner, O. Avrutina, H. Kolmar, *Organic & Biomolecular Chemistry* **2013**, *11*, 2224-2236.

[40] S. Horner, S. Fabritz, H. D. Herce, O. Avrutina, C. Dietz, R. W. Stark, M. C. Cardoso, H. Kolmar, *Organic & Biomolecular Chemistry* **2013**, *11*, 2258-2265.

[41] a) A.-M. Meredith, C. R. Dass, *Journal of Pharmacy and Pharmacology* **2016**, *68*, 729-741; b) Y. Sun, X. Yan, T. Yuan, J. Liang, Y. Fan, Z. Gu, X. Zhang, *Biomaterials* **2010**, *31*, 7124-7131; c) S. Wesselborg, I. H. Engels, E. Rossmann, M. Los, K. Schulze-Osthoff, *Blood* **1999**, *93*, 3053-3063.

[42] S. Hörner, C. Uth, O. Avrutina, H. Frauendorf, M. Wiessler, H. Kolmar, *Chemical Communications* **2015**, *51*, 11130-11133.

4. Summary

Cube-octameric silsesquioxanes (COSS) were investigated in the present cumulative dissertation as modular scaffolds for the application in biomedical engineering and associated research areas. Chemical modification of these unique organic-inorganic hybrids endowed them with novel features, aimed at functional tailoring towards executing certain biologic tasks.

Within the frames of this PhD research, the chemical and structural peculiarities of COSS nanoparticles were used to address two parallel issues, the first one being development of a viable route to peptide multimers, and the second one – elaboration of a molecular platform for efficient cellular transport. The results of the respective studies provided the basis for four full papers and one review in peer-reviewed scientific journals.

As octakis ammonium COSS provide eight addressable sites suitable for the conjugation with peptide ligands, the methods allowing for their efficient functionalization were established. Taking into consideration poor stability of COSS scaffold in the presence of hydroxyl nucleophiles, the chemical route to peptide oligomers was based on efficient oxime ligation that proceeds smoothly under slightly acidic conditions. Thus, the amine groups crowning the flanking arms were converted to highly reactive aminooxy functions and those reacted with the respective peptide aldehydes. As the introduction of addressable carbonyls in peptides is rather good elaborated and can be achieved both by the methods of organic synthesis and enzymatically, the developed procedure can be applied to a vast number of monomers possessing peptidic structure. In the frames of present PhD research, a set of peptides of different size, molecular complexity and biologic functions were oligomerized on COSS scaffolds, among them antimicrobial and integrin-binding peptides, K-coils, and inhibitors of serine proteases, i.e. the therapeutically relevant ones comprising up to three disulfide bridges. It was shown that the bioactivity of peptide ligands was not compromised upon conjugation to COSS scaffold.

Besides the establishment of the oximation method allowing for the simultaneous attachment of multiple peptides, different strategies were elaborated for the single-corner modification of a COSS framework in order to enable attachment of a solitaire peptide or other construct of interest. To this end, redox-labile covalent connection was realized by closure of an S-S bond at a thiol moiety installed by amide coupling of a single cysteine under stoichiometric control. The formation of a required disulfide proceeded either via oxidation with hydrogen peroxide, or upon pre-activation of one of the mercapto functions by 4,4'-dipyridyl disulfide. The formed bond could be easily opened as soon as the conjugate is exposed to the reducing environment of e.g. the cytoplasm. In addition to cleavable disulfide, the irreversible connection between COSS and the peptide of interest was established applying the version of Diels-Alder cycloaddition with inverse electron demand (DAR_{INV}). In the frame of the present PhD research, this pericyclic reaction was systematically investigated with respect to the applicability for the conjugation of structurally complex peptides and miniproteins. This highly efficient method was shown applicable to bioorthogonal attachment of individual peptides to the COSS framework.

The unique molecular structure of COSS offers not only the possibility to attach multiple copies of desired ligands at the termini of its pendant arms. Rigid and compact, but at the same time easily ruptured under physiological conditions, the silsesquioxane cage provides almost perfect framework for the development of new-generation biodegradable cell-penetrating compounds. Indeed, manipulating the charge and arrangement of residues surrounding the siloxane core caused certain biological effects in view of membrane permeation. Thus, COSS bearing seven aminopropyl groups was able to deliver a 17 amino acid peptide that binds to the proliferating cell nuclear antigen in the nucleus of living HeLa cells. Flow-cytometry studies in mammalian revealed cellular uptake efficacy comparable to common cell-penetrating peptides.

For the functional improvement of COSS-based transporters, selected functional groups were covalently grafted onto the inorganic core of COSS, and linkers of different length separated both structural motifs. In the resulting COSS constructs, the siloxane counterpart enabled compactness of the whole construct and biodegradability, and the pendant groups ensured both dense positive charge and the hydrophobic elements required for the passage through biological membranes. The cellular uptake of these novel derivatives was investigated by live-cell confocal microscopic imaging and flow-cytometry. These studies revealed improved cellular uptake for the derivatives comprising a more compact arrangement of the functional groups. In comparison to common cell-penetrating peptides (Tat, Penetratin, polyarginine) COSS bearing seven guanidinopropyl groups (GuCOSS) was 157 times more efficient as the Tat peptide and 35 times more efficient as the heptaarginine one. Since the number, nature and structure of the moieties inducing cell-penetration properties was similar for both transporters, this finding impressively confirms the importance of the COSS platform, which allows for compact and rigid assembly of guanidinium groups. In addition, unlike cell-penetrating peptides which need to be present above a certain concentration in order to permeate membranes, no minimal threshold was found for GuCOSS. Moreover, besides mammalian cells, GuCOSS-mediated cell penetration was observed in bacteria, yeast, and archaea.

As the highly efficient GuCOSS delivery module could represent an alternative for cell-penetrating peptides, it was thoroughly investigated and its ability to serve as a molecular transporter was verified by intracellular delivery of the cytotoxic drug Doxorubicin in an *in vitro* assay. By using an XTT cell viability test, its toxicity was found comparable to cell-penetrating peptides. Furthermore, the half-life of the hydrolytic disassembly of the inorganic core in living HeLa cells was determined as $t_{1/2}=149$ min. As the carrier degrades under physiological conditions, intracellular as well as renal accumulation is prevented and the risk of an immune response is considered low. Whereas the bioavailability of free Doxorubicin is limited due to its poor cell permeation, its activity could be significantly improved by using the GuCOSS transport system.

Due to the simple synthesis, highly efficient cell-penetration and a defined half-live under physiological conditions, the GuCOSS transport system could contribute to the toolbox of biomolecular research. As a platform technology for the transport of a vast number of drugs, among them small molecules, antibiotics, peptides, proteins, antibodies, and nucleic acids it could enable novel therapeutic approaches and find its way into clinical practice (potential areas for the application of COSS are presented in section 5.1).

5. Zusammenfassung

Die vorliegende kumulative Dissertationsarbeit behandelt die Erforschung von Silsesquioxan Gerüstmolekülen im Hinblick auf unterschiedliche biomedizinische Anwendungen. Durch die chemische Modifikation dieser einzigartigen organisch-anorganischen Hybridmoleküle konnten verschiedene biologische Effekte erzielt werden.

Im Rahmen der vorliegenden Forschungsarbeit wurden die chemischen und strukturellen Besonderheiten von Cube-octameric Silsesquioxanen (COSS) verwendet, um zwei Ziele zu erreichen: Erstens die Etablierung einer geeigneten Methode zur Multimerisierung von Peptiden und zweitens, die Entwicklung einer Plattformtechnologie für effizienten Wirkstofftransport. Die dabei erlangten Erkenntnisse waren die Basis für vier Manuskripte, welche nach der Begutachtung durch Experten in einem Peer-Review-Verfahren in Fachzeitschriften veröffentlicht wurden.

Die beschriebenen Methoden ermöglichen die effiziente Biofunktionalisierung von COSS mit Peptiden, Miniproteinen und niedermolekularen Verbindungen. Für die Kopplung von bis zu acht strukturell anspruchsvollen Peptiden wurde dazu die säurekatalysierte Oxim-Ligation angewandt. Mittels dieser Methode konnten auch bis zu drei Cystinknoten-Miniproteine binnen weniger Stunden ans COSS Gerüst gekoppelt werden, wobei deren inhibitorische Aktivität gegenüber der Serinprotease Matriptase erhalten blieb. Da die Integrität des Hydrolyse-empfindlichen anorganischen Kerns von COSS unter den sauren Reaktionsbedingungen nicht gefährdet wird und die zur Kopplung benötigten Aldehydfunktionalitäten leicht in Biomoleküle wie Peptide, Proteine und (Poly)Saccharide eingebacht werden können, ermöglicht die Etablierung dieser Funktionalisierungsstrategie die Anwendung von COSS in der biomedizinischen Forschung.

Neben der Methode zur Anbindung mehrerer Peptide wurden auch verschiedene Methoden zur Kopplung eines einzelnen Peptids etabliert. Die reversible Anbindung von Peptiden wurde dabei über eine Disulfidbrücke realisiert. Dazu wurde die Aminosäure Cystein in einer stöchiometrisch kontrollierten Reaktion via Amidkopplung an eine Ecke des COSS-Gerüsts gekoppelt. Das Schließen der Disulfidbindung gelang im Folgenden sowohl unter oxidativen Bedingungen durch den Einsatz von Wasserstoffperoxid als auch durch die Aktivierung mittels *4,4'*-Dipyridyldisulfid. Diese Bindung kann leicht unter reduzierenden Bedingungen gespalten werden, welche beispielsweise im Zytoplasma vorherrschen. Neben dieser reversiblen Anbindung wurde die Diels-Alder-Reaktion mit inversem Elektronenbedarf (DAR_{INV}) systematisch auf Ihre Eignung zur Konjugation von strukturell anspruchsvollen Peptiden und Miniproteinen untersucht. Damit steht diese Methode ebenfalls zur bioorthogonalen Anbindung einzelner Peptide an das COSS-Gerüst zur Verfügung.

Die einzigartige Struktur von COSS erlaubt nicht nur die Multimerisierung von Peptiden, sondern eignet sich auf grund der kompakten und starren Anordnung der den anorganischen Kern umgebenden Gruppen geradezu ideal für die Entwicklung neuer zellpenetrierender Verbindungen. So konnte mittels eines mit sieben Aminopropylgruppen funktionalisierten COSS ein 17 Aminosäuren langes, das Proliferating Cell Nuclear Antigen bindendes Peptid funktional in lebende HeLa Zellen transportiert werden. Im Rahmen durchflusszytometrischer Studien mit Säugetierzellen zeigte dieser molekulare Transporter trotz einer geringeren Anzahl von die Zellaufnahme vermittelnden funktionellen Gruppen eine mit gängigen zellpenetrierenden Peptiden vergleichbare Aufnahmeeffizienz.

Um verbesserte molekulare Transportsysteme zu entwickeln, wurden die funktionellen Gruppen am COSS Gerüst systematisch modifiziert. Dazu wurden kationische, die Zellaufnahme vermittelnde Gruppen, welche auch hydrophobe Strukturelemente enthalten in unterschiedlichem Abstand zum anorganischen Kern eingebracht. Die einzigartige Struktur von COSS ermöglichte dabei eine besonders kompakte Anordnung der kationischen funktionellen Gruppen. Darüber hinaus sind die auf diese Weise hergestellten molekularen Transporter durch den hydrolytischen Abbau des anorganischen Kerns unter physiologischen Bedingungen bioabbaubar.

Die Zellaufnahme der neu synthetisierten Derivate wurde in konfokalmikroskopischen und durchflusszytometrischen Studien untersucht. Dabei konnte eine verstärkte zelluläre Aufnahme im Falle von kompakter angeordneten funktionellen Gruppen gefunden werden. Im Vergleich zu den gängigen zellpenetrierenden Peptiden (Tat, Penetratin, Polyarginine) war der mit sieben Guanidinopropylgruppen funktionalisierte COSS (GuCOSS) rund 157 mal effizienter als Tat und ca. 35 mal effizienter als Heptaarginin. Diese deutliche Steigerung der Aktivität bei identischer Anzahl an die Zellaufnahme vermittelnden funktionellen Gruppen zeigt eindrucksvoll den Einfluss der Struktur von COSS. Diese erlaubt die gleichermaßen kompakte und rigide Anordnung der Guanidinogruppen. Im Gegensatz zu zellpenetrierenden Peptiden, welche oberhalb einer minimalen Konzentration vorliegen müssen um zellpenetrierend zu wirken konnte für GuCOSS kein minimaler Schwellwert für die Zellaufnahme gezeigt werden. Im Rahmen fluoreszenzmikroskopischer Untersuchungen wurden zudem Hinweise auf die Penetration von Bakterien, Hefen und Archaeen gefunden.

Da der hocheffiziente molekulare Transporter GuCOSS eine Alternative zu zellpenetrierenden Peptiden darstellt wurde er vollständig charakterisiert und als Modellsubstanz wurde das Chemotherapeutikum Doxorubicin im Zellkulturversuch in HeLa Zellen transportiert. Im Rahmen von XTT-basierten Zellviabilitätstests wurde eine mit zellpenetrierenden Peptiden vergleichbare Toxizität gefunden. Darüber hinaus wurde der hydrolytische Abbau des anorganischen Kerns mittels verschiedener Methoden untersucht und seine Halbwertszeit $t_{1/2}$ in lebenden HeLa Zellen zu 149 Minuten bestimmt. Da GuCOSS sich unter physiologischen Bedingungen mit der Zeit zersetzt, kann sowohl die Akkumulation im Gewebe als auch in den Nieren verhindert werden. Zudem ist das Risiko einer Immunantwort als gering anzusehen. Während das freie Doxorubicin eine geringe Membrangängigkeit und damit eine geringe Bioverfügbarkeit aufweist, konnte seine Effizienz durch den Transport mittels des GuCOSS Transportsystems erheblich verbessert werden.

Dank der einfacheren Synthese, der hohen Zellpenetration und einer klar definierten Halbwertszeit im physiologischen Umfeld könnte das GuCOSS System die biomolekulare Forschung vereinfachen. Als Plattformtechnologie für den Transport einer Vielzahl von Wirkstoffen wie niedermolekulare Verbindungen, Antibiotika, Peptide, Proteine, Antikörper und Nukleinsäuren könnte es praktische Anwendung im klinischen Umfeld finden und neue Therapieformen ermöglichen (potentielle Anwendungen für COSS werden im Abschnitt 5.1 vorgestellt).

6. Danksagungen

Den folgenden Personen möchte ich meinen aufrichtigen Dank aussprechen:

Meinem Doktorvater **Prof. Dr. Harald Kolmar** danke ich dafür, dass ich meine Doktorarbeit in seinem Arbeitskreis anfertigen durfte. Damit ermöglichte er es mir, meine Ausbildung gemäß meiner Interessen abzuschließen. Die von ihm bereitgestellt Infrastruktur in Kombination mit seinem interdisziplinären Team boten dafür das perfekte Umfeld. Im Rahmen seiner sehr guten Betreuung ließ er mir immer Freiräume, in welchem ich eine Vielzahl eigener Ideen umsetzen konnte. Dank ihm konnte ich mir mit dieser Forschungsarbeit einen Traum erfüllen, auf welchen ich zuvor lange hingearbeitet hatte. Dafür bin ich ihm sehr dankbar.

Ich danke **Dr. Olga Avrutina** für eine Vielzahl von wissenschaftlichen Diskussionen und ihre immerwährende Unterstützung. Sie vermittelte mir die Fertigkeit wissenschaftliche Texte zu verfassen und war stets eine in höchstem Maße kompetente und jederzeit hilfsbereite Ansprechpartnerin. Dank ihres unermüdlichen Engagements verstehe ich mich heute als Wissenschaftler. Vielen Dank dafür!

Ebenfalls danke ich **Dr. Andreas Christmann** für seine Unterstützung und seine Hilfsbereitschaft im Hinblick auf fachübergreifende Fragestellungen.

Ich möchte mich bei **allen derzeitigen und ehemaligen Mitgliedern des Arbeitskreises** um Prof. Kolmar für eine großartige Zeit bedanken. Die Zusammenarbeit mit allen Kollegen war für mich stets ein Genuss und ich möchte allen für ihren Beitrag zur freundschaftlichen Atmosphäre im Arbeitskreis danken. Auf Grund der erfolgreichen engen Zusammenarbeit und den teilweise über die Grenzen des Arbeitskreises hinausreichenden Beziehungen gilt mein besonderer Dank **Dr.-Ing. Christina Uth**, **Carolin Patricia Mai**, **Dr. Maren Paschke**, **Dr. Thomas Hofmeyer**, **Dr.-Ing. Sebastian Fabritz**, **Nicklas Weber**, **Dr. Stefan Zielonka**, **Sascha Knauer** und **Janine Becker**. Ohne Euch wäre die Zeit niemals so großartig gewesen und ich danke euch für diese wertvollen Erinnerungen.

Allen **Kooperationspartnern und Koautoren** danke ich für die ergiebige Zusammenarbeit. Gerade durch die fachübergreifenden gemeinsamen Arbeiten ergaben sich oft besondere Synergien. Die Interdisziplinarität der Fragestellungen, welche wir in unseren Publikationen behandelten machten für mich immer den besonderen Reiz aus.

Ferner danke ich **Dr. Anna-Lena Krause**, **Michael Haag**, **Jan Willing**, **Sven Messerschmidt** und **Dr.-Ing. Tobias Larem** für eine großartige Zeit außerhalb der Universität. Die Zeit die ich mit euch verbracht habe hat mir immer sehr geholfen die Balance zu wahren. Danke für eure langjährige Freundschaft und eine Menge Spaß.

Zu guter Letzt danke ich meinen Eltern **Annette und Bernhard Hörner** dafür, dass diese mir eine solch hervorragende Ausbildung ermöglicht haben. Ihr unermüdliches Investment machte diesen erfolgreichen Abschluss letztlich erst möglich. Dafür, dass ich mich uneingeschränkt persönlich entfalten konnte danke ich ihnen von ganzem Herzen.

7. Introduction

7.1. Bioconjugation on Cube-octameric Silsesquioxanes (COSS)

Title:

Bioconjugation on Cube-octameric Silsesquioxane

Authors:

Sebastian Fabritz,[‡] Sebastian Hörner,[‡] Olga Avrutina und Harald Kolmar.

Bibliographic data:

Organic & Biomolecular Chemistry
Volume 11, pages 2224-2236, October 24th 2012
DOI: 10.1039/C2OB26807H
For the first time published in the internet on October 24th 2012

Graphical abstract:

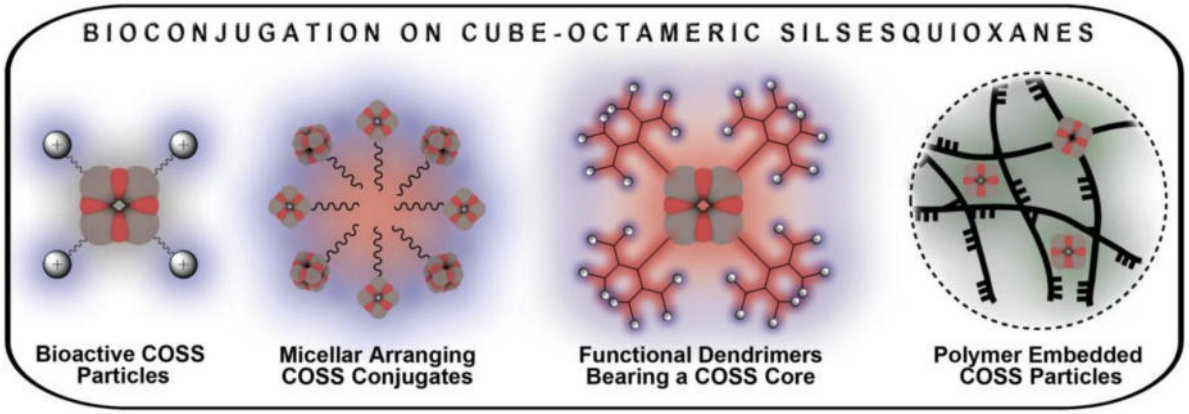

Summary:

The present article summarizes current applications of silsesquioxanes in biomedical research. Key subjects as chemical and bioothogonal modification, stability, toxicity, molecular self-organization, bioconjugation, as well as application as molecular probe and drug delivery module are addressed in detail.

Contributions by Dipl.-Ing. Sebastian Hörner:

Dipl.-Ing. Sebastian Hörner und Dr.-Ing. Sebastian Fabritz contributed equally to the review article and the corresponding front page.

‡ shared lead author

Organic & Biomolecular Chemistry

www.rsc.org/obc

Volume 11 | Number 14 | 14 April 2013 | Pages 2215–2378

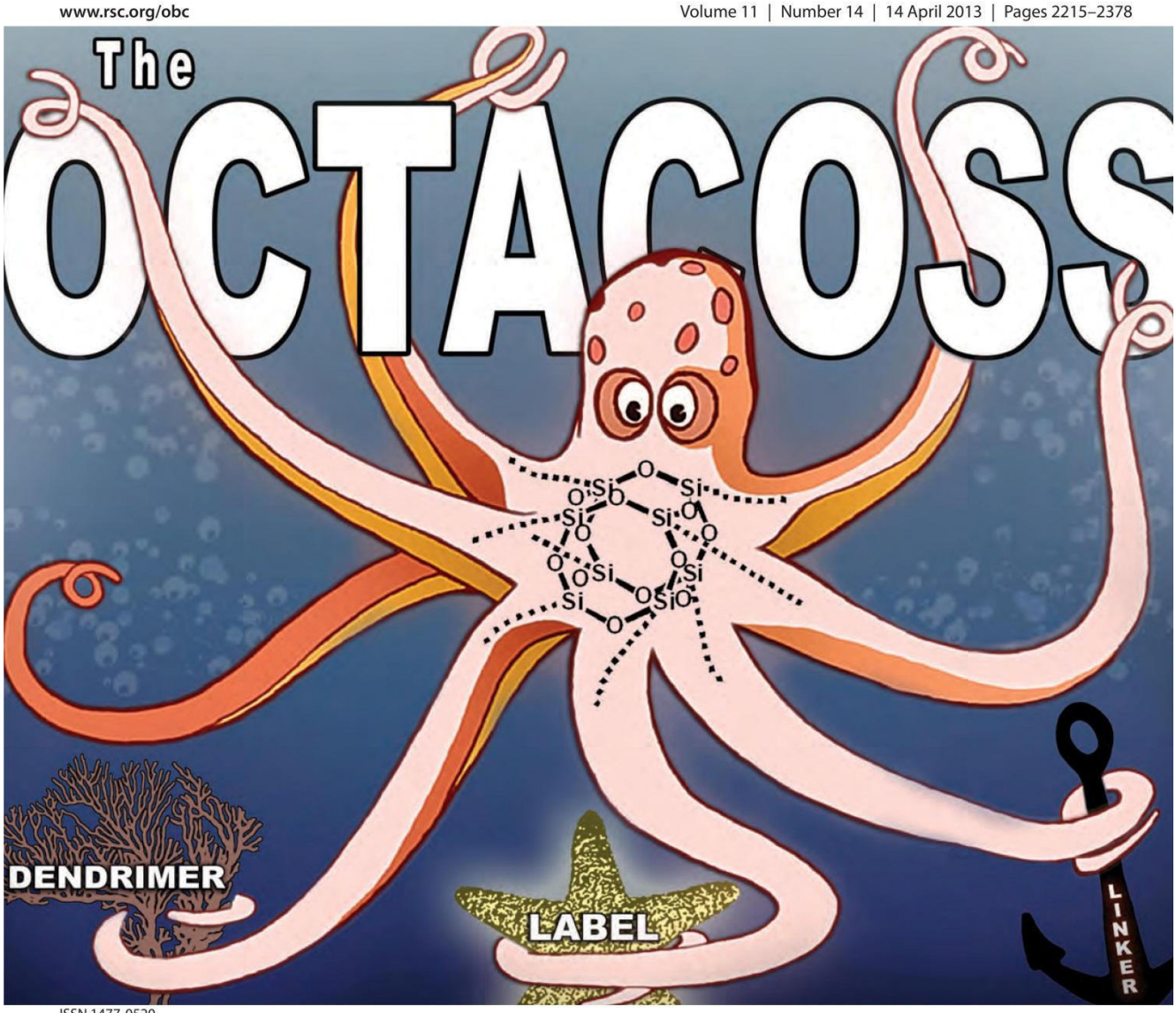

ISSN 1477-0520

RSC Publishing

PERSPECTIVE
Sebastian Fabritz *et al.*
Bioconjugation on cube-octameric silsesquioxanes

1477-0520(2013)11:14;1-C

Cover page of „Organic and Biomolecular Chemistry“ (issue 14, 2013). Reproduced with permission of the Royal Society of Chemistry.

Organic & Biomolecular Chemistry

RSC Publishing

PERSPECTIVE

View Article Online
View Journal | View Issue

Bioconjugation on cube-octameric silsesquioxanes

Cite this: *Org. Biomol. Chem.*, 2013, **11**, 2224

Sebastian Fabritz,†* Sebastian Hörner,† Olga Avrutina and Harald Kolmar

Received 14th September 2012,
Accepted 23rd October 2012

DOI: 10.1039/c2ob26807h

www.rsc.org/obc

Small, compact, and highly symmetric cube-octameric silsesquioxanes have recently attracted increased attention as scaffolds for tailor-made bioconjugates. The expanded arsenal of effective conjugation methods (CuAAC, TEC, oxime ligation) allows one to decorate these nanoparticles bearing up to eight addressable organic substituents, with a wide range of biorelevant ligands, among them carbohydrates, peptides, miniproteins, reporter molecules, and rare-earth chelates. Low toxicity of COSS-based molecules combined with solubility in aqueous systems and half-life sufficient for *in vivo* studies make these structures attractive targets for a number of applications, among them drug delivery, tumor diagnostics and therapy.

1 Introduction

Cube-octameric silsesquioxanes (COSS), widely used in fine-tuned polymeric compositions (the topic is reviewed in ref. 1–3), have recently found biochemical application in their monomeric form. A broad range of COSS-based hybrid systems has been developed, which are used in drug development, delivery, and diagnostics.[4–6] Currently, bio-inspired research taking advantage of these versatile scaffolds is a fast-growing field, and it seems like the era of COSS has just begun.

COSS belong to the group of silica nanoparticles and are highly symmetric hybrid molecules comprising an inorganic core composed of silicon and oxygen. Every silicon atom is linked to an organic residue allowing for further modifications. The molecular composition of silsesquioxanes, first reported in 1874,[7] is given by the empirical formula $(RSiO_{1,5})_{2n}$ where n is an integer and R substitutes hydrogen or aliphatic organic groups.[8,9] The synthesis of cube-octameric silsesquioxanes corresponding to the formula $(RSiO_{1.5})_8$ was first described in 1955 by Sprung and Guenther.[10] In an analogous manner, silsesquioxanes bearing pendant functional groups were first synthesized in the 1990s by hydrolytic condensation of organosilicon monomers $RSiX_3$ (Fig. 1, R = organic residue; X = halogen or alkoxide).[11,12] Today, fine-tuned experimental procedures employing tetra-*n*-butylammonium fluoride[13] or di-*n*-butyltin dilaurate[14] as a catalyst allow for multigram production of COSS within several days.

Polyhedral silsesquioxanes are classified depending on either the number of silicon atoms within their core (T_6, T_8, T_{10},

Clemens-Schöpf Institute of Organic Chemistry and Biochemistry, Technische Universität Darmstadt, Petersenstr. 22, 64287 Darmstadt, Germany. E-mail: SFabritz@Biochemie-TUD.de
†These authors contributed equally to this work.

Sebastian Fabritz

Sebastian Fabritz, born 1982, studied chemistry in Darmstadt and spent an academic year at the University of Bristol, UK. He received the Dr. Anton Keller Foundation award for exceptional achievements in the diploma chemist main exams. He is currently at the final stage of his PhD thesis dealing with biofunctionalization of COSS under the supervision of Prof. Harald Kolmar.

Sebastian Hörner

Sebastian Hörner, born 1982, studied chemistry at the Technische Universität Darmstadt and spent an academic year at the University of Alcalá de Henares (Spain). Currently he is working on his PhD thesis focused on bioconjugation on nanoparticle scaffolds, under the supervision of Prof. Harald Kolmar.

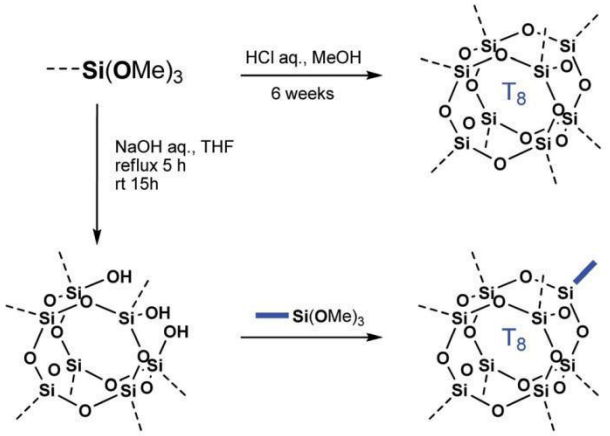

Fig. 1 Organosilicon monomers SiX_3 (exemplary depicted as a methoxy derivative) can be condensed to form a cube-like cage structure. The formation of a desired condensation product is solvent- and time dependent and can be therefore controlled.[12,15] Incompletely condensed COSS allow for the introduction of a heterogeneous residue at one corner of the cage. Dotted and fat blue bonds depict organic ligands.

T_{12},...T_n; T stands for a silicon atom bearing three oxygens also connected to silicon) or according to their geometry (octahedral, decahedral, *etc.*). Interestingly, the cubic cage architecture is favored in organo-silsesquioxanes due to steric effects,[13] while silsesquioxanes bearing small organic residues form polyhedrals with n = 10, 12, 14, and 16.[8,9]

To date, two approaches have been generally applied to the synthesis of functional COSS derivatives. Functional moieties can be introduced upon corner capping of incompletely condensed COSS cores[15] (see section 3.1) or, alternatively, an intact T_8 cage can be modified towards COSS derivatives with tailor-made reactive moieties. Improvements of synthetic strategies allowing for the manipulation of pendant organic groups (see sections 2 and 3), as well as recent commercial availability of a wide range of silsesquioxane monomers, have contributed to the rapid development of COSS chemistry within the last few decades.

2 Functionalization of COSS scaffolds

Several different approaches for the functionalization of the inorganic COSS core have been reported to date (reviewed in ref. 16). Although the main efforts in this field are aimed at the derivatization of fully condensed COSS particles, chemical modifications of their monomeric precursors are known as well.[17]

To date, the condensation of commercially available halo- or aminopropyl-substituted alkoxysilanes is the most popular method as it provides diverse COSS particles allowing for the variation of their pendant functional residues. Indeed, taking the octachloropropyl COSS as a starting compound, a number of functional groups can be introduced by nucleophilic substitution, among them azides,[18–20] nitriles,[21] thiocyanates,[12] ethanthiolates,[22] as well as bromides[19] and iodides.[12] These groups allow for further modifications towards *e.g.* carboxylic acids[21] or alcohols.[23]

Another versatile COSS particle is the 3-aminopropyl-substituted one. Besides direct conversion into azides,[24,25] carboxylates,[23] and alkenes,[23] various functionalities could be introduced onto this framework by amide coupling using respective derivatives of carboxylic acids.[23,26] Finally, octaphenyl silsesquioxanes allow for the incorporation of aminophenyl, azidophenyl,[27] carboxyphenyl,[28] and maleimidophenyl[29] groups by aromatic nitration with subsequent hydrogenation followed by further modifications (the synthesis and modification of polyhedral phenylsilsesquioxanes are also reviewed in ref. 30). COSS modifications resulting in addressable functional groups are listed in Table 1.

Interestingly, several enzymes have been recently identified which are able to catalyze siloxane bond formation.[31–33] Enzyme-mediated modifications of COSS ligands have been reported by Ihara *et al.*[31–34] Hence, transformations employing enzymatic catalysis can be considered as interesting alternatives to chemical methods that merit further exploration.

Starting from hydrido-silsesquioxanes as the simplest COSS derivatives, epoxides[35] and nitriles[12] can be installed in the

Olga Avrutina

Olga Avrutina, born 1970, studied chemistry in Belarusian State University (Minsk). In 2006, she completed her doctorate under the supervision of Prof. Ulf Diederichsen at Georg-August-Universität Göttingen. She is currently working in the research group of Prof. Harald Kolmar. Her interests focus on design and synthesis of bioactive multivalent peptides and proteins.

Harald Kolmar

Harald Kolmar, born 1961, is full professor at the Technische Universität Darmstadt, where he has been the head since 2005 of the Department of Applied Biochemistry. His current scientific interests mainly focus on protein engineering and design, nanobiotechnology, chemical biology and development of tailor-made peptides for applications in diagnostics and therapy.

Table 1 Alphabetical list of COSS scaffolds allowing for bioconjugation

Ligand/functionality	Precursor	Applied reaction	Yield	Subsequent conjugation chemistry	Year	Ref.
α–β Unsaturated carboxylic acid	Octaammonium	Anhydride opening	64%	Amide coupling/esterification	1999	23
Acetophenone	Octaphenyl	Friedel–Crafts reaction	n.a.	Oxime ligation	2012	28
Allyl	Octaammonium	Addition	90%	Cross-metathesis/hydrosilylation/thiol–ene	1999	23
Amine	Monomer	Condensation	93%	Amide coupling/S_N	2005	58
Amine (hydrochloride)	Monomer	Condensation	30%	Amide coupling/S_N	1998	59
Aminooxy	Octaammonium	Amide coupling	4–33%	Oxime ligation	2012	26
Aminophenyl	Octaphenyl	Nitration/hydrogenation	68%	Amide coupling/S_N	2011	27
Azide	Octaiodo	S_N	90%	CuAAC/SPAAC/Staudinger ligation	2010	20
Azide	Octaammonium	Diazotransfer	60–73%	CuAAC/SPAAC/Staudinger ligation	2010	24, 25
Azide	Q8	Hydrosilylation/oxirane opening	90–91%	CuAAC/SPAAC/Staudinger ligation	2012	36
Azidophenyl	Octaaminophenyl	Diazotation/S_N	76%	CuAAC/SPAAC/Staudinger ligation	2012	27
Benzaldehyde	Octavinyl	Hydrosilylation	92%	Schiff base formation	2001	37
Bromo	Octachloro	S_N	91%	S_N/Grignard/cross-coupling	2010	19
Carboxylic acid	Octaammonium	Anhydride opening	58%	Amide coupling/esterification	1999	23
Carboxylic acid	Octanitrile	Hydrolysis	quant.	Amide coupling/esterification	2012	21
Carboxyphenyl	Octaphenyl	Friedel–Crafts reaction	85%	Amide coupling/esterification	2012	28
Chloro	Monomer	Condensation	25–35%	S_N/Grignard	1995/2008	12, 14
Epoxide	Monomer	Condensation	n.a.	Oxirane opening	2006	60
Epoxide	Q8	Hydrosilylation	>80%	Oxirane opening	2001	35
Hydroxy	Octaammonium	Amide coupling	23%	Esterification/ether bond formation/S_N	1999	23
Hydroxy	Octaiodo	Nitration/hydrogenolysis	85%	Esterification/ether bond formation/S_N	1999	23
Iodo	Octachloro	Finkelstein reaction	quant.	S_N/Grignard/cross-coupling	1995	12
Iodophenyl	Octaphenyl	Iodination	80–90%	S_N/Grignard/cross-coupling	2010	61
Maleimidephenyl	Octaaminophenyl	Dehydration	79%	Thioether formation	2001	29
Nitrile[a]	Octachloro	S_N	98%	Hydrolysis/hydration	2012	21
Nitrile[a]	Octahydrido	Hydrosilylation	93%	Hydrolysis/hydration	1995	12
Nitrophenoxy[b]	Octaepoxy	Oxirane opening	99%	Hydration	2012	36
Nitrophenyl[b]	Octaphenyl	Nitration	90%	Hydration	2001/2011	27, 29
Sulfhydryl	Monomer	Condensation	>50%	Thioether/disulfide formation	1995	12

[a] Precursor for carboxy-functionalized COSS. [b] Precursor for amine-functionalized COSS, n.a.: not available.

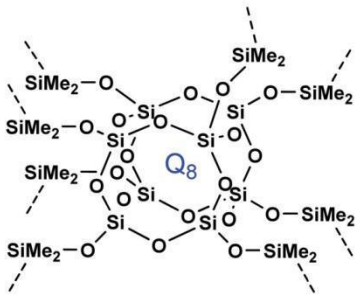

Fig. 2 Schematic depiction of a Q_8 silica particle. Q indicates that each core silicon atom features four oxygen interactions. Dotted bonds depict organic ligands.

siloxane framework upon hydrosilation using alkene-bearing building blocks. In the same manner olefinic residues carrying epoxide[35,36] groups can be incorporated into spherosilicates, COSS-like particles bearing additional eight silicon atoms (Fig. 2, Q8 particles). The introduced epoxide moieties allow for a subsequent transformation into hydroxy, azide, or nitrophenyl functionalities by oxirane ring-opening reaction.[36] Conversely, silicon-bearing benzaldehyde building blocks can be attached to olefinic COSS derivatives.[37]

3 Bioorthogonal functionalized COSS scaffolds

3.1 Homofunctional COSS scaffolds

COSS scaffolds that allow for bioconjugation are listed in Table 1. For biochemical applications, azidopropyl-functionalized COSS are widely used (see section 7) as they are bioorthogonally addressable either *via* the copper-catalyzed azide–alkyne cycloaddition (CuAAC)[38,39] or by the strain-promoted cycloaddition (SPAAC)[40] employing cyclooctyne derivatives. Alternatively, the oxime ligation turned out to be a particularly powerful method for the oligomerization of aldehyde-bearing ligands on a COSS scaffold.[26] Aminooxy moieties can be grafted onto octaaminopropyl COSS by amide coupling using a respective carboxylic acid derivative.[26] Oximation provides the selectivity required for biochemical applications, addressing bioorthogonal aldehyde or ketone groups[41] which can be easily incorporated into peptides and proteins by mild sodium periodate oxidation of *N*-terminal serine residues.[42] Conversely, aldehyde-bearing silsesquioxanes[37] can be considered as potential candidates for the conjugation with aminooxy-decorated biomolecules. Another substituted silsesquioxane is the octavinyl COSS as it can be addressed *via* thiol–ene[43] or cross-coupling reactions.[44]

Apart from the discussed amine, azide, and vinyl substituents which have already demonstrated their utility for COSS-based ligations with biomolecules, a number of other functional moieties were applied for bioconjugation. Thus, introduction of epoxides allows for the reaction with amine- or hydroxyl-bearing coupling partners *via* nucleophilic ring opening,[45] while maleimide-functionalized COSS could be decorated with substituted thiols through the formation of stable thioethers.[29] Additionally, innovative bioorthogonal coupling strategies as the inverse electron-demand Diels–Alder reaction[46] could contribute to the tool set of COSS-based bioconjugations.

3.2 Heterofunctional COSS scaffolds

Bifunctional COSS derivatives combining two selectively addressable functionalities can be generated either by stoichiometrically controlled single-corner ligation on a fully condensed particle or *via* the corner capping of incompletely condensed COSS. Resulting molecules can be used as a starting point for the design of compounds with higher structural hierarchy and peculiar properties. Vinyl-modified silsesquioxanes are especially suited for the synthesis of heterobifunctional COSS constructs as vinyl groups are bioorthogonal (Fig. 3). Recently, COSS molecules bearing seven vinyl and one hydroxyethyl substituent have been synthesized by stoichiometrically controlled reactions.[47] Thus, to a single-corner hydroxy group of heptavinyl COSS a hydrophobic polymer was attached upon polymerization. Subsequent modification of the remaining seven alkenes with hydrophilic moieties such as alcohols,[48,49] carboxylic acids,[48,50] or carbohydrates[48] resulted in a number of amphiphilic siloxane derivatives which exhibit potentially useful biophysical properties.[48] Moreover, fluorescent dyes and amino acids have been single-corner grafted onto azide-[19,51] or amine-bearing[4,51,52] COSS. The resulting conjugates are of particular interest for biomedical microscopic studies.[4,52]

Bifunctional COSS may serve as scaffolds for the oligomerization of bioactive molecules, such as peptides and carbohydrates, allowing for the additional attachment of reporter molecules. Therefore, they are well-suited for *e.g.* theranostic *in vivo* studies.

The addition of functional groups to partially condensed COSS using the corner-capping approach is limited to the modification of aliphatic- and aromatic-substituted cages and results in single-corner-functionalized scaffolds bearing carboxy,[53] halogen,[53] azide,[53] amine[54] or hydroxy[53] groups. Additionally, it appeared possible to cap multiple corners of COSS with monomeric building blocks that bear functional molecules such as *e.g.* fluorescein. Thus, a cell-penetrating fluorescein-labeled, heterobifunctionalized aliphatic COSS particle comprising an additional amino or carboxy site for successive attachment of cargo molecules was examined in microscopic studies on human cancer cells.[55]

Today, incompletely condensed cages and suitable monomers bearing a broad range of functional groups are commercially available (Hybrid Plastics Inc., USA; SiKÉMIA, France). Therefore, the modular approach to the synthesis of novel heterobifunctional COSS derivatives becomes possible.

Finally, the application of heterobifunctional COSS can be extended if heterodimeric COSS conjugates are considered. Li *et al.* recently approached this strategy by fusing an aliphatic and a vinylic COSS through esterification using a dicarboxy linker.[56]

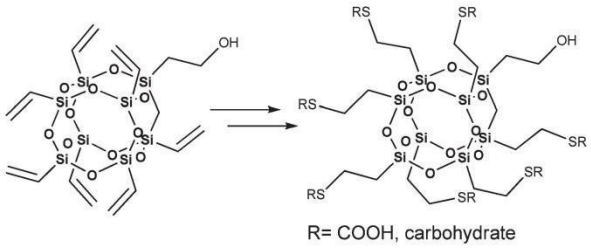

Fig. 3 Heptavinyl hydroxyethyl COSS is a heterobifunctional scaffold allowing for additional functionalization *via* thiol–ene click reactions.

4 Hydrolytic stability of COSS particles

A remarkable feature of the COSS cage is its stability that is highly dependent on the environment. Although the rigid inorganic core endows COSS with chemical and thermal robustness,[54] the nature of its corner substituents crucially influences the stability, *i.e.* integrity of the whole framework. Considering the latter issue, it is essential to distinguish between cage rearrangement and its breakdown.

Rearrangement of a T_8 cage to T_{10} and T_{12} structures was observed in potassium carbonate or sodium hydroxide solutions, where the tendency to undergo such rearrangements seemed to correlate with the electronegativity of a terminal moiety X within the pendant ligands in octa(3-X-propyl) COSS ($X = H < I < C_6F_6 < Br < Cl < NCS$).[57]

As the inorganic core of COSS is formed upon condensation under acidic conditions, the incubation in a basic medium might cause hydrolytic decomposition of the system. Furthermore, it was shown that amines accelerate the degradation of COSS in wet solvents.[23] Therefore, it is advisable to use dry organic solvents or acidic aqueous media for silsesquioxane reactions or storage. Interestingly, the breakdown of aminopropyl-substituted siloxanes has been suggested to follow a back-bite mechanism. In this case, the amino groups themselves may intramolecularly attack the core, thus promoting decomposition.[23]

In recent years, extensive studies concerning the half-life of different monomeric COSS derivatives and their breakdown products were performed. The degradation of carbohydrate-functionalized COSS in different buffer systems under different pH was studied. Both, the buffer composition and the pH, were found to influence the half-life of the COSS scaffold. In 4-(2-hydroxyethyl)-1-piperazineethanesulfonic acid (HEPES) buffer at pH 6.55 the degradation was completed within 48 hours as determined by comparison of ^{29}Si-NMR

shifts. In contrast, at pH 7.20 the signal corresponding to the breakdown products was found already after 21 hours. In phosphate buffer at pH 6.35 degradation occurred much faster and was completed within 24 hours.[62] More detailed studies that extended analytics to the breakdown products of COSS were performed using silsesquioxanes decorated with macrocyclic Gd^{3+} chelates (2D ^{1}H, ^{29}Si HSQC-NMR, ESI-MS and relaxivity measurements). At pH 7.0 in deuterated water NMR signals corresponding to the completely degraded species were observed only after 7 days. Further core stability tests were based on water relaxivity measurements that quantified the rigidity of the core-attached Gd^{3+} chelates. Combination with ESI-MS measurements provided detailed insights into the degradation of the core. In aqueous solution at pH 7.0 the MS signal corresponding to the intact COSS species faded within 48 h. After 14 days a complex mixture of partially degraded COSS was formed. For complete degradation at neutral pH it was necessary to heat the mixture to 75 °C for several days.[63] A further test that was performed under physiological conditions (HEPES buffer, pH 7.4–7.6, 37 °C) with and without fetal calf serum (FCS) indicated no additional destabilization of COSS caused by enzymatic degradation. Relaxivity measurements showed a first-order exponential decay corresponding to a half-life of 11–18 h for these special COSS derivatives. A plateau indicating no further degradation was reached after 5 days. These experiments clearly showed that the stability of the COSS framework is pH dependent as its half-life was dramatically shortened to about 55 min when measured in solution at pH 8.1–8.6.[63]

The tunable decomposition of COSS has been exploited for the synthesis of biodegradable polymers such as poly(L-lactide),[64,65] polycaprolactone, and polycarbonate polyurethane.[66] They were found to degrade faster when aliphatic COSS substituents have been incorporated into the framework.[64,65] However, the presence of COSS units in these polymers was supposed to have a stabilizing effect in the case of enzyme-mediated degradation.[66]

In conclusion, the hydrolytic stability of the COSS core depends on its ligands and the chemical environment, *e.g.* the applied solvent or the buffer system. Hence, a crude estimation of the integrity of novel COSS compounds is possible, but stability tests in each particular case should be conducted.

5 Cell toxicity of COSS

As COSS derivatives are potential scaffold molecules or drug carriers for *in vivo* applications, the biocompatibility of COSS and its breakdown products is an important issue.

COSS precursors, monomeric primary silsesquioxanes, are known to possess low *in vitro* and *in vivo* toxicity.[67] Therefore, low toxicity of the silsesquioxane component of a COSS particle may be assumed. Nevertheless, the nature of ligands attached to a COSS core may influence its toxicity. For the assessment of toxicological risks of COSS derivatives from literature data it is essential to note that the direct comparison is not possible due to the distinct assay setups (choice of cell line, incubation times, *etc.*). Hence, we strongly recommend an independent and comprehensive evaluation of the toxicity of novel COSS compounds, as even within one cell line toxic concentrations differ depending on external stimuli as *e.g.* hormone concentration.[68]

Although *in vivo* toxicity of COSS derivatives has not been studied extensively to date, potential risks depending on the nature of the COSS derivative and the initial concentration may be ascertained based on *in vitro* assays. For example, the effect of 3-aminopropyl-substituted COSS on the Cos-1 cells was quantified using a cell viability test. Incubation with COSS taken at different concentrations (0.05 mM to 1 mM) did not lead to decreased enzyme activity within 36 hours, indicating low or no toxicity.[4] However, in another study, HeLa cells were incubated with a single-corner cysteine-modified 3-aminopropyl COSS and an IC_{50} was determined as 70 μM.[52]

In addition to monomeric silsesquioxanes, the toxicity of COSS-based amphiphiles and COSS-containing polymers has been extensively analyzed. COSS-derived amphiphiles showed low toxicity in NIH/3T3 and L929 cells as indicated by an MTT cell viability test.[69,70] Hydrido-COSS copolymers used in tissue engineering and cell culture have demonstrated low toxicity in MC3T3-E1[71] and human stem cells[72] as well. Both the copolymer and its degradation products did not affect cell growth and viability.

6 Self-assembly of COSS

Aggregation of biomolecules is supposed to play a crucial role in a number of pathologic disorders, *e.g.* neurodegenerative diseases. On the other hand, important biological processes, among them cell penetration, may be governed by the formation of highly ordered structures from monomeric precursors.[73,74] The implementation of tailor-made ordering segments into bioactive molecular blocks may influence the shape of the resulting structures, thus stimulating the formation of ordered aggregates. The effect of an individual component is therefore enhanced.[75] Indeed, Bode *et al.* have recently shown that aggregation of small cationic peptides multiplied their efficiency upon cell penetration.[76]

Due to their unique structure, COSS provide additional ordering effects during self-assembly. Thus, linear and dendrimer-like assemblies of silsesquioxane monomers were observed upon crystallization.[52,77] These findings are in accordance with theoretical studies which propose a particular mode of interaction between COSS molecules resulting in face-to-face stacking.[78–80] Being one of the energetically preferable siloxane modifications, the cubic core of COSS is formed spontaneously from amorphous Si. Therefore, this modification could be essential for biological processes aiming at the construction of diverse silica frameworks.[81] Moreover, COSS can potentially serve as building blocks for the controlled assembly of nanoscale structures possessing different architectures.[82] Recent publications reported the synthesis of nanostructured hybrid materials with distinct characteristics that are attributed to the ordering effect of COSS.[56,83–87] Potential applications

Table 2 List of biofunctionalized cubic siloxanes and COSS based probes

Ligand/precursor for bioconjugation	COSS functionalization	Conjugation chemistry	Yield	No. of copies	Year	Ref.
δ-Lactonolactone	Octaaminopropyl	Amide bond	53%	8	1998/99	23, 90
δ-Maltonolactone	Octaaminopropyl	Amide bond	26%	8	1998/99	23, 90
Thiol-modified mannosyl derivative	Octavinyl	Thiol radical addition	70%	8	2004	89
Thiol-modified lactosyl derivative	Octavinyl	Thiol radical addition	66, 73%	8	2004	89
Propargyl β-D-galactopyranoside	Octaazidopropyl	CuAAC	~80%	8	2010	20
Propargyl α-D-mannopyranoside	Octaazidopropyl	CuAAC	~80%	8	2010	20
Propargyl α-D-mannopyranoside	Octaazidopropyl	CuAAC	≤76%	8	2010	24
C-glucosylpropyl thiol	Octavinyl	TEC	94%	8	2012	43
C-mannosylpropyl thiol	Octavinyl	TEC	93%	8	2012	43
1-Thio-β-D-glucopyranose	PEGylated octaallyl	TEC	79%	8	2012	43
1-Thio-β-D-lactopyranose	PEGylated octaallyl	TEC	50%	8	2012	43
α-D-Mannopyranoside	Octaazidopropyl	CuAAC	78%	8	2012	62
α-D-Mannopyranoside	PEGylated octaazidopropyl	CuAAC	80%	8	2012	62
β-Cyclodextrin oligomer	Mono-adamantane	Non-covalent	n.a.	1	2012	70
Single amino acids (Z-Gly, Z-Ala, Z-Pro)	Octaaminopropyl	Amide bond	91/98/44%	8	1998	92
Dipeptides (Z-Phe-Leu, Z-Ala-Pro)	Octaaminopropyl	Amide bond	94/100%	8	1998	92
Tripeptides (Z-Phe-Leu-Ala, Z-Ala-Phe-Leu)	Octaaminopropyl	Amide bond	73/92%	8	1998	92
$(L\text{-Lys})_8$-$(L\text{-Lys})_4$-$(L\text{-Lys})_2$-$(L\text{-Lys})_1$	Octaaminopropyl	Amide bond	16%	8	2007	93
$(L\text{-Lys})_2$-$(L\text{-Lys})_1$, ELLLLLLLLL	Octaaminopropyl	Amide bond, non-covalent	n.a.	—	2012	69
$(CGLIIQKNEC)_{0.25}$-(Gd or Mn-DOTA)$_{3.2}$-$(L\text{-Lys})_4$-$(L\text{-Lys})_2$-$(L\text{-Lys})_1$	Octaaminopropyl	Amide bond, CuAAC	n.a.	8	2010–12	5, 95–97
$(L\text{-Glu})_4$-$(L\text{-Glu})_2$-$(L\text{-Glu})_1$	Succinic acid terminated octaaminopropyl	Amide bond	57%	8	2010	6
Poly(benzyl-L-glutamate)$_{5-53}$	Monoazidophenyl	CuAAC	n.a.	1	2011	83
Propynyl poly(benzyl-L-glutamate)$_{16\text{ and }36}$	Monomercaptopropyl	Thiol–alkyne chemistry	73%[a]	1	2011	98
(γ-Propargyl-L-glutamate)$_{5-50}$	Monoazidophenyl	CuAAC	n.a.	n.a.	2012	99
ECG	PEGylated octaallyl	TEC	78%	8	2012	43
RGDC	PEGylated octaallyl	TEC	61%	8	2012	43
Hexynyl-IPRGDYRG	Octaazidopropyl	CuAAC	91%[a]	8	2010	19
Glyoxylyl-IPRGDYRKG	Boc-aminooxy derivative	Oximation	90%	8	2012	26
Glyoxylyl-LHLSLKFPG	Boc-aminooxy derivative	Oximation	99%	6	2012	26
Glyoxylyl-GVCPKILKKCRRDSDCPGACICRG-NGYCG	Boc-aminooxy derivative	Oximation	n.a.	3	2012	26
Glyoxylyl-WGVCPKVLRNCRRDSDCPGACIC-LGNGYCG	Boc-aminooxy derivative	Oximation	n.a.	3	2012	26
Glyoxylyl-$(KVSALKE)_5$	Boc-aminooxy derivative	Oximation	n.a.	2	2012	26
Fluorescein	Octaazidopropyl	CuAAC	100%[a]	1	2010	19
BODIPY	Octaamino/vinyl-heptaisobutyl	Amide bond/Heck reaction	14–88%	1	2005/11	4, 100, 101
Cationic oligofluorene	Octavinyl	Heck reaction	45%	8	2010	102
Trifluoroacetic acid	Octaamino	Amide bond	83%	3–5	2008	103
C_{60} fullerene	Heptaisobutyl-hydroxylpropyl	Esterification	70%	1	2011	104
Ferrocene carboxylic acid	Octaamino	Amide bond	70%	3–5	2009	105

[a] Conversion; n.a.: not available.

of COSS-based amphiphilic nanostructures as drug delivery units are detailed in section 8.

7 COSS-based bioconjugation

Over the years, an increasing number of COSS-based bioconjugates have been reported that are listed in Table 2.

7.1 Carbohydrates

Molecular interactions and cell signalling in living cells involve a range of small- to medium-sized molecules, often presented in multiple copies. Therefore, COSS particles offering eight (or more) conjugation sites are viable molecular scaffolds for oligomerization of peptides and carbohydrates. Thus, the eightfold presentation of gluco- or mannosyl residues on a COSS core allowed for an efficient synthesis of glycoclusters. These spherical macromolecules enable, for example, the investigation of structural, thermodynamic, kinetic and mechanistic aspects of lectin[88]–carbohydrate interactions. Feher *et al.* reported a pioneering work in the field of COSS-based glycoclusters, having synthesized octagalactose and –maltose frameworks.[23] The reaction of carbohydrate lactones with octaamino COSS resulted in a respective glycocluster, albeit in a moderate yield (26–53%), within 24–72 h.

Hence, improved synthetic routes towards the synthesis of COSS glycoclusters were established. In 2004, the photoactivated conjugation of thiol-terminated glycoside residues to the cubic silsesquioxane (66–70% yield) was reported.[89] Six years later, the research groups of Chiara and Fessner further improved coupling efficacies by using CuAAC.[20,24,62] Taking the sensitivity of a COSS core into account (see section 4), a biphasic base-free $CuSO_4$–sodium ascorbate system was found to perform best (~80% yield, 2–36 h). Finally, Dondoni and co-workers could perfect the conjugation of carbohydrates and T_8 silsesquioxanes applying the photoinduced free-radical thiol–ene coupling (TEC).[43]

The bioactivity of COSS-derived glycoclusters was generally validated *via* lectin precipitation[20,62,90] or inhibition.[43,62,89] Yet, the recent contribution to this field by Trastoy *et al.*[62] allowed for further understanding of COSS–glycocluster–lectin interactions. The comparison between the lectin binding properties of two octamannosyl COSS derivatives with maximal ligand distances of ~25 Å (Fig. 4) and ~50 Å (PEG linker applied) allowed not only for an evaluation of the sterical accessibility of ligands presented on a COSS core, but also for an assessment of the increased binding affinities achieved *via* eightfold presentation of the ligands.[62]

Although the covalent attachment of carbohydrates is most common, examples for the non-covalent presentation of sugar derivatives on cube-octameric silsesquioxanes are noteworthy. They are generally based on cyclodextrin (CD) host–guest interactions, *e.g.* rotaxane formation *via* complexation of PEGylated COSS with α-CDs[91] or on exploiting the interaction of adamantane silsesquioxanes[20] and β-CDs.[70] The latter allows for the formation of supramolecular amphiphiles that might be applicable in tissue engineering and cell culture by promoting adhesion and proliferation of cells.[70]

7.2 Peptides/amino acids

The presentation of amino acids and peptides in multiple copies on a defined scaffold allows for the targeting of diverse biological functions, *e.g.* cell surface receptors or enzymes. They can be added to a scaffold using either a divergent or a convergent approach. The first one is usually based on amide chemistry. Thus, an excess of a benzotriazole-activated amino acid and a hindered nitrogenous base (*e.g. N*,*N*-diisopropylethylamine) in an aprotic solvent are added to an amine-functionalized COSS scaffold (water and humidity must be excluded). Straightforward examples for divergently synthesized amino acid-bearing silsesquioxane are the functionalization of COSS with single amino acids[92] and the generation of lysine dendrimers comprising cube-octameric silsesquioxanes as a core unit (see also section 7.3).[93]

For the convergent attachment of peptides directly to the nanoparticle only highly effective conjugation chemistry is applicable. Considering 85% conversion for a single ligation, the respective overall yield for the octa-functionalization of silsesquioxanes drops to 27%. Therefore, only reactions that allow for full conversion are recommended for the functionalization of COSS. Click reactions, as defined by Sharpless and co-workers in 2001,[94] easily comply with this requirement. Hence, it is not surprising that the first direct coupling of a biologically relevant peptide was conducted applying the CuAAC[19] on an octaazido COSS scaffold.[18–20,24] Within the last two years, not only the application of the CuAAC was optimized for the COSS conjugations,[62] but also a new set of biocompatible ligations was established. Lo Conte *et al.* used the photoinduced free-radical thiol–ene coupling to attach a tetrapeptide RGDC.[43] Additionally, the conjugation of a heptadecapeptide to a cysteine-bearing silsesquioxane *via* disulfide bond formation appeared possible.[52] Taking the sensitivity of COSS towards nucleophiles into account (see section 4), acid-catalyzed reactions are preferable over base-catalyzed conjugation methods. Hence, COSS bearing aminooxy functionalities were developed.[26] These particles readily react with aldehydes and allow for the multiple presentation of diverse peptide-based ligands, among them a derivative of antimicrobial peptide jelleine, a three-disulfide trypsin inhibitor MCoTI (Fig. 5), or a

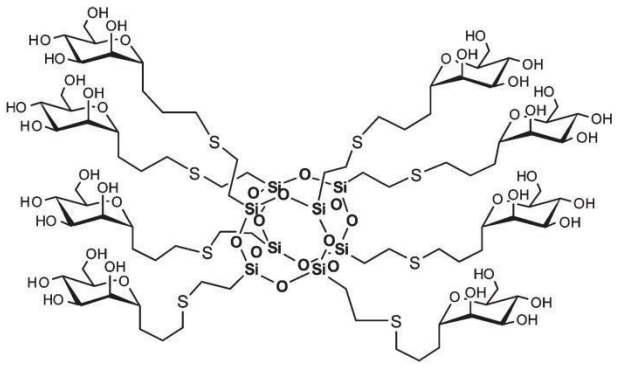

Fig. 4 Mannopyranoside glycocluster synthesized *via* photoinduced free-radical thiol–ene coupling of the respective glycol-thiol and octavinyl COSS.[43]

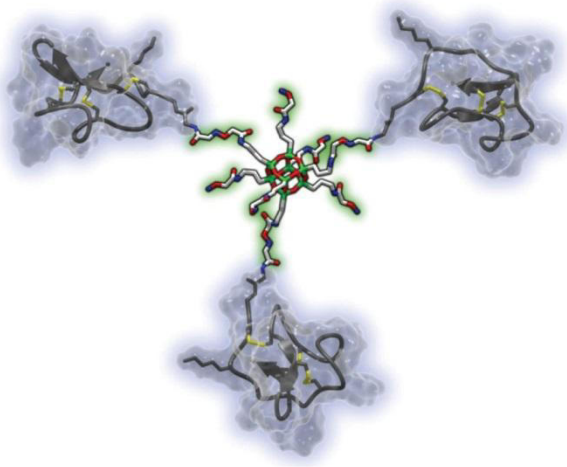

Fig. 5 Proposed model of a miniprotein–COSS conjugate (YASARA calculation; pale blue: cysteine-knot peptide MCoTI with disulfide bridges depicted as yellow sticks; red: oxygen, blue: nitrogen, green: silicon, grey: carbon). For the chemical structure see Table 2.[26]

35 amino acid K-coil peptide, a possible interface for non-covalent protein binding.[26] The aminooxy-based conjugation chemistry might also be exploited to decorate cubic siloxanes with cancer-targeting peptides and reporter molecules, *e.g.* DOTA (see section 9), promising its future pharmaceutical use as a biodegradable scaffold. Considering the novelty of functional peptide–COSS conjugates, the actual research is focused on proof-of-principle experiments, and biological applications are limited. Noteworthy are efforts to elucidate hierarchical self-assembly processes of peptidic COSS.[26,69,83,98,99] These can be exploited to form *e.g.* vesicles using lipid surrogates[98] or peptisomes that mimic viral capsids[69] allowing for new approaches towards drug delivery.

7.3 Biofunctional COSS-based dendrimers

Dendrimers are a special class of branched and short-chained polymers. For biomedical applications, dendrimers based on polyamidoamine (PAMAM)[106] and polylysine[5,69,93,95–97,107] are of special interest. Due to the presentation of multiple positive surface charges, they exhibit cell-membrane-targeting properties that can result in membrane permeation or disruption.[108] These properties were utilized for the development of antimicrobial compounds[108] or to facilitate drug delivery into cells.[69,93,107]

In 2007, Kaneshiro *et al.*[93] demonstrated the general applicability of poly-L-lysine octaaminopropyl COSS dendrimers as drug carriers. In 2008, Chujo's research group[106] reported an increased cargo capacity of COSS-based dendrimers. These findings gave rise to growing interest in the synthesis of cube-octameric silsesquioxane dendrimers.

Amphiphilic dendrimers allow either for an entrapment of small hydrophobic molecules in their interior or for a covalent ligand attachment to their external functionalities enabling them to act as a supramolecular scaffold. The specific chemical environment of a COSS dendrimer interior keeps trapped molecules well dispersed and can regulate their molecular rotation.[109] This freezing effect caused not only an improvement of quantum yields and the elongation of fluorescent lifetimes for an *in vivo* imaging relevant fluorophore emitting in the deep red region,[109] but also resulted in the effective inhibition of fluorescence bleaching of a rhodamine dye.[106]

Concerning the surface modification of globular COSS-based dendrimers, their functionalization with metal chelators is of special interest as it allows for magnetic resonance imaging (MRI) in tumor diagnostics. In this context, it is important to mention Lu and his co-workers who developed surface-modified polylysine dendrimers with a cube-octameric silsesquioxane core. Thus, gadolinium 1,4,7,10-tetraazacyclododecane-1,4,7,10-triacetic acid (Gd-DOTA), manganese 1,4,7-triaazacyclononane-1,4,7-triacetic acid (Mn-NOTA) and tumor targeting peptides were attached to surface-exposed lysine residues.[5,95–97] The resulting particles have been applied in a murine animal model as MRI contrast agents targeting human breast and prostate carcinoma xenografts *via* CTL1[110] peptide-mediated interaction with extracellular abundantly present fibrin–fibronectin complexes.[95–97] The size of one of these second generation (G2) COSS dendrimers was determined as ~5.6 nm allowing for a fast renal clearance.[96] This finding is of special importance due to the toxicity of paramagnetic gadolinium (Gd) generally used for MRI studies.[111] Interestingly, Tan *et al.*[5,97] also considered that *in vivo* dissociation and trans-metallation of complexed Gd can result in harmful side effects *e.g.* nephrogenic systemic fibrosis.[111] Therefore, Gd was substituted with manganese, a less toxic paramagnetic metal.[5,97] In summary, the development of COSS-dendrimer-based contrast agents is an advanced research field. After appropriate safety experiments, the synthesized compounds can be considered as excellent candidates for initial clinical studies. Nevertheless, approaches have been reported to evaluate the direct attachment of Gd-chelates to cubic silsesquioxanes (see also section 9).[63]

Another interesting example for surface-modified COSS dendrimers was given by Gu and colleagues.[6] They designed a dendrimer skeleton on the basis of poly-L-glutamic acid with a cube-octameric silsesquioxane as a core unit. The reaction of terminal carboxylic moieties with hydrazine towards corresponding hydrazides allowed for the pH-sensitive attachment of a respective biotin derivative and doxorubicin. The biotin targeted overexpressed biotin receptors on the surface of HeLa cancer cells and doxorubicin destroyed the cells *via* DNA intercalation upon a receptor-mediated uptake.[6] Considering pharmacokinetics and, especially, the clearance of these particles in potentially upcoming animal model experiments, it is noteworthy that these glutamic acid hydrazide particles seemed to be prone to aggregation and their diameter increases of 30–50 nm.[6] This topic is also reviewed in ref. 114.

8 COSS-mediated drug delivery

Due to their hydrophobic nature, potent drugs (*e.g.* paclitaxel) very often feature low solubility in aqueous systems. Furthermore, their efficacy might be limited to special body or cell compartments. In this context, DNA-intercalating drugs such as doxorubicin are good examples. Accordingly, carriers are needed to overcome these limitations. COSS-based drug delivery systems follow four general design principles (Fig. 6): (a) the particle itself facilitates cell penetration,[4,52,55] upon its derivatization; (b) an amphiphile[48,50,69,70,98,115] is formed allowing for the self-assembly of micelle-like structures; (c) COSS constitutes the core structure of a dendrimer[6,93,107] (see section 7.3); (d) it is incorporated into biocompatible polymers.[112,116]

In the recent literature the development of COSS amphiphiles gained particular attention. To highlight the structural similarities of these constructs and small molecules surfactants such as *e.g.* sodium dodecyl sulfate (SDS), the term "giant surfactants"[50] was coined. Compact COSS cages presenting alcohols,[48] carboxylic acids[50] or carbohydrates[48] are expedient hydrophilic tenside head groups, whereas cubic silsesquioxanes bearing aliphatic ligands are also viable analogs of a tensides hydrophobic tail.[70,98,115] Amphiphilic

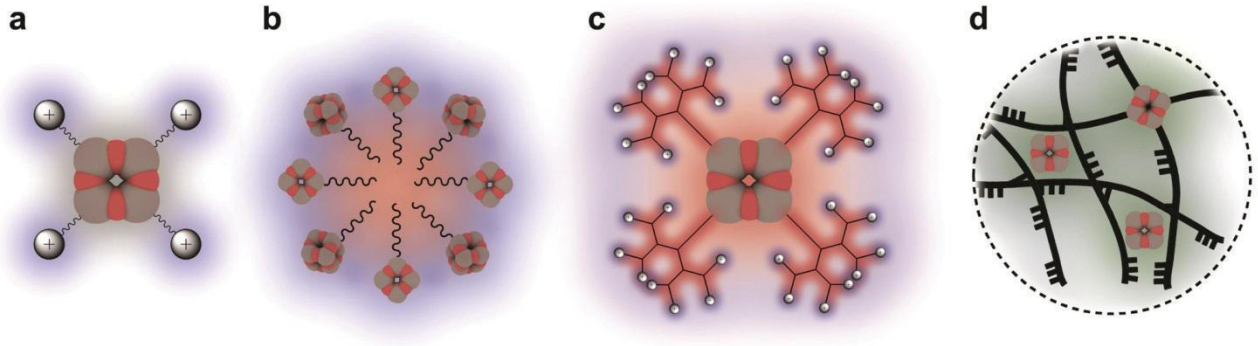

Fig. 6 Schematic depiction of COSS constructs used in drug delivery: a, direct cell penetration of *e.g.* polycationic octaamino COSS;[4] b, formation of nanocontainers by self-assembly of amphiphilic silsesquioxane derivatives;[48,50,98] c, dendrimers with a highly symmetric and compact COSS core;[6,107] d, incorporation of cubic silsesquioxanes into cell-penetrating polymeric nanoparticles.[112,113] (Silicon atoms are depicted in grey colour, oxygen in red; blue shadows indicate hydrophilic environment, red shadows indicate a hydrophobic milieu.)

COSS derivatives are able to hierarchically self-assemble.[70,115] Thus, they are able to form nanocontainers that might host a drug.[48] Considering the cell penetration potential of micelle- and liposome-like assemblies,[117] amphiphilic COSS are promising candidates for new drug delivery studies.

COSS-based drug delivery must be considered as an expanding research field, still suffering from a difficult generalization of obtained results. Identified uptake mechanisms are not only strongly dependent on the functionalities decorating a COSS surface, but also on the used cell lines, incubation methods, *etc.* For example, polycationic octaamino COSS are able to transport an attached cargo across a cell membrane,[4] but depending on the cell line its distribution pattern differs. Whereas in the COS-1 cell the BODIPY–siloxane derivative exclusively labeled the cytoplasm,[4] a similar compound showed accumulation in HeLa cell nucleoli, allowing for nuclear drug targeting.[52]

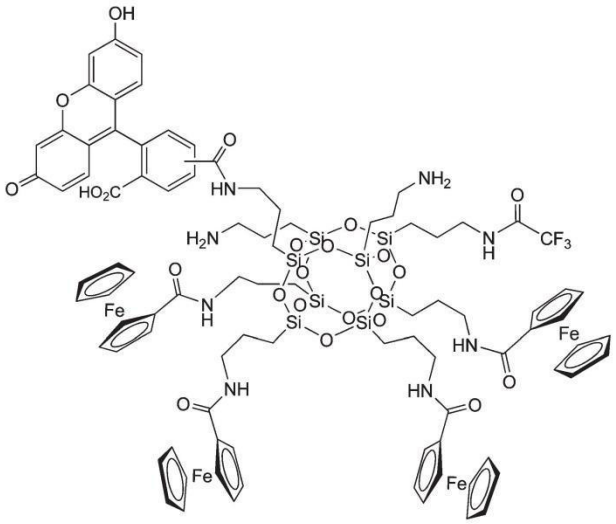

Fig. 7 Proposed structure of a bimodal probe for fluorescence microscopy and ^{19}F-NMR.[105]

9 COSS-based molecular probes

Good water solubility, low toxicity, compact and precise 3D architecture of amine-terminated cube-octameric silsesquioxanes (see section 1 and 5) make these particles a versatile framework for the construction of environment-sensitive molecular probes.

In this context, the decoration of COSS with fluorinated ligands is intriguing. The resulting particles, often called F-POSS,[103,118] are applicable for ^{19}F-NMR experiments[103,105,119,120] and exhibit tunable melting properties relevant for polymer science.[118]

The recent literature offers two different approaches for the synthesis of fluorinated COSS. Fluoroalkyl ligands are introduced either *via* corner capping[118] or by a stoichiometrically controlled conjugation between octaamino COSS and trifluoroacetic acid.[103] Chujo and co-workers implemented F-POSS units in experimental setups allowing for the monitoring of enzymatic activities[103,119,120] and redox reactions.[105] The attachment of fluorinated COSS to macromolecular silica particles resulted in decreased intensity of signals in the ^{19}F-NMR spectrum, due to restricted molecular rotation.[103] Depending on the conjugation pattern, the activity of different enzyme classes was assessed. Thus, alkaline phosphatase cleaved COSS bound *via* a phosphorodiamidate linker.[103,119] Reduced glutathione generated by glutathione reductase detached disulfide-bound fluorinated silsesquioxane cages[120] from their macromolecular support. The respective COSS release resulted in a measurable ^{19}F-NMR signal enhancement due to the regained rotational freedom of the fluorinated ligands and allowed for the calculation of enzyme activities. COSS scaffolds bearing Fe^{3+} ferrocenyl ligands are, therefore, of interest as powerful electrochemical probes.[121] Furthermore, the addition of Fe^{3+} ferrocenyl groups to F-POSS transforms the resulting construct (Fig. 7) into a switchable redox-sensitive ^{19}F-NMR probe. Conjugation of this construct with an additional fluorescein moiety yields a versatile redox sensor that allows for bimodal measurements.[105]

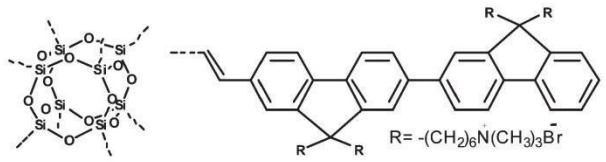

Fig. 8 Chemical structure of a water-soluble oligoelectrolyte-COSS.[102]

It will be interesting to see if the synthesis of functional COSS cages with entrapped fluoride ions[122] is possible as these derivatives could allow for even more sophisticated F-POSS probes.

Other NMR applications of COSS exploit its octavalent framework for the development of MRI contrast agents. Apart from the already discussed dendrimeric design, the eightfold presentation of Gd^{3+} chelates reported by Henig *et al.*[63] is noteworthy. Interestingly, Gd^{3+} is not only applicable as DOTA chelates. Fullerene-encapsulated gadolinium species ($Gd@C_{82}(OH)_n$, $n > 32$)[123] allow for enhanced *in vivo* MRI studies.[123,124] The recent report on C_{60} fullerene–COSS conjugates[104,125,126] might allow for the development of a new class of COSS-based contrast agents.

Fluorescently labelled silsesquioxanes are common COSS-based probes. Cubic siloxanes decorated with fluorescein[19,105] and BODIPY[4,100,101] allow for confocal microscopy studies on live cells. Oligoelectrolyte-polyhedral oligomeric silsesquioxanes (O-POSS) designed by Bin Liu and co-workers[102,116,127–129] are of interest as special fluorescent COSS particles (Fig. 8).

These water-soluble molecules feature low toxicity, whole cell permeability and high fluorescence quantum yields.[102] Hence, O-POSS were used as nuclear-staining agents[116] and as efficient Förster resonance energy (FRET) donors that enhanced the ethidium bromide labelling of DNA.[102] Further biological applications are based on O-POSS derivatives incorporated into polymeric nanoparticles that were used for folic acid[116] or HER2 antibody-targeted[128] tumor imaging.

Finally, Xiong and co-workers[130] nicely highlighted the opto-physical properties of COSS. They demonstrated that the photoluminescence of quantum dots increased upon their surface decoration with cubic silsesquioxanes.[130] This enhancement was attributed to the special 3D structure of a COSS cage. It reflects emitted light and allows for a multiple excitation of the quantum dots.[130] In summary, light-harvesting COSS particles[102,130] can be considered as promising agents for enhanced *in-vitro* microscopy studies. The topic is also reviewed in ref. 131.

10 Conclusions

Cube-octameric silsesquioxanes are small silica nanoparticles featuring an extremely compact structural framework, high symmetry and up to eight addressable organic ligands. Low toxicity of these molecules combined with solubility in aqueous systems and half-life under physiological conditions sufficient for *in vivo* studies make them attractive scaffolds for the development of tailor-made bioconjugates or hybrid molecules of biologic relevance. Thus, conjugation of cubic silsesquioxanes with carbohydrates resulted in glycoclusters used to study sugar–lectin interactions. Coupling of functional peptides onto COSS scaffolds yielded oligomeric peptidic constructs without loss of bioactivity, while surface-modified silsesquioxane-based dendrimers have been used in drug delivery and MRI. Development of molecular probes comprising a COSS core is, probably, the most advanced application of these unique nanoparticles. The recently expanded arsenal of effective conjugation methods (CuAAC, TEC, oxime ligation) made COSS-based bioconjugation a rapidly growing research field with large potential for further developments, particularly for tumor diagnostics and therapy.

Acknowledgements

This project was funded in part by the LOEWE Soft Control consortium.

References

1 J. Wu and P. T. Mather, *Polym. Rev.*, 2009, **49**, 25–63.
2 Y. Kawakami, Y. Kakihana, A. Miyazato, S. Tateyama and M. A. Hoque, *Adv. Polym. Sci.*, 2011, **235**, 185–228.
3 H. Ghanbari, A. de Mel and A. M. Seifalian, *Int. J. Nanomed.*, 2011, **6**, 775–786.
4 C. McCusker, J. B. Carroll and V. M. Rotello, *Chem. Commun.*, 2005, 996–998.
5 M. Q. Tan, Z. Ye, E. K. Jeong, X. M. Wu, D. L. Parker and Z. R. Lu, *Bioconjugate Chem.*, 2011, **22**, 931–937.
6 H. Yuan, K. Luo, Y. S. Lai, Y. J. Pu, B. He, G. Wang, Y. Wu and Z. W. Gu, *Mol. Pharmaceutics*, 2010, **7**, 953–962.
7 A. Ladenburg, *Liebigs Ann. Chem.*, 1874, **173**, 143–166.
8 A. J. Barry, W. H. Daudt, J. J. Domicone and J. W. Gilkey, *J. Am. Chem. Soc.*, 1955, **77**, 4248–4252.
9 C. L. Frye and W. T. Collins, *J. Am. Chem. Soc.*, 1970, **92**, 5586–5588.
10 M. M. Sprung and F. O. Guenther, *J. Am. Chem. Soc.*, 1955, **77**, 3996–4002.
11 R. Weidner, N. Zellner, B. Deubzer and V. Frey, *Germany Pat.*, DE 383797-A1, 1990.
12 U. Dittmar, B. J. Hendan, U. Florke and H. C. Marsmann, *J. Organomet. Chem.*, 1995, **489**, 185–194.
13 A. R. Bassindale, Z. H. Liu, I. A. MacKinnon, P. G. Taylor, Y. X. Yang, M. E. Light, P. N. Horton and M. B. Hursthouse, *Dalton Trans.*, 2003, 2945–2949.
14 B. Marciniec, M. Dutkiewicz, H. Maciejewski and M. Kubicki, *Organometallics*, 2008, **27**, 793–794.
15 J. F. Brown and L. H. Vogt, *J. Am. Chem. Soc.*, 1965, **87**, 4313–4317.
16 D. B. Cordes, P. D. Lickiss and F. Rataboul, *Chem. Rev.*, 2010, **110**, 2081–2173.

17 C. H. Ni, G. Wu, C. P. Zhu and B. L. Yao, *J. Phys. Chem. C*, 2010, **114**, 13471–13476.
18 V. Ervithayasuporn, X. Wang and Y. Kawakami, *Chem. Commun.*, 2009, 5130–5132.
19 S. Fabritz, D. Heyl, V. Bagutski, M. Empting, E. Rikowski, H. Frauendorf, I. Balog, W. D. Fessner, J. J. Schneider, O. Avrutina and H. Kolmar, *Org. Biomol. Chem.*, 2010, **8**, 2212–2218.
20 D. Heyl, E. Rikowski, R. C. Hoffmann, J. J. Schneider and W. D. Fessner, *Chem.–Eur. J.*, 2010, **16**, 5509–5548.
21 A. Boullanger, G. Gracy, N. Bibent, S. Devautour-Vinot, S. Clement and A. Mehdi, *Eur. J. Inorg. Chem.*, 2012, 143–150.
22 V. Ervithayasuporn, T. Tomeechai, N. Takeda, M. Unno, A. Chaiyanurakkul, R. Hamkool and T. Osotchan, *Organometallics*, 2011, **30**, 4475–4478.
23 F.J. Feher, K. D. Wyndham, D. Soulivong and F. Nguyen, *J. Chem. Soc., Dalton Trans.*, 1999, 1491–1497.
24 B. Trastoy, M. E. Perez-Ojeda, R. Sastre and J. L. Chiara, *Chem.–Eur. J.*, 2010, **16**, 3833–3841.
25 J. R. Suarez, B. Trastoy, M. E. Perez-Ojeda, R. Marin-Barrios and J. L. Chiara, *Adv. Synth. Catal.*, 2010, **352**, 2515–2520.
26 S. Fabritz, S. Hörner, D. Könning, M. Empting, M. Reinwarth, C. Dietz, B. Glotzbach, H. Frauendorf, H. Kolmar and O. Avrutina, *Org. Biomol. Chem.*, 2012, **10**, 6287–6293.
27 H. B. Fan and R. J. Yang, *J. Appl. Polym. Sci.*, 2012, **124**, 4389–4397.
28 H. Cai, K. Xu, X. Liu, Z. Fu and M. Chen, *Dalton Trans.*, 2012, **41**, 6919–6921.
29 R. Tamaki, Y. Tanaka, M. Z. Asuncion, J. W. Choi and R. M. Laine, *J. Am. Chem. Soc.*, 2001, **123**, 12416–12417.
30 R. M. Laine and M. F. Roll, *Macromolecules*, 2011, **44**, 1073–1109.
31 V. Abbate, A. R. Bassindale, K. F. Brandstadt and P. G. Taylor, *J. Inorg. Biochem.*, 2011, **105**, 268–275.
32 M. Frampton, R. Simionescu and P. M. Zelisko, *Silicon*, 2009, **1**, 47–56.
33 M. B. Frampton and P. M. Zelisko, *Silicon*, 2012, **4**, 51–56.
34 N. Ihara, M. Kurisawa, J. E. Chung, H. Uyama and S. Kobayashi, *Appl. Microbiol. Biotechnol.*, 2005, **66**, 430–433.
35 R. M. Laine, J. W. Choi and I. Lee, *Adv. Mater.*, 2001, **13**, 800–803.
36 M. Dutkiewicz, H. Maciejewski and B. Marciniec, *Synthesis*, 2012, 881–884.
37 B. W. Manson, J. J. Morrison, P. I. Coupar, P. A. Jaffres and R. E. Morris, *J. Chem. Soc., Dalton Trans.*, 2001, 1123–1127.
38 V. V. Rostovtsev, L. G. Green, V. V. Fokin and K. B. Sharpless, *Angew. Chem., Int. Ed.*, 2002, **41**, 2596–2599.
39 C. W. Tornoe, C. Christensen and M. Meldal, *J. Org. Chem.*, 2002, **67**, 3057–3064.
40 J. M. Baskin, J. A. Prescher, S. T. Laughlin, N. J. Agard, P. V. Chang, I. A. Miller, A. Lo, J. A. Codelli and C. R. Bertozzi, *Proc. Natl. Acad. Sci. U. S. A.*, 2007, **104**, 16793–16797.
41 A. Dirksen, T. M. Hackeng and P. E. Dawson, *Angew. Chem., Int. Ed.*, 2006, **45**, 7581–7584.
42 K. F. Geoghegan and J. G. Stroh, *Bioconjugate Chem.*, 1992, **3**, 138–146.
43 M. Lo Conte, S. Staderini, A. Chambery, N. Berthet, P. Dumy, O. Renaudet, A. Marra and A. Dondoni, *Org. Biomol. Chem.*, 2012, **10**, 3269–3277.
44 Y. Itami, B. Marciniec and M. Kubicki, *Chem.–Eur. J.*, 2004, **10**, 1239–1248.
45 J. Choi, J. Harcup, A. F. Yee, Q. Zhu and R. M. Laine, *J. Am. Chem. Soc.*, 2001, **123**, 11420–11430.
46 E. M. Sletten and C. R. Bertozzi, *Angew. Chem., Int. Ed.*, 2009, **48**, 6974–6998.
47 F. J. Feher, K. D. Wyndham, R. K. Baldwin, D. Soulivong, J. D. Lichtenhan and J. W. Ziller, *Chem. Commun.*, 1999, 1289–1290.
48 W. B. Zhang, Y. W. Li, X. P. Li, X. H. Dong, X. F. Yu, C. L. Wang, C. Wesdemiotis, R. P. Quirk and S. Z. D. Cheng, *Macromolecules*, 2011, **44**, 2589–2596.
49 Y. Li, X.-H. Dong, H. Guo, Z. Wang, Z. Chen, C. Wesdemiotis, R. P. Quirk, W. B. Zhang and S. Z. D. Cheng, *ACS Macro Lett.*, 2012, **1**, 834–839.
50 X. F. Yu, S. Zhong, X. P. Li, Y. F. Tu, S. G. Yang, R. M. Van Horn, C. Y. Ni, D. J. Pochan, R. P. Quirk, C. Wesdemiotis, W. B. Zhang and S. Z. D. Cheng, *J. Am. Chem. Soc.*, 2010, **132**, 16741–16744.
51 S. Kuwahara, K. Yamamoto and J. Kadokawa, *Chem. Lett.*, 2010, **39**, 1045–1047.
52 S. Hörner, S. Fabritz, H. D. Herce, O. Avrutina, C. Dietz, R. W. Stark, M. C. Cardoso and H. Kolmar, *Org. Biomol. Chem.*, 2012, DOI: 10.1039/c2ob26808f.
53 H. Liu, M. Puchberger and U. Schubert, *Chem.–Eur. J.*, 2011, **17**, 5019–5023.
54 J. L. Zhou, Y. C. Zhao, K. C. Yu, X. P. Zhou and X. L. Xie, *New J. Chem.*, 2011, **35**, 2781–2792.
55 F. Olivero, F. Renò, F. Carniato, M. Rizzi, M. Cannas and L. Marchese, *Dalton Trans.*, 2012, **41**, 7467–7473.
56 Y. W. Li, W. B. Zhang, I. F. Hsieh, G. L. Zhang, Y. Cao, X. P. Li, C. Wesdemiotis, B. Lotz, H. M. Xiong and S. Z. D. Cheng, *J. Am. Chem. Soc.*, 2011, **133**, 10712–10715.
57 E. Rikowski and H. C. Marsmann, *Polyhedron*, 1997, **16**, 3357–3361.
58 G. Jungang, Z. Xuejian, W. Shichen and R. Mingtao, *Chem. J. Internet*, 2005, **7**, 48 (http://www.chemistrymag.org/cji/2005/077048ne.htm).
59 F. J. Feher and K. D. Wyndham, *Chem. Commun.*, 1998, 323–324.
60 T. L. Lu, G. Z. Liang and Z. Guo, *J. Appl. Polym. Sci.*, 2006, **101**, 3652–3658.
61 M. F. Roll, J. W. Kampf, Y. Kim, E. Yi and R. M. Laine, *J. Am. Chem. Soc.*, 2010, **132**, 10171–10183.
62 B. Trastoy, D. A. Bonsor, M. E. Pérez-Ojeda, M. L. Jimeno, A. Méndez-Ardoy, J. M. García-Fernández, E. J. Sundberg and J. L. Chiara, *Adv. Funct. Mater.*, 2012, **22**, 3191–3201.

63 J. Henig, E. Toth, J. Engelmann, S. Gottschalk and H. A. Mayer, *Inorg. Chem.*, 2010, **49**, 6124–6138.
64 Z. B. Qiu and H. Pan, *Compos. Sci. Technol.*, 2010, **70**, 1089–1094.
65 H. Pan and Z. B. Qiu, *Macromolecules*, 2010, **43**, 1499–1506.
66 J. Raghunath, G. Georgiou, D. Armitage, S. N. Nazhat, K. M. Sales, P. E. Butler and A. M. Seifalian, *J. Biomed. Mater. Res., Part A*, 2009, **91A**, 834–844.
67 W. H. Siddiqui and R. G. York, *Fundam. Appl. Toxicol.*, 1993, **21**, 66–70.
68 V. Edwards, E. Markovic, J. Matisons and F. Young, *Biotechnol. Appl. Biochem.*, 2008, **51**, 63–71.
69 X. Xu, H. Yuan, J. Chang, B. He and Z. Gu, *Angew. Chem., Int. Ed.*, 2012, **51**, 3130–3133.
70 B. B. Jiang, W. Tao, X. Lu, Y. Liu, H. B. Jin, Y. Pang, X. Y. Sun, D. Y. Yan and Y. F. Zhou, *Macromol. Rapid Commun.*, 2012, **33**, 767–772.
71 K. Wang, L. Cai and S. F. Wang, *Polymer*, 2011, **52**, 2827–2839.
72 J. Raghunath, H. Zhang, M. J. Edirisinghe, A. Darbyshire, P. E. Butler and A. M. Seifalian, *Biotechnol. Appl. Biochem.*, 2009, **52**, 1–8.
73 C. Munch, J. O'Brien and A. Bertolotti, *Proc. Natl. Acad. Sci. U. S. A.*, 2011, **108**, 3548–3553.
74 P. H. Ren, J. E. Lauckner, I. Kachirskaia, J. E. Heuser, R. Melki and R. R. Kopito, *Nat. Cell Biol.*, 2009, **11**, 219–232.
75 Y. B. Lim, E. Lee and M. Lee, *Angew. Chem., Int. Ed.*, 2007, **46**, 9011–9014.
76 S. A. Bode, M. Thevenin, C. Bechara, S. Sagan, S. Bregant, S. Lavielle, G. Chassaing and F. Burlina, *Chem. Commun.*, 2012, **48**, 7179–7181.
77 C. Y. Jung, H. S. Kim, H. J. Hah and S. M. Koo, *Chem. Commun.*, 2009, 1219–1221.
78 E. R. Chan, X. Zhang, C. Y. Lee, M. Neurock and S. C. Glotzer, *Macromolecules*, 2005, **38**, 6168–6180.
79 X. Zhang, E. R. Chan and S. C. Glotzer, *J. Chem. Phys.*, 2005, **123**, 184718.
80 S. W. Hu, Y. J. Sheng and H. K. Tsao, *J. Phys. Chem. C*, 2012, **116**, 1789–1797.
81 M. Z. Asuncion, I. Hasegawa, J. W. Kampf and R. M. Laine, *J. Mater. Chem.*, 2005, **15**, 2114–2121.
82 T. T. Toth-Fejel, *IEEE Sens. J.*, 2008, **8**, 1036–1040.
83 Y. C. Lin and S. W. Kuo, *J. Polym. Sci., Part A: Polym. Chem.*, 2011, **49**, 2127–2137.
84 Y. C. Wu and S. W. Kuo, *J. Mater. Chem.*, 2012, **22**, 2982–2991.
85 Y. L. Chu, C. C. Cheng, Y. P. Chen, Y. C. Yen and F. C. Chang, *J. Mater. Chem.*, 2012, **22**, 9285–9292.
86 R. S. Shih, C. H. Lu, S. W. Kuo and F. C. Chang, *J. Phys. Chem. C*, 2010, **114**, 12855–12862.
87 J. J. Miao and L. Zhu, *J. Phys. Chem. B*, 2010, **114**, 1879–1887.
88 Y. Kamiya, M. Yagi-Utsumi, H. Yagi and K. Kato, *Curr. Pharm. Des.*, 2011, **17**, 1672–1684.
89 Y. Gao, A. Eguchi, K. Kakehi and Y. C. Lee, *Org. Lett.*, 2004, **6**, 3457–3460.
90 F. J. Feher, K. D. Wyndham and D. J. Knauer, *Chem. Commun.*, 1998, 2393–2394.
91 J. C. Huang, X. Li, T. T. Lin, C. B. He, K. Y. Mya, Y. Xiao and J. Li, *J. Polym. Sci., Part B: Polym. Phys.*, 2004, **42**, 1173–1180.
92 F. J. Feher, K. D. Wyndham, M. A. Scialdone and Y. Hamuro, *Chem. Commun.*, 1998, 1469–1470.
93 T. L. Kaneshiro, X. Wang and Z. R. Lu, *Mol. Pharmaceutics*, 2007, **4**, 759–768.
94 H. C. Kolb, M. G. Finn and K. B. Sharpless, *Angew. Chem., Int. Ed.*, 2001, **40**, 2004–2021.
95 M. Q. Tan, X. M. Wu, E. K. Jeong, Q. J. Chen and Z. R. Lu, *Biomacromolecules*, 2010, **11**, 754–761.
96 M. Tan, S. M. Burden-Gulley, W. Li, X. Wu, D. Lindner, S. M. Brady-Kalnay, V. Gulani and Z. R. Lu, *Pharm. Res.*, 2012, **29**, 953–960.
97 M. Q. Tan, X. M. Wu, E. K. Jeong, Q. J. Chen, D. L. Parker and Z. R. Lu, *Mol. Pharmaceutics*, 2010, **7**, 936–943.
98 J. G. Ray, J. T. Ly and D. A. Savin, *Polym. Chem.*, 2011, **2**, 1536–1541.
99 Y. C. Lin and S. W. Kuo, *Polym. Chem.*, 2012, **3**, 162–171.
100 M. Liras, M. Pintado-Sierra, F. Amat-Guerri and R. Sastre, *J. Mater. Chem.*, 2011, **21**, 12803–12811.
101 M. E. Perez-Ojeda, B. Trastoy, I. Lopez-Arbeloa, J. Banuelos, A. Costela, I. Garcia-Moreno and J. L. Chiara, *Chem.–Eur. J.*, 2011, **17**, 13258–13268.
102 K. Y. Pu, K. Li and B. Liu, *Adv. Mater.*, 2010, **22**, 643–646.
103 K. Tanaka, N. Kitamura, K. Naka and Y. Chujo, *Chem. Commun.*, 2008, 6176–6178.
104 H. J. Sun, Y. F. Tu, C. L. Wang, R. M. Van Horn, C. C. Tsai, M. J. Graham, B. Sun, B. Lotz, W. B. Zhang and S. Z. D. Cheng, *J. Mater. Chem.*, 2011, **21**, 14240–14247.
105 K. Tanaka, N. Kitamura, Y. Takahashi and Y. Chujo, *Bioorg. Med. Chem.*, 2009, **17**, 3818–3823.
106 K. Tanaka, K. Inafuku, K. Nakab and Y. Chujo, *Org. Biomol. Chem.*, 2008, **6**, 3899–3901.
107 T. L. Kaneshiro and Z. R. Lu, *Biomaterials*, 2009, **30**, 5660–5666.
108 M. A. Mintzer, E. L. Dane, G. A. O'Toole and M. W. Grinstaff, *Mol. Pharmaceutics*, 2012, **9**, 342–354.
109 K. Tanaka, J. H. Jeon, K. Inafuku and Y. Chujo, *Bioorg. Med. Chem.*, 2012, **20**, 915–919.
110 J. Pilch, D. M. Brown, M. Komatsu, T. A. Jarvinen, M. Yang, D. Peters, R. M. Hoffman and E. Ruoslahti, *Proc. Natl. Acad. Sci. U. S. A.*, 2006, **103**, 2800–2804.
111 J. L. Abraham and C. Thakral, *Eur. J. Radiol.*, 2008, **66**, 200–207.
112 X. J. Loh, Z. X. Zhang, K. Y. Mya, Y. L. Wu, C. B. He and J. Li, *J. Mater. Chem.*, 2010, **20**, 10634–10642.
113 M. Tarini, P. Cignoni and C. Montani, *IEEE Trans. Visualization Comput. Graphics*, 2006, **12**, 1237–1244.
114 K. Tanaka and Y. Chujo, *Polym. J.*, 2012, DOI: 10.1038/pj.2012.154.
115 L. Ma, H. P. Geng, J. X. Song, J. Z. Li, G. X. Chen and Q. F. Li, *J. Phys. Chem. B*, 2011, **115**, 10586–10591.

116 D. Ding, K. Y. Pu, K. Li and B. Liu, *Chem. Commun.*, 2011, **47**, 9837–9839.
117 V. P. Torchilin, *Adv. Drug Delivery Rev.*, 2006, **58**, 1532–1555.
118 S. C. Kettwich, S. N. Pierson, A. J. Peloquin, J. M. Mabry and S. T. Iacono, *New J. Chem.*, 2012, **36**, 941–946.
119 K. Tanaka, N. Kitamura and Y. Chujo, *Bioconjugate Chem.*, 2011, **22**, 1484–1490.
120 K. Tanaka, N. Kitamura and Y. Chujo, *Bioorg. Med. Chem.*, 2012, **20**, 96–100.
121 S. Bruna, D. Nieto, A. M. Gonzalez-Vadillo, J. Perles and I. Cuadrado, *Organometallics*, 2012, **31**, 3248–3258.
122 P. G. Taylor, A. R. Bassindale, Y. El Aziz, M. Pourny, R. Stevenson, M. B. Hursthouse and S. J. Coles, *Dalton Trans.*, 2012, **41**, 2048–2059.
123 L. Qu, W. B. Cao, G. M. Xing, J. Zhang, H. Yuan, J. Tang, Y. Cheng, B. Zhang, Y. L. Zhao and H. Lei, *J. Alloys Compd.*, 2006, **408–412**, 400–404.
124 M. Mikawa, H. Kato, M. Okumura, M. Narazaki, Y. Kanazawa, N. Miwa and H. Shinohara, *Bioconjugate Chem.*, 2001, **12**, 510–514.
125 D. J. Clarke, J. G. Matisons, G. P. Simon, M. Samoc and A. Samoc, *Appl. Organomet. Chem.*, 2010, **24**, 184–188.
126 F. F. Yang, C. C. Li, H. Y. Guo, J. Q. Ye and Z. Y. Jiao, *Synth. Commun.*, 2012, **42**, 3664–3669.
127 K. Y. Pu, Z. T. Luo, K. Li, J. P. Xie and B. Liu, *J. Phys. Chem. C*, 2011, **115**, 13069–13075.
128 K. Li, Y. T. Liu, K. Y. Pu, S. S. Feng, R. Y. Zhan and B. Liu, *Adv. Funct. Mater.*, 2011, **21**, 287–294.
129 K. Y. Pu and B. Liu, *Adv. Funct. Mater.*, 2011, **21**, 3408–3423.
130 Q. Li, L. J. Dong, X. Wang, J. Huang, H. A. Xie and C. X. Xiong, *Scr. Mater.*, 2012, **66**, 646–649.
131 K. Tanaka and Y. Chujo, *J. Mater. Chem.*, 2012, **22**, 1733–1746.

8. Cumulative part

This section contains the following manuscripts published in peer-reviewed journals:

8.1 Sebastian Fabritz,[‡] **Sebastian Hörner**,[‡] Martin Empting, Doreen Könning, Michael Reinwarth, Christian Dietz, Bernhard Glotzbach, Holm Frauendorf, Harald Kolmar[*] and Olga Avrutina[*]. From Pico to Nano: Biofunctionalization of Cube-octameric Silsesquioxanes by Peptides and Miniproteins. *Org. Biomol. Chem*., **2012**, *10*, 6287-6293. Reproduced with permission of the Royal Society of Chemistry.

8.2 **Sebastian Hörner**,[‡] Sebastian Fabritz,[‡] Henry D. Herce,[*] Olga Avrutina, Christian Dietz, Robert W. Stark, M. Cristina Cardoso and Harald Kolmar[*]. Cube-octameric silsesquioxane-mediated cargo peptide delivery into living cancer cells. *Org. Biomol. Chem*., **2013**, *11*, 2258-2265. Reproduced with permission of the Royal Society of Chemistry.

8.3 **Sebastian Hörner**,[‡] Christina Uth,[‡] Olga Avrutina, Holm Frauendorf, Manfred Wiessler, Harald Kolmar[*]. Combination of inverse electron-demand Diels–Alder reaction with highly efficient oxime ligation expands the toolbox of site-selective peptide conjugations. *Chem. Commun*., **2015**, *51*, 11130-11133. Reproduced with permission of the Royal Society of Chemistry.

8.4 **Sebastian Hörner**,[‡] Sascha Knauer,[‡] Christina Uth,[‡] Marina Jöst, Volker Schmidts, Holm Frauendorf, Christina M. Thiele, Olga Avrutina, and Harald Kolmar[*]. Nanoscale biodegradable organic-inorganic hybrids for efficient cell penetration and drug delivery. *Angew. Chem. Int. Ed*., **2016**, *55*, DOI: 10.1002/anie.201606065. Reproduced with permission of John Wiley and Sons.

8.1. Biofunctionalization of COSS by peptides and Miniproteins

Title:

From pico to nano: Biofunctionalization of cube-octameric silsesquioxanes by peptides and miniproteins

Authors:

Sebastian Fabritz,[‡] Sebastian Hörner,[‡] Martin Empting, Doreen Könning, Michael Reinwarth, Christian Dietz, Bernhard Glotzbach, Holm Frauendorf, Harald Kolmar, and Olga Avrutina.

Bibliographic data:

Organic & Biomolecular Chemistry
Volume 10, pages 6287-6293, June 11th 2012
DOI: 10.1039/C2OB25728A
For the first time published in the internet on June 13th 2012

Graphical abstract:

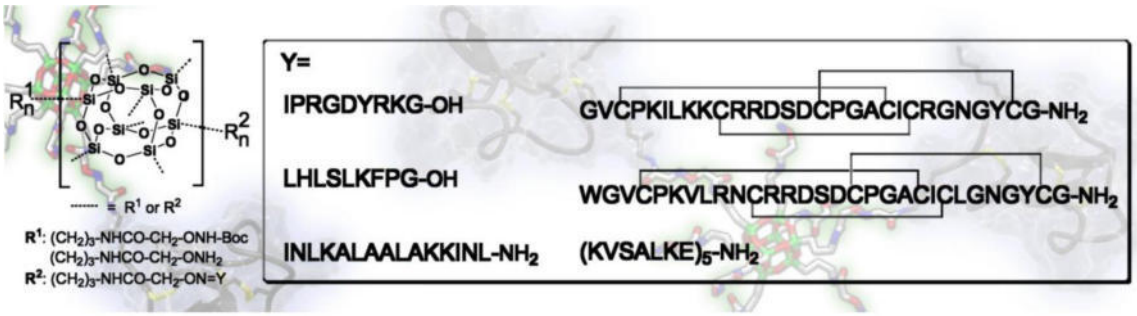

Summary:

The present publication introduces a conjugation strategy allowing for efficient functionalization of COSS nanoparticles with peptides and miniproteins. By using the acid-catalyzed oxime ligation between aminooxy and aldehydic groups, multimerization of different peptides and mini-proteins was achieved within several hours.

Contributions by Dipl.-Ing. Sebastian Hörner:

- Synthesis of compounds **2** and **p5**
- NMR-Analysis of compound **2**

Organic & Biomolecular Chemistry

Cite this: *Org. Biomol. Chem.*, 2012, **10**, 6287

www.rsc.org/obc

PAPER

From pico to nano: biofunctionalization of cube-octameric silsesquioxanes by peptides and miniproteins†

Sebastian Fabritz,‡[a] Sebastian Hörner,‡[a] Doreen Könning,[a] Martin Empting,[a] Michael Reinwarth,[a] Christian Dietz,[b] Bernhard Glotzbach,[a] Holm Frauendorf,[c] Harald Kolmar*[a] and Olga Avrutina*[a]

Received 13th April 2012, Accepted 11th June 2012
DOI: 10.1039/c2ob25728a

Polyhedral silsesquioxanes are considered valuable conjugation scaffolds. Nevertheless, only a few examples of silsesquioxane-assembled peptide oligomers have been reported to date. We developed a new bioorthogonal cube-octameric silsesquioxane (COSS) scaffold bearing eight aminooxy coupling sites allowing for the conjugation of diverse peptides *via* oxime ligation. We found that the coupling efficacy depends on the ligand in view of steric hindrance and electrostatic repulsion. For the first time scaffold-based conjugation of cystine-knot miniproteins having a backbone of about thirty amino acids was successfully accomplished without loss of bioactivity. Atomic force microscopy (AFM) provided further knowledge on the size of COSS verifying them as picoscaffolds growing upon bioconjugation to nano-dimension.

Introduction

Combining several ligands on a single scaffold often results in improved characteristics of a formed oligomer compared to its individual constituents. Nature extensively uses this phenomenon known as multivalency to effect biomolecular interactions[1] in living organisms by enhancing affinity and specificity of binding.[2] This inspires research efforts towards creation of synthetic molecules in which the benefits of simultaneous multiple contacts are achieved through the oligomerization of bioactive modules – small molecules,[3] carbohydrates,[4] peptides,[5] and proteins.[1] Properties of scaffold-grafted molecular blocks are often governed by the peculiar architecture that implies shape, size, and valency of the framework, as well as spatial orientation of ligands.[6]

In recent years, cube-octameric silsesquioxanes (COSS)[7,8] have been brought into focus as promising oligomerization scaffolds due to their unique characteristics. These monodisperse particles with a core size of 0.5 nm[9] are considered the smallest known nanoscaffolds with a high degree of symmetry. Their hybrid molecules are composed of a siloxane inorganic core decorated with organic ligands which combine an aliphatic linker with a terminal active group. From a broad repertoire of functionalized COSS molecules reported to date, amine,[10] azide,[11–13] alkyne,[12] thiol,[14] aldehyde[15] or maleimide bearing[16] particles are potentially applicable for bioconjugations.

To date, several COSS-based bioconjugates have been reported, among them lysine dendrimers for drug delivery,[17,18] oligomers of peptides[12,19] and carbohydrates,[13,20] as well as macrocyclic Gd^{3+} chelates as potential magnetic resonance imaging contrast agents.[21]

The convergent synthesis of peptidic COSS is limited to homopolypeptides where one amino acid unit with a protected or non-reactive side chain is propagated,[22,23] or to rather short (up to 8 residues) RGD oligomers.[12] In these bioconjugations, copper-catalyzed azide–alkyne cycloaddition (CuAAC) is currently the established method to obtain a linkage between an azide-bearing silsesquioxane and an alkyne-modified peptidic ligand usually added in stoichiometric excess.[24,25] Due to the instability of a COSS core in the presence of aqueous nucleophiles,[21,26] CuAAC with silsesquioxanes is generally performed in water-free DMF.[12,27,28] In this aprotic solvent, the copper catalyst often appeared to be coordinated by an amide backbone[29] or functional side chains[30] of peptides leading to a drastic decrease of active catalytic species and, as a consequence, to prolonged reaction times (up to several weeks) and low yields.[12] Very recently, an elegant alternative approach to silsesquioxane-based peptide conjugations has been reported which utilized the photo-induced free-radical thiol–ene coupling and resulted in eightfold presentation of the tripeptide glutathione on a COSS scaffold.[31,32] Interestingly, for a tetrapeptide RGDC complete

[a]*Clemens-Schöpf Institute of Organic Chemistry and Biochemistry, Technische Universität Darmstadt, Petersenstr. 22, 64287 Darmstadt, Germany.*
E-mail: Kolmar@Biochemie-TUD.de; Avrutina@Biochemie-TUD.de
[b]*Center of Smart Interfaces, Technische Universität Darmstadt, Petersenstr. 32, 64287 Darmstadt, Germany*
[c]*Institute of Organic and Biomolecular Chemistry, Georg-August Universität Göttingen, Tamannstraße 2, 37077 Göttingen, Germany*

†Electronic supplementary information (ESI) available: ^{1}H-NMR and ^{29}Si-NMR data of **2**, **3**; ESI-MS data of **2–9**; IR spectra of **2**, **3**. See DOI: 10.1039/c2ob25728a

‡These authors contributed equally to this work.

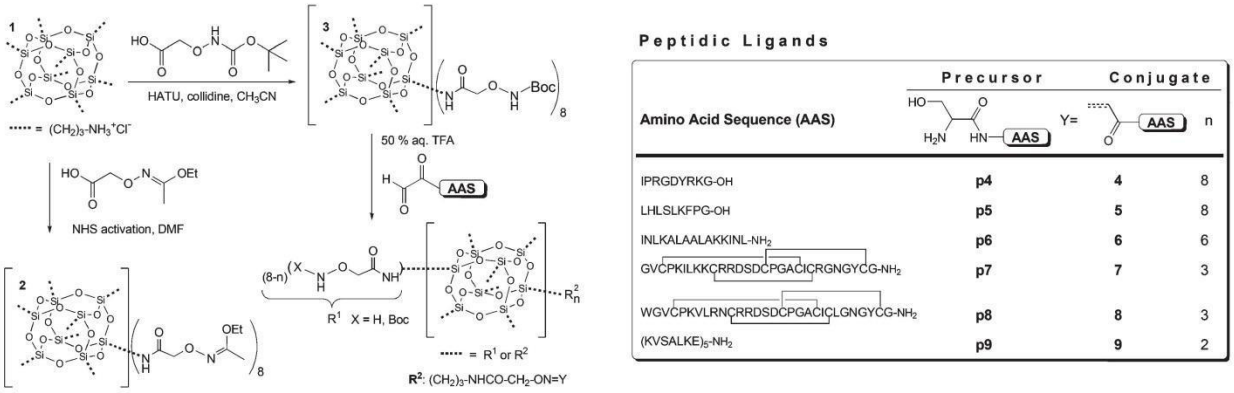

Scheme 1 Synthetic approaches to protected aminooxy COSS **2** and **3**. Octakis (Boc-aminooxy) COSS was used as a scaffold for bioconjugation. Ligands: an octapeptide with an RGD motif (**p4**), a derivative of the antimicrobial peptide Jelleine 1 (**p5**), mastoparan (**p6**), MCoTI-based miniproteins (**p7**, **p8**) and Kcoil, a basic α-helical coil (**p9**), were chosen.

hydrothiolation of vinyl coupling sites was achieved only after the introduction of elongation linkers.[31]

Herein, we report bioconjugation on a COSS scaffold in acidic aqueous media based on the oxime ligation[33,34] between an aldehyde and an aminooxy functionality (Scheme 1). This approach provides several advantages compared to other methods reported for COSS–peptide conjugations[12,27,28,31,32] as it ensures both stability of the silsesquioxane core and good solubility of biological ligands. The introduction of aldehyde moieties into biomolecules is well-established and can easily be achieved *via* periodate oxidation of an N-terminal serine residue.[35] Moreover, building blocks for solid phase peptide synthesis[36,37] containing a masked side-chain aldehyde function enable the generation of this moiety at any desired sequence position. Aminooxy functionality can be easily introduced in peptides by N-acylation of side-chain or terminal amines by butoxycarbonyl (Boc)[38] or ethoxyethylidene (Eei)[39,40] protected aminooxy acetic acid. Protection is essential to avoid side reactions and overacylation of target compounds. In the present research, the applicability of the oxime ligation to the synthesis of hybrid COSS–peptide conjugates was studied highlighting the benefits and the limitations of the method.

Results and discussion

As a conjugation scaffold an octaaminopropyl-COSS **1** was used. The reaction with commercially available mono-Boc aminooxy acetic acid towards **3** appeared strongly dependent on the activation conditions leading to overacylated species (Table 1).

Decostaire *et al*. have recently reported[38] that the control over these undesired processes could be achieved by the proper choice of used activator, base, and solvent as well as their excess. Corroborating the reported data,[38] 2-(7-aza-1*H*-benzotriazole-1-yl)-1,1,3,3-tetramethyluronium hexa-fluoro-phosphate (HATU) activation in the presence of collidine was found to be the optimal reaction conditions, and 20 equivalents of the base per silsesquioxane octamer were used (Fig. 1). Although no overacylated COSS species have been found in both acetonitrile- and DMF-based reaction mixtures (Table 1, entries 5 and 6), dry acetonitrile appeared to be the solvent of choice as no complete

Table 1 Reaction conditions for the synthesis of **3**

No.	Solvent	Base equiv. (collidine)	Activator (8 × 5.2 equiv.)	Overacylated 0	×1	×2	×3
1	DMF	85	HBTU	X	X	X	X
2	DMF	43	HBTU	X	X	nd	nd
3	DMF	53	HATU	X	X	nd	nd
4	MeCN	53	HATU	X	X	X	X
5	MeCN	20	HATU	X	nd	nd	nd
6	DMF	20	HATU	X[a]	nd	nd	nd

X: detected; nd: not detected. [a] Reaction showed incomplete conversion. Heptameric Boc-aminooxy COSS species were detected *via* LC-MS analysis.

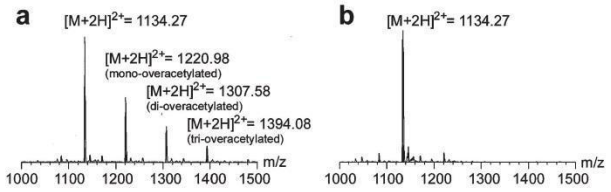

Fig. 1 ESI-MS spectra for the synthesis of **3**. (a) Reaction in DMF using HBTU and 85 equiv. collidine; (b) reaction in MeCN using HATU and 20 equiv. collidine.

conversion was observed in DMF after an overnight reaction. Contrary to this procedure, reaction of **1** with *N*-hydroxysuccinimide-activated 2-(1-ethoxy-ethylidene-aminooxy) acetic acid[40] resulted in octakis Eei-protected aminooxy-COSS **2** without overacylation. Due to the instability of COSS in the presence of aqueous nucleophiles,[21,26] the cage integrity of **2** and **3** was verified by ^{29}Si-NMR and IR spectroscopy (see ESI Fig. S3, S4 and S6†). The NMR spectra showed exclusively the shifts corresponding to COSS cages **2** and **3** (δ −66.87 and δ −66.75, respectively). The IR spectra showed a Si–O–Si stretch characteristic band at 1115 cm^{-1}. Both Boc and Eei groups were cleaved in 50% aqueous trifluoroacetic acid (TFA) within 3 hours, and one-pot conjugation with aldehyde functionalized peptides[35] succeeded. In our study, ligands with diverse primary

and secondary structures and different bioactivity were used (Scheme 1).

For the initial experiment, an integrin-binding octapeptide bearing an RGD functional motif (**p4**) was chosen.[41,42] It was shown previously that this ligand could be coupled onto the COSS scaffold in eightfold copies *via* CuAAC.[12] We found that oxime ligation had obvious benefits compared to CuAAC as the reaction time needed for full conversion was drastically reduced – from several weeks to an overnight reaction at room temperature. LC-MS monitoring of the reaction progress showed the presence of COSS species bearing both protected aminooxy coupling sites and oxime-ligated peptides (see ESI Fig. S8†), indicating that Boc cleavage was the rate-determining step. Nevertheless, as soon as full deprotection was achieved, the steric hindrance and electrostatic repulsion caused by the growing number of peptidic ligands seemed to have a major influence on the reaction progress.

Consequently, we explored the ligand-dependent limitations of the proposed COSS-based oximation. It is obvious that direct coupling of bulky peptide ligands onto constrained COSS scaffolds can be hindered due to steric reasons. On the other hand, often the oligomerization of peptides and full-size proteins is desirable without implementation of elongation linkers. Therefore, in a series of coupling experiments the size of bioactive peptidic ligands was progressively increased from eight (**p4**) to 35 (**p9**) amino acid residues.

To that end, a derivative of natural antimicrobial peptide Jelleine 1[43,44] from the royal jelly of honey bees (**p5**) was used. The successful eightfold presentation of this octapeptide on the COSS scaffold encouraged us to approach more sophisticated ligands. Thus, an α-helical calmodulin[45] binding peptide mastoparan (**p6**)[46] comprising 14 residues, trypsin inhibitors[47] **p7** and **p8** having 29 and 30 residues, respectively, and the inherent Kcoil part of a heterodimeric coiled coil (**p9**)[48–50] with a length of 35 amino acids were used. Moreover, miniproteins[51] **p7** and **p8** contained a characteristic tri-disulfide pattern known as a cystine knot[52] that is absolutely essential for the function; the damage of this motif results in the loss of three-dimensional structure and, as a consequence, of bioactivity.[52]

All peptidic ligands contained, compared to their parent sequences, an additional N-terminal serine and were assembled by standard microwave-assisted Fmoc-SPPS as previously described.[53] After chain assembling and cleavage from the support, sodium periodate oxidation resulted in peptide aldehydes.[35] In the case of miniproteins **p7** and **p8**, oxidative folding[54] into a cystine knot preceded the formation of an N-terminal glyoxal.

One-step deprotection of **3** followed by conjugation with peptidic ligands **p5**–**p9** was performed in 50% aqueous TFA as described above. The LC-MS monitoring of the conjugation reaction with cystine-free ligands revealed the formation of COSS–peptide intermediates after 10 min. Within 12 hours the reactions were completed. The formation of miniprotein–COSS conjugates **7** and **8** was only observed after an overnight reaction. This might be attributed to a hindered accessibility of the miniprotein aldehyde functionalities.

The amount of ligand copies attached to the COSS core correlated with the primary structure of the peptides and the increasing steric demand. Thus, the conjugation with the Jelleine-derived octapeptide **p5** yielded an octameric product. Mastoparan **p6** with just 6 additional amino acids formed a hexameric conjugate. In miniproteins **p7** and **p8** the amount of amino acids is doubled compared to **p6** resulting in a decreased coupling efficacy. Accordingly, only di- as well as trimeric constructs were observed for these ligands (Fig. 2). Finally, the pronounced steric hindrance as well as the possibility of strong electrostatic

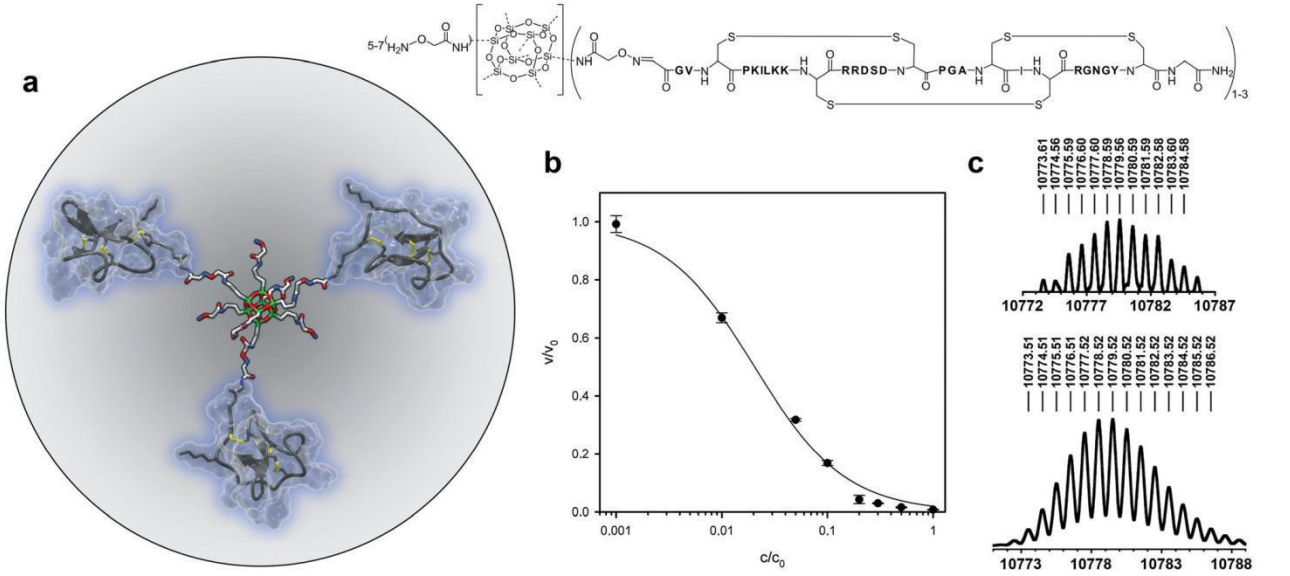

Fig. 2 (a) Proposed YASARA model of a miniprotein–COSS conjugate (pale blue: MCoTI miniproteins with disulfide bridges depicted as yellow sticks; red: oxygen; blue: nitrogen; green: silicon; grey: carbon) and its chemical structure. (b) Inhibition of trypsin-catalyzed proteolysis of chromogenic substrate *Boc*-QAR-*pNA* by conjugate **7**. Trypsin fractional activity is plotted as a function of inhibitor concentration on a log scale.[56] (c) Observed (top) and simulated (bottom) HR-MS spectra of **7**.

repulsion allowed only for the formation of mono- and dimeric products with the α-helical Kcoil peptide **p9**.

To the best of our knowledge, to date the dimerization of miniproteins was only facilitated *via* chemical cross-linking using a bis-succinimidyl suberate.[55] Herein, we present the first scaffold-based approach to the oligomerization of miniproteins. To examine whether cystine knot protease inhibitors retained their unique three-dimensional structure after conjugation, we studied the bioactivity of formed hybrid molecules. To that end, an RP-HPLC fraction containing conjugate **7** and lower substituted COSS–**p7** conjugates was tested for inhibitory activity against trypsin (Fig. 2).[56] Although a precise determination of inhibitor concentrations in the mixture of tri-, bi- and monoconjugated miniproteins was not possible and corresponding inhibition constants were not calculated, the concentration-dependent inhibition of trypsin-mediated proteolysis provided clear evidence that the bioactivity of **p7** was preserved under oximation conditions.

The bioactivity and toxicity of nanoparticles as well as their potential for drug delivery is greatly dependent on the size. Therefore, we conducted atomic force microscopy (AFM) experiments using the particles **1**, **4**, and **5**. We considered mica (negatively charged sheet silica) an optimal substrate, as the eight amino groups of **1** and the peptidic side chains of **4** and **5** promised a good binding to this surface. The dropcasting of an acidic solution of **1** (~1 ng mL^{-1}) allowed us to visualize singular particles. The enumeration of 60 particles (see ESI Fig. S7† and Fig. 3d) resulted in an average particle size of 743 ± 211 pm. This value is in good accordance with the literature stating ~500 pm for the POSS core.[8,9] For further measurements a mica substrate was dipcoated with an RP-HPLC fraction containing **4**. An analysis of the particle size distribution revealed an average size of 1810 ± 300 pm. Hence, the peptidic shell induced a measurable size increase of 1050 pm. On a first glance, this value seemed to be rather small compared to a rough simulation of **4** predicting 6.42 ± 0.69 nm as its maximal diameter in solution (see ESI Fig. S12†). However, it has to be taken into account that the particle is absorbed on a mica surface and might adopt a pancake-like structure. Furthermore, the recorded topography of a sample always depends on several parameters. Being operated in tapping mode, the AFM *z*-piezo detects changes upon the interaction of its tip with an analyzed sample keeping the amplitude of the vibrating cantilever constant. If attractive van der Waals forces change due to differences in the Hamaker constant[57] between two materials, the *z*-piezo will compensate this difference by varying the mean distance between the tip and the sample. On soft materials, compared to the sample substrate, an additional difference of the indentation depth of the tip into the material is compensated by the *z*-piezo. As a consequence, even for atomically flat surfaces a non-negligible height profile can be measured for inhomogeneous samples.[58] Hence, the measured height differences should only be used to classify the nanoparticle dimension.

The subsequent analysis of **5** revealed, in accordance with the expectations, particles with a similar height profile. Therefore, we chose a random particle and continuously increased its mapping resolution using bimodal atomic force microscopy. Fig. 4a shows the high resolution phase image of the second eigenmode. Phase images in AFM are related to mechanical properties of the sample. Three regions with a distinctive phase shift between cantilever oscillation and excitation were identified. The difference in phase values of mica ($\Delta\varphi_2$ = 120°) and the main body of the particle ($\Delta\varphi_2$ = 119°) can be attributed to the mechanical dissimilarity of the materials. A region with a relatively low phase shift ($\Delta\varphi_2$ = 110°) was found in the right part of the particle (Fig. 4b). An image artefact can be excluded since the same area was successively scanned several times depicting comparable contrast. We presume that this region might visualize the position of the mica-adsorbed silsesquioxane core surrounded by randomly oriented peptide chains (Fig. 4d).

Conclusion

A new bioorthogonal COSS scaffold was developed comprising a highly symmetric silsesquioxane core decorated with aminooxy functional modules. We demonstrated the applicability of this scaffold for the oligomerization of aldehyde-bearing peptidic ligands through oxime ligation. Our scheme has an obvious advantage as all involved reactions proceed in an acidic medium that does not affect the COSS core known to be extremely unstable in the presence of nucleophiles. We found that the coupling efficacy depends on the ligand in view of steric hindrance and electrostatic repulsion. Thus, octapeptide derivatives were eightfold presented on a COSS scaffold, whereas for more bulky ligands lower oligomers were detected. Nevertheless, for the first time the scaffold-based conjugation of miniproteins comprising a backbone of about thirty amino acids with a structure-defining cystine knot was successfully accomplished without the loss of ligand bioactivity.

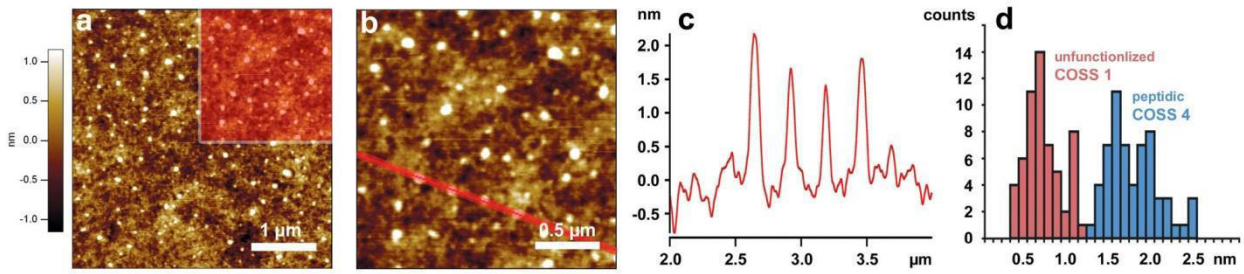

Fig. 3 (a) AFM topography image of a uniformly distributed COSS–peptide particle **3** on a mica surface; (b) image extension displaying the trend of the section line; (c) profile of four adjacent particles; (d) comparative histogram depicting the size distribution of **1** and **4**.

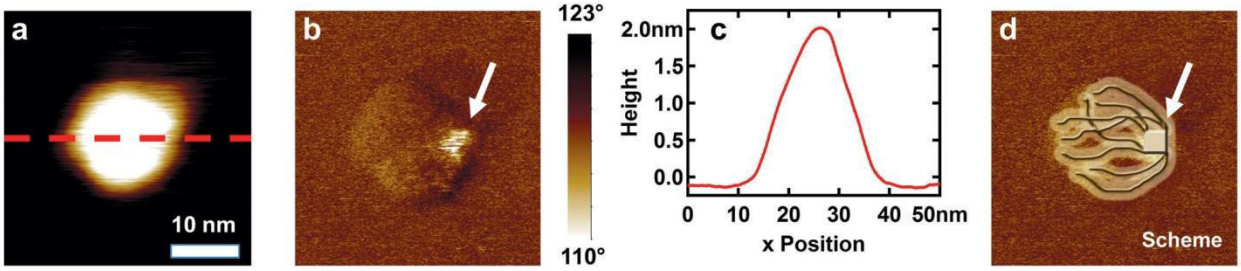

Fig. 4 High-resolution image of a single COSS–peptide particle **4** using bimodal atomic force microscopy. (a) Topography image and (b) profile of a single particle. (c) Corresponding second eigenmode phase image. The image reveals a bright region at the right area of the particle. (d) Schematic structure of the particle deduced from the phase image shown in (b).

AFM experiments conducted in the present study provided further knowledge on the size of COSS allowing us to consider them as picoscaffolds growing upon bioconjugation to nano-dimension.

Detailed studies concerning the bioactivity of COSS-assembled conjugates are currently ongoing, with constructs **6** and **9** being of particular interest. They can provide an interface for the non-covalent oligomerization of proteins fused either to a complementary Ecoil or to calmodulin. Thus, oligomerization can occur *via* the formation of a Kcoil/Ecoil leucine zipper,[48] or through tight binding to mastoparan,[46] respectively.

Experimental

Peptide synthesis

Microwave-assisted Fmoc-SPPS of peptide ligands was performed on a CEM *liberty*® peptide synthesizer equipped with a CEM *discover*® SPS microwave (CEM GmbH). As solid supports 2-CT-resin-Gly-OH from Iris Biotech GmbH (**p4** and **p5**), AmphiSphere™ 40 RAM resin from Varian Inc. (**p6**, **p7** and **p8**) and NovaSyn®TGR resin from Merck KGaA (**p8**) were used. After cleavage, cysteine-free crude products were oxidized using 10 equiv. of sodium periodate in PBS buffer for 10 min. The reaction product was isolated by RP-HPLC using a Varian 940-LC equipped with a YMC Europe GmbH C18 column (250 × 20 mm; S- 4 µm, 8 nm). Oxidative folding[59] of hexathiol precursors was followed by RP-HPLC purification. The resulting cystine knots were submitted to the above-described periodate oxidation procedure.

Synthesis of octa(aminopropyl) COSS 1

The synthesis of **1** was performed according to the reported procedure.[10]

Synthesis of scaffold 2

10 mg (1 equiv., 0.009 mmol) of **1**, 90 mg (5 equiv. per ammonium group, 0.35 mmol) of Eei protected and NHS activated aminooxyacetic acid[40] and 240 µL (20 equiv. per ammonium group, 178.1 mg, 1.38 mmol) of dry DIEA were dissolved in 3 mL of dry DMF. After 12 hours of stirring, full conversion of **1** into **2** was confirmed by LC-MS monitoring. Subsequently, the solvent and base were removed *in vacuo*. The resulting crude product was purified *via* RP-HPLC using a semi-preparative C4 column (300 × 20 mm, 5 µ, PSS Polymer Standards Service GmbH) and a linear gradient of 90% aq. MeCN (10 → 100% B in 63 min) preceded by 10 min isocratic 10% B at a flow rate of 10 mL min^{-1} with t_R = 48.0 min. Yield after RP-HPLC purification: 5.7 mg (33%).

HR-MS: calc. for $C_{72}H_{136}N_{16}O_{36}Si_8$ (+2): 1013.3801, meas. 1013.3800 $[M + 2H]^{2+}$, 1024.3710 $[M + H + Na]^{2+}$, 1035.3622 $[M + 2Na]^{2+}$; ATR-IR: ν 702 w, 1114 vs, 1308 m, 1378 w, 1540 w, 1651 m, 2933 vw, 3332 vw cm^{-1}, ^{29}Si NMR IGATED (99 MHz, $CDCl_3$): δ −66.85.

Synthesis of scaffold 3

50 mg (1 equiv., 0.043 mmol) of **1**, 347 mg Boc-aminooxy acetic acid (5.3 equiv. per ammonium group, 1.815 mmol), 674 mg HATU (5.2 equiv. per ammonium group, 1.773 mmol) and 112.5 µL dry collidine (120.8 mg, 2.9 equiv. per ammonium group, 0.997 mmol) were dissolved in 8 mL dry MeCN. After 12 hours of stirring full conversion of **1** into **3** was confirmed *via* LC-MS monitoring. Subsequently, the solvent and base were removed *in vacuo*. The resulting crude product was purified *via* RP-HPLC using a semi-preparative C8 column (250 × 20 mm, 5 µ, Phenomenex Inc.) and a linear gradient of 90% aq. MeCN in 0.1% aq. TFA (40 → 100% B in 20 min) preceded by 5 min isocratic 40% B at a flow rate of 18 mL min^{-1} with t_R = 16.5 min. Yield after RP-HPLC purification: 3.6 mg (4%).

HR-MS: calc. for $C_{80}H_{154}N_{16}O_{44}Si_8$ (+2): 1133.4224, meas. 1133.4216 $[M + 2H]^{2+}$; ATR-IR: ν 1115 vs, 1286 m, 1371 w, 1567 w, 1661 m, 1729 m, 2944 vw, 2989 vw, 3327 vw, ^{29}Si NMR (99 MHz, $CDCl_3$): δ −66.90.

Conjugation of peptidic ligands on aminooxy COSS 3

0.1 mg (1 equiv., 0.041 µmol) of **3** were dissolved in 500 µL 50% aq. TFA and 9 equiv. (0.39 µmol) of a corresponding peptidic ligand were added. The reaction process was monitored for 12 hours by LC-MS. The conjugates were isolated *via* RP-HPLC using an analytical C4 column (50 × 1 mm, 5 µ, Phenomenex Inc.) and a linear gradient of MeCN in 0.1% aq. formic acid (2 → 100% in 10 min) at a flow rate of 0.2 mL min^{-1}.

HR-MS: calc. for **4** $C_{424}H_{689}N_{144}O_{140}Si_8$ (+9): 1140.4375, meas. 1140.4393 $[M + 9H]^{9+}$ (see Fig. S9 and S10†), calc. for **5**

$C_{448}H_{705}N_{112}O_{124}Si_8$ (+9): 1096.0051, meas. 1096.0042 $[M + 9H]^{9+}$ (see ESI Fig. S14 and S15†), calc. for **6** $C_{472}H_{862}N_{130}O_{124}Si_8$: 10 565.34, meas. 10 565.37 (see ESI Fig. S17 and S18†), calc. for **7** $C_{418}H_{697}N_{145}O_{139}S_{18}Si_8$: 10 773.51, meas. 10 773.61 (see ESI Fig. S20 and S21†), calc. for **8** $C_{308}H_{496}N_{104}O_{106}S_{12}Si_8$: 7957.15, meas. 7957.22 (see ESI Fig. S23 and S24†), calc. for **9** $C_{384}H_{700}N_{108}O_{130}Si_8$: 9132.97, meas. 9132.98 (see ESI Fig. S26 and S27†).

Yields based on the integration of HPLC traces at 220 nm: 90% (conjugate **4**) and 99% (conjugate **5**).

See the ESI† for full LC-MS and HR-MS data.

Trypsin inhibition assay

The trypsin inhibition assay of **7** was performed according to the reported procedure.[56]

High resolution imaging of COSS–peptide particles using bimodal atomic force microscopy

Tapping mode atomic force microscopy measurements were performed on COSS–peptide particles randomly distributed on a mica surface. The resonance frequency of the cantilever (PPP-ZEIHR and PPP-NCH from NanoandMore GmbH, Wetzlar, Germany) was f_1 = 120–320 kHz and a free amplitude of $A_{01} \approx 10$ nm was chosen. We paid careful attention to operate the AFM in the net attractive regime where van der Waals forces dominate the tip–sample interaction by keeping the free amplitude low and using a relatively high setpoint amplitude $A_1/A_{01} \approx 0.9$. This operation regime is comparably gentle to the sample surface avoiding excessive indentation of the tip apex into the surface structure.

High-resolution images on single COSS–peptide particles were accomplished using bimodal atomic force microscopy.[60–66] Compared to the conventional tapping mode, the cantilever was excited simultaneously at the first two flexural eigenmodes. The amplitude of the first eigenmode was kept constant varying the distance between a tip and a sample (as in conventional tapping). Additionally, the amplitude and phase shift of the second eigenmode sensed compositional variations of the sample with very high accuracy. The cantilevers' resonance frequencies (PPP-ZEIHR Cantilever) were as follows: f_1 = 127 kHz and f_2 = 781 kHz for the first and second oscillations, respectively. The free amplitude of the oscillating cantilever was excited to A_{01} = 5 nm and A_{02} = 0.5–1 nm.

AFM image processing

All topography images were 1st order flattened in order to remove image tilt. A Gauss filter was applied to enhance the signal-to-noise ratio.

Acknowledgements

We acknowledge the collaboration with Prof. Dr Robert Stark (Center of Smart Interfaces, Technische Universität Darmstadt) with respect to AFM measurements in the frame of the LOEWE Soft Control consortium. We thank Volker Schmidts (Clemens-Schöpf Institute of Organic Chemistry and Biochemistry, Technische Universität Darmstadt) for the performance of ^{29}Si-NMR experiments on **3**.

References

1 P. H. Ehrlich, *J. Theor. Biol.*, 1979, **81**, 123–127.
2 S. M. Deyev and E. N. Lebedenko, *Bioassays*, 2008, **30**, 904–918.
3 D. Wright and L. Usher, *Curr. Org. Chem.*, 2001, **5**, 1107–1131.
4 R. J. Pieters, *Org. Biomol. Chem.*, 2009, **7**, 2013–2025.
5 S. P. Liu, L. Zhou, R. Lakshminarayanan and R. W. Beuerman, *Int. J. Pept. Res. Ther.*, 2010, **16**, 199–213.
6 J. E. Gestwicki, C. W. Cairo, L. E. Strong, K. A. Oetjen and L. L. Kiessling, *J. Am. Chem. Soc.*, 2002, **124**, 14922–14933.
7 J. F. Brown, L. H. Vogt and P. I. Prescott, *J. Am. Chem. Soc.*, 1964, **86**, 1120–1125.
8 D. B. Cordes, P. D. Lickiss and F. Rataboul, *Chem. Rev.*, 2010, **110**, 2081–2173.
9 H. Mori, Y. Miyamura and T. Endo, *Langmuir*, 2007, **23**, 9014–9023.
10 F. J. Feher and K. D. Wyndham, *Chem. Commun.*, 1998, 323–324.
11 V. Ervithayasuporn, X. Wang and Y. Kawakami, *Chem. Commun.*, 2009, 5130–5132.
12 S. Fabritz, D. Heyl, V. Bagutski, M. Empting, E. Rikowski, H. Frauendorf, I. Balog, W.-D. Fessner, J. J. Schneider, O. Avrutina and H. Kolmar, *Org. Biomol. Chem.*, 2010, **8**, 2212–2218.
13 B. Trastoy, M. Eugenia Perez-Ojeda, R. Sastre and J. Luis Chiara, *Chem.–Eur. J.*, 2010, **16**, 3833–3841.
14 U. Dittmar, B. J. Hendan, U. Flörke and H. C. Marsmann, *J. Organomet. Chem.*, 1995, **489**, 185–194.
15 B. W. Manson, J. J. Morrison, P. I. Coupar, P. A. Jaffres and R. E. Morris, *J. Chem. Soc., Dalton Trans.*, 2001, 1123–1127.
16 R. Tamaki, Y. Tanaka, M. Z. Asuncion, J. W. Choi and R. M. Laine, *J. Am. Chem. Soc.*, 2001, **123**, 12416–12417.
17 T. L. Kaneshiro, X. Wang and Z.-R. Lu, *Mol. Pharm.*, 2007, **4**, 759–768.
18 K. Tanaka, K. Inafuku, K. Nakab and Y. Chujo, *Org. Biomol. Chem.*, 2008, **6**, 3899–3901.
19 F. J. Feher, K. D. Wyndham, M. A. Scialdone and Y. Hamuro, *Chem. Commun.*, 1998, 1469–1470.
20 D. Heyl, E. Rikowski, R. C. Hoffmann, J. J. Schneider and W.-D. Fessner, *Chem.–Eur. J.*, 2010, **16**, 5544–5548.
21 J. Henig, E. Toth, J. Engelmann, S. Gottschalk and H. A. Mayer, *Inorg. Chem.*, 2010, **49**, 6124–6138.
22 Y.-C. Lin and S.-W. Kuo, *Polym. Chem.*, 2012, **3**, 162–171.
23 S.-W. Kuo, H.-F. Lee, W.-J. Huang, K.-U. Jeong and F.-C. Chang, *Macromolecules*, 2009, **42**, 1619–1626.
24 V. V. Rostovtsev, L. G. Green, V. V. Fokin and K. B. Sharpless, *Angew. Chem., Int. Ed.*, 2002, **41**, 2596–2599.
25 O. Avrutina, M. Empting, S. Fabritz, M. Daneschdar, H. Frauendorf, U. Diederichsen and H. Kolmar, *Org. Biomol. Chem.*, 2009, **7**, 4177–4185.
26 E. Rikowski and H. C. Marsmann, *Polyhedron*, 1997, **16**, 3357–3361.
27 S.-W. Kuo and H.-T. Tsai, *Polymer*, 2010, **51**, 5695–5704.
28 Y.-C. Lin and S.-W. Kuo, *J. Polym. Sci., Part A: Polym. Chem.*, 2011, **49**, 2127–2137.
29 H. Sigel and R. B. Martin, *Chem. Rev.*, 1982, **82**, 385–426.
30 A. Jancso, K. Andras, B. Gyurcsik, N. V. Nagy and T. Gajda, *J. Inorg. Biochem.*, 2009, **103**, 1634–1643.
31 M. Lo Conte, S. Staderini, A. Chambery, N. Berthet, P. Dumy, O. Renaudet, A. Marra and A. Dondoni, *Org. Biomol. Chem.*, 2012, **10**, 3269–3277.
32 A. Dondoni, A. Massi, P. Nanni and A. Roda, *Chem.–Eur. J.*, 2009, **15**, 11444–11449.
33 A. Dirksen, T. M. Hackeng and P. E. Dawson, *Angew. Chem., Int. Ed.*, 2006, **45**, 7581–7584.
34 O. Renaudet, D. Boturyn and P. Dumy, *Bioorg. Med. Chem. Lett.*, 2009, **19**, 3880–3883.
35 K. F. Geoghegan and J. G. Stroh, *Bioconjugate Chem.*, 1992, **3**, 138–146.
36 J. C. Spetzler and T. Hoeg-Jensen, *Tetrahedron Lett.*, 2002, **43**, 2303–2306.
37 T. Groth and M. Meldal, *J. Comb. Chem.*, 2001, **3**, 34–44.
38 I. P. Decostaire, D. Lelievre, H. Zhang and A. F. Delmas, *Tetrahedron Lett.*, 2006, **47**, 7057–7060.

39 S. Foillard, M. O. Rasmussen, J. Razkin, D. Boturyn and P. Dumy, *J. Org. Chem.*, 2008, **73**, 983–991.
40 V. Dulery, O. Renaudet and P. Dumy, *Tetrahedron*, 2007, **63**, 11952–11958.
41 R. O. Hynes, *Cell*, 1992, **69**, 11–25.
42 R. H. Kimura, A. M. Levin, F. V. Cochran and J. R. Cochran, *Proteins*, 2009, **77**, 359–369.
43 R. Fontana, M. A. Mendes, B. M. de Souza, K. Konno, L. M. M. Cesar, O. Malaspina and M. S. Palma, *Peptides*, 2004, **25**, 919–928.
44 A. Romanelli, L. Moggio, R. C. Montella, P. Campiglia, M. Iannaccone, F. Capuano, C. Pedone and R. Capparelli, *J. Pept. Sci.*, 2011, **17**, 348–352.
45 A. R. Means and J. R. Dedman, *Nature*, 1980, **285**, 73–77.
46 D. A. Malencik and S. R. Anderson, *Biochem. Biophys. Res. Commun.*, 1983, **114**, 50–56.
47 O. Avrutina, H. U. Schmoldt, D. Gabrijelcic-Geiger, D. Le Nguyen, C. P. Sommerhoff, U. Diederichsen and H. Kolmar, *Biol. Chem.*, 2005, **386**, 1301–1306.
48 B. Tripet, L. Yu, D. L. Bautista, W. Y. Wong, R. T. Irvin and R. S. Hodges, *Protein Eng.*, 1996, **9**, 1029–1042.
49 B. Steinmann, A. Christmann, T. Heiseler, J. Fritz and H. Kolmar, *Appl. Environ. Microbiol.*, 2010, **76**, 5563–5569.
50 B. Apostolovic, M. Danial and H.-A. Klok, *Chem. Soc. Rev.*, 2010, **39**, 3541–3575.
51 C. P. Sommerhoff, O. Avrutina, H.-U. Schmoldt, D. Gabrijelcic-Geiger, U. Diederichsen and H. Kolmar, *J. Mol. Biol.*, 2010, **395**, 167–175.
52 A. Heitz, O. Avrutina, D. Le-Nguyen, U. Diederichsen, J.-F. Hernandez, J. Gracy, H. Kolmar and L. Chiche, *BMC Struct. Biol.*, 2008, 8.
53 I. Coin, M. Beyermann and M. Bienert, *Nat. Protocols*, 2007, **2**, 3247–3256.
54 L. Moroder, D. Besse, H. J. Musiol, S. RudolphBohner and F. Siedler, *Biopolymers*, 1996, **40**, 207–234.
55 S. Krause, H.-U. Schmoldt, A. Wentzel, M. Ballmaier, K. Friedrich and H. Kolmar, *FEBS J.*, 2007, **274**, 86–95.
56 M. Empting, O. Avrutina, R. Meusinger, S. Fabritz, M. Reinwarth, M. Biesalski, S. Voigt, G. Buntkowsky and H. Kolmar, *Angew. Chem., Int. Ed.*, 2011, **50**, 5207–5211.
57 J. N. Israelachvili, *Intermolecular and Surface Forces*, Elsevier Inc., 2011.
58 A. Knoll, R. Magerle and G. Krausch, *Macromolecules*, 2001, **34**, 4159–4165.
59 O. Avrutina, H. U. Schmoldt, H. Kolmar and U. Diederichsen, *Eur. J. Org. Chem.*, 2004, 4931–4935.
60 T. R. Rodriguez and R. Garcia, *Appl. Phys. Lett.*, 2004, **84**, 449–451.
61 S. Patil, N. F. Martinez, J. R. Lozano and R. Garcia, *J. Mol. Recognit.*, 2007, **20**, 516–523.
62 R. W. Stark, N. Naujoks and A. Stemmer, *Nanotechnology*, 2007, **18**, 065502.
63 N. F. Martinez, J. R. Lozano, E. T. Herruzo, F. Garcia, C. Richter, T. Sulzbach and R. Garcia, *Nanotechnology*, 2008, **19**, 163118.
64 C. Dietz, M. Zerson, C. Riesch, A. M. Gigler, R. W. Stark, N. Rehse and R. Magerle, *Appl. Phys. Lett.*, 2008, **92**, 143107.
65 J. W. Li, J. P. Cleveland and R. Proksch, *Appl. Phys. Lett.*, 2009, **94**, 163118.
66 C. Dietz, E. T. Herruzo, J. R. Lozano and R. Garcia, *Nanotechnology*, 2011, **22**, 125708.

8.2. Combination of inverse electron-demand Diels–Alder reaction with highly efficient oxime ligation expands the toolbox of site-selective peptide conjugations

Title:

Combination of inverse electron-demand Diels–Alder reaction with highly efficient oxime ligation expands the toolbox of site-selective peptide conjugations.

Authors:

Sebastian Hörner,[‡] Christina Uth,[‡] Olga Avrutina, Holm Frauendorf, Manfred Wiessler und Harald Kolmar.

Bibliographic data:

Chemical Communications
Issue 51, Pages11130-11133, 10. June 2015.
DOI: 10.1039/C5CC03434E.
For the first time published in the internet on June 10th 2015.

Graphical abstract:

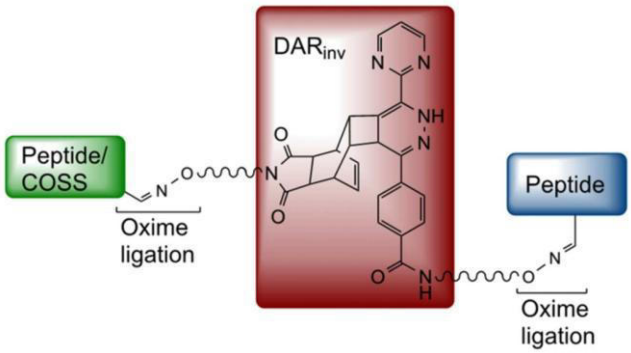

Summary:

For the synthesis of defined peptide heterodimers and peptide conjugation to cell-penetrating COSS modules, the Diels-Alder reaction with inverse electron demand was combined with the oxime ligation between aminooxy and aldehydic groups. This conjugation strategy allows for highly efficient peptide conjugate synthesis.

Contributions by Dipl.-Ing. Sebastian Hörner:

- Conception of the manuscript
- Design and accomplishment of all chemical synthesis and interpretation of the corresponding physicochemical analysis except for compounds **3**, **5**, and **32**
- Writing of the experimental section of the manuscript

‡ shared lead author

ChemComm

COMMUNICATION

View Article Online
View Journal | View Issue

Cite this: *Chem. Commun.*, 2015, 51, 11130

Received 24th April 2015,
Accepted 10th June 2015

DOI: 10.1039/c5cc03434e

www.rsc.org/chemcomm

Combination of inverse electron-demand Diels–Alder reaction with highly efficient oxime ligation expands the toolbox of site-selective peptide conjugations†

S. Hörner,‡[a] C. Uth,‡[a] O. Avrutina,[a] H. Frauendorf,[b] M. Wiessler[c] and H. Kolmar*[a]

A modular approach combining inverse electron-demand Diels–Alder coupling (DAR_{inv}) and oxime ligation expands the toolbox of bioorthogonal peptide chemistry. Applicability of versatile site-specific bifunctional building blocks is demonstrated by generation of defined conjugates comprising linear, cystine-bridged and multi-disulfide functional peptides as well as their conjugation with hybrid silsesquioxane nanoparticles.

Covalent linkage of certain peptidic units, being an alternative or a complementary strategy to recombinant production, often becomes a method of choice for the synthesis of sophisticated macromolecular constructs with tailored properties.[1] Indeed, to date a vast number of bioconjugates and the respective techniques have been reported,[2] ranging from relatively simple fluorescently[3] or small-molecule-labelled peptides[4] to complex, multifunctional architectures like antibody–drug conjugates.[5] Obviously, chemical transformations suitable for bioconjugations must satisfy at least two obligatory requirements, chemoselectivity and efficiency.[6] In view of the variety of inherent functional groups present in peptidic molecules, the development of a viable orthogonal chemistry for their effective junction at a certain position still remains a challenge.

Generally, the strategy towards site-specific bioconjugations[7] relies on incorporation of a uniquely addressable group at the desired position in the molecule of interest followed by its peculiar reaction with the respective counterpart. Such a uniquely addressable moiety could be incorporated into peptidic molecules through a vast number of post-synthetic modifications, *e.g.* periodate oxidation of β-aminoalcohols,[8,9] or *via* the non-natural building blocks[10] either upon recombinant production[11] or in the course of chemical synthesis. Bioorthogonal reactions to target these non-natural functional groups often make use of rich ketone and aldehyde chemistry[12] as well as numerous click-type reactions,[3,13] with the azide–alkyne cycloaddition being the most prominent representative.[14–16] During the last decade, a special class of pericyclic reactions has got the highest priority as they utilize the ring strain to promote increased reactivity upon cycloaddition.[17–19] In particular, the Diels–Alder reaction with inverse electron-demand (DAR_{inv})[20–22] between numerous dienophiles[23–25] and tetrazines[21,26,27] was found to be a valuable tool for effective bioorthogonal conjugations.[28–30] Followed by a retro-Diels–Alder reaction to eliminate nitrogen gas, this so-called tetrazine ligation is characterized by extremely fast kinetics with second-order rate constants up to 2×10^3 M^{-1} s^{-1} and has been already used in a number of both *in situ* and *in vivo* studies.[25,31,32]

In this study we present a modular approach to the conjugation of biomolecules based on the combination of two efficient chemical transformations, oxime ligation and DAR_{inv}. For the proof-of-concept experiments we designed bifunctional building blocks to incorporate the bioorthogonal DAR_{inv} coupling site in a peptide site-specifically *via* oximation of the respective aldehyde. Following this step, attachment of a DAR_{inv} counterpart would accomplish a desired conjugate. The choice of the strategy was specified by two arguments, feasible generation of required aldehydes in biomolecules[8,9,33] and fast kinetics of an irreversible DAR_{inv}. We reasoned that our approach, initially investigated on peptides of different size and molecular complexity, could be further extended to orthogonal conjugations featuring a broad spectrum of biomacromolecules, *i.e.* proteins, sugars, or other biopolymers.

Here it is important to mention that, while having been used for numerous labeling approaches,[34,35] the DAR_{inv} reaction was surprisingly rarely applied to connect functional peptides site-specifically.[28,36] This could be explained taking into account that both the diene and the dienophile counterparts have been

[a] *Technische Universität Darmstadt, Clemens-Schöpf-Institut für Organische Chemie und Biochemie, Alarich-Weiss Straße 4, 64287 Darmstadt, Germany. E-mail: kolmar@biochemie-tud.de*
[b] *Georg-August-Universität Göttingen, Institut für Organische und Biomolekulare Chemie, Zentrale Analytik/Massenspektrometrie, Tammannstraße 2, 37077 Göttingen, Germany*
[c] *Deutsches Krebsforschungszentrum, Medizinische Physik in der Radiologie, Projektgruppe Biologische Chemie E020, Im Neuenheimer Feld, 69120 Heidelberg, Germany*

† Electronic supplementary information (ESI) available: Combination of inverse electron-demand Diels–Alder reaction with highly efficient oxime ligation expands the toolbox of site-selective peptide conjugations. See DOI: 10.1039/c5cc03434e

‡ These authors contributed equally to this work.

to date installed into partner biomolecules using either amide[37,38] or maleimide chemistry[39] which cannot provide the required orthogonality, especially with regard to cysteine/cystine-bearing molecules. Though the installation of DAR_{inv} building blocks into peptide-like molecules on solid support has been reported, this approach did not find broad application. Moreover, the on-resin assembly is very rarely used for the production of full-size proteins.

Since oxime ligation has been applied to couple *exo*-norbornene as a dienophile handle onto aldehydes of the reducing ends of oligosaccharides[40] and taking into consideration that this moiety is easily generated in both recombinant and synthetic peptides[41] without interference with functional side chains, we decided to use this highly efficient reaction to decorate the peptides of interest with the respective diene and dienophile partners.

Our modular approach relies on the tailor-made bifunctional building blocks equipped with an aminooxy moiety for the primary incorporation into peptidic counterparts along with the DAR_{inv} site for the successive ligation (Fig. 1). In our proof-of-concept study we installed the DAR_{inv} building blocks **5** and **8** into the next functional peptides: a Sortase A recognition heptapeptide **12**,[42,43] an integrin-binding RGD decapeptide **9**,[12] an antimicrobial decapeptide Jelleine derivative **13**,[44] a disulfide-bridged pentadecapeptide matriptase inhibitor **10**,[45] and two cystine knots comprising three disulfides and a backbone of more than thirty amino acids **11**, **14**[46] (Scheme S2, ESI†). An additional *N*-terminal serine was introduced into each peptide to provide the orthogonally addressable site upon post-synthetic modification.[9] The resulted glyoxylyl moieties generated by periodate oxidation (Scheme S1, ESI†) were oximated by the aminooxy-bearing derivatives of Reppe anhydride **5** and tetrazine **8**, respectively (Fig. 1 and 2). The dienes **15–17** were synthesized from peptide-glyoxals **9–11**, and the dienophiles **18–20** – from peptide-glyoxals **12–14** (Fig. 2 and ESI 1.2.12†). Peptides were assembled by microwave-assisted Fmoc-SPPS.[47] Following cleavage from the support with successive oxidative folding if required, the *N*-terminal serines were oxidized by $NaIO_4$ to generate the aminooxy-reactive glyoxals **9–14** for further conjugations (ESI 1.2.9–1.2.11†).

Prior to the installation into synthetic peptides, the bifunctional DAR_{inv} building blocks were synthesized following a two-step procedure as illustrated in Fig. 1.

Thus, mono-Boc-protected miniPEG **1** was reacted with Reppe anhydride **2** or tetrazine derivative **6**, respectively, and the resulting constructs **3** and **7** were transformed into *N*-ethoxyethylidene (Eei)-protected aminooxy building blocks **5** and **8** upon acidolytic cleavage of *N*-Boc protection followed by the *N*-acylation with *N*-hydroxysuccinimide-activated (NHS) Eei-protected aminooxy acetic acid **4** (Fig. 1 and ESI 1.2.1–1.2.8†).[48] The oxime ligation was performed in 50% (v:v) aqueous TFA overnight leading to peptide-tetrazines **15–17** and peptide-dienophiles **18–20** (Fig. 2 and ESI 1.2.12†).

After the conjugation partners have been decorated with the respective DAR_{inv} building blocks, the resulted diene and dienophile counterparts were reacted with each other in 10% aq. acetonitrile containing 0.1% TFA overnight at ambient temperature giving conjugates **21–29** (Fig. 3 and 4, ESI 1.2.15†). The exemplified monitoring of DAR_{inv} reaction progress presented in Fig. 4 and in ESI 1.2.15† clearly indicates that conversion into the desired

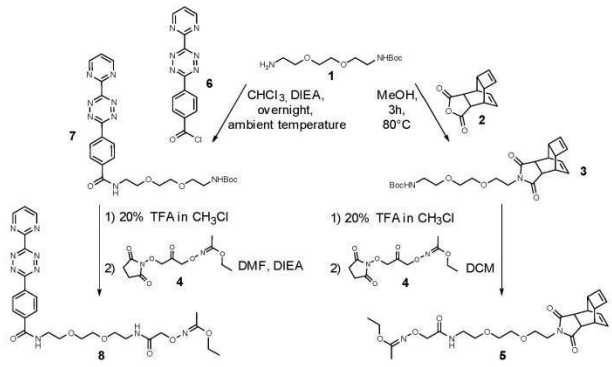

Fig. 1 Synthesis of DAR_{inv} building blocks.

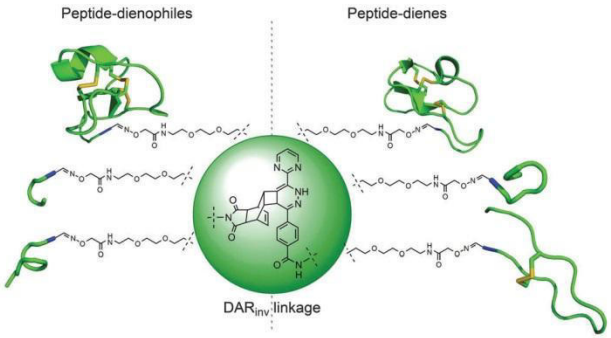

Fig. 3 Schematic representation of peptide conjugates synthesized by DAR_{inv} between the counterparts depicted on the left and the right panels.

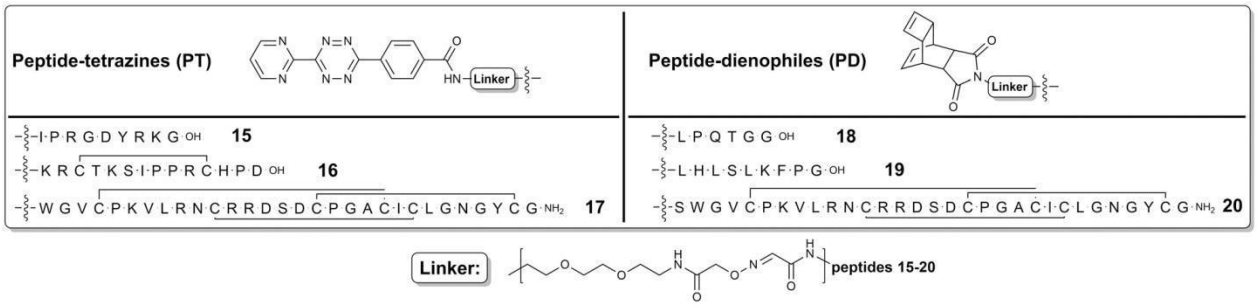

Fig. 2 Synthesized peptidic ligands for successive DAR_{inv} conjugations.

A)

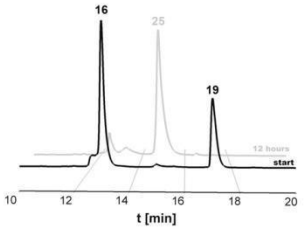

B)

	15	16	17
18	**21** (73.3%)	**24** (87.7%)	**27** (n.d.)
19	**22** (85%)	**25** (100%)	**28** (93.8%)
20	**23** (92.5%)	**26** (87%)	**29** (n.d.)

Fig. 4 (A) HPLC monitoring of an exemplified DAR_{inv} conjugation between Jelleine–Reppe construct **19** and SDMI-3 tetrazine partner **16**. (B) Conversion rate for DAR_{inv} conjugations calculated from the HPLC traces (n.d.: not determined).

products has been achieved for all constructs. Interestingly, upon evaluation of the mass spectrometric data, we observed for some DAR_{inv} conjugates the recovery of the aromatic system in the tetrazine, as previously reported.[49,50] The mass spectra can be seen in Fig. 5 as well as in ESI 1.2.21–1.2.29.†

As the proof-of-concept study showed the viability of our approach, it was further expanded towards a more sophisticated (in view of architecture and functional properties) molecular construct. Thus, we attached a peptidic cargo to the smallest nanoparticle known, a cell-penetrating organic–inorganic hybrid molecule comprising cube-octameric silsesquioxane (COSS).[44] This highly symmetric octavalent compound has recently attracted keen attention, being used as a scaffold in a number of biomedical applications, including delivery of

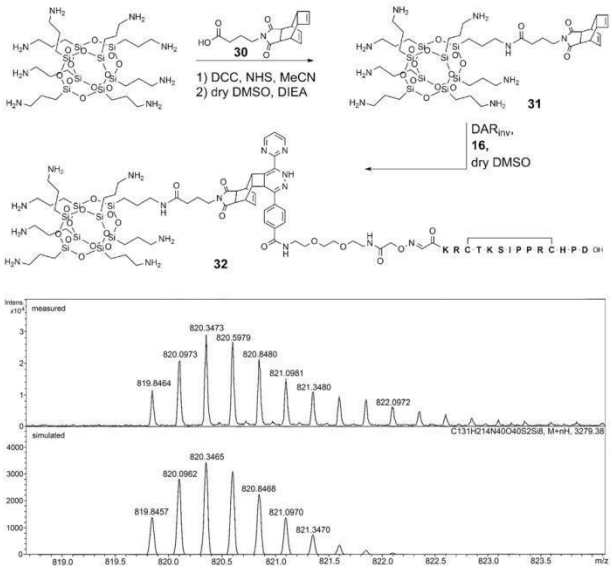

Fig. 5 Top: formation of conjugate **32** by DAR_{inv} between cell-penetrating COSS **31** and peptide **16**. Bottom: exemplary ESI-HR-MS analysis of conjugate **32** $[M + 4H]^{4+}$.

bioactive payloads into cancer cells and development of novel tailor-made conjugates of pharmacological interest.[44]

Compared to the modification of peptides with a dienophile, a different procedure was applied. Thus, Reppe anhydride **2** was equipped with a linker comprising the NHS-activated γ-amino-butyric acid (ESI 1.2.13†). Building block **30** was attached to a single corner of octaamino COSS through an amide bond (Fig. 5 and ESI 1.2.14†) resulting in COSS-dienophile **31** which was reacted with peptide-diene **16** giving conjugate **32**. The reaction was carried out in dry DMSO to assure stability of the siloxane core in the presence of the pendant propylamine groups (Fig. 5).

The combination of oxime ligation and DAR_{inv} is a convenient method for site-specific conjugation of complex peptidic molecules. What is the rationale behind using the set of two transformations rather than the individual reactions, each of which is bioorthogonal, selective, and fast *per se*? First, at physiological pH oxime ligation is rather slow and requires catalysis. This could pose a problem if two functional biological macromolecules are ligated directly, whereas the introduction of small bifunctional linker proceeds unhampered, and the next step is irreversible and uncatalyzed. Second, although the direct introduction of DAR_{inv} moieties on solid support has been reported for short peptides,[21,30,36,51] their introduction in recombinant proteins requires extensive modification of the cellular translation machinery.[10,32,52] And, third, our approach provides certain modularity, giving an option to choose between the reactive sites according to reaction environment and nature of the conjugation partners.

In general, our bifunctional building blocks are readily synthetically accessible and can be introduced into peptides site-selectively, without affecting their architecture. The generation of the required carbonyl moieties in peptidic macromolecules is a routine procedure as it proceeds smoothly both upon post-synthetic modification[8] and in the course of recombinant production.[33] Successive oxime ligation was highly efficient and orthogonal to the side-chain functionalities. Subsequently, the generated DAR_{inv}-modified peptides were reacted without a catalyst with the respective counterpart giving defined peptidic constructs with good to quantitative conversion rates. So far, only few DAR_{inv} site-specific conjugations of peptides have been reported restricted either to junction of rather short peptidic sequences[28] or to the generation of macromolecular constructs of undefined stoichiometry.[34,36] Our approach offers the advantage of being suitable for all synthetic peptides, particularly the recombinant ones.

In our hands, being incorporated into peptides and hybrid silsesquioxanes, the strained four-membered ring system of the Reppe anhydride reacted with the respective tetrazine, smoothly converting it into the desired product. This reactivity can be easily explained considering the non-reversible character of DAR_{inv} coupling and the fact that cyclobutene is amongst the most reactive species classified *via* their activation free energies.[53]

Interestingly, for some peptide conjugates we observed the regeneration of the aromatic system within the tetrazine moiety after DAR_{inv} reaction. This observation has previously been reported, but detailed study of the mechanism is still required.[49,50]

To demonstrate modularity and versatility of our approach, we applied it to covalently graft a bioactive peptide[45] onto a

cell-penetrating COSS nanoparticle. The success of this reaction opens new avenues for the facile generation of peptide–COSS conjugates for intracellular delivery, thus expanding the toolbox for the chemical modifications of these promising compounds. In a perspective, our system could be applied to the generation of peptide–protein conjugates under physiological conditions.[54] Taking into consideration that stability of oxime linkage is context-dependent and at physiological pH a catalyst is required to assure efficient transformation, an adequately high-performance chemistry should be considered to replace this ligation step. To this end, recently reported trapped Knoevenagel condensation[55] could be applied as an alternative strategy.

This work was partially funded by the DFG priority program SPP 1623. The authors thank Peter Lorenz (DKFZ, Heidelberg) for his advice regarding tetrazine synthesis.

Notes and references

1 A. Angelini and C. Heinis, *Curr. Opin. Chem. Biol.*, 2011, **15**, 355–361.
2 J. Kalia and R. T. Raines, *Curr. Org. Chem.*, 2010, **14**, 138–147.
3 A. Chakraborty, D. Wang, Y. W. Ebright and R. H. Ebright, *Methods Enzymol.*, 2010, **472**, 19–30.
4 N. K. Devaraj, S. Hilderbrand, R. Upadhyay, R. Mazitschek and R. Weissleder, *Angew. Chem.*, 2010, **49**, 2869–2872.
5 B. M. Zeglis, P. Mohindra, G. I. Weissmann, V. Divilov, S. A. Hilderbrand, R. Weissleder and J. S. Lewis, *Bioconjugate Chem.*, 2011, **22**, 2048–2059.
6 J. C. Jewett and C. R. Bertozzi, *Chem. Soc. Rev.*, 2010, **39**, 1272–1279.
7 G. C. Rudolf, W. Heydenreuter and S. A. Sieber, *Curr. Opin. Chem. Biol.*, 2013, **17**, 110–117.
8 D. Chelius and T. A. Shaler, *Bioconjugate Chem.*, 2003, **14**, 205–211.
9 K. F. Geoghegan and J. G. Stroh, *Bioconjugate Chem.*, 1992, **3**, 138–146.
10 C. H. Kim, J. Y. Axup and P. G. Schultz, *Curr. Opin. Chem. Biol.*, 2013, **17**, 412–419.
11 W. P. Heal, S. R. Wickramasinghe, P. W. Bowyer, A. A. Holder, D. F. Smith, R. J. Leatherbarrow and E. W. Tate, *Chem. Commun.*, 2008, 480–482.
12 S. Fabritz, S. Horner, D. Konning, M. Empting, M. Reinwarth, C. Dietz, B. Glotzbach, H. Frauendorf, H. Kolmar and O. Avrutina, *Org. Biomol. Chem.*, 2012, **10**, 6287–6293.
13 P. V. Chang, J. A. Prescher, E. M. Sletten, J. M. Baskin, I. A. Miller, N. J. Agard, A. Lo and C. R. Bertozzi, *Proc. Natl. Acad. Sci. U. S. A.*, 2010, **107**, 1821–1826.
14 M. Meldal and C. W. Tornoe, *Chem. Rev.*, 2008, **108**, 2952–3015.
15 J. E. Moses and A. D. Moorhouse, *Chem. Soc. Rev.*, 2007, **36**, 1249–1262.
16 K. Nwe and M. W. Brechbiel, *Cancer Biother. Radiopharm.*, 2009, **24**, 289–302.
17 N. J. Agard, J. A. Prescher and C. R. Bertozzi, *J. Am. Chem. Soc.*, 2004, **126**, 15046–15047.
18 X. Ning, R. P. Temming, J. Dommerholt, J. Guo, D. B. Ania, M. F. Debets, M. A. Wolfert, G. J. Boons and F. L. van Delft, *Angew. Chem.*, 2010, **49**, 3065–3068.
19 N. E. Mbua, J. Guo, M. A. Wolfert, R. Steet and G. J. Boons, *ChemBioChem*, 2011, **12**, 1912–1921.
20 M. Wiessler, W. Waldeck, C. Kliem, R. Pipkorn and K. Braun, *Int. J. Med. Sci.*, 2009, **7**, 19–28.
21 R. Pipkorn, W. Waldeck, B. Didinger, M. Koch, G. Mueller, M. Wiessler and K. Braun, *J. Pept. Sci.*, 2009, **15**, 235–241.
22 A. Niederwieser, A. K. Spate, L. D. Nguyen, C. Jungst, W. Reutter and V. Wittmann, *Angew. Chem.*, 2013, **52**, 4265–4268.
23 S. B. Engelsma, L. I. Willems, C. E. van Paaschen, S. I. van Kasteren, G. A. van der Marel, H. S. Overkleeft and D. V. Filippov, *Org. Lett.*, 2014, **16**, 2744–2747.
24 D. N. Kamber, L. A. Nazarova, Y. Liang, S. A. Lopez, D. M. Patterson, H. W. Shih, K. N. Houk and J. A. Prescher, *J. Am. Chem. Soc.*, 2013, **135**, 13680–13683.
25 M. L. Blackman, M. Royzen and J. M. Fox, *J. Am. Chem. Soc.*, 2008, **130**, 13518–13519.
26 Z. Li, H. Cai, M. Hassink, M. L. Blackman, R. C. Brown, P. S. Conti and J. M. Fox, *Chem. Commun.*, 2010, **46**, 8043–8045.
27 M. R. Karver, R. Weissleder and S. A. Hilderbrand, *Bioconjugate Chem.*, 2011, **22**, 2263–2270.
28 S. Ameta, J. Becker and A. Jaschke, *Org. Biomol. Chem.*, 2014, **12**, 4701–4707.
29 T. S. Elliott, F. M. Townsley, A. Bianco, R. J. Ernst, A. Sachdeva, S. J. Elsasser, L. Davis, K. Lang, R. Pisa, S. Greiss, K. S. Lilley and J. W. Chin, *Nat. Biotechnol.*, 2014, **32**, 465–472.
30 B. M. Zeglis, F. Emmetiere, N. Pillarsetty, R. Weissleder, J. S. Lewis and T. Reiner, *ChemistryOpen*, 2014, **3**, 48–53.
31 J. Seckute and N. K. Devaraj, *Curr. Opin. Chem. Biol.*, 2013, **17**, 761–767.
32 J. L. Seitchik, J. C. Peeler, M. T. Taylor, M. L. Blackman, T. W. Rhoads, R. B. Cooley, C. Refakis, J. M. Fox and R. A. Mehl, *J. Am. Chem. Soc.*, 2012, **134**, 2898–2901.
33 D. Rabuka, J. S. Rush, G. W. deHart, P. Wu and C. R. Bertozzi, *Nat. Protoc.*, 2012, **7**, 1052–1067.
34 F. Emmetiere, C. Irwin, N. T. Viola-Villegas, V. Longo, S. M. Cheal, P. Zanzonico, N. Pillarsetty, W. A. Weber, J. S. Lewis and T. Reiner, *Bioconjugate Chem.*, 2013, **24**, 1784–1789.
35 K. S. Yang, G. Budin, C. Tassa, O. Kister and R. Weissleder, *Angew. Chem.*, 2013, **52**, 10593–10597.
36 R. Hassert, M. Pagel, Z. Ming, T. Haupl, B. Abel, K. Braun, M. Wiessler and A. G. Beck-Sickinger, *Bioconjugate Chem.*, 2012, **23**, 2129–2137.
37 J. B. Haun, N. K. Devaraj, S. A. Hilderbrand, H. Lee and R. Weissleder, *Nat. Nanotechnol.*, 2010, **5**, 660–665.
38 R. Rossin, P. R. Verkerk, S. M. van den Bosch, R. C. Vulders, I. Verel, J. Lub and M. S. Robillard, *Angew. Chem.*, 2010, **49**, 3375–3378.
39 J. D. Thomas, H. Cui, P. J. North, T. Hofer, C. Rader and T. R. Burke, Jr., *Bioconjugate Chem.*, 2012, **23**, 2007–2013.
40 H. S. Beckmann, A. Niederwieser, M. Wiessler and V. Wittmann, *Chemistry*, 2012, **18**, 6548–6554.
41 O. El-Mahdi and O. Melnyk, *Bioconjugate Chem.*, 2013, **24**, 735–765.
42 R. G. Kruger, B. Otvos, B. A. Frankel, M. Bentley, P. Dostal and D. G. McCafferty, *Biochemistry*, 2004, **43**, 1541–1551.
43 C. Uth, S. Zielonka, S. Hörner, N. Rasche, A. Plog, H. Orelma, O. Avrutina, K. Zhang and H. Kolmar, *Angew. Chem.*, 2014, **53**, 12618–12623.
44 S. Fabritz, S. Horner, O. Avrutina and H. Kolmar, *Org. Biomol. Chem.*, 2013, **11**, 2224–2236.
45 H. Fittler, O. Avrutina, M. Empting and H. Kolmar, *J. Pept. Sci.*, 2014, **20**, 415–420.
46 B. Glotzbach, M. Reinwarth, N. Weber, S. Fabritz, M. Tomaszowski, H. Fittler, A. Christmann, O. Avrutina and H. Kolmar, *PLoS One*, 2013, **8**, e76956.
47 R. B. Merrifield, *J. Am. Chem. Soc.*, 1963, **85**, 2149–2154.
48 S. Foillard, M. O. Rasmussen, J. Razkin, D. Boturyn and P. Dumy, *J. Org. Chem.*, 2008, **73**, 983–991.
49 A. C. Knall and C. Slugovc, *Chem. Soc. Rev.*, 2013, **42**, 5131–5142.
50 R. Hoogenboom, B. C. Moore and U. S. Schubert, *J. Org. Chem.*, 2006, **71**, 4903–4909.
51 M. Wiessler, W. Waldeck, R. Pipkorn, C. Kliem, P. Lorenz, H. Fleischhacker, M. Hafner and K. Braun, *Int. J. Med. Sci.*, 2010, **7**, 213–223.
52 K. Lang, L. Davis, S. Wallace, M. Mahesh, D. J. Cox, M. L. Blackman, J. M. Fox and J. W. Chin, *J. Am. Chem. Soc.*, 2012, **134**, 10317–10320.
53 F. Liu, Y. Liang and K. N. Houk, *J. Am. Chem. Soc.*, 2014, **136**, 11483–11493.
54 E. M. Sletten and C. R. Bertozzi, *Angew. Chem.*, 2009, **48**, 6974–6998.
55 R. Kudirka, R. M. Barfield, J. McFarland, A. E. Albers, G. W. de Hart, P. M. Drake, P. G. Holder, S. Banas, L. C. Jones, A. W. Garofalo and D. Rabuka, *Chem. Biol.*, 2015, **22**, 293–298.

ChemComm

CORRECTION

View Article Online
View Journal | View Issue

Cite this: *Chem. Commun.*, 2015, 51, 11727

Correction: Combination of inverse electron-demand Diels–Alder reaction with highly efficient oxime ligation expands the toolbox of site-selective peptide conjugations

S. Hörner,[a] C. Uth,[a] O. Avrutina,[a] H. Frauendorf,[b] M. Wiessler[c] and H. Kolmar*[a]

DOI: 10.1039/c5cc90302e

www.rsc.org/chemcomm

Correction for 'Combination of inverse electron-demand Diels–Alder reaction with highly efficient oxime ligation expands the toolbox of site-selective peptide conjugations' by S. Hörner, *et al.*, *Chem. Commun.*, 2015, DOI: 10.1039/c5cc03434e.

In Fig. 1 of the published article the structures for compound **4** were displayed incorrectly. Fig. 1 should appear as follows:

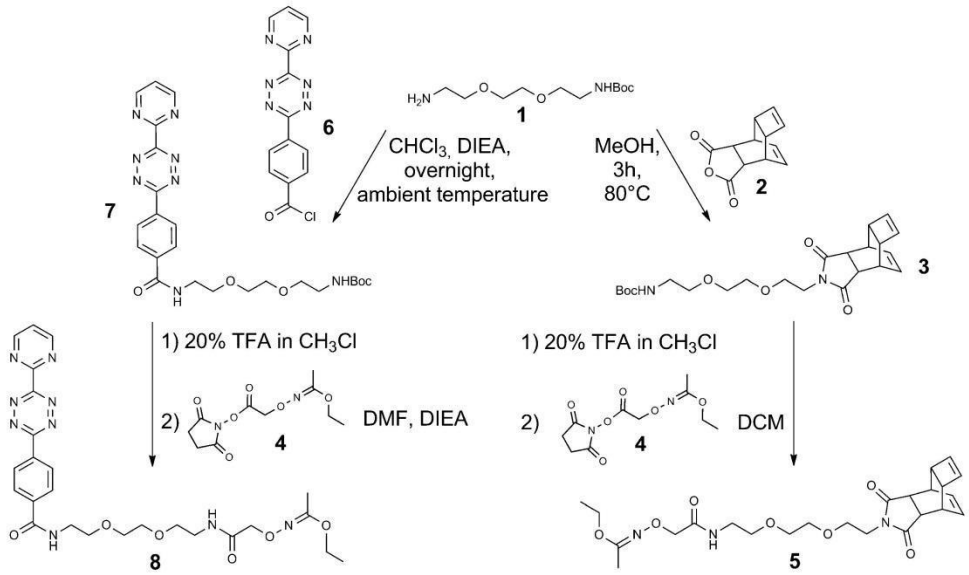

The Royal Society of Chemistry apologises for these errors and any consequent inconvenience to authors and readers.

[a] *Technische Universität Darmstadt, Clemens-Schöpf-Institut für Organische Chemie und Biochemie, Alarich-Weiss Straße 4, 64287 Darmstadt, Germany. E-mail: kolmar@biochemie-tud.de*

[b] *Georg-August-Universität Göttingen, Institut für Organische und Biomolekulare Chemie, Zentrale Analytik/Massenspektrometrie, Tammannstraße 2, 37077 Göttingen, Germany*

[c] *Deutsches Krebsforschungszentrum, Medizinische Physik in der Radiologie, Projektgruppe Biologische Chemie E020, Im Neuenheimer Feld, 69120 Heidelberg, Germany*

8.3. Cube-octameric silsesquioxanes-mediated cargo peptide delivery into living cancer cells

Title:

Cube-octameric silsesquioxanes-mediated cargo peptide delivery into living cancer cells

Authors:

Sebastian Hörner,[‡] Sebastian Fabritz,[‡] Henry D. Herce, Olga Avrutina, Christian Dietz, Robert W. Stark, M. Cristina Cardoso und Harald Kolmar.

Bibliographic Data:

Organic & Biomolecular Chemistry
Issue 11, pages 2258-2265, December 6th 2012
DOI: 10.1039/C2OB26808F
For the first time published in the internet on December 6th 2012

Graphical abstract:

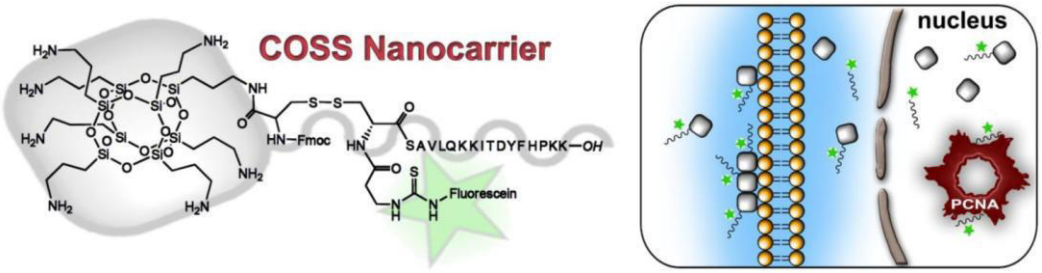

Summary:

COSS were investigated as drug delivery modules for peptide delivery into living cancer cells. A peptide comprising high affinity to the Proliferating Cell Nuclear Antigen (PCNA) was delivered into human cancer cell-line HeLa. Functionality of the peptide was proven by intracellular co-localization with its target.

Contributions by Dipl.-Ing. Sebastian Hörner:

- Conception of the chemical part of the manuscript
- Design and accomplishment of all chemical synthesis and interpretation of corresponding physicochemical analysis
- Support of writing of the manuscript
- Writing of the experimental section of the manuscript

‡ shared lead author

Organic & Biomolecular Chemistry

RSC Publishing

PAPER

View Article Online
View Journal | View Issue

Cube-octameric silsesquioxane-mediated cargo peptide delivery into living cancer cells†

Cite this: *Org. Biomol. Chem.*, 2013, **11**, 2258

Sebastian Hörner,‡[a] Sebastian Fabritz,‡[a] Henry D. Herce,*[b,c] Olga Avrutina,[a] Christian Dietz,[d] Robert W. Stark,[d] M. Cristina Cardoso[c] and Harald Kolmar*[a]

Received 14th September 2012,
Accepted 6th December 2012

DOI: 10.1039/c2ob26808f

www.rsc.org/obc

Cube octameric silsesquioxanes (COSS) are among the smallest nanoparticles known to date with a diameter of only 0.7 nm. We describe a COSS-based delivery system which allows for the drug targeting in human cells. It comprises a siloxane core with seven pendant aminopropyl groups and a fluorescently labeled peptidic ligand attached to one cage corner *via* a reversible disulfide bond to ensure its intracellular release. Bimodal amplitude-modulated atomic force microscopy (AFM) experiments revealed the formation of dendritic COSS structures by a self-assembly of single particles on negatively charged surfaces. Nuclear targeting was demonstrated in HeLa cells by selective binding of released $p21^{Cip1/Waf1}$-derived cargo peptide to PCNA, a protein involved in DNA replication and repair.

Introduction

Nanomaterials and nanoparticles with tailor-made functionalities attract growing interest in the fields of gene therapy,[1] DNA protection,[2] or cancer targeting.[1–3] In molecular oncology, they enable cell penetration acting as modules for drug delivery into tumor cells. *In vivo*, the enhanced permeability and retention effect[4,5] as well as the leaky vasculature of cancer cells result in a passive targeting of nanoparticle-delivered drugs.[6,7] Size, shape, surface charge, and the functional groups of a nanoparticle control its interaction with biological systems.[8,9] Thus, the functionality but also the toxicity of nanoparticle-based delivery units strongly depends on their design.[10,11] Therefore, it is essential to ensure a balance between the desired biological function and cytotoxicity due to *e.g.* reactive oxygen species[10] or vasculature obstruction resulting in organ-associated toxicity.[11] Considering these requirements, a wide range of cell membrane-permeable nanoparticles has been developed, among them core–shell fluorescent,[12] mesoporous dye-doped,[13,14] TAT[15]-peptide-conjugated[16,17] silica nanoparticles (SNP) and nanovalves.[18–20]

Cube-octameric silsesquioxanes (COSS)[21] can be considered as special members of the SNP family. They are highly symmetric molecules of pico dimension comprising a 500 pm silica core that is decorated with organic ligands.[22] COSS with pendant azide,[23–25] aminooxy,[22] vinyl,[26] thiol[27] or amine[28] functionalities allow for the presentation of biomolecules such as carbohydrates,[19,25,26,29] peptides,[22,23] and miniproteins[22] using the respective conjugation chemistry. Thus, up to eight ligands can be covalently attached to the silsesquioxane scaffold (Scheme 1a).

Comparing the size of COSS nanoparticles with the dimensions of other nanomaterials (*e.g.* silica and gold nanoparticles or biocompatible polymers), it is evident that a COSS cage is significantly smaller. This feature could be advantageous *e.g.* for enhanced vascular distribution or deeper tissue penetration. The cubic structure of the inorganic core allows for extremely dense presentation of functional ligands within an exactly defined architecture. Hydrolytic degradation of the inorganic COSS core into well-known primary silsesquioxanes at physiological pH[19,30] makes these molecules biodegradable scaffolds with potentially reduced risk of renal accumulation. However, the aspect of biodistribution and biostability of modified cube-octameric silsesquioxanes is largely unexplored and requires further systematic studies.

Among others, COSS carrying either lysine dendrimers[31] or poly(2-dimethylamino)ethyl methacrylate chains,[32] respectively, have been reported as DNA delivery systems into cells.

[a]*Clemens-Schöpf Institute of Organic Chemistry and Biochemistry, Technische Universität Darmstadt, Petersenstr. 22, 64287 Darmstadt, Germany. E-mail: Kolmar@Biochemie-TUD.de*
[b]*Department of Physics, Rensselaer Polytechnic Institute, Center for Biotechnology and Interdisciplinary Studies, Building 3237, 110 8th Street, Troy, NY 12180, USA. E-mail: hdherce@gmail.com*
[c]*Fachbereich Biologie, Technische Universität Darmstadt, Schnittspahnstraße 10, 64287 Darmstadt, Germany*
[d]*Center of Smart Interfaces, Technische Universität Darmstadt, Petersenstr. 32, 64287 Darmstadt, Germany*
†Electronic supplementary information (ESI) available: RP-HPLC spectra of **2**, **2a**, **3**, **4**, **5**, **5a**; ESI-MS data of **2**, **3**, **5**, **5a**, **5b**; HR-MS data of **2a**, **4**; IR spectrum of **4**. See DOI: 10.1039/c2ob26808f
‡These authors contributed equally to this work.

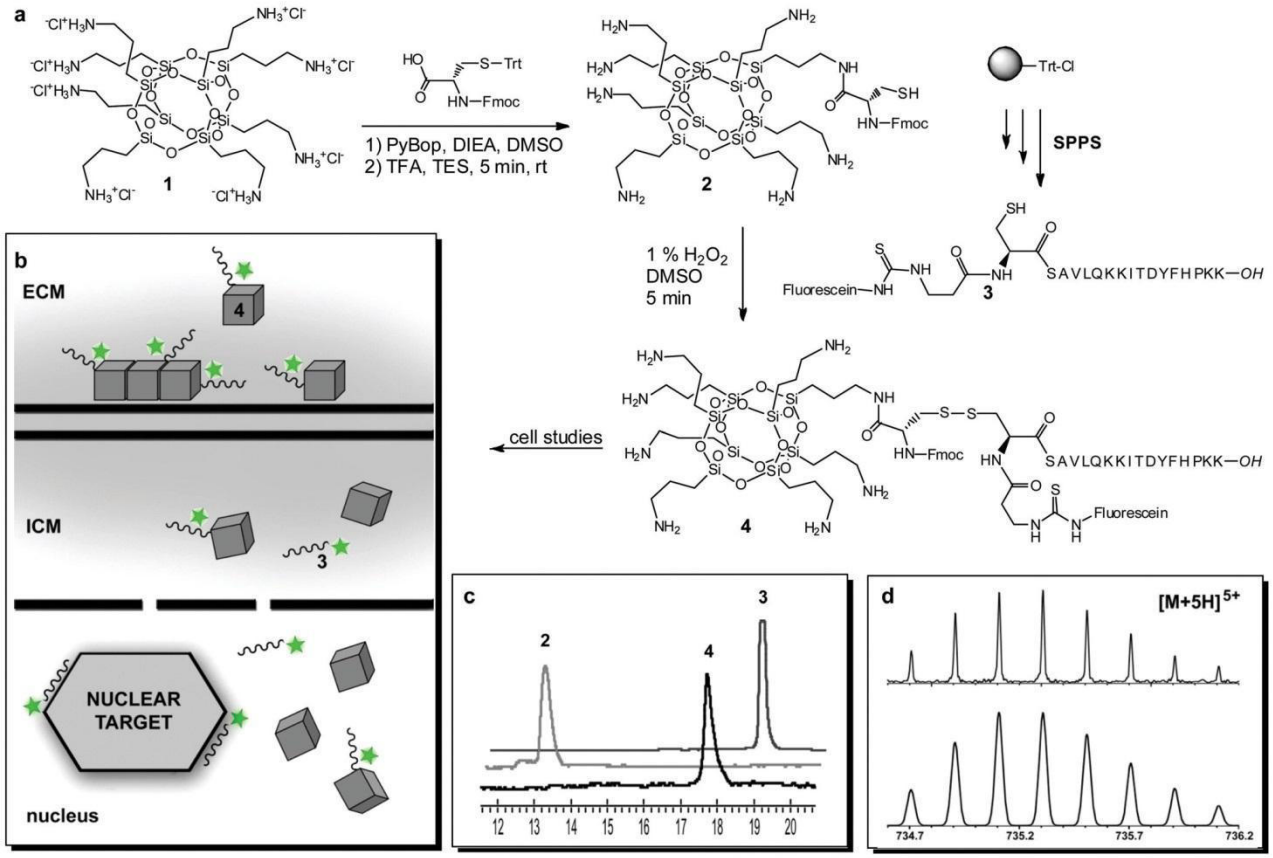

Scheme 1 (a) Synthesis of a biodegradable COSS–peptide conjugate **4**. The sequence of a $p21^{Cip1/Waf1}$-based peptide cargo is shown using a one-letter code; SPPS – solid phase peptide synthesis; (b) studies in HeLa cells using **4** are depicted as cartoon. **4** was applied to the extracellular medium (ECM) and penetrated the cell outer membrane. In the intracellular medium (ICM) the nanoparticle was accumulated in the nucleoli allowing for the targeting of the nucleus abundant protein PCNA; (c) HPLC traces (220 nm, 25% → 50% aq. CH_3CN in 20 min) recorded upon synthesis of **4**; (d) high-resolution mass spectrometric isotopic pattern; calc. for **4** $C_{158}H_{246}N_{35}O_{45}S_3Si_8$ (5+): 734.7065, meas. 734.7077.

Nanodots composed of a COSS cage surrounded by cationic-conjugated electrolyte arms could be targeted to the cell nucleus upon folic acid functionalization.[33]

In addition to nanoparticles that contain large and branched side chains extending from the inorganic silica core, cell-penetrating COSS derivatives have been described that bear relatively short arms, *i.e.* an isobutyl[34] or aminopropyl side chain.[35] Interestingly, McCusker *et al.* have demonstrated that fluorescently labeled water-soluble ammonium-functionalized COSS penetrated the outer membrane of Cos-1 cells[36] while exhibiting very low toxicity.[35] Based on these findings, the general applicability of octaamino COSS as a very small nanoparticle drug carrier was postulated, albeit an experimental proof is still missing.[35]

Herein, we investigated the applicability of octaamino COSS nanoparticles as a delivery system for targeting a peptidic cargo molecule to the nucleus of human HeLa[37] cancer cells.

As a model peptide for cargo delivery a 16-mer peptide SAVLQKKITDYFHPKK[38] was chosen that is known to bind an abundant nuclear protein, the proliferating cell nuclear antigen (PCNA).[39] PCNA is an essential component of the DNA replication and repair machinery and plays a fundamental role in cell proliferation and genome stability.[38–40] Tumor theranostic-related research in this field is concentrated on the development of a cancer biomarker based on the immunostaining of cancer-associated PCNA isoforms[41] and the inhibition of DNA replication *via* binding of peptidic ligands to PCNA.[38] The peptide mentioned above is derived from protein $p21^{Cip1/Waf1}$ that is known to bind PCNA,[42] thus playing a crucial role in regulating its activity.[43] An oligopeptide comprising the PCNA binding sequence of $p21^{Cip1/Waf1}$ was delivered into C2C12[44] mouse myoblast cells *via* TAT-mediated transduction. It caused cell cycle arrest indicating direct interference with protein–protein interaction that is crucial for DNA replication and repair.[45]

Results and discussion

For initial experiments, a single corner of the octaamino COSS particle was modified with a C-terminally fluorescein-labeled Cys-*β*Ala dipeptide (Fig. 1a) and human HeLa cells were

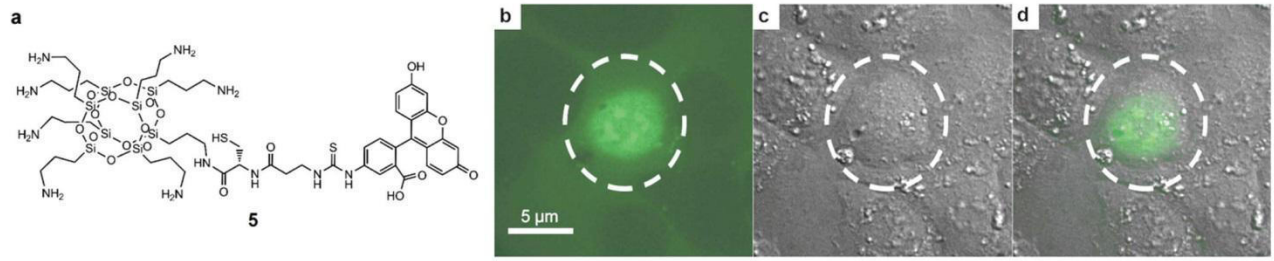

Fig. 1 Cellular uptake of fluorescein-labeled octaamino COSS **5** (a). The nanoparticle was added to the extracellular medium (final concentration of 20 μM) and after 30 min incubation the cells were washed with phosphate buffered saline and imaged. (b) Fluorescence image, (c) contrast image, (d) overlay. The location of the nucleus is indicated by a dotted circle.

incubated with the resulting conjugate (20 μM) for 30 min. Confocal microscopy studies revealed the distinct accumulation of silsesquioxanes in the multiple nucleoli of HeLa cells and also, to a lower extent, throughout the nucleoplasm and cytoplasm (Fig. 1b–d). This is in accordance with previous findings for nuclear localization of gold nanoparticles having the size of 2400 pm.[46] Due to their small size, the transit of COSS derivatives (700–800 pm) through the nuclear pore complex with an internal diameter of about 30 to 50 nm[47–49] might be achieved by passive diffusion. The observed accumulation in the nucleoli could be enhanced *via* electrostatic interactions of positively charged SNPs and phosphate-rich RNA. Providing clear evidence that amino silsesquioxanes are accumulated in the nucleoli of HeLa cells, our data differ from the reported lack of nuclear uptake of octaammonium COSS in a Cos-1 cell assay.[35] This discrepancy might be caused by the distinct nature of the used cell lines. Indeed, Cos-1 is a monkey-derived immortalized fibroblast-like cell line,[50] whereas HeLa is a human-derived cervical cancer cell line.[51]

After having confirmed intracellular and nuclear accumulation of COSS, the p21-derived peptide was covalently attached to a single-corner cysteine-modified octaamino COSS through a reversible disulfide bond (Scheme 1). Being sensitive to reducing conditions inside living cells,[52] the disulfide bond is well known to dissociate after cell penetration thereby releasing the attached cargo molecule from the carrier.[52] An additional fluorescein moiety was introduced into this hybrid construct allowing for live-cell confocal[53] microscopy studies.

As cell penetration, toxicity and nuclear targeting depend on the size and shape of the applied SNPs, bimodal amplitude-modulated atomic force microscopy (AFM)[54–56] was used to further characterize particle **4**. Depending on the particle concentration in the initial solution, we observed two types of particle arrangements on a mica surface: globular particle assembly (Fig. 2a and 2b) and dendritic structures (Fig. 2c–2h). Fig. 2a shows an amplitude-modulated AFM topography image of solitary and assembled COSS particle **4**. The cross-section analysis (Fig. 2a and 2b) reveals three distinctive heights: ≈700 pm, 1400 pm and 2100 pm, suggesting a single particle size of 700 pm and multiples of it. At higher

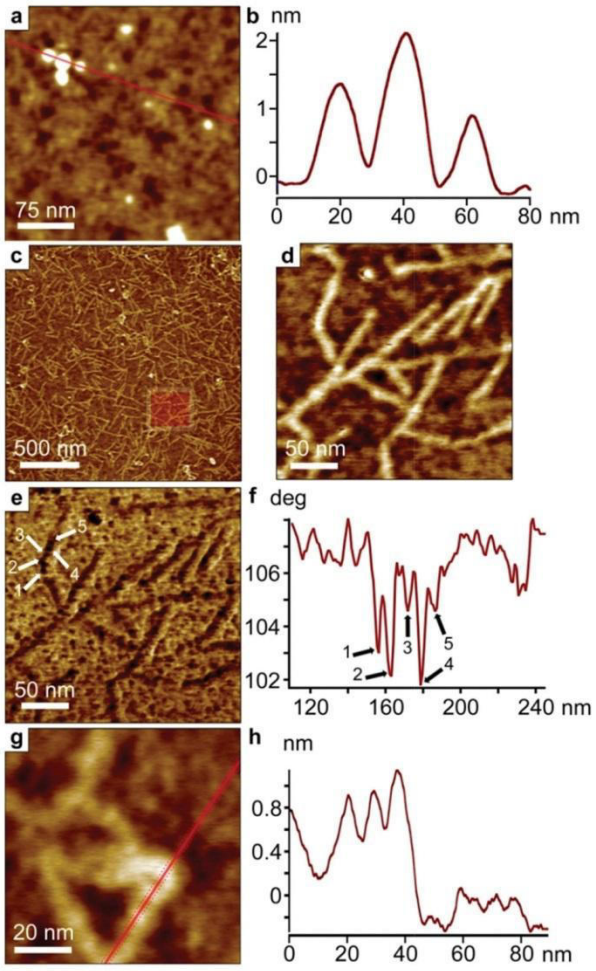

Fig. 2 (a) AFM topography image of singular and globular COSS–peptide particles **4**; (b) three particle profile from a section along the red line in (a); (c) and (d) AFM topography image of self-assembled SNP **4**; (e) second eigenmode phase image corresponding to (d). The image allows for the detection of single particles within the dendritic structure; (g) high-resolution frequency modulated AFM image of self-assembled **4**; (h) corresponding particle profile.

concentrations dendritic structures of **4** can be seen in the topographical image of Fig. 2c. Here, bimodal AFM was applied to enhance the lateral resolution of the phase images,

giving the height of the ordered structures as ≈700–800 pm (Fig. 2d). The corresponding second eigenmode phase image (Fig. 2e) clearly depicts the arrangement of single particles within one chain. Particles appear as dark dots (phase shift ≈102–104°), whereas the mica substrate shows a phase shift of ≈108°. In the profile (Fig. 2f) these particles are well separated. This leads to the conclusion that the dendritic structures are formed by a self-assembly of single SNPs **4** arranged next to each other. Frequency-modulated AFM topography images (Fig. 2g and 2h) corroborated these findings. Because this technique is extremely sensitive to topographical variations, even single particles were distinguished in the height profile. A similar self-assembly of silsesquioxane monomers may occur on a cell surface as well. However, the issue remains open whether the monomeric octaammonium COSS or self-assembled polymers are preferably involved in uptake and cell penetration. We suppose that the difference between heptalysine which lacks membrane permeability[57] and cell-penetrating octaaminosilsesquioxanes could be explained by the higher charge density within COSS and its shape-dependent self-assembly.[58–60] It might allow these cube-octameric SNPs to act as polycationic polymers (*e.g.* polylysine or polyethyleneimine) which are known to penetrate cell membranes.[61] It will be interesting to see, whether variation of the spatial arrangement and nature of the cationic groups have an influence on cellular uptake of COSS and on the uptake mechanism, which has to be elucidated yet.

It remained to be investigated, whether the COSS-bound cargo peptide displays biological activity which, in this experimental setting, is binding to PCNA. To address this question, co-localization experiments were performed involving fluorescein-labeled peptide **3** and PCNA, which was expressed as a fusion protein with red fluorescent protein (mRFP)[62] *via* transient transfection of HeLa cells with a mammalian expression plasmid coding for mRFP-tagged PCNA. PCNA is known to accumulate at sites of DNA damage that can be induced locally *via* UV microbeam irradiation (Fig. 3 and S18†).[63] To this end, a spot in a nucleus of a HeLa cell treated with a 20 μM solution of **4** was micro-irradiated for 1.2 seconds. Within 20 min RFP-labeled PCNA could be visualized at the site of DNA damage.[63] Co-localization of the fluorescent signal of **3** provided evidence of its accumulation at the DNA repair site (Fig. 3b and 3d). This clearly demonstrates that a significant portion of the cargo is able to freely address a target site in a HeLa cell nucleus.

Release of a peptide from a disulfide-bound cell-penetrating peptide carrier in the reducing milieu of a cell is a process that occurs relatively fast.[52,64] This is corroborated by our finding that the fluorescently labeled nanoparticle **5** is predominantly found in the nucleus while the COSS-bound labeled peptide **3** is also detected in the cytoplasm 30 min after incubation (Fig. S18†), which indicates a release from the carrier. Hence, it is most likely the liberated peptide **3** that interacts with PCNA rather than the COSS–peptide complex **4**.

For drug delivery, interactions of the carrier with a biological system that may eventually result in cell toxic effects are not desired, except those important for directed transit. Indeed, non-porous SNPs presenting primary amines at their surface have been reported to exhibit low toxicity[11,35] and degrade[65,66] under physiological conditions.[19,30] Here we corroborate these findings for amino-functionalized COSS with a cell viability assay based on the enzymatic reduction of the tetrazole XTT[67] using a single-corner cysteine-modified octaamino COSS. Within 12 hours, an SNP solution with a concentration of ~70 μM was needed to kill half of the cell population. Considering the reported lack of toxicity for non-functionalized octaaminopropyl COSS,[19,35] concentration-dependent reduced cell viability may be caused by the presence of the Fmoc-L-cysteine moiety attached to one of the cage corners rather than the COSS itself. Nevertheless, the concentration of SNP, which was used for the targeted delivery into the cell, is significantly lower than the concentration at which toxicity was observed (Fig. 4).

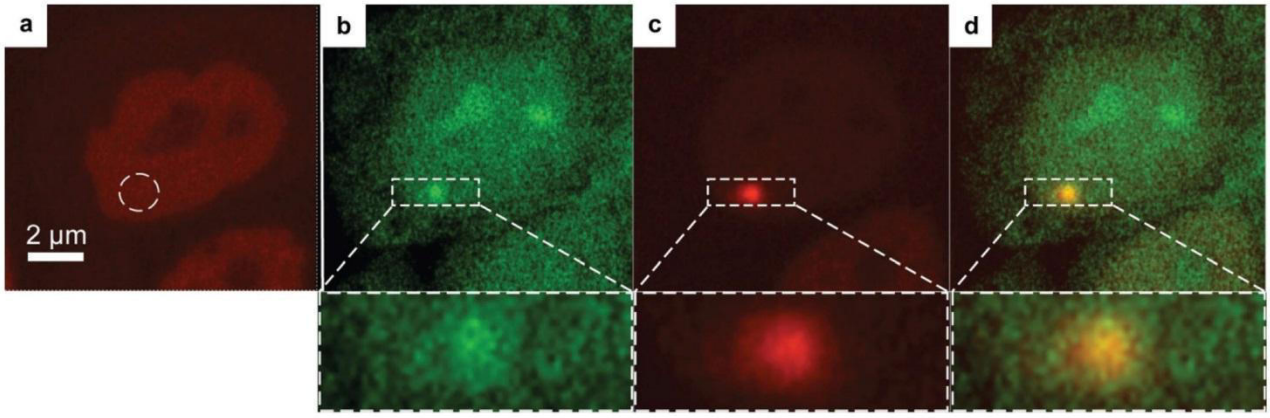

Fig. 3 (a) Micro-irradiation at the circle position (1.2 s) of a HeLa cell using a 405 nm laser; (b)–(d) co-localization of **3** and PCNA after cell incubation with **4** for 30 minutes at 37 °C. PCNA is recruited to repair micro-irradiated damaged DNA; (b) fluorescence signal of **3** (green); (c) fluorescence signal of red fluorescent protein labeled PCNA; (d) overlay of (b) and (c).

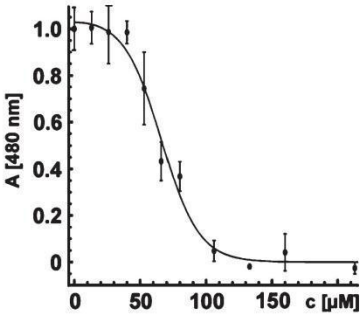

Fig. 4 The cell viability test using a single-corner cysteine-modified octaamino COSS. At a nanoparticle concentration of ~70 μM half of the observed cell population died, whereas a concentration of ~120 μM killed all cells within 12 hours.

Conclusion

In conclusion, a COSS derivative was synthesized which comprised a siloxane core with seven pendant aminopropyl groups and a peptidic ligand attached to one cage corner through a reversible disulfide bond. This architecture allowed for the penetration of human cells and peptide accumulation in the cell nucleus. Nuclear drug targeting was demonstrated in HeLa cells using a fluorescently labeled $p21^{Cip1/Waf1}$-derived peptide as a COSS cargo, which selectively bound PCNA, a protein involved in DNA replication and repair. In perspective, it might be interesting to study the octaamino COSS uptake mechanism in further detail by AFM and fluorescence microscopy studies on artificial lipid membranes[68,69] and cells. Finally, it remains to be elucidated whether silsesquioxane-based cargo delivery allows for the targeting of other proteins both in the nucleus and cytoplasm.

Experimental

HPLC analysis and purification

For RP-HPLC analysis a Varian 940-30 LC equipped with a Phenomenex Luna C_{18} column (5u, 100 A, 250 × 4.60 mm, 5 μm) was used at a flow rate of 1 mL min^{-1}. For isolation of products by RP-HPLC a C_{18} column (250 × 20 mm; S-4 μm, 8 nm) was employed at a flow rate of 18 mL min^{-1}. Eluent A: 0.1% aq. trifluoroacetic acid (TFA), eluent B: 90% aq. MeCN in 0.1% aq. TFA. 5 min of isocratic flow (starting concentration of eluent B) was followed by 20 min of gradient flow.

Compound 1

Synthesis of octaammonium COSS. According to a modified procedure reported by Feher and Wyndham,[70] 25 mL (23.7 g, 0.107 mol) 3-(triethoxysilyl)-1-propanamine were dissolved in 600 mL methanol. 34.0 mL concentrated hydrochloric acid (HCl) were added and the reaction mixture was stirred at room temperature. After 4 weeks, a white precipitate was formed. The suspension was stirred for additional two weeks. The precipitate was separated by filtration, washed 2 times with ice-cold acetone and dried in a desiccator. 3.08 g of white solid were obtained (23.0%).

^{1}H NMR [300.0 MHz, DMSO-d_6, room temp.] δ 8.25 (s, NH_3^+, 24 H), 2.79 (t, $CH_2NH_3^+$, 16 H), 1.74 (m, $SiCH_2CH_2$, 16 H), 0.74 (t, $SiCH_2$, 16 H). ^{13}C NMR [75.4 MHz, DMSO-d_6, room temp.] δ 40.95 (s, $CH_2NH_3^+$), 20.55 (s, $SiCH_2CH_2$), 8.37 (s, $SiCH_2$). ^{29}Si NMR [59.6 MHz, DMSO-d_6, room temp.] δ −66.41. ESI-MS calc. for **1** $C_{24}H_{64}N_8O_{12}Si_8$ *m/z*: 881.5, meas. 881.5 $[M + H]^+$; calc. 441.8, meas. 441.8 $[M + 2H]^{2+}$.

Compound 2

Synthesis of Fmoc-(S-trityl)-L-cysteine heptaammonium-COSS (2a). To a mixture of 10.5 mg (0.018 mmol, 2.1 equiv.) of Fmoc-(S-trityl)-L-cysteine and 8.9 μL dry DIEA (6.6 mg, 0.051 mmol, 6.0 equiv.) in 1 mL dry dimethylsulfoxide (DMSO), 8.9 mg (0.017 mmol, 2.0 equiv.) of (benzotriazol-1-yloxy)tripyrrolidinophosphonium hexafluorophosphate (PyBOP) in 1 mL dry DMSO were added dropwise. The mixture was incubated for 10 min at room temperature and afterwards diluted with dry DMSO to a volume of 12 mL.

10 mg (0.0085 mmol, 1.0 equiv.) of **1** were dissolved in 0.5 mL dry DMSO and vigorously stirred. The previously described mixture was added slowly using a peristaltic pump (flow: 0.05 mL min^{-1}). After complete addition, the mixture was stirred for 1 hour at room temperature. The solvent was removed by lyophilization. The resulting oil was suspended in 5 mL of 0.01 M HCl and again lyophilized. The white powder was suspended in dry acetonitrile and the insoluble part was washed two times with dry acetonitrile. The precipitate was dried *in vacuo* and purified by semipreparative RP-HPLC. After lyophilization, 3.0 mg of white solid were obtained (24.4%).

RP-HPLC, 10 → 80% B, t_R = 20.1 min. HR-MS calc. for **2a** $C_{24}H_{79}N_9O_{15}SSi_8$ *m/z*: 724.7406, meas. 724.7409 $[M + 2H]^{2+}$ (see Fig. S2 and S3†).

Deprotection of Fmoc-(S-trityl)-L-cysteine heptaammonium-COSS. 3.0 mg of Fmoc-(S-trityl)-L-cysteine heptaammonium-COSS were dissolved in 500 μL TFA and 5 μL (1 vol%) triethylsilane (TES) were added. The mixture was shaken for 30 min at room temperature and the solvent was removed *in vacuo*. The colorless residue was dissolved in deionized water and the solvent was removed by lyophilization. The product was used without further purification.

RP-HPLC 10 → 80% B, t_R = 16.7 min. ESI-MS calc. for **2** $C_{42}H_{79}N_9O_{15}SSi_8$ *m/z*: 1206.9, meas. 1206.6 ($[M + H]^+$); calc. 604.4, meas. 604.4 $[M + 2H]^{2+}$; calc. 403.3, meas. 403.3 $[M + 3H]^{3+}$ (see Fig. S4†).

Compound 3

Synthesis of fluorescein-labeled PCNA binding peptide. Microwave-assisted Fmoc-SPPS of PCNA binding peptide **3** was performed on 2-chlorotrityl resin (*Iris Biotech* GmbH) (0.25 mmol) using a CEM *Liberty*® peptide synthesizer equipped with a CEM *Discover*® SPS microwave (CEM GmbH). All amino acids were attached by triple coupling using 4.0 equiv. of the amino acid, 3.9 equiv. of *O*-(benzotriazol-1-yl)-*N*,*N*,*N*′,*N*′-tetramethyluroniumhexafluorophosphate (HBTU)

(*Iris Biotech* GmbH), and 8 equiv. of base (DIEA for all amino acids except cysteine; for coupling of Fmoc-(S-trityl)-L-cysteine, collidine (*Sigma-Aldrich*) was used) in *N*,*N*′-dimethylformamide (DMF). Triple coupling (30 W, 50 °C, 15 min) and double deprotection (30 W, 50 °C, 5 min) of the amino acids were performed upon microwave assistance. Fluorescein isothiocyanate (FITC) was coupled manually to the resin-bound peptide. 194.7 mg (0.50 mmol, 2 equiv.) FITC and 87.2 μL (64.7 mg, 4.0 equiv.) dry DIEA were dissolved in 5 mL dry DMF and the solution was added to the resin-bound peptide. The mixture was heated 3 times in a microwave (30 W, 50 °C, 30 min). Afterwards, the mixture was shaken at room temperature overnight. The peptide was cleaved from the resin and purified by semi-preparative RP-HPLC yielding 37.0 mg of a yellow solid after lyophilization (6.0%).

RP-HPLC, 30 → 40% B, t_R = 20.0 min. ESI-MS calc. for **3** $C_{116}H_{164}N_{26}O_{30}S_2$ *m*/*z*: 1234.4, meas. 1234.5 $[M + 2H]^{2+}$; calc. 823.3, meas. 823.3 $[M + 3H]^{3+}$; calc. 617.7, meas. 617.8 $[M + 4H]^{4+}$; calc. 494.4, meas. 494.5 $[M + 5H]^{5+}$ (see Fig. S6 and S7†).

Compound 4

Coupling of PCNA binding peptide to 2. 1.6 mg (0.0014 mmol, 1 equiv.) of **2** and 10.0 mg (0.0040 mmol, 3 equiv.) of compound **3** were dissolved in 200 μL dry DMSO. 10 μL 30 vol% aqueous hydrogen peroxide were mixed with 100 μL dry DMSO and quickly added to the mixture resulting in a 1 vol% solution of hydrogen peroxide. The probe was vigorously shaken for 5 min at room temperature. Immediately, 1 mL of deionized water was added and the probe was frozen in liquid nitrogen. The solvent was removed by lyophilization and the resulting solid was purified by RP-HPLC. After lyophilization, 1.4 mg of yellow solid was obtained (23.0%).

RP-HPLC, 27 → 40% B, t_R = 17.8 min. HR-MS calc. for **4** $C_{158}H_{241}N_{35}O_{45}S_3Si_8$ *m*/*z*: 734.7065, meas. 734.7077 $[M + 5H]^{5+}$. IR: 2912, 1629, 1530, 1104 cm^{-1} (see Fig. S9, S10, and S11†).

Compound 5

Synthesis of Cys-(S-trityl)-β-Ala-fluorescein (5a). Microwave-assisted Fmoc-SPPS of dipeptide Cys-(S-trityl)-β-alanine-fluorescein was performed at 0.10 mmol scale on 2-chlorotrityl resin (*Iris Biotech* GmbH). 58.6 mg (0.10 mmol, 1 equiv.) Fmoc-(S-trityl)-L-cysteine (*IRIS Biotech* GmbH) and 52.9 μL (48.5 mg, 0.40 mmol, 4 equiv.) collidine (*Sigma-Aldrich*) were dissolved in 3 mL dry DCM and the solution was added to the resin and shaken for 2 hours at room temperature. The Fmoc protecting group was removed by double deprotection using a CEM *Discover*® SPS microwave (CEM GmbH) (30 W, 50 °C, 5 min). Coupling of Fmoc-β-alanine (*IRIS Biotech* GmbH) was performed as a triple coupling using 4.0 equiv. Fmoc-β-alanine, 3.9 equiv. HBTU, and 8 equiv. DIEA in DMF in a microwave (30 W, 50 °C, 15 min). 78.0 mg (0.20 mmol, 2 equiv.) FITC and 69.5 μL (51.6 mg, 4.0 equiv.) dry DIEA were dissolved in 2 mL dry DMF and the solution was added to the resin-bound dipeptide. The mixture was heated 3 times (30 W, 50 °C, 30 min) in a microwave. Afterwards, the mixture was shaken at room temperature overnight. For cleavage of the peptide, 5.0 mL of a mixture of acetic acid, methanol, and DCM (5 : 1 : 4, v : v : v) were added. The mixture was shaken for 3 hours at room temperature. Afterwards the solution was added dropwise to 45.0 mL of ice-cold methyl *tert*-butyl ether (MTBE). The yellow precipitate was purified by semi-preparative RP-HPLC. Lyophilization gave 52.4 mg of a yellow solid (63.6%).

RP-HPLC, 10 → 100% B, t_R = 23.7 min. ESI-MS calculated for **5a** $C_{46}H_{37}N_3O_8S_2$ *m*/*z*: 823.9, meas. 824.4 $[M + H]^+$ (see Fig. S13 and S14†).

Synthesis of Cys-(S-trityl)-β-Ala-fluorescein heptaammonium-COSS (5b). 7.7 mg (0.0094 mmol, 1.1 equiv.) of the dipeptide Cys-(S-trityl)-β-alanine-fluorescein, 1.6 mg (0.0085 mmol, 1 equiv.) of 1-ethyl-3-(3-dimethylaminopropyl)-carbodiimide (DIC) and 6 μL (4.4 mg, 0.034 mmol, 4 equiv.) of dry DIEA were dissolved in 500 μL dry DMSO. The mixture was shaken for 10 min at room temperature and 10.0 mg (0.0085 mmol, 1 equiv.) of compound **1** dissolved in 500 μL dry DMSO were added. The mixture was shaken for 4 days in the dark and poured into 12 mL of dry acetonitrile. The yellow precipitate was washed two times with dry acetonitrile. It was purified by semi-preparative RP-HPLC. After lyophilization, 4.4 mg of yellow solid were obtained (27.8%).

RP-HPLC, 10 → 100% B, t_R = 16.0 min. ESI-MS calc. for **5b** $C_{70}H_{99}N_{11}O_{19}S_2Si_8$ *m*/*z*: 844.7, meas. 844.8 $[M + 2H]^{2+}$; calc. 563.5, meas. 563.5 $[M + 3H]^{3+}$; calc. 422.9, meas. 422.9 $[M + 4H]^{4+}$ (see Fig. S16†).

Deprotection of Cys-(S-trityl)-β-Ala-fluorescein heptaammonium-COSS. 4.4 mg of Cys-(S-trityl)-β-Ala-fluorescein heptaammonium-COSS were dissolved in 0.5 mL TFA and 5 μL (1 vol%) of triethylsilane (TES) (*Alfa Aesar*) were added. The mixture was shaken for 30 min at room temperature and the solvent was removed *in vacuo*. The yellow residue was purified by semi-preparative RP-HPLC. After lyophilization, 2.0 mg of yellow solid were obtained (53.0%).

RP-HPLC, 10 → 100% B, t_R = 14.0 min. ESI-MS calc. for **5** $C_{51}H_{85}N_{11}O_{19}S_2Si_8$ *m*/*z*: 723.6, meas. 723.5 $[M + 2H]^{2+}$; calc. 482.7, meas. 482.7 $[M + 3H]^{3+}$ (see Fig. S17†).

Atomic force microscopy. We conducted atomic force microscopy experiments on air using a Cypher AFM (*Asylum Research*, Santa Barbara, CA, USA) and PPP-ZEIHR cantilevers (*NanoandMore* GmbH, Wetzlar, Germany). Bimodal AFM was done with the first two eigenfrequencies at $f_1 \approx 130$ kHz and $f_2 \approx 820$ kHz. The free oscillation amplitudes were driven to $A_{01} \approx 10$ nm and $A_{02} \approx 1$ nm, respectively. A high amplitude setpoint ratio $A_{sp}/A_{01} \approx 0.9$ was chosen ensuring that the AFM is operated in the net attractive regime where mechanical repulsion is minimized and hence, the impact of the tip on the sample is small.

High-resolution frequency-modulated AFM measurements were accomplished using the same type of cantilever. For tracking the frequency, an external phase-locked-loop PLLPro2 (*RHK Technology*, Troy, MI, USA) was integrated into the feedback loop of the AFM. We kept the cantilever vibrating at a constant frequency shift of $\Delta f = 50$ Hz with respect to the free oscillation and the amplitude was maintained at $A_0 \approx 10$ nm. Images (512 × 512 pixel) were obtained with a scan speed of 500 nm s^{-1}.

Cell culture and fluorescein-labeled COSS cellular uptake. HeLa cells were seeded at 80% confluency into 24-well microscope observation chambers (*Ibidi*, Munich, Germany) and the growth medium (Dulbecco's modified Eagle medium; PAA) DMEM supplemented with 10% fetal calf serum (*Life Technologies*) and gentamycin was exchanged against the COSS solutions. COSS were diluted to 20 μM final concentration in 400 μL DMEM and incubated with the HeLa cells for 30 min at 37 °C prior to imaging.

Cell viability assay. HeLa cells were seeded at 70% confluency in 24-well plates and incubated for one hour at different COSS concentrations. The media were subsequently exchanged for DMEM without COSS and the cells were incubated for 12 hours. Then the media were exchanged with serum-free DMEM and 0.3 mg mL^{-1} of XTT (2,3-bis-(2-methoxy-4-nitro-5-sulfophenyl)-2*H*-tetrazolium-5-carboxanilide) and incubated for three hours. The XTT enzymatic reduction was measured by reading the absorbance at 490 nm, with a reference wavelength of 630 nm. This procedure was repeated four times for each concentration.

HeLa cells expressing RFP labeled PCNA. HeLa cells were plated on 24 well optical dishes (*Ibidi*, Munich, Germany) and transfected with a mammalian expression plasmid coding for mRFP-tagged PCNA[62] using polyethylenimine (PEI). Time lapse microscopy was performed on an UltraView spinning disc confocal microscopy system (*PerkinElmer*, UK) equipped with temperature, humidity and CO_2 incubation controller (*Olympus*) and a 63×/1.4 Plan-Fluor oil immersion lens (*Nikon*).

Microirradiation and confocal microscopy. COSS compound **4** was added at 20 μM concentration to the HeLa cells expressing RFP-labeled PCNA. After 30 min of incubation, a cell was first imaged and then irradiated at the micrometer spot within the nucleus for 1.2 s using a 405 nm laser. The same cell was imaged after 5 min using a laser excitation of 488 nm to detect the fluorescein-labeled peptide and 561 nm to detect the RFP labeled PCNA.

Acknowledgements

We thank Dr. Holm Frauendorf (Georg-August University, Göttingen) for the HR-MS measurements. We acknowledge the collaboration with Prof. Dr. Robert Stark (Center of Smart Interfaces, Technische Universität Darmstadt) with respect to AFM measurements in the frame of the LOEWE Soft Control consortium.

References

1 M. Mahmood, D. Casciano, Y. Xu and A. S. Biris, *J. Appl. Toxicol.*, 2011, **32**, 10–19.
2 K. Ariga, Q. M. Ji, M. J. McShane, Y. M. Lvov, A. Vinu and J. P. Hill, *Chem. Mater.*, 2012, **24**, 728–737.
3 M. R. Longmire, M. Ogawa, P. L. Choyke and H. Kobayashi, *Bioconjugate Chem.*, 2011, **22**, 993–1000.
4 J. Fang, H. Nakamura and H. Maeda, *Adv. Drug Delivery Rev.*, 2011, **63**, 136–151.
5 V. Torchilin, *Adv. Drug Delivery Rev.*, 2011, **63**, 131–135.
6 F. Danhier, O. Feron and V. Preat, *J. Controlled Release*, 2010, **148**, 135–146.
7 M. Das, C. Mohanty and S. K. Sahoo, *Expert Opin. Drug Delivery*, 2009, **6**, 285–304.
8 A. E. Nel, L. Madler, D. Velegol, T. Xia, E. M. Hoek, P. Somasundaran, F. Klaessig, V. Castranova and M. Thompson, *Nat. Mater.*, 2009, **8**, 543–557.
9 A. Verma and F. Stellacci, *Small*, 2010, **6**, 12–21.
10 D. Napierska, L. C. Thomassen, D. Lison, J. A. Martens and P. H. Hoet, *Part. Fibre Toxicol.*, 2010, **7**, 39.
11 T. Yu, K. Greish, L. D. McGill, A. Ray and H. Ghandehari, *ACS Nano*, 2012, **6**, 2289–2301.
12 J. E. Fuller, G. T. Zugates, L. S. Ferreira, H. S. Ow, N. N. Nguyen, U. B. Wiesner and R. S. Langer, *Biomaterials*, 2008, **29**, 1526–1532.
13 S. W. Bae, W. Tan and J. I. Hong, *Chem. Commun.*, 2012, **48**, 2270–2282.
14 V. Lebret, L. Raehm, J. O. Durand, M. Smaihi, C. Gerardin, N. Nerambourg, M. H. V. Werts and M. Blanchard-Desce, *Chem. Mater.*, 2008, **20**, 2174–2183.
15 M. Green and P. M. Loewenstein, *Cell*, 1988, **55**, 1179–1188.
16 S. Santra, H. Yang, D. Dutta, J. T. Stanley, P. H. Holloway, W. Tan, B. M. Moudgil and R. A. Mericle, *Chem. Commun.*, 2004, 2810–2811.
17 L. Pan, Q. He, J. Liu, Y. Chen, M. Ma, L. Zhang and J. Shi, *J. Am. Chem. Soc.*, 2012, **134**, 5722–5725.
18 S. Angelos, Y. W. Yang, K. Patel, J. F. Stoddart and J. I. Zink, *Angew. Chem., Int. Ed.*, 2008, **47**, 2222–2226.
19 B. Trastoy, D. A. Bonsor, M. E. Perez-Ojeda, M. L. Jimeno, A. Mendez-Ardoy, J. M. G. Fernandez, E. J. Sundberg and J. L. Chiara, *Adv. Funct. Mater.*, 2012, **22**, 3191–3201.
20 Y. W. Yang, *Med. Chem. Commun.*, 2011, **2**, 1033–1049.
21 D. B. Cordes, P. D. Lickiss and F. Rataboul, *Chem. Rev.*, 2010, **110**, 2081–2173.
22 S. Fabritz, S. Hörner, D. Könning, M. Empting, M. Reinwarth, C. Dietz, B. Glotzbach, H. Frauendorf, H. Kolmar and O. Avrutina, *Org. Biomol. Chem.*, 2012, **10**, 6287–6293.
23 S. Fabritz, D. Heyl, V. Bagutski, M. Empting, E. Rikowski, H. Frauendorf, I. Balog, W. D. Fessner, J. J. Schneider, O. Avrutina and H. Kolmar, *Org. Biomol. Chem.*, 2010, **8**, 2212–2218.
24 Y. C. Lin and S. W. Kuo, *Polym. Chem.*, 2012, **3**, 162–171.
25 B. Trastoy, M. E. Perez-Ojeda, R. Sastre and J. L. Chiara, *Chem.–Eur. J.*, 2010, **16**, 3833–3841.
26 M. Lo Conte, S. Staderini, A. Chambery, N. Berthet, P. Dumy, O. Renaudet, A. Marra and A. Dondoni, *Org. Biomol. Chem.*, 2012, **10**, 3269–3277.
27 U. Dittmar, B. J. Hendan, U. Florke and H. C. Marsmann, *J. Organomet. Chem.*, 1995, **489**, 185–194.
28 F. J. Feher, K. D. Wyndham, M. A. Scialdone and Y. Hamuro, *Chem. Commun.*, 1998, 1469–1470.

29 D. Heyl, E. Rikowski, R. C. Hoffmann, J. J. Schneider and W. D. Fessner, *Chem.–Eur. J.*, 2010, **16**, 5544–5548.
30 J. Henig, E. Toth, J. Engelmann, S. Gottschalk and H. A. Mayer, *Inorg. Chem.*, 2010, **49**, 6124–6138.
31 T. L. Kaneshiro, X. Wang and Z. R. Lu, *Mol. Pharmaceutics*, 2007, **4**, 759–768.
32 X. J. Loh, Z. X. Zhang, K. Y. Mya, Y. L. Wu, C. B. He and J. Li, *J. Mater. Chem.*, 2010, **20**, 10634–10642.
33 D. Ding, K. Y. Pu, K. Li and B. Liu, *Chem. Commun.*, 2011, **47**, 9837–9839.
34 F. Olivero, F. Reno, F. Carniato, M. Rizzi, M. Cannas and L. Marchese, *Dalton Trans.*, 2012, **41**, 7467–7473.
35 C. McCusker, J. B. Carroll and V. M. Rotello, *Chem. Commun.*, 2005, 996–998.
36 Y. Gluzman, *Cell*, 1981, **23**, 175–182.
37 W. F. Scherer, J. T. Syverton and G. O. Gey, *J. Exp. Med.*, 1953, **97**, 695–710.
38 D. I. Zheleva, N. Z. Zhelev, P. M. Fischer, S. V. Duff, E. Warbrick, D. G. Blake and D. P. Lane, *Biochemistry*, 2000, **39**, 7388–7397.
39 T. Paunesku, S. Mittal, M. Protic, J. Oryhon, S. V. Korolev, A. Joachimiak and G. E. Woloschak, *Int. J. Radiat. Biol.*, 2001, **77**, 1007–1021.
40 S. M. Görisch and M. C. Cardoso, in *Proliferating Cell Nuclear Antigen*, ed. H. Lee and M. Szyf, Research SignPost, 2006, pp. 51–70.
41 L. H. Malkas, B. S. Herbert, W. Abdel-Aziz, L. E. Dobrolecki, Y. Liu, B. Agarwal, D. Hoelz, S. Badve, L. Schnaper, R. J. Arnold, Y. Mechref, M. V. Novotny, P. Loehrer, R. J. Goulet and R. J. Hickey, *Proc. Natl. Acad. Sci. U. S. A.*, 2006, **103**, 19472–19477.
42 J. Cmielova and M. Rezacova, *J. Cell. Biochem.*, 2011, **112**, 3502–3506.
43 J. M. Gulbis, Z. Kelman, J. Hurwitz, M. O'Donnell and J. Kuriyan, *Cell*, 1996, **87**, 297–306.
44 D. Yaffe and O. Saxel, *Nature*, 1977, **270**, 725–727.
45 G. Tunnemann, R. M. Martin, S. Haupt, C. Patsch, F. Edenhofer and M. C. Cardoso, *FASEB J.*, 2006, **20**, 1775–1784.
46 E. Oh, J. B. Delehanty, K. E. Sapsford, K. Susumu, R. Goswami, J. B. Blanco-Canosa, P. E. Dawson, J. Granek, M. Shoff, Q. Zhang, P. L. Goering, A. Huston and I. L. Medintz, *ACS Nano*, 2011, **5**, 6434–6448.
47 W. Yang, J. Gelles and S. M. Musser, *Proc. Natl. Acad. Sci. U. S. A.*, 2004, **101**, 12887–12892.
48 J. E. Hinshaw, B. O. Carragher and R. A. Milligan, *Cell*, 1992, **69**, 1133–1141.
49 J. M. de la Fuente and C. C. Berry, *Bioconjugate Chem.*, 2005, **16**, 1176–1180.
50 F. C. Jensen, H. Koprowski, A. J. Girardi and R. V. Gilden, *Proc. Natl. Acad. Sci. U. S. A.*, 1964, **52**, 53–59.
51 W. F. Scherer, J. T. Syverton and G. O. Gey, *J. Exp. Med.*, 1953, **97**, 695–710.
52 G. Saito, J. A. Swanson and K. D. Lee, *Adv. Drug Delivery Rev.*, 2003, **55**, 199–215.
53 *Handbook of Biological Confocal Microscopy*, Springer Science + Business Media, LLC, James B. Pawley, 3rd edn, 2006.
54 T. R. Rodriguez and R. Garcia, *Appl. Phys. Lett.*, 2004, **84**, 449–451.
55 C. Dietz, E. T. Herruzo, J. R. Lozano and R. Garcia, *Nanotechnology*, 2011, **22**, 125708.
56 R. Garcia and E. T. Herruzo, *Nat. Nanotechnol.*, 2012, **7**, 217–226.
57 G. Tunnemann, G. Ter-Avetisyan, R. M. Martin, M. Stockl, A. Herrmann and M. C. Cardoso, *J. Pept. Sci.*, 2008, **14**, 469–476.
58 W. A. Zhang, J. Y. Yuan, S. Weiss, X. D. Ye, C. L. Li and A. H. E. Muller, *Macromolecules*, 2011, **44**, 6891–6898.
59 X. Zhang, E. R. Chan and S. C. Glotzer, *J. Chem. Phys.*, 2005, **123**, 184718.
60 Y. C. Lin and S. W. Kuo, *J. Polym. Sci., Part A: Polym. Chem.*, 2011, **49**, 2127–2137.
61 H. J. Ryser, *Nature*, 1967, **215**, 934–936.
62 A. Sporbert, P. Domaing, H. Leonhardt and M. C. Cardoso, *Nucleic Acids Res.*, 2005, **33**, 3521–3528.
63 P. Perucca, O. Cazzalini, O. Mortusewicz, D. Necchi, M. Savio, T. Nardo, L. A. Stivala, H. Leonhardt, M. C. Cardoso and E. Prosperi, *J. Cell Sci.*, 2006, **119**, 1517–1527.
64 M. Hallbrink, A. Floren, A. Elmquist, M. Pooga, T. Bartfai and U. Langel, *Biochim. Biophys. Acta Biomembranes*, 2001, **1515**, 101–109.
65 E. Rikowski and H. C. Marsmann, *Polyhedron*, 1997, **16**, 3357–3361.
66 F. J. Feher, K. D. Wyndham, D. Soulivong and F. Nguyen, *J. Chem. Soc., Dalton Trans.*, 1999, 1491–1497.
67 D. A. Scudiero, R. H. Shoemaker, K. D. Paull, A. Monks, S. Tierney, T. H. Nofziger, M. J. Currens, D. Seniff and M. R. Boyd, *Cancer Res.*, 1988, **48**, 4827–4833.
68 P. R. Leroueil, S. Hong, A. Mecke, J. R. Baker Jr., B. G. Orr and M. M. Banaszak Holl, *Acc. Chem. Res.*, 2007, **40**, 335–342.
69 P. R. Leroueil, S. A. Berry, K. Duthie, G. Han, V. M. Rotello, D. Q. McNerny, J. R. Baker Jr., B. G. Orr and M. M. Holl, *Nano Lett.*, 2008, **8**, 420–424.
70 F. J. Feher and K. D. Wyndham, *Chem. Commun.*, 1998, 323–324.

8.4. Nanoscale biodegradable organic-inorganic hybrids for efficient cell penetration and drug delivery

Title:

Nanoscale biodegradable organic-inorganic hybrids for efficient cell penetration and drug delivery

Authors:

Sebastian Hörner,[‡] Sascha Knauer,[‡] Christina Uth,[‡] Marina Jöst, Volker Schmidts, Holm Frauendorf, Christina M. Thiele, Olga Avrutina und Harald Kolmar.

Bibliographic Data:

Angewandte Chemie International Edition
Volume 55, Issue 47, November 1, 2016, Pages: 14842–14846, DOI: 10.1002/anie.201606065.
For the first time published in the internet on October 24th 2016

Graphical abstract:

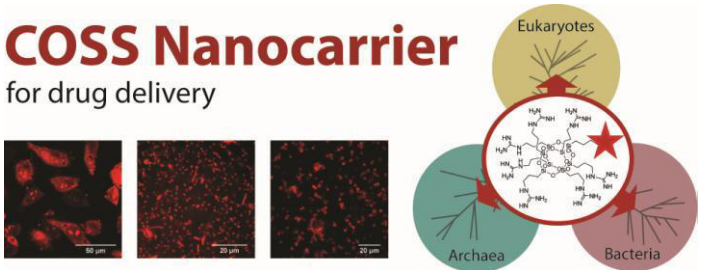

Summary:

Novel cell-penetrating COSS derivatives were synthesized and cellular uptake was compared to cell-penetrating peptides in three different mammalian cell lines. COSS with guanidinium groups (GuCOSS) efficiently translocates cellular membranes of mammalien cells, yeast, archeae, and bacteria. By using this biodegradable delivery module, the efficacy of cytotoxic drug Doxorubicin was significantly improved in an *in vitro* experiment.

Contributions by Dipl.-Ing. Sebastian Hörner:

- Conception of the manuscript
- Design and accomplishment of chemical synthesis and interpretation of corresponding physicochemical analysis of compounds **2**, **4**, **8**, **9**, **12**, **13**, **18**, **22**, **23**, **27**, and **28**
- Design, accomplishment (50%), analysis and interpretation of flow-cytometrc experiments
- Design, accomplishment, analysis, and interpretation of confocal microscopy and fluorescence microscopy studies
- Design, accomplishment, analysis, and interpretation of degradation studies
- Writing of the manuscript
- Writing of the experimental section of the manuscript

‡ shared lead author

Nanoscale Biodegradable Organic–Inorganic Hybrids for Efficient Cell Penetration and Drug Delivery

*Sebastian Hörner[+], Sascha Knauer[+], Christina Uth[+], Marina Jöst, Volker Schmidts, Holm Frauendorf, Christina Marie Thiele, Olga Avrutina, and Harald Kolmar**

Abstract: *We report a comprehensive study on novel, highly efficient, and biodegradable hybrid molecular transporters. To this end, we designed a series of cell-penetrating, cube-octameric silsesquioxanes (COSS), and investigated cellular uptake by confocal microscopy and flow cytometry. A COSS with dense spatial arrangement of guanidinium groups displayed fast uptake kinetics and cell permeation at nanomolar concentrations in living HeLa cells. Efficient uptake was also observed in bacteria, yeasts, and archaea. The COSS-based carrier was significantly more potent than cell-penetrating peptides (CPPs) and displayed low toxicity. It efficiently delivered a covalently attached cytotoxic drug, doxorubicin, to living tumor cells. As the uptake of fluorescently labeled carrier remained in the presence of serum, the system could be considered particularly attractive for the in vivo delivery of therapeutics.*

Since Linus Pauling's groundbreaking publication in *Science*[1] in 1949, achievements in the rapidly advancing field of molecular medicine and related areas are very impressive. However, while today a vast arsenal of potent and selective drugs is available, an efficient strategy to deliver these therapeutic compounds inside the cell, in particular, in the cell nucleus, has become as important as the design and optimization of the pharmacophore itself. Considering that promising newly developed potential drug candidates, such as peptides and proteins, are water-soluble, a bottleneck in their application in living systems is the passage across the cellular membrane. As a consequence, drug delivery has emerged as one of the major fields in biomedical research. In 1994, the first cell-penetrating peptide (CPP) penetratin was described as a vehicle for cargo delivery into cells.[2] Since then, CPPs were thoroughly investigated and improved.[3] However, several issues associated with toxicity, stability, and efficacy of cellular uptake still require work. As the peptidic structure of CPPs intrinsically limits the scope of improvements, recent efforts are focused on nanoparticles or small non-peptidic molecular scaffolds.[4] These simple, uniform molecular architectures can be easily tailored, leading to cell-penetrating molecules with entirely new properties. In contrast to the macromolecular delivery systems, such as (bio)polymers, dendrimers, lipid-based or viral-like carriers, some of which are actually on the market or under clinical trials,[4c] the next-generation molecular transporters still require optimization.

General strategies towards the improvement of cellular uptake include the reduction of conformational freedom by backbone cyclization of cell-penetrating peptides or by the usage of scaffolds which induce spatial organization of the uptake-mediating functional groups.[3a,4d,5] Interestingly, the proximity of the charged groups to the backbone was found to influence the efficiency of cell uptake as well.[3c,d,5c,6]

Herein, we chose the cube-octameric silsesquioxane scaffold (COSS) as the starting point for the development of new-generation cell-penetrating compounds. COSS are highly ordered organic–inorganic hybrid molecules with a cage-like core of alternating silicon and oxygen atoms surrounded by eight pendant organic residues. Such an architecture with charged groups located at the flanking arms tethered to a compact (0.7 nm)[7] core ensures a compact, rigid, and symmetric construct. Generally, COSS are used in certain medical fields, for example, tissue engineering, or for the oligomerization of bioactive ligands, among them peptides and carbohydrates.[7,8] They are considered non-toxic and the hydrolytic degradation of the inorganic core under physiological conditions has been thoroughly investigated.[7]

COSS bearing seven ammonium groups were found to penetrate cells.[7,9] We have previously shown that these molecules enable the delivery of a functional peptidic cargo into living HeLa cells.[10] To improve this drug delivery system, we synthesized a series of COSS-based molecular transporters and investigated the uptake efficacy of a covalently attached cytotoxic drug.

Compounds **2**–**7** were synthesized following a two-step procedure (Scheme 1). Thus, inexpensive octaammonium COSS hydrochloride **1** was functionalized with a) guanidinium groups positively charged under physiological conditions or b) permanent positive charges installed by quaternary amines. Additionally, we investigated the influence of the flanking arm's length on cellular uptake. To visualize the constructs in cell assays, tetramethylrhodamine (TAMRA) was attached to a single corner of COSS **1** in a stoichiometri-

[*] S. Hörner,[+] S. Knauer,[+] C. Uth,[+] M. Jöst, Dr. O. Avrutina, Prof. Dr. H. Kolmar
Clemens-Schöpf-Institut für Organische Chemie und Biochemie
Technische Universität Darmstadt
Alarich-Weiss-Strasse 4, 64287 Darmstadt (Germany)
E-mail: kolmar@biochemie-tud.de
Dr. V. Schmidts, Prof. Dr. C. M. Thiele
Clemens-Schöpf-Institut für Organische Chemie und Biochemie
Technische Universität Darmstadt
Alarich-Weiss-Strasse 16, 64287 Darmstadt (Germany)
Dr. H. Frauendorf
Institut für Organische und Biomolekulare Chemie
Georg-August Universität Göttingen
Tammannstrasse 2, 37077 Göttingen (Germany)
[+] These authors contributed equally to this work.

Supporting information for this article can be found under: http://dx.doi.org/10.1002/anie.201606065.

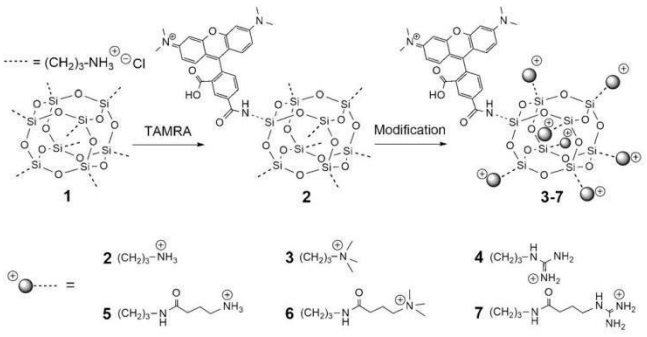

Scheme 1. Synthesis of fluorescently labeled cell-penetrating COSS derivatives **2**–**7** equipped with cationic functional groups separated from the core by spacers of different lengths. Counterions are excluded for clarity. Sequences of CPPs are shown in Supporting Information 5.2.

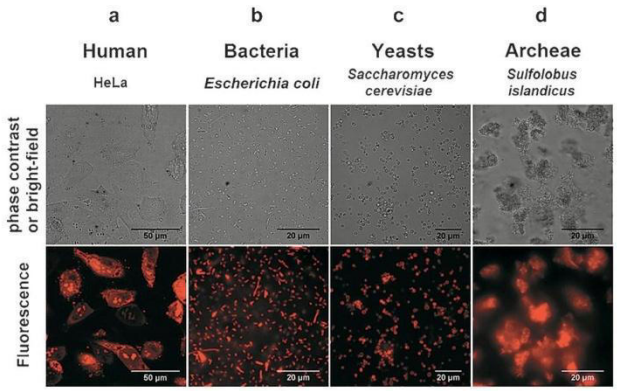

Figure 1. Cell uptake of TAMRA-GuCOSS (**4**). a) Live-cell laser scanning confocal microscopy imaging of HeLa cells incubated with **4** at 37 °C; b)–d) fluorescence microscopy imaging of cells incubated with **4**; b) Gram-negative bacterium (*E. coli*); c) yeast (*Saccharomyces cerevisiae*), both incubated at 37 °C; d) archaeon (*Sulfolobus islandicus*) incubated at 80 °C.

cally controlled reaction leading to TAMRA-aminoCOSS (**2**). Subsequently, the remaining seven amine functionalities of **2** were converted into the corresponding quaternary amines by N-methylation (TAMRA-quartCOSS **3**) or guanidinylation (TAMRA-GuCOSS **4**). Alternatively, for the introduction of a linker separating the siloxane core and the charged elements, 4-aminobutyric, 4-trimethylaminobutyric, or 4-guanidinobutyric acids were installed via amide coupling leading to, respectively, TAMRA-aminoCOSS-L (**5**), TAMRA-quartCOSS-L (**6**), and TAMRA-GuCOSS-L (**7**) (Scheme 1). To investigate toxicity of molecular transporters we synthesized amino-GuCOSS (**8**) lacking a fluorescent label (Supporting Information 5.2). Fluorescein-TAMRA-GuCOSS (**9**) was designed to assess biodegradation of the carriers (Figure 3a). The integrity of the cage-like siloxane core was confirmed by NMR spectroscopy (compounds **2**–**7**; Supporting Information 5.3).

Fluorescently labeled derivatives **2**–**7** were investigated for their ability to penetrate living cells. To qualitatively estimate the uptake, we performed live-cell imaging using confocal laser scanning microscopy. Thus, HeLa cells were incubated with compounds **2**–**7** at a concentration of 20 μM in serum-free Dulbecco's modified eagle medium (DMEM) for 30 min. The cells were washed three times with phosphate buffered saline (PBS) and imaged in DMEM with fetal bovine serum (FBS). Compounds **2**–**4** bearing shorter linkers (Figure 1a, Figure S1) demonstrated enhanced cellular uptake and prominent accumulation inside the nucleus, the nucleoli, and the cytoplasm, whereas an increase of the spacer's length led to reduced cellular uptake and primarily cytoplasmic localization (compounds **5**–**7**, Figure S1). In view of predominant accumulation in the nucleus, molecular transporters **2**–**4** are particularly attractive for the delivery of drugs addressing this cellular compartment.

As the guanidinylated carrier TAMRA-GuCOSS (**4**) exhibited the highest uptake in HeLa cells, its ability to penetrate cells from all three domains of life was further studied. The microscopic images obtained suggest that it is able to enter both eukaryotic and prokaryotic cells, among them yeast (*S. cerevisiae*) and mammalian cells (HeLa), as well as bacteria (*E. coli*) and archaea (*S. islandicus*, *S. tokodaii*, *Halobacterium salinarum*) (Figure 1b–d, Figure S2). These observations are of particular interest in view of the exceptional membrane composition of archaea.[11] As guanidinylated COSS could be of interest for the delivery of antibiotics, we investigated its uptake in *E. coli* in detail (Figure S2c).

To quantify the cellular uptake in eukaryotic cells, we performed comprehensive flow-cytometric experiments with COSS derivatives **2**–**7** and TAMRA-labeled cell-penetrating peptides: TAT (**10**), penetratin (**11**), heptaarginine (**12**), and decaarginine (**13**).[12] We incubated HeLa cells with these compounds at a final concentration of 20 μM in serum-free DMEM at 37 °C up to 60 min. To remove surface-bound carrier molecules, cells were trypsinized (Supporting Information 5.1). Assays were performed in triplicate, the results were verified in three independent experiments (Figure S3a–g) with carrier **4** having shown the best cellular uptake. Indeed, the intensity of the fluorescence signal was found 155 times higher than that for the TAT peptide **10**. Interestingly, compound **4** carrying seven guanidinium groups displayed a 78-fold higher cellular uptake than heptaarginine (**12**; Figure 2a). In agreement with our microscopy studies, shorter linkers correlated with enhanced fluorescence intensity (Figure S4). Similar results were obtained for HEK 293 and CHO cells (Figure S5a–c). This higher uptake of **4** can be attributed to its more compact arrangement, hence increased density of uptake-mediating functional groups. Indeed, cyclization of CPPs, leading to more constrained and rigid structures, is an efficient strategy to improve cellular uptake.[5c]

To evaluate whether the cellular uptake is energy-dependent, we compared the fluorescence intensity of HeLa cells incubated with **4** at 37 °C and at 4 °C (Figure 2d). As the uptake was only negligibly decreased at 4 °C, an energy-independent mechanism was assumed. Time-resolved flow cytometry indicated fast uptake kinetics with a first shift of the population within an incubation time of 1 min at 37 °C (Figure S6). To determine the minimal internalization threshold, cells were incubated with **4** at different concentrations. Even at the lowest concentration (80 nM) a shift in fluores-

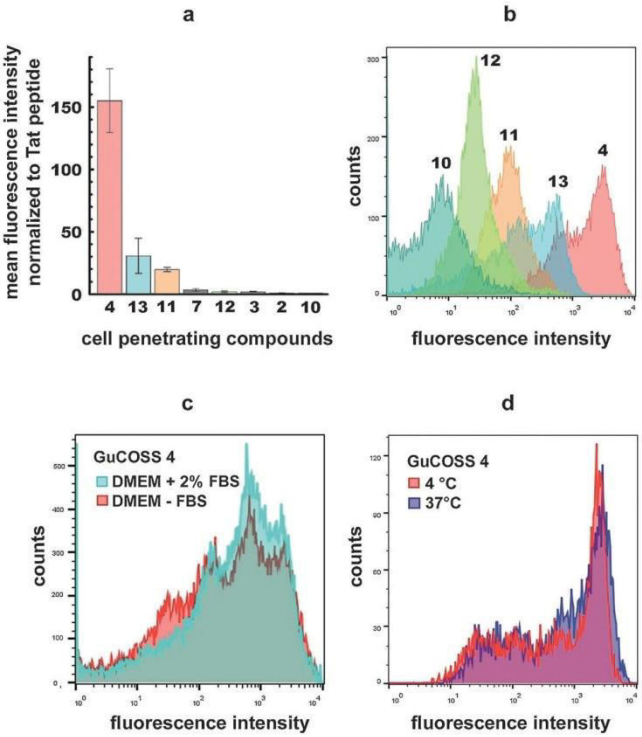

Figure 2. Flow-cytometric experiments using HeLa cells. a) mean fluorescence intensity of selected COSS derivatives and cell-penetrating peptides. b) representative histogram of TAMRA-GuCOSS (**4**) and cell-penetrating peptides (petrol-green: TAT (**10**); yellow-green: heptaarginine (**12**); orange: penetratin (**11**), light blue: decaarginine (**13**); red: TAMRA-GuCOSS (**4**). c) HeLa cells incubated with **4** in the presence and the absence of 2% FBS in DMEM. d) Cellular uptake of **4** in HeLa cells incubated in serum-free DMEM for 10 min with 20 μM **4** at 37 °C or 4 °C.

cence intensity was observed and 1 μM **4** was needed to reach full shift of the population after an incubation time of 10 min at 37 °C (Figure S7). In contrast to cell-penetrating peptides, no minimal internalization threshold within the investigated concentrations was observed.[13] As recent studies suggest that both the silsesquioxane core and guanidine groups promote clustering,[7,14] it could be supposed that high local concentration of **4** (as a result of its assembly on the cell surface) ensures cell penetration even at low concentrations. Our observations point to an energy-independent direct cell translocation, in accordance with the uptake mechanism of other polyguanidines.[13]

The uptake of cell-penetrating peptides is generally retarded in serum-containing media.[15] Impaired CPP-mediated permeation efficacy has been reported for polyarginines both in serum-containing media and in in vivo experiments, presumably owing to their aggregation with serum proteins. Therefore, we imaged **4** in the presence of 10% FBS in DMEM (Figure S8) and found that 40% of the mean fluorescence intensity was retained, compared to that for serum-free media.[3c,15a,16] This tolerance of serum proteins, combined with fast and effective cellular uptake, makes **4** a promising carrier for in vivo applications.

Since many cell-penetrating compounds were found to be toxic above a certain concentration, we investigated the toxicity of amino-GuCOSS (**8**) lacking a fluorescent label (Supporting Information 5.2) in HeLa cells using an XTT cell viability assay. Thereby the LC_{50} was determined to be 84 μM (Figure 3e), which is comparable to that of polyarginines (76 μM), TAT (86.6% viability at 50 μM), and penetratin (88.2% at 50 μM).[17] This low toxicity may be caused by biodegradation of the inorganic core under physiological conditions. Indeed, the pH-dependent degradation of polyhedral silsesquioxanes resulting in primary siloxanes is well established.[7]

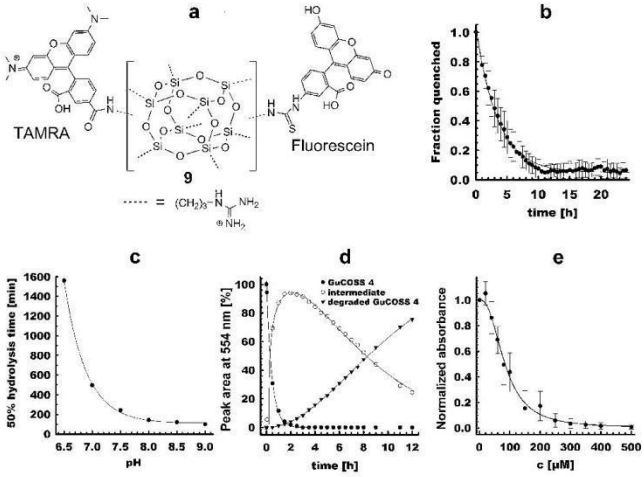

Figure 3. GuCOSS degradation studies. a) Guanidinylated COSS construct bearing the two fluorophores, fluorescein and TAMRA (Fluorescein-TAMRA-GuCOSS (**9**)). b) Decrease of the quenched fraction of fluorescein in the in vitro degradation studies in living HeLa cells. c) 50% hydrolysis of TAMRA-GuCOSS (**4**) as a function of the pH in PBS. d) Kinetics of the degradation of **4** at pH 7.0 in PBS analyzed by HPLC. e) XTT assay of the in vitro toxicity of guanidinylated COSS (**8**) bearing no fluorescent label.

For characterization of pH-dependent degradation of **4**, we monitored decomposition of the inorganic core by RP-HPLC. To that end, **4** was incubated in PBS at pH 6.5–9.0 (37 °C) and time-resolved HPLC traces were recorded within 12 h at 554 nm (absorption maximum of TAMRA). Hydrolysis intermediates and the degradation products were quantified by determination of the peak areas. Although hydroxyl-bearing intermediates were eluted earlier from the column, the completely hydrolyzed TAMRA-decorated siloxanes had longer retention times. Typical HPLC traces at pH 7.0 are shown at Figure S9, and respective half-life values at pH 6.5–9.0 in Figure 3c. Thereby, the $t_{1/2}$ at pH 7.4 (PBS) was determined to be 252 min. The degradation at neutral pH is shown in Figure 3d.

To assess the biodegradation of the GuCOSS-based carriers, we synthesized derivative **9** carrying two fluorescent markers, fluorescein and TAMRA (Figure 3a). As both dyes are attached to the same siloxane core in spatial proximity, the fluorescence of fluorescein is quenched upon Förster resonance energy transfer (FRET; Figure S10). As the inorganic core loses its integrity during breakdown, either fluorescein or TAMRA separates from the siloxane cage, and the fluorescence of fluorescein is restored. Along with excitation at

488 nm the increase of the emission at 520 nm was used to quantify the fraction of partially disassembled carriers. Based on the fluorescence recovery of fluorescein, a half-life of 186 min was found in human serum, indicating sufficient stability for in vivo applications (Figure S11). As HPLC analysis allowed the erosion process to be monitored up to the final degradation products, the half-life determined using this approach was significantly longer (252 min at pH 7.4). In former studies, the half-life of cell-penetrating peptides in the presence of serum was found to be in the range of minutes (e.g. $t_{1/2} = 5$ min for penetratin).[18] This fast decay is most likely caused by proteolysis. It is clear that the hybrid GuCOSS construct does not serve as a substrate for proteolytic enzymes. The enhanced half-life of derivative **9** in serum is an additional indication that the degradation of the COSS core is predominantly pH dependent.

To better understand how the degradation proceeds in living cells, we monitored the recovery of fluorescein fluorescence by live-cell confocal laser scanning microscopy upon internalization of construct **9** in HeLa cells (Figure 3b, Figure S12). The fluorescent markers were disconnected in half of the starting material within 149 min, and complete disassembly (reappearance of fluorescence) occurred in 11 h. The half-lives obtained in these experiments are on the same order of magnitude as those observed upon incubation in human serum ($t_{1/2} = 186$ min).

Applicability of GuCOSS as a molecular transporter was examined upon cellular delivery of a cytotoxic cargo doxorubicin (DOX, **14**)—a widely applied antitumor drug.[19] Being able to intercalate DNA, this agent induces apoptosis in cancer cells by activating the intrinsic death pathway.[20] Therefore, it is clear that the therapeutic effect of DOX could be exerted only if the drug gains access to the cell nucleus. However, because only passive diffusion ensures its penetration into tumor tissues, the efficiency of DOX is strongly compromised, which represents the major limitation of this highly potent compound.[21] In a model construct, we connected the GuCOSS delivery module to a DOX functional cargo via a disulfide yielding the conjugate **15** (Supporting Information 5.2). This bond is rapidly reduced in the reductive environment of cytosol, enabling drug release inside the cell.[22]

Cellular delivery was studied in HeLa cells. First, an incubation time-dependent cell assay with the free antibiotic was performed (Supporting Information 4.0, 5.1). Because of the slow uptake of free doxorubicin, the number of cancer cells killed correlated with the duration of incubation (Figure S13). The conjugate **15** as well as the controls (free doxorubicin (**14**) and untreated cells) were incubated at the same concentrations for 1 h (Supporting Information 3.0). Then the cells were washed with DMEM, and after 18 h an MTT assay was performed (Figure 4). The results clearly show that the hybrid construct **15** had an enhanced cytotoxic effect compared to the free drug **14**.

Although it is one of the cornerstones of cancer therapy, free doxorubicin causes irreversible cardiac damage.[23] Whereas its liposomal formulation[24] mitigates the toxic side effects,[23] the potency is unaltered compared to the conventional drug.[25] While the recently reported formulation

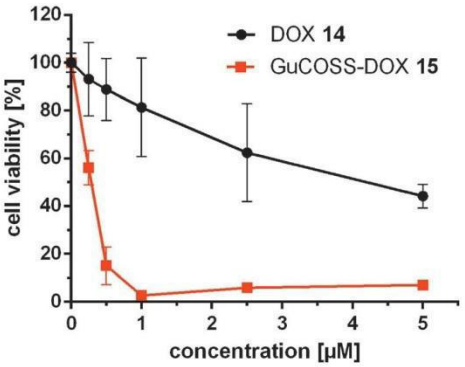

Figure 4. Cell viability assay (MTT) of free doxorubicin (DOX, **14**) and the doxorubicin-GuCOSS conjugate (**15**). Error bars indicate standard deviations from three independent measurements.

based on liposomal coencapsulation of DOX with Listeriolysin O enables enhancement of nuclear targeting in certain carcinoma cell lines, it is supposed to be highly immunogenic.[26] Therefore, we believe that our delivery platform combining highly efficient cell penetration with small size, low toxicity, and biodegradability might provide clear benefits. Nevertheless, further validation by animal studies is required, which particularly addresses cardiotoxic effects in comparison to liposomal doxorubicin formulations. It may also be interesting to investigate whether the cellular uptake of other cytotoxins with particularly low cell-penetrating efficacy, such as for example, hygromycin,[27] can be enhanced upon COSS conjugation.

To summarize, we developed new-generation hybrid cell-penetrating compounds based on the cube-octameric silsesquioxane scaffold. Thus, the guanidinylated fluorescent COSS derivative was found to efficiently penetrate cells from all three domains of life with a 155-fold enhanced, compared to the cell-penetrating peptide TAT, cellular uptake in HeLa cells. The carrier has fast uptake kinetics and penetrates cells at double-digit nanomolar concentrations. It has low toxicity and decomposes under physiological conditions within 11 h. This novel molecular transporter retains its activity in the presence of serum, which makes it a promising candidate for in vivo delivery of drugs. Taking into consideration that these organic–inorganic hybrids are very small and compact, no or weak immune response could be assumed. We believe that our delivery platform may enrich the toolbox of low-toxic and highly efficient molecular systems needed for the development of future-oriented therapeutics.

Acknowledgements

We thank Dr. Anna-Lena Krause (Nationales Centrum für Tumorerkrankungen, DKFZ, Heidelberg, Germany) for assistance during flow cytometry interpretation, Thomas Pirzer for providing HeLa cells, and PD Dr. Arnulf Kletzin (Fachbereich Biologie, Technische Universität Darmstadt) for providing *sulfobacter* and *archaea*.

Keywords: cell penetration · cell-penetrating compound · COSS · drug delivery · silsesquioxanes

[1] L. Pauling, H. A. Itano, S. J. Singer, I. C. Wells, *Science* **1949**, *110*, 543 – 548.
[2] D. Derossi, M. H. Joliot, G. Chassaing, M. Prochiantz, *J. Biol. Chem.* **1994**, *269*, 10444 – 10450.
[3] a) A. Ho, S. R. Schwarze, S. J. Mermelstein, G. Waksman, S. F. Dowdy, *Cancer Res.* **2001**, *61*, 474 – 477; b) A. Nasrolahi Shirazi, R. Tiwari, B. S. Chhikara, D. Mandal, K. Parang, *Mol. Pharm.* **2013**, *10*, 488 – 499; c) P. A. Wender, D. J. Mitchell, K. Pattabiraman, E. T. Pelkey, L. Steinman, J. B. Rothbard, *Proc. Natl. Acad. Sci. USA* **2000**, *97*, 13003 – 13008; d) P. A. Wender, J. B. Rothbard, T. C. Jessop, E. L. Kreider, B. L. Wylie, *J. Am. Chem. Soc.* **2002**, *124*, 13382 – 13383.
[4] a) V. Bagnacani, V. Franceschi, M. Bassi, M. Lomazzi, G. Donofrio, F. Sansone, A. Casnati, R. Ungaro, *Nat. Commun.* **2013**, *4*, 1721; b) S. Bersani, S. Salmaso, F. Mastrotto, E. Ravazzolo, A. Semenzato, P. Caliceti, *Bioconjugate Chem.* **2012**, *23*, 1415 – 1425; c) Z. G. Chen, *Trends Mol. Med.* **2010**, *16*, 594 – 602; d) N. W. Luedtke, P. Carmichael, Y. Tor, *J. Am. Chem. Soc.* **2003**, *125*, 12374 – 12375; e) M. Okuyama, H. Laman, S. R. Kingsbury, C. Visintin, E. Leo, K. L. Eward, K. Stoeber, C. Boshoff, G. H. Williams, D. L. Selwood, *Nat. Methods* **2007**, *4*, 153 – 159; f) J. Valero, M. Van Gool, R. Perez-Fernandez, P. Castreno, J. Sanchez-Quesada, P. Prados, J. de Mendoza, *Org. Biomol. Chem.* **2012**, *10*, 5417 – 5430.
[5] a) Y. A. Fillon, J. P. Anderson, j. Chmielewski, *J. Am. Chem. Soc.* **2005**, *127*, 11798 – 11803; b) N. P. Gabrielson, H. Lu, L. Yin, D. Li, F. Wang, J. Cheng, *Angew. Chem. Int. Ed.* **2012**, *51*, 1143 – 1147; *Angew. Chem.* **2012**, *124*, 1169 – 1173; c) G. Lättig-Tünnemann, M. Prinz, D. Hoffmann, J. Behlke, C. Palm-Apergi, I. Morano, H. D. Herce, M. C. Cardoso, *Nat. Commun.* **2011**, *2*, 453; d) D. Mandal, A. Nasrolahi Shirazi, K. Parang, *Angew. Chem. Int. Ed.* **2011**, *50*, 9633 – 9637; *Angew. Chem.* **2011**, *123*, 9807 – 9811; e) A. Nasrolahi Shirazi, R. K. Tiwari, D. Oh, B. Sullivan, K. McCaffrey, D. Mandal, K. Parang, *Mol. Pharm.* **2013**, *10*, 3137 – 3151; f) H. Tang, L. Yin, K. H. Kim, J. Cheng, *Chem. Sci.* **2013**, *4*, 3839.
[6] K. K. Maiti, W. S. Lee, T. Takeuchi, C. Watkins, M. Fretz, D. C. Kim, S. Futaki, A. Jones, K. T. Kim, S. K. Chung, *Angew. Chem. Int. Ed.* **2007**, *46*, 5880 – 5884; *Angew. Chem.* **2007**, *119*, 5984 – 5988.
[7] S. Fabritz, S. Hörner, O. Avrutina, H. Kolmar, *Org. Biomol. Chem.* **2013**, *11*, 2224 – 2236.
[8] a) S. Fabritz, S. Hörner, D. Konning, M. Empting, M. Reinwarth, C. Dietz, B. Glotzbach, H. Frauendorf, H. Kolmar, O. Avrutina, *Org. Biomol. Chem.* **2012**, *10*, 6287 – 6293; b) D. Heyl, E. Rikowski, R. C. Hoffmann, J. J. Schneider, W. D. Fessner, *Chem. Eur. J.* **2010**, *16*, 5544 – 5548.
[9] C. McCusker, J. B. Carroll, V. M. Rotello, *Chem. Commun.* **2005**, 996 – 998.
[10] S. Hörner, S. Fabritz, H. D. Herce, O. Avrutina, C. Dietz, R. W. Stark, M. C. Cardoso, H. Kolmar, *Org. Biomol. Chem.* **2013**, *11*, 2258 – 2265.
[11] M. De Rosa, A. Gambacorta, A. Gliozzi, *Microbiol. Rev.* **1986**, *50*, 70 – 80.
[12] a) D. Derossi, S. Calvet, A. Trembleau, A. Brunissen, G. Chassaing, A. Prochiantz, *J. Biol. Chem.* **1996**, *271*, 18188 – 18193; b) S. Futaki, T. Suzuki, W. Ohashi, T. Yagami, S. Tanaka, K. Ueda, Y. Sugiura, *J. Biol. Chem.* **2001**, *276*, 5836 – 5840; c) E. Vivès, P. Brodin, B. Lebleu, *J. Biol. Chem.* **1997**, *272*, 16010 – 16017.
[13] F. Duchardt, M. Fotin-Mleczek, H. Schwarz, R. Fischer, R. Brock, *Traffic* **2007**, *8*, 848 – 866.
[14] M. Vazdar, E. Wernersson, M. Khabiri, L. Cwiklik, P. Jurkiewicz, M. Hof, E. Mann, S. Kolusheva, R. Jelinek, P. Jungwirth, *J. Phys. Chem. B* **2013**, *117*, 11530 – 11540.
[15] a) M. Kosuge, T. Takeuchi, I. Nakase, A. T. Jones, S. Futaki, *Bioconjugate Chem.* **2008**, *19*, 656 – 664; b) I. Nakase, Y. Konishi, M. Ueda, H. Saji, S. Futaki, *J. Controlled Release* **2012**, *159*, 181 – 188; c) K. Park, *J. Controlled Release* **2012**, *159*, 153.
[16] A. F. Saleh, A. Arzumanov, R. Abes, D. Owen, B. Lebleu, M. J. Gait, *Bioconjugate Chem.* **2010**, *21*, 1902 – 1911.
[17] S. W. Jones, R. Christison, K. Bundell, C. J. Voyce, S. M. Brockbank, P. Newham, M. A. Lindsay, *Br. J. Pharmacol.* **2005**, *145*, 1093 – 1102.
[18] M. Hällbrink, J. Oehlke, G. Papsdorf, M. Bienert, *Biochim. Biophys. Acta Biomembr.* **2004**, *1667*, 222 – 228.
[19] A. M. Meredith, C. R. Dass, *J. Pharm. Pharmacol.* **2016**, *68*, 729.
[20] a) Y. Sun, X. Yan, T. Yuan, J. Liang, Y. Fan, Z. Gu, X. Zhang, *Biomaterials* **2010**, *31*, 7124 – 7131; b) S. Wesselborg, I. H. Engels, E. Rossmann, M. Los, K. Schulze-Osthoff, *Blood* **1999**, *9*, 3053 – 3063.
[21] A. I. Minchinton, I. F. Tannock, *Nat. Rev. Cancer* **2006**, *6*, 583 – 592.
[22] G. Saito, J. A. swanson, K. D. Lee, *Adv. Drug Delivery Rev.* **2003**, *55*, 199 – 215.
[23] T. Safra, *Oncologist* **2003**, *8*, 17 – 24.
[24] A. L. B. Seynhaeve, B. M. Dicheva, S. Hoving, G. A. Koning, T. L. M. ten Hagen, *J. Controlled Release* **2013**, *172*, 330 – 340.
[25] a) L. Harris, G. Batist, R. Belt, D. Rovira, R. Navari, N. Azarnia, K. Welles, E. Winer, T. D.-S. Grp, *Cancer* **2002**, *94*, 25 – 36; b) E. Rivera, *Oncologist* **2003**, *8*, 3 – 9.
[26] a) J. A. Carrero, H. Vivanco-Cid, E. R. Unanue, *Plos One* **2012**, *7*, e32310; b) Z. F. Walls, H. Gong, R. J. Wilson, *Mol. Pharm.* **2016**, *13*, 1185 – 1190.
[27] J. C. Lacal, L. Carrasco, *Antimicrob. Agents Chemother.* **1983**, *24*, 273 – 275.

Received: June 22, 2016
Revised: September 27, 2016
Published online: ■■ ■■, ■■■■

9. Additional experimental and analytical data

9.1. Experimental and analytical data appending to section 8.1

Electronic Supplementary Material (ESI) for Organic & Biomolecular Chemistry

From Pico to Nano: Biofunctionalization of Cube-octameric Silsesquioxanes by Peptides and Miniproteins

Sebastian Fabritz,‡ Sebastian Hörner,‡ Doreen Könning, Martin Empting, Michael Reinwarth, Christian Dietz, Bernhard Glotzbach, Holm Frauendorf, Harald Kolmar* and Olga Avrutina

Electronic Supplemental Information

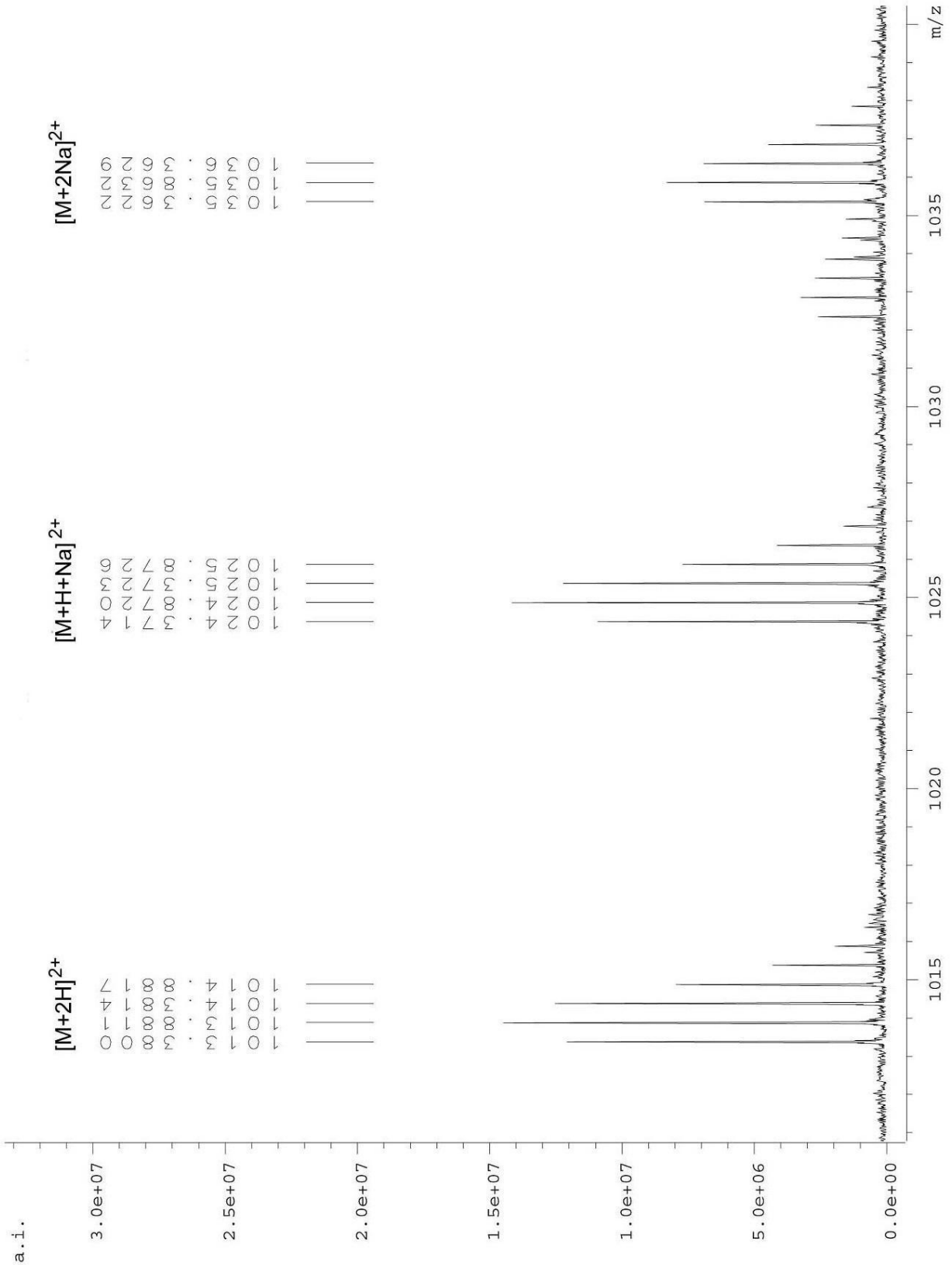

Fig. S1: HR-MS spectrum of **2**.

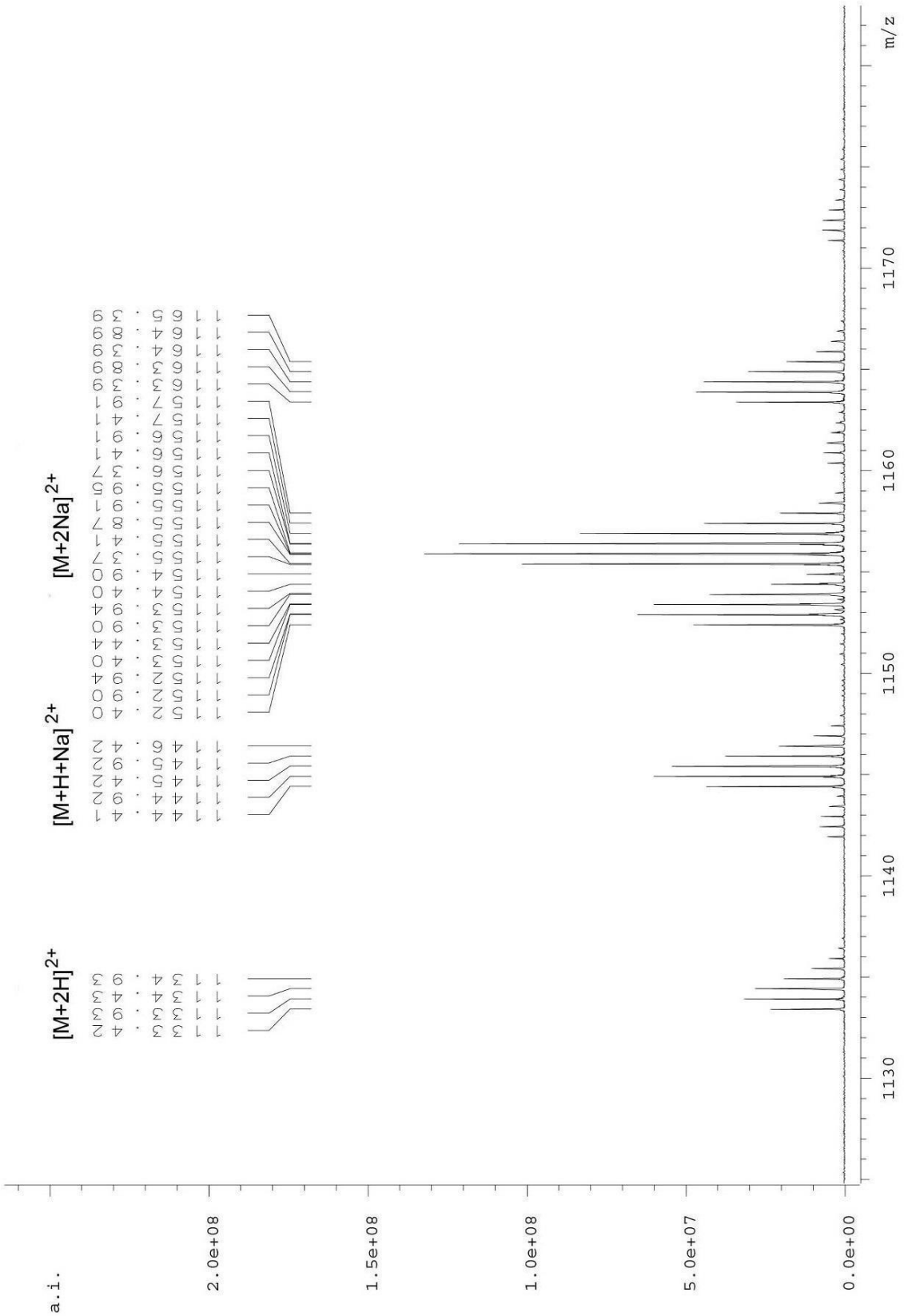

Fig. S2: HR-MS spectrum of **3**.

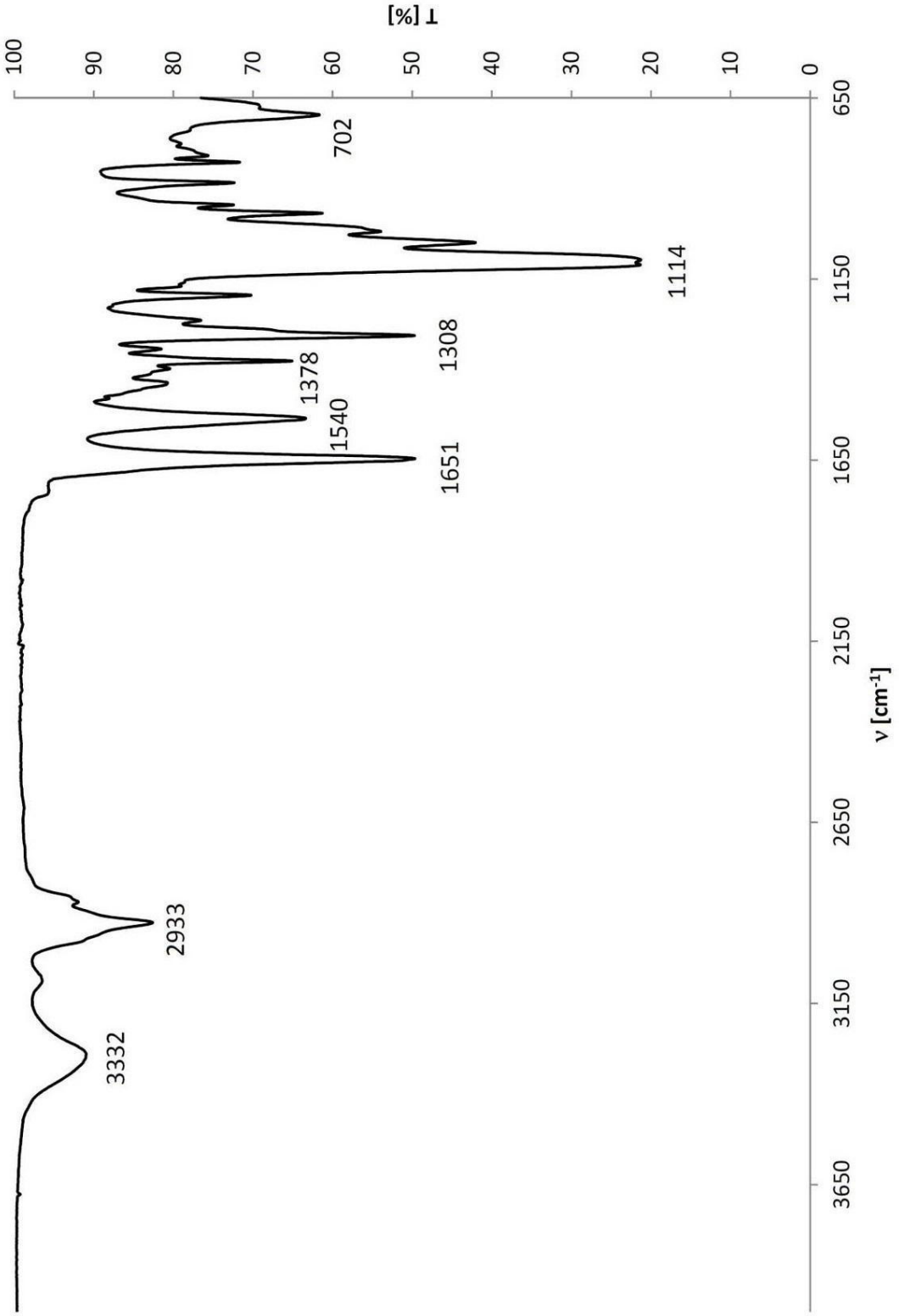

Fig. S3: ATR-IR spectrum of **2**

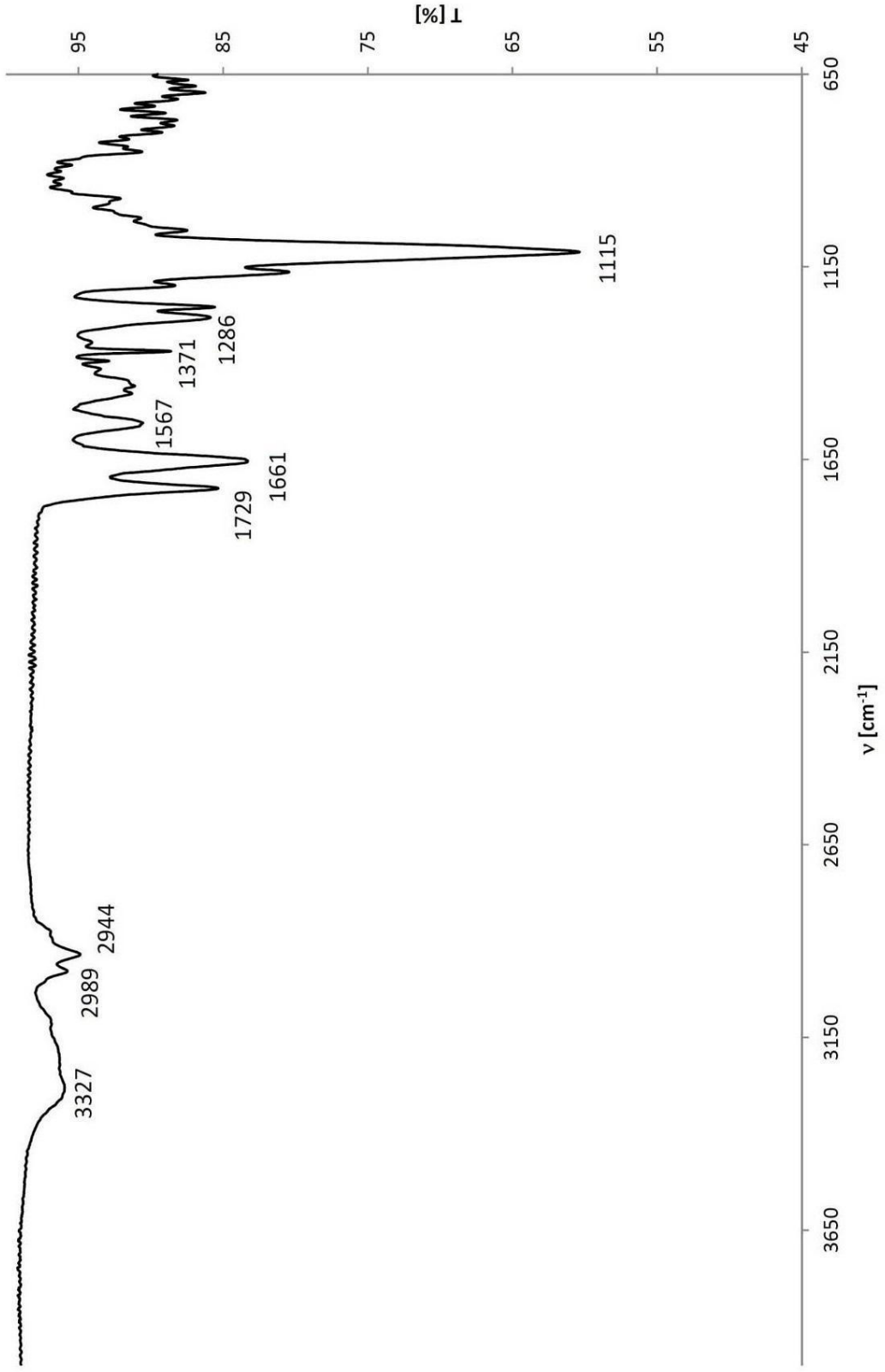

Fig. S4: ATR-IR spectrum of **3**.

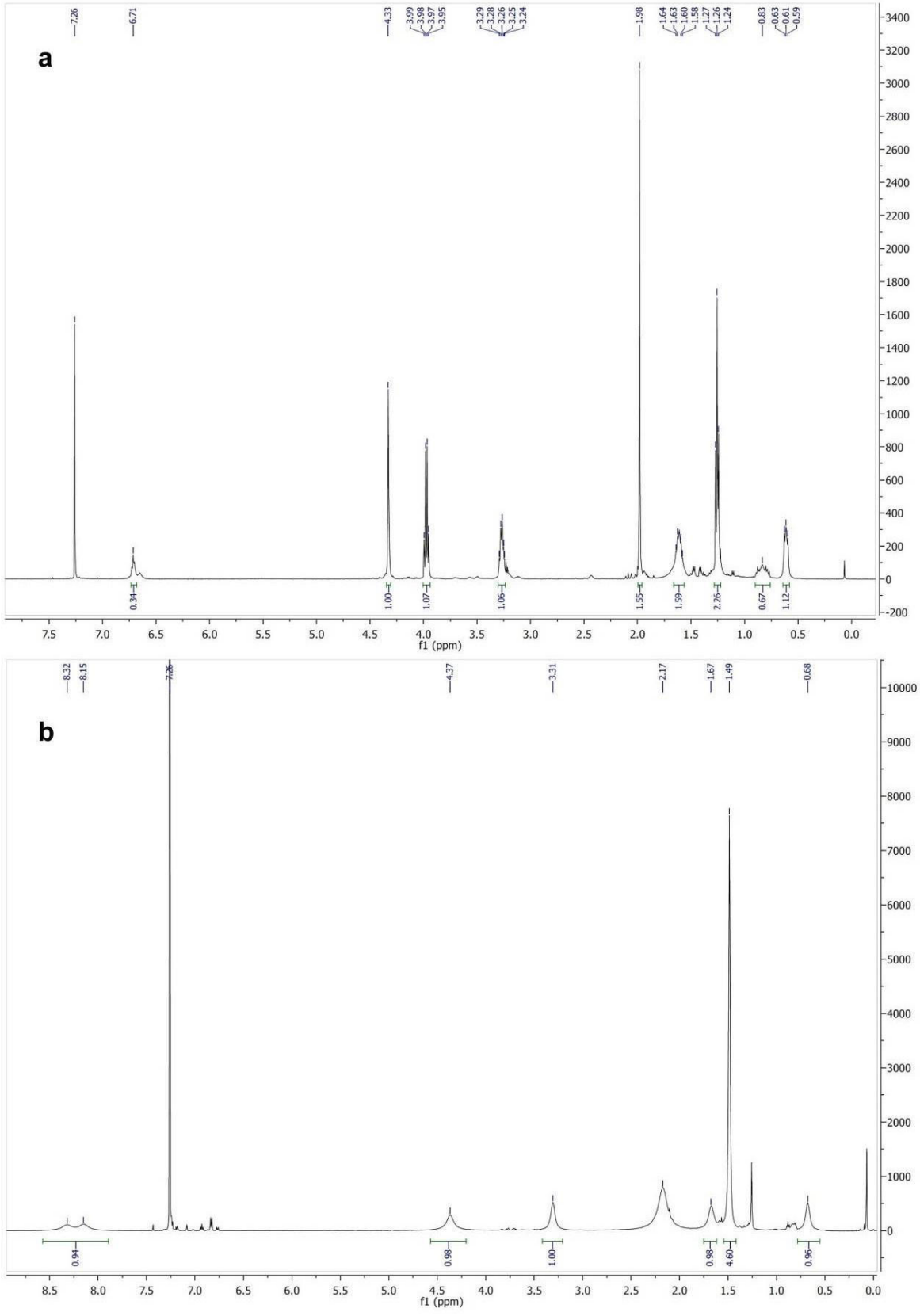

Fig. S5: (a) ^{1}H-NMR of **2**, (b) ^{1}H-NMR of **3**.

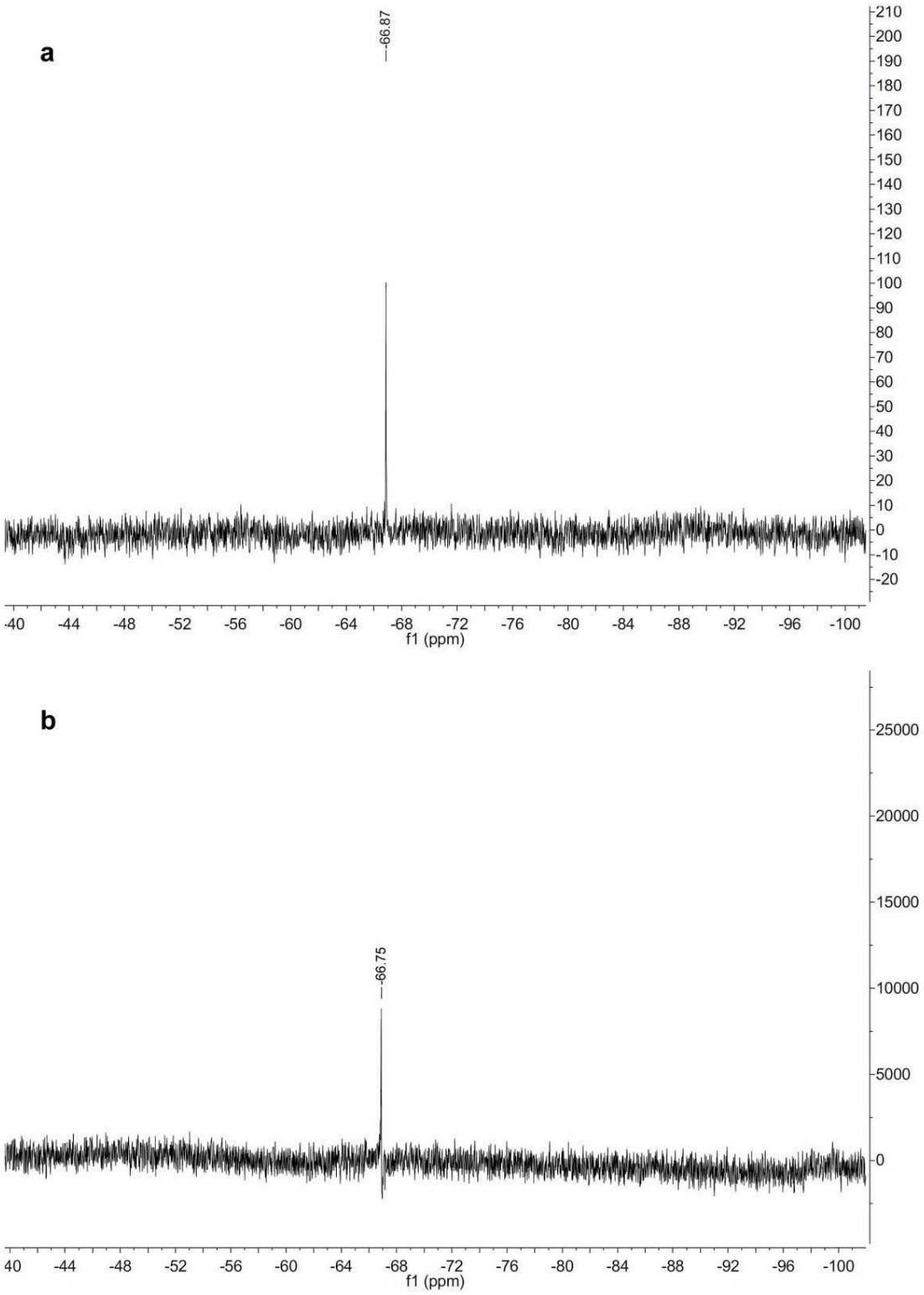

Fig. S6: (a) ^{29}Si-NMR of **2**, (b) ^{29}Si-NMR of **3**, the NMR spectra were base-line corrected using MestReNova.

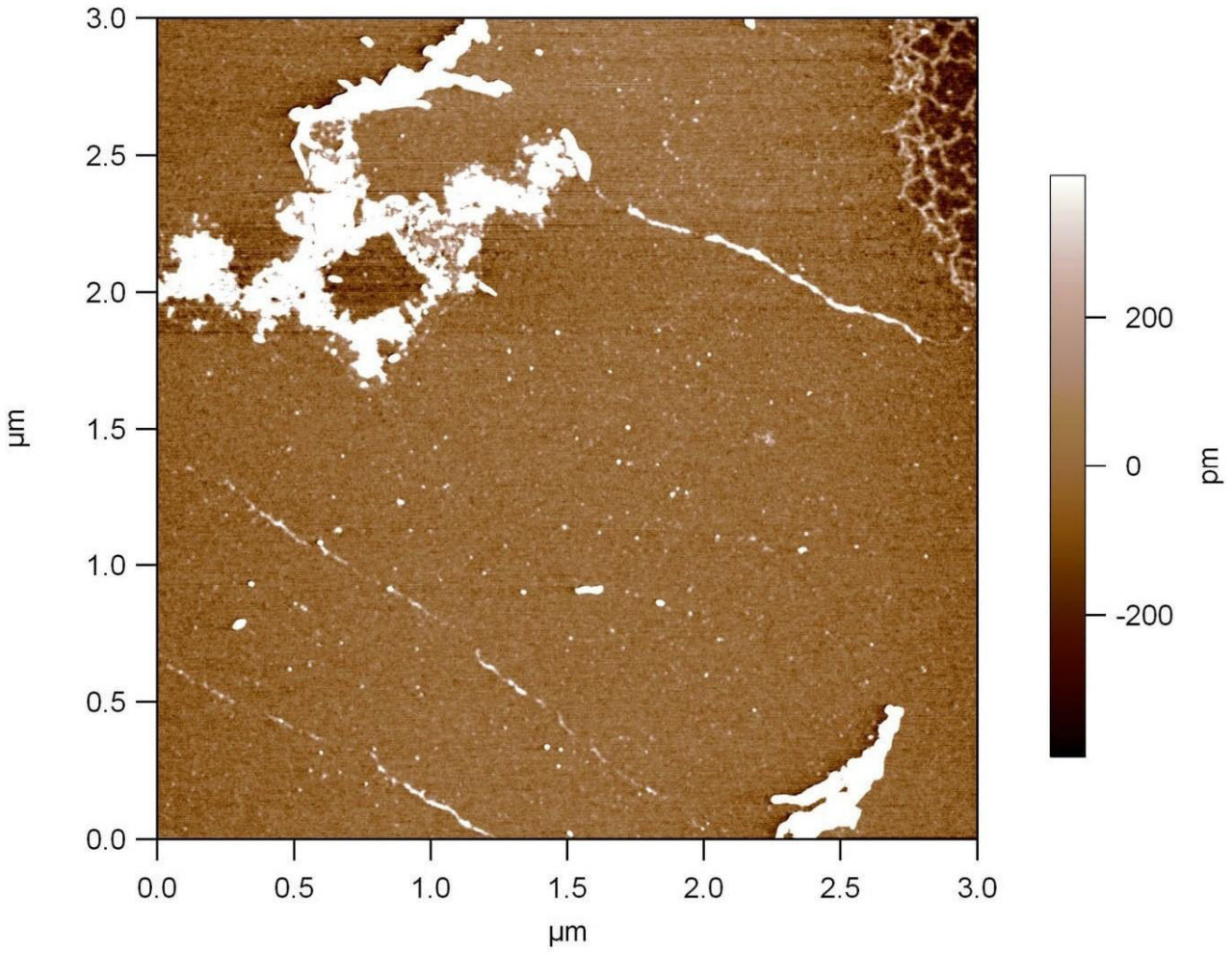

Fig. S7: AFM image of aggregated and randomly distributed COSS particles **1**.

a

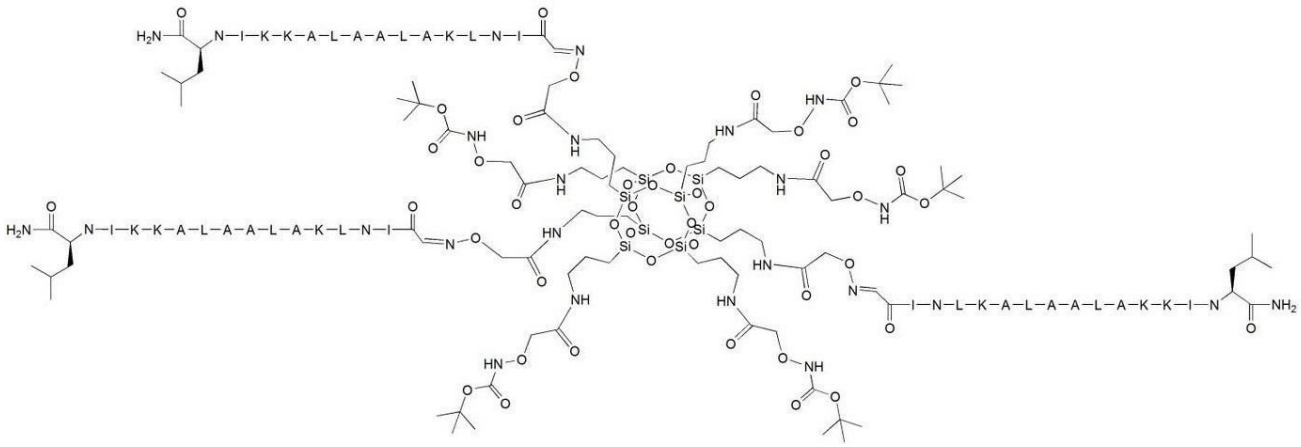

b

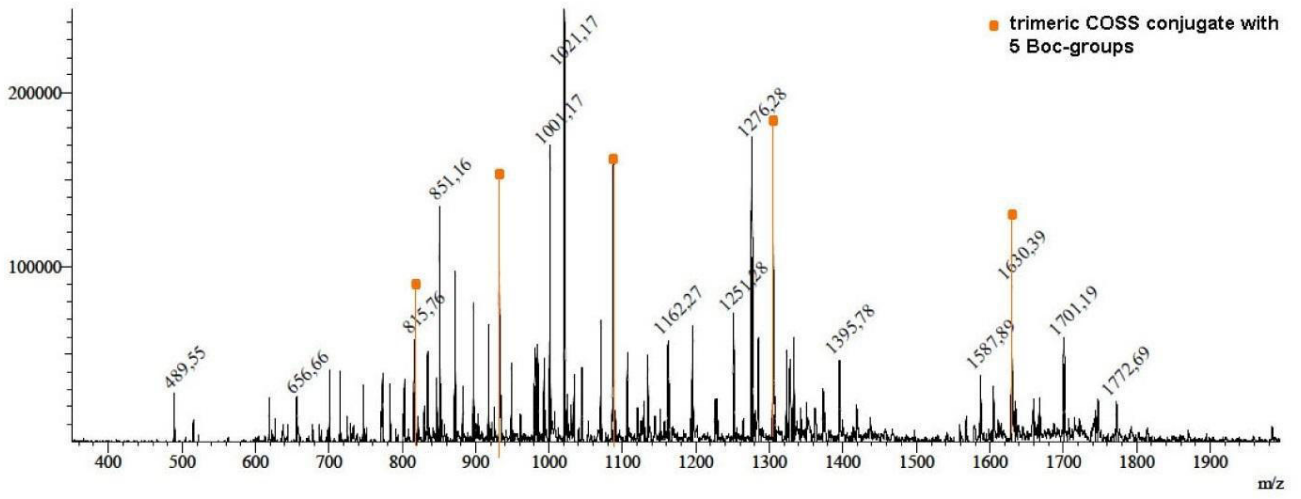

Fig. S8: (a) proposed structure of reaction intermediates in the synthesis of **6**. (b) ESI-MS spectrum of the reaction mixture after 30 min.

a

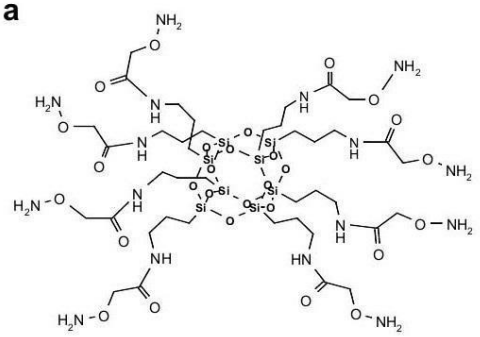

Molecular Weight =1465.93
Molecular Formula =$C_{40}H_{88}N_{16}O_{28}Si_8$

b

Molecular Weight =1117.24
Molecular Formula =$C_{48}H_{76}N_{16}O_{15}$

c

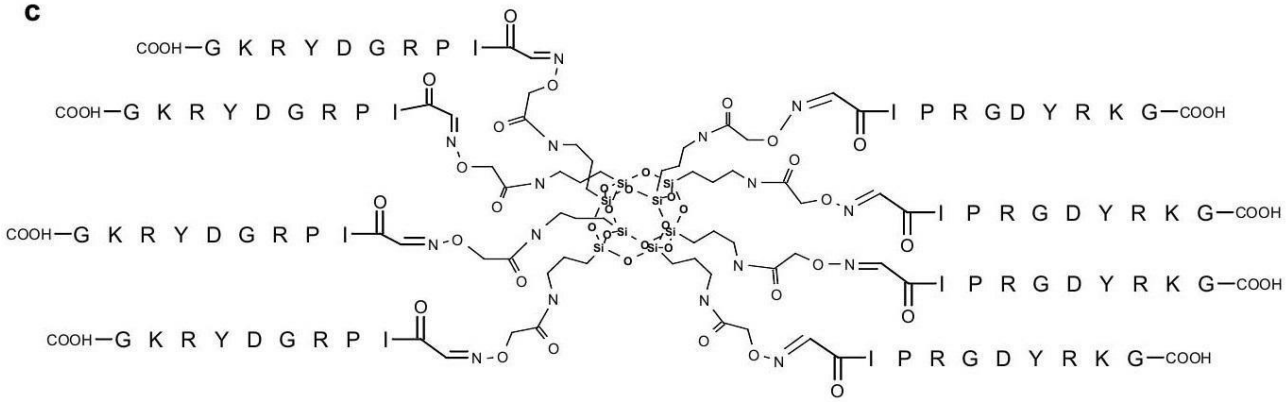

d

Monoconjugate
Molecular Weight =2565.15
Molecular Formula =$C_{88}H_{162}N_{32}O_{42}Si_8$

Diconjugate
Molecular Weight =3664.37
Molecular Formula =$C_{136}H_{236}N_{48}O_{56}Si_8$

Triconjugate
Molecular Weight =4763.60
Molecular Formula =$C_{184}H_{310}N_{64}O_{70}Si_8$

Tetraconjugate
Molecular Weight =5862.82
Molecular Formula =$C_{232}H_{384}N_{80}O_{84}Si_8$

Pentaconjugate
Molecular Weight =6962.04
Molecular Formula =$C_{280}H_{458}N_{96}O_{98}Si_8$

Hexaconjugate
Molecular Weight =8061.27
Molecular Formula =$C_{328}H_{532}N_{112}O_{112}Si_8$

Heptaconjugate
Molecular Weight =9160.49
Molecular Formula =$C_{376}H_{606}N_{128}O_{126}Si_8$

Octaconjugate
Molecular Weight =10259.72
Molecular Formula =$C_{424}H_{680}N_{144}O_{140}Si_8$

Fig. S9: (a) unprotected aminooxy COSS particle, (b) periodate oxidized **p4**, (c) possible conjugation products **4**.

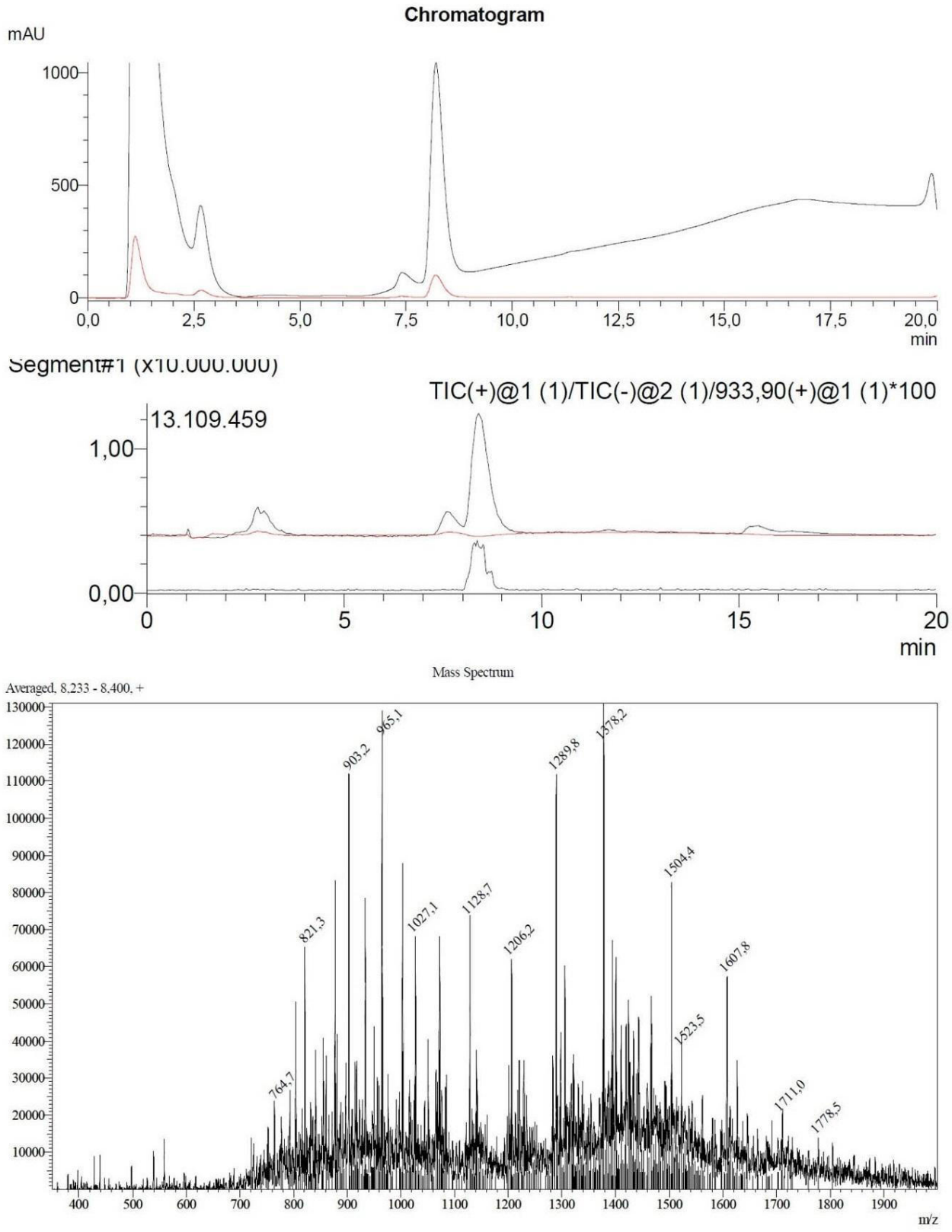

Fig. S10: LC-MS monitoring of the synthesis of **4**: analysis after overnight reaction.

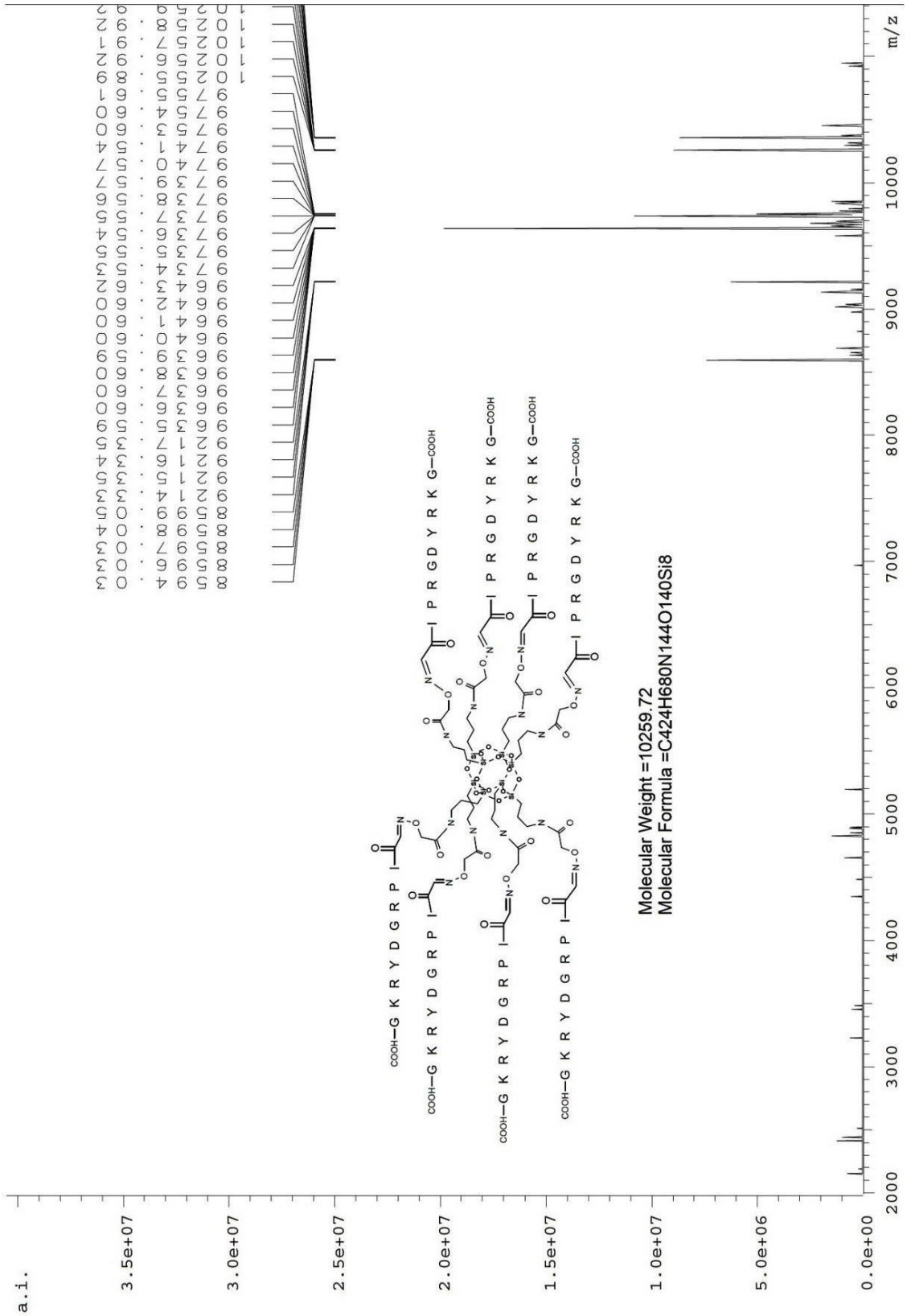

Fig. S11: Synthesis of **4**: deconvoluted ESI MS spectrum of the reaction mixture.

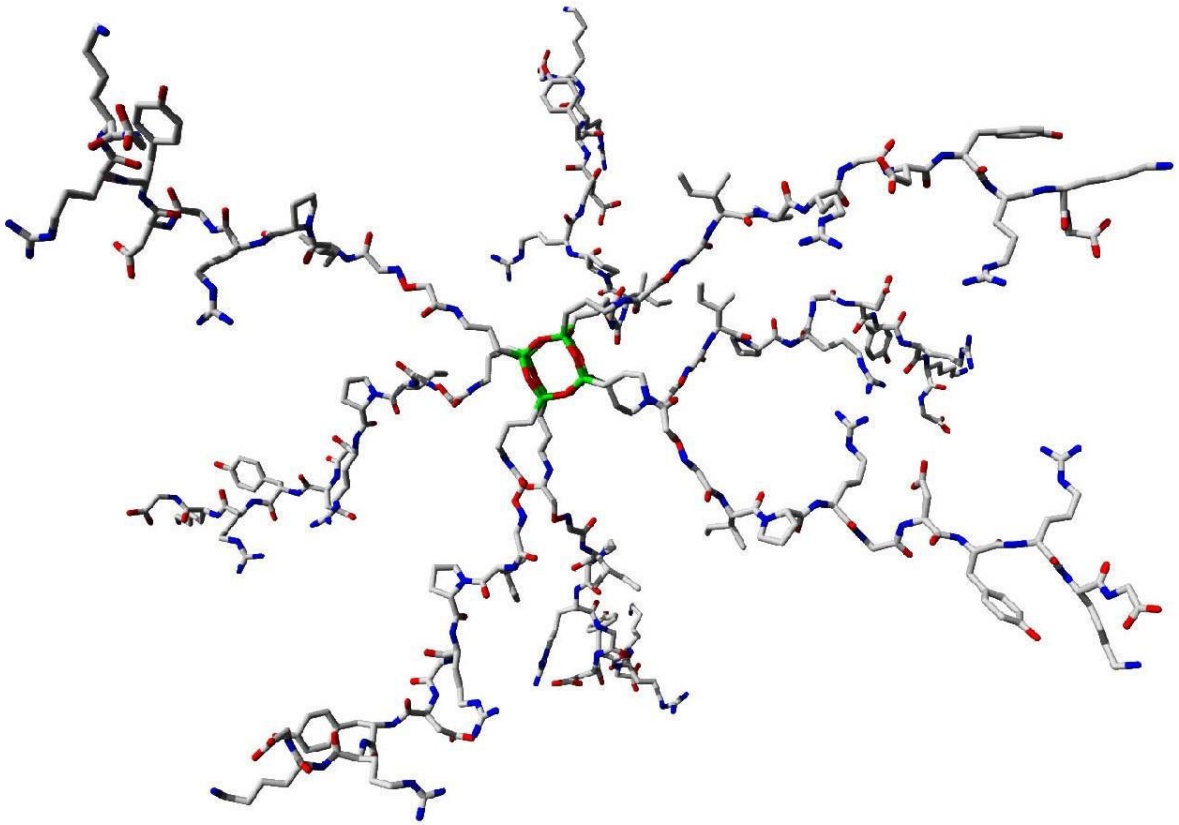

Fig. S12: 3D representation (sticks) of compound **4**. The model was generated using the YASARA structure package. After modelling of the COSS core atoms and connectivities an energy minimization procedure was applied. The respective peptide structures (compare **p4**) were attached, and the core coordinates were fixed. The resulting conjugate **4** was simulated in 0.9 % (m/v) NaCl aq. at pH 7 and 298 K for 0.1 ns using the AMBER03 force field. Blue: nitrogen, green: silicon, red: oxygen, grey: carbon, hydrogen was left out for clarity. Representative diameters were measured as distances of *C*-terminal carboxylic carbons of peptide ligands attached to opposing corners of the COSS cage. The measured values were: 7.21 nm, 6.69 nm, 6.16 nm, and 5.61 nm. The resulting average diameter was 6.42 ± 0.69 nm.

a

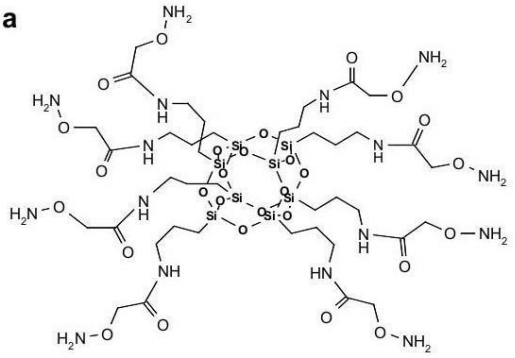

Molecular Weight =1465.93
Molecular Formula =$C_{40}H_{88}N_{16}O_{28}Si_8$

b

Molecular Weight =1067.26
Molecular Formula =$C_{51}H_{78}N_{12}O_{13}$

c

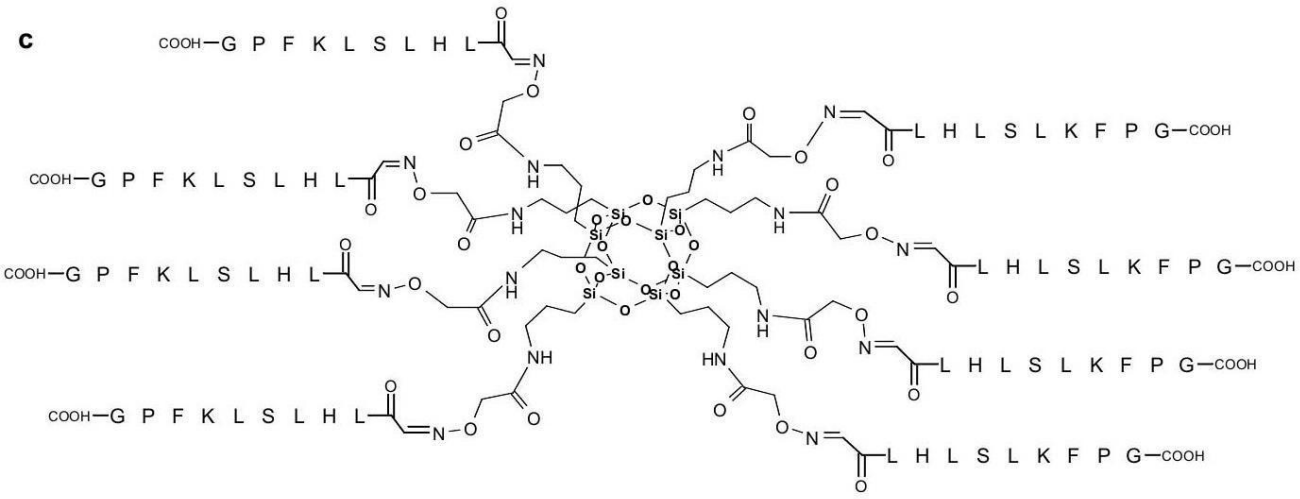

d

Monoconjugate
Molecular Weight =2515.17
Molecular Formula =$C_{91}H_{164}N_{28}O_{40}Si_8$

Diconjugate
Molecular Weight =3564.42
Molecular Formula =$C_{142}H_{240}N_{40}O_{52}Si_8$

Triconjugate
Molecular Weight =4597.65
Molecular Formula =$C_{193}H_{314}N_{51}O_{64}Si_8$

Tetraconjugate
Molecular Weight =5662.92
Molecular Formula =$C_{244}H_{392}N_{64}O_{76}Si$-

Pentaconjugate
Molecular Weight =6712.16
Molecular Formula =$C_{295}H_{468}N_{76}O_{88}Si_8$

Hexaconjugate
Molecular Weight =7761.41
Molecular Formula =$C_{346}H_{544}N_{88}O_{100}Si_8$

Heptaconjugate
Molecular Weight =8810.66
Molecular Formula =$C_{397}H_{620}N_{100}O_{112}Si_8$

Octaconjugate
Molecular Weight =9859.91
Molecular Formula =$C_{448}H_{696}N_{112}O_{124}Si_8$

Fig. S13: (a) unprotected aminooxy COSS particle, (b) periodate oxidized **p5**, (c) possible conjugation products **5**.

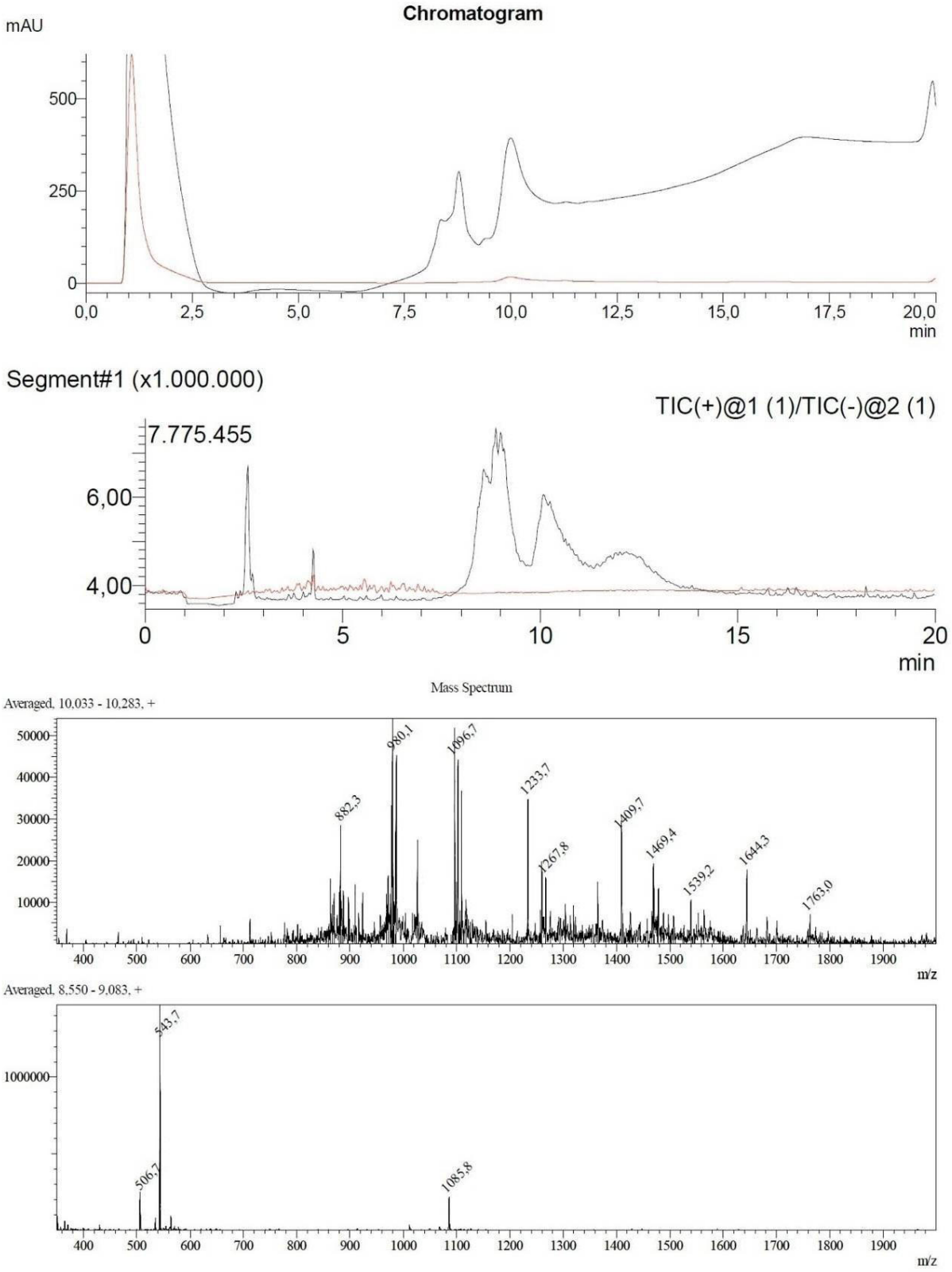

Fig. S14: LC-MS monitoring of the synthesis of **5**: analysis after overnight reaction.

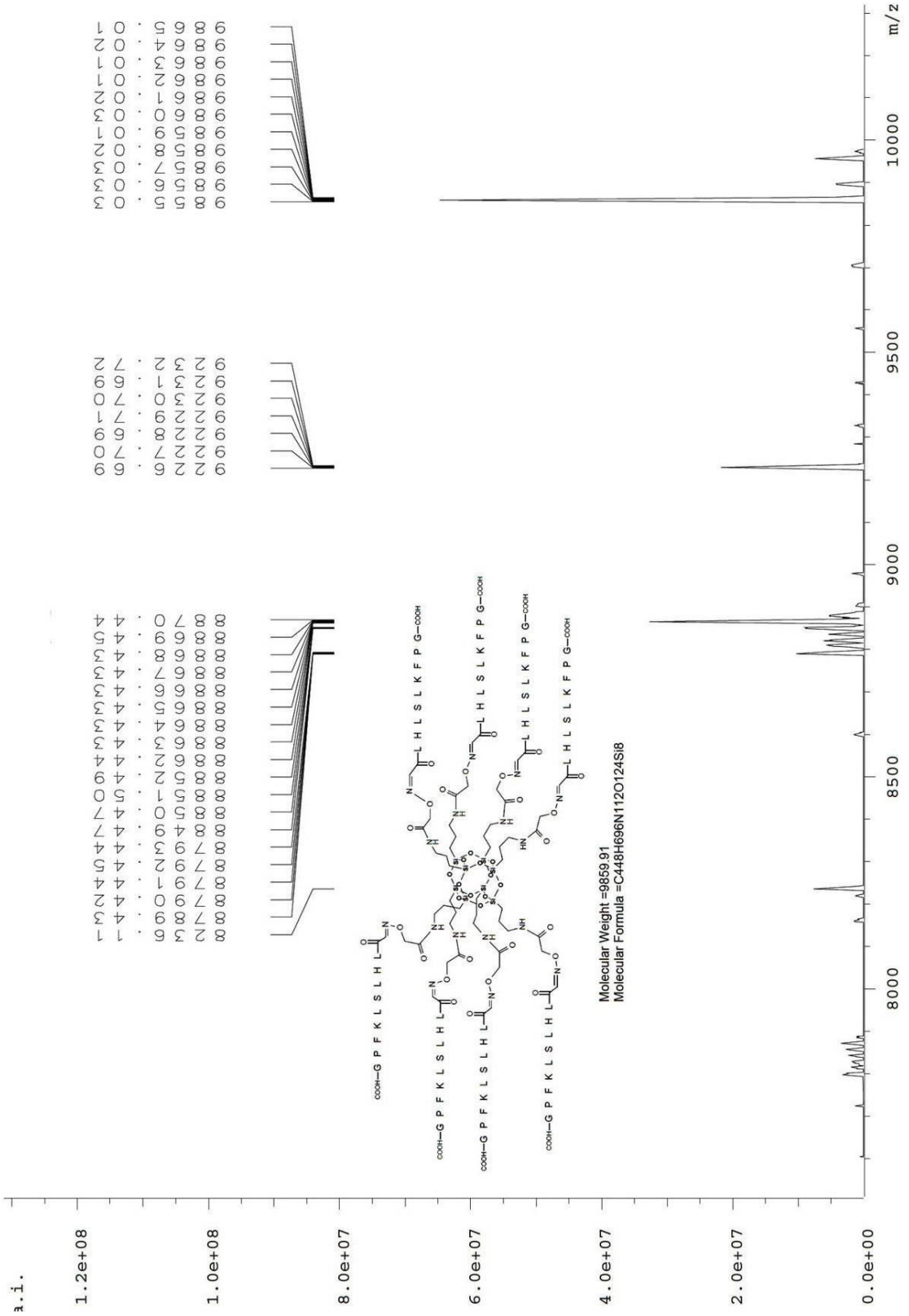

Fig. S15: Synthesis of **5**: deconvoluted ESI MS spectrum of the reaction mixture.

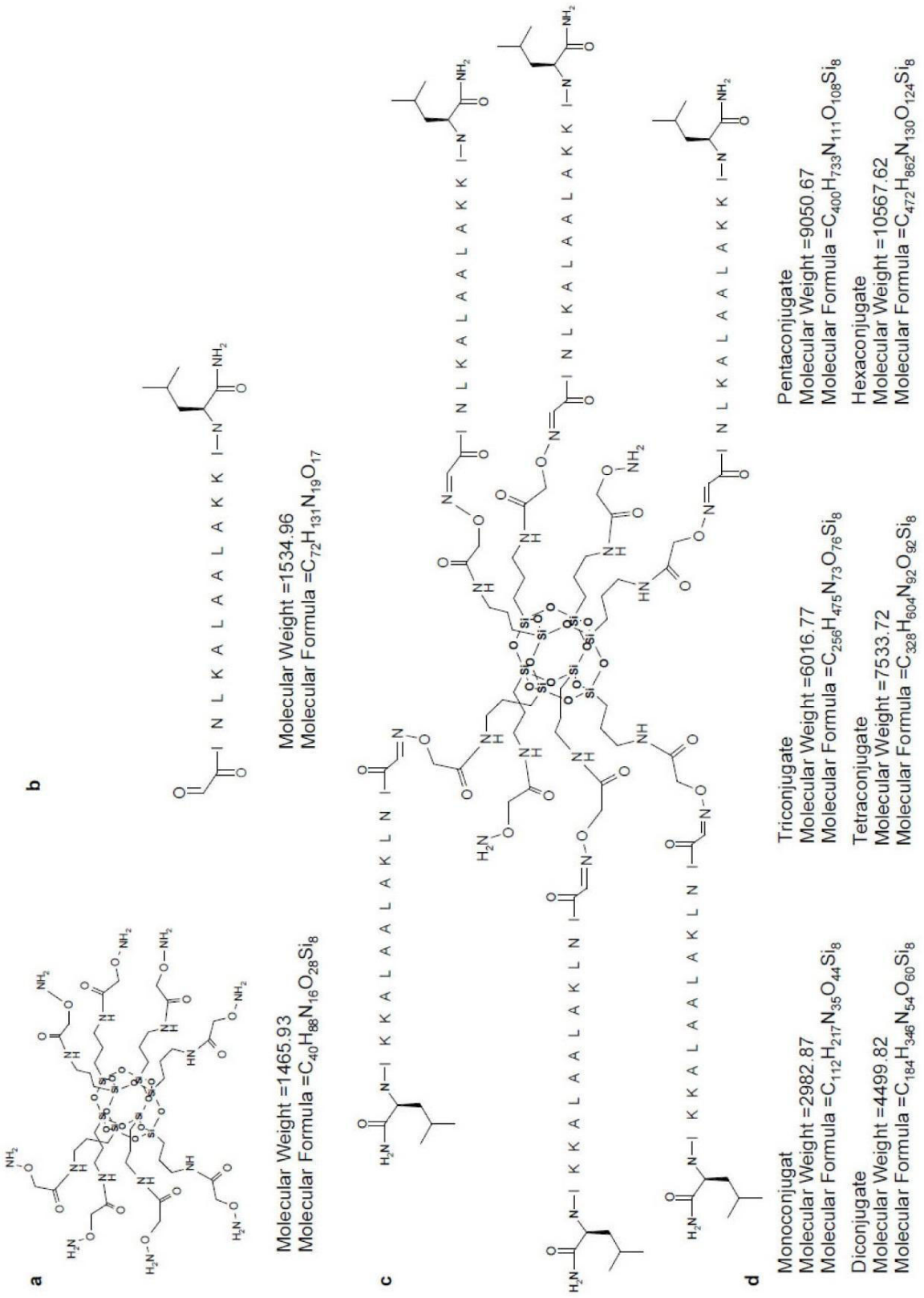

Fig. S16: (a) unprotected aminooxy COSS particle, (b) periodate oxidized **p6**, (c) possible conjugation products **6**.

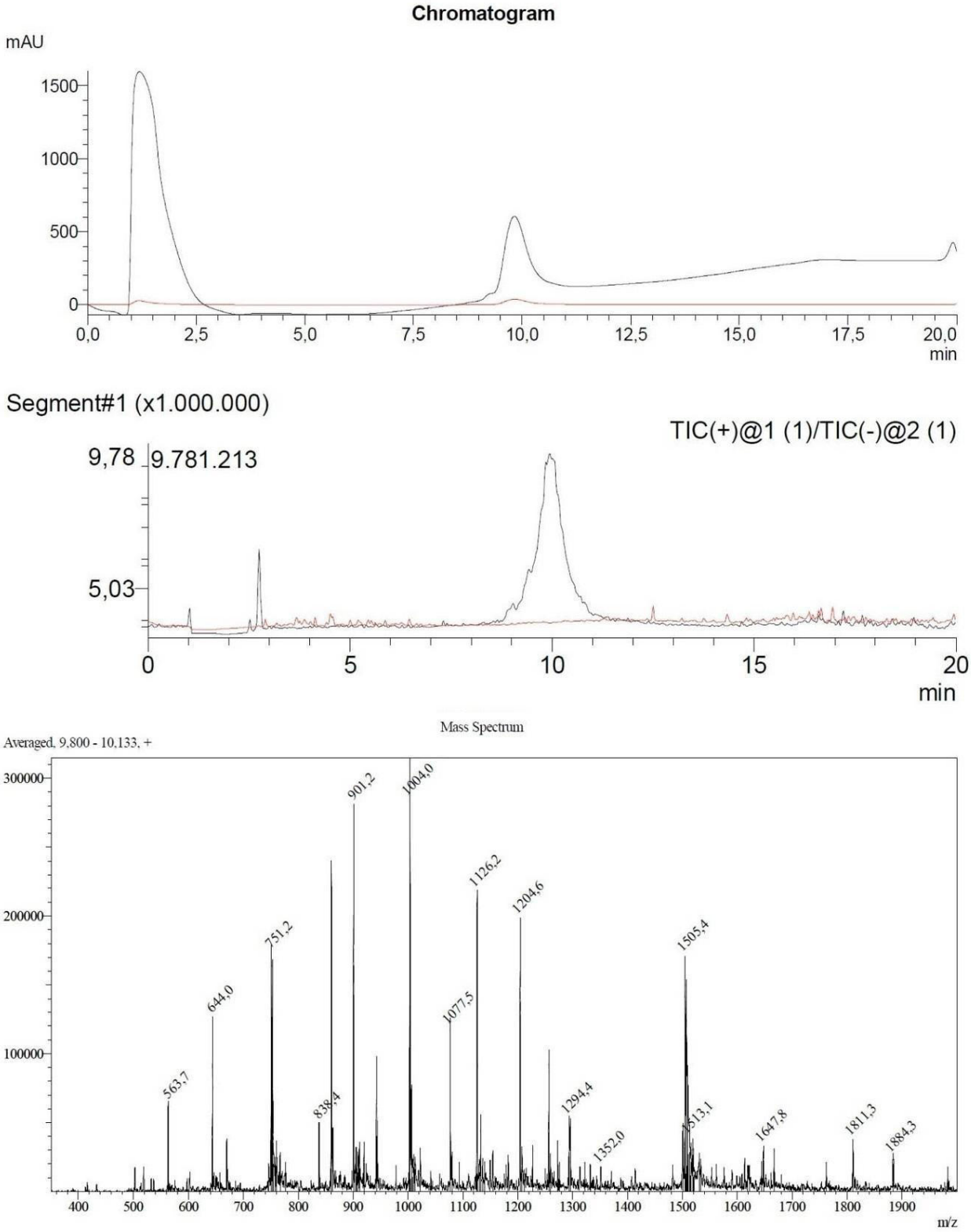

Fig. S17: LC-MS monitoring of the synthesis of **6**: analysis after overnight reaction.

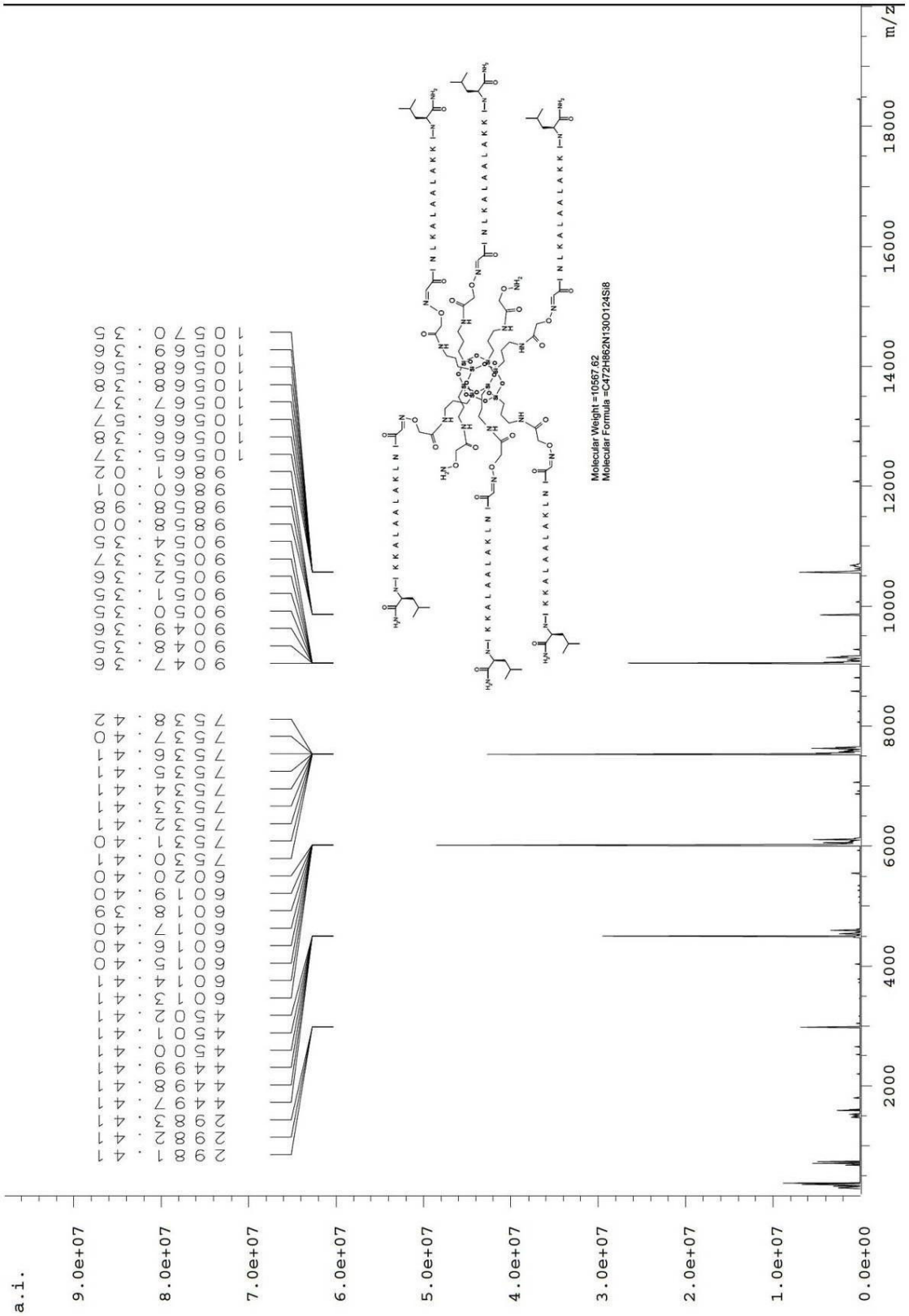

Fig. S18: Synthesis of **6**: deconvoluted ESI MS spectrum of the reaction mixture.

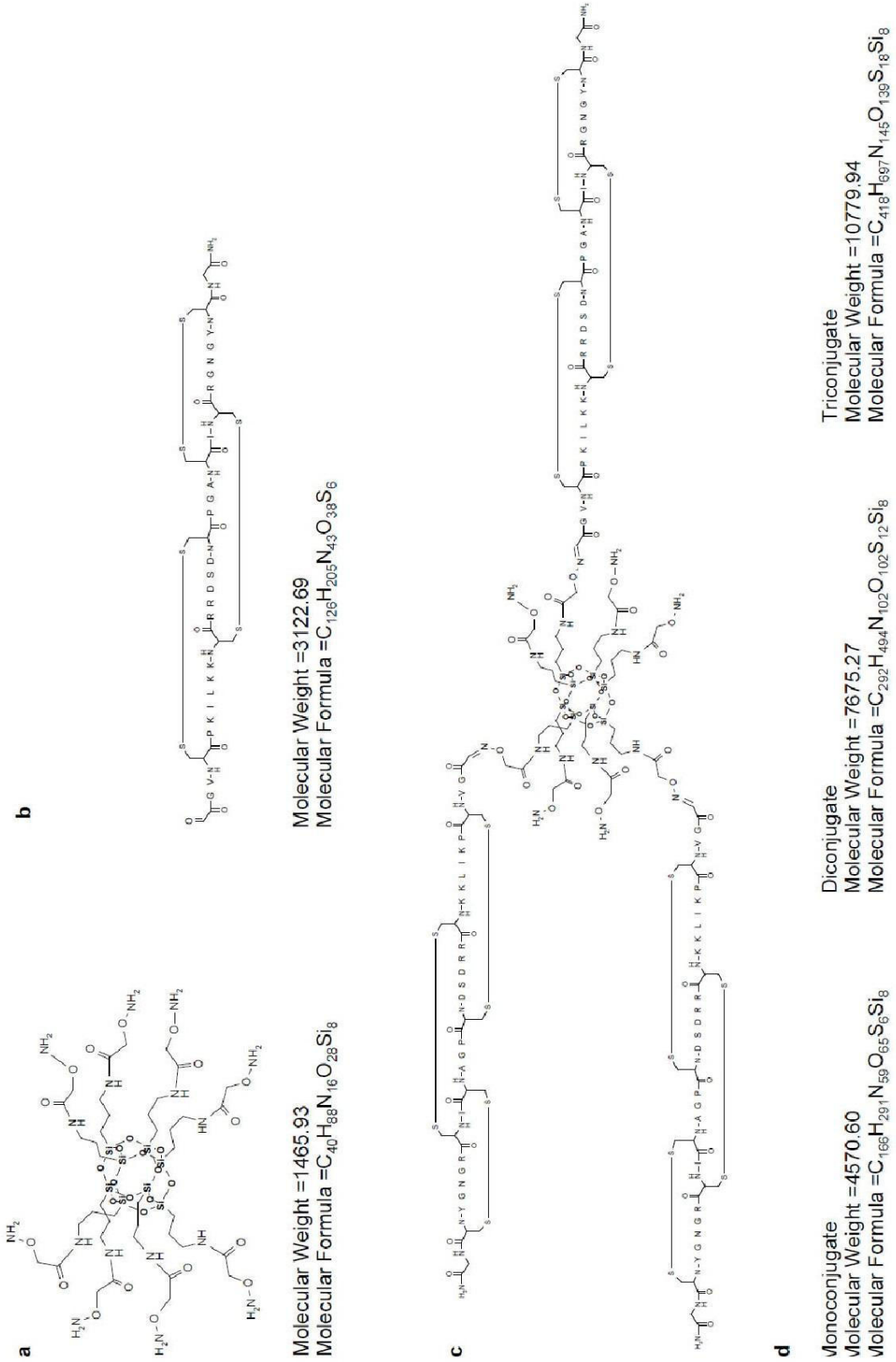

Fig. S19: (a) unprotected aminooxy COSS particle, (b) periodate oxidized **p7**, (c) possible conjugation products.

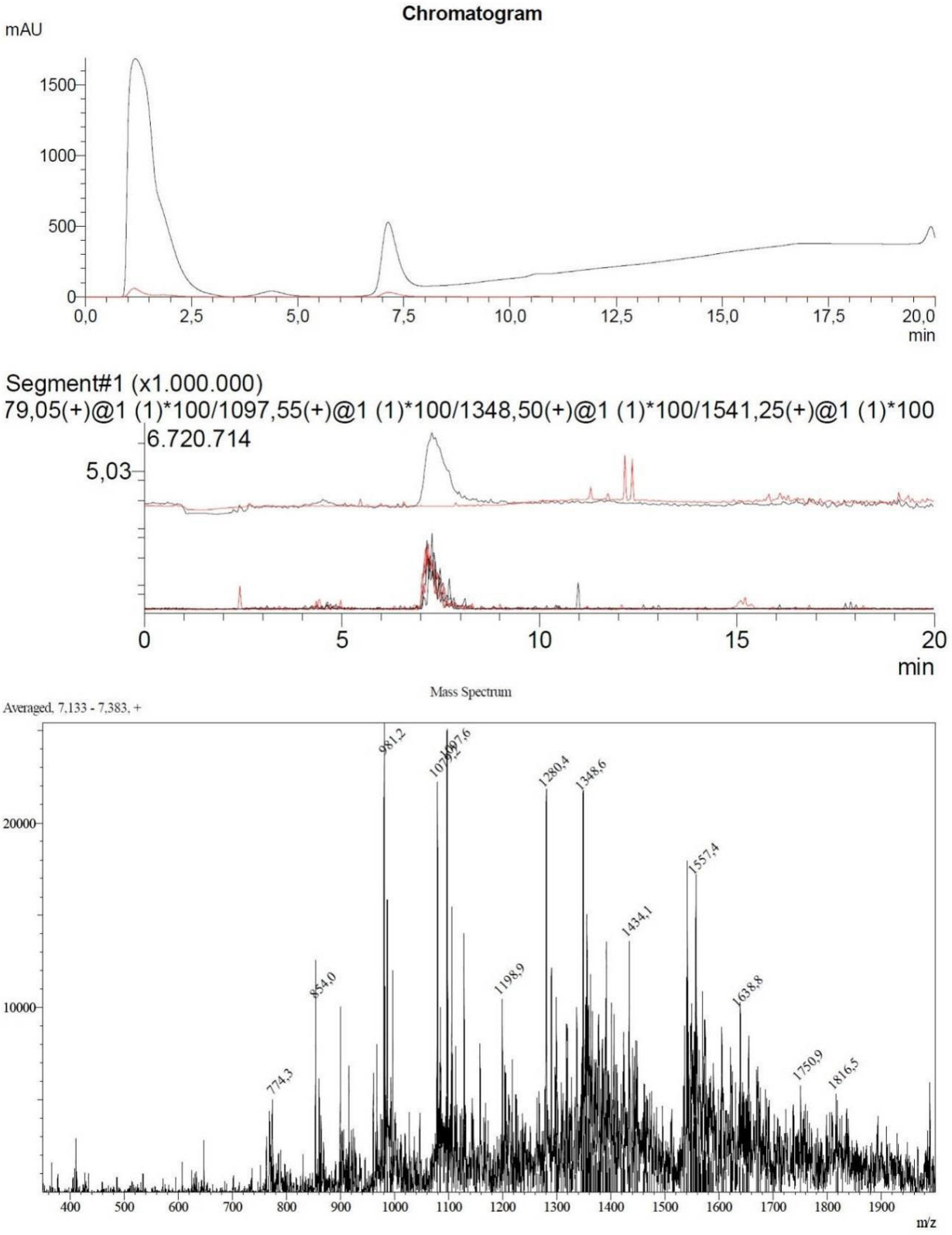

Fig. S20: LC-MS monitoring of the synthesis of **7**: analysis after overnight reaction.

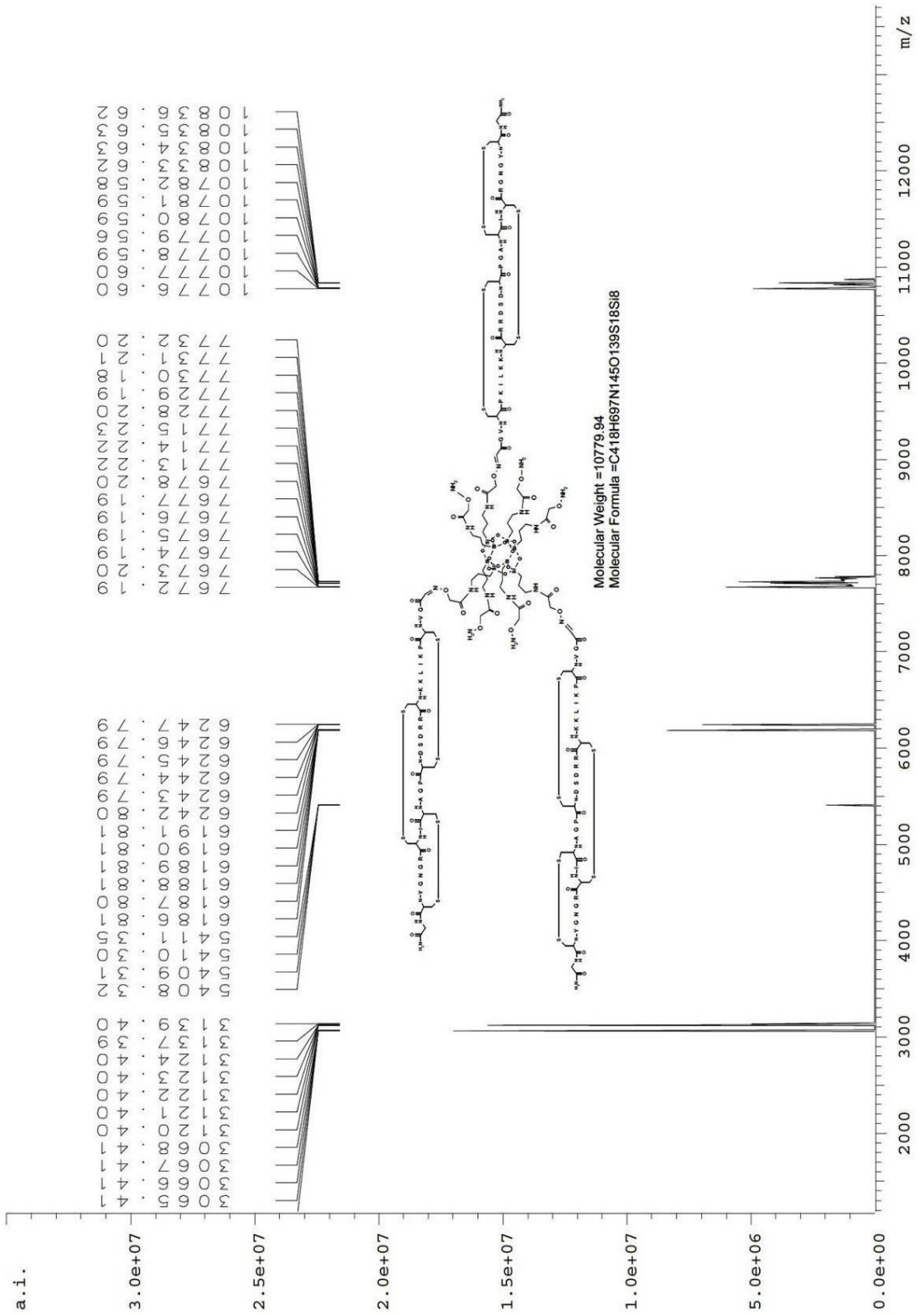

Fig. S21: Synthesis of **7**: deconvoluted ESI MS spectrum of the reaction mixture.

a

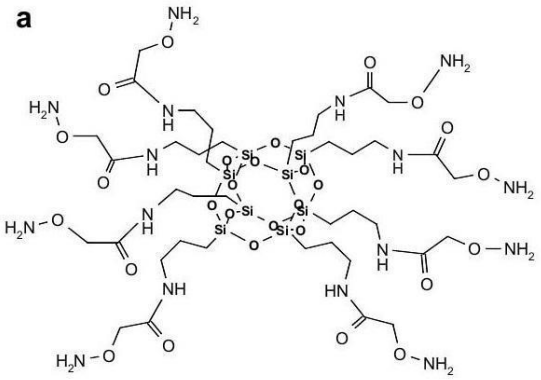

Molecular Weight =1465.93
Molecular Formula =$C_{40}H_{88}N_{16}O_{28}Si_8$

b

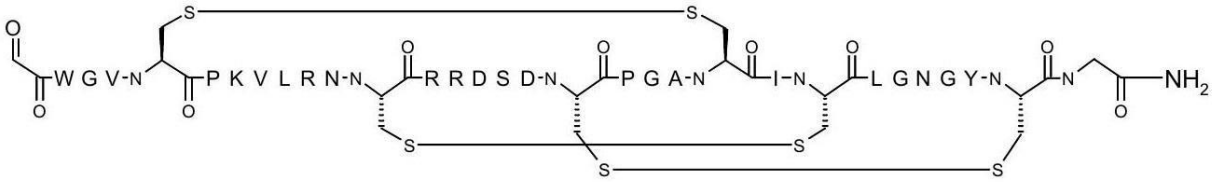

Molecular Weight =3265.79
Molecular Formula =$C_{134}H_{206}N_{44}O_{40}S_6$

c

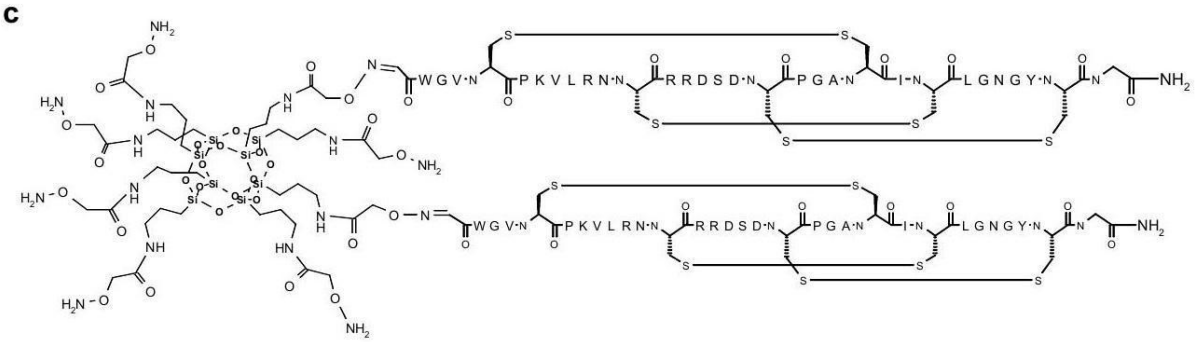

d

Monoconjugate
Molecular Weight =4713.70
Molecular Formula =$C_{174}H_{292}N_{60}O_{67}S_6Si_8$

Diconjugate
Molecular Weight =7961.48
Molecular Formula =$C_{308}H_{496}N_{104}O_{106}S_{12}Si_8$

Fig. S22: (a) unprotected aminooxy COSS particle, (b) periodate oxidized **p8**, (c) possible conjugation products **8**.

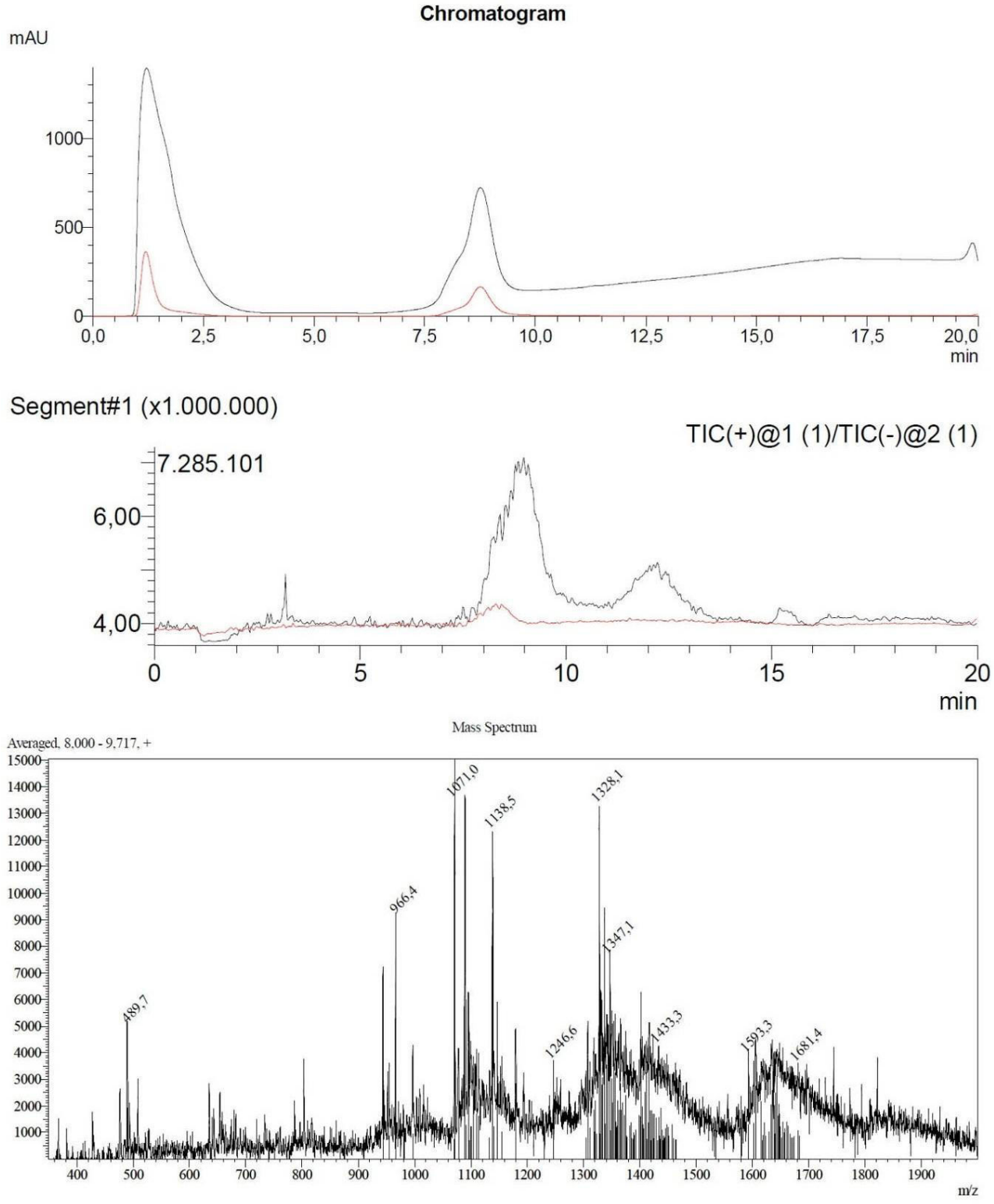

Fig. S23: LC-MS monitoring of the synthesis of **8**: analysis after overnight reaction.

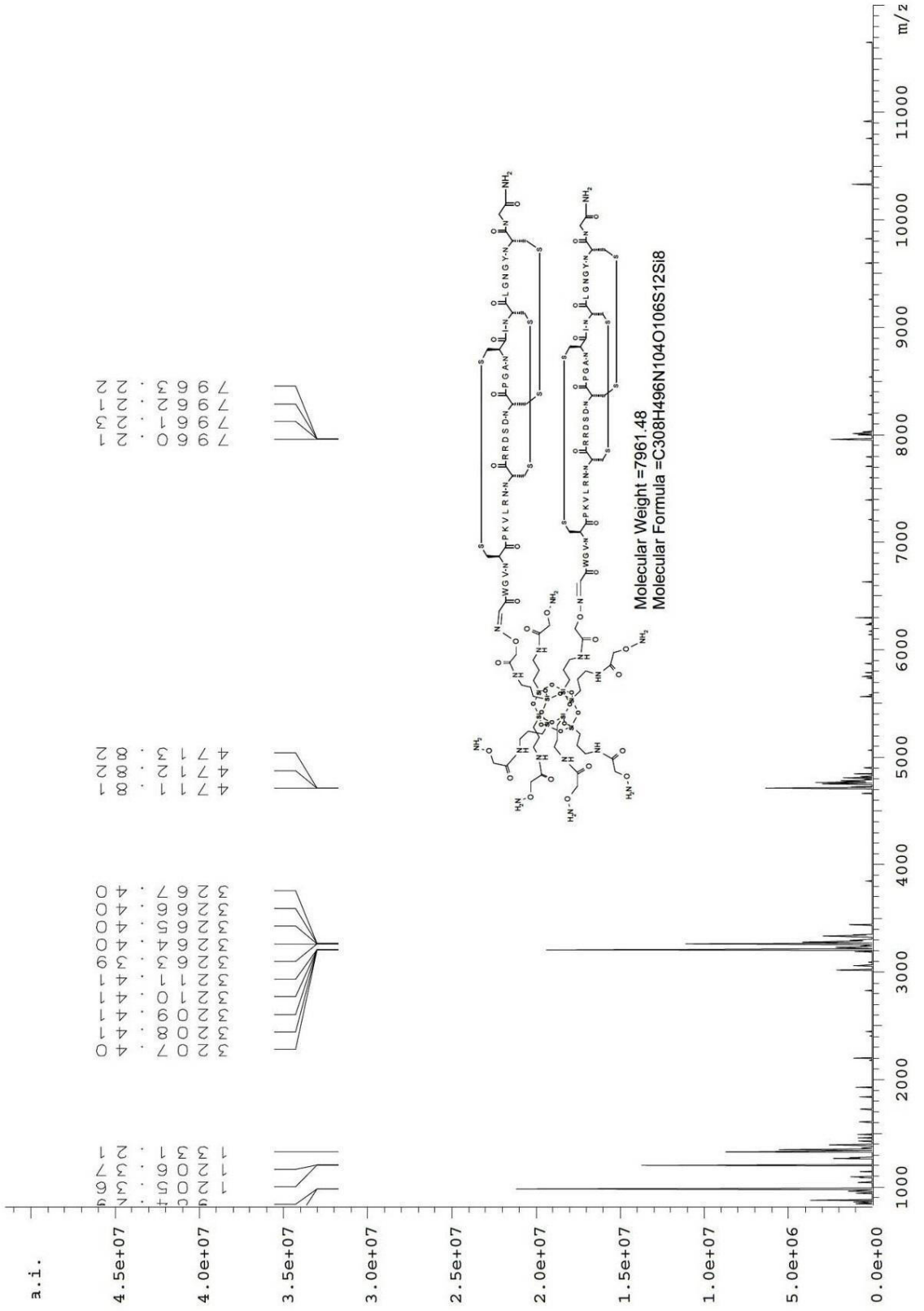

Fig. S24: Synthesis of **8**: deconvoluted ESI MS spectrum of the reaction mixture.

a

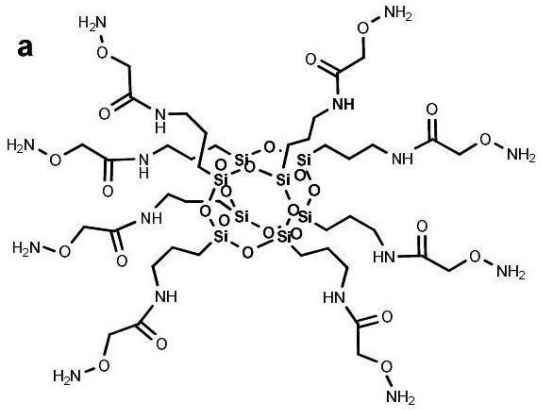

Chemical Formula: C40H88N16O28Si8 $C_{40}H_{88}N_{16}O_{28}Si_8$
Molecular Weight: 1465.901465.9011

b

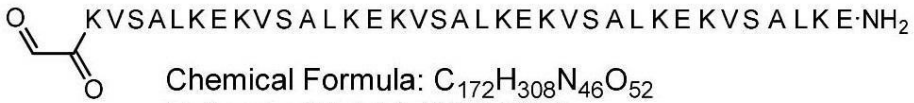

Chemical Formula: $C_{172}H_{308}N_{46}O_{52}$
Molecular Weight: 3852.5629

c

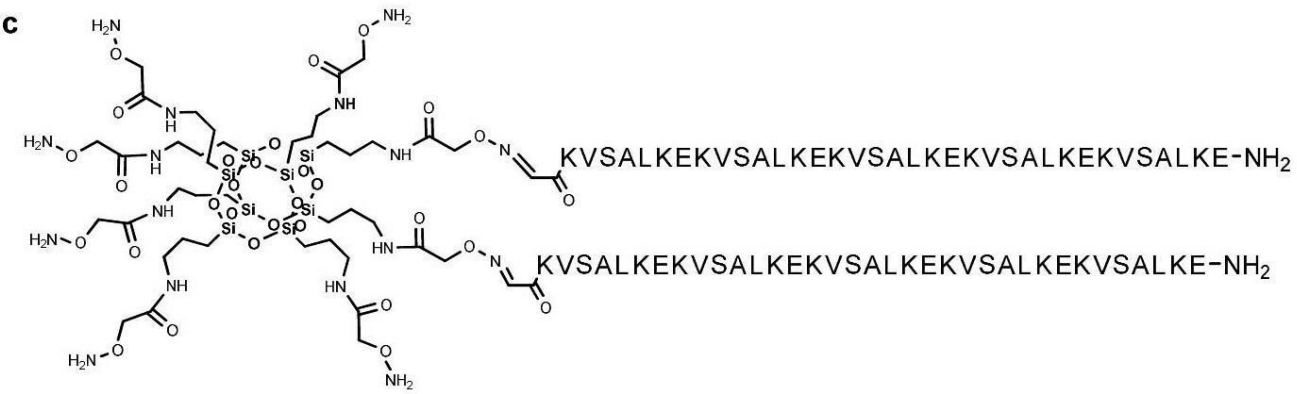

d

Monoconjugate
Chemical Formula: $C_{212}H_{394}N_{62}O_{79}Si_8$
Molecular Weight: 5300.44

Diconjugate
Chemical Formula: $C_{384}H_{700}N_{108}O_{130}Si_8$
Molecular Weight: 9134.99

Fig. S25: (a) unprotected aminooxy COSS particle, (b) periodate oxidized **p9**, (c) possible conjugation products **9**.

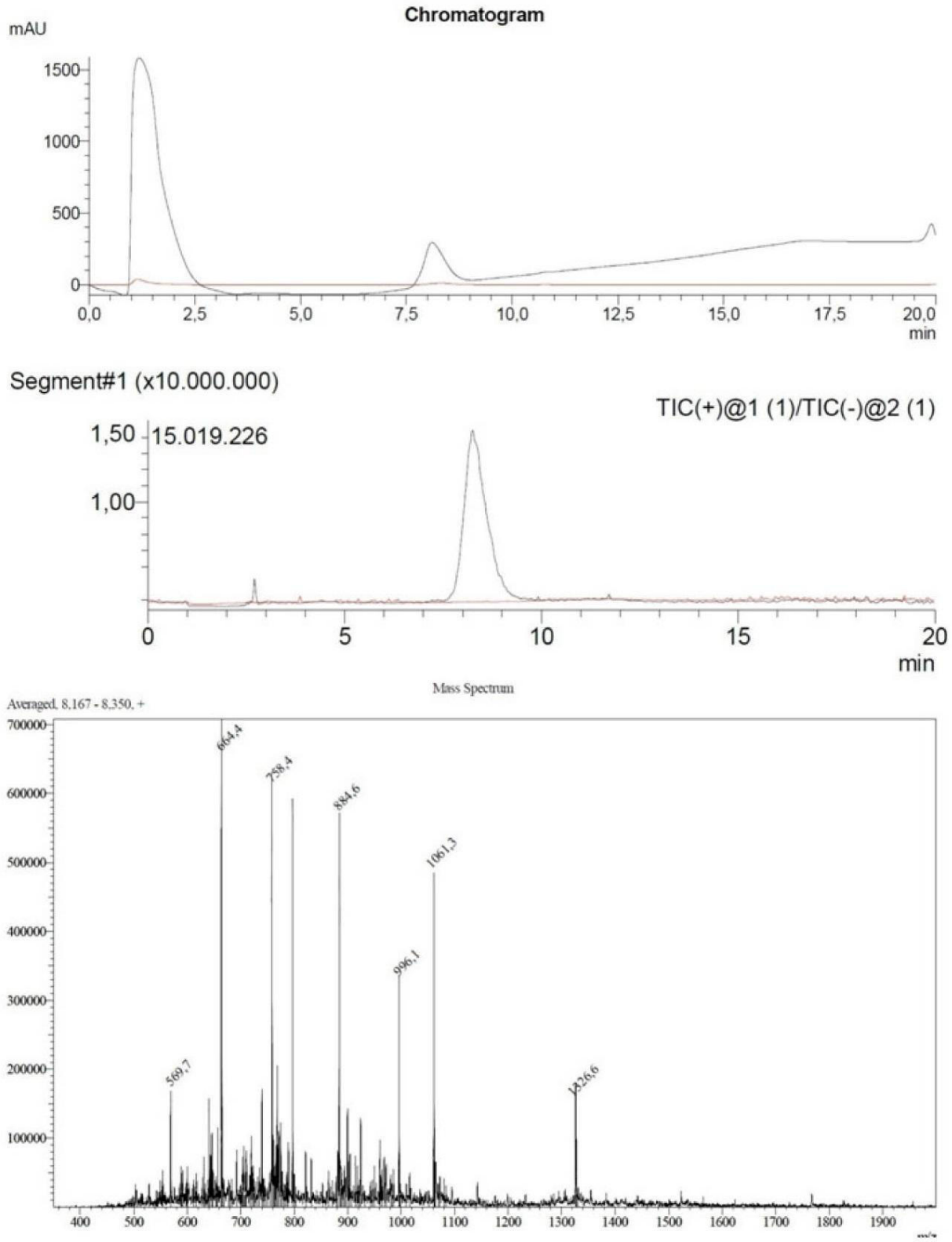

Fig. S26: LC-MS monitoring of the synthesis of **9**: analysis after overnight reaction.

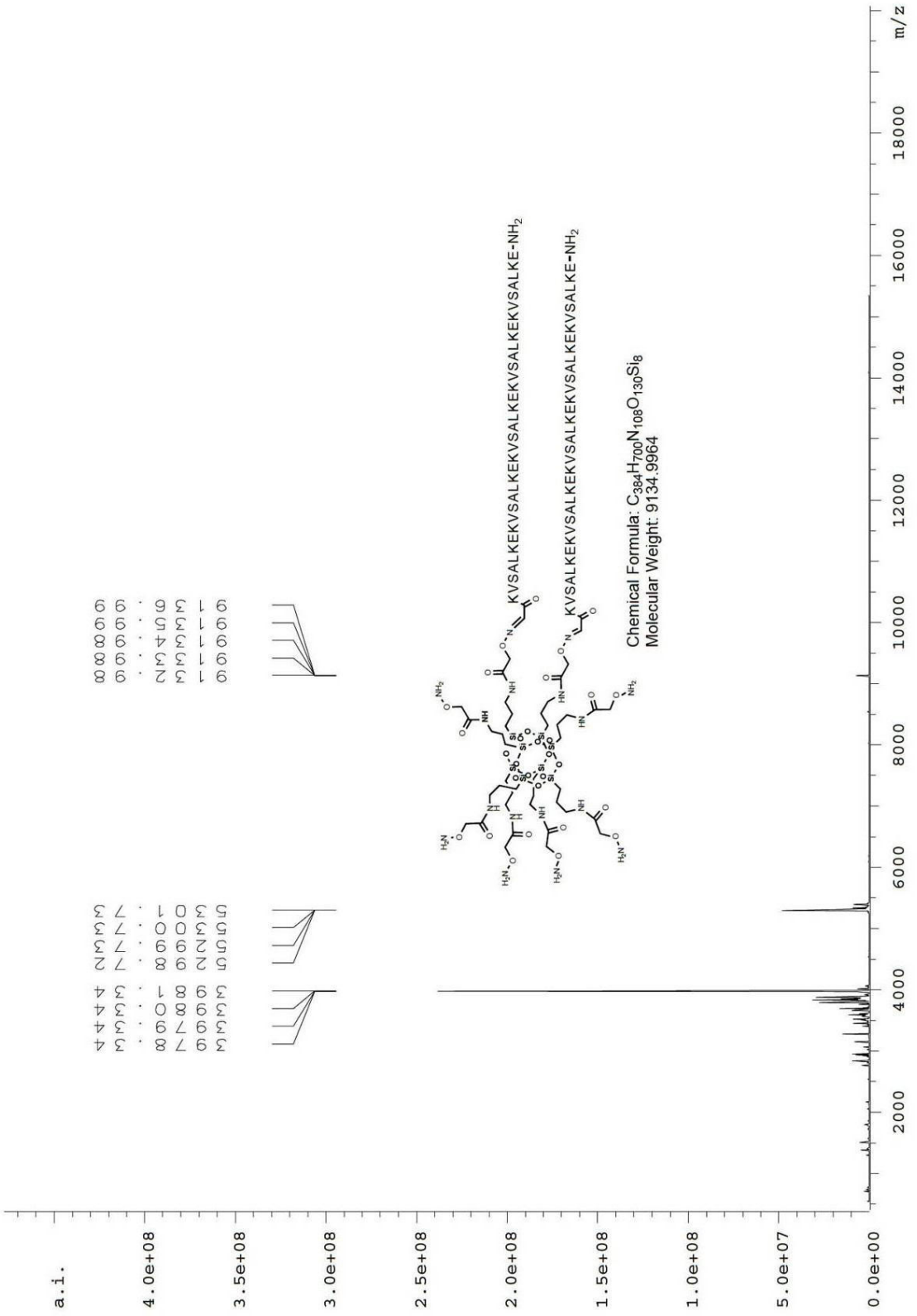

Fig. S27: Synthesis of **9**: deconvoluted ESI MS spectrum of the reaction mixture.

9.2. Experimental and analytical data appending to section 8.2

Electronic Supplemental Information (ESI):

Combination of inverse electron-demand Diels-Alder reaction with highly efficient oxime ligation expands the toolbox of site-selective peptide conjugations

S. Hörner,[‡] C. Uth,[‡] O. Avrutina, H. Frauendorf, M. Wiessler, and H. Kolmar[*]

Content

1 Experimental

1.1 General

1.1.1 Reagents

All reagents were used as supplied by *Sigma Aldrich, Alfa Aesar,* or *Acros Organics* without further purification. Amino acids and resins for solid-phase peptide synthesis (SPPS) were purchased from *Novabiochem* (brand of *Merck KGaA*, Darmstadt, Germany), *CEM* (Kamp-Lintfort, Germany) or *Iris Biotech* (Marktredwitz, Germany).

1.1.2 Mass spectrometry

Electrospray ionization mass spectrometry (ESI-MS) spectra were obtained using a *Shimadzu LCMS-2020* mass spectrometer equipped with a *Phenomenex Jupiter 5u C4 LC* column (50x1 mm, 5 µm, 300 Å). The eluent system consisted of 0.1% (v/v) aq. formic acid (LC-MS grade, *Sigma-Aldrich* (St. Louis, USA)) (eluent A) and acetonitrile containing 0.1% (v/v) formic acid (LC-MS grade, *Karl Roth GmbH*, Karlsruhe, Germany)) (eluent B).

ESI-HRMS measurements were performed on a maXis Q-TOF mass spectrometer (Bruker Daltonik) equipped with an electrospray ion source. 2 µL solution of the dissolved analytes were injected (autoinjector G1313A, Agilent) and transferred into the ion source together with methanol (flow 0.2 mL/min) provided by a pump (G1311A, Agilent). Electrospray mass spectra were measured in the positive ion mode. Mass calibration using a mixture of calibrants (Agilent) was applied. Compound 31: ESI(+)-HRMS was carried on a FTICR mass spectrometer (APEX IV, Bruker Daltonik). Analyte solution was introduced into the electrospray ion source *via* a syringe pump. MALDI mass spectra were acquired applying a MALDI-TOF instrument Autoflex (Bruker). 2,5-dihydroxy benzoic acid (DHB) was used as a matrix.

‡ shared lead author

1.1.3 Liquid chromatography

Analytical reversed-phase high performance liquid chromatography (RP-HPLC) was performed on a *Varian 920 LC* equipped with a *Phenomenex Luna Hypersil* 5u BDS C_{18} LC column (5 u, 130 Å, 150×4.60 mm, 5 µm) at a flow rate of 1 mL/min. For isolation of peptides by semi-preparative RP-HPLC a *Varian 940 LC* equipped with a preparative C_{18} column (*Phenomenex Luna* 5u C_{18} (250×20 mm; S-4 µm, 8 nm)) was used. At a flow rate of 18 mL/min, 5 min of isocratic flow (starting concentration of eluent B) was followed by 20 min of gradient flow. Eluent A: with 0.1% (v/v) aq. trifluoroacetic acid (TFA), eluent B: 90% (*v*/*v*) aq. MeCN with 0.1% (*v*/*v*) TFA. Absorption was measured by an UV/VIS detector at 220 nm and 280 nm or 220 nm and 534 nm.

1.2 Synthetic procedures:

1.2.1 Synthesis of compound 1

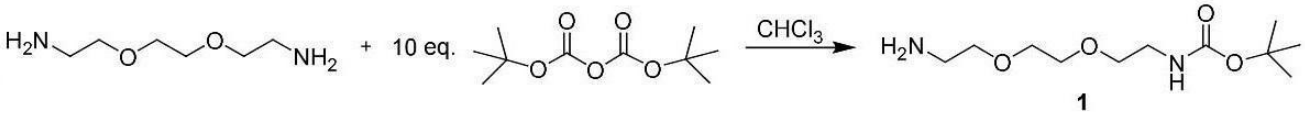

To a cooled solution (0°C) of 30.0 g (202.5 mmol) 2'2-(ethylenedioxy)bis(ethylamine) in 200 mL chloroform, a solution of 4.425 g (20.3 mmol) di-*tert.*-butyl dicarbonate in 200 mL chloroform was drop-wise added under inert atmosphere (N_2). After complete addition, the mixture was allowed to warm to ambient temperature and then stirred overnight. The organic solvent was removed and the colorless liquid was dissolved in 300 mL deionized water. It was extracted three times with each 100 mL methylene chloride. The combined organic phases were washed with 100 mL brine and dried over $MgSO_4$. The solvent was removed resulting in 4.74 g of turbid, colorless oil (yield: 94.1%).

^{1}H-NMR: (300 MHz, DMSO-d_6) δ: 1.37 (s, 9H), 2.63 (t, *J*=5.8 Hz, 2H), 3.05 (q, *J*=6.1 Hz, 2H), 3.35 (t, *J*=5.7 Hz, 2H), 3.38 (t, *J*=6.1 Hz, 2H), 3.49 (s, 4H).

1.2.2 Synthesis of compound 2

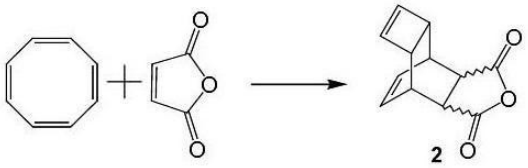

Reppe anhydride **2** was synthesized as described in reference **1**. 5 g (48 mmol) cyclooctatetraene and 4.708 g (48 mmol) maleic anhydride were converted in 1,2-dichlorobenzene. The crude product had a melting point of 162°C (lit. 165-168°C). It was purified by sublimation on high vacuum resulting in 6.123 g of colorless crystals with a melting point of 167°C (yield: 63%).

^{1}H-NMR (500 MHz, DMSO-d_6) δ: 2.81 (s, 2H), 3.04 (s, 2H), 3.25 (s, 2H), 5.89 (s, 2H), 5.97 (dd, *J*=4.6 Hz, 2H).

^{13}C-NMR (125 MHz, DMSO-d_6) δ: 36.42, 42.68, 43.71, 128.90, 138.10, 173.72.

1.2.3 Synthesis of compound 3

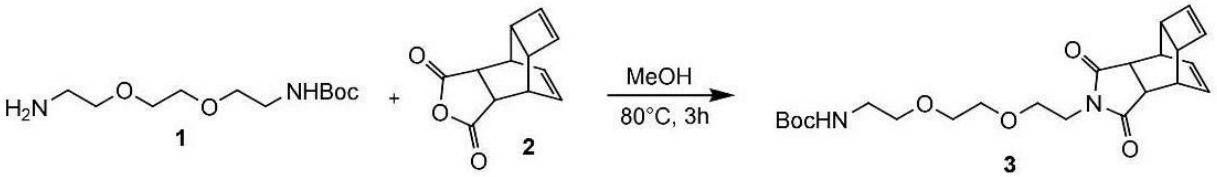

To obtain compound **3**, 0.870 g (1.1 eq., 3.54 mmol) Boc-PEG **1** were reacted with 0.651 g (1 eq., 3.22 mmol) Reppe anhydride **2** in 80 mL MeOH. The reaction mixture was heated for 3 h at 80°C under reflux. As the TLC analysis verified the completion of the reaction, the solution was cooled down and methanol was evaporated under reduced pressure. The crude product was dissolved in water and extracted twice with each 30 mL diethyl ether. The organic phase was dried over $MgSO_4$ and the solvent was removed. 1.1 g of compound **3** were obtained (yield: 82%).

^{1}H-NMR (300 MHz, $CDCl_3$) δ: 1.376 (s, 9H), 2.715 (s, 2H), 2.744 (s, 2H), 3.092 (m, 2H), 3.242 (t, *J*=5.6 Hz, 2H), 3.443 (m, 2H), 3.489 (m, 2H), 3.549 (m, 2H), 5.804 (m, 4H), 5.818 (s, 2H).

ESI-MS calc. for $C_{23}H_{32}N_2O_6$ 432.23; meas.: 433.4 $[M+H]^+$.

1.2.4 Synthesis of compound 4

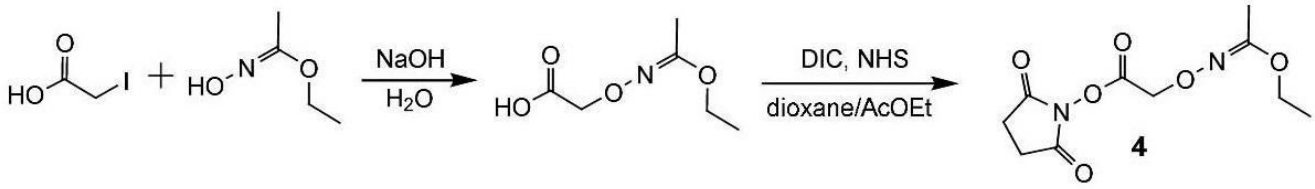

Synthesis of compound **4** was performed as described in reference **2**. 15 g (80.7 mmol) iodoacetic acid were dissolved in 30 mL deionized water and 5 mL aq. NaOH (40% (*w*/*w*)) were slowly added at 0°C. The solution was allowed to warm to ambient temperature. 9.56 g (92.8 mmol) ethyl-acetohydroxamate were added drop-wise to the stirring solution followed by the addition of 7.5 mL aq. NaOH (40% (*w*/*w*)) and 20 mL deionized water. The mixture was heated to 80°C for four hours. During this time, the pH was retained above pH 12 using aq. NaOH (40% (*w*/*w*)). The yellow solution was cooled down to ambient temperature and 100 mL deionized water were added. The solution was washed twice with each 50 mL methylene chloride. The pH of the solution was adjusted to pH 2.0 using 1 M aq. hydrochloric acid. The solution was extracted four times with each 50 mL methylene chloride. Between the extraction steps, the pH was adjusted to pH 2.0 using 1 M aq. hydrochloric acid. The combined organic phases were washed with 50 mL brine and dried over $CaSO_4$. Evaporation of the solvent resulted in 6.98 g colorless oil (yield: 53.8%). This compound is the precursor for compound **4**.

^{1}H-NMR (300 MHz, DMSO-d_6) δ: 1.26 (t, *J*=6.8 Hz, 3H), 2.01 (s, 3H), 4.00 (q, *J*=7.0 Hz, 2H), 4.49 (s, 2H).

^{13}C-NMR (75 MHz, DMSO-d_6) δ: 13.95, 14.21, 62.68, 70.11, 164.73, 175.45.

The colorless oil (6.98 g, 43.2 mmol) and 4.973 g (43.2 mmol) *N*-hydroxysuccinimide were dissolved in a mixture containing 100 mL dioxane and 120 mL AcOEt. The solution was cooled to 0°C and 6.69 mL (5.452 g, 43.2 mmol) *N*,*N*'-diisopropylcarbodiimide (DIC) were added drop-wise. After complete addition the cooled mixture was stirred for additional 30 min and was afterwards allowed to warm to ambient temperature and stirred overnight. The white precipitate was separated by filtration and the solvent was reduced to a volume of 50 mL *in vacuo*. The colorless precipitate was removed by filtration and the remaining solvent was removed. The colorless oil was dissolved in 200 mL chloroform and washed three times with each 40 mL aq. $NaHCO_3$ (5% (*w*/*w*)) and three times with each 40 mL brine. The organic phase was dried over $MgSO_4$. After removing the solvent a colorless oil containing a white precipitate was obtained. The precipitate was removed by filtration using a syringe equipped with a Teflon filter. 8.421 g colorless oil were obtained which crystallized quickly upon freezing at -20°C (yield: 75.5%). Compound **4** should be stored sealed below -20°C.

^{1}H-NMR (300 MHz, DMSO-d_6) δ: 1.26 (t, *J*=7.0 Hz, 3H), 2.01 (s, 3H), 2.84 (s, 4H), 4.02 (q, *J*=7.1 Hz, 2H), 4.78 (s, 2H).

^{13}C-NMR (75 MHz, DMSO-d_6) δ: 13.89, 14.23, 25.57, 62.76, 68.51, 164.77, 165.70, 168.74.

ESI-MS calc. for $C_{10}H_{14}N_2O_6$ m/z: 258.09 meas. 259.05 $[M+H]^+$.

1.2.5 Synthesis of compound 5

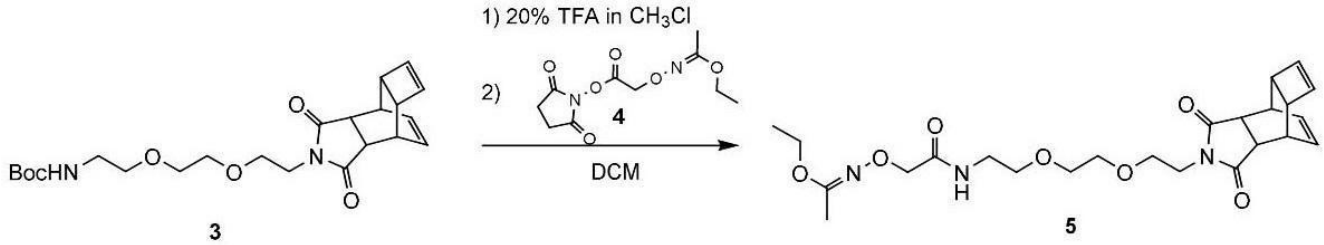

The deprotection of the Boc group was conducted in 20% TFA in chloroform for 1 h at ambient temperature. As LC-MS analysis confirmed the complete Boc elimination, TFA was removed under reduced pressure. 0.8 g (1.0 eq., 1.85 mmol) of the deprotected Reppe-PEG **3** were reacted with 1.01 g (2.0 eq., 3.7 mmol) NHS activated aminooxy building block **4** in 30 mL dichloromethane for 16 h at ambient temperature. After complete reaction dichloromethane was removed under reduced pressure and the crude product was dissolved in deionized water. The aqueous solution was extracted thrice with chloroform. The organic phase was dried over $MgSO_4$ and the solvent evaporated *in vacuo*. Final purification was done by flash column chromatography, applying an isocratic DCM:MeOH (9.5:0.5) mixture giving 0.167 g light yellow oil (yield: 19%).

^{1}H-NMR (300 MHz, $CDCl_3$) δ: 1.196 (t, *J*=7.1 Hz, 3H), 1.918 (s, 3H), 2.713 (s, 2H), 2.745 (s, 2H), 3.087 (s, 2H), 3.484 (m, 12H), 3.912 (q, *J*=7.0 Hz, 2H), 4.299 (s, 2H), 5.799 (q, *J*=4.6 Hz 2 H), 5.819 (s, 2 H).

ESI-MS calc. for $C_{24}H_{33}N_3O_7$ m/z: 475.24 meas. 476.45 $[M+H]^+$.

1.2.6 Synthesis of compound 6

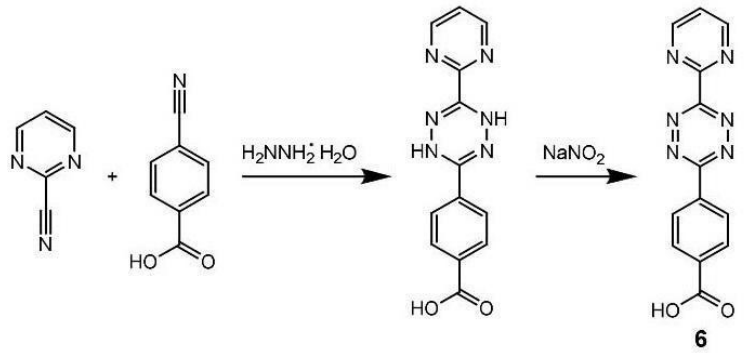

Compound **6** was synthesized according to reference **3**. 5 g (47.57 mmol) 2-pyrimidine-carbonitrile and 7 g (47.57 mmol) 4-cyanobenzoic acid were employed as described in reference **3**. 2.915 g of a yellow solid were obtained (yield: 21.7%). This substance is the precursor for compound **6**.

^{1}H-NMR (300 MHz, DMSO-d_6) δ: 7.61 (t, *J*=4.9 Hz, 1H), 7.93 (d, *J*=9.6 Hz, 2H), 8.00 (d, *J*=8.4 Hz, 2H), 8.83 (s, 1H), 8.92 (d, *J*=4.8 Hz, 2H), 9.52 (s, 1H).

^{13}C-NMR (75 MHz, DMSO-d_6) δ: 122.09, 126.27, 129.41, 132.20, 133.65, 145.62, 146.64, 155.89, 157.67, 166.72.

2.8 g (9.9 mmol) of the yellow solid were oxidized as described in reference **3**. 2.37 g of purple solid **6** were obtained (yield: 85.5%).

^{1}H-NMR (300 MHz, DMSO-d_6) δ: 7.83 (t, *J*=4.4 Hz, 1H), 8.24 (d, *J*=8.5 Hz, 2H), 8.68 (d, *J*=8.5 Hz, 2H), 9.17 (d, *J*=4.8 Hz, 2H)

^{13}C-NMR (75 MHz, DMSO-d_6) δ: 123.00, 128.31, 130.23, 134.63, 135.25, 158.50, 159.01, 162.89, 163.16, 166.68.

1.2.7 Synthesis of compound 7

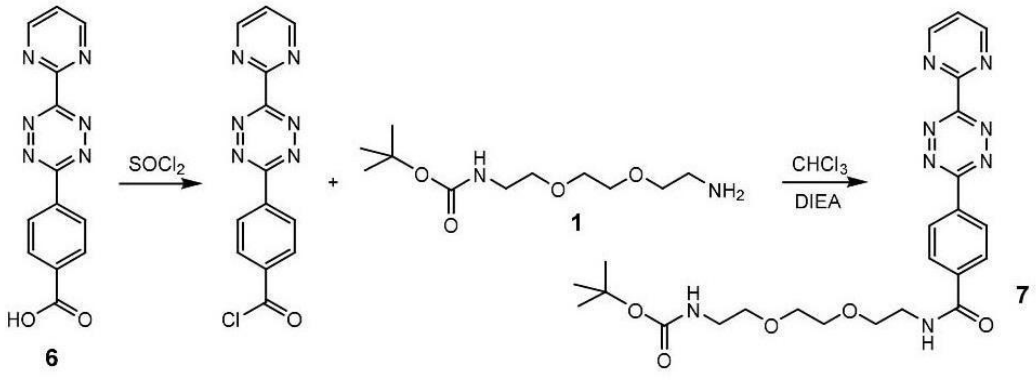

0.62 g (2.08 mmol) of compound **6** were suspended in 10 mL thionyl chloride and 10 drops of DMF were added. The setup was equipped with a dry pipe filled with $MgSO_4$. The mixture was stirred for three hours at 90°C. Afterwards the mixture was allowed to cool to ambient temperature and the excess of thionyl chloride was removed *in vacuo*.

The residue was dissolved in 100 mL chloroform and 1.445 mL (1.072 g, 8.3 mmol) *N*,*N*'-diisopropylethylamine (DIEA) were added. The mixture was cooled to 0°C. 1.031 g

(4.16 mmol) of compound **1** were dissolved in 10 mL chloroform and the solution was added drop-wise. The setup was equipped with a dry pipe filled with $MgSO_4$ and the mixture was stirred overnight at ambient temperature. The reaction mixture was washed five times with each 30 mL deionized water and the organic phase was dried over $MgSO_4$. After removing the solvent the purple residue was purified by flash column chromatography using the solvent mixture EtOH:DCM 1:9 (*v*:*v*) (R_f=0.44). 0.452 g purple solid were obtained (yield: 42.6%).

^{1}H-NMR (500 MHz, $CDCl_3$) δ: 1.35 (s, 9H), 3.25 (d, *J*=4.2 Hz, 2H), 3.50 (s, 2H), 3.59 (s, 2H), 3.60 (s, 2H), 3.66 (s, 4H), 4.94 (s, 1H), 6.94 (s, 1H), 7.54 (t, *J*=4.9 Hz, 1H), 7.99 (d, *J*=9.4 Hz, 2H), 8.73 (d, *J*=5.0 Hz, 2H), 9.07 (d, *J*=4.8 Hz, 2H).

^{13}C-NMR (125 MHz, $CDCl_3$) δ: 28.40, 39.97, 40.28, 70.34, 122.58, 128.05, 128.92, 133.88, 138.79, 158.45, 159.46, 163.18, 164.04, 166.51.

ESI-MS calc. for $C_{24}H_{30}N_8O_5$ m/z: 510.24 meas. 511.45 $[M+H]^+$.

1.2.8 Synthesis of compound 8

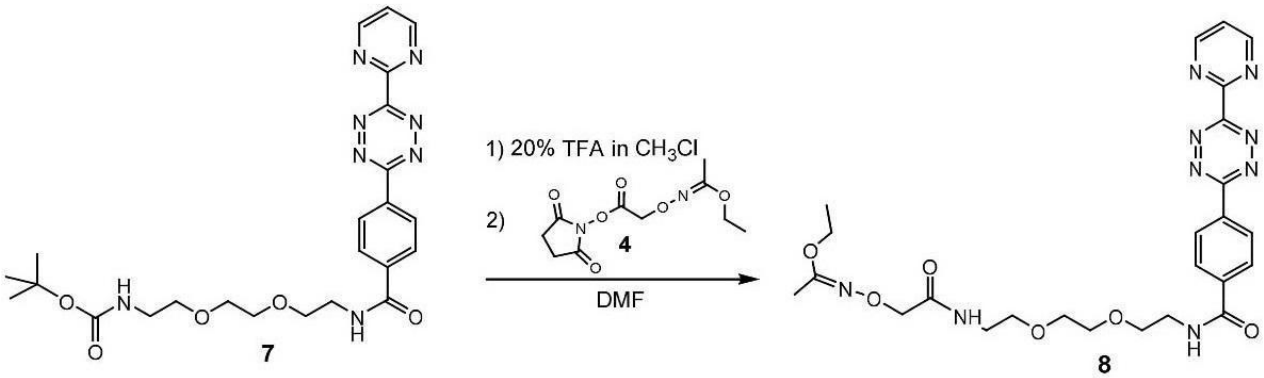

0.452 g (0.885 mmol) of compound **7** were dissolved in 5 mL 20% TFA (*v*:*v*) in chloroform. After two hours at ambient temperature, complete deprotection of compound **7** was confirmed by thin-layer chromatography (TLC). The solvent was removed and a purple oil containing residual TFA was obtained. To remove remaining TFA, the oil was dissolved in a mixture of methanol and cyclohexane and the solvent was removed *in vacuo*. After several steps, the remaining oil was dissolved in water and dried by lyophilization. The purple solid was dissolved in 60 mL DMF and 0.462 mL (0.343 g, 2.66 mmol) DIEA were added. 0.457 g (1.77 mmol) of compound **4** were dissolved in 10 mL DMF and were added drop-wise to the mixture. After complete addition, the mixture was stirred for additional three hours at ambient temperature. The solvent was removed in high vacuum and the excess of DIEA was removed thoroughly. The remaining purple oil was dissolved in 70 mL deionized water and the aqueous phase was extracted twice with each 30 mL chloroform. The solvent was removed and 0.584 g of a purple solid were obtained which was purified by flash column chromatography using the solvent mixture DCM:MeOH (9.5:1 (*v*:*v*)) (R_f=0.59). 0.302 g of yellow solid were obtained (yield: 61.2%).

^{1}H-NMR (500 MHz, $CDCl_3$) δ: 1.18 (t, *J*=7.2 Hz, 3H), 1.90 (s, 3H), 3.44 (q, *J*=5.0 Hz, 2H), 3.53 (t, *J*=5.0 Hz, 2H), 3.59 (m, 4H), 3.65 (m, 4H), 3.89 (q, *J*=7.2 Hz, 2H), 4.28 (s, 2H), 6.64 (s, 1H), 6.99 (s, 1H), 7.54 (t, *J*=4.8 Hz, 1H), 8.00 (d, *J*=8.5 Hz, 2H), 8.74 (d, *J*=8.5 Hz, 2H), 9.08 (d, *J*=4.8 Hz, 2H)

^{13}C-NMR (125 MHz, $CDCl_3$) δ: 13.85, 14.28, 38.59, 39.97, 62.69, 69.80, 69.91, 70.24, 70.36, 72.85, 122.60, 128.07, 128.91, 133.88, 138.74, 158.45, 159.44, 163.19, 164.02, 166.51, 170.50.

RP-HPLC, 10→100% B, t_R=12.62 min.

ESI-MS calc. for $C_{25}H_{31}N_9O_6$ m/z: 553.25 meas. 554.46 $[M+H]^+$.

Deprotection of compound **8** towards **8a**:

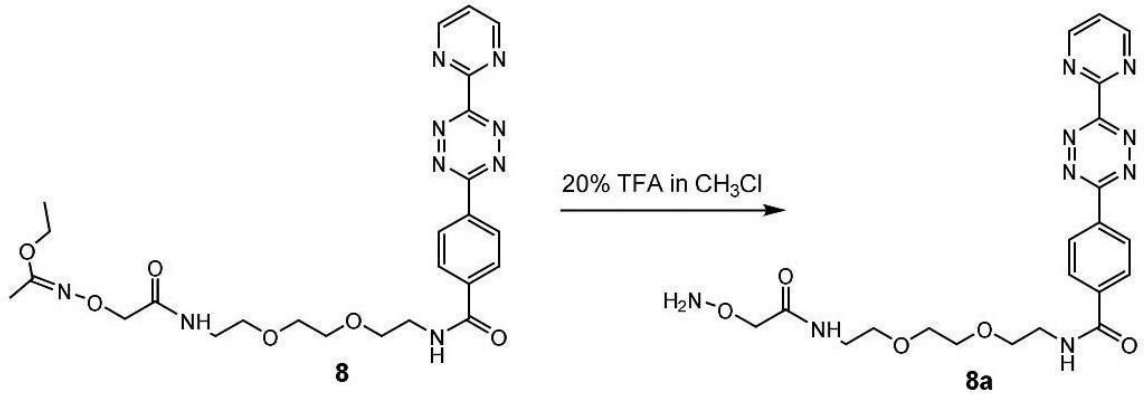

For deprotection of compound **8** it was dissolved in 20% (*v*:*v*) TFA in chloroform and stirred for 120 min at ambient temperature (the deprotected compound forms a second phase). The solvent was removed and residual TFA removed by dissolving the purple oil in water followed by lyophilization.

RP-HPLC, 10→100% B, t_R=9.11 min.

ESI-MS calc. for $C_{21}H_{25}N_9O_5$ m/z: 483.20 meas. 484.45 $[M+H]^+$.

1.2.9 Microwave-assisted solid-phase peptide synthesis (SPPS) of peptides 9-14

Microwave-assisted Fmoc-SPPS was performed on a CEM *liberty*® peptide synthesizer equipped with a CEM *discover*® SPS microwave (CEM GmbH) using DMF as solvent. As solid supports 2-chlorotrityl resin from Iris Biotech GmbH (peptides **9**, **10**, **12**, and **13**) and AmphiSphere™ 40 RAM resin from Varian Inc. (peptides **11** and **14**) were used. Triple coupling of the amino acids and double deprotection was performed upon microwave assistance. For all amino acids except arginine, coupling was performed at 30 W and 50°C for 15 min. Coupling of arginine was performed at ambient temperature for 60 min. Deprotection was performed at 30 W at 50°C for 5 min). Each amino acid was attached using 4 eq. of the respective Fmoc-protected amino acid, 3.9 eq. of *O*-(benzotriazol-1-yl)-*N,N,N',N'*-tetramethyluronium hexafluorophosphate (HBTU) (*Iris Biotech* GmbH), and 8 eq. base (DIEA for all amino acids except cysteine; for coupling of Fmoc-S-trityl-L-cysteine, collidine (*Sigma-Aldrich*) was used).

1.2.10 Peptide cleavage and workup

All peptides were cleaved from the resin using 92% (*v*:*v*) trifluoroacetic acid (TFA), 2% (*v*:*v*) H_2O, 4% (*v*:*v*) triethylsilane (TES), and 2% (*v*:*v*) anisole. In case of cysteine-containing

peptides, a spatula tip of dithiothreitol (DTT) was added to the cleavage cocktail. After shaking 2 h at room temperature, the solution was filtered and injected into ice-cold diethyl ether. The mixture was cooled down to -20°C for one hour and the precipitate was separated by centrifugation. The supernatant was discharged and the precipitate resuspended in ice-cold diethyl ether. The procedure was repeated additionally two times and the precipitate was dried in a desiccator. The obtained solid was dissolved in 10% (*v*:*v*) aqueous MeCN and the solvent was removed by lyophilization resulting in a fluffy consistency of the solid.

1.2.11 Oxidation of *N*-terminal serine residues

Cysteine-free crude products were oxidized using 10 eq. of sodium periodate in PBS buffer for 10 min. The reaction product was isolated by RP-HPLC using a Varian 940-LC equipped with a YMC Europe GmbH C_{18} column (250 × 20mm; S- 4 µm, 8 nm). Thereby, aldehyde-bearing peptides **9**, **12**, and **13** were obtained. For the synthesis of aldehyde-bearing folded peptides **10**, **11** and **14**, oxidative folding was followed by the above-described periodate oxidation procedure and by RP-HPLC purification.[4,5] The structures of all synthesized peptides are given in scheme ESI-2.

Scheme ESI-1: *Mechanism of periodate oxidation of N-terminal serine residues.*

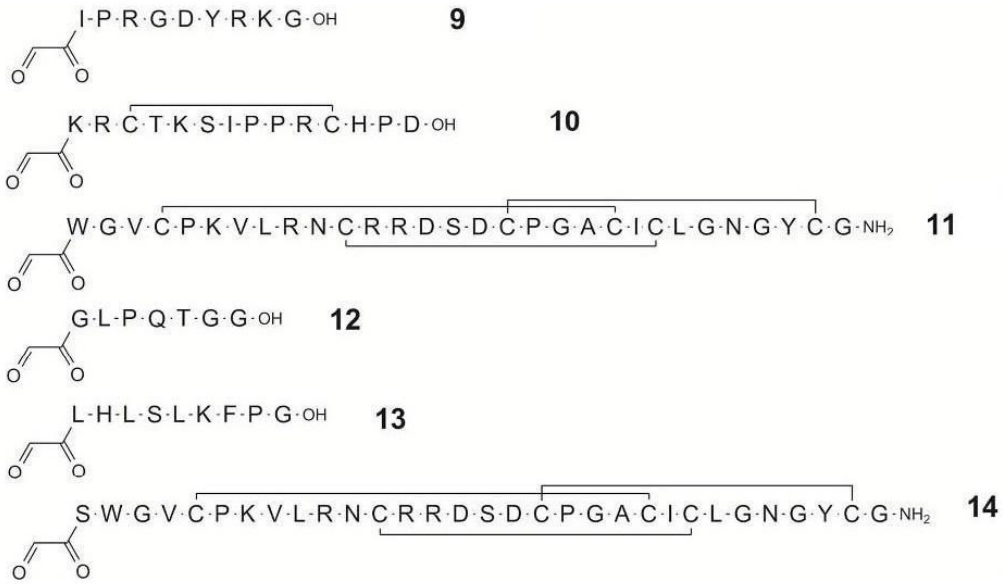

Scheme ESI-2: *Bioactive peptides **9-14** equipped with aldehyde functionality.*

Table ESI-1: *Analytical data of compounds **9-14**.*

Compound	HPLC gradient	t_R [min]	Formula and calculated molar mass	ESI-MS measured	Yield
9	10→100 B	13.22	$C_{48}H_{76}N_{16}O_{15}$ 1116.57	1117.8 $[M+H]^+$, 559.5 $[M+2H]^{2+}$, 373.2 $[M+3H]^{3+}$.	43%

10	10→100 B	11.54	$C_{70}H_{114}N_{24}O_{21}S_2$ 1690.80	846.9 $[M+2H]^{2+}$, 571.0 $[M+3H+H_2O]^{3+}$, 428.5 $[M+4H+H_2O]^{4+}$.	12.5%
11	10→100 B	14.27	$C_{134}H_{206}N_{44}O_{40}S_6$ 3263.38	1642.89 $[M+2H+H_2O]^{2+}$, 1095.57 $[M+3H+H_2O]^{3+}$, 821.86 $[M+4H+H_2O]^{4+}$.	16.3%
12	10→100 B	10.76	$C_{28}H_{45}N_9O_{11}$ 683.32	684.4 $[M+H]^{+}$, 702.4 $[M+H+H_2O]^{+}$.	32%
13	10→100 B	15.06	$C_{51}H_{78}N_{12}O_{13}$ 1066.58	1085.87 $[M+H+H_2O]^{+}$, 543.55 $[M+2H+H_2O]^{2+}$.	23.8%
14	10→100 B	13.56	$C_{137}H_{211}N_{45}O_{42}S_6$ 3350.41	1686.39 $[M+2H+H_2O]^{2+}$, 1124.67 $[M+3H+H_2O]^{3+}$, 843.76 $[M+4H+H_2O]^{4+}$.	18.1%

1.2.12 General procedure for oxime ligation of inverse electron-demand Diels-Alder building blocks 5 and 8 to peptides 9-14

Each 1 eq. of the aldehyde-bearing peptides **9-14** and varying equivalents of the aminooxy-bearing inverse electron-demand Diels-Alder building blocks **5** and **8** were mixed in 50% (*v*:*v*) aq. TFA and the mixture was shaken overnight at ambient temperature. The TFA was removed under reduced pressure and the aqueous solution was purified by semi-preparative HPLC. Reaction details are listed in table ESI-1 and table ESI-2. The structures of peptides **15-20** equipped with inverse electron-demand Diels-Alder functional groups are shown in scheme ESI-3.

Table ESI-2: *reaction details of the synthesis of bioactive peptides* ***15-17*** *equipped with inverse electron-demand Diels-Alder functionality.*

Synthesis of:	Peptide no.	# mg peptide	# mmol peptide	# equiv. of **8**	# mg of **8**	# mmol of **8**	Yield [mg]	Yield [%]
15	9	2.0	0.0018	5.0	5.0	0.0090	1.4	49.4
16	10	10.0	0.0059	5.0	16.4	0.0030	1.7	13.3
17	11	13.0	0.0040	5.0	10.9	0.0198	2.0	13.6

Table ESI-3: *reaction details of the synthesis of bioactive peptides* ***18-20*** *equipped with inverse-electron-demand Diels-Alder functionality.*

Synthesis of	Peptide no.	# mg peptide	# mmol peptide	# equiv. of **5**	# mg of **5**	# mmol of **5**	Yield [mg]	Yield [%]
18	12	19.0	0.0278	1.2	15.4	0.0334	3.0	10.1
19	13	10.0	0.0092	1.2	5.1	0.0110	1.4	10.3
20	14	8.0	0.0024	1.5	1.7	0.0036	0.8	8.9

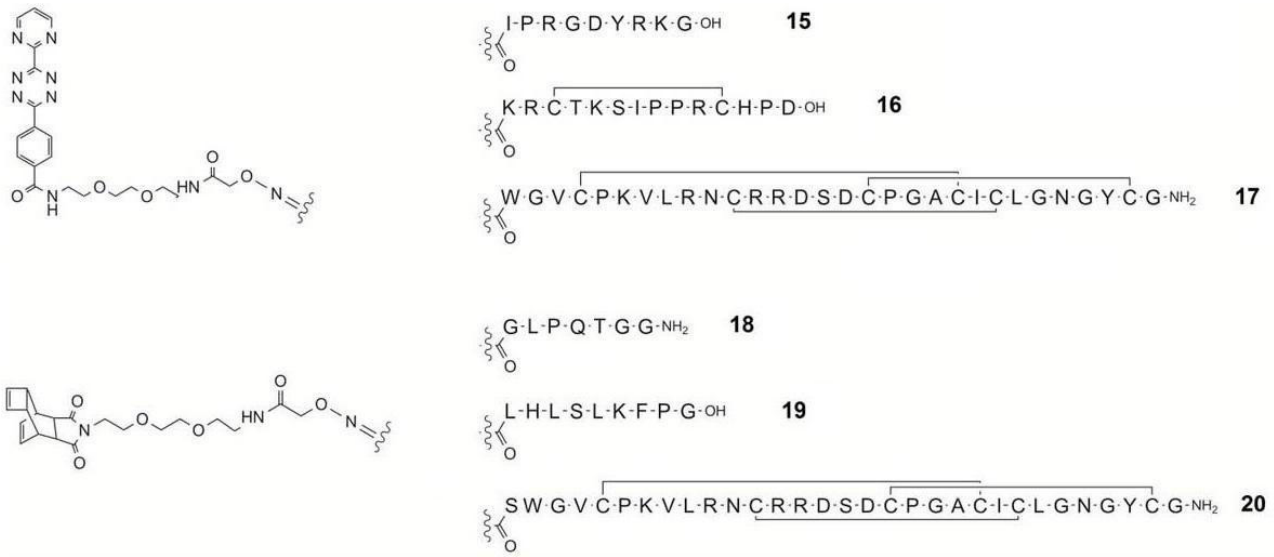

Scheme ESI-3: *Inverse electron-demand Diels-Alder building blocks grafted to diverse bioactive peptides.*

Table ESI-4: *Analytical data of compounds* ***15-20****.*

Compound	HPLC gradient	t_R [min]	Formula and mass calculated	MS type	MS measured
15	10→100 B	12.98	$C_{69}H_{99}N_{25}O_{19}$ 1581.7549	ESI-HR-MS	791.8851 $[M+2H]^{2+}$, 528.2598 $[M+3H]^{3+}$.
16	10→100 B	12.20	$C_{91}H_{137}N_{33}O_{25}S_2$ 2155.9905	ESI-HR-MS	1079.0016 $[M+2H]^{2+}$, 719.6713 $[M+3H]^{3+}$ 540.0067 $[M+4H]^{4+}$.
17	10→100 B	14.67	$C_{155}H_{229}N_{53}O_{44}S_6$ 3728.5635	ESI-HR-MS	1243.8574 $[M+3H]^{3+}$, 933.1459 $[M+4H]^{4+}$.
18	10→100 B	14.78	$C_{48}H_{70}N_{12}O_{16}$ 1070.5033	ESI-HR-MS	1071.5077 $[M+H]^{+}$, 1093.4910 $[M+Na]^{+}$, 536.2598 $[M+2H]^{2+}$, 547.2502 $[M+H+Na]^{2+}$.
19	10→100 B	16.72	$C_{71}H_{103}N_{15}O_{18}$ 1453.7606	ESI-HR-MS	1454.7668 $[M+H]^{+}$, 727.8883 $[M+2H]^{2+}$.
20	10→100 B	15.07	$C_{157}H_{236}N_{48}O_{47}S_6$ 3737.5877	ESI-HR-MS	1246.8713 $[M+3H]^{3+}$, 935.4055 $[M+4H]^{4+}$.

1.2.13 Synthesis of compound 30

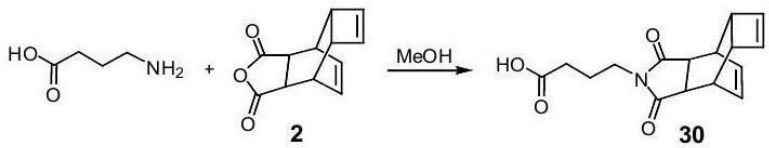

0.51 g (4.94 mmol) 4-aminobutyric acid and 0.5 g (2.47 mmol) of compound **2** were suspended in 10 mL methanol. The mixture was stirred for two hours at 100°C. After cooling down to ambient temperature, the solvent was removed *in vacuo*. The colorless solid was

purified by flash column chromatography by using a solvent mixture of toluene and methanol in a ratio of 9:1 (*v*:*v*) (R_f=0.43). 472.1 mg of a colorless solid were obtained (yield: 66.6%).

^{1}H-NMR (300 MHz, DMSO-d_6) δ: 1.60 (q, *J*=7.1 Hz, 2H), 2.13 (t, *J*=7.5 Hz, 2H), 2.80 (s, 2H), 2.85 (s, 2H), 2.98 (s, 2H), 3.31 (t, *J*=6.7 Hz, 2H), 5.80 (d, *J* =4.5 Hz, 2H), 5.88 (d, *J* =4.5 Hz, 2H).

^{13}C-NMR (75 MHz, DMSO-d_6) δ: 22.61, 30.80, 36.21, 37.06, 42.62, 43.58, 128.03, 137.93, 173.73, 178.50.

1.2.14 Synthesis of compound 31

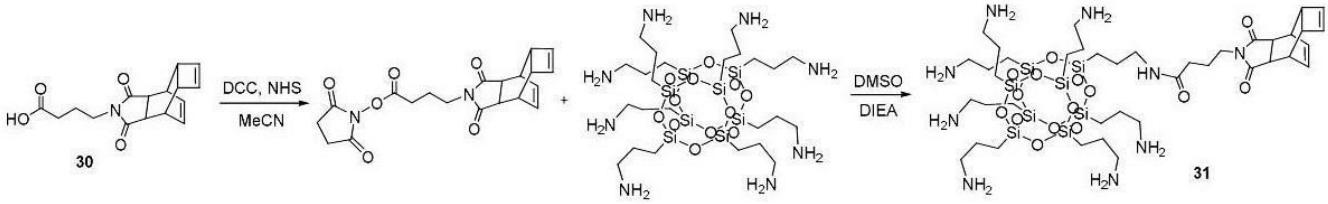

0.1 g (0.348 mmol) of compound **30** were dissolved in 5 mL dry acetonitrile and the solution was cooled to 0°C. 0.121 mL (0.09 g, 0.696 mmol) DIEA were added to the cooled solution. 0.093 g (0.452 mmol) dicyclohexylcarbodiimide (DCC) and 0.06 g (0.522 mmol) *N*-hydroxysuccinimide (NHS) were dissolved in 3 mL acetonitrile and were added drop-wise to the cooled solution. After complete addition, the mixture was stirred for one hour on ice and afterwards stirred at ambient temperature overnight. The colorless precipitate was separated by filtration. The solvent was removed *in vacuo* and the colorless solid dissolved in 40 mL dry DMSO. 1.225 g (1.044 mmol) of octammonium POSS (Hybrid Plastics) were dissolved in 10 mL dry DMSO. To this vigorously stirred solution, activated compound **30** was added drop-wise at ambient temperature and after complete addition, the mixture was stirred overnight. The solvent was removed by lyophilization and the colorless oil was purified by semi-preparative RP-HPLC (gradient: 10→100). The solvent was removed by lyophilization and 0.113 g of a white solid were obtained (yield: 28.3%).

RP-HPLC, 10→100% B, t_R=12.64 min.

ESI-HR-MS calc. for $C_{40}H_{79}N_9O_{15}Si_8$ 1149.3850 meas. 575.7000 $[M+3H]^{3+}$, 384.1356 $[M+4H]^{4+}$.

1.2.15 General procedure for inverse electron-demand Diels-Alder reactions of peptides 15-20

Inverse electron-demand Diels-Alder functional groups grafted peptides **15** to **20** were dissolved in 10% aq. acetonitrile containing 0.1% TFA at a concentration of 10 mg/mL (*w*:*v*). Equimolar amounts were mixed according to table ESI-5 and were shaken at ambient temperature overnight. The reaction is schematically shown in scheme ESI-4. The reaction mixtures were analyzed by RP-HPLC and the turnover was determined by comparing the area of the absorption at 220 nm corresponding to the peptides **15** to **20** before and after the reaction. The HPLC-traces of the reactions are shown in figure ESI-1 and ESI-2. The

reaction products of the Diels-Alder reaction with inverse electron-demand (DAR_{inv}) reactions are shown in scheme ESI-5.

Table ESI-5: *Overview of the DAR_{inv} building block bearing bioactive peptides **15-20** and the formed reaction products **21-29**.*

		Peptides		
		15	**16**	**17**
Peptides	**18**	**21**	**24**	**27**
	19	**22**	**25**	**28**
	20	**23**	**26**	**29**

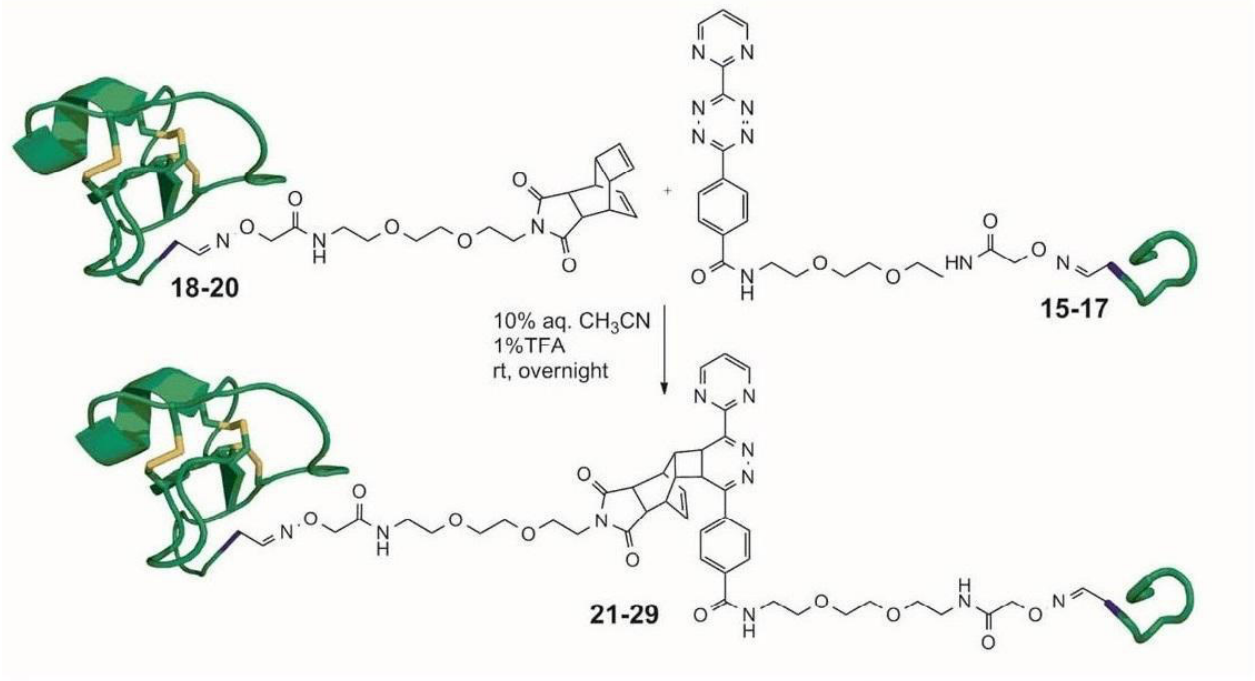

Scheme ESI-4: *DAR_{inv} reaction for the synthesis of heterodimers of bioactive peptides.*

In the frame of our proof-of-concept study, the products **21-29** were HPLC purified in the amounts required to perform the HR-MS analysis. As we did not plan further activity assays, the fractions from the analytical purification runs were collected and analyzed. Therefore no isolated yields but HPLC conversions are given (**Fig. 4B**).

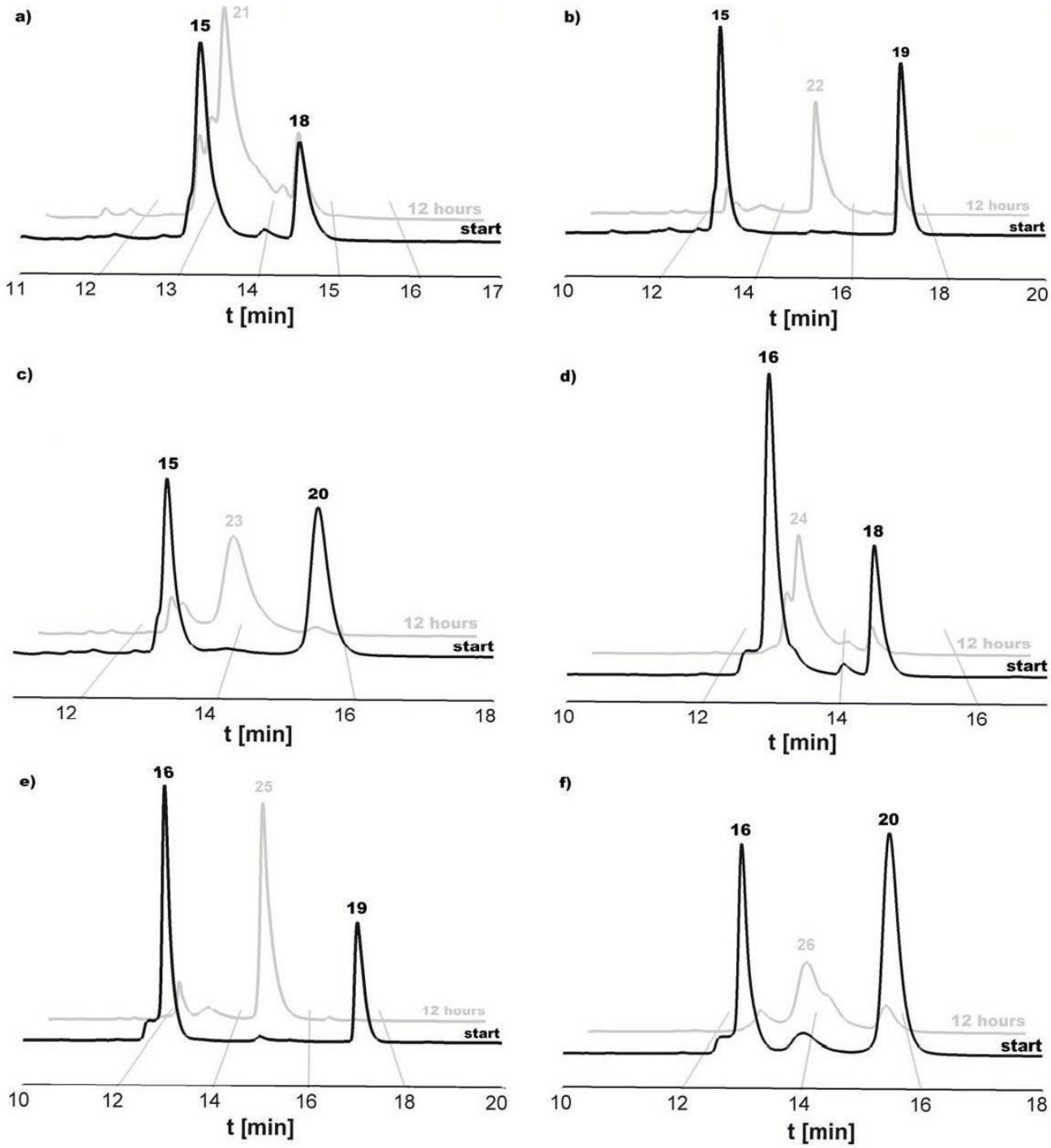

Figure ESI-1: *HPLC traces of DAR_{inv} reactions for generation of heterodimers comprising different bioactive peptides. The reaction mixtures were investigated at the beginning and after a reaction time of 12 hours. Absorbance at 220 nm. Reaction of: a)* ***15*** *and* ***18****; b)* ***15*** *and* ***19****; c)* ***15*** *and* ***20****; d)* ***16*** *and* ***18****; e)* ***16*** *and* ***19****; f)* ***16*** *and* ***20****.*

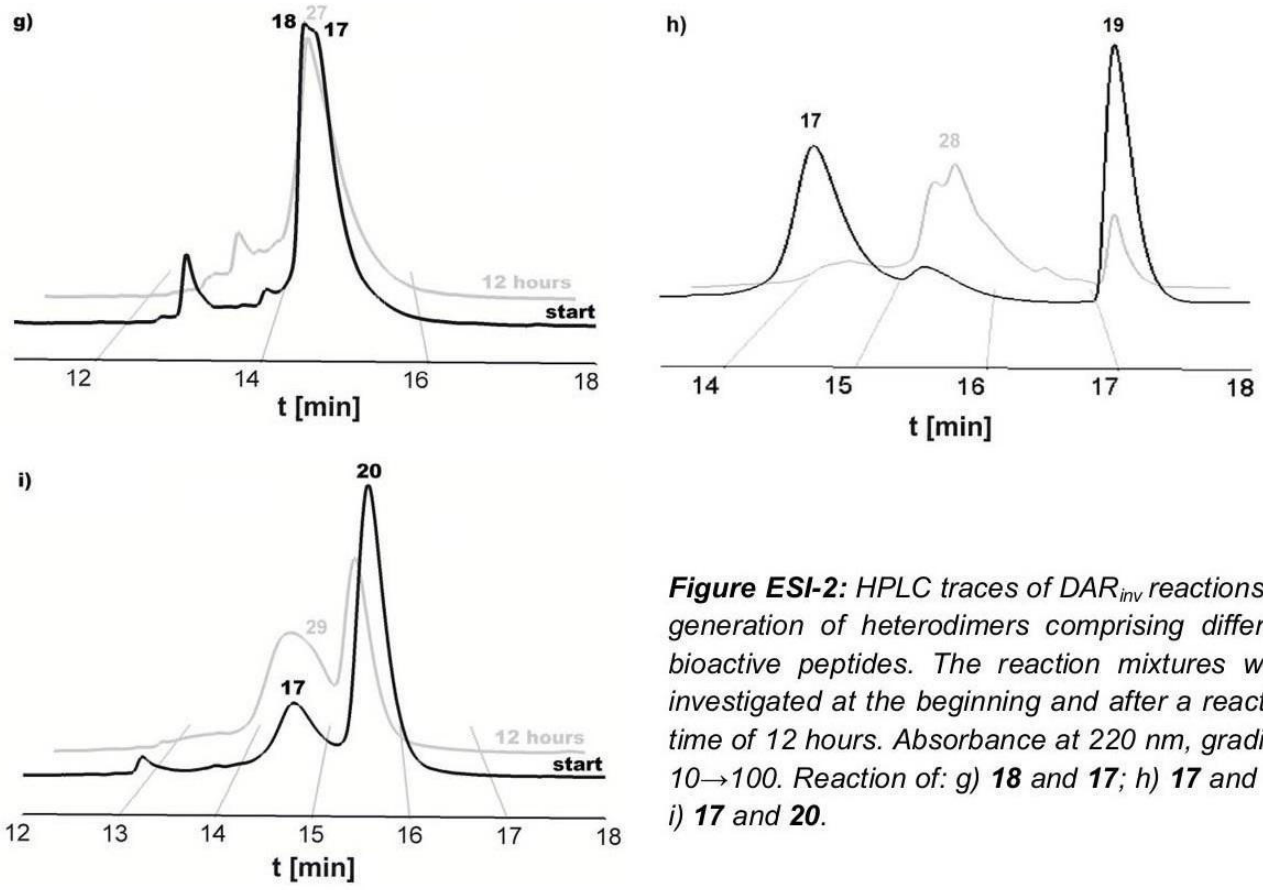

Figure ESI-2: *HPLC traces of DAR_{inv} reactions for generation of heterodimers comprising different bioactive peptides. The reaction mixtures were investigated at the beginning and after a reaction time of 12 hours. Absorbance at 220 nm, gradient 10→100. Reaction of: g)* ***18*** *and* ***17****; h)* ***17*** *and* ***19****; i)* ***17*** *and* ***20****.*

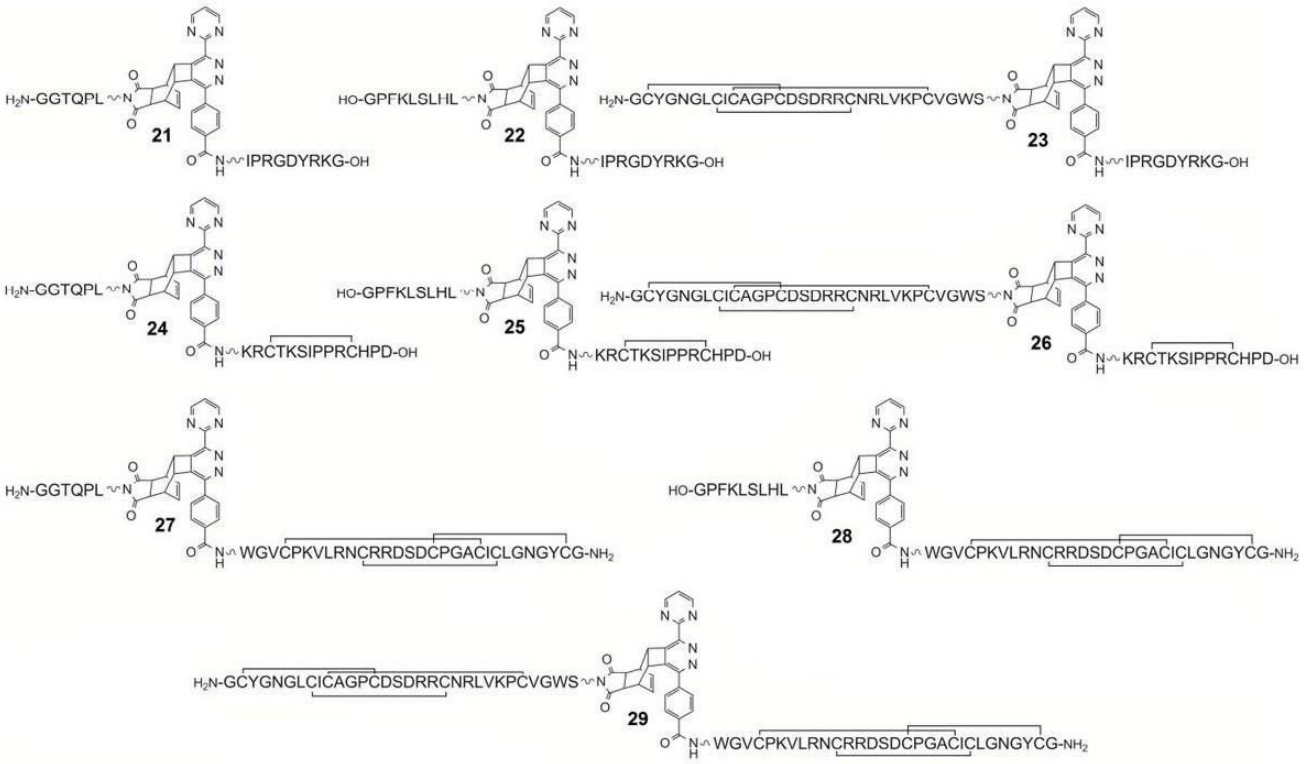

Scheme ESI-5*: Structures of DAR_{inv} conjugates* ***21-29****.*

Table ESI-6: *Mass spectrometric data of DAR_{inv} conjugates **21-29** and **32**.*

compound	Formula and calculated molar mass	MS method	MS measured
21	$C_{117}H_{167}N_{35}O_{35}$ 2622.2364	HR ESI	875.0857 $[M+3H]^{3+}$, 656.5662 $[M+3H]^{3+}$.
22	$C_{140}H_{200}N_{38}O_{37}$ 3005.4937	HR ESI	1002.8383 $[M+3H]^{3+}$, 752.3804 $[M+4H]^{4+}$, 602.1064 $[M+5H]^{5+}$.
23	$C_{226}H_{333}N_{71}O_{66}S_6$ 5289.3208	HR ESI	1058.8703 $[M+5H]^{5+}$, 882.5639 $[M+6H]^{6+}$.
24	$C_{139}H_{205}N_{43}O_{41}S_2$ 3196.4720	HR ESI	800.1251 $[M+4H]^{4+}$, 640.2998 $[M+5H]^{5+}$.
25	$C_{162}H_{238}N_{46}O_{43}S_2$ 3579.7292	HR ESI	1194.2505 $[M+3H]^{3+}$, 895.9390 $[M+4H]^{4+}$, 716.9526 $[M+5H]^{5+}$, 597.6290 $[M+6H]^{6+}$, 512.3984 $[M+7H]^{7+}$.
26	$C_{248}H_{371}N_{79}O_{72}S_8$ 5863.5564	HR ESI	978.2661 $[M+6H]^{6+}$, 838.6411 $[M+7H]^{7+}$, 733.9730 $[M+8H]^{8+}$.
27	$C_{203}H_{299}N_{63}O_{60}S_6$ 4771.0606	MALDI	4775.3 $[M+H]^{+}$.
28	$C_{226}H_{332}N_{66}O_{62}S_6$ 5154.3179	HR ESI	1031.6788 $[M+5H]^{5+}$, 860.0650 $[M+6H]^{6+}$.
29	$C_{312}H_{463}N_{99}O_{91}S_{12}$ 7436.1294	MALDI	7482.0 $[M+K]^{+}$.
32	$C_{131}H_{214}N_{40}O_{40}S_2Si_8$ 3275.3537	HR ESI	819.8464 $[M+4H]^{4+}$, 656.0783 $[M+5H]^{5+}$, 546.8998 $[M+6H]^{6+}$.

1.2.16 Inverse electron-demand Diels-Alder reaction for the synthesis of compound 32

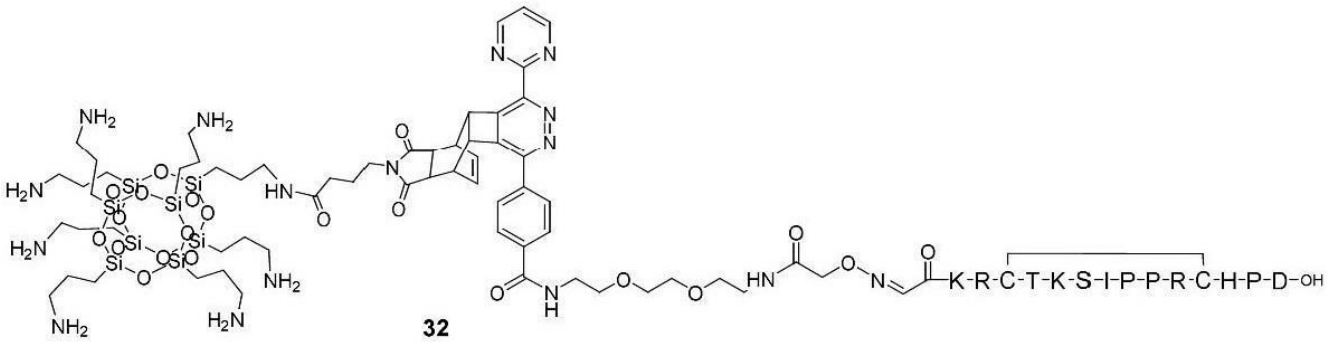

32

Compound **32** was synthesized using 1.0 mg of **31** (1 eq., 0.87 µmol) and 2.3 mg of **16** (1.2 eq., 1.044 µmol). Both compounds were dissolved in dry DMSO and reacted overnight at ambient temperature. The reaction completion was confirmed via LC-MS.

ESI-HR-MS calc. for $C_{131}H_{214}N_{40}O_{40}S_2Si_8$ 3275.3537 meas. 819.8464 $[M+4H]^{4+}$, 656.0783 $[M+5H]^{5+}$, 546.8998 $[M+6H]^{6+}$.

1.2 Analytical data

1.2.1 Compound 1

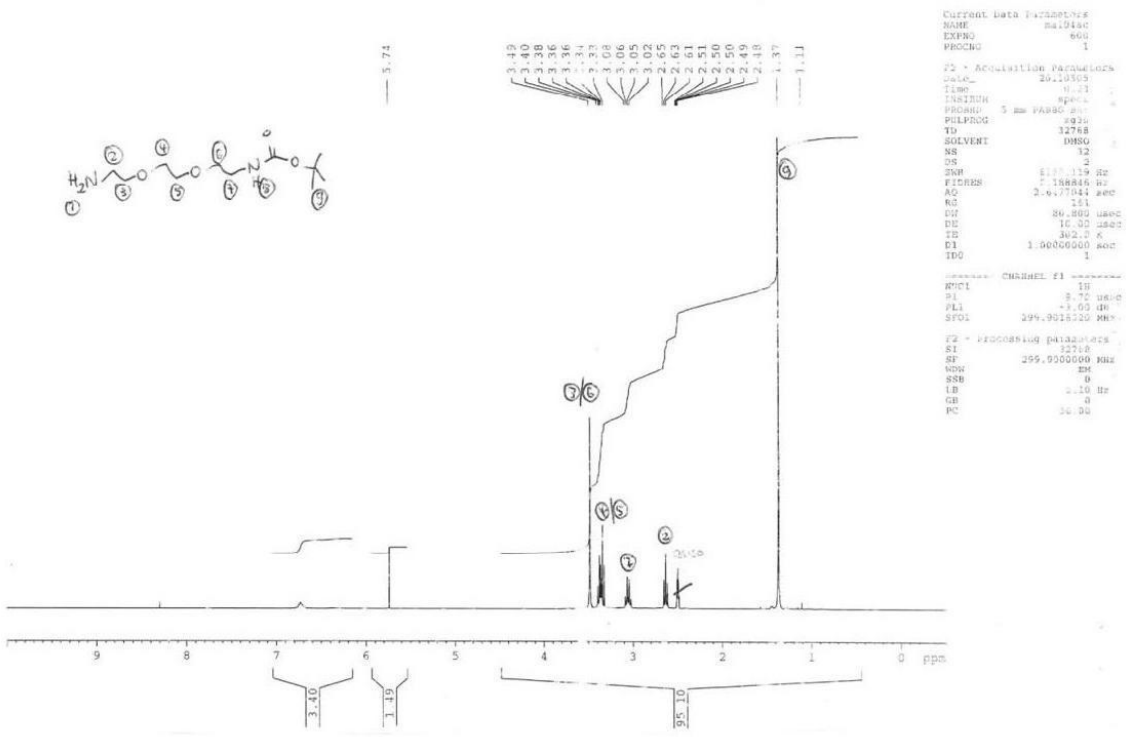

***Figure ESI-3**: [1]H-NMR spectrum of compound **1**.*

1.2.2 Compound 2

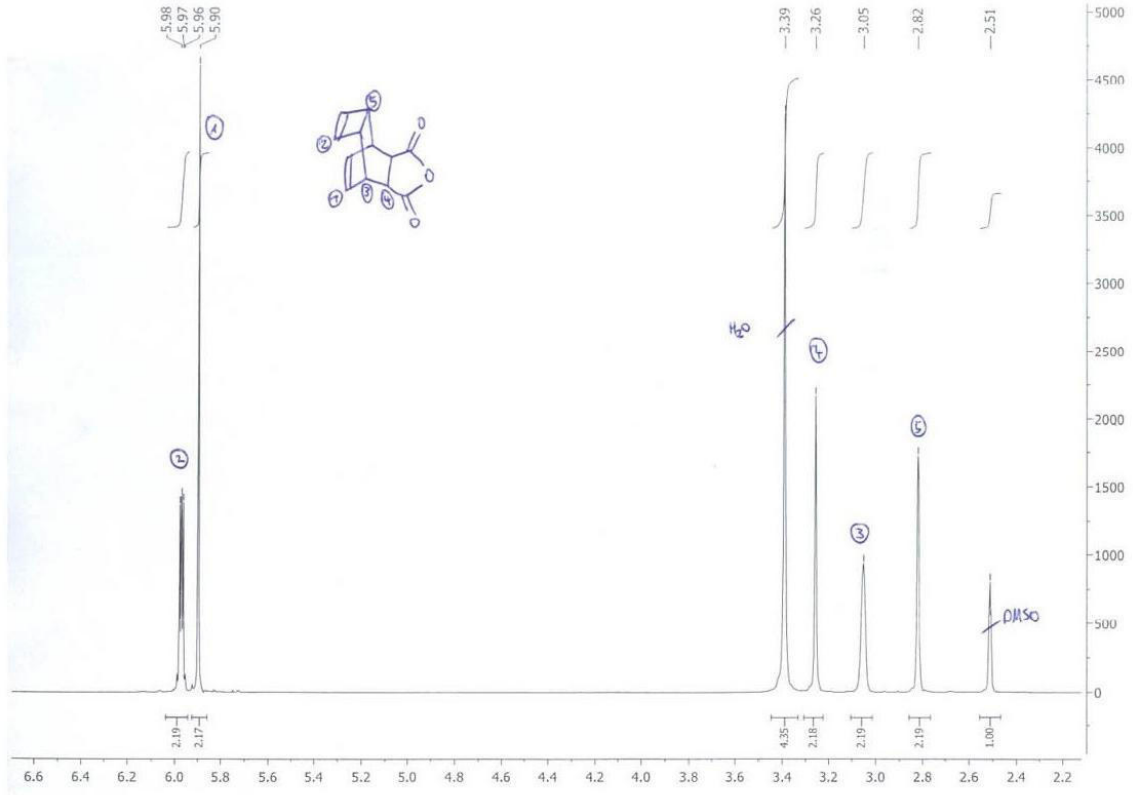

***Figure ESI-4:** [1]H-NMR spectrum of compound **2**.*

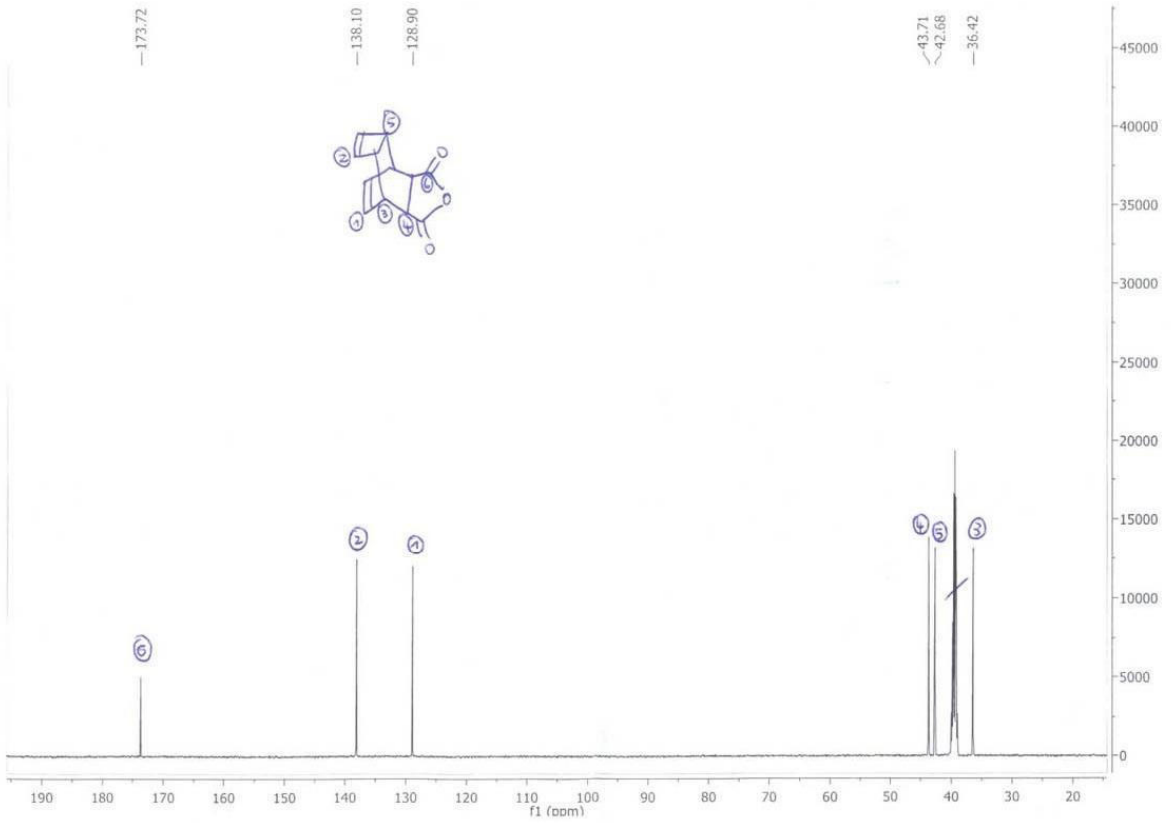

Figure ESI-5: *^{13}C-NMR spectrum of compound* ***2****.*

1.2.3 Compound 3

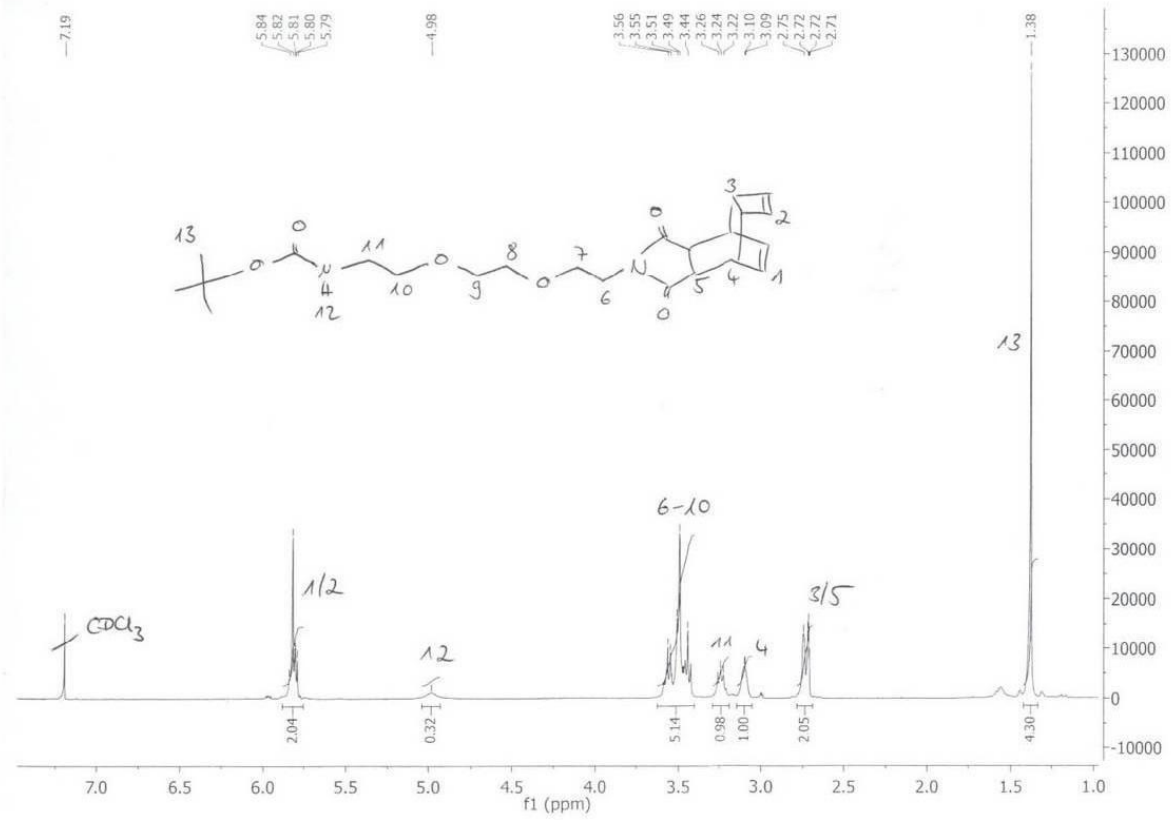

Figure ESI-6*: ^{1}H-NMR spectrum of compound* ***3****.*

1.2.4 Compound 4

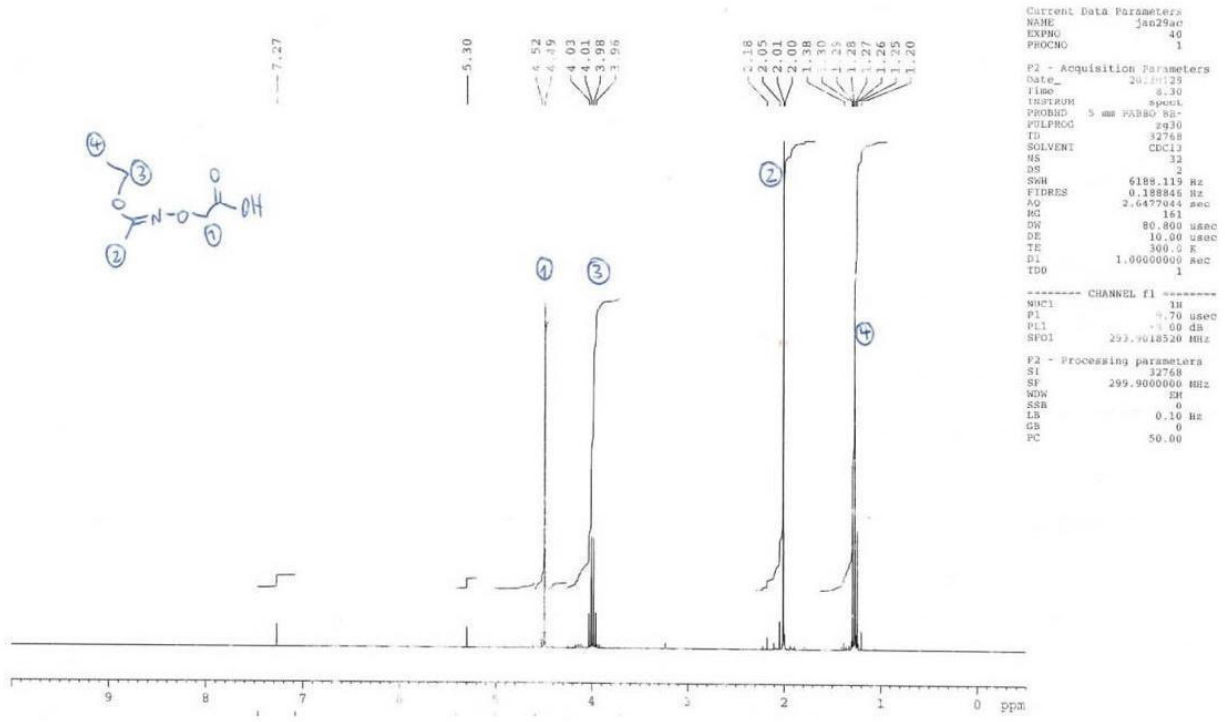

Figure ESI-7: *^{1}H-NMR spectrum of the precursor compound **4**.*

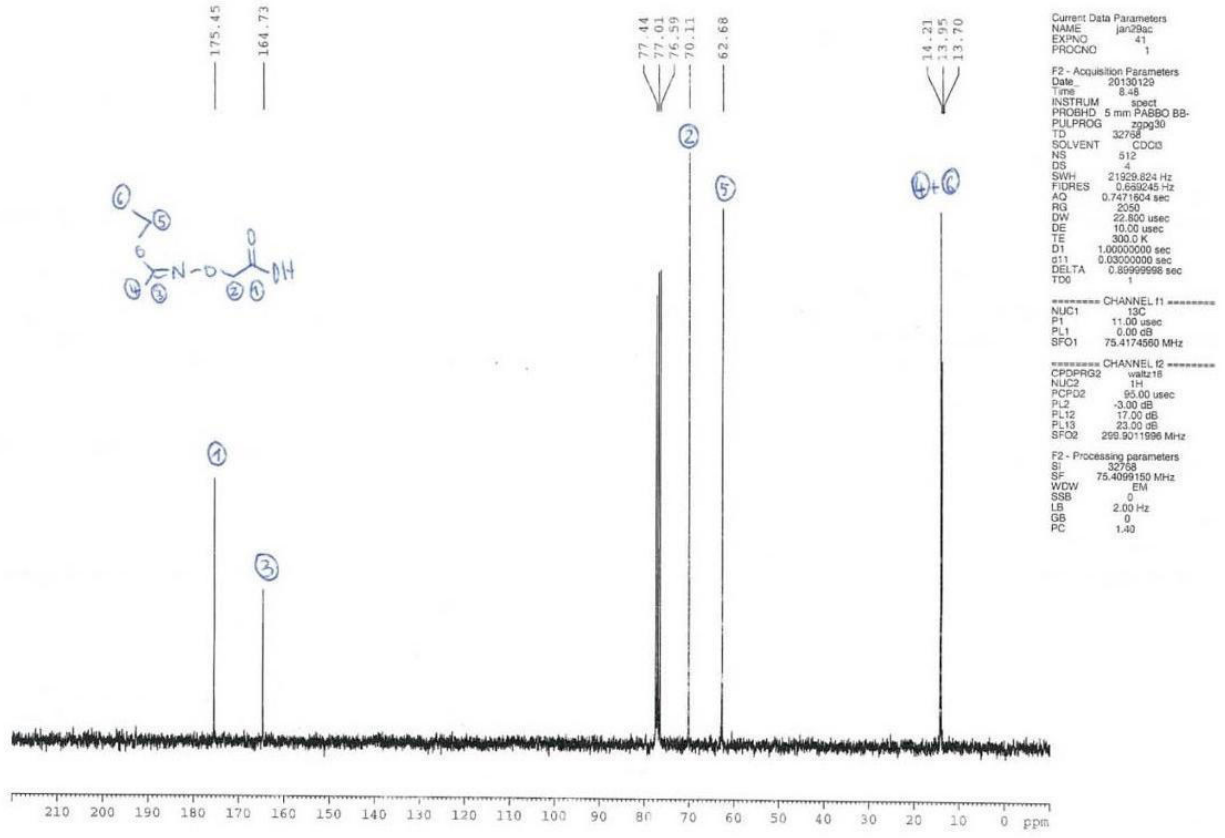

Figure ESI-8: *^{13}C-NMR spectrum of the precursor of compound **4**.*

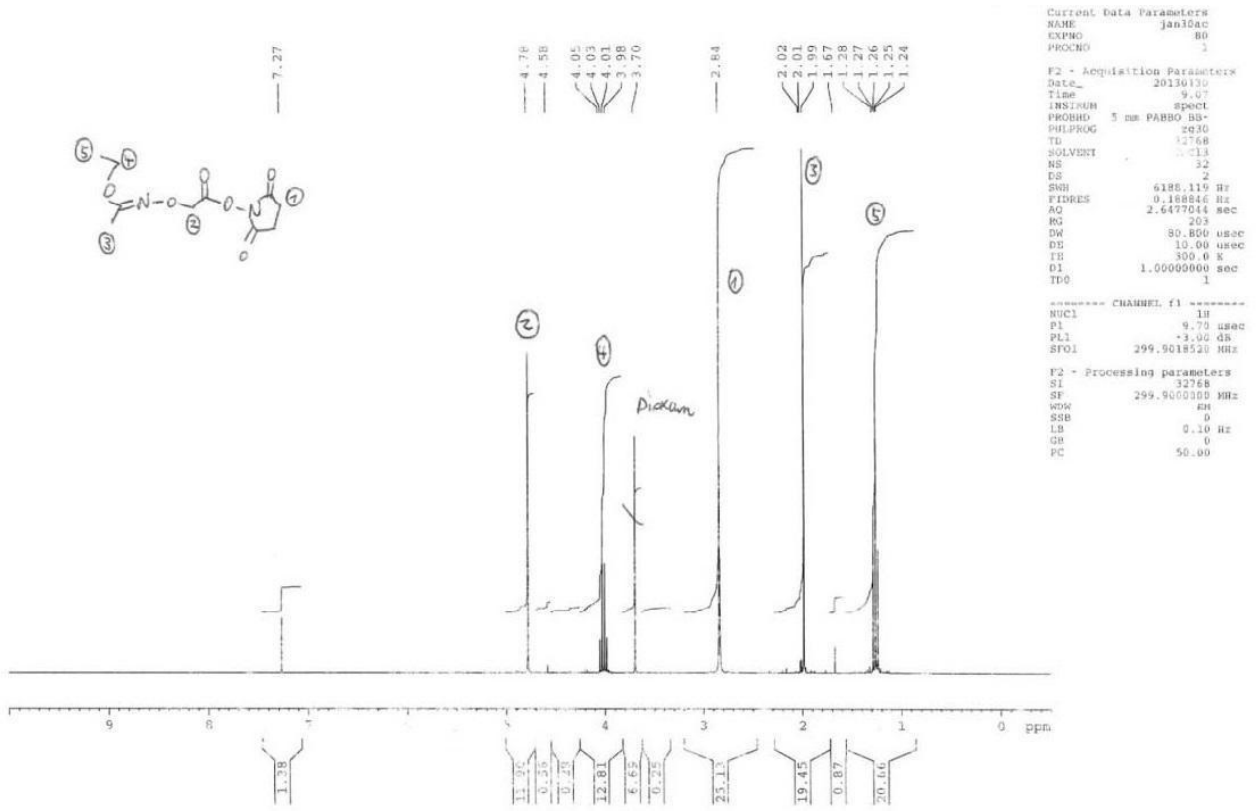

Figure ESI-9: *^{1}H-NMR spectrum of compound **4**.*

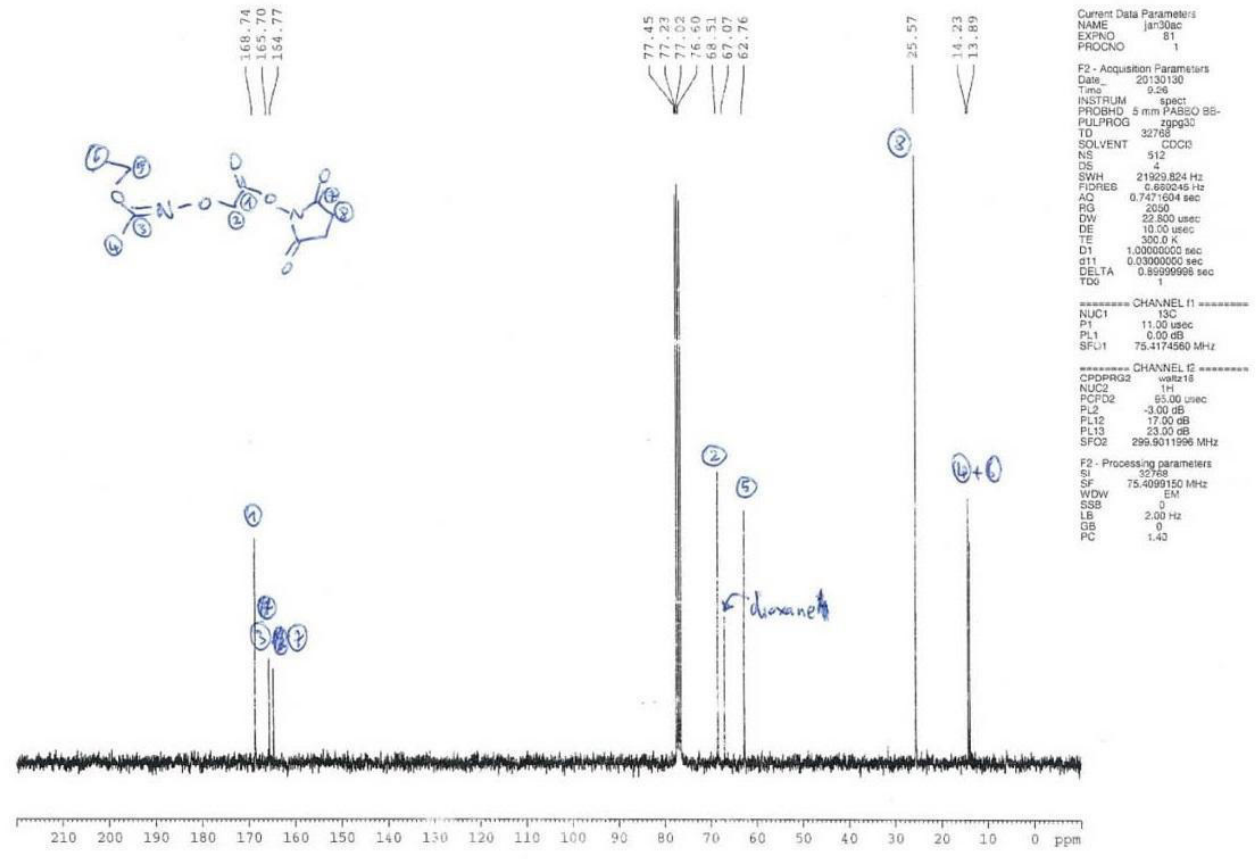

Figure ESI-10: *^{13}C-NMR spectrum of compound **4**.*

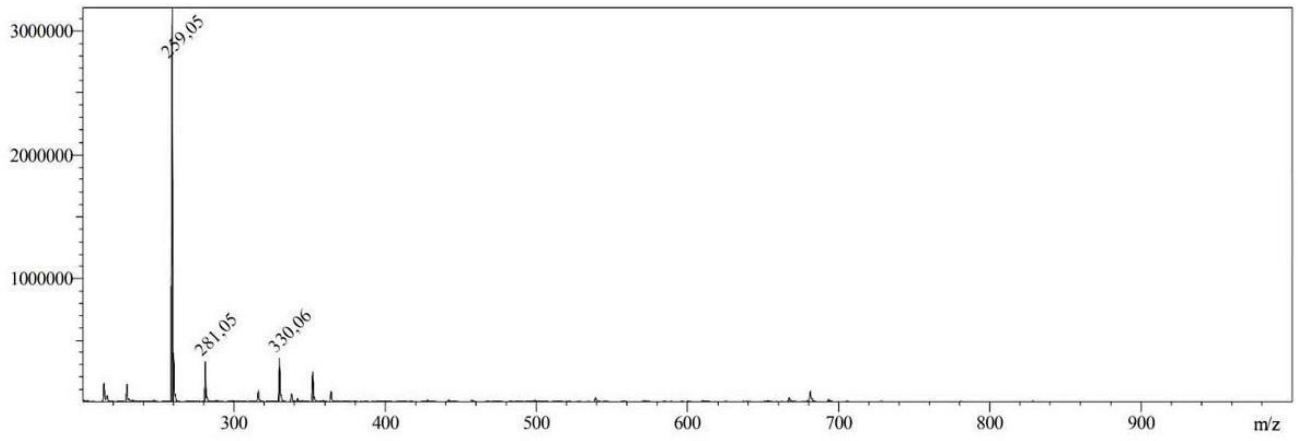

Figure ESI-11: *ESI-MS spectrum of compound* ***4****; calc. for* $C_{10}H_{14}N_2O_6$ *M: 258.09 m/z meas.: 259.05* $[M+H]^+$.

1.2.5 Compound 5

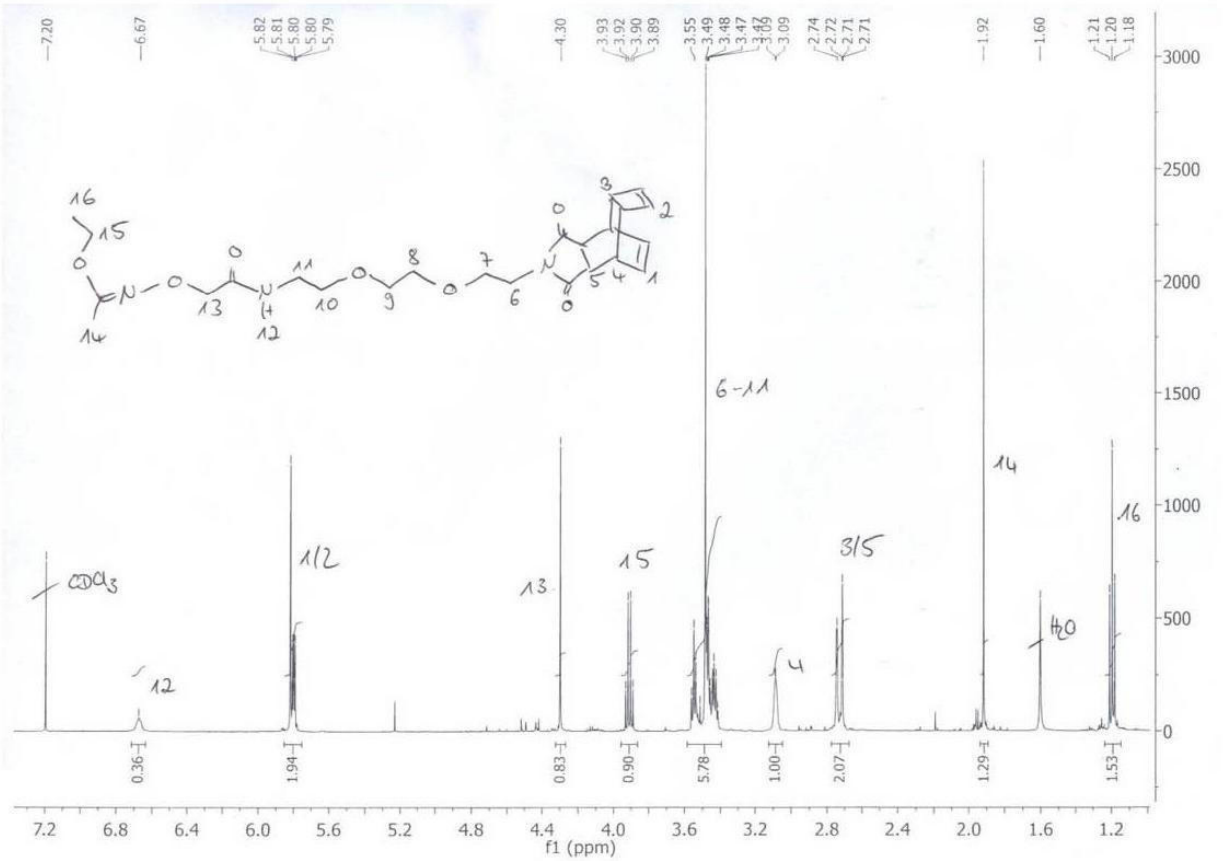

Figure ESI-12: *^{1}H-NMR spectrum of compound* ***5****.*

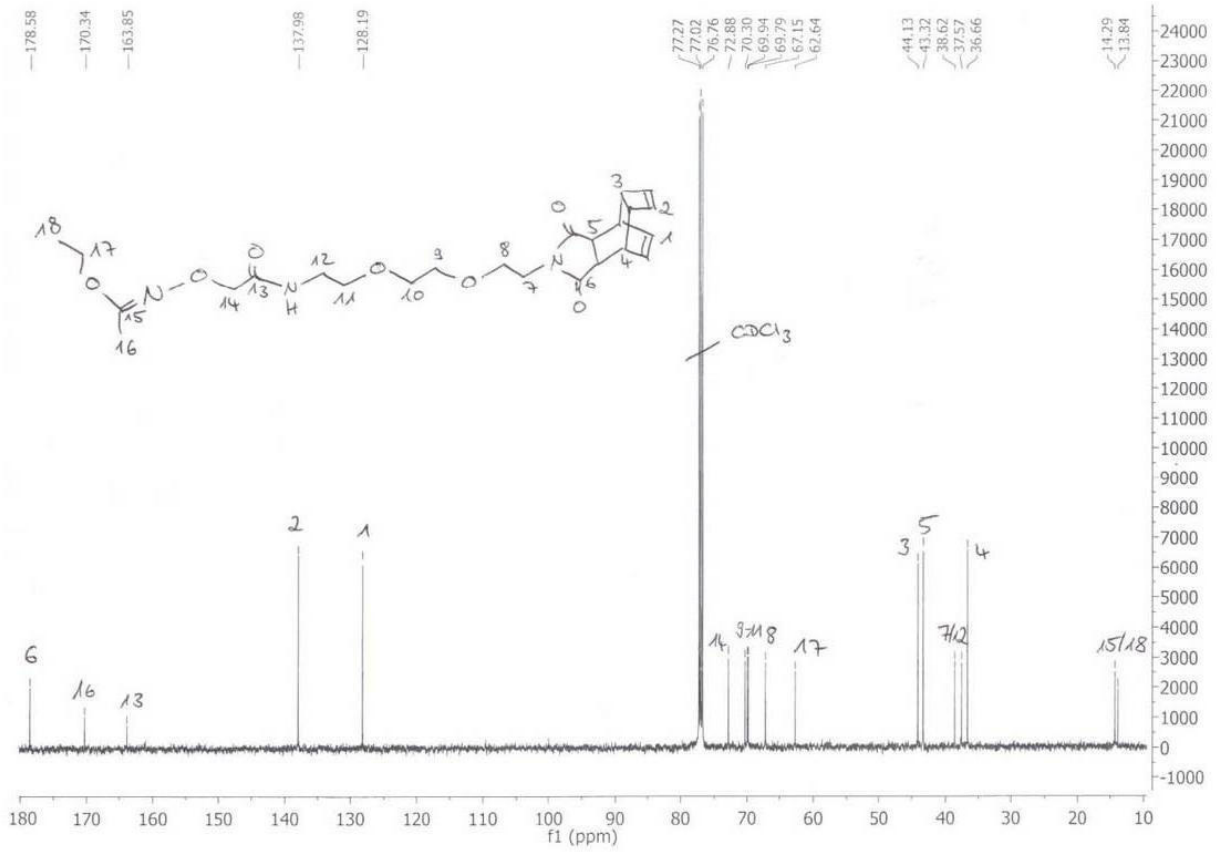

Figure ESI-13: *^{13}C-NMR spectrum of compound **5**.*

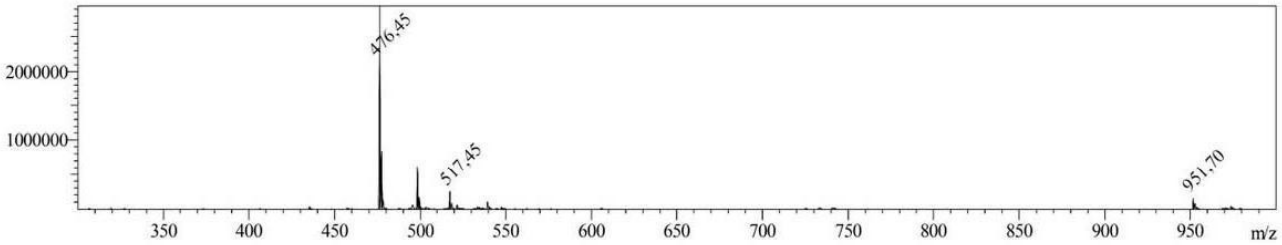

Figure ESI-14: *ESI-MS spectrum of compound **5**; calc. for $C_{24}H_{33}N_3O_7$ M: 475.24, m/z meas.: 476.45 $[M+H]^+$.*

1.2.6 Compound 6

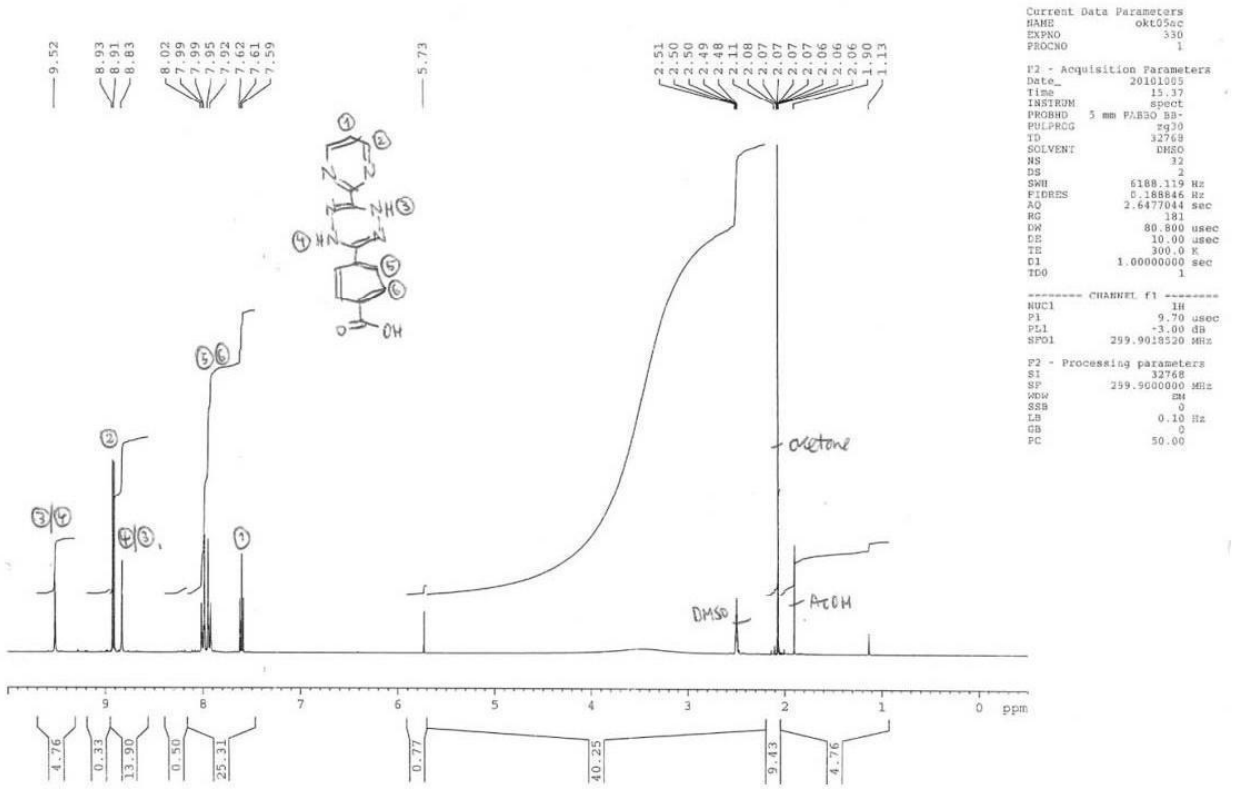

Figure ESI-15: *[1]H-NMR spectrum of the precursor of compound* ***6****.*

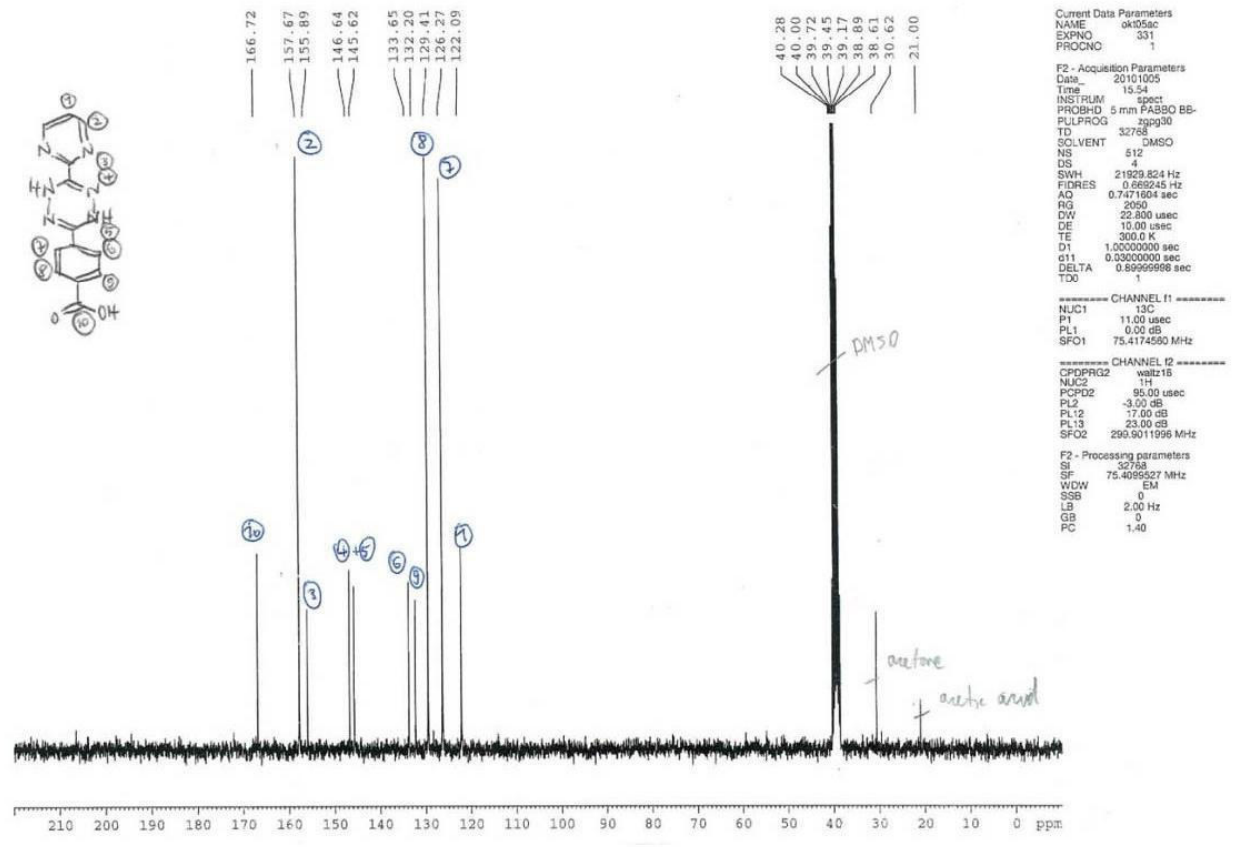

Figure ESI-16: *[13]C-NMR spectrum of the precursor of compound* ***6****.*

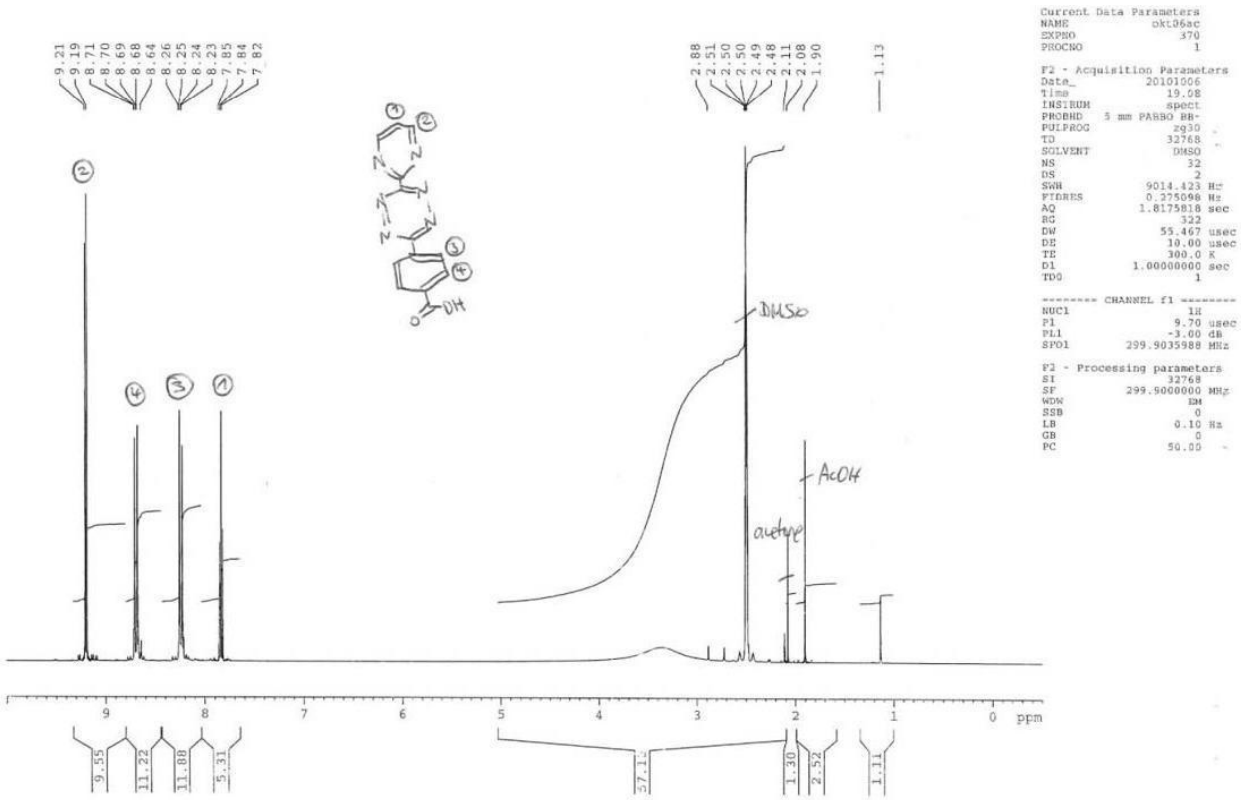

Figure ESI-17: *^{1}H-NMR spectrum of compound **6**.*

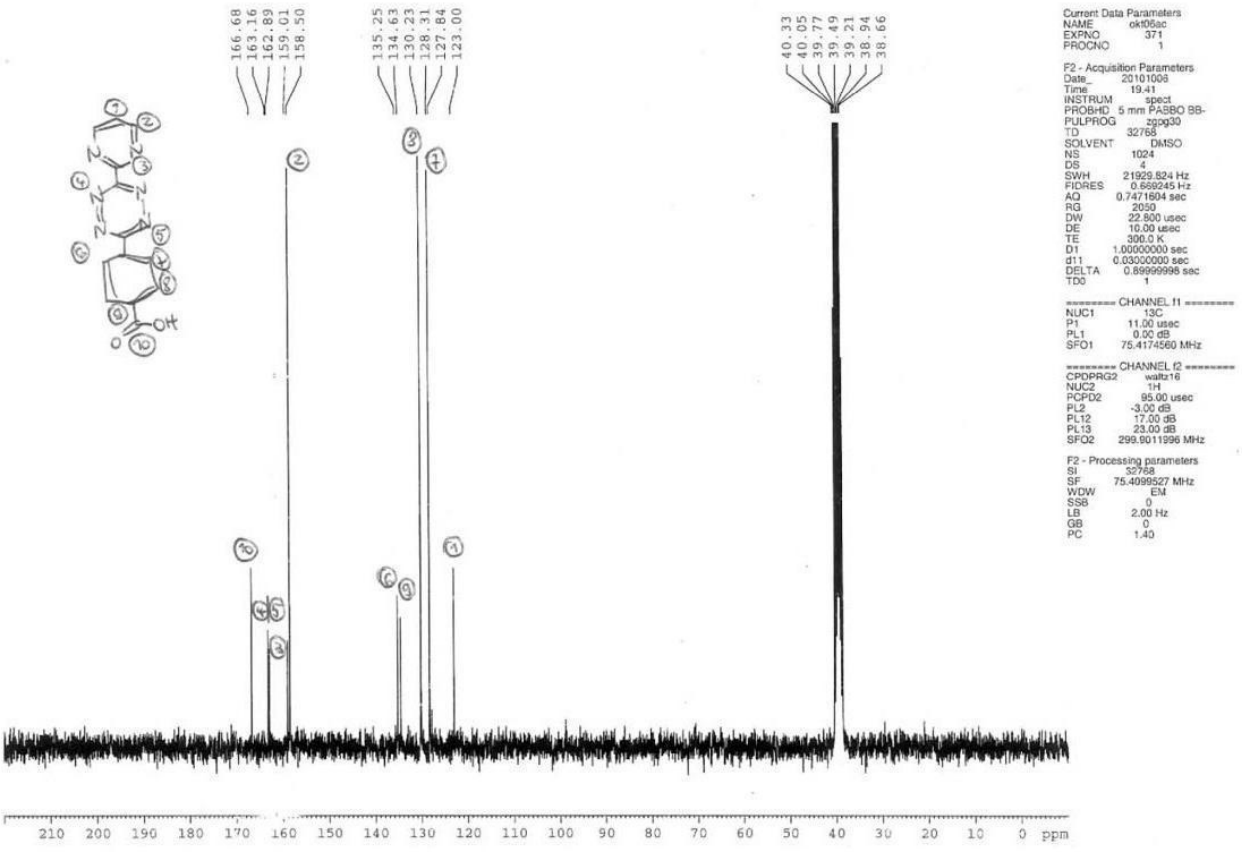

Figure ESI-18: *^{13}C-NMR spectrum of compound **6**.*

1.2.7 Compound 7

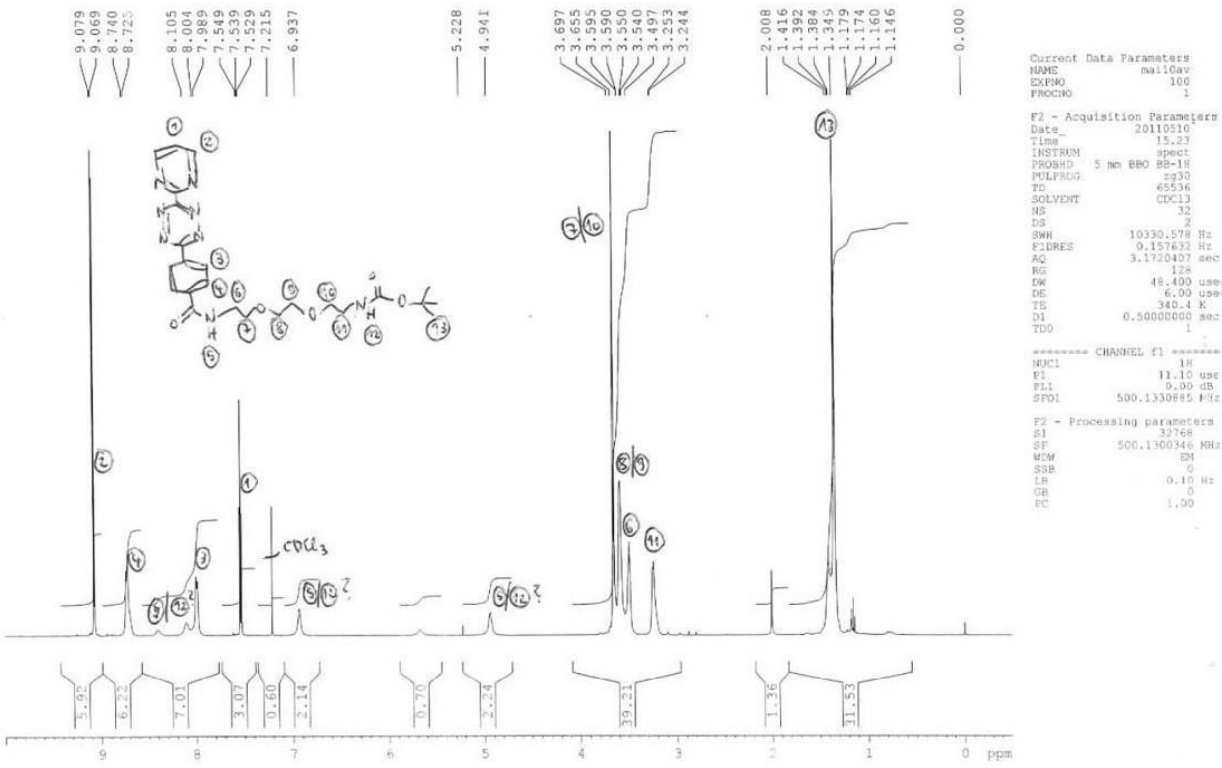

Figure ESI-19: *^{1}H-NMR spectrum of compound **7**.*

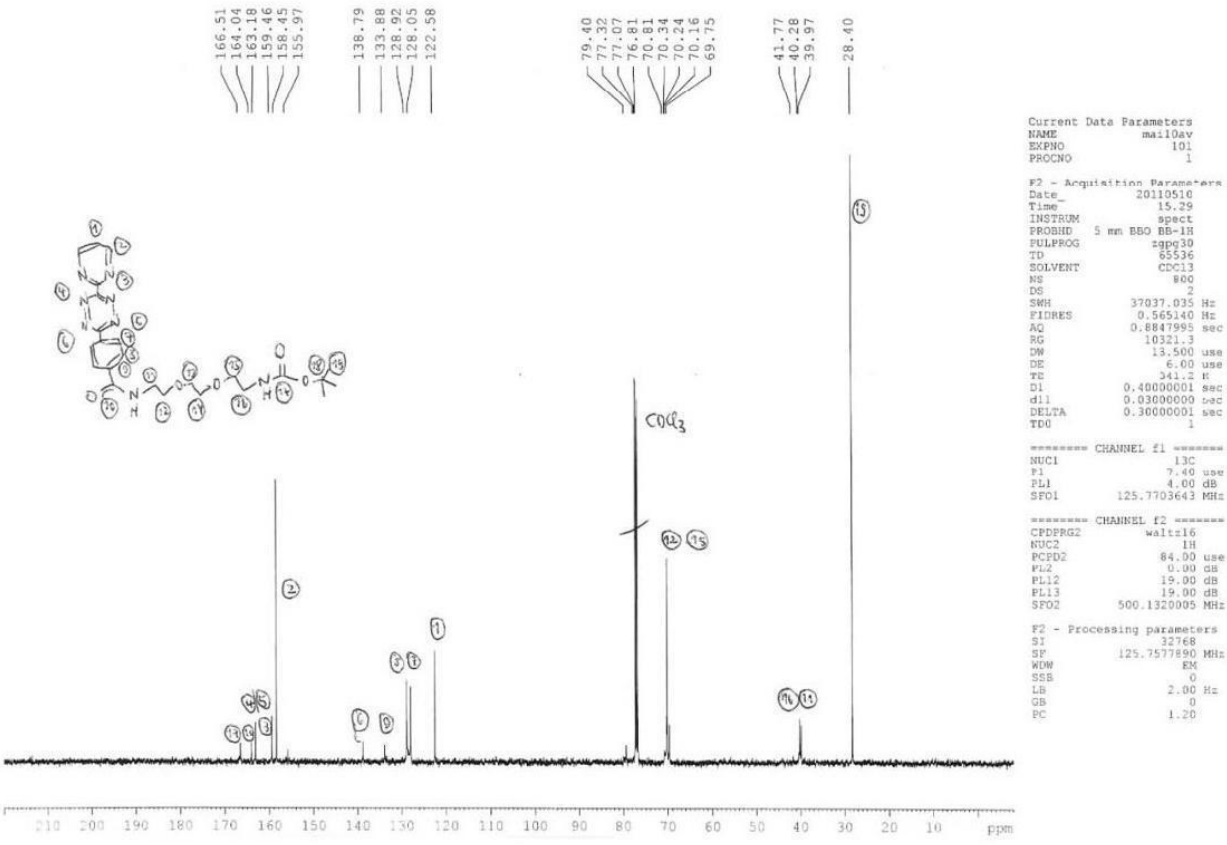

Figure ESI-20: *^{13}C-NMR spectrum of compound **7**.*

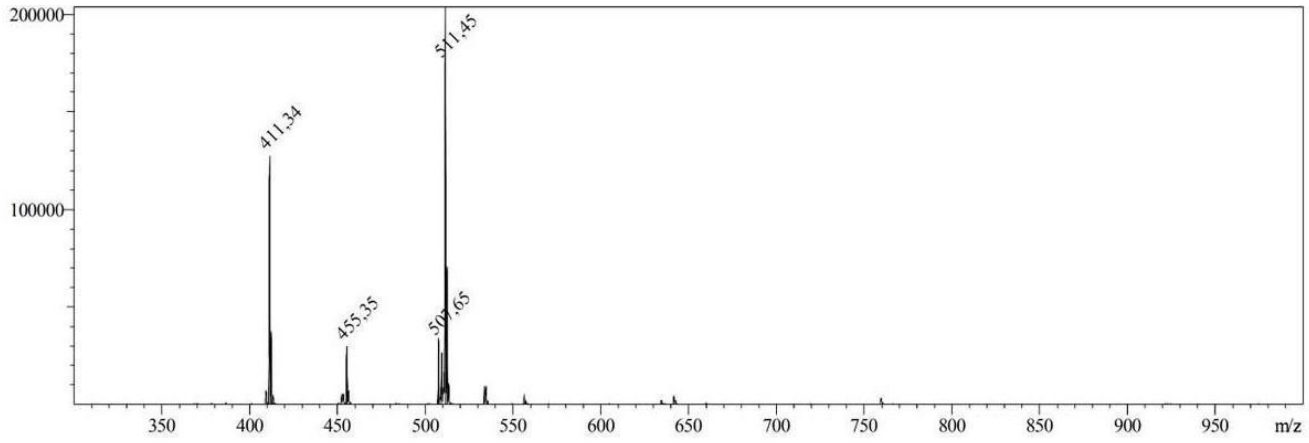

Figure ESI-21: *ESI-MS spectrum of compound* ***7****; calc. for* $C_{24}H_{30}N_8O_5$ *M: 510.24, m/z meas.: 511.45* $[M+H]^+$.

1.2.8 Compound 8

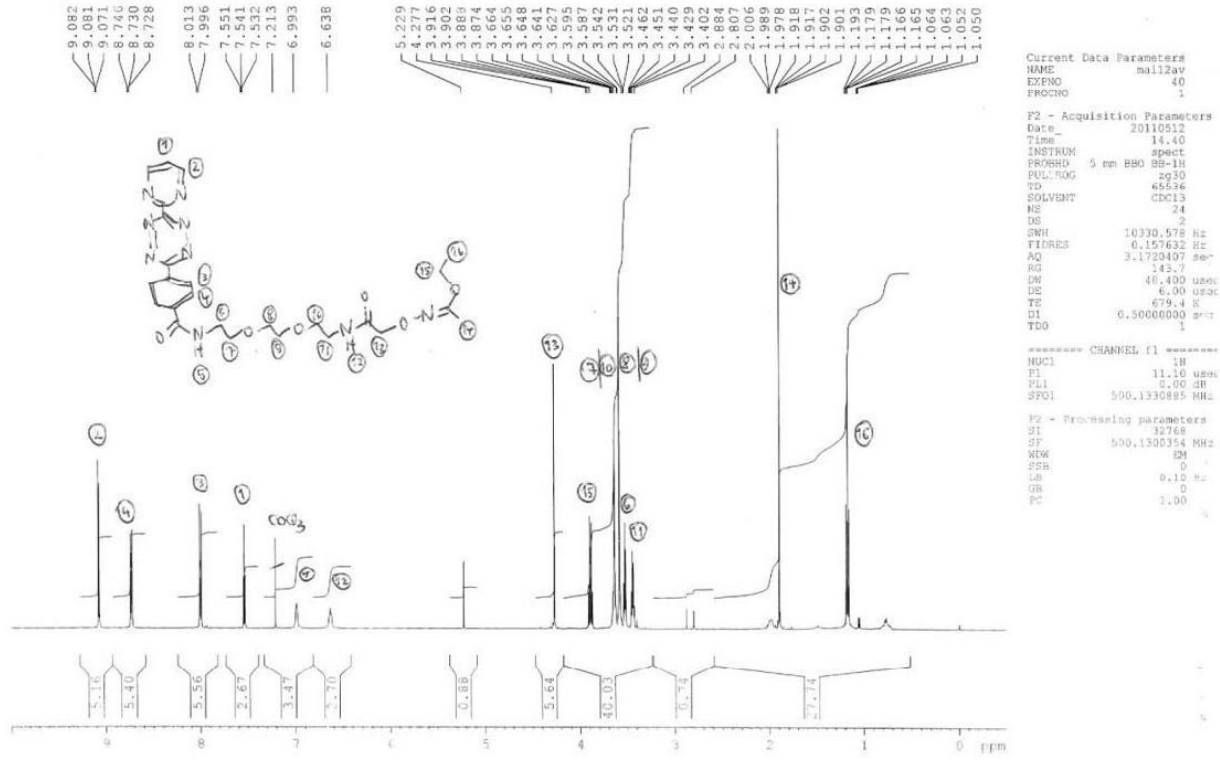

Figure ESI-22: *^{1}H-NMR spectrum of compound* ***8****.*

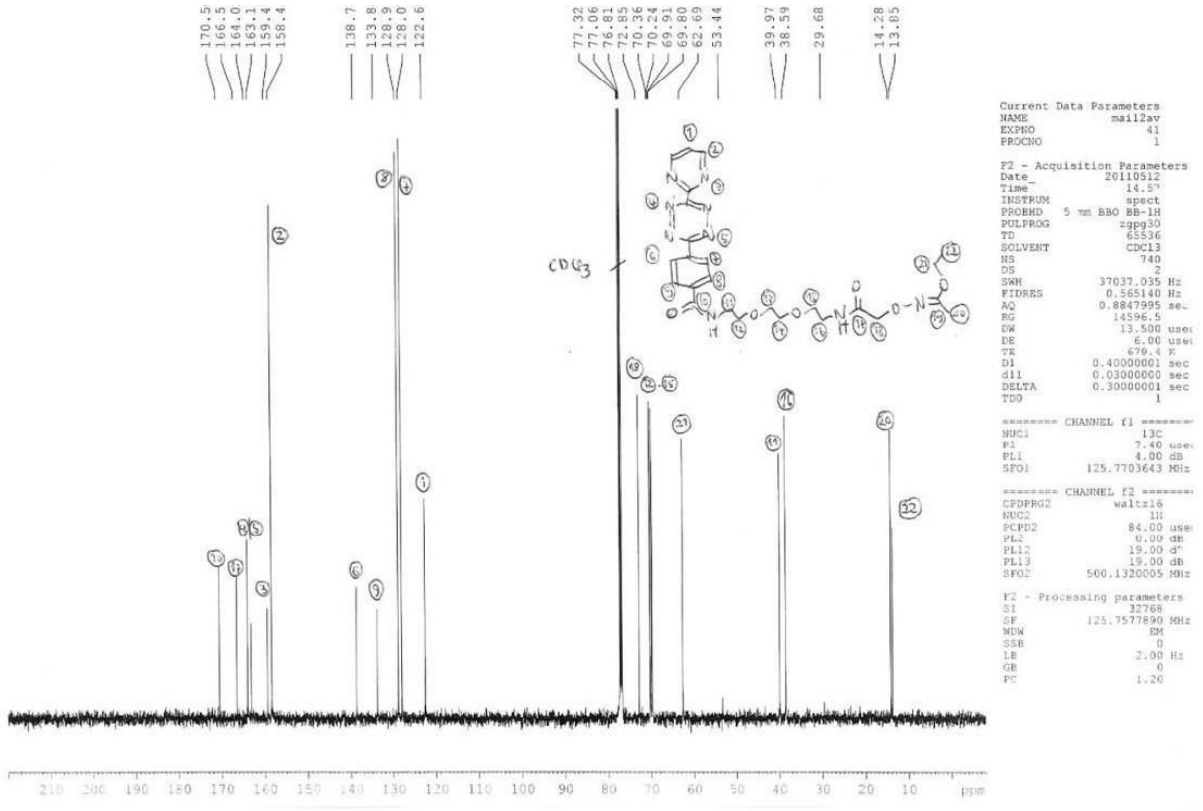

Figure ESI-23: *^{13}C-NMR spectrum of compound **8**.*

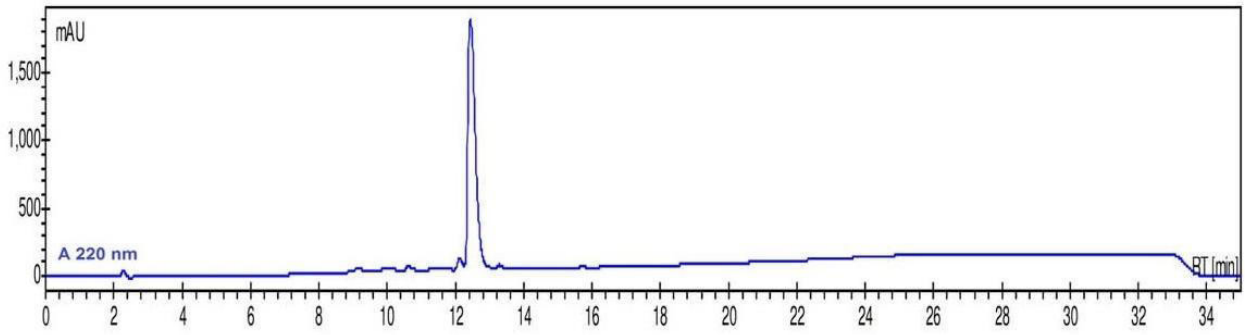

Figure ESI-24: *HPLC trace of compound **8**. Absorbance at 220 nm; gradient 10→100 B; t_R=12.62 min.*

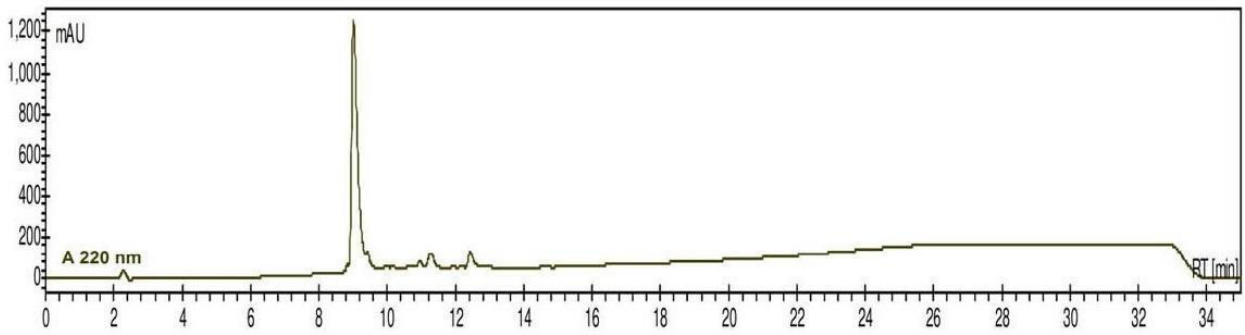

Figure ESI-25: *HPLC trace of compound **8a**. Absorbance at 220 nm; gradient 10→100 B; t_R=9.11 min.*

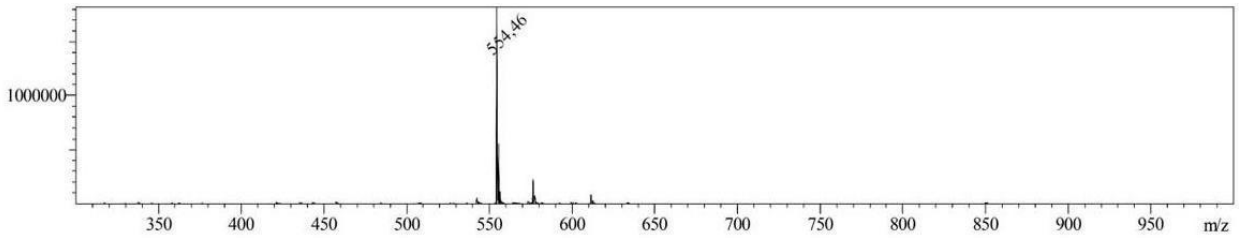

Figure ESI-26: *ESI-MS spectrum of compound **8**; calc. for $C_{25}H_{31}N_9O_6$ M: 553.25, m/z meas.: 554.46 $[M+H]^+$.*

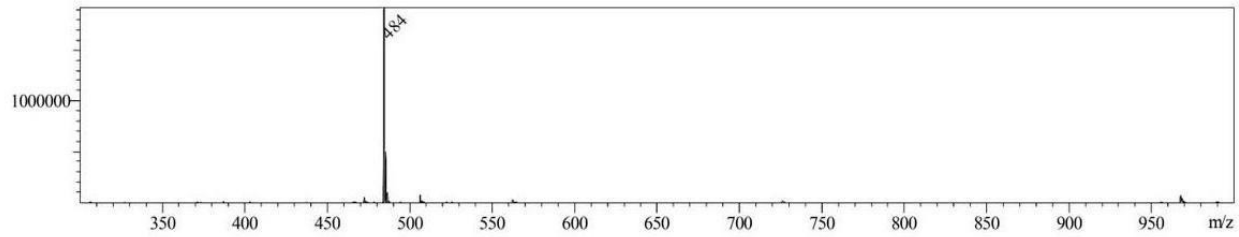

Figure ESI-27: *ESI-MS spectrum of compound **8a**; calc. for $C_{21}H_{25}N_9O_5$ M: 483.20, m/z meas.: 484.45 $[M+H]^+$.*

1.2.9 Compound 9

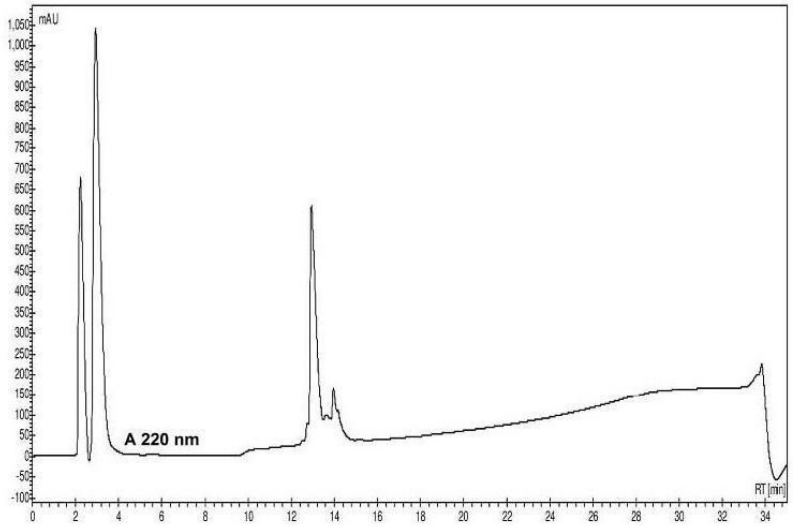

Figure ESI-28: *HPLC trace of compound **9**. Absorbance at 220 nm; gradient 10→100 B; t_R=13.22 min.*

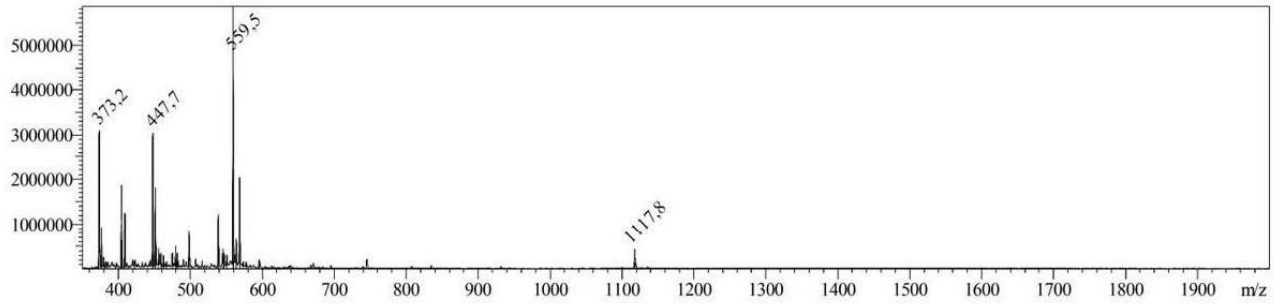

Figure ESI-29: *ESI-MS spectrum of compound **9**; calc. for $C_{48}H_{76}N_{16}O_{15}$ M: 1116.57, m/z meas.: 1117.8 $[M+H]^+$, 559.62 meas. 559.5 $[M+2H]^{2+}$, 373.41 meas. 373.2 $[M+3H]^{3+}$.*

1.2.10 Compound 10

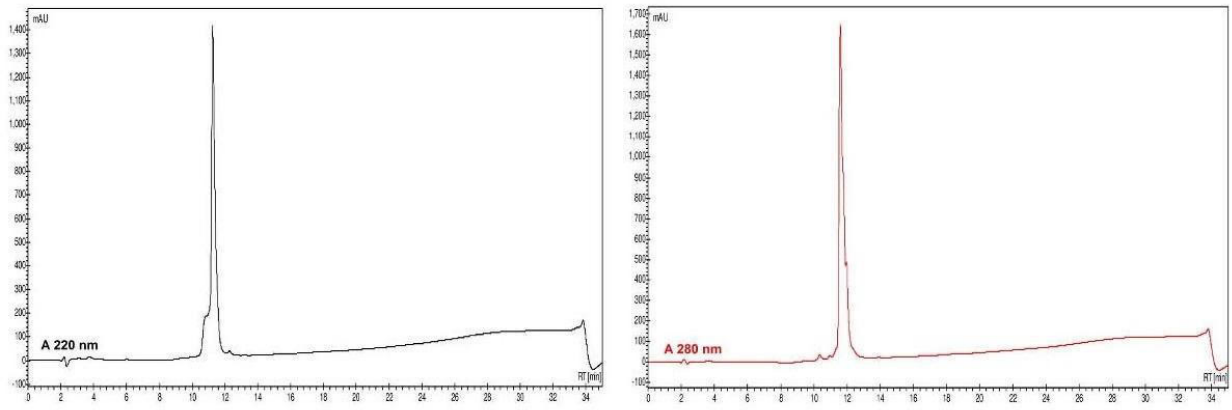

Figure ESI-30: *HPLC trace of compound* ***10****. Left: absorbance at 220 nm; right: absorbance at 220 nm; gradient 10→100 B;* t_R*=11.54 min.*

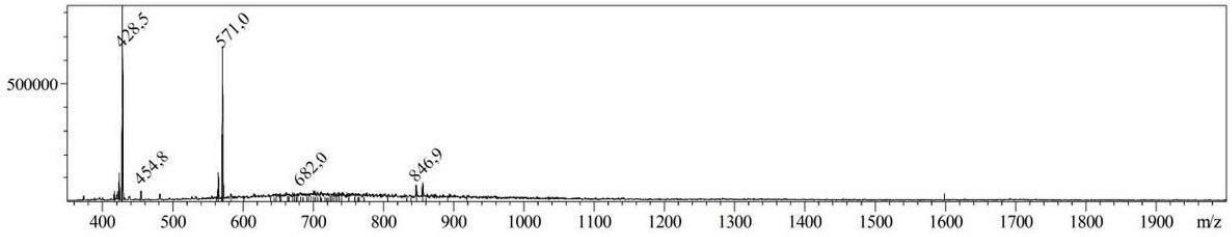

Figure ESI-31: *ESI-MS spectrum of compound* ***10****; calc. for* $C_{70}H_{114}N_{24}O_{21}S_2$ *M: 846.98, m/z meas.: 846.9* $[M+2H]^{2+}$*, calc. 564.98 meas. 571.0* $[M+3H+H_2O]^{3+}$*, calc. 423.99 meas. 428.5* $[M+4H+H_2O]^{4+}$*.*

1.2.11 Compound 11

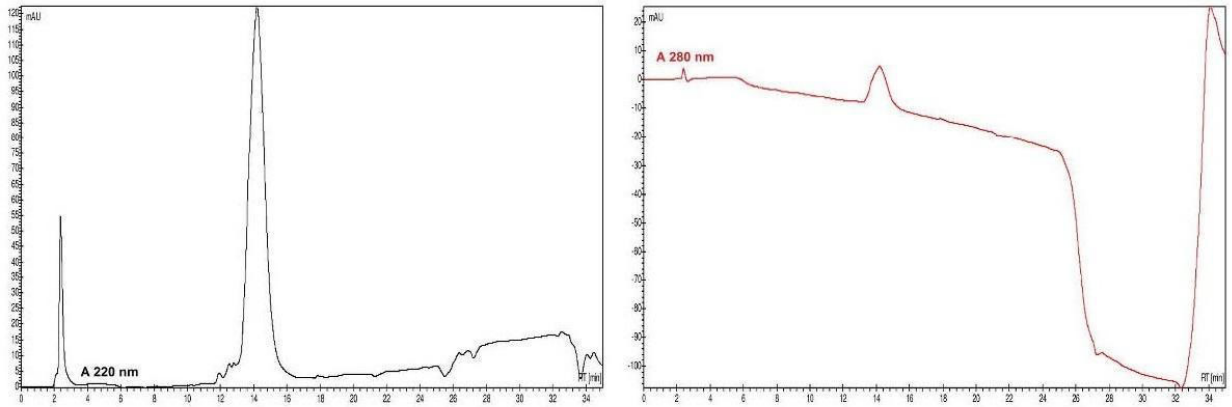

Figure ESI-32: *HPLC trace of compound* ***11****. Left: absorbance at 220 nm; right: absorbance at 280 nm; gradient 10→100 B;* t_R*=14.27 min.*

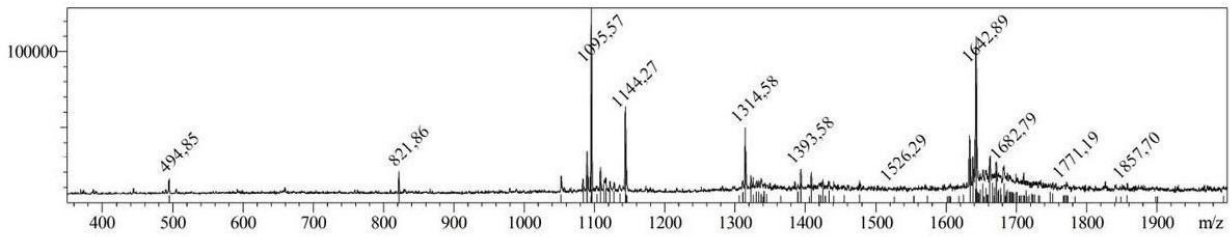

Figure ESI-33: *ESI-MS spectrum of compound* ***11****; calc. for* $C_{134}H_{206}N_{44}O_{40}S_6$ *M: 1633.88, m/z meas.: 1642.89* $[M+2H+H_2O]^{2+}$*, calc. 1095.59 meas. 1095.57* $[M+3H+H_2O]^{3+}$*, calc. 821.95 meas. 821.86* $[M+4H+H_2O]^{4+}$*.*

1.2.12 Compound 12

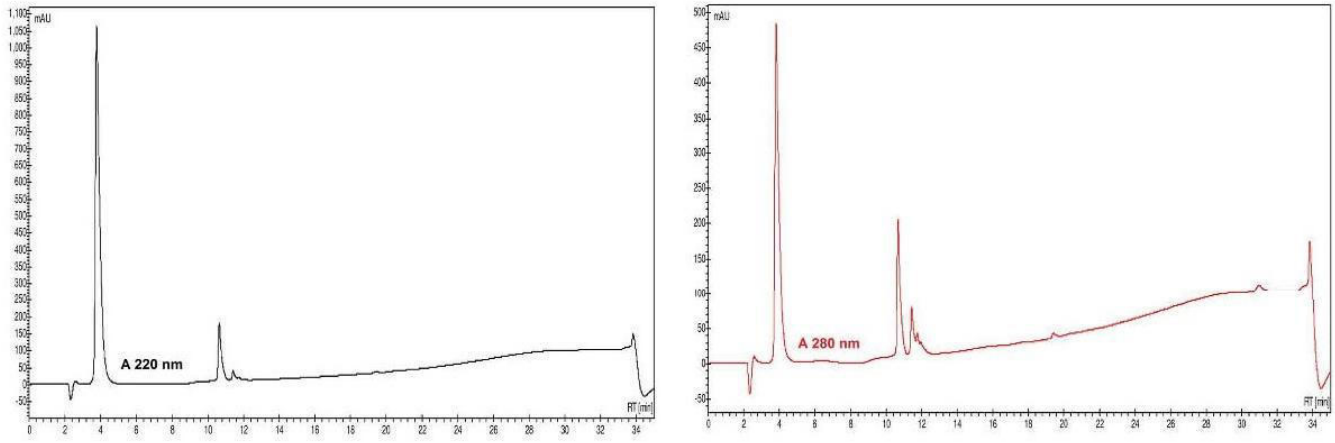

Figure ESI-34: *HPLC trace of compound* ***12****. Left: absorbance at 220 nm; right: absorbance at 280 nm; gradient 10→100 B;* t_R*=10.76 min.*

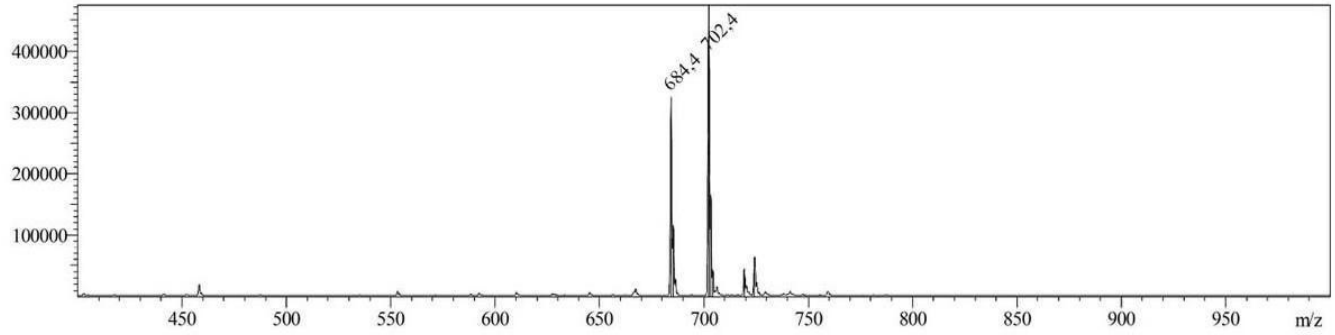

Figure ESI-35: *ESI-MS spectrum of compound* ***12****; calc. for* $C_{28}H_{45}N_9O_{11}$ *M: 683.32, m/z meas.: 684.4* $[M+H]^+$*, 702.4* $[M+H+H_2O]^+$*.*

1.2.13 Compound 13

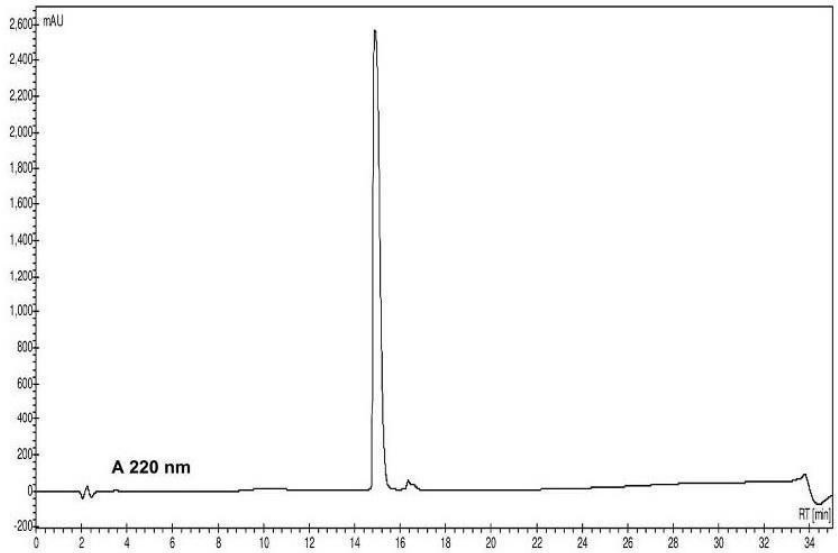

Figure ESI-36: *HPLC trace of compound* ***13****. Absorbance at 220 nm; gradient 10→100 B;* t_R*=15.06 min.*

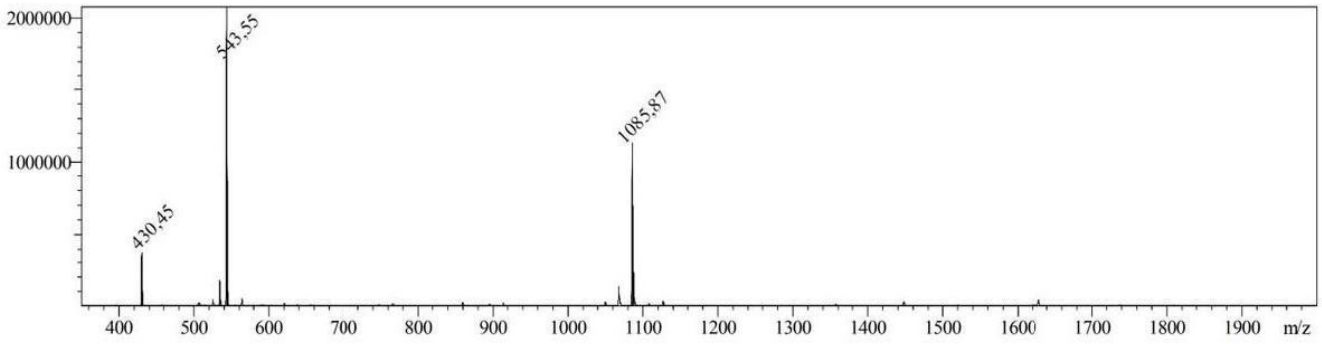

Figure ESI-37: *ESI-MS spectrum of compound* ***13****; calc. for* $C_{51}H_{78}N_{12}O_{13}$ *M: 1067.26, m/z meas.: 1085.87* $[M+H+H_2O]^+$*, 534.63 meas. 543.55* $[M+2H+H_2O]^{2+}$.

1.2.14 Compound 14

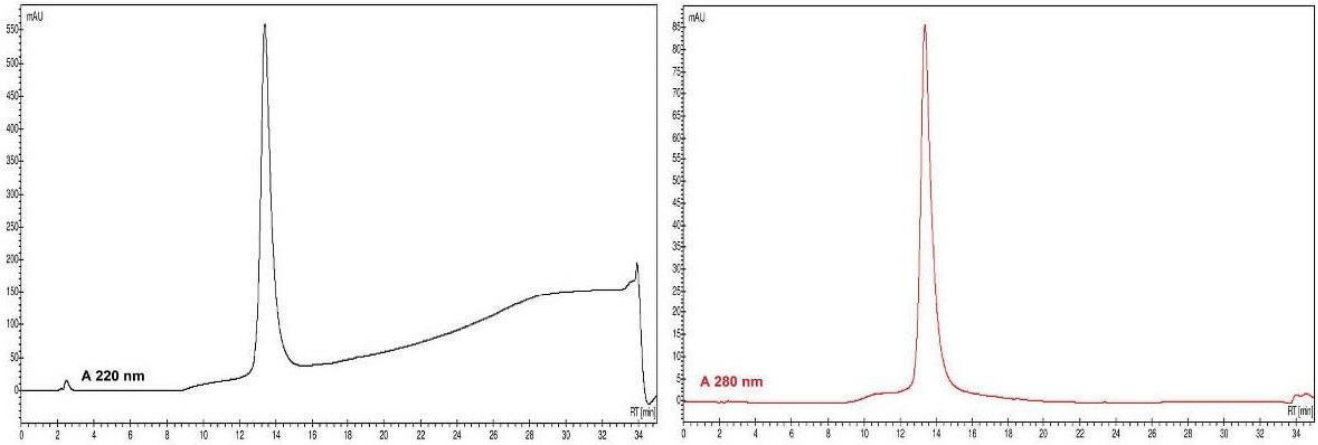

Figure ESI-38: *HPLC trace of compound* ***14****. Left: absorbance at 220 nm; right: absorbance at 280 nm; gradient 10→100 B;* t_R*=13.56 min.*

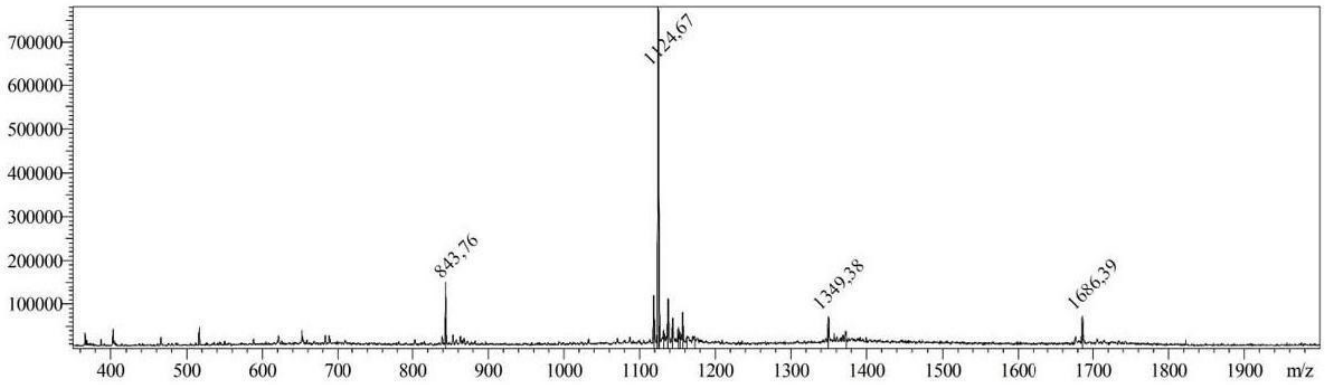

Figure ESI-39: *ESI-MS spectrum of compound* ***14****; calc. for* $C_{137}H_{211}N_{45}O_{42}S_6$ *M: 1677.42, m/z meas.: 1686.39* $[M+2H+H_2O]^{2+}$*, 1118.61 meas.1124.67* $[M+3H+H_2O]^{3+}$*, 839.21 meas.843.76* $[M+4H+H_2O]^{4+}$.

1.2.15 Compound 15

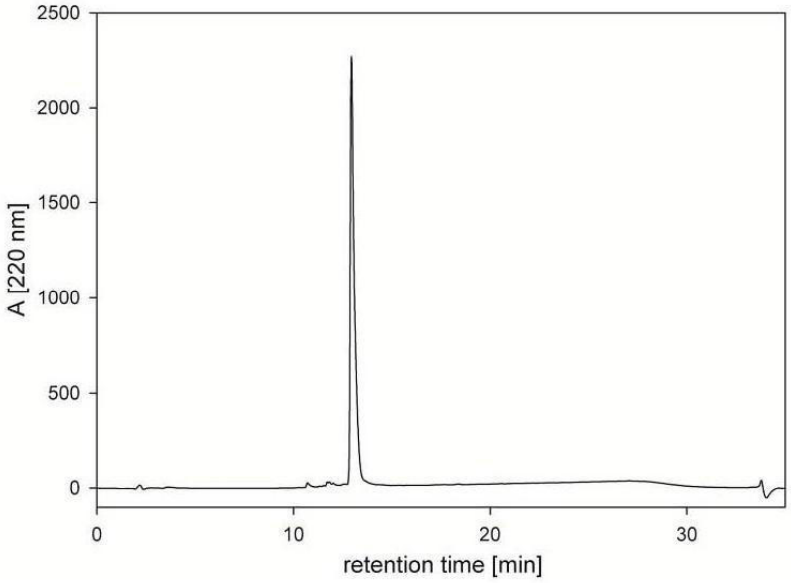

Figure ESI-40: *HPLC trace of compound* ***15****. Absorbance at 220 nm; gradient 10→100 B;* t_R*=12.98 min.*

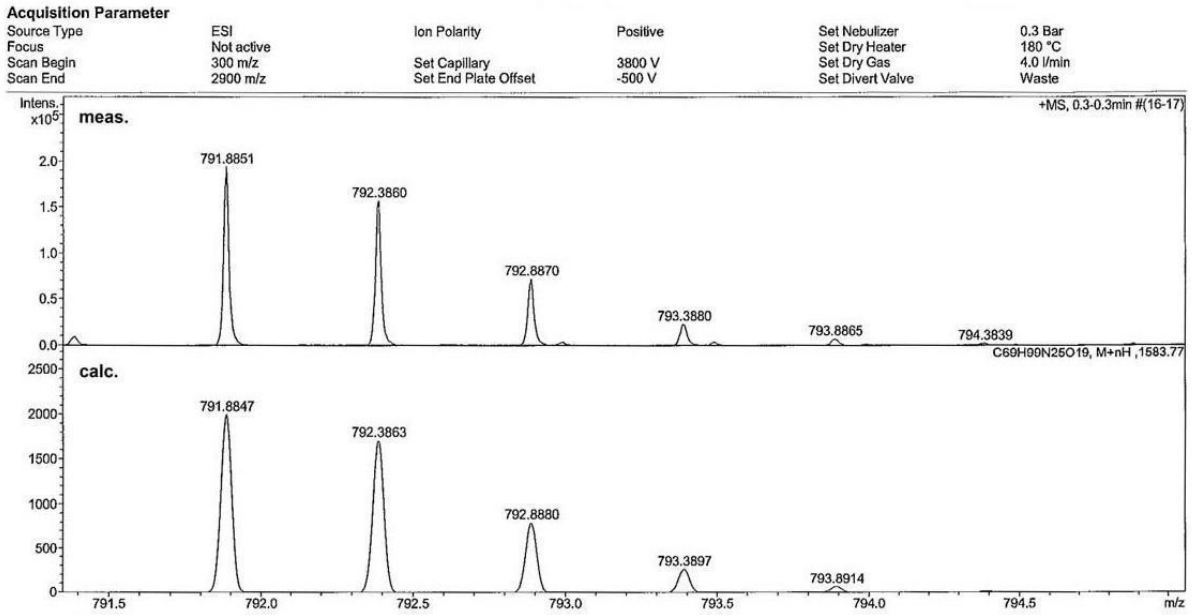

Figure ESI-41: *Section of HR ESI-MS spectrum of compound* ***15****. Upper panel: measured isotopic pattern* $[M+2H]^{2+}$*. Lower panel: simulated isotopic pattern* $[M+2H]^{2+}$*.*

1.2.16 Compound 16

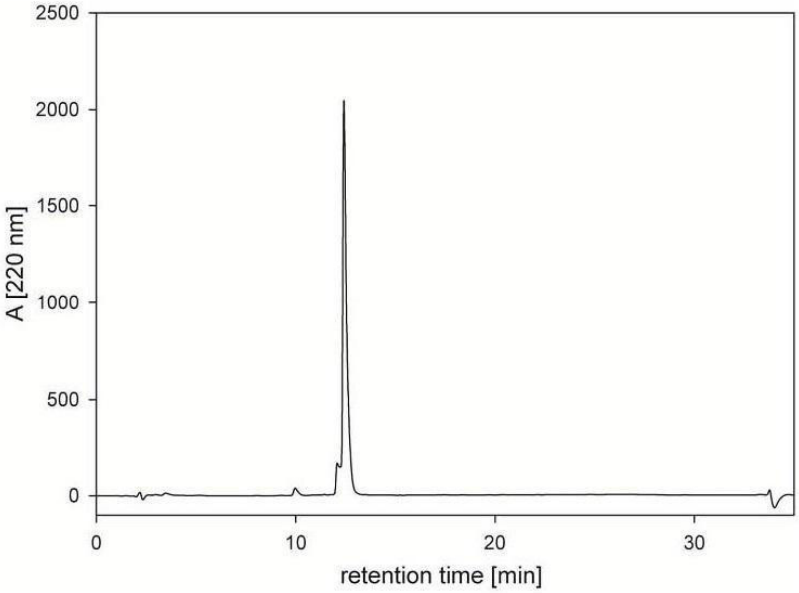

Figure ESI-42: *HPLC trace of compound* ***16****. Absorbance at 220 nm; gradient 10→100 B;* t_R*=12.20 min.*

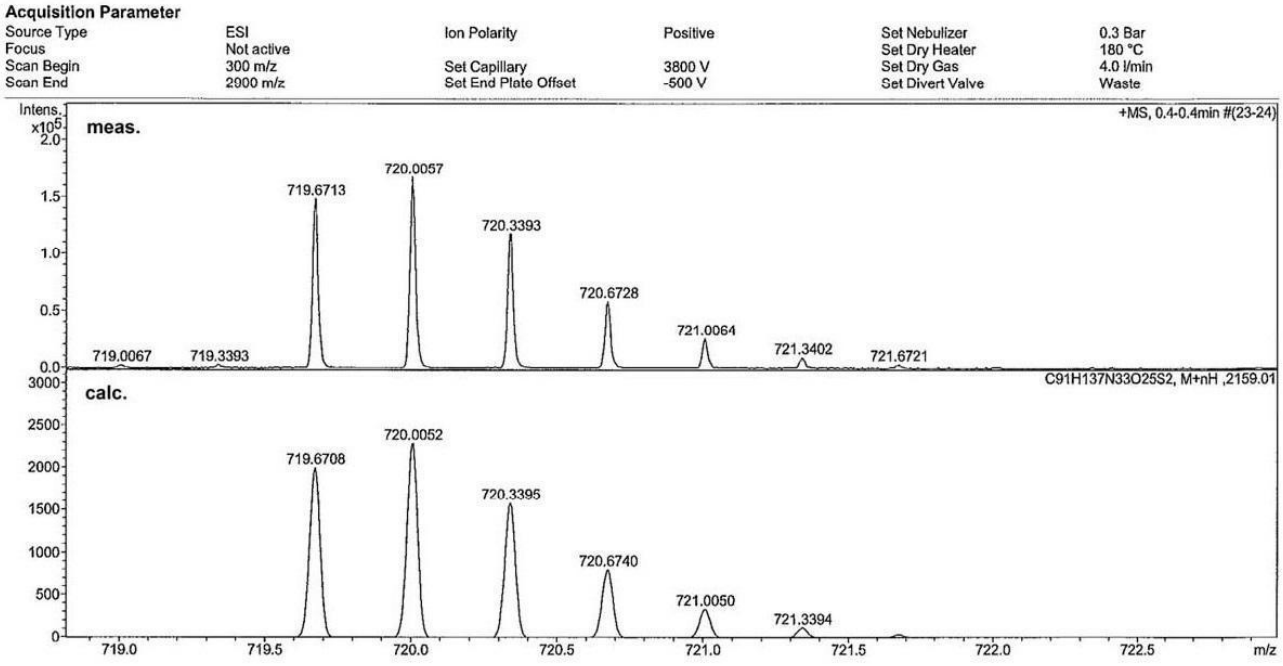

Figure ESI-43: *Section of HR ESI-MS spectrum of compound* ***16****. Upper panel: measured isotopic pattern* $[M+3H]^{3+}$*. Lower panel: simulated isotopic pattern* $[M+3H]^{3+}$*.*

1.2.17 Compound 17

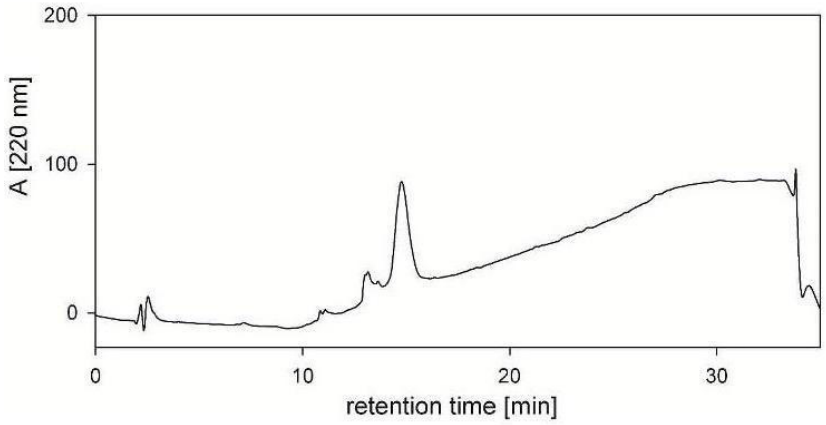

Figure ESI-44: *HPLC trace of compound* ***17****. Absorbance at 220 nm; gradient 10→100 B;* t_R*=14.67 min.*

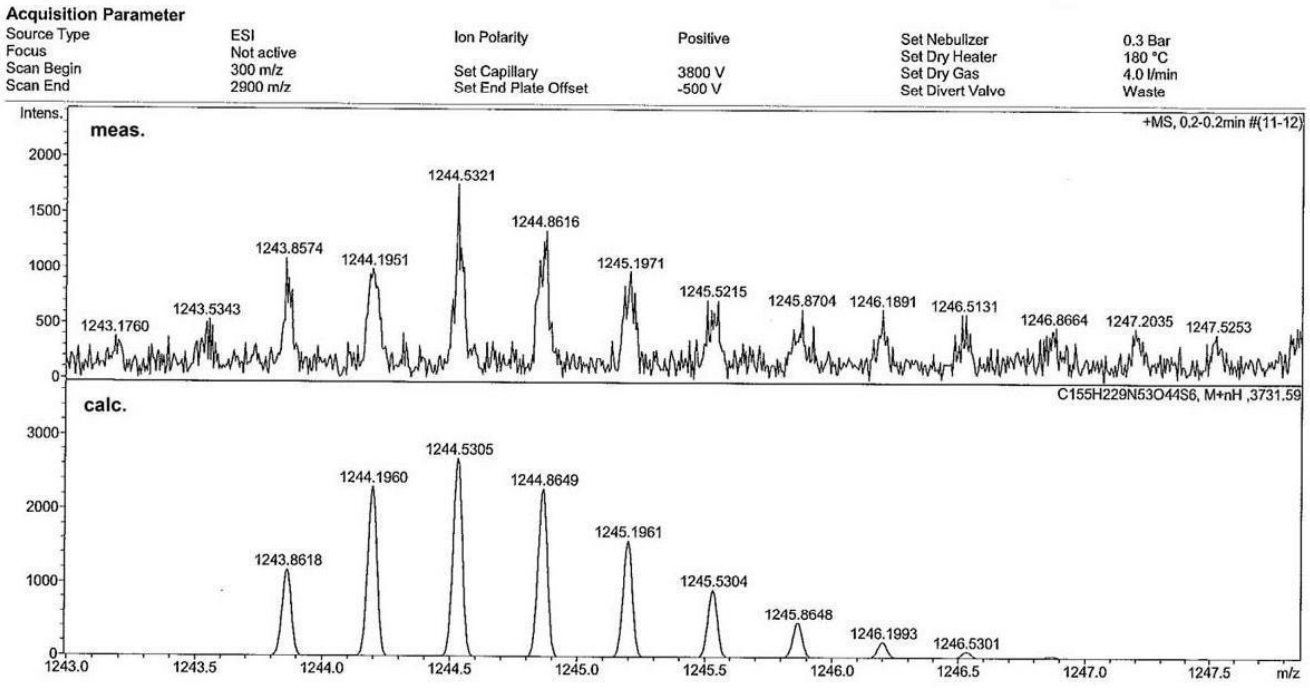

Figure ESI-45: *Section of HR ESI-MS spectrum of compound* ***17****. Upper panel: measured isotopic pattern* $[M+3H]^{3+}$*. Lower panel: simulated isotopic pattern* $[M+3H]^{3+}$*.*

1.2.18 Compound 18

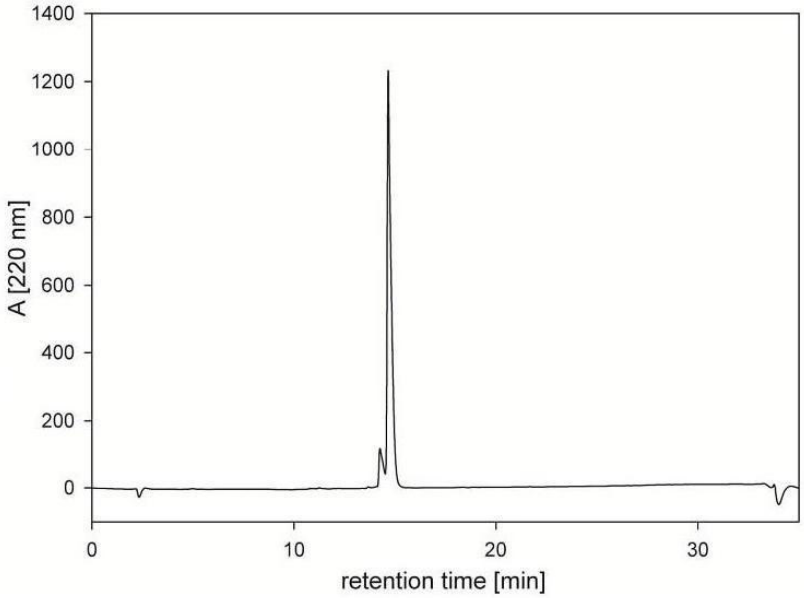

Figure ESI-46: *HPLC trace of compound* ***18****. Absorbance at 220 nm; gradient 10→100 B;* t_R*=14.78 min.*

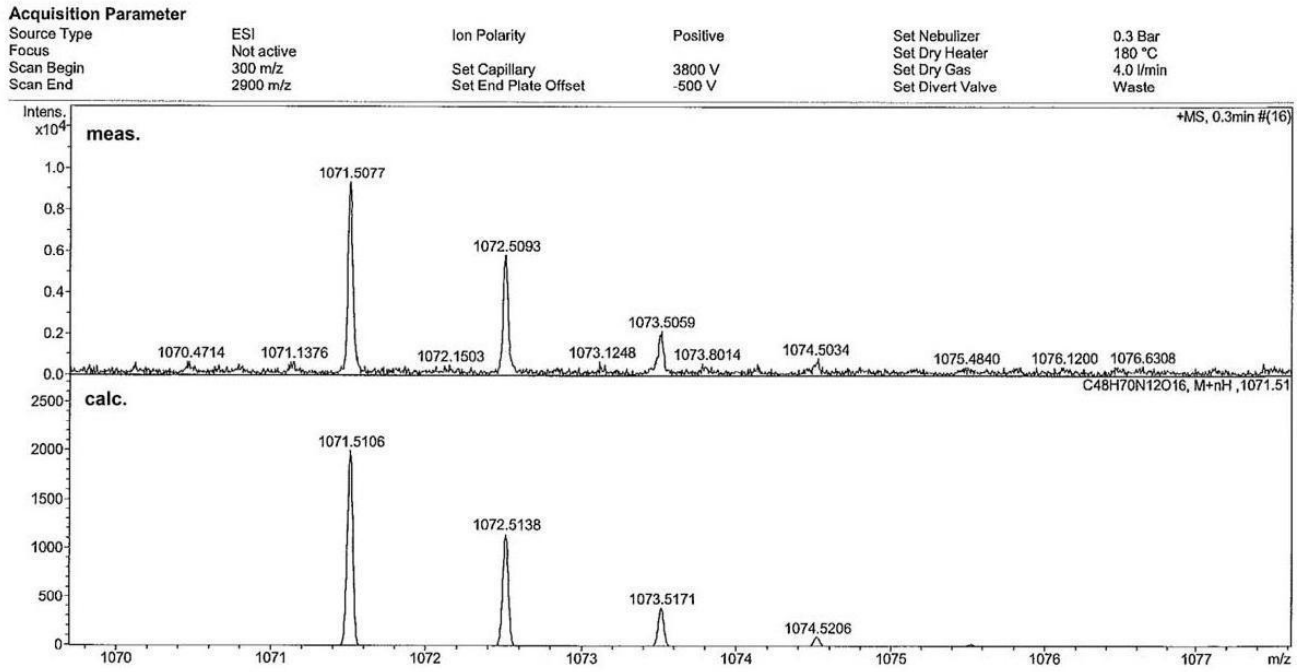

Figure ESI-47: *Section of HR ESI-MS spectrum of compound* ***18****. Upper panel: measured isotopic pattern* $[M+H]^+$*. Lower panel: simulated isotopic pattern* $[M+H]^+$*.*

1.2.19 Compound 19

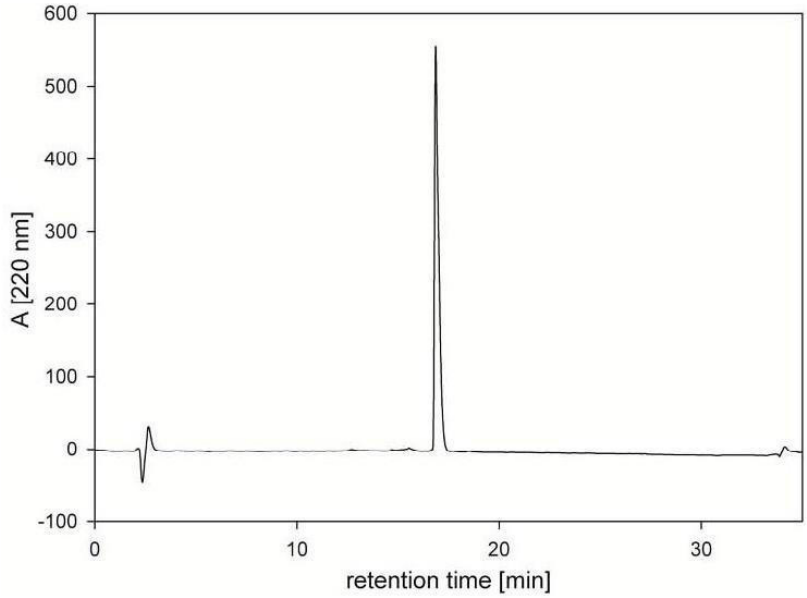

Figure ESI-48: *HPLC trace of compound* ***19****. Absorbance at 220 nm; gradient 10→100 B;* t_R*=16.72 min.*

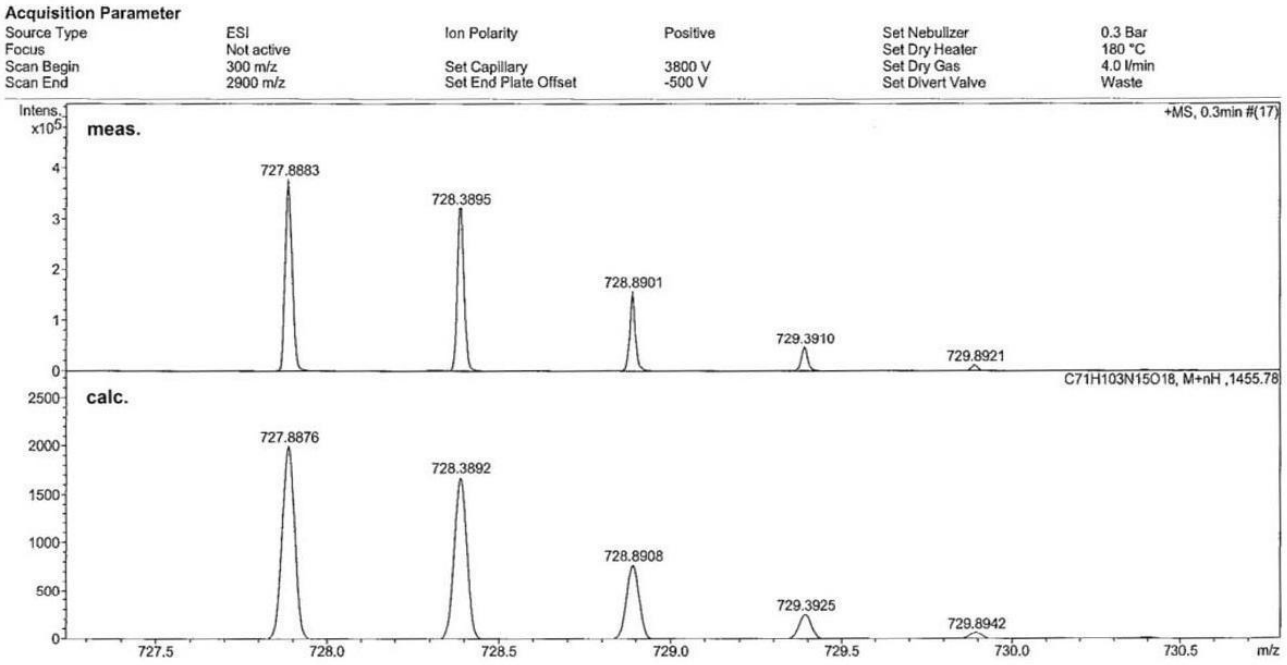

Figure ESI-49: *Section of HR ESI-MS spectrum of compound* ***19****. Upper panel: measured isotopic pattern* $[M+2H]^{2+}$*. Lower panel: simulated isotopic pattern* $[M+2H]^{2+}$*.*

1.2.20 Compound 20

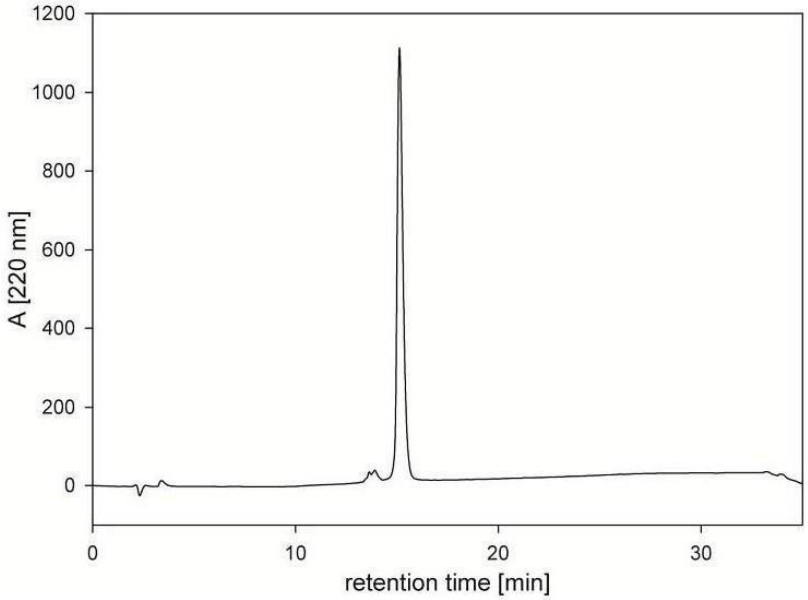

Figure ESI-50: *HPLC trace of compound* ***20****. Absorbance at 220 nm; gradient 10→100 B;* t_R*=15.07 min.*

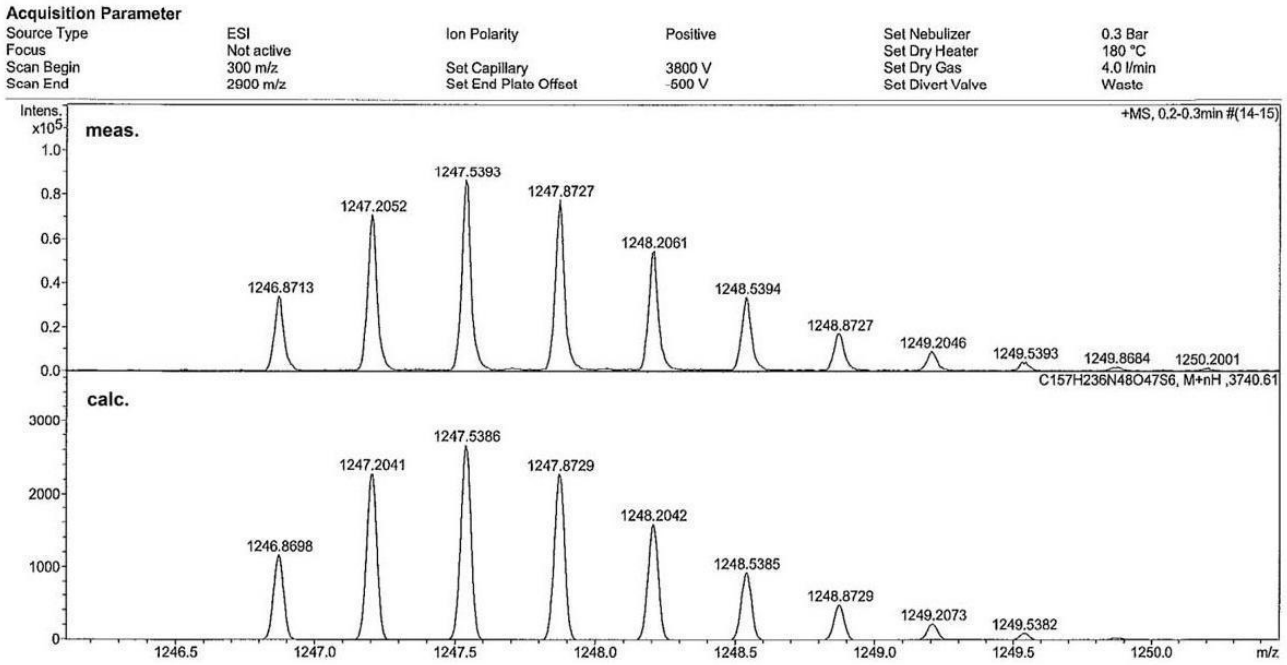

Figure ESI-51: *Section of HR ESI-MS spectrum of compound* ***20****. Upper panel: measured isotopic pattern* $[M+3H]^{3+}$*. Lower panel: simulated isotopic pattern* $[M+3H]^{3+}$*.*

1.2.21 Compound 21

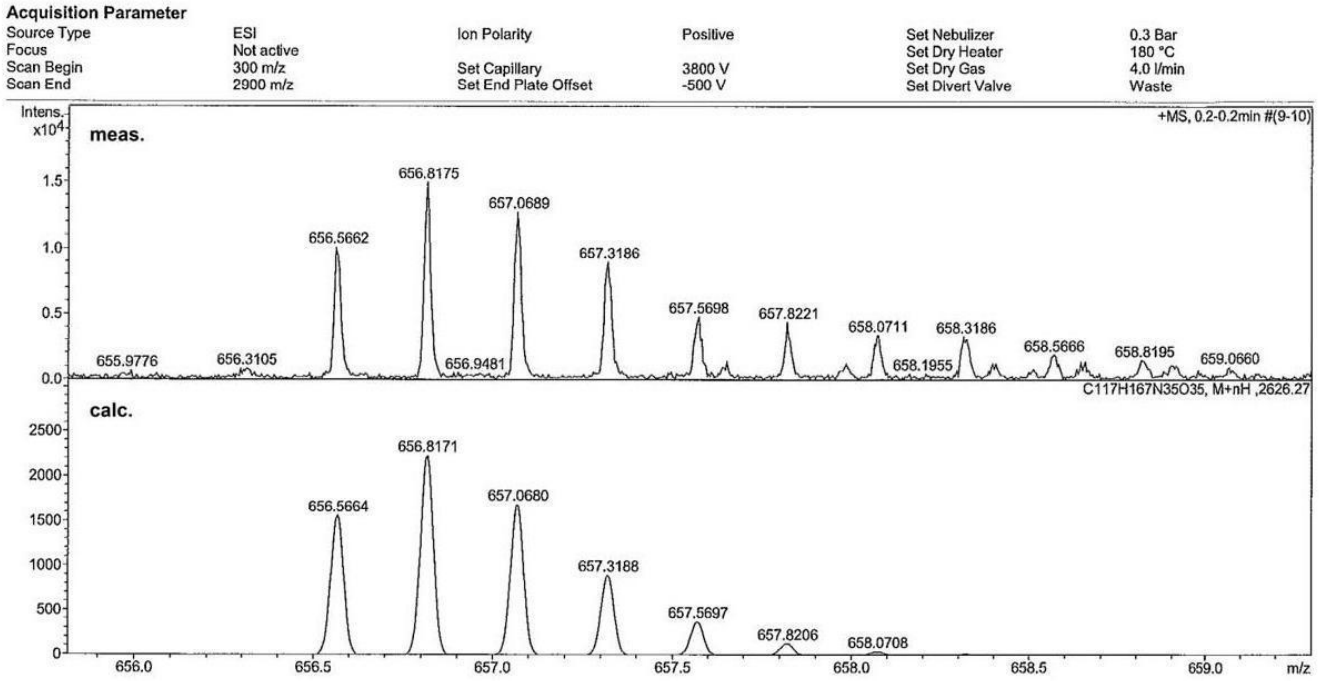

Figure ESI-52: *Fragment of HR ESI-MS spectrum of compound* ***21****. Upper panel: measured isotopic pattern* $[M+4H]^{4+}$*. Lower panel: simulated isotopic pattern* $[M+4H]^{4+}$*.*

1.2.22 Compound 22

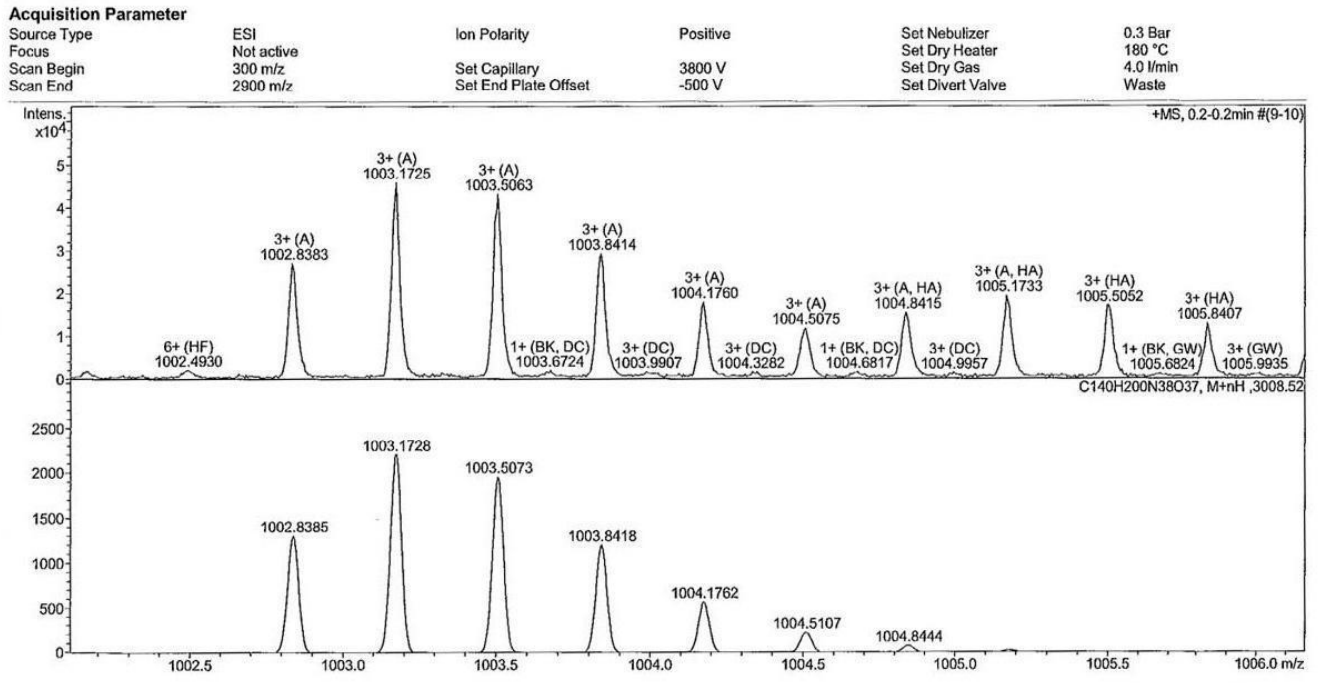

Figure ESI-53: *Section of HR ESI-MS spectrum of compound* ***22****. Upper panel: measured isotopic pattern* $[M+3H]^{3+}$*. Lower panel: simulated isotopic pattern* $[M+3H]^{3+}$*.*

1.2.23 Compound 23

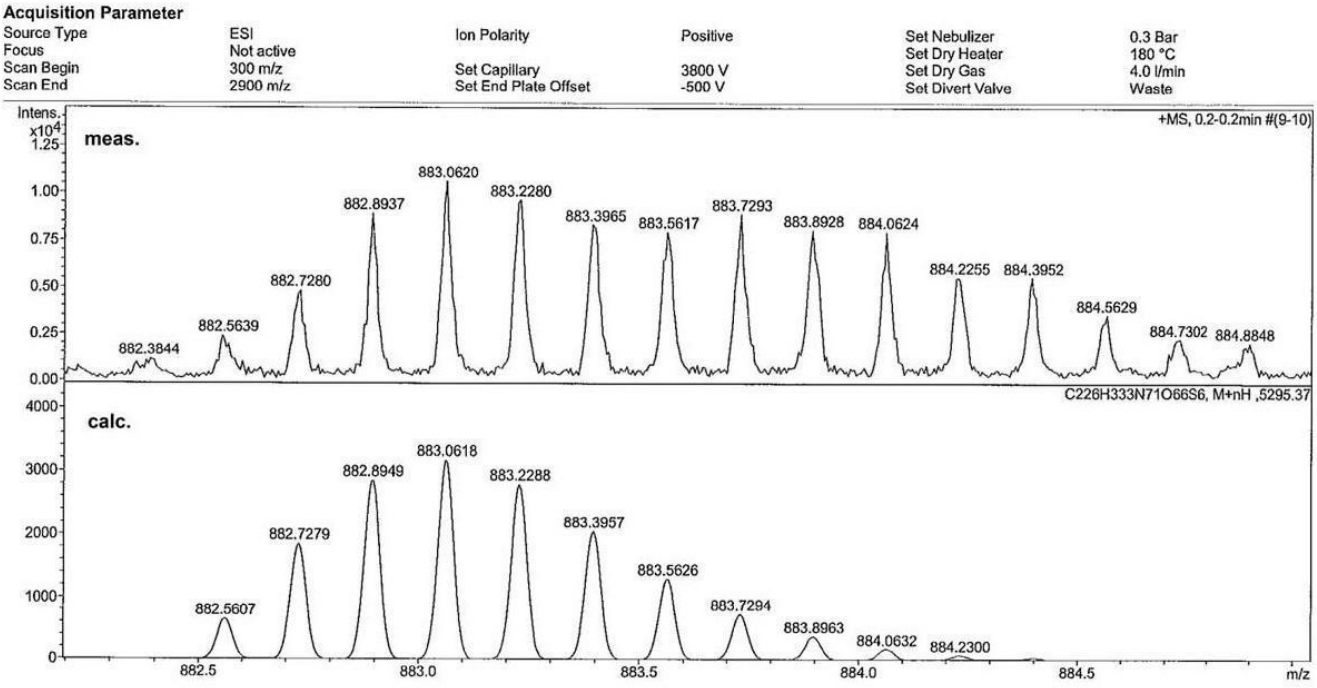

Figure ESI-54: *Section of HR ESI-MS spectrum of compound* ***23****. Upper panel: measured isotopic pattern* $[M+6H]^{6+}$*. Lower panel: simulated isotopic pattern* $[M+6H]^{6+}$*.*

1.2.24 Compound 24

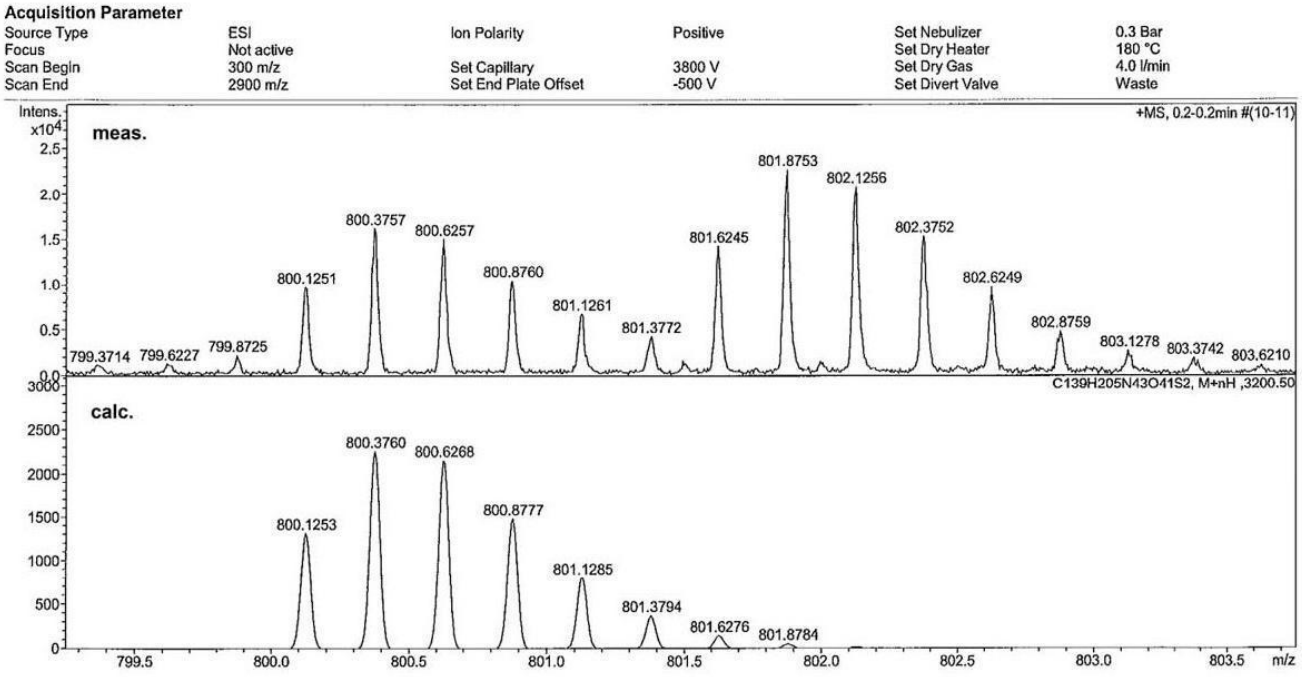

Figure ESI-55: *Section of HR ESI-MS spectrum of compound* ***24****. Upper panel: measured isotopic pattern* $[M+4H]^{4+}$*. Lower panel: simulated isotopic pattern* $[M+4H]^{4+}$*.*

1.2.25 Compound 25

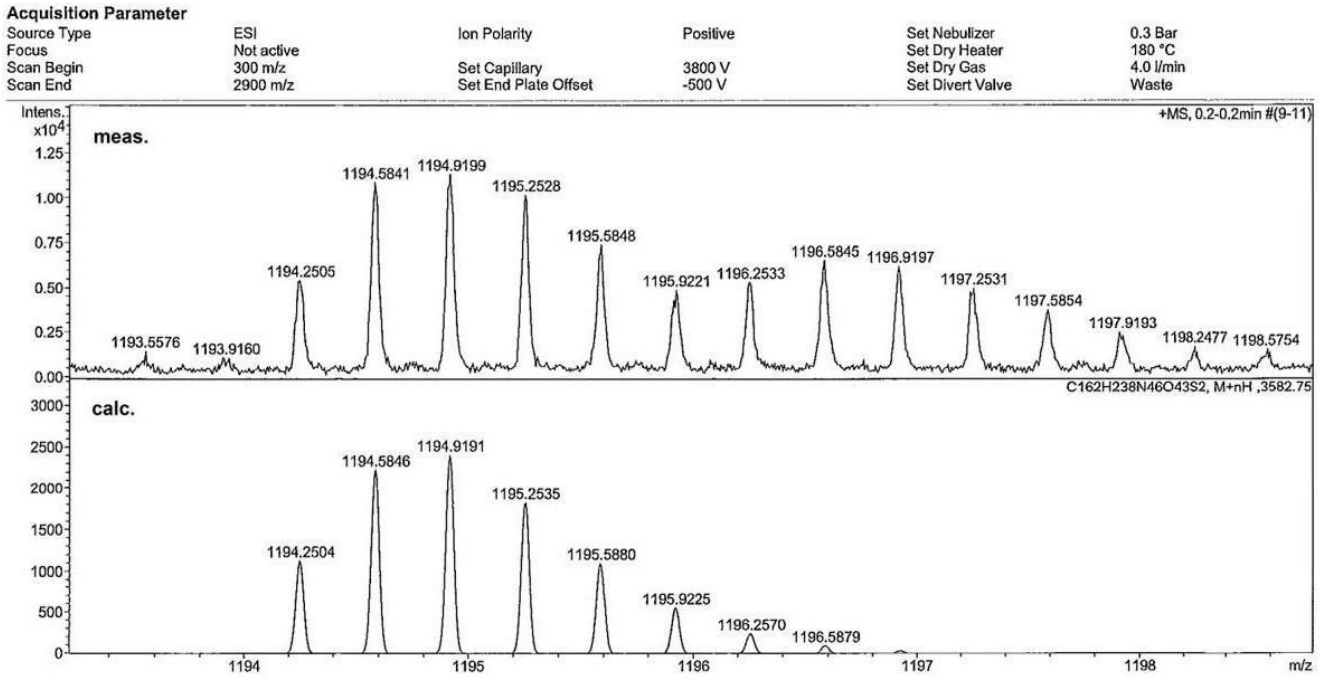

Figure ESI-56: *Section of HR ESI-MS spectrum of compound* ***25****. Upper panel: measured isotopic pattern* $[M+3H]^{3+}$*. Lower panel: simulated isotopic pattern* $[M+3H]^{3+}$*.*

1.2.26 Compound 26

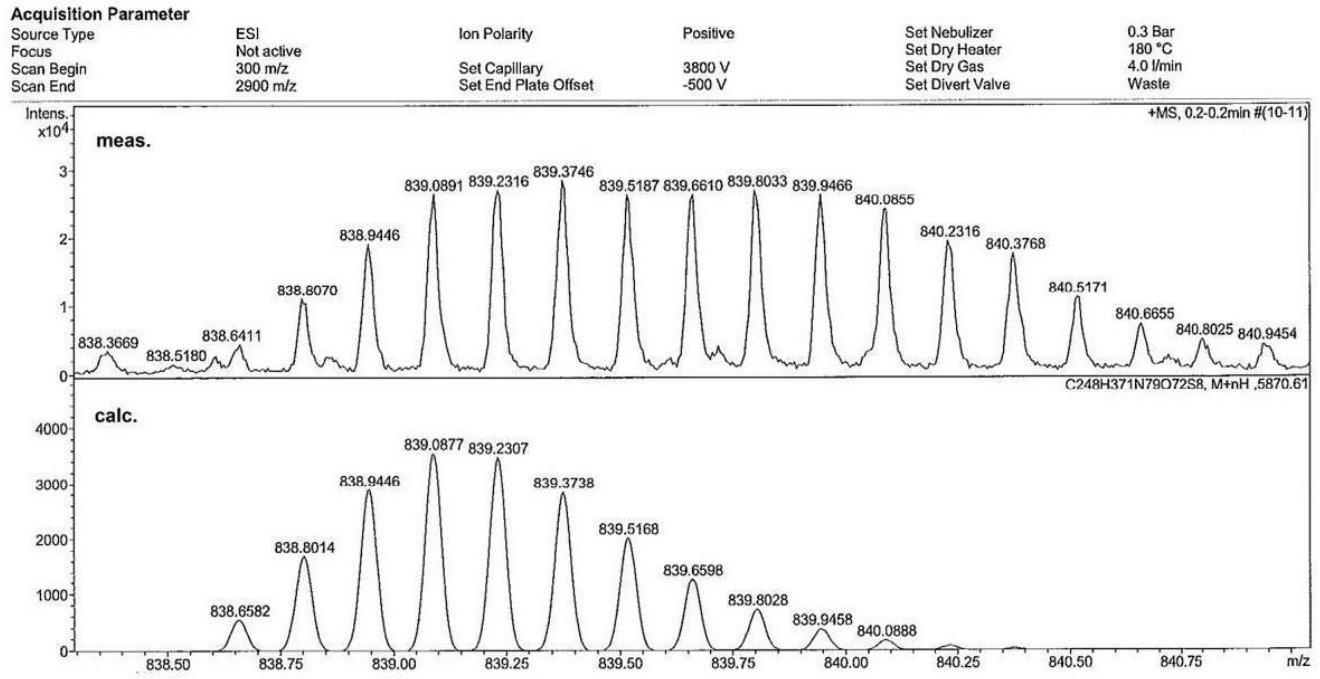

Figure ESI-57: *Section of HR ESI-MS spectrum of compound* ***26****. Upper panel: measured isotopic pattern* $[M+7H]^{7+}$*. Lower panel: simulated isotopic pattern* $[M+7H]^{7+}$*.*

1.2.27 Compound 27

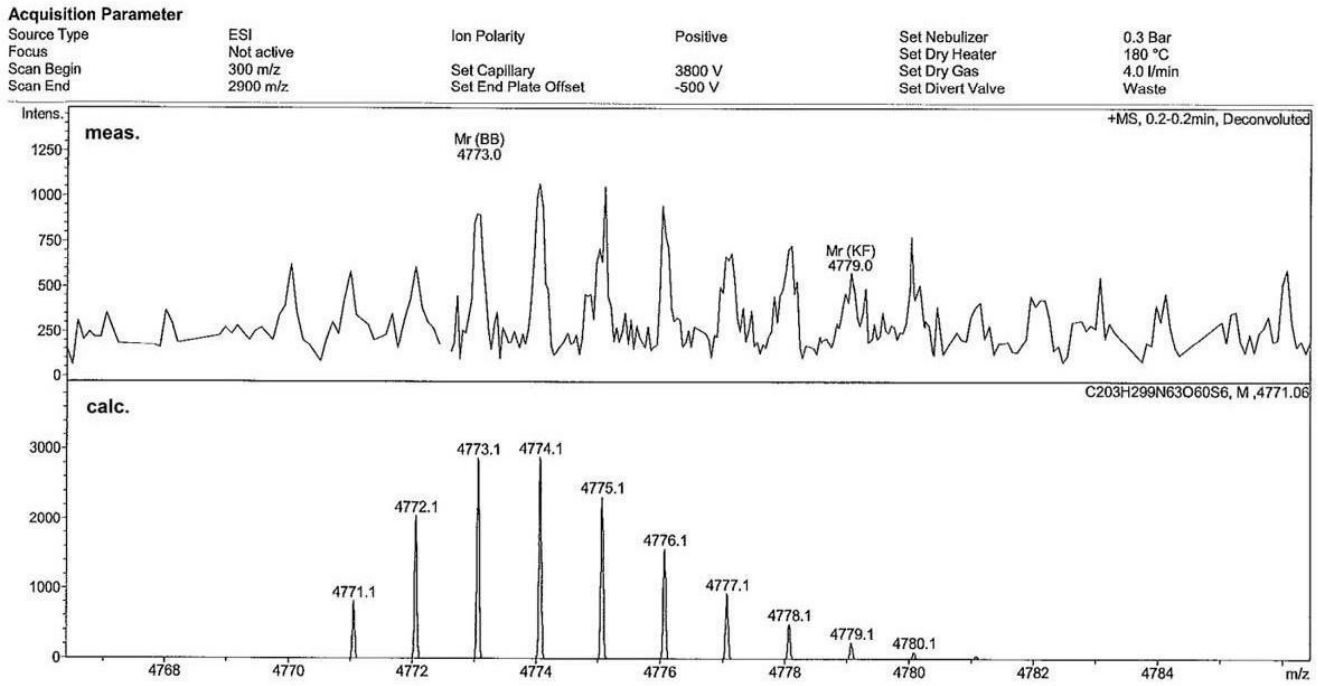

Figure ESI-58: *Section of deconvoluted HR ESI-MS spectrum of compound* ***27****. Upper panel: deconvoluted isotopic pattern measured. Lower panel: calculated isotopic pattern.*

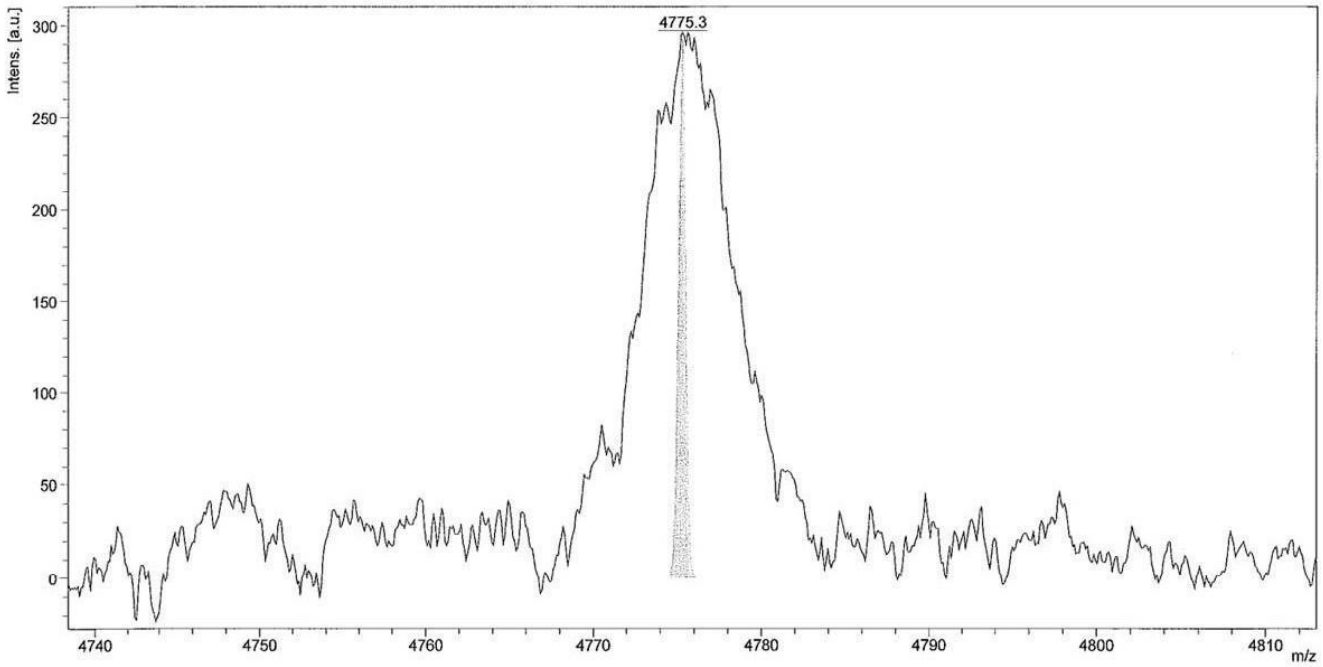

Figure ESI-59: *Fragment of a MALDI-MS spectrum of compound* ***27****.Calc. for* $C_{203}H_{299}N_{63}O_{60}S_6$ *4774.4 meas. 4775.3* $[M+H]^+$.

1.2.28 Compound 28

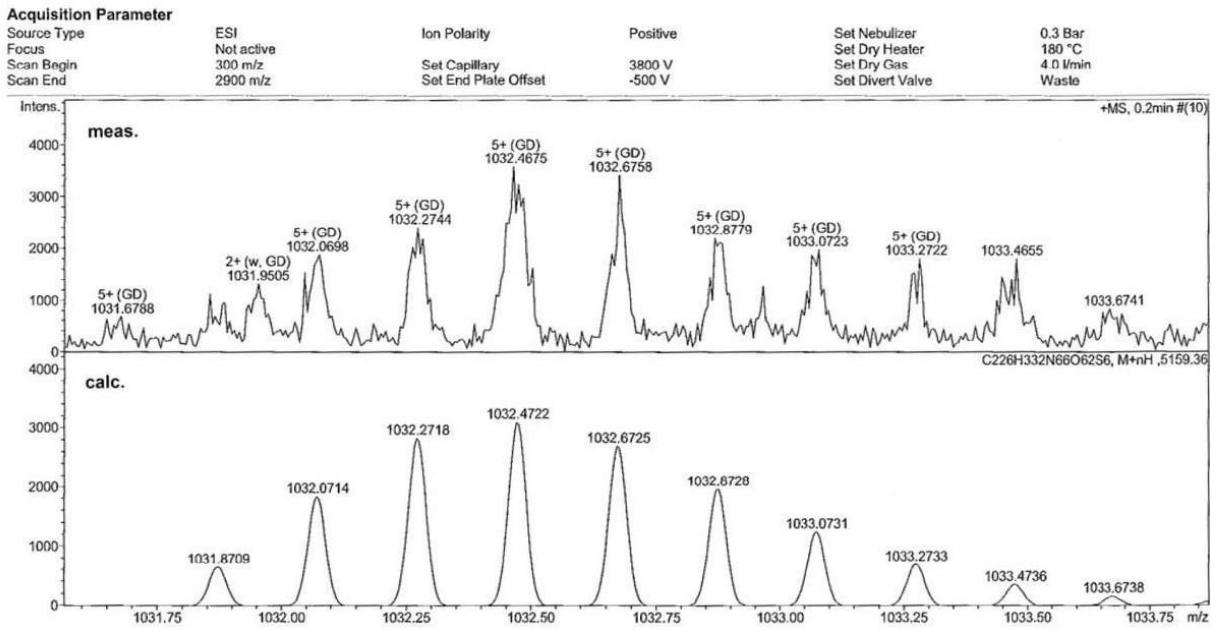

Figure ESI-60: *Section of HR ESI-MS spectrum of compound* ***28****. Upper panel: measured isotopic pattern [M+5H]$^{5+}$. Lower panel: simulated isotopic pattern [M+5H]$^{5+}$.*

1.2.29 Compound 29 possessed extremely poor ionization upon mass-spectrometric analysis, combined with strong aggregation tendency. Therefore, although mass peaks corresponding to [M+K^{+}+H^{+}] species were found in MALDI-MS spectrum, it was not used for characterization, and analysis relied on chromatographic methods (see Fig. ESI-2).

1.2.30 Compound 30

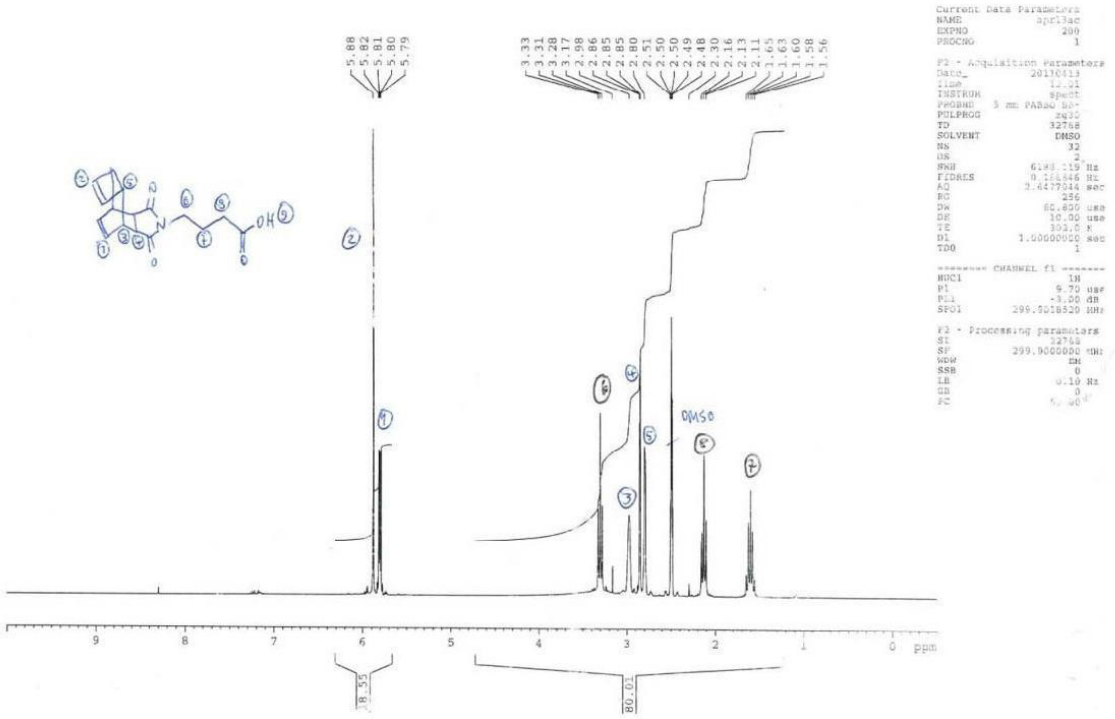

Figure ESI-62: *^{1}H-NMR spectrum of compound* ***30****.*

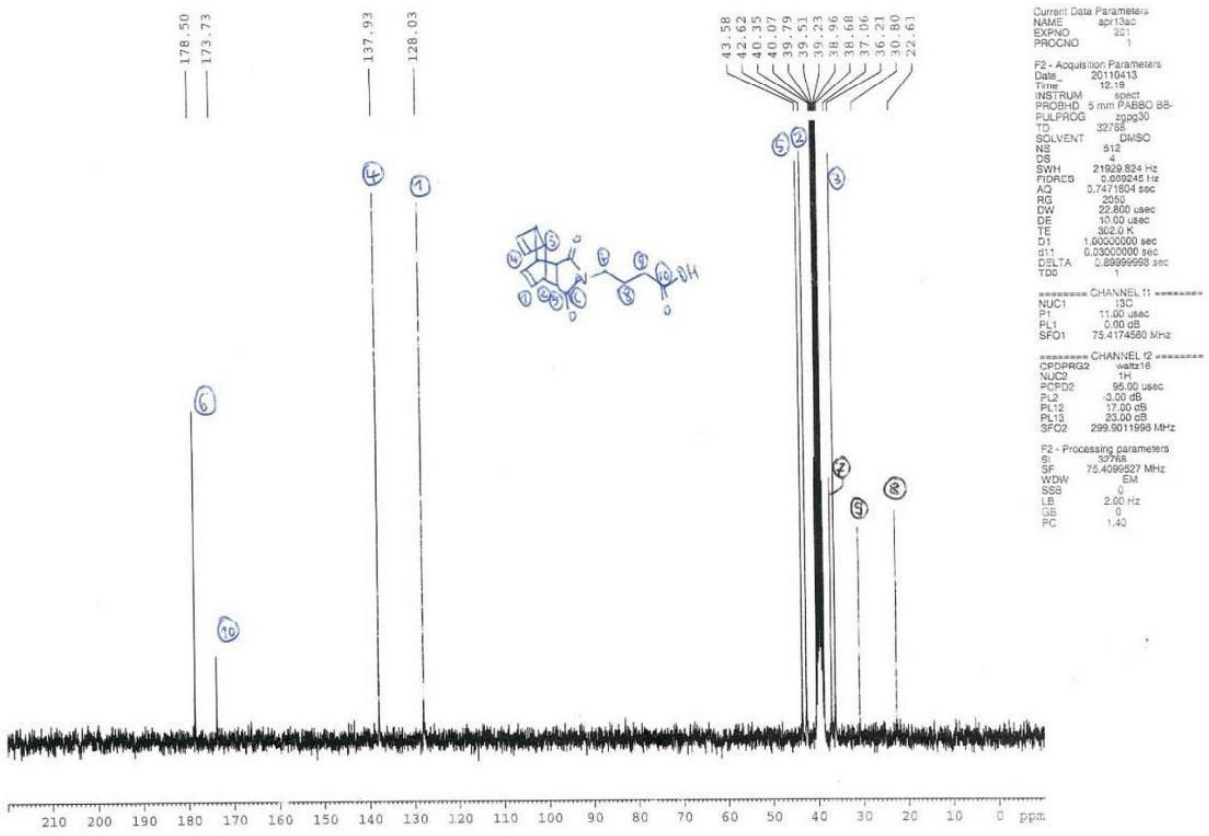

Figure ESI-63: *^{13}C-NMR spectrum of compound **30**.*

1.2.31 Compound 31

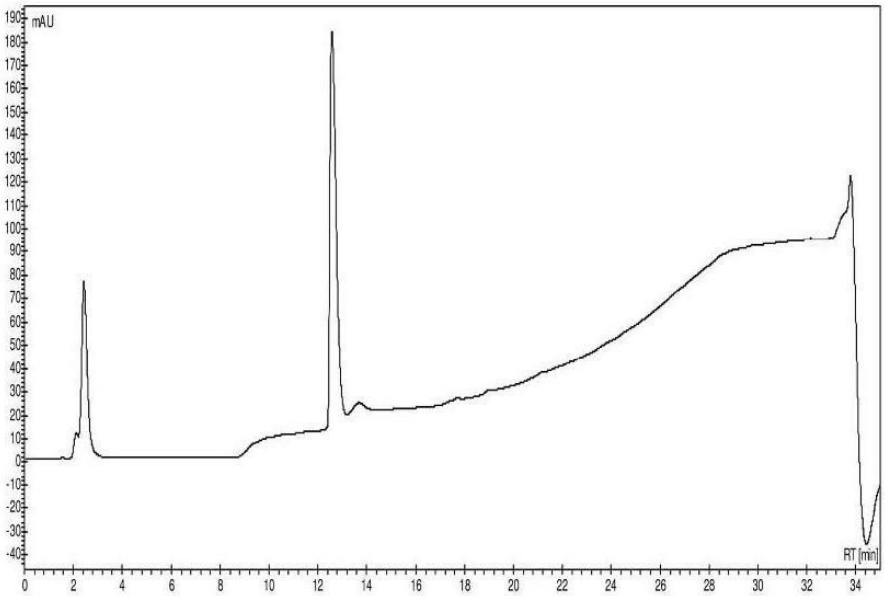

Figure ESI-64: *HPLC trace of compound **31**. Absorbance at 220 nm; gradient 10→100 B; t_R=12.27 min.*

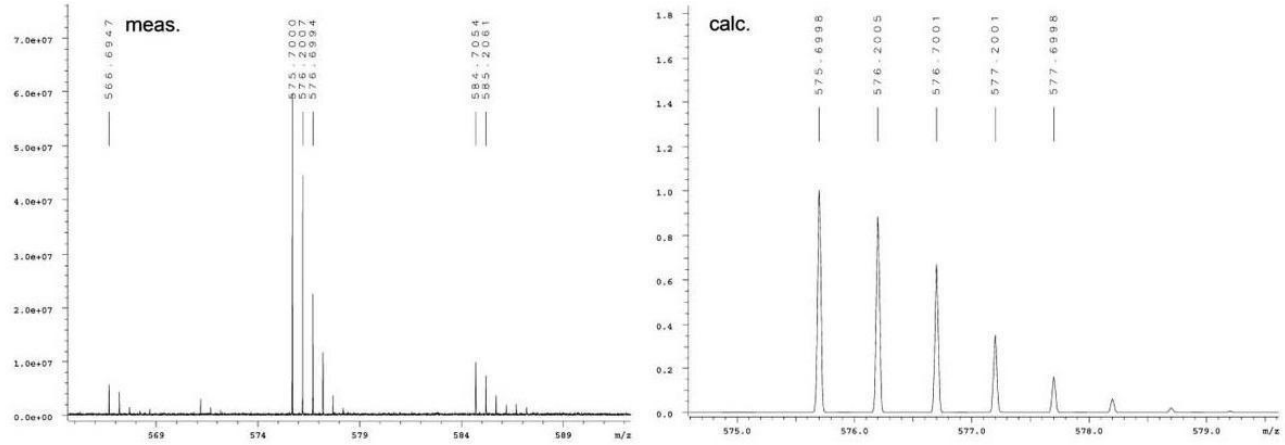

Figure ESI-65: *Section of ESI-HR-MS spectrum of compound* ***31****. Left: measured isotopic pattern* $[M+3H]^{3+}$*; right: calculated isotopic pattern* $[M+3H]^{3+}$*.*

1.2.32 Compound 32

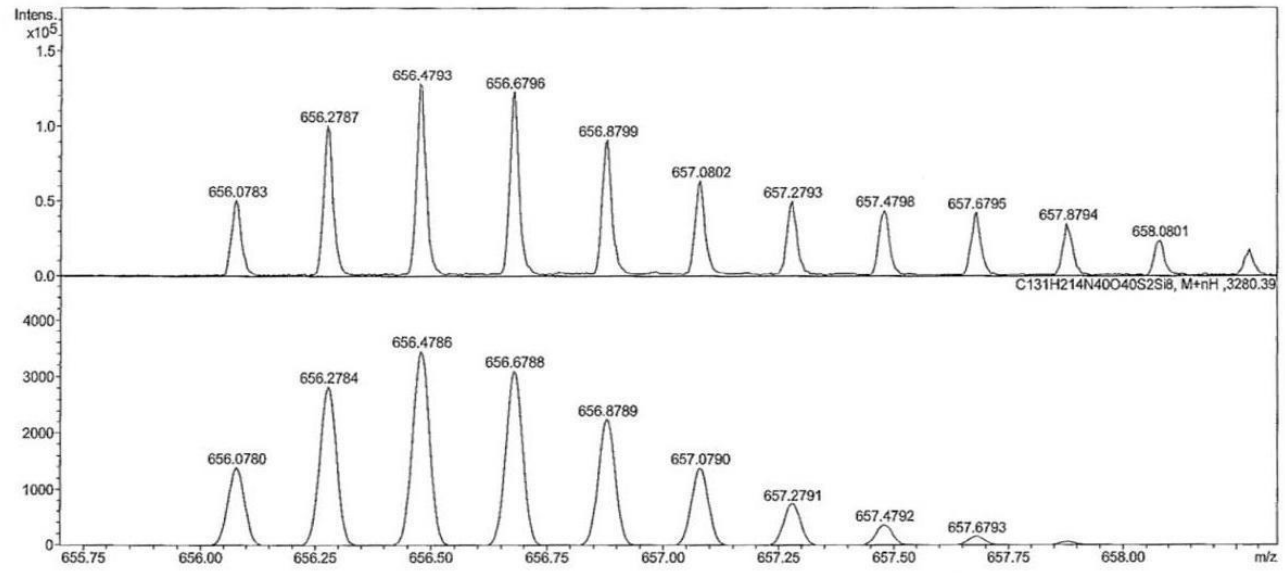

Figure ESI-66: *Section of HR ESI-MS spectrum of compound* ***32****. Upper panel: measured isotopic pattern* $[M+5H]^{5+}$*. Lower panel: simulated isotopic pattern* $[M+5H]^{5+}$*.*

2 References

[1] W. Reppe, *Justus Liebigs Ann. Chem.,* **1948**, *560*, 1-92. (page 66)

[2] V. Dulery, O. Renaudet, P. Dumy, Tetrahedron, **2007**, *63*, 11952–11958.

[3] R. Pipkorn, W. Waldeck, B. Didinger, M. Koch, G. Mueller, M. Wiessler, K. J. Braun, *J. Pept. Sci.,* **2009**, *15*, 235−241.

[4] H. Fittler, O. Avrutina, B. Glotzbach, M. Empting, H. Kolmar, *Org. Biomol. Chem*., **2013**, *11*, 1848–1857.

[5] M. Reinwarth, B. Glotzbach, M. Tomaszowski, S. Fabritz, O. Avrutina, H. Kolmar, *ChemBioChem*, **2013**, *14*, 137–146.

9.3. Experimental and analytical data appending to section 8.3

Electronic Supplementary Material (ESI) for Organic & Biomolecular Chemistry

Supplemental Information

Cube-octameric silsesquioxane-mediated cargo peptide delivery into living cancer cells

Sebastian Hörner, Sebastian Fabritz, Henry D. Herce, Olga Avrutina, Christian Dietz, Robert W. Stark, M. Cristina Cardoso, and Harald Kolmar

Content

Compound 2 (Fmoc-L-cysteine heptaamino-COSS) and 2a (Fmoc-(S-trityl)-L-cysteine heptaamino-COSS)

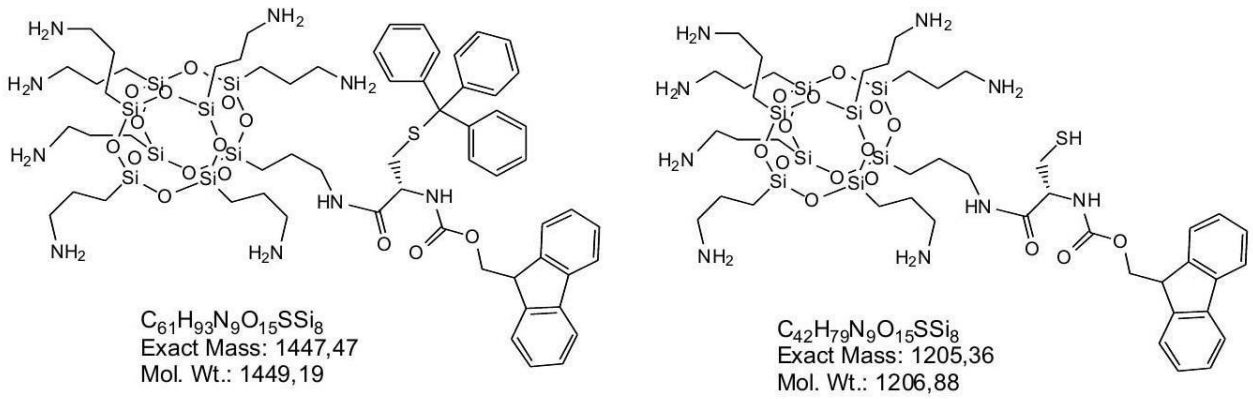

Fig. S1: Chemical structure of Fmoc-(S-trityl)-L-cysteine heptaamino-COSS **2a** (left) and unprotected Fmoc-L-cysteine heptaamino-COSS **2** (right).

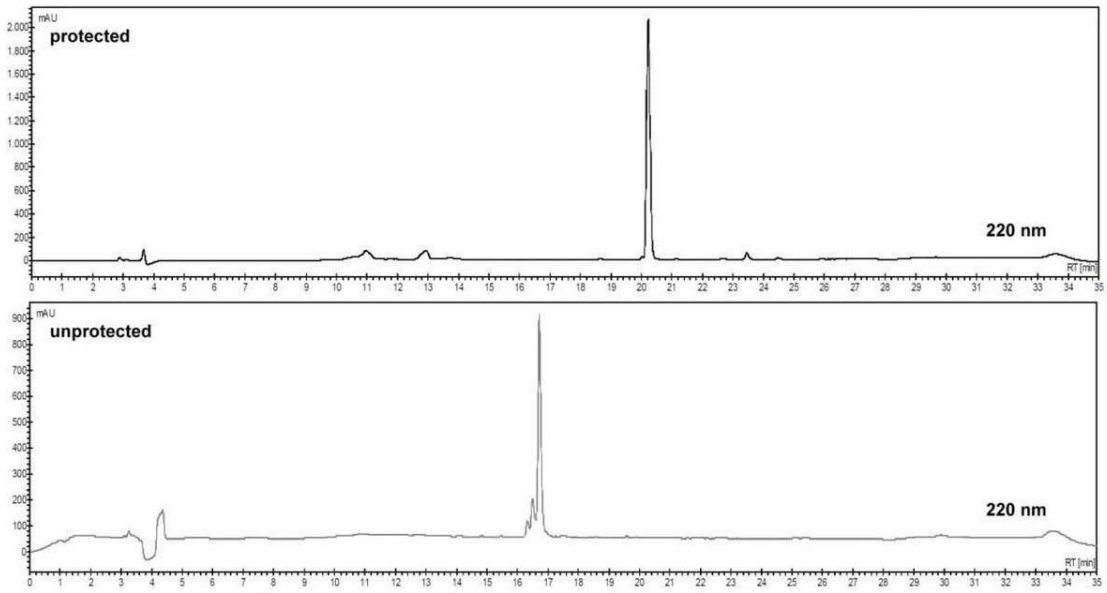

Fig. S2: Analytical RP-HPLC traces of trityl-protected (**2a**) and deprotected Fmoc-L-cysteine heptaamino-COSS **2**. (*Varian* 940-LC equipped with a *Phenomenex* Luna C_{18} column (5u, 100 A, 250×4.60 mm, 5 µm). Eluent A: 0.1% aq. trifluoroacetic acid (TFA), eluent B: 90 % aq. acetonitrile in 0.1% aq. TFA; 10 → 80% B in 20 min preceded by 5 min isocratic 10 % B at a flow rate of 1 mL min^{-1}).

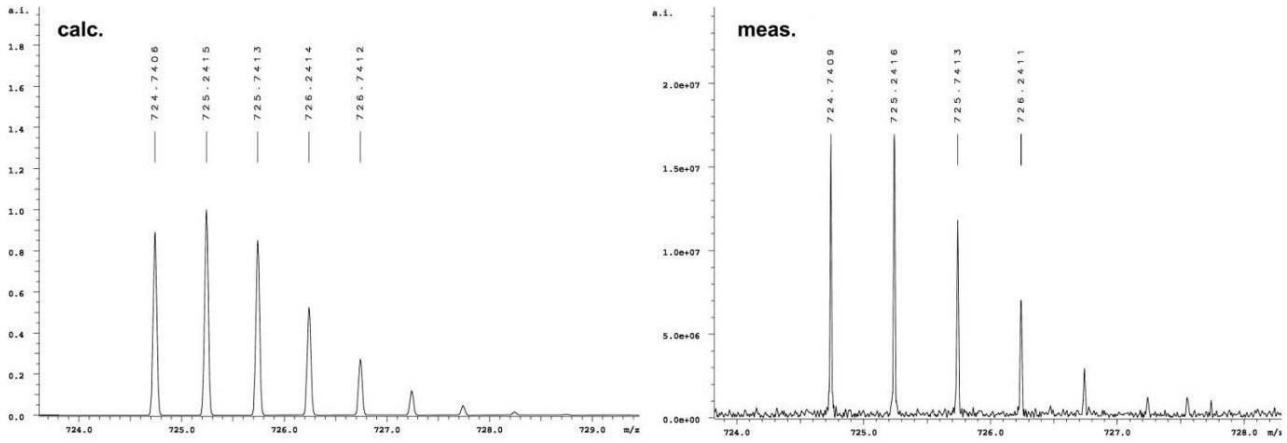

Fig. S3: HR-MS measurement of compound **2a**; left: calculated isotopic pattern $[M+2H]^{2+}$= 724.7406; right: measured isotopic pattern $[M+2H]^{2+}$= 724.7409.

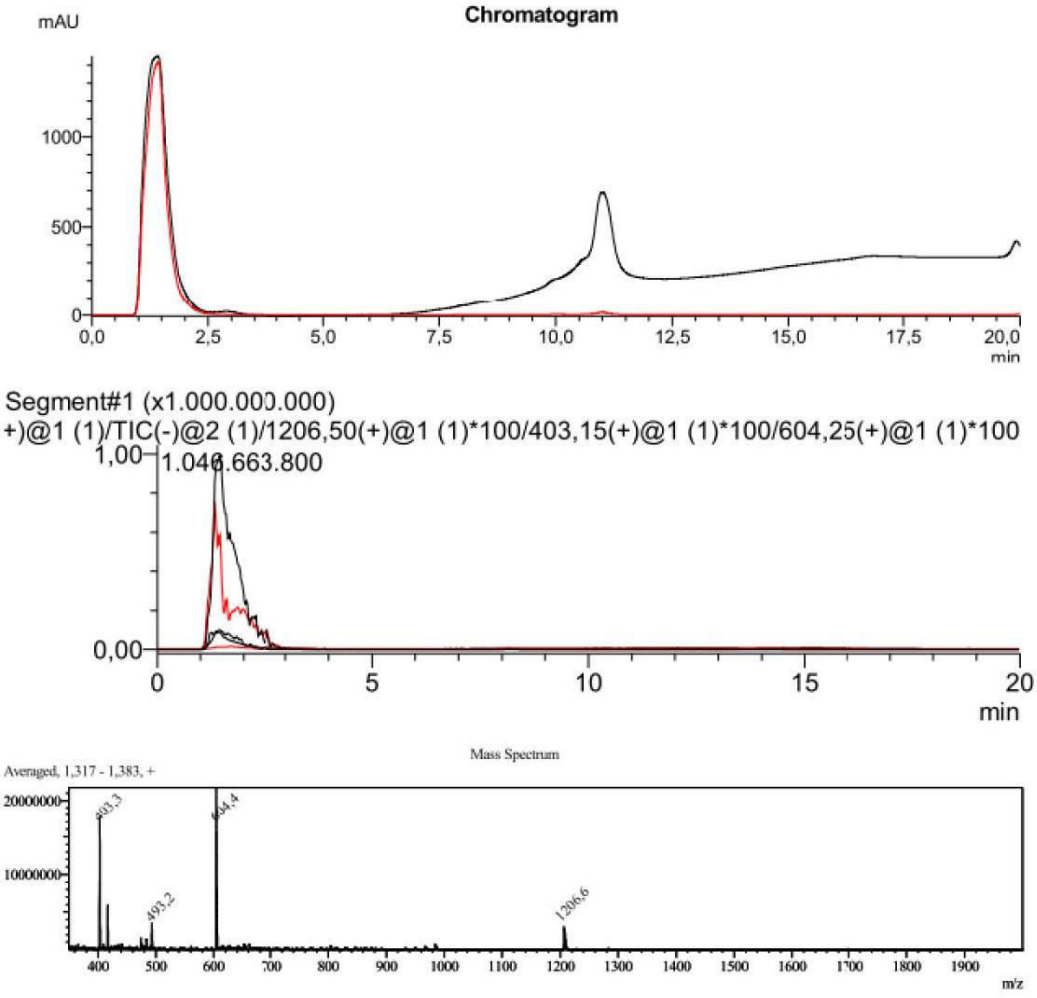

Fig. S4 LC-MS (ESI) measurement of compound **2**.

Compound 3 (fluorescein-labeled PCNA binding peptide)

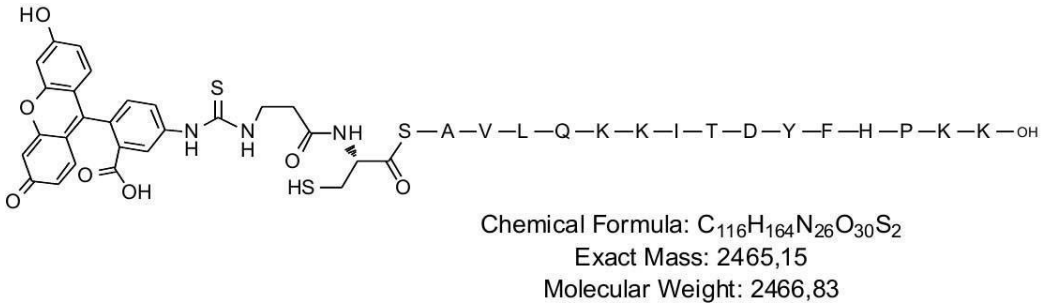

Chemical Formula: $C_{116}H_{164}N_{26}O_{30}S_2$
Exact Mass: 2465,15
Molecular Weight: 2466,83

Fig. S5: Amino acid sequence and chemical structure of fluorescein-labeled PCNA binding peptide **3**.

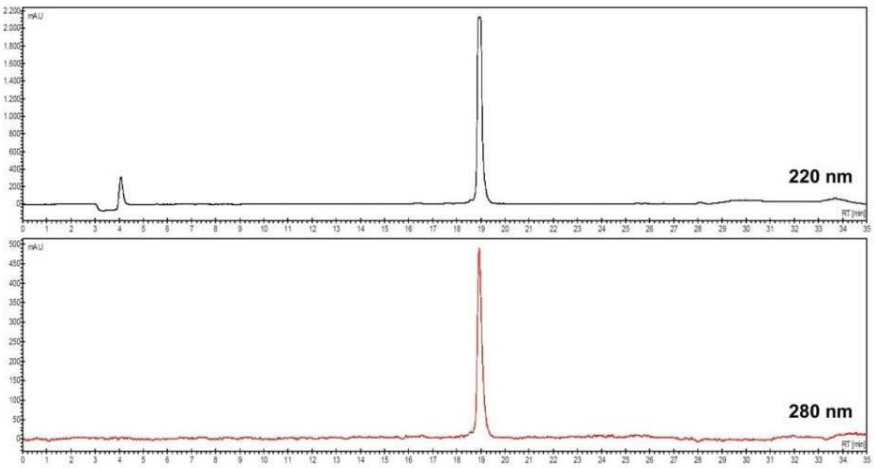

Fig. S6: Analytical RP-HPLC traces of FITC-labeled PCNA binding peptide **3** (*Varian* 940-LC equipped with a *Phenomenex* Luna C_{18} column (5u, 100 A, 250×4.60 mm, 5 µm). Eluent A: 0.1% aq. trifluoroacetic acid (TFA), eluent B: 90 % aq. acetonitrile in 0.1% aq. TFA; 25 → 50% B in 20 min preceded by 5 min isocratic 25 % B at a flow rate of 1 mL min^{-1}).

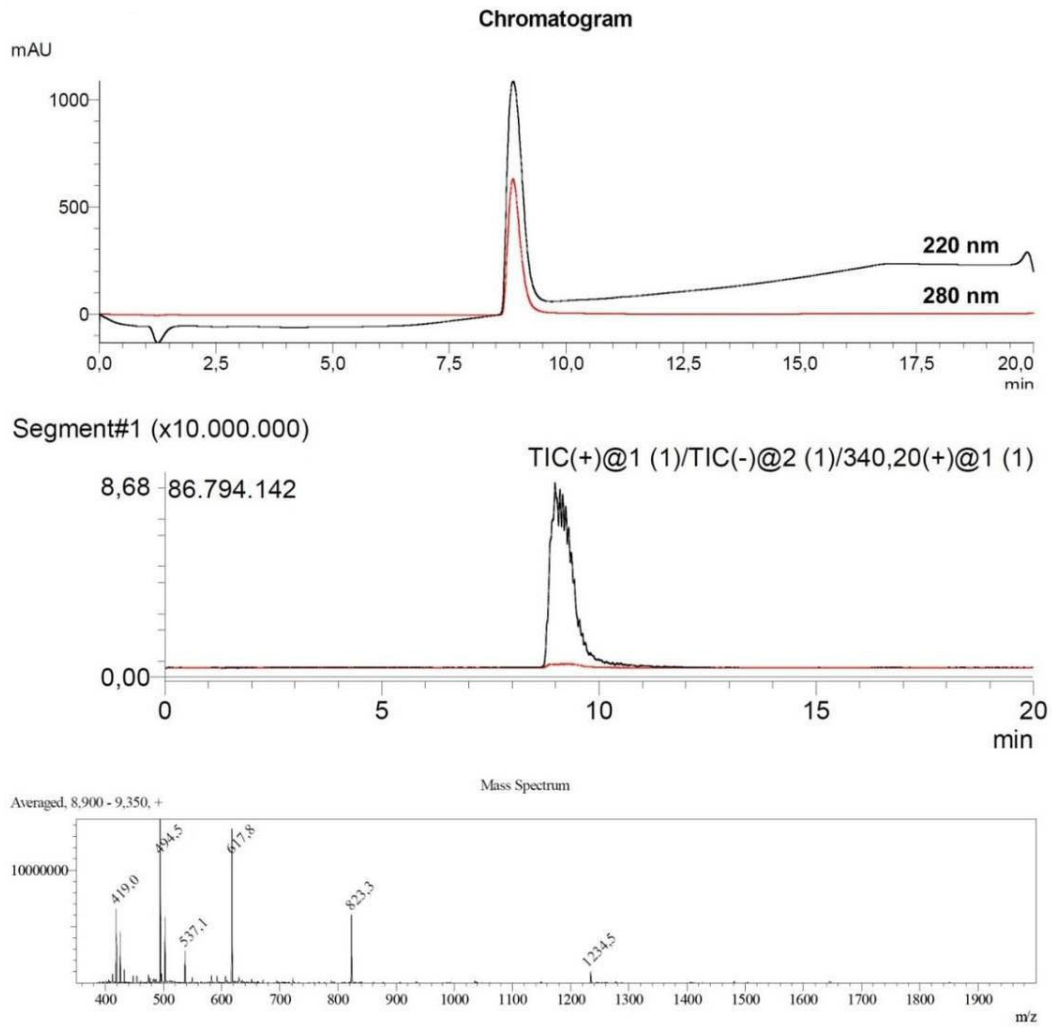

Fig. S7: LC-MS (ESI) measurement of the purified fluorescein-labeled PCNA binding peptide **3**.

Compound 4 (fluorescently labeled PCNA binding peptide coupled to Fmoc-L-cysteine heptaamino-COSS)

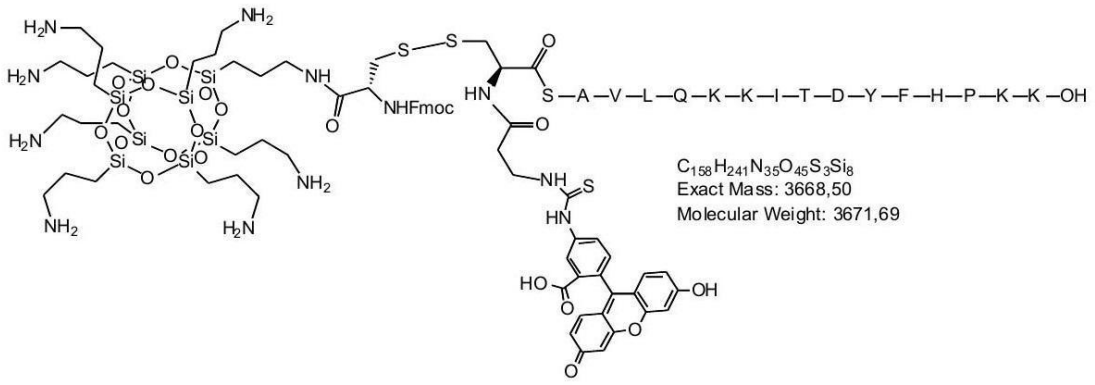

Fig. S8: Chemical structure of compound **4**.

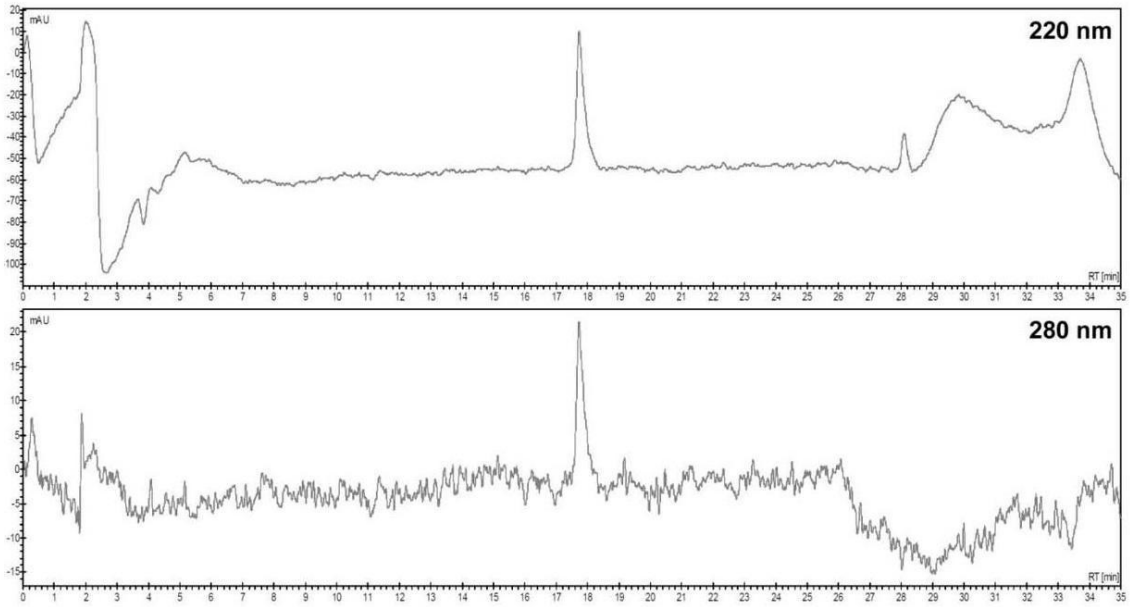

Fig. S9: Analytical RP-HPLC traces of compound **4** (*Varian* 940-LC equipped with a *Phenomenex* Luna C_{18} column (5u, 100 A, 250×4.60 mm, 5 µm). Eluent A: 0.1% aq. trifluoroacetic acid (TFA), eluent B: 90 % aq. acetonitrile in 0.1% aq. TFA; 25 → 50% B in 20 min preceded by 5 min isocratic 10 % B at a flow rate of 1 mL min^{-1}).

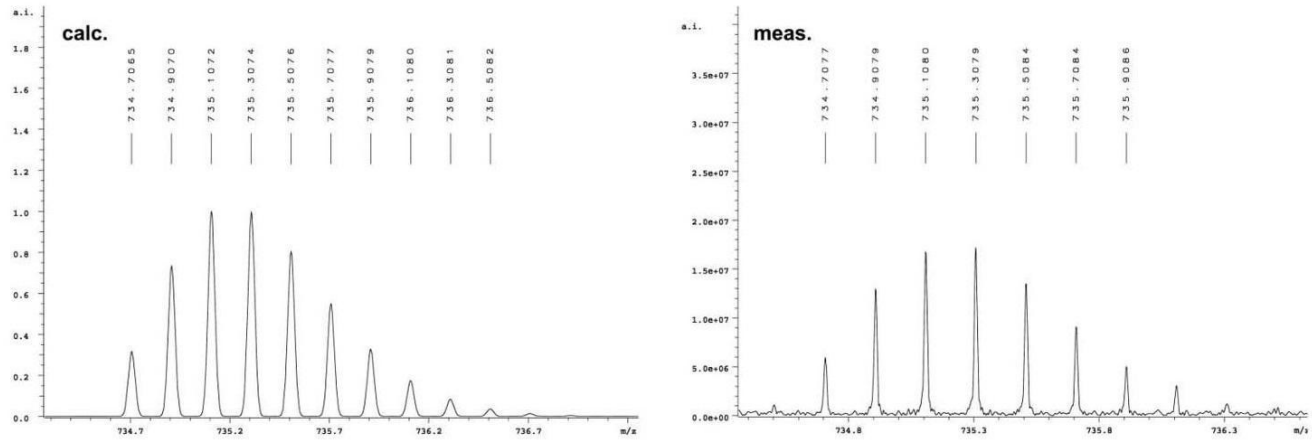

Fig. S10: HR-MS measurement of compound **4**; left: calculated isotopic pattern $[M+5H]^{5+}$= 734.7065; right: measured isotopic pattern $[M+5H]^{5+}$= 734.7077.

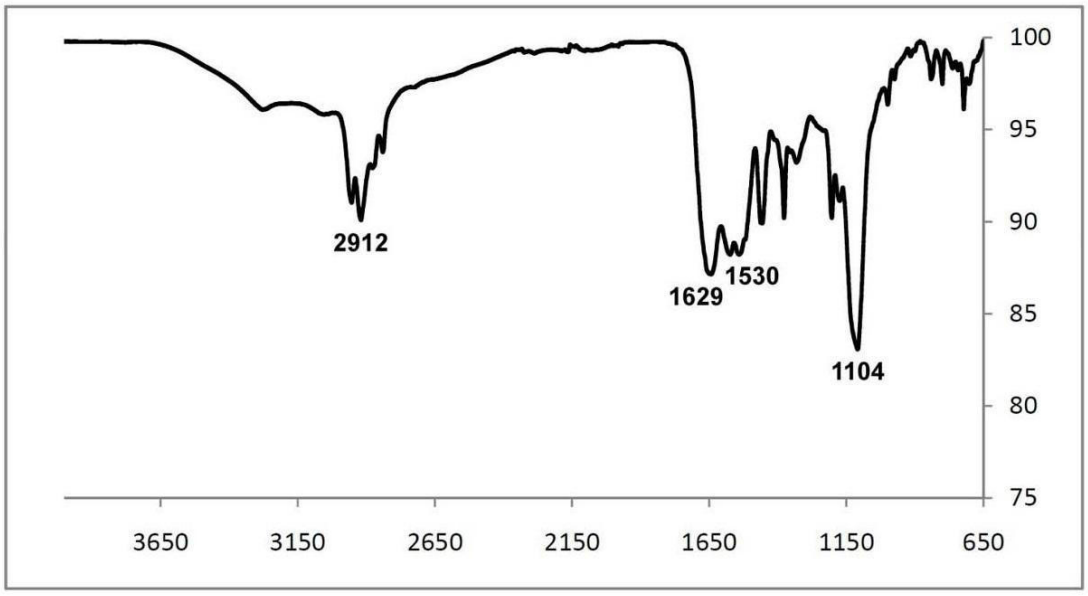

Fig. S11: FT-IR spectrum of compound **4**.

Compound 5 (cysteine-β-alanine-fluorescein hepataamino-COSS), 5a (cysteine-(S-trityl)-β-alanine-fluorescein), and 5b (cysteine-(S-trityl)-β-alanine-fluorescein hepataamino-COSS)

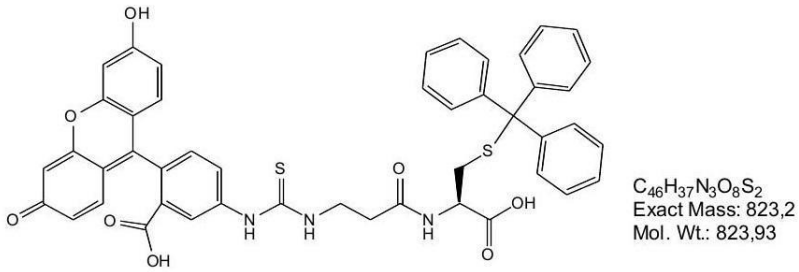

Fig. S12: Chemical structure of compound **5a**.

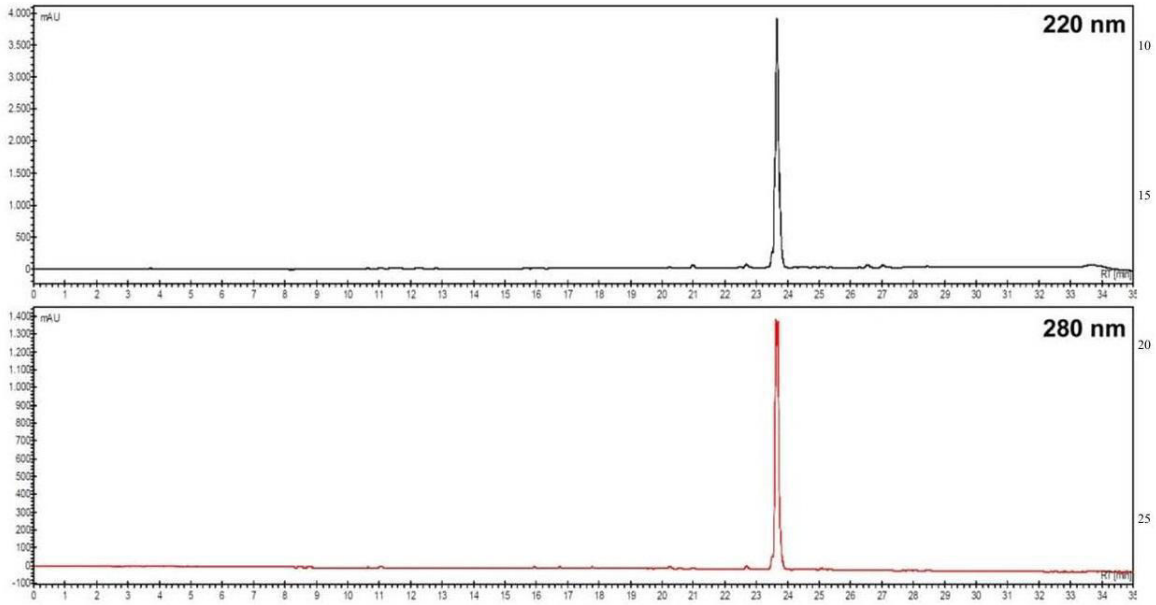

Fig. S13: Analytical RP-HPLC traces of compound **5a**. (*Varian* 940-LC equipped with a *Phenomenex* Luna C_{18} column (5u, 100 A, 250×4.60 mm, 5 µm). Eluent A: 0.1% aq. trifluoroacetic acid (TFA), eluent B: 90 % aq. acetonitrile in 0.1% aq. TFA; 10 → 100% B in 20 min preceded by 5 min isocratic 10 % B at a flow rate of 1 mL min^{-1}).

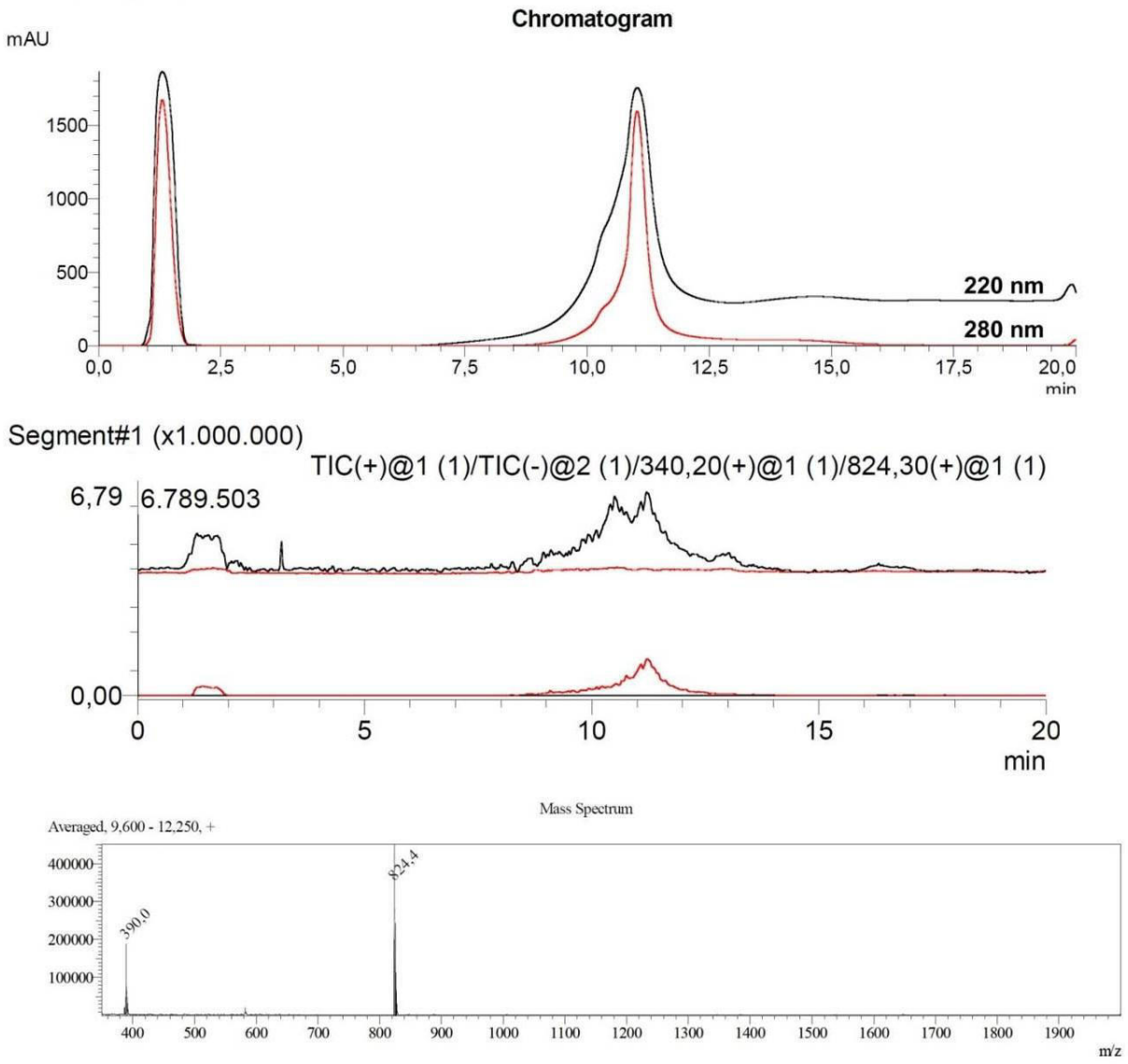

Fig. S14: LC-MS (ESI) measurement of compound **5a**.

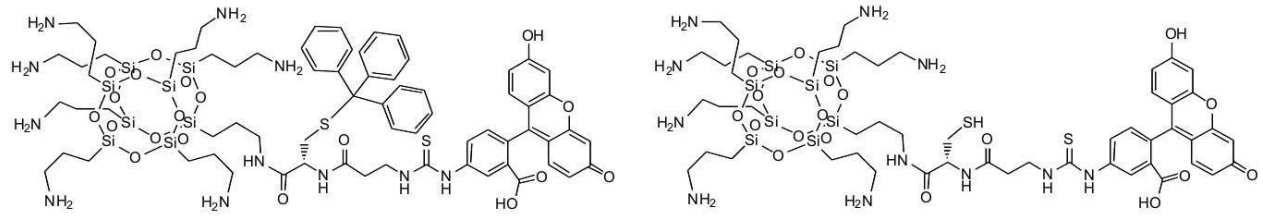

$C_{70}H_{99}N_{11}O_{19}S_2Si_8$
Exact Mass: 1685,47
Molecular Weight: 1687,41

$C_{51}H_{85}N_{11}O_{19}S_2Si_8$
Exact Mass: 1443,36
Molecular Weight: 1445,10

Fig. S15: Chemical structures of trityl protected **5b** (left) and unprotected cysteine-β-alanine-fluorescein hepataamino-COSS **5** (right).

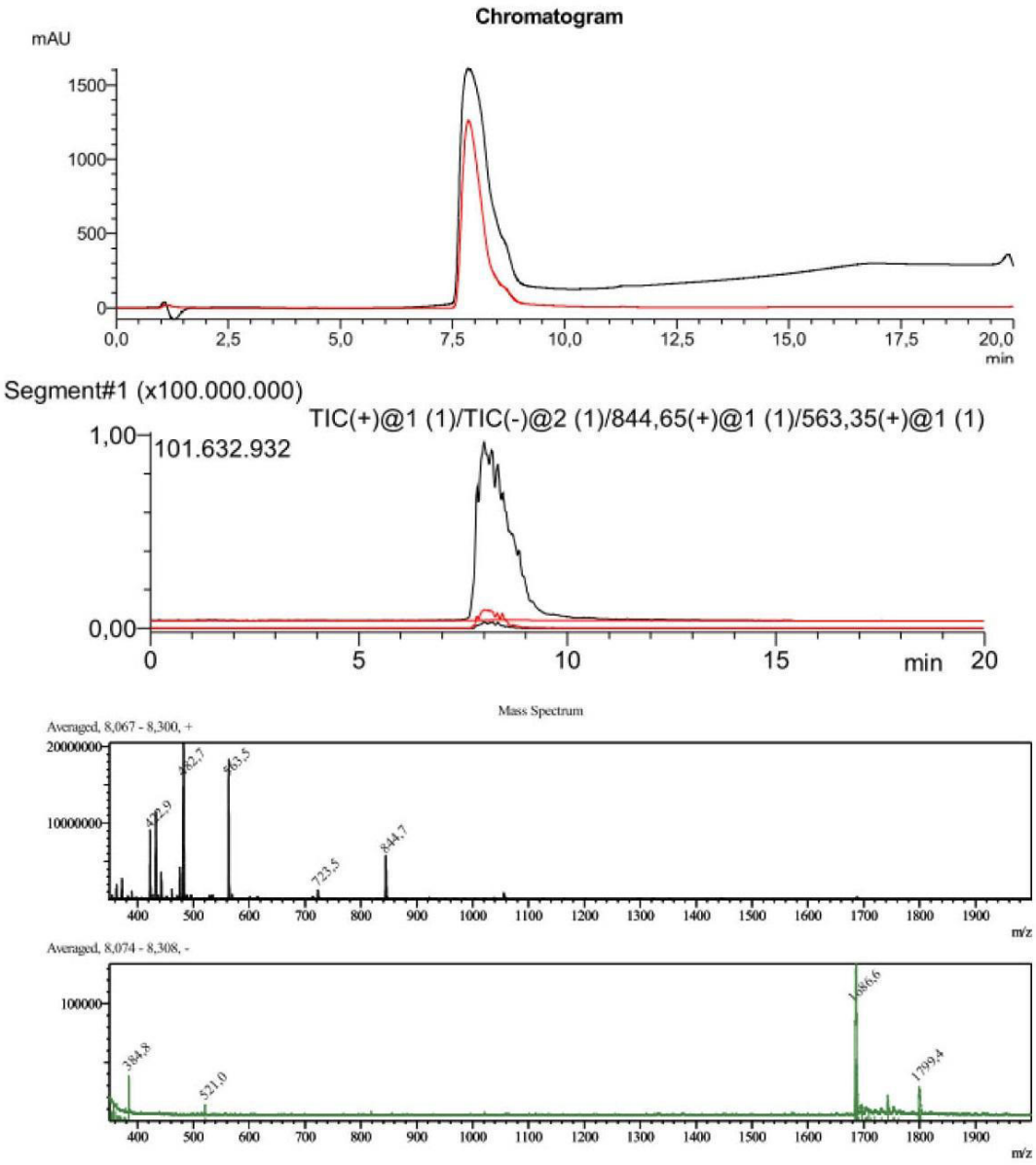

Fig. S16: LC-MS (ESI) measurement of cysteine-(S-trityl)-β-alanine-fluorescein hepataamino-COSS **5b**.

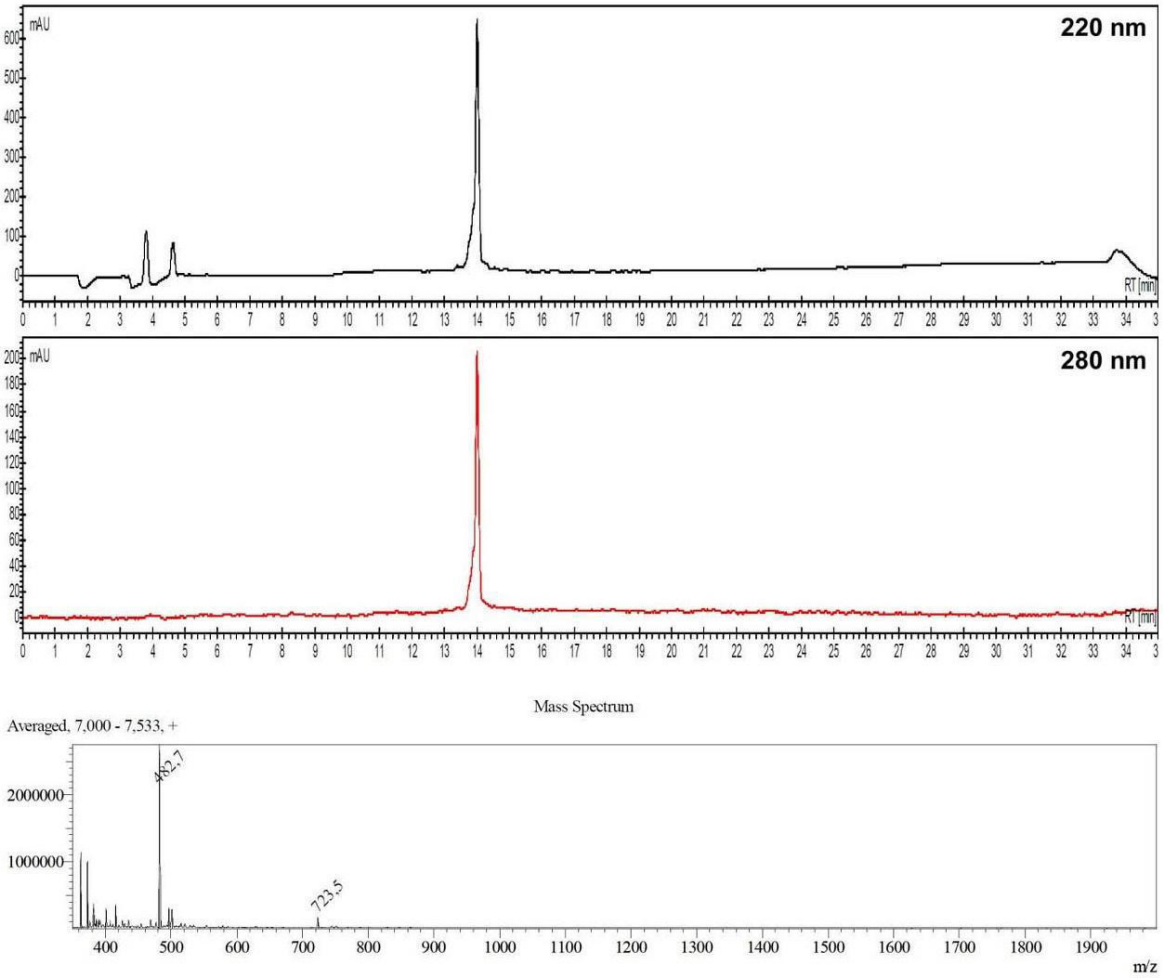

Fig. S17: Analytical RP-HPLC traces (*Varian* 940-LC equipped with a *Phenomenex* Luna C_{18} column (5u, 100 A, 250×4.60 mm, 5 µm). Eluent A: 0.1% aq. trifluoroacetic acid (TFA), eluent B: 90 % aq. acetonitrile in 0.1% aq. TFA; 10 → 100% B in 20 min preceded by 5 min isocratic 10 % B at a flow rate of 1 mL min^{-1}) and MS analysis of cysteine-β-alanine-fluorescein hepataamino-COSS **5**.

Microirradiation experiment and subsequent co-localization of fluorescently labeled PCNA binding peptide and RFP labeled PCNA after the addition of compound 4

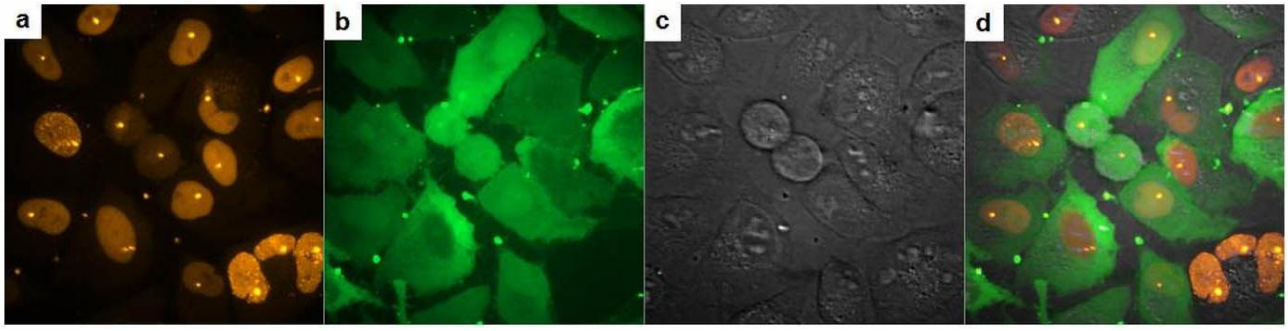

Fig. S18: Fluorescence microscopic analysis of irradiated HeLa cells 30 minutes after the addition of compound **4**. (a) PCNA (red); (b) cleaved fluorescein-labeled peptide **3** (green); (c) contrast image ; (d) overlay.

9.4. Experimental and analytical data appending to section 8.4

Supporting Information

Nanoscale Biodegradable Organic–Inorganic Hybrids for Efficient Cell Penetration and Drug Delivery

*Sebastian Hörner[+], Sascha Knauer[+], Christina Uth[+], Marina Jöst, Volker Schmidts, Holm Frauendorf, Christina Marie Thiele, Olga Avrutina, and Harald Kolmar**

Content

‡ shared lead author

1. Live-cell laser scanning confocal microscopy and fluorescence microscopy studies

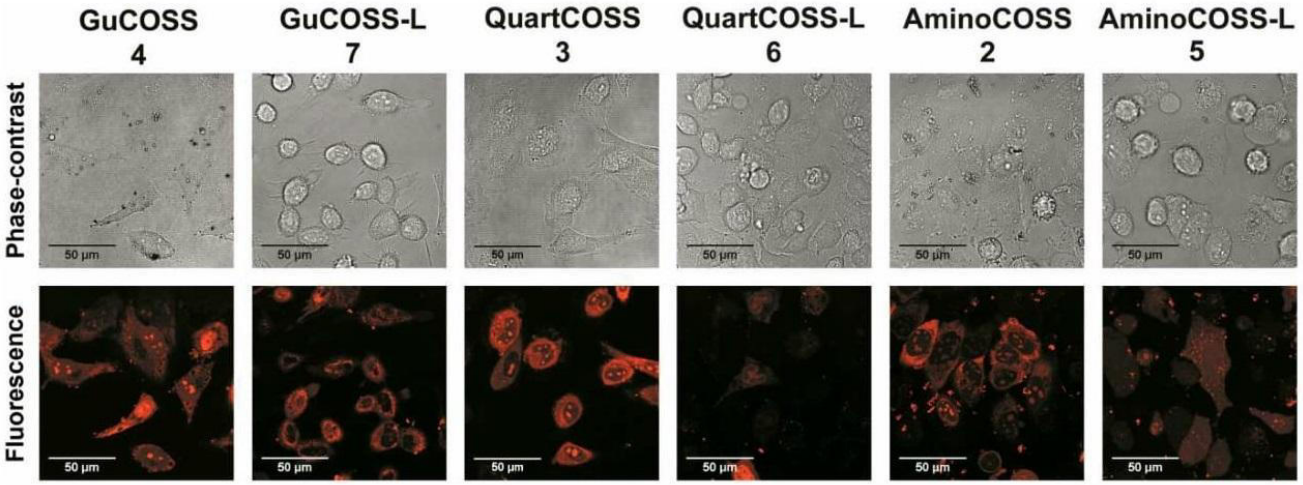

Figure S1: *Live-cell laser scanning confocal microscopy imaging of cellular uptake of TAMRA-labeled COSS derivatives 2-7. Cells were incubated with 20 µM of the respective COSS derivative in DMEM media lacking fetal bovine serum (FBS) for 30 min at 37°C. After incubation, the cells were washed thrice with PBS and investigated in DMEM media containing 2 vol% FBS. Controls with cells similarly treated in the absence of the respective COSS derivative showed no fluorescence (not shown).*

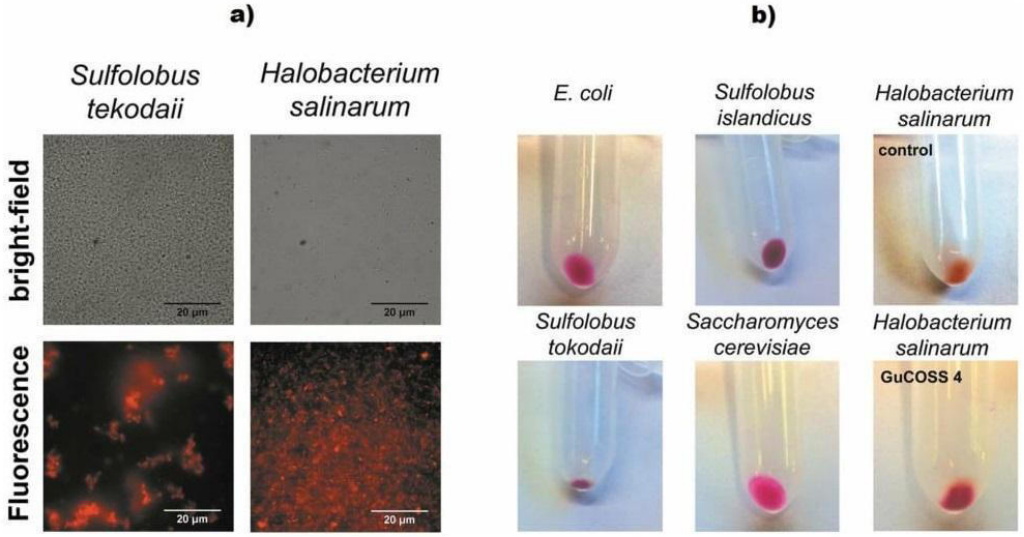

Figure S2: *Fluorescence microscopy imaging of cells incubated with TAMRA-labeled GuCOSS **4** at a concentration of 20 µM for 30 min: a) Sulfolobus tekodaii incubated at 80°C and Halobacterium salinarum incubated at ambient temperature. Controls with cells similarly treated in the absence of the respective COSS derivative showed no fluorescence. b) Pellets of cells incubated with GuCOSS **4** at a concentration of 20 µM for 30 min; E. coli incubated at 37°C; Sulfolobus islandicus incubated at 80°C; Sulfolobus tokodaii incubated at 80°C; Saccharomyces cerevisiae incubated at ambient temperature; Halobacterium salinarium incubated at ambient temperature. Due to background color of Halobacterium salinarium untreated cells are shown.*

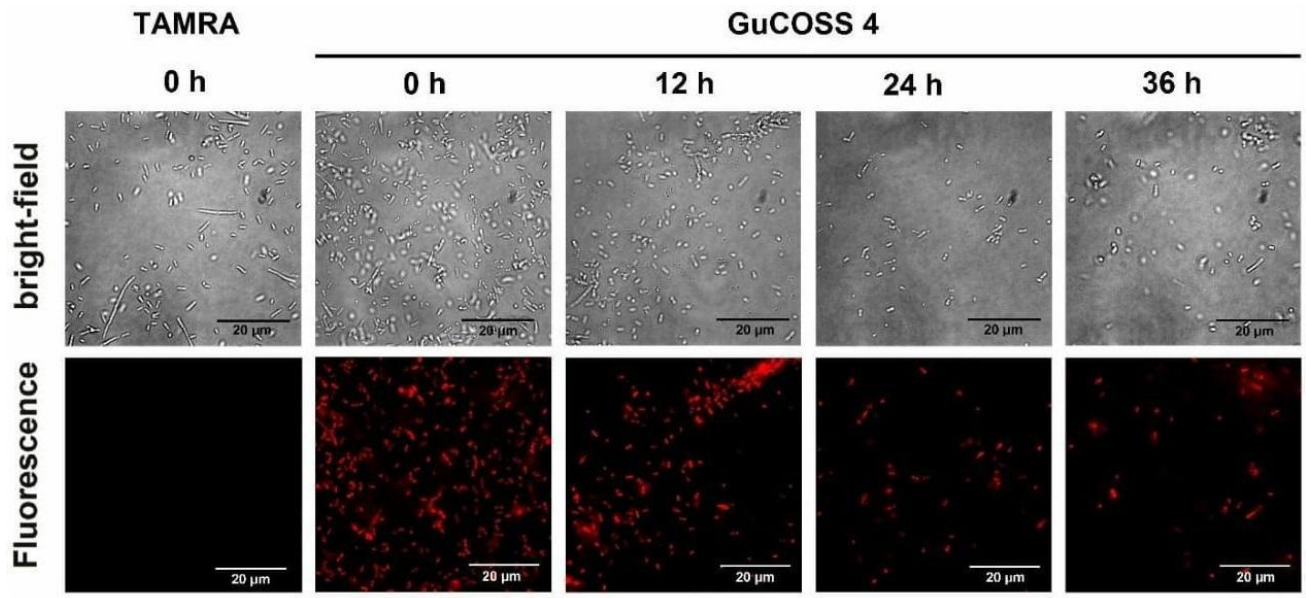

Figure S2: *c) Incubation of E.coli with GuCOSS **4** and 5-carboxytetramethylrhodamine (TAMRA) at a concentration of each 20 µM for 30 min at 37 °C. No fluorescence was observed when E. coli were incubated with solitaire TAMRA (same exposure time as for GuCOSS **4** was used). Fluorescence of E. coli incubated with GuCOSS **4** was still detectable after an incubation time of 36 h in PBS at pH 7.4, 37 °C.*

Discussion on figure S 2c:

As GuCOSS **4** could be of interest for the delivery of antibiotics, we investigated its ability to penetrate *E. coli* in detail. To that end, we incubated bacteria with 5-carboxytetramethylrhodamine (TAMRA) or TAMRA-labelled GuCOSS **4**. After incubation with **4** strong fluorescence was observed in microscopy experiments, whereas after incubation with solitaire dye no fluorescence signal was detected, suggesting that TAMRA was not associated with the cell membrane of *E. coli*. To exclude the possibility that the recorded fluorescence was attributed to the accumulation of **4** on the cell membrane *via* its GuCOSS part, we examined stained bacteria under COSS degradation-promoting conditions. Indeed, we found that bacterial cells treated with **4** retained their fluorescence after incubation in PBS (pH 7.4) for 36 hours (Figure S 2c). As it is known that the COSS carrier degrades at pH 7.4 within 18 h (Figure 3c-d, Figure S9), this observation clearly indicates that the TAMRA fluorophore is trapped inside the bacteria.

2. Flow-cytometric studies

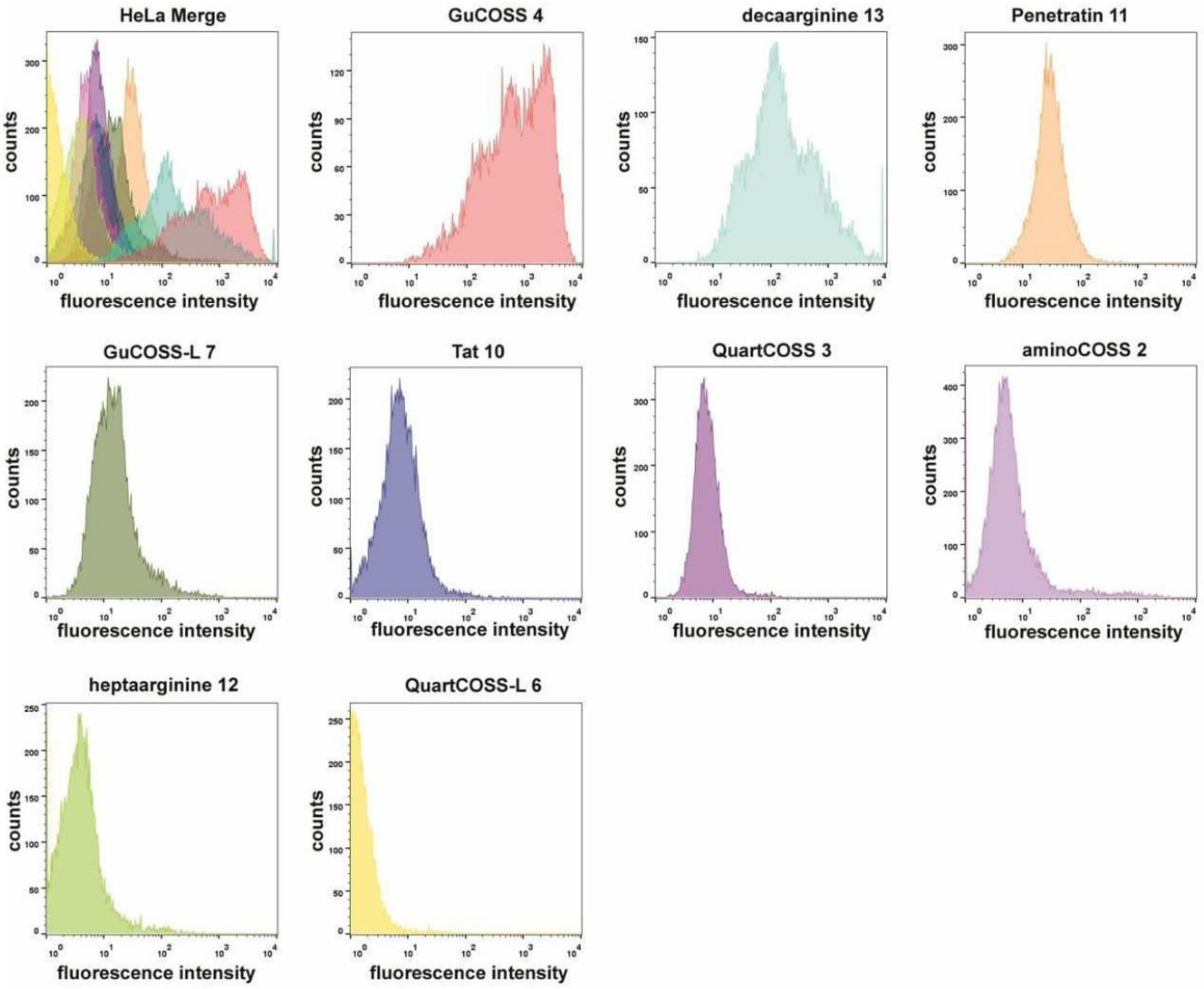

Figure S3 a: *First of three independent flow-cytometric studies of the cellular uptake of highly efficient COSS derivatives (**2**, **3**, **4**, **6**, and **7**) and cell-penetrating peptides **10-13** in HeLa cells. Cells were incubated with 20 µM of the respective compound in DMEM lacking fetal bovine serum (FBS) for 10 min at 37°C. After incubation, the cells were washed thrice with PBS both before and after trypsinization for 10 min at ambient temperature. Afterwards cells were kept on ice. Experiments with HeLa cells were performed in triplicates, each comprising 10000 events; average values are shown.*

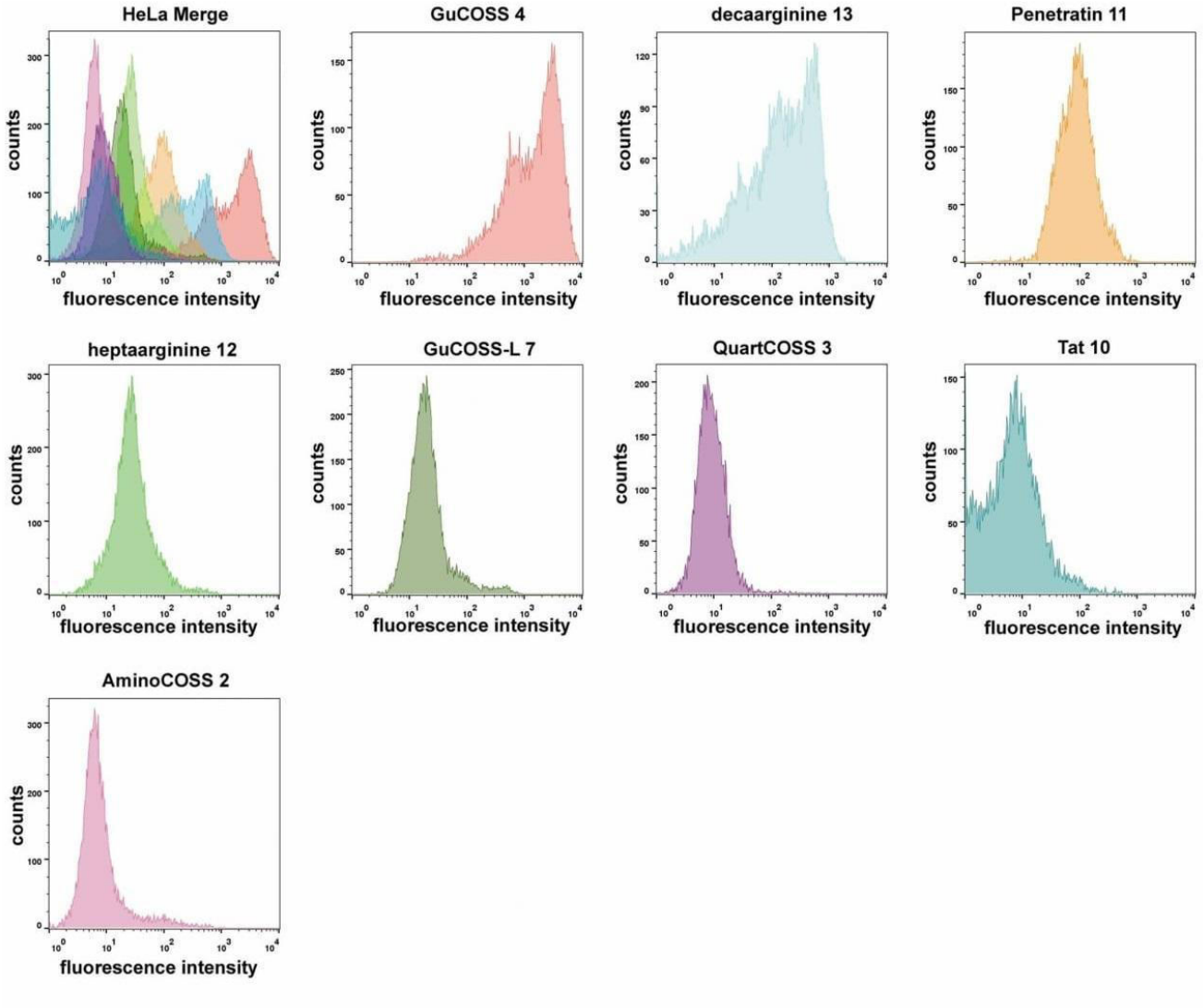

Figure S3 b: *Second of three independent flow-cytometric studies of the cellular uptake of highly efficient COSS derivatives (**2**, **3**, **4**, and **7**) and cell-penetrating peptides **10-13** in HeLa cells. Cells were incubated with 20 μM of the respective compound in DMEM lacking fetal bovine serum (FBS) for 10 min at 37°C. After incubation, the cells were washed thrice with PBS both before and after trypsinization for 10 min at ambient temperature. Afterwards cells were kept on ice. Experiments with HeLa cells were performed in triplicates, each comprising 10000 events; average values are shown.*

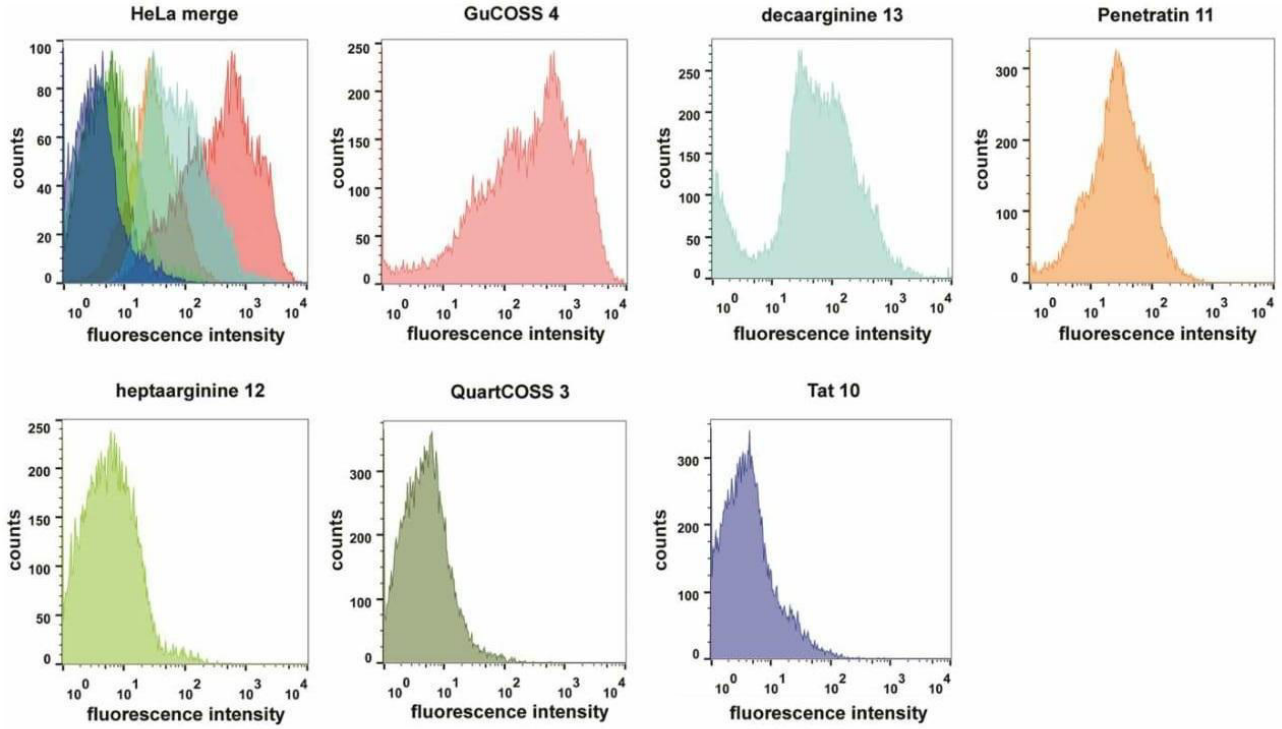

Figure S3 c: *Third of three independent flow-cytometric studies of the cellular uptake of highly efficient COSS derivatives (**3** and **4**) and cell-penetrating peptides **10-13** in HeLa cells. Cells were incubated with 20 µM of the respective compound in DMEM lacking fetal bovine serum (FBS) for 10 min at 37°C. After incubation, the cells were washed thrice with PBS both before and after trypsinization for 10 min at ambient temperature. Afterwards cells were kept on ice. Experiments with HeLa cells were performed in triplicates, each comprising 10000 events; average values are shown.*

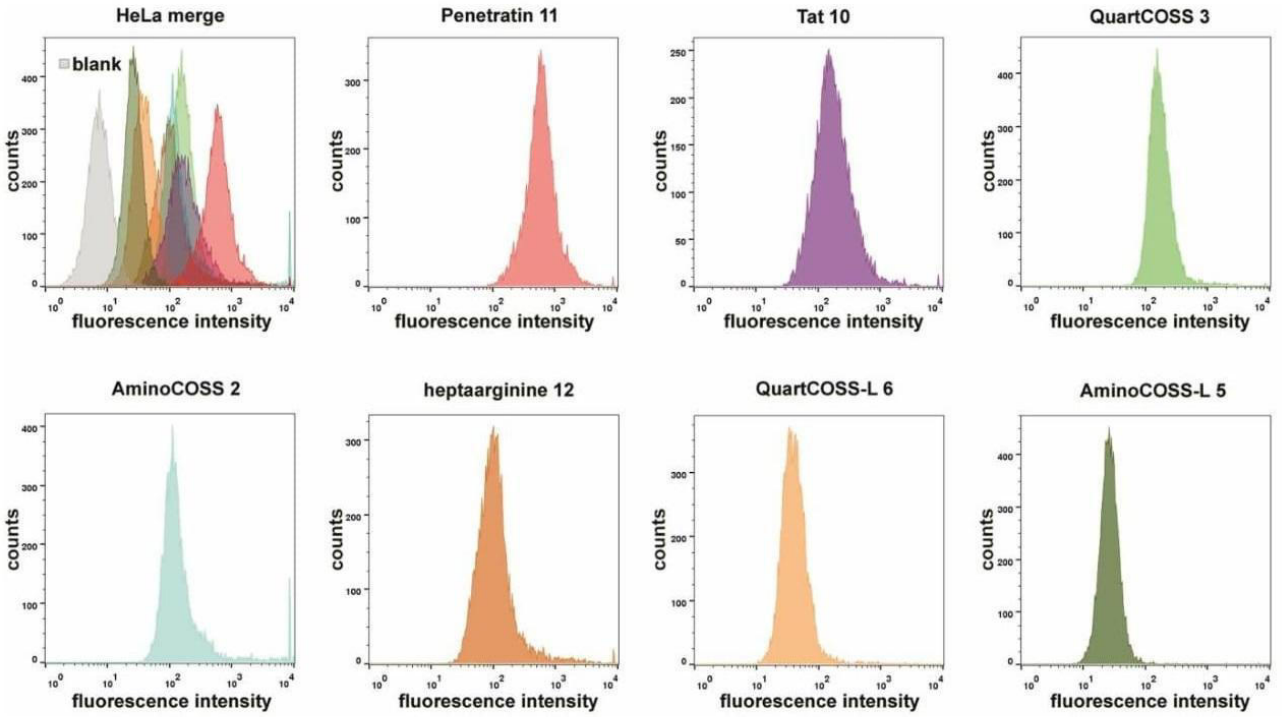

Figure S3 d: *First of three independent flow-cytometric studies of the cellular uptake of COSS derivatives (**2**, **3**, **5**, and **6**) and cell-penetrating peptides **10-12** in HeLa cells. Cells were incubated with 20 µM of the respective compound in DMEM lacking fetal bovine serum (FBS) for 10 min at 37°C. After incubation, the cells were washed thrice with PBS both before and after trypsinization for 10 min at ambient temperature. Afterwards cells were kept on ice. Experiments with HeLa cells were performed in triplicates, each comprising 10000 events; average values are shown.*

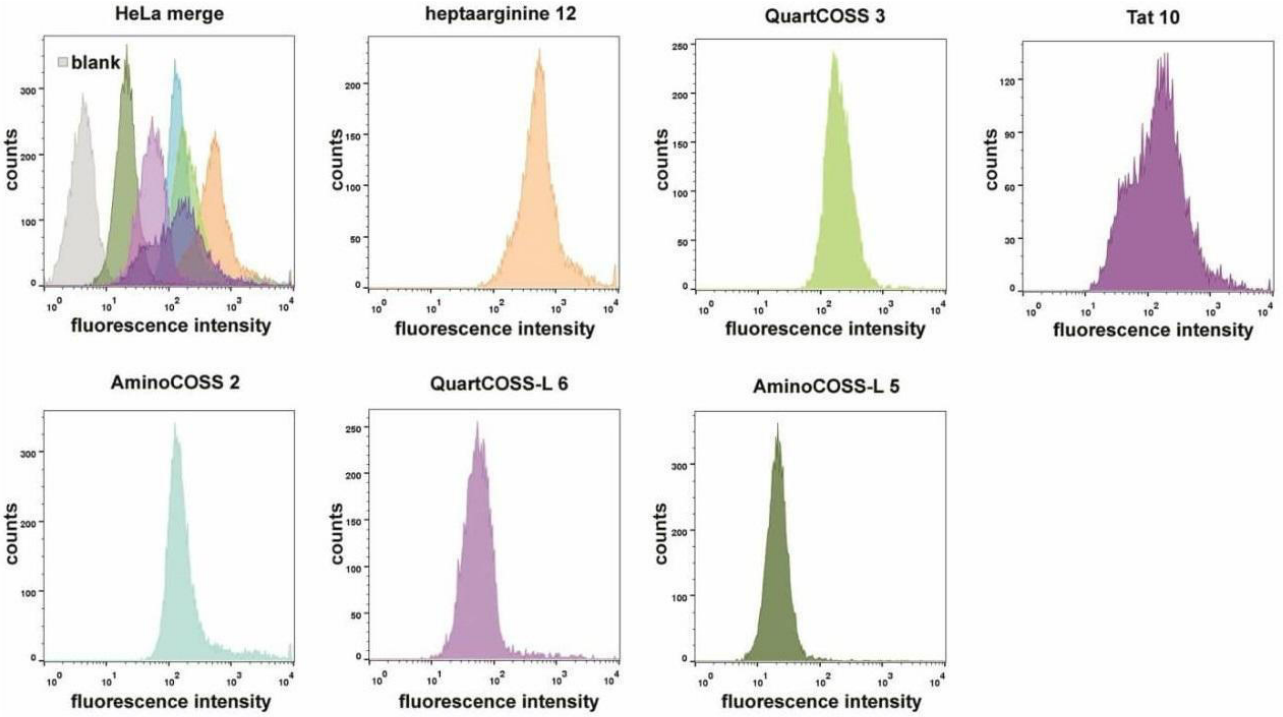

Figure S3 e: *Second of three independent flow-cytometric studies of the cellular uptake of COSS derivatives (**2**, **3**, **5**, and **6**) and cell-penetrating peptides **10** and **12** in HeLa cells. Cells were incubated with 20 µM of the respective compound in DMEM lacking fetal bovine serum (FBS) for 10 min at 37°C. After incubation, the cells were washed thrice with PBS both before and after trypsinization for 10 min at ambient temperature. Afterwards cells were kept on ice. Experiments with HeLa cells were performed in triplicates, each comprising 10000 events; average values are shown.*

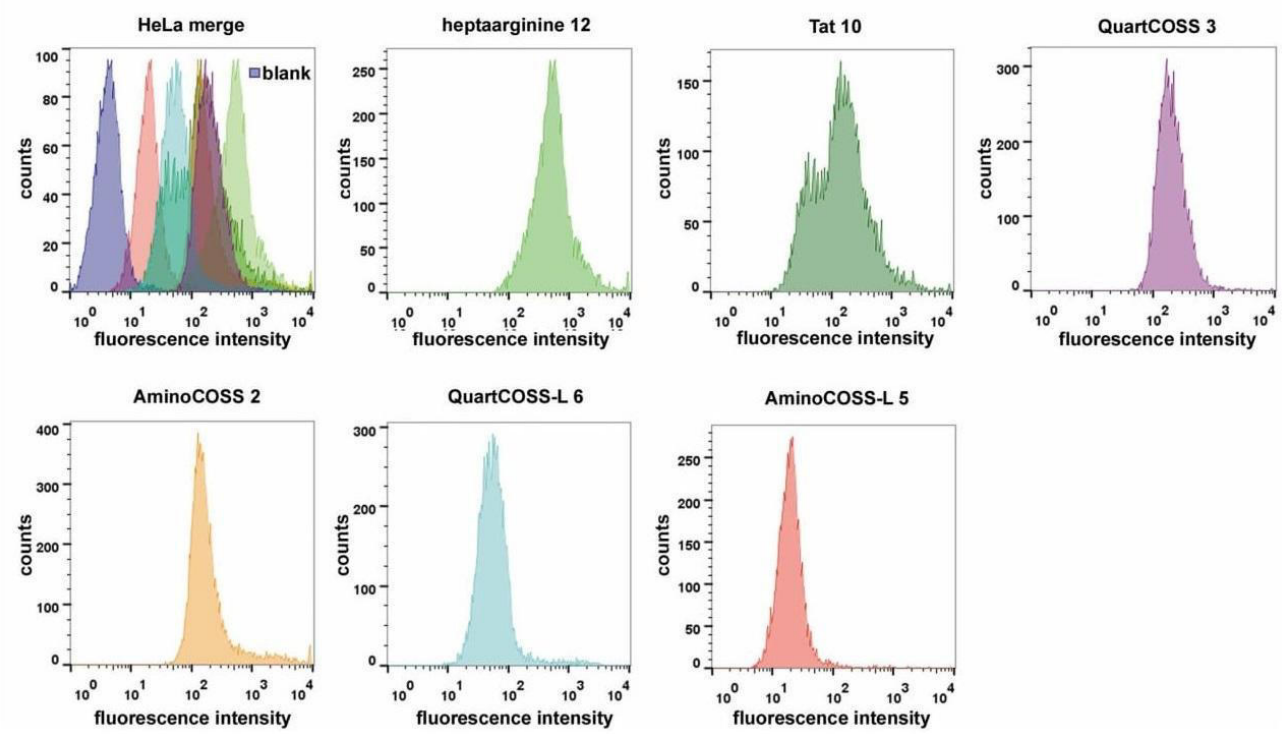

Figure S3 f: *Third of three independent flow-cytometric studies of the cellular uptake of COSS derivatives (**2**, **3**, **5**, and **6**) and cell-penetrating peptides **10** and **12** in HeLa cells. Cells were incubated with 20 µM of the respective compound in DMEM lacking fetal bovine serum (FBS) for 10 min at 37°C. After incubation, the cells were washed thrice with PBS both before and after trypsinization for 10 min at ambient temperature. Afterwards cells were kept on ice. Experiments with HeLa cells were performed in triplicates, each comprising 10000 events; average values are shown.*

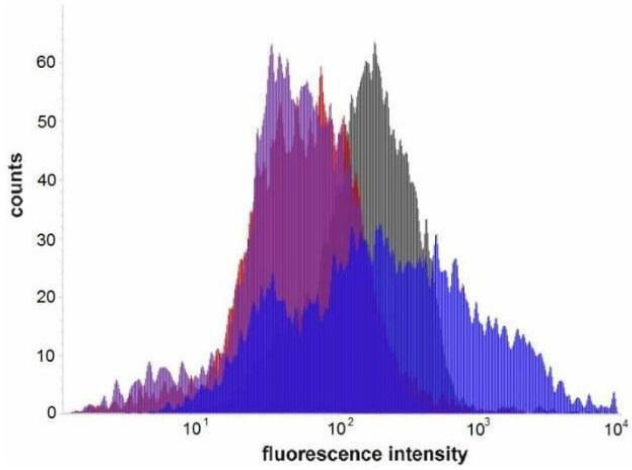

Figure S3 g: *Flow-cytometric studies of the cellular uptake of COSS derivative* ***4*** *and cell-penetrating peptides* ***10, 11*** *and* ***12*** *in HeLa cells. Cells were incubated with 20 µM of the respective compound in DMEM lacking fetal bovine serum (FBS) for 60 min at 37°C. After incubation, the cells were washed thrice with PBS both before and after trypsinization for 10 min at ambient temperature. Afterwards cells were kept on ice. Experiments with HeLa cells were performed in triplicates, each comprising 10000 events; average values are shown. Violet:* ***12****, red:* ***10****, grey:* ***11****, blue:****4****.*

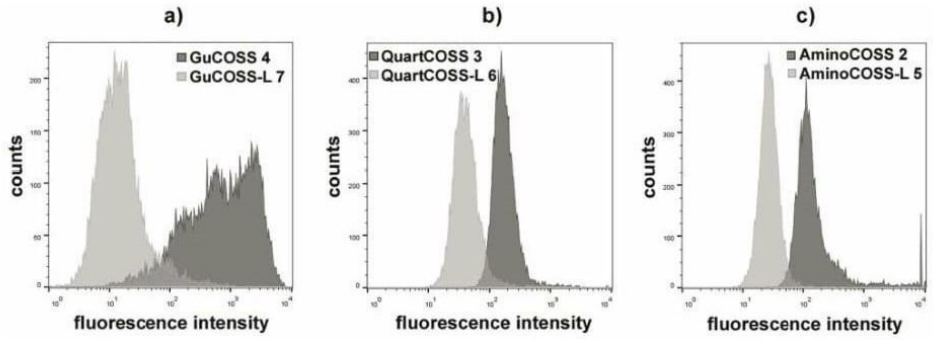

Figure S4: *Direct comparison of cellular uptake of COSS derivatives equipped with similar functional groups and varying in the linker length (in HeLa cells). a) GuCOSS* ***4*** *and GuCOSS-L* ***7*** *bearing an elongated linker; b) QuartCOSS* ***3*** *and QuartCOSS-L* ***6*** *bearing an elongated linker; c) AminoCOSS* ***2*** *and AminoCOSS-L* ***5*** *bearing an elongated linker. Cells were incubated with 20 µM of the respective compound in DMEM lacking fetal bovine serum (FBS) for 10 min at 37°C. After incubation, the cells were washed thrice with PBS both before and after trypsinization for 10 min at ambient temperature. Afterwards cells were kept on ice. Experiments with HeLa cells were performed in triplicates, each comprising 10000 events; average values are shown. In general, shorter linkers (compounds* ***2-4****) led to enhanced cellular uptake whereas cellular uptake of linker-bearing derivatives* ***5-7*** *was reduced when compared to the directly modified derivative.*

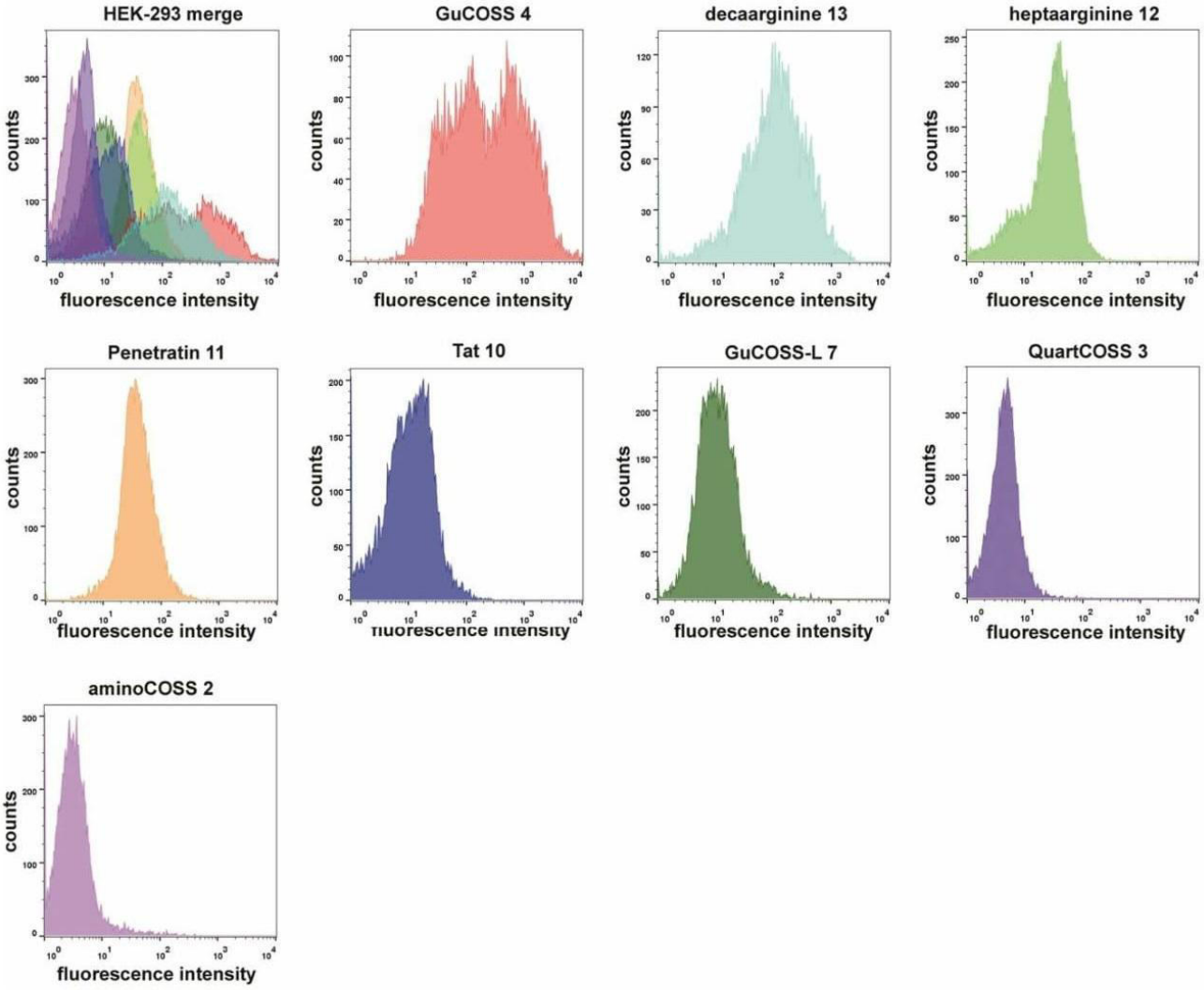

Figure S5 a: *Flow-cytometric studies of the cellular uptake of COSS derivatives (**2**, **3**, **4**, and **7**) and cell-penetrating peptides **10-13** in HEK-293 cells. Cells were incubated with 20 µM of the respective compound in DMEM lacking fetal bovine serum (FBS) for 10 min at 37°C. After incubation, the cells were washed thrice with PBS both before and after trypsinization for 10 min at ambient temperature. Afterwards cells were kept on ice. Experiments with HEK-293 cells were performed in triplicates, each comprising 10000 events; average values are shown.*

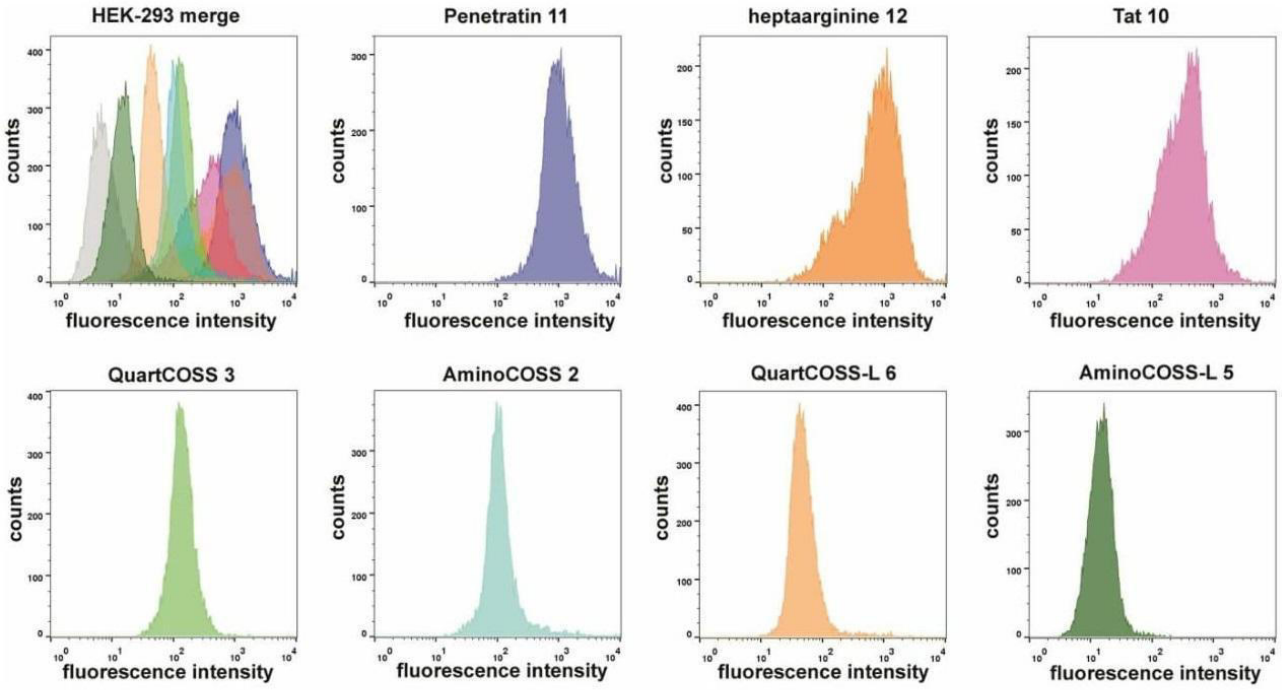

Figure S5 b: *Flow-cytometric studies of the cellular uptake of COSS derivatives (**2**, **3**, **5**, and **6**) and cell-penetrating peptides **10-12** in HEK-293 cells. Cells were incubated with 20 µM of the respective compound in DMEM lacking fetal bovine serum (FBS) for 10 min at 37°C. After incubation, the cells were washed thrice with PBS both before and after trypsinization for 10 min at ambient temperature. Afterwards cells were kept on ice. Experiments with HEK-293 cells were performed in triplicates, each comprising 10000 events; average values are shown.*

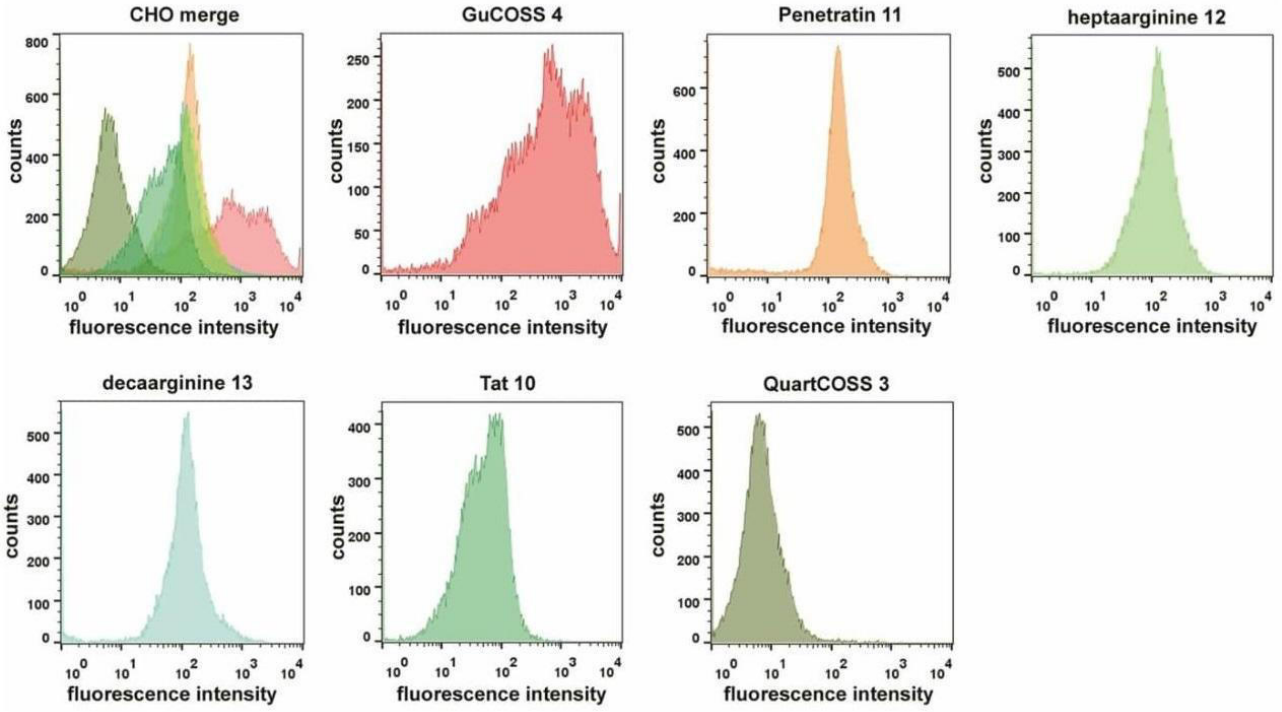

Figure S5 c: *Flow-cytometric studies of the cellular uptake of COSS derivatives (**3** and **4**) and cell-penetrating peptides **10-13** in CHO cells. Cells were incubated with 20 µM of the respective compound in DMEM lacking fetal bovine serum (FBS) for 10 min at 37°C. After incubation, the cells were washed thrice with PBS both before and after trypsinization for 10 min at ambient temperature. Afterwards cells were kept on ice. Experiments with CHO cells were performed in triplicates, each comprising 10000 events; average values are shown.*

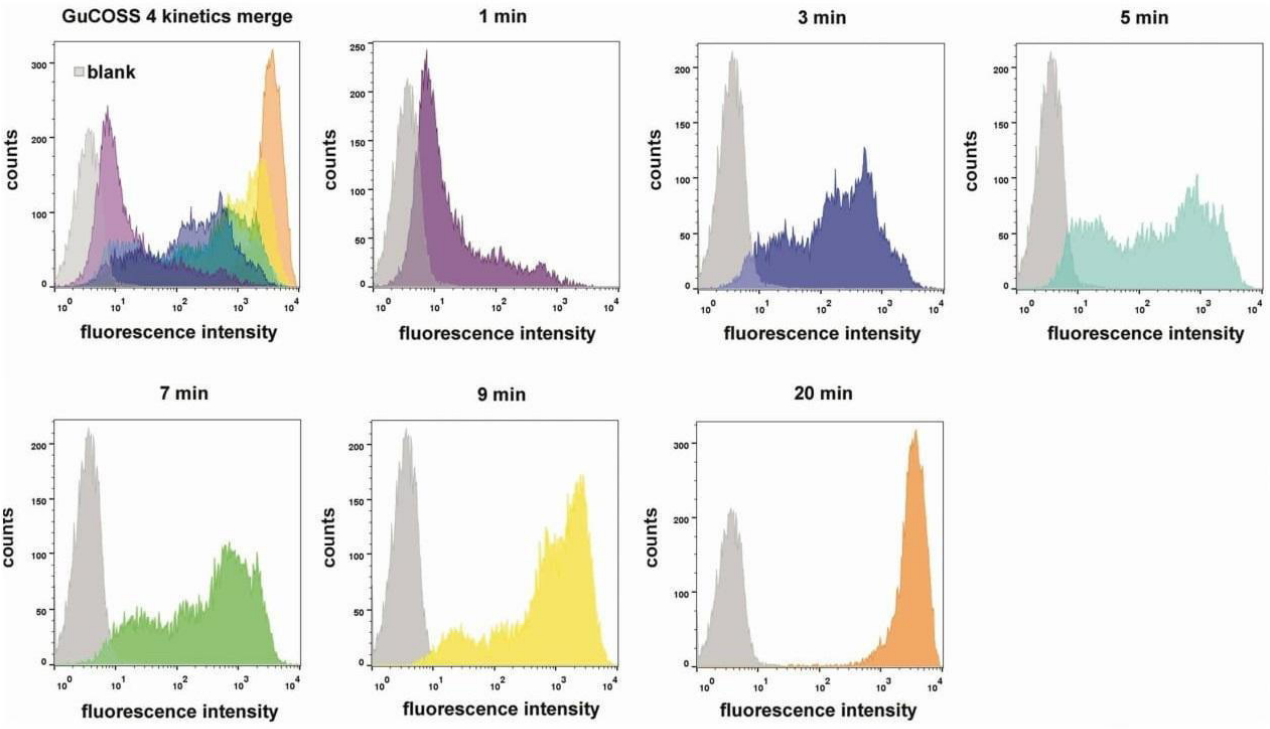

Figure S6: *Time-resolved flow-cytometric studies of the cellular uptake of GuCOSS* ***4*** *in HeLa cells. Cells were incubated for indicated times with 20 µM of compound* ***4*** *in DMEM lacking fetal bovine serum (FBS) at 37°C. After incubation, the cells were washed thrice with PBS both before and after trypsinization for 10 min at ambient temperature. Afterwards cells were kept on ice. Experiments with HeLa cells were performed in triplicates, each comprising 10000 events; average values are shown.*

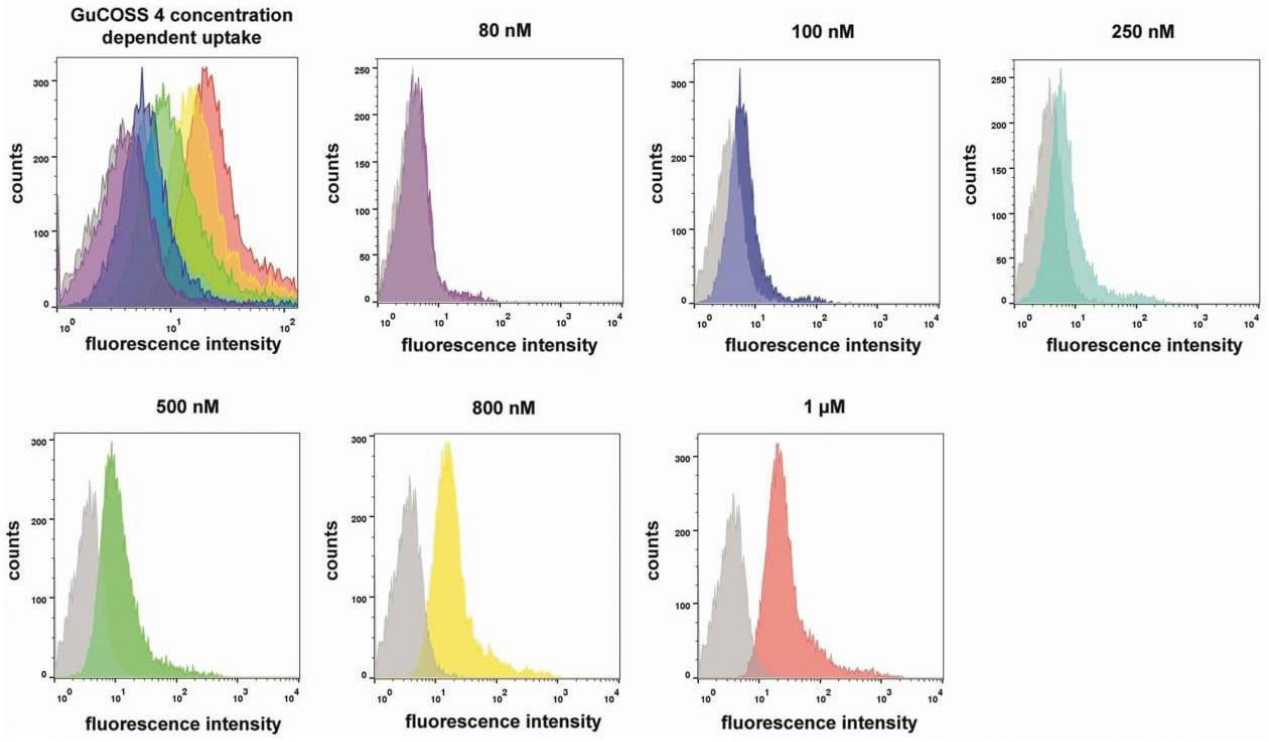

Figure S7: *Flow-cytometric studies of the cellular uptake of GuCOSS* ***4*** *in HeLa cells. Cells were incubated with compound* ***4*** *(at the indicated concentration) in DMEM lacking fetal bovine serum (FBS) for 10 min at 37°C. After incubation, the cells were washed thrice with PBS both before and after trypsinization for 10 min at ambient temperature. Afterwards cells were kept on ice. Experiments with HeLa cells were performed in triplicates, each comprising 10000 events; average values are shown.*

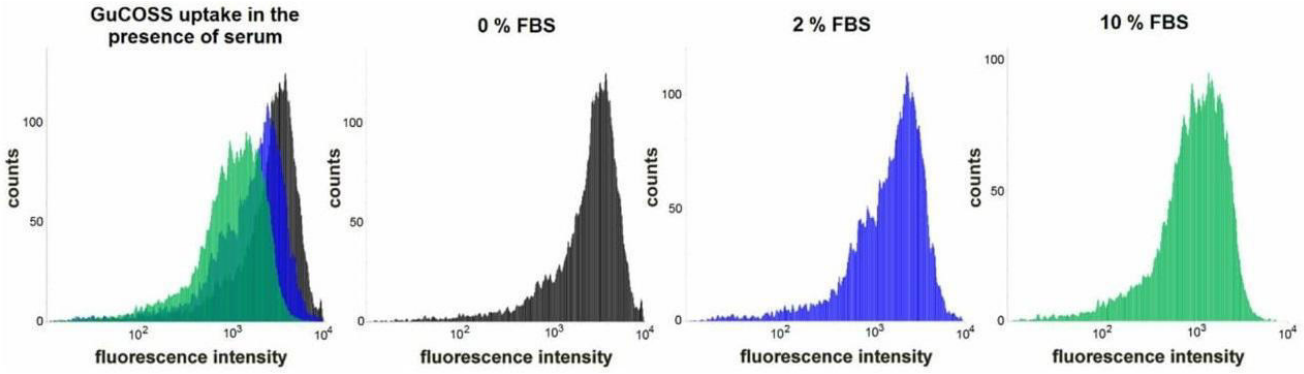

Figure S8: *Flow-cytometric studies of the cellular uptake of GuCOSS **4** in HeLa cells. Cells were incubated with compound **4** (20 µM) either in DMEM lacking fetal bovine serum (FBS) or in DMEM containing 2% or 10% FBS at 37°C for 10 min. After incubation, the cells were washed thrice with PBS both before and after trypsinization for 10 min at ambient temperature. Afterwards cells were kept on ice. Experiments with HeLa cells were performed in triplicates, each comprising 10000 events; average values are shown. Upon incubation with 2 % or 10 % FBS, mean fluorescence decreased to 72 % and 40 % of the intensity measured with DMEM lacking FBS (mean fluorescence data from three independent experiments; data not shown).*

3. Degradation studies

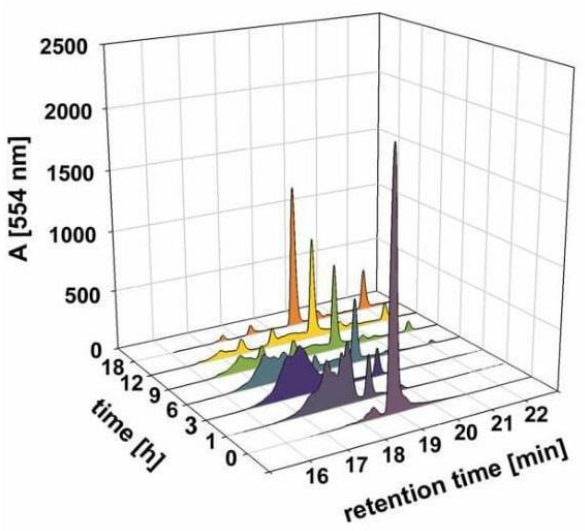

Figure S9: *Exemplary HPLC traces showing the time-resolved monitoring of the hydrolysis of GuCOSS **4**. To that end, compound **4** was investigated at a concentration of 50 µM in PBS at pH 7.0. Hydrolysis intermediates and the degradation products were identified and quantitatively analyzed by the change of the retention time and by determination of the peak area at 554 nm, which corresponds to the absorption maximum of TAMRA. Although hydroxyl-bearing hydrolysis intermediates of **4** are eluted earlier from the RP-HPLC column, the completely hydrolyzed TAMRA-bearing siloxanes have enhanced retention times.*

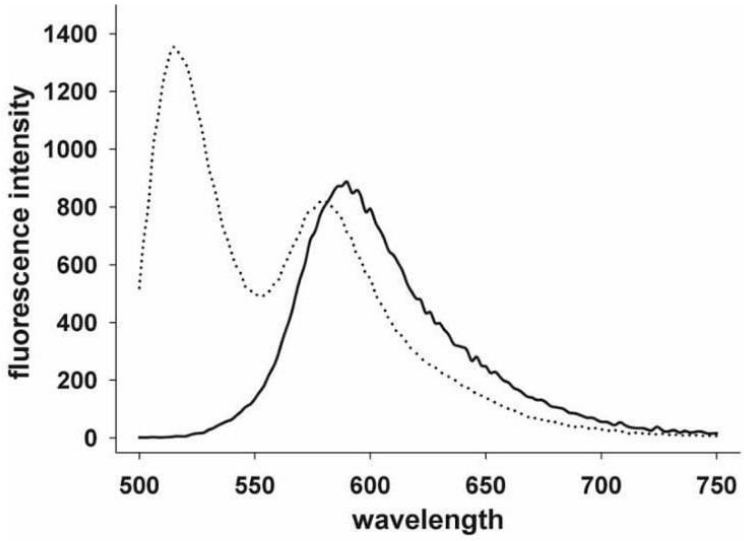

Figure S10: *Fluorescence emission spectra of intact and disassembled COSS derivative* ***9*** *bearing fluorescein and TAMRA. Samples of COSS derivative* ***9*** *(20 µM) were incubated for 30 min in 0.2 M HCl (solid line) and in 0.2 M NaOH (dotted line). Both samples were excited at 488 nm and fluorescence emission spectra were recorded using a Tecan infinite M1000 microplate reader. At acidic pH, the inorganic core of compound* ***9*** *is intact and the fluorescence of fluorescein is efficiently quenched by Förster resonance energy transfer due to the spatial proximity of TAMRA. Therefore, only the emission of TAMRA can be measured (580 nm; solid line). Upon hydrolytic disassembly of the inorganic core under aqueous basic conditions, the fluorescence of fluorescein is restored (520 nm; dotted line).*

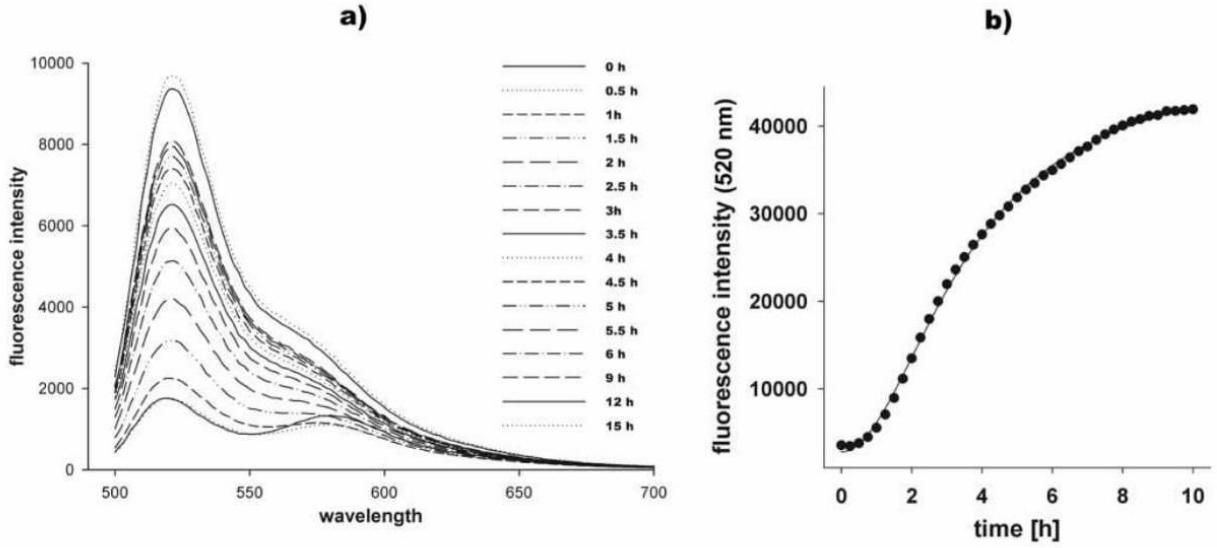

Figure S11: *Degradation studies of COSS derivative* ***9*** *in human blood serum at 37°C. COSS derivative* ***9*** *was incubated at a concentration of 20 µM in triplicates in 200 µL human serum (Sigma-Aldrich). The samples were excited at 488 nm and the fluorescence intensity at 520 nm was quantified for 15 h using a Tecan infinite M1000 microplate reader. a) Emission spectra of COSS derivative* ***9*** *(excitation at 488 nm). The recovery of the fluorescence of fluorescein was monitored by the increase of the emission at 520 nm. b) Fluorescence recovery of fluorescein measured at 520 nm. 50% fluorescence recovery was reached after 186 min.*

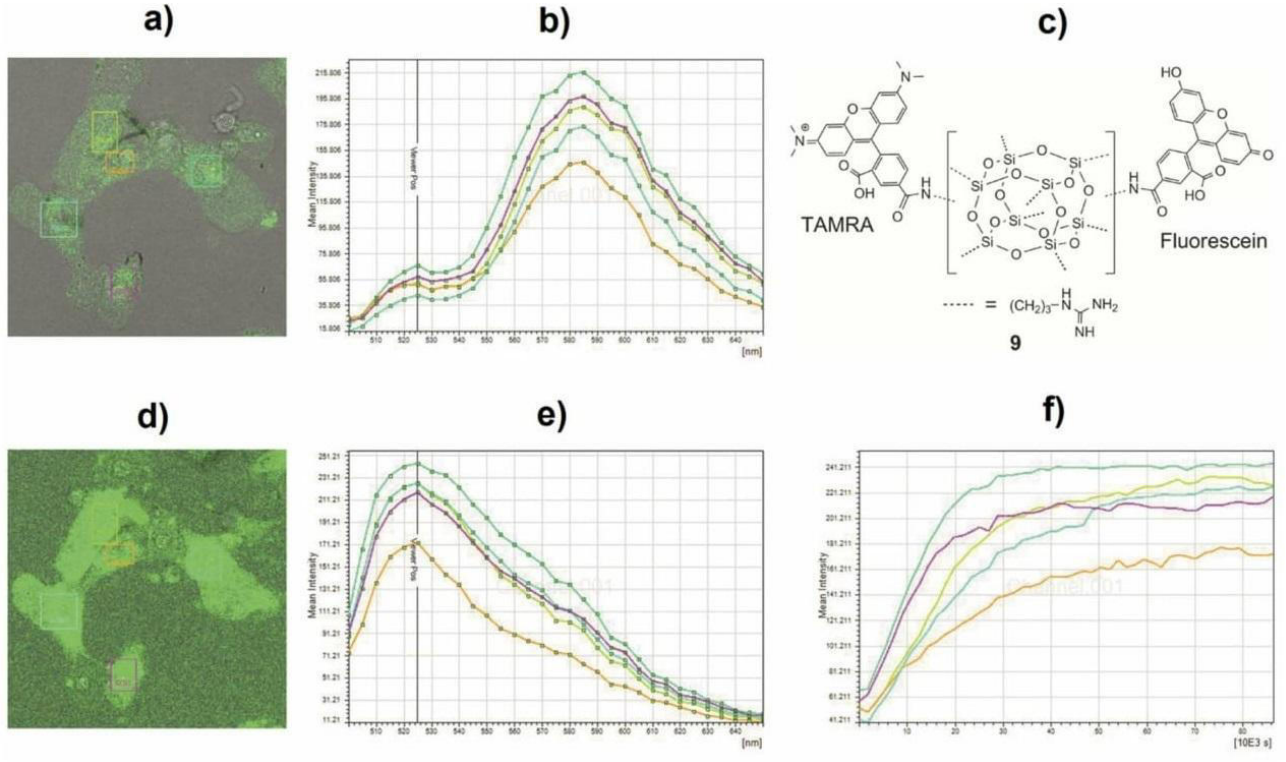

Figure S12: *Degradation studies of COSS derivative* ***9*** *in HeLa cells using live-cell laser scanning confocal microscopy. Cells were incubated with compound* ***9*** *(25 µM) in DMEM lacking FBS at 37°C for 20 min. After incubation, the cells were washed thrice with PBS and investigated in DMEM with 2 vol% FBS at 37°C and 5% CO_2 for 24 h. Every 30 min, excitation at 488 nm was performed and an emission spectrum was recorded. a) Fluorescence of fluorescein after an incubation time of 30 min. Colored windows indicate the selected areas for the emission scans. b) Emission scans after an incubation time of 30 min. The fluorescence of fluorescein is efficiently quenched (520 nm) and the emission of TAMRA (580 nm) is dominating. c) Structure of guanidine-bearing COSS derivative* ***9*** *comprising two fluorescent markers, fluorescein and TAMRA. d) Fluorescence of fluorescein after 24 h. e) Emission scans after 24 h. The fluorescence of fluorescein (520 nm) is restored and the emission of TAMRA (580 nm) is reduced. f) Time-resolved recovery of the fluorescence of fluorescein at 520 nm.*

4. Cellular delivery of a cytotoxic drug

Time-dependent delivery of free doxorubicin

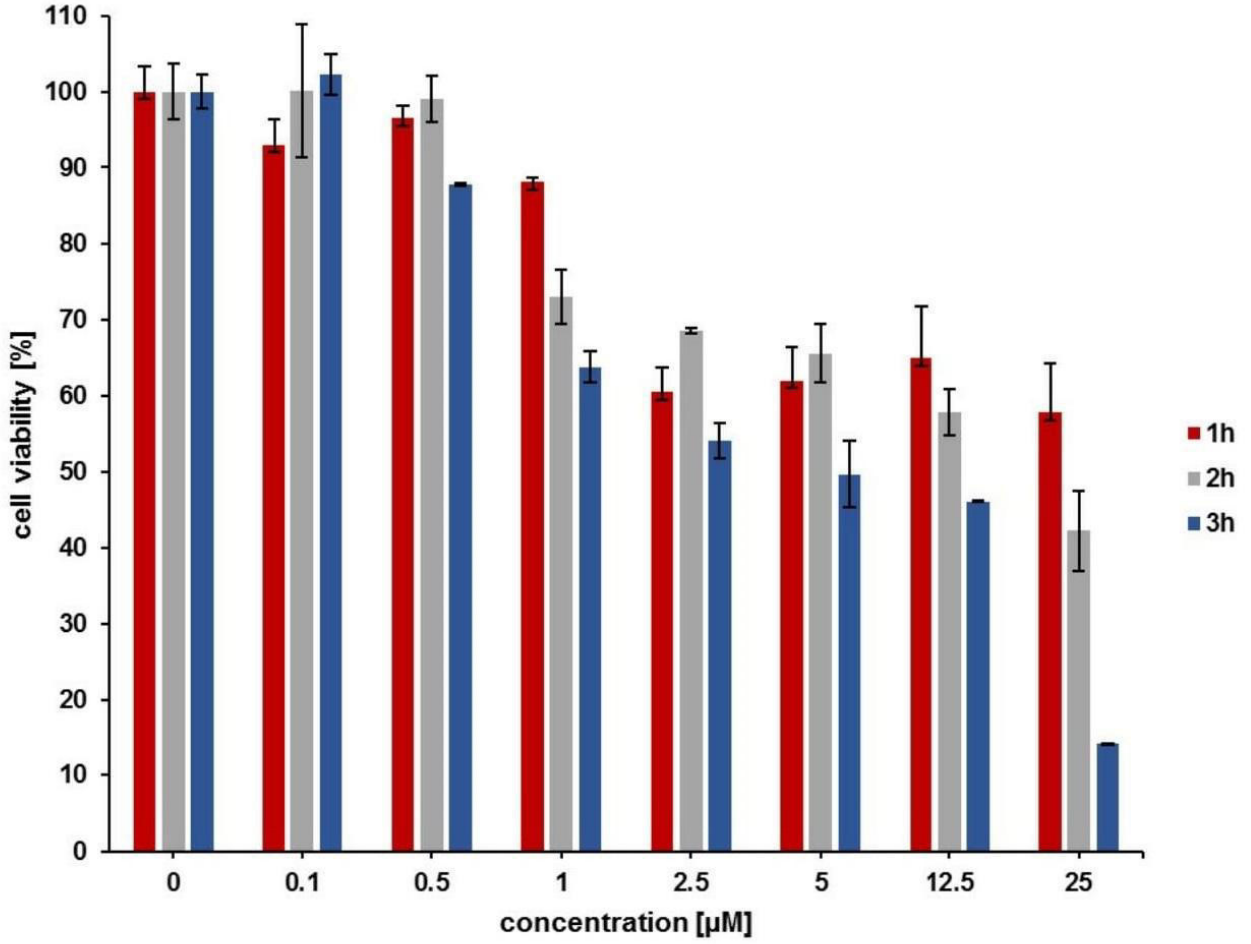

Figure S13: *Time-dependent cytotoxicity of free doxorubicin in HeLa cells. Serial dilutions of doxorubicin**14** in PBS (pH 5.5) were prepared and the resulting solutions were incubated in duplicates for 1 h, 2 h and 3 h with HeLa cells. After 18 h a MTT assay was performed. Upon co-incubation of unconjugated GuCOSS derivatives **8** or **28** and doxorubicin **14** at 1 µM, a concentration where the covalent GuCOSS-DOX conjugate showed a strong cytotoxic effect, no effect on cell viability was observed (data not shown)*

5. Experimental details

5.1 Cell culture assays

Cell culture

Human cervical cancer (HeLa), Chinese hamster ovary (CHO) and human embryonic kidney (HEK293) cells were maintained in Dulbecco`s modified eagle`s medium (DMEM, *Sigma-Aldrich*), supplemented with 2 mM L-glutamine, 10% (*v*/*v*) fetal bovine serum (FBS, *Sigma-Aldrich*) and penicillin (100 U/mL), streptomycin (100 µg/mL). *Sulfolobus islandicus*, and *Sulfolobus tokodaii* were cultured in 0.2% bacto-trypton (Difco) media as reported by Grogan *et al* and Brock *et al*.[1] *Halobacterium salinarum* were cultured in peptone (oxoid No. 37) media

as reported by Hechtler *et al*.[2] *E. coli* cells were cultured in dYT media and *Saccharomyces cerevisiae* were cultured in YPD media.

Live-cell confocal laser scanning microscopy

HeLa cells were grown to 70% confluence on *Lab Tek®II Chambered Coverglass System Nunc ThermoScientific 8 Chamber* (brand of *Merck KGaA*, Darmstadt, Germany). Cells were washed with Dulbecco's modified eagle medium without serum and then incubated with 20 µM of the labeled compounds in DMEM media lacking FBS at 37°C for 30 min. Afterwards the cells were washed thrice with PBS and investigated in DMEM supplemented with 2 mM L-glutamine, 10% (*v*/*v*) FBS (*Sigma-Aldrich*), and penicillin (100 U/mL), streptomycin (100 µg/mL) at 37°C and 5% CO_2. With a *Leica TCS SP5 II* TAMRA-labeled compounds were excited at 561 nm and detected at 580-650 nm. Exposure time settings were adjusted in the software to achieve the optimal quality of images. For controls lacking the COSS derivative, the same exposure time was used.

Fluorescence microscopy

Cells were incubated with 20 µM of GuCOSS **4** for 30 min in different buffers (*Saccharomyces cerevisiae, E. coli (BMH 71-18), Sulfolobus islandicus*, and *Sulfolobus tokodaii in PBS; Halobacterium salinarum in 3 M NaCl)* at different temperature (*Saccharomyces cerevisiae, and Halobacterium salinarum:* ambient temperature*; Sulfolobus islandicus*, and *Sulfolobus tokodaii*: 80°C; *E. coli*: 37°C). Cells were centrifuged for 3 min at 2500 rpm. The cell pellet was resuspended and centrifuged for 3 min at 2500 rpm; this procedure was repeated. The cells were investigated *on Millicell EZ SLIDE 4-well glass* (brand of *Merck KGaA*, Darmstadt, Germany). Microscopy images were acquired with *Zeiss Observer Z.1 microscope* (*Carl Zeiss AG*, Oberkochen, Germany) using an *EC Plan-Neofluar 63x/1.25 Oil objective* (*Carl Zeiss AG*, Oberkochen, Germany). The TAMRA moiety was excited at 543 nm and emission was detected at 565–615 nm. Exposure time settings were adjusted in the *Zeiss AxioVision SE64 Rel. 4.9* software to achieve the optimal quality of images. For controls lacking the COSS derivative, the same exposure time was used.

Flow-cytometric analysis

Cell-lines were subcultured overnight in 24-well plates to 70% confluence (*Costar*, *24-well cell culture cluster, Corning Incorporation*). Cells were grown on *CELLSTAR* 6-well slides (*Greiner Bio-One GmbH*, Frickenhausen, Germany). Cells were washed once with serum-free DMEM and then incubated with the labeled compounds at a concentration of 20 µM in DMEM lacking FBS for 10 min at 37°C. Afterwards the cells were washed thrice with PBS and trypsinized for 10 min at ambient temperature (0.05% trypsin/0.02% EDTA in PBS). Trypsinization was

terminated by adding 400 µL growth medium with 2 vol% FBS per well. Afterwards the cells were centrifuged for 3 min at 2500 rpm. The cell pellet was resuspended in PBS and centrifuged for 3 min at 2500 rpm. This procedure was repeated one more time. The cells have been resuspended in PBS and hold on ice until they were analyzed in a *BD Influx* cell sorter (*Becton, Dickinson and Company*, Franklin Lakes, USA), excited with a *BD Influx Yellow-Green Laser* (561 nm) (*Becton, Dickinson and Company*, Franklin Lakes, USA), emission detected between 573-613 nm (593/40 Filter). 10000 events were analyzed in each experiment.

Doxorubicin delivery

Cellular delivery of doxorubicin **14** (DOX) was studied in HeLa cells. First, an incubation time-dependent cell assay with the free antibiotic was conducted. To this end, the medium was exchanged with high glucose DMEM without L-methionine, L-cystine and L-glutamine. Free Doxorubicin was dissolved in phosphate buffered saline (PBS, pH 5.5), incubated at 37°C at different concentrations for 1 h, 2 h and 3 h with 1×10^4 HeLa cells/well (48-well plates, *Sigma Aldrich*) and subsequently washed with DMEM. After 18 h a cell proliferation assay (*CellTiter 96® Aqueous One Solution Cell Proliferation Assay, Promega Corporation*) was carried out (**figure S9**). For the investigation of the doxorubicin delivery *via* GuCOSS, the conjugate **15** as well as the controls were dissolved in PBS (pH 5.5), incubated at the different concentrations for 1 h at 37°C, in triplicates. To preserve the disulfide bond, the medium was exchanged with high glucose DMEM without L-methionine, L-cystine and L-glutamine prior to the incubation. After incubation, the cells were washed with DMEM and after 18 h a MTT assay was performed (**figure 3**).

Cell toxicity test: XTT assay

Cell proliferation assay XTT was purchased from *Applichem* and performed according to the manufacturer's instructions. 5,000 HeLa-cells per well were seeded in triplicates into 96-well plates the day before the experiment (Cellstar, 96-Well Cell Culture Plate, Greiner Bio-one) and used at 70% confluency. Cells were washed with serum-free DMEM and incubated for one h at 37°C and 5% CO_2 with different concentrations with COSS derivative **8** (0 µM; 20 µM; 40 µM; 60 µM; 80 µM; 100 µM; 150 µM; 200 µM; 250 µM; 300 µM; 400 µM; 500 µM) in DMEM lacking FBS. Additionally, cells were incubated with 50% (v/v) DMSO in DMEM lacking FBS (positive control). Cells were cultured 12 h at 37°C and 5% CO_2 in DMEM media supplemented with 2 mM L-glutamine, 10% (*v/v*) fetal bovine serum (FBS, Sigma-Aldrich) and penicillin (100 U/mL), streptomycin (100 µg/mL). The media was exchanged to DMEM lacking FBS and 0.3 mg/mL of 2,3-bis(2-methoxy-4-nitro-5-sulfophenyl)-5-((phenylamino)-carbonyl)-2H-

tetrazolium-hydroxide (XTT) (*AppliChem*, brand of *Illinois Tool Works Inc.*, Glenview, USA) in DMEM media including 25 mM HEPES (Life technologies) were added. After an incubation time of 4 h, the XTT enzymatic reduction was measured by measuring the absorbance at 450 nm, with a reference wavelength of 630 nm in a *Tecan Infinite M1000* (*Tecan Group AG*, Männedorf, Switzerland) microplate reader. Each measurement was conducted in triplicate and the toxicity was determined in three independent experiments.

Cell toxicity test: MTT assay

Cell proliferation assay *CellTiter 96® AQ_{ueous} One Solution* was purchased from *Promega Corporation* and performed according to the manufacturer's instructions. 1×10^4 HeLa cells/well were seeded into 48-well plates (48-well cell culture plate, *Sigma Aldrich*). After 24 h culturing, the cells were washed with serum-free high glucose DMEM lacking L-methionine, L-cystine and L-glutamine (*D0422, Sigma Aldrich*) and incubated with 150 µL medium and 50 µL of the respective probe. After the corresponding incubation period the cells were washed with DMEM. After 18 h 40 µL of the MTT solution was added and the absorbance at 485 nm was measured in a *Tecan Infinite M1000* (*Tecan Group AG*, Männedorf, Switzerland) microplate reader. Each measurement was conducted in triplicate or duplicate and the toxicity was determined in two independent experiments.

5.2 Synthetic procedures

Solvents

Solvents were obtained from *Carl Roth GmbH* (Karlsruhe, Germany), *Acros* (Taufkirchen, Germany), *Fluka* (Buchs, Switzerland) or *Sigma-Aldrich* (St. Louis, USA) and had the following quality: acetone: synthesis grade; dimethyl sulfoxide (DMSO): spectroscopic grade; acetonitrile (MeCN): HPLC grade. Millipore quality water was used for the HPLC analysis. Some solvents were dried und purified using the following procedures:

MeCN: 1 g/L sodium hydride dispersion was added to the solvent. After being heated to reflux for 1 h, the solvent was distilled. 2 g/L P_2O_5 were added and the mixture was heated to reflux for 1 h. It was subsequently distilled and stored in the dark under argon atmosphere over activated 4 Å molecular sieve.

DMSO: The solvent was pre-dried by stirring over 25 g/L calcium hydride at ambient temperature for one day. Afterwards it was distilled and stored in the dark under argon atmosphere over activated 4 Å molecular sieve.

N,N-diisopropylethylamine (DIEA): The solvent was refluxed over 50 g/L potassium hydroxide for 1 h. After cooling to ambient temperature, it was decanted and 50 g/L fresh potassium hydroxide was added. The solvent was refluxed for 1 h and afterwards decanted. After distillation, the obtained solvent was refluxed for 3 h over calcium hydride, distilled and stored in the dark under argon atmosphere over activated 4 Å molecular sieve.

Reagents

All reagents were used as supplied by *Sigma Aldrich* or *Acros Organics* without further purification or drying. Amino acids and resins were purchased from *Novabiochem* (brand of *Merck KGaA*, Darmstadt, Germany), *CEM* (Kamp-Lintfort, Germany) or *Iris Biotech* (Marktredwitz, Germany).

Microwave-assisted solid-phase peptide synthesis (SPPS)

Microwave-assisted SPPS was performed using a *CEM Liberty*® peptide synthesizer equipped with a *CEM Discover*® SPS microwave.

Manual SPPS

Coupling of Fmoc-protected amino acids was performed as triple coupling. 4 eq. of the respective amino acid, 3.9 eq. of the activator *O*-benzotriazole-*N,N,N′,N′*-tetramethyl-uronium-hexafluoro-phosphate (HBTU) and 8 eq. DIEA, were diluted in a minimal amount of *N,N*-dimethylformamide (DMF) and pre-activated for 10 min. Coupling was performed at ambient temperature for 1 h. *N*-Terminal deprotection of amino acids was performed as double deprotection step with 20% piperidine in DMF for 5 and 15 min at ambient temperature. Afterwards the resin was washed thrice with DMF and dichloromethane (DCM).

Peptide cleavage and work-up

All peptides were cleaved from the resin using 92 vol% trifluoroacetic acid (TFA), 2 vol% H_2O, 4 vol% triethylsilane (TES), 2 vol% anisole and a spatula tip of dithiothreitol (DTT). After 1-2 h of shaking at ambient temperature the solution was filtered and poured into ice-cold MTBE. The mixture was cooled to -20°C for at least 30 min and centrifuged for 15 min at 4000 rpm at 4°C. The supernatant was discharged and the precipitate was washed by MTBE twice and dried in a desiccator. The peptide was dissolved in a mixture of MeCN and water and the solvent mixture was removed by lyophilization.

Mass spectrometry

Electrospray ionization mass spectrometry (ESI-MS) spectra were obtained using a *Shimadzu*

LCMS-2020 mass spectrometer equipped with a *Phenomenex Jupiter 5u C4 LC* column (50x1 mm, 5 µm, 300 Å). Eluent system consisted of eluent A comprising 0.1 vol% aq. formic acid, LC-MS grade (*Sigma-Aldrich*, St. Louis, USA) and eluent B comprising 100% acetonitrile with 0.1 vol% formic acid, LC-MS grade (*Carl Roth GmbH*, Karlsruhe, Germany). High-resolution ESI-MS were performed using a *maXis Q-TOF* (*Bruker*) or an *APEX IV FTICR-MS* (*Bruker*).

Liquid chromatography

Analytical reversed-phase high-performance liquid chromatography (RP-HPLC) was performed on a *Varian 920 LC* equipped with a *Phenomenex Luna Hypersil 5u BDS C_{18} LC* column (5 u, 130 Å, 150×4.60 mm, 5 µm) at a flow rate of 1 mL/min. For isolation of peptides a semi-preparative RP-HPLC *Varian 940 LC* equipped with a preparative C_{18} column (*Phenomenex Luna 5u C_{18}* (250×20 mm; S-4 µm, 8 nm)) was used at a flow rate of 18 mL/min. Eluent A: 0.1 vol% aq. trifluoroacetic acid (TFA), eluent B: 90 vol% aq. MeCN with 0.1 vol% TFA. 5 min of isocratic flow (starting concentration of eluent B) was followed by 20 min of gradient flow. Absorption was measured by UV/VIS detector at 220 nm and 280 nm or 220 nm and 534 nm

NMR

NMR spectra were recorded with a *Bruker DRX 500 MHz NMR spectrometer* (*Bruker Biospin*, Karlsruhe) equipped with a 5mm TBI probe (^{1}H, ^{2}H, ^{31}P, BB, z-gradient) and a *Bruker AV III HD 400 MHz spectrometer* equipped with a 5mm BBFO smart probe. Unless noted otherwise, the sample temperature was held constant at 300 K using a *BCU-Xtreme chiller*. All samples were dissolved in deuterated DMSO-d_6 purchased from *Euriso Top* (Gif-Sur-Yvette, France). Samples were prepared inside PTFE tube liners to improve the signal to noise ratio of the dilute solutions.

Experiments (1D: ^{1}H, ^{13}C, ^{29}Si, 2D: ^{1}H-^{13}C HSQC, ^{1}H-^{1}H COSY and ^{1}H-^{29}Si HMBC) were performed using standard pulse sequences from the Bruker library and default settings. ^{29}Si 1D spectra were acquired with inverse gated decoupling of protons, 32k FID data points, and a relaxation delay of 30s and a spectral offset of -50ppm. Some spectra acquired on the older hardware showed a spike at the carrier frequency of the experiment, presumably due to a DC offset caused by the amplifiers. Acquisition was performed under *XWinNMR 3.5* on older hardware and *TopSpin 3.2pl5* on the newer hardware. Processing was performed with *MestreNova 10.0.1*. For ^{29}Si 1D spectra the FID was apodized by exponential multiplication with a broadening factor of 0.2 – 2 Hz, followed by zero-filling to 128k data points (incl. linear prediction), manual phase correction, and automatic baseline correction (Whittaker smoothing, 5 Hz filter). For ^{1}H 1D spectra the FID was apodized by exponential multiplication with a

broadening factor of 0.3 Hz, followed by zero-filling to 128k data points (incl. linear predition), manual phase correction and automatic baseline correction (Whittaker smoothing, 8 -15 Hz filter).

As a first step of structural characterization, ^{1}H and ^{29}Si spectra were analyzed. Quantitative analysis of the ^{1}H spectra was performed with the multiplet analysis tool in *MestreNova 10.0.1*, giving the line-shape fitted numerical integrals even in overlapping spectral regions. In several spectra the integrals of labile amine protons are difficult to quantify due to an undetermined protonation state. Similarly, a strong residual water signal around 3.50 ppm leads to perturbed integrals in some spectra. The chemical shift of the Si-nuclei in the cage-like siloxane core was used as an indicator for stability. Within an intact structure where all Si-nuclei are connected to three other Si-nuclei *via* oxygen atoms (denoted as T_8 structure), the chemical shifts of the four non-isochronous Si-sites are expected around -65 ppm. Hydrolysis (or other decomposition) products would be expected around -40 ppm. The spectra confirmed the integrity of the cage-like T_8 core and the unsymmetrical substitution pattern allowed for full assignment of all non-isochronous resonances in favorable cases, where resonance overlap is minimal.

COSS derivative 2 (TAMRA-aminoCOSS)

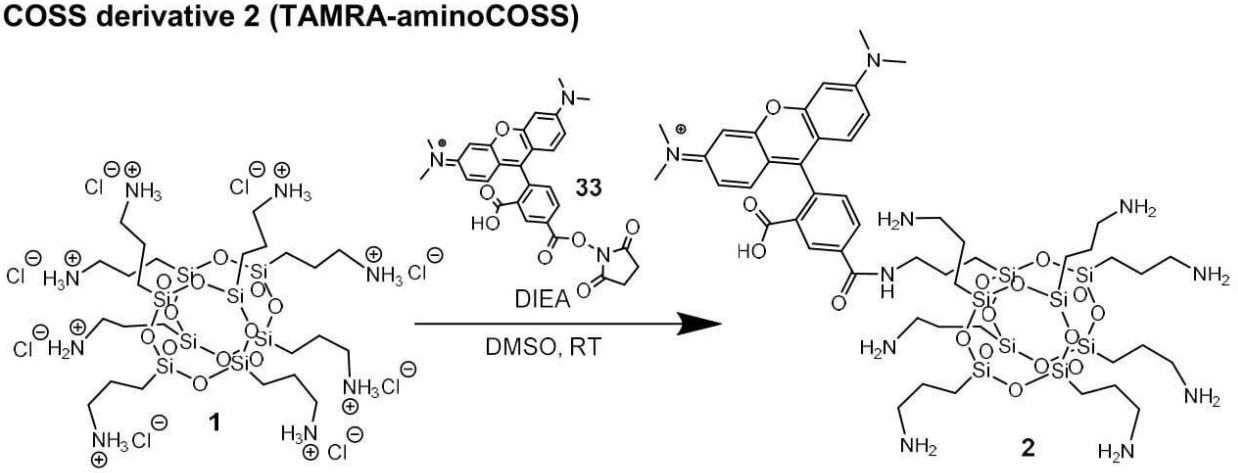

100 mg (85.2 µmol, 6.4 eq.) of octaammonium COSS hydrochloride **1** (purchased from *Hybrid Plastics* Inc., USA) were dissolved in 0.5 mL dry DMSO and vigorously stirred. The solution comprising 7 mg (13.2 µmol, 1 eq.) of TAMRA-NHS ester **33** (*Thermo Fischer Scientific*) and 13.8 µL (79.5 µmol, 6 eq.) of dry DIEA in 8 mL dry DMSO was added slowly using a peristaltic pump (flow: 0.05 mL/min). The resulting mixture was stirred for additional 2 h at room temperature and the solvent was removed by lyophilization. The purple residue was suspended in dry acetonitrile and the insoluble part was washed twice with dry acetonitrile. The precipitate was dissolved in 10 vol% aq. MeCN with 0.1 vol% TFA and purified by semi-

preparative RP-HPLC (gradient 10to40% B). After lyophilization, 13 mg of a purple solid **2** were obtained (76.3%).

RP-HPLC, 10→40% B, t_R= 19.35 min.

HR-MS calc. for $C_{49}H_{84}N_{10}O_{16}Si_8$ m/z: 431.8146 meas. 431.8134 $[M+3H]^{3+}$.

^{1}H NMR (500 MHz, DMSO-d_6) δ: 9.00 (t, *J* = 5.6 Hz, 1H), 8.65 (s, 1H), 8.30 (d, *J* = 8.0 Hz, 1H), 8.01 (s, 29H), 7.54 (d, *J* = 8.1 Hz, 1H), 7.15 – 6.75 (m, 6H), 3.38 – 3.29 (m, 2H), 3.23 (s, 12H), 2.94 – 2.60 (m, 20H, expected 14H), 1.88 – 1.41 (m, 23H, expected 16H), 0.96 – 0.32 (m, 23H, expected 16H).

The integral mismatch between the TAMRA and C_3-NH_2 side chains might indicate an incomplete reaction.

^{29}Si NMR (99 MHz, DMSO-d_6) δ: -65.94, -66.62, -66.67.

COSS derivative 3 (TAMRA-quartCOSS)

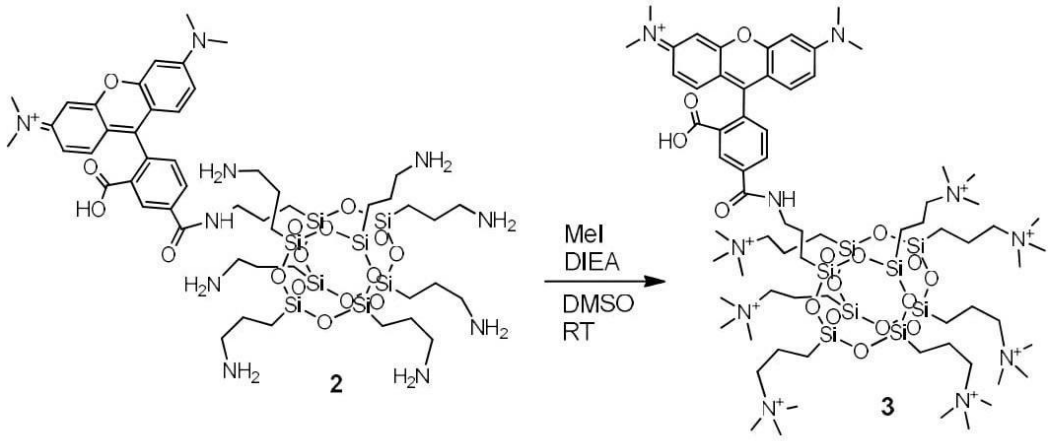

A mixture of 25 mg (19.3 µmol, 1 eq.) of TAMRA-aminoCOSS **2**, 84 µL (482.8 µmol, 25 eq.) dry DIEA and 42 µL (674.7 µmol, 35 eq.) methyl iodide are dissolved in 5 mL dry DMSO. After being stirred for 5 days the solvent was removed using a rotary evaporator. The purple residue was dissolved in 10 vol% aq. MeCN with 0.1 vol% TFA and purified by semi-preparative RP-HPLC (gradient 10to40% B). After lyophilization, 14.9 mg of a purple solid **3** were obtained (48.8%).

RP-HPLC, 10→40% B, t_R=19.81 min.

^{1}H NMR (500 MHz, DMSO-d_6) δ: 9.32 – 9.11 (m, 1H), 8.71 (s, 1H), 8.37 (d, *J* = 8.1 Hz, 1H), 7.63 (d, *J* = 8.0 Hz, 1H), 7.13 – 7.02 (m, 2H), 7.04 – 6.92 (m, 4H), 3.47 – 3.18 (m, 28H), 3.08 (s, 63H), 1.96 – 1.52 (m, 16H), 0.91 – 0.74 (m, 2H), 0.74 – 0.48 (m, 14H).

^{29}Si NMR (99 MHz, DMSO-d_6) δ: -65.89, -67.26, -67.32, -67.39.

COSS derivative 4 (TAMRA-GuCOSS)

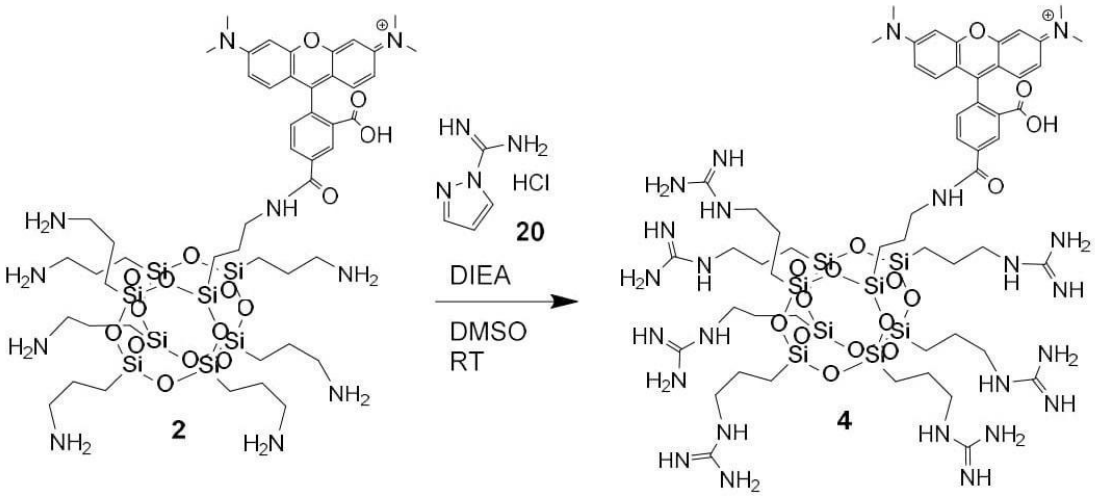

19.2 mg of TAMRA-aminoCOSS **2** (1 eq., 14.8 µmol), 45.6 mg of 1*H*-pyrazole-1-carboxamidine hydrochloride (21 eq., 311.4 µmol) and 126 µL of DIEA (50 eq., 741 µmol) were dissolved in 5 mL dry DMSO and stirred at room temperature for 4 days. The mixture was freeze-dried. The oily residue was suspended in dry acetonitrile and the insoluble part was washed twice with dry acetonitrile. The purple solid was dissolved in 10 vol% aq. MeCN with 0.1 vol% TFA and purified by semi-preparative RP-HPLC (gradient 10to100% B). After lyophilization, 5.5 mg of a purple solid **4** were obtained (23.6%).

RP-HPLC, 10→40% B, t_R=21.50 min.

HR-MS calc. for $C_{56}H_{98}N_{24}O_{16}Si_8$ m/z: 318.3222, meas. 318.3221 $[M+5H]^{5+}$.

^{1}H NMR (500 MHz, DMSO-d_6) δ: 8.91 (s, 1H), 8.72 – 8.07 (m, 2H), 8.02 – 7.67 (m, 7H), 7.67 – 6.63 (m, 29H), 3.35 (s, 89H, expected 12H), 3.09 (m, 16H, expected 14H), 3.05 – 2.90 (m, 2H), 1.69 – 1.60 (m, 2H), 1.60 – 1.44 (m, 14H), 0.78 – 0.69 (m, 2H), 0.69 – 0.50 (m, 14H).

TAMRA resonances mostly overlap with guanidinyl resonances and a strong residual water signal at ~3.53 ppm disturbs the baseline, such that the affected resonances cannot be integrated cleanly.

^{29}Si NMR (99 MHz, DMSO-d_6) δ: -66.41, -66.42.

COSS derivative 5 (TAMRA-aminoCOSS-L)

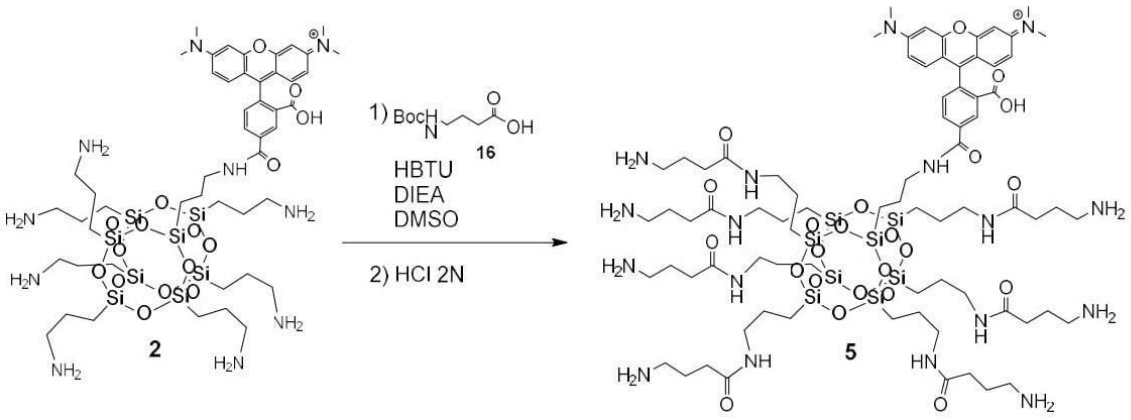

A mixture of 65.9 mg (324.3 µmol, 21 eq.) 4-Boc-aminobutyric acid (*Sigma-Aldrich*) **16**, 134.6 µL (772.2 µmol, 50 eq.) dry DIEA and 117.2 mg (308.9 µmol, 20 eq.) of HBTU were dissolved in 4 mL dry DMSO and pre-activated for 10 min at room temperature. 20 mg (15.4 µmol, 1 eq.) of TAMRA-aminoCOSS **2** were added and the mixture was stirred for 2 h. The solvent was removed by lyophilization. Boc deprotection was performed in 50 vol% aq. TFA for 7 h. The solvent was removed using a rotary evaporator and the residue was dissolved in 10 vol% aq. MeCN with 0.1 vol% TFA and purified by semi-preparative RP-HPLC (gradient 10to40% B). After lyophilization, 18.3 mg of a purple solid **5** were obtained (45.7%).

RP-HPLC, 10→40% B, t_R=19.82 min.

HR-MS calc. for $C_{77}H_{133}N_{17}O_{23}Si_8$ m/z: 378.5656 meas. 378.5661 $[M+5H]^{5+}$.

^{1}H NMR (500 MHz, DMSO-d_6) δ: 8.92 (s, 1H), 8.53 (s, 1H), 8.25 (s, 1H), 8.11 – 7.70 (m, 28H), 7.67 – 6.08 (m, 7H), 3.65 – 3.21 (m, 148H, expected 12H), 3.07 – 2.97 (m, 16H), 2.85 – 2.69 (m, 14H), 2.24 – 2.08 (m, 14H), 1.83 – 1.68 (m, 14H), 1.68 – 1.58 (m, 2H), 1.53 – 1.38 (m, 14H), 0.74 – 0.65 (m, 2H), 0.65 – 0.46 (m, 14H).

A strong residual water signal at ~3.40 ppm prevents the clean integration of some resonances.

^{29}Si NMR (99 MHz, $CDCl_3$) δ: -66.23, -66.25.

COSS derivative 6 (TAMRA-quartCOSS-L)

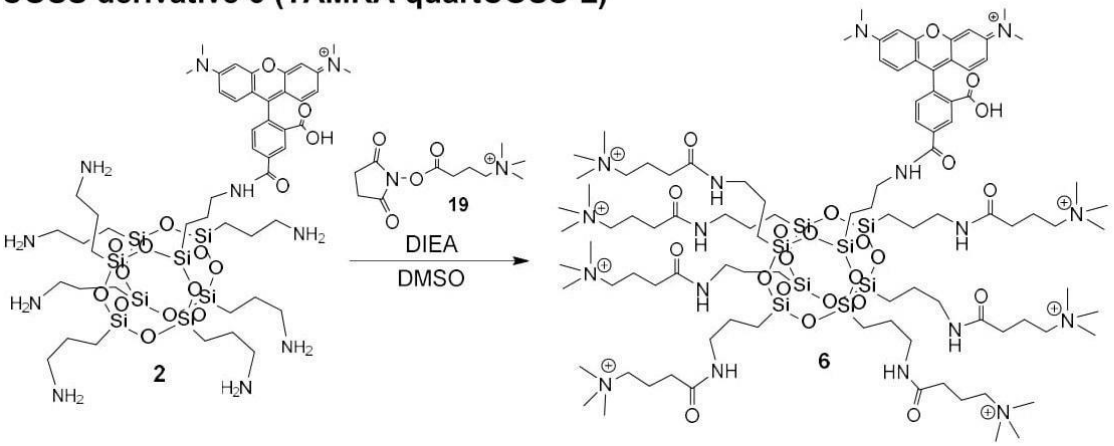

A mixture of 25 mg (19.3 µmol, 1 eq.) TAMRA-aminoCOSS **2**, 98.6 mg (324.3 µmol, 21 eq.) 4-trimethylammoniumbutyric acid NHS ester **19** and 134.4 µL (772.2 µmol, 50 eq.) dry DIEA were dissolved in 5 mL dry DMSO and stirred for 8 days. The solvent was removed by lyophilization. The residue was dissolved in 10 vol% aq. MeCN with 0.1 vol% TFA and purified by semi-preparative RP-HPLC (gradient 10to40% B). After lyophilization, 18.3 mg of a purple solid **6** were obtained (45.7%).

RP-HPLC, 10→40% B, t_R=18.87 min.

HR-MS calc. for $C_{98}H_{182}N_{17}O_{23}Si_8^{7+}$ m/z: 312.7387, meas. 312.7384 $[M]^{7+}$.

^{1}H NMR (500 MHz, DMSO-d_6) δ: 9.00 (t, J = 5.5 Hz, 1H), 8.67 (s, 1H), 8.31 (d, J = 7.9 Hz, 1H), 8.09 – 7.98 (m, 7H), 7.55 (d, J = 8.0 Hz, 1H), 7.42 – 6.59 (m, 6H), 3.37 – 3.14 (m, 28H), 3.10 – 3.01 (m, 77H), 2.15 (t, J = 7.2 Hz, 14H), 1.95 – 1.83 (m, 14H), 1.73 – 1.57 (m, 2H), 1.53 – 1.39 (m, 14H), 0.74 – 0.67 (m, 2H), 0.66 – 0.50 (m, 14H).

^{29}Si NMR (99 MHz, DMSO-d_6) δ: -66.22, -66.23, -66.25.

COSS derivative 7 (TAMRA-GuCOSS-L)

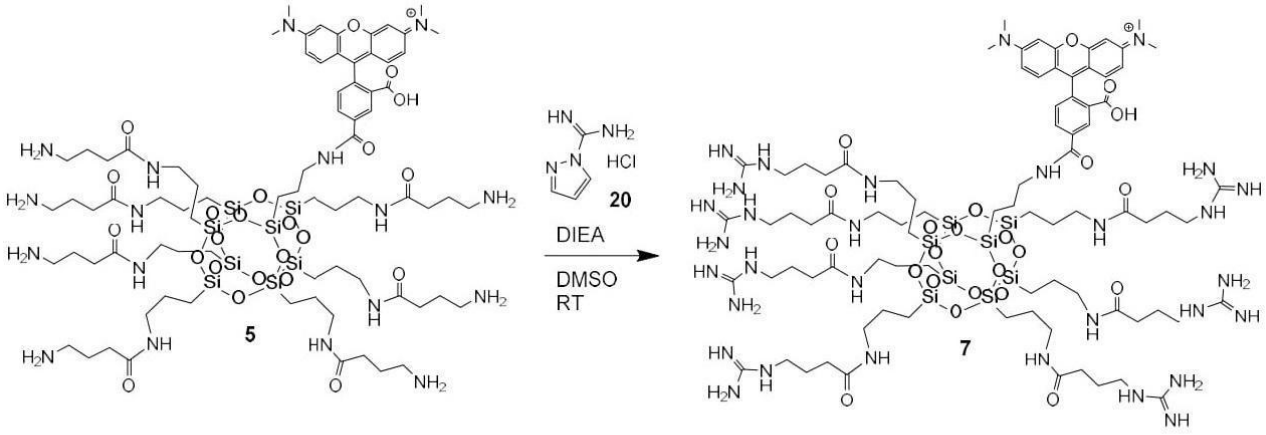

A mixture of 12 mg (6.4 µmol, 1 eq.) COSS derivative **5**, 44.1 µL (253.9 µmol, 40 eq.) dry DIEA and 22.3 mg (152.4 µmol, 24 eq.) 1*H*-pyrazole-1-carboxamidine hydrochloride **20** were dissolved in 10 mL dry DMSO and stirred for 8 days. The solvent was removed by lyophilization and the residue was dissolved in 10 vol% aq. MeCN with 0.1 vol% TFA and purified by semi-preparative RP-HPLC. After lyophilization 3.6 mg of a purple solid **7** were obtained (26%).

RP-HPLC, 10→40% B, t_R=20.9 min.

HR-MS calc. for $C_{84}H_{147}N_{31}O_{23}Si_8$ m/z: 364.6646, meas. 364.6643 $[M+6H]^{6+}$.

^{1}H NMR (500 MHz, DMSO-d_6) δ: 8.94 (s, 1H), 8.68 (s, 1H), 8.30 (d, *J* = 8.3 Hz, 1H), 7.94 (s, 7H), 7.86 – 7.75 (m, 7H), 7.68 – 6.70 (m, 28H), 3.67 – 3.44 (m, 410H, expected 12H), 3.34 – 3.31 (m, 2H), 3.17 – 3.00 (m, 28H), 2.12 (t, *J* = 7.4 Hz, 14H), 1.74 – 1.60 (m, 16H), 1.52 – 1.39 (m, 14H), 0.75 – 0.66 (m, 2H), 0.66 – 0.49 (m, 14H).

A strong residual water signal at ~3.50 ppm prevents the clean integration of some resonances.

^{29}Si NMR (99 MHz, $CDCl_3$) δ: -66.23, -66.26.

COSS derivative 8 (amino-GuCOSS)

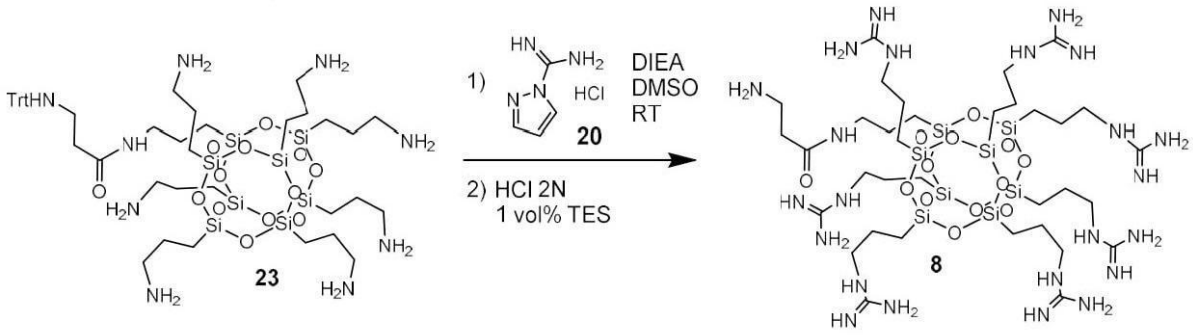

123 mg (0.103 mmol, 1 eq.) single-corner amidated and trityl-protected COSS **23**, 317 mg (2.16 mmol, 21 eq.) 1*H*-pyrazole-1-carboxamidine hydrochloride **20** and 666 mg (5.2 eq., 897 µL) dry DIEA were mixed in 5 mL dry DMSO and the mixture was stirred for 2 days at ambient temperature. The solvent was removed by lyophilization and the oily residue was suspended in dry acetonitrile. The insoluble part was washed twice with dry acetonitrile. The precipitate was dissolved in 5 vol% aq. AcOH and purified by semi-preparative RP-HPLC (gradient 0to60% B) with 0.1 vol% AcOH. After lyophilization 44.5 mg of colorless trityl-protected intermediate **24** were obtained (29%). For deprotection of the trityl protecting group, 1 mL 2 N aq. HCl and 1 mL $CHCl_3$ were added and the solution was shaken for 3 h at ambient temperature. The organic phase was removed and the aqueous phase was extracted twice with each 1 mL $CHCl_3$. The combined organic phases were abolished and 9 mL deionized water was added to the aqueous phase. The solvent was removed by lyophilization. The

remaining colorless solid was dissolved in 5 mL 5 vol% aq. AcOH and the solvent was removed by lyophilization. 37.1 mg of colorless solid **8** were obtained (99%).

Trt protected **24**:

ESI-MS calc. for $C_{53}H_{97}N_{23}O_{13}Si_8$ m/z: 745.58 meas. 745.61 $[M+2H]^{2+}$, calc. 497.39 meas. 497.32 $[M+3H]^{3+}$.

RP-HPLC, 10→60% B, t_R= 20.38 min.

^{1}H NMR (400 MHz, DMSO-d_6) δ: 8.50 (s, 7H), 8.13 (t, *J* = 5.6 Hz, 1H), 7.62 (s, 21H), 7.38 (d, *J* = 7.9 Hz, 6H), 7.29 (t, *J* = 7.6 Hz, 6H), 7.18 (t, *J* = 7.2 Hz, 3H), 3.19 – 2.95 (m, 16H), 2.72 (s, 1H), 2.39 – 2.25 (m, 2H), 2.24 – 2.09 (m, 2H), 1.61 – 1.36 (m, 16H), 0.91 – 0.27 (m, 16H).

^{29}Si NMR (79 MHz, DMSO) δ: -66.03, -66.21, -66.25, -66.32.

Amino-GuCOSS **8**:

^{1}H NMR (400 MHz, DMSO-d_6) δ: 8.07 – 7.88 (m, 8H), 7.72 – 6.91 (m, 26H, expected 23H), 3.31 – 3.14 (m, 14H), 3.11 – 3.02 (m, 2H), 3.01 – 2.91 (m, 2H), 2.67 – 2.54 (m, 2H), 1.69 – 1.34 (m, 16H), 0.95 – 0.24 (m, 16H).

COSS derivative 9 (Fluorescein-TAMRA-GuCOSS)

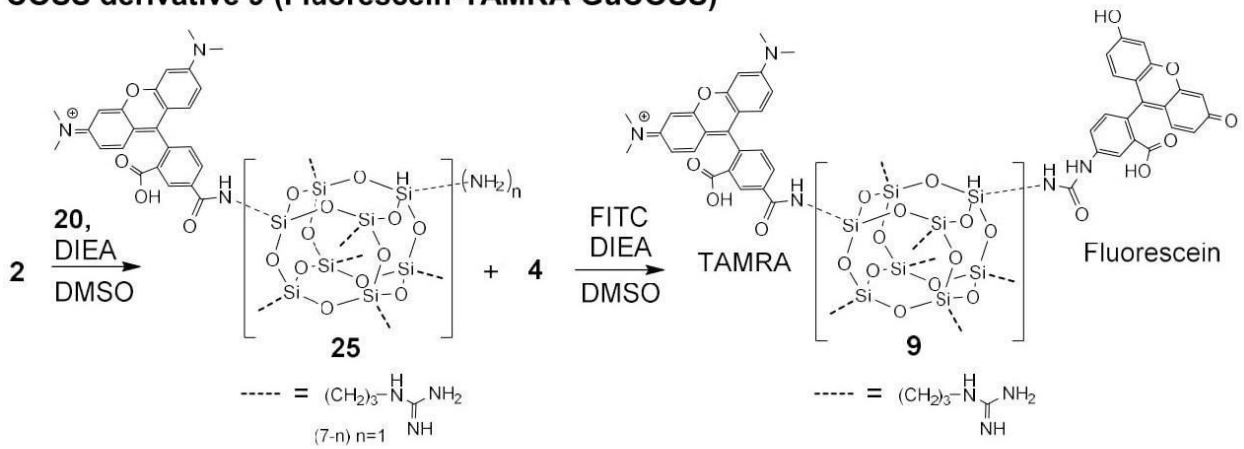

20 mg of TAMRA-aminoCOSS **2** (1 eq., 15.4 µmol), 47.5 mg of 1*H*-pyrazole-1-carboxamidine hydrochloride **20** (21 eq., 324.2 µmol) and 99.5 mg (134.5 µL, 50 eq, 770 µmol) of dry DIEA were dissolved in 5 mL dry DMSO and stirred at room temperature for 3 days. The formation of six- and sevenfold guanidinylated COSS was verified by LC-MS analysis of the reaction mixture. The mixture was freeze-dried and the oily residue was suspended in dry acetonitrile. The insoluble part was washed twice with dry acetonitrile. The purple solid was dissolved in 10 vol% aq. MeCN with 0.1 vol% TFA and purified by semi-preparative RP-HPLC (gradient 10to100% B). After lyophilization, 5.6 mg of a mixture of compound **25** and TAMRA-GuCOSS **4** were obtained. The product mixture was treated with 2.7 mg fluoresceinisothiocyanate (FITC, *Applichem*) (2 eq., 6.9 µmol) and 1.8 mg dry DIEA (2.4 µL, 4 eq., 13.9 µmol) in 2 mL

dry DMSO at ambient temperature overnight. The solvent was removed by lyophilization and the oily residue purified by RP-HPLC. After lyophilization, 1.9 mg of red solid **9** were obtained (6.6%).

RP-HPLC, 10→100% B, t_R=14.57 min.

HR-MS calc. for $C_{76}H_{107}N_{23}O_{21}SSi_8$ m/z: calc. 645.5368, meas. 645.5362 $[M+3H]^{3+}$.

TAMRA-β-alanine-Tat peptide 10

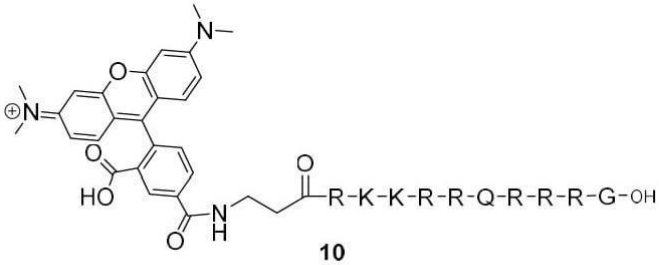

10

The synthesis was performed on 100 mg preloaded *TentaGel S AC-Gly(Fmoc)* with a binding capacity of 0.2-0.25 mmol/g (0.23 mmol, 1 eq.) by manual Fmoc-SPPS.

Afterwards 6.4 µL (36.8 µmol, 8 eq.) DIEA and 4.9 mg (9.2 µmol, 2 eq.) of TAMRA-NHS ester **33** were dissolved in a minimal amount of DMF and added to 25 mg of resin-bound peptide. The reaction mixture was gently shaken overnight at room temperature and afterwards washed four times with DMF and DCM, respectively. Cleavage and workup was performed as previously described. After lyophilization, 2.2 mg of a purple solid **10** were obtained (25.4%).

RP-HPLC, 10→40% B, t_R=17.03 min.

ESI-MS calc. for $C_{83}H_{135}N_{34}O_{17}^+$ m/z: 628.06, meas. 627.6 $[M+3H]^{3+}$, calc. 471.30 meas. 470.94 $[M+4H]^{4+}$, 377.24 meas. 376.89 $[M+5H]^{5+}$.

TAMRA-β-alanine-penetratin 11

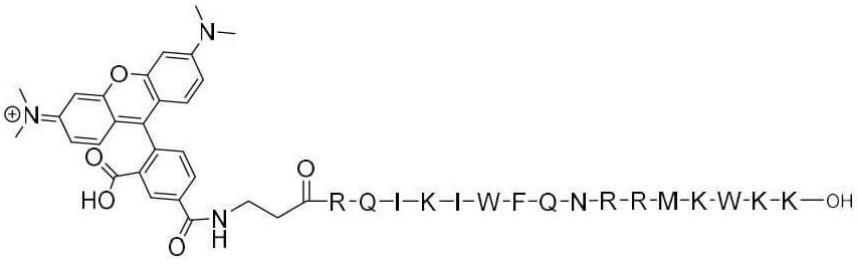

11

The synthesis was performed on 1 g preloaded *TentaGel S AC-Lys(Boc) Fmoc* with a binding capacity of 0.22 mmol/g (0.22 mmol, 1 eq.) by manual Fmoc-SPPS. After the attachment of β-

alanine, the resin-bound peptide was split and one-half (11 mmol) was fluorescently labeled. Therefore, 85.2 mg (114.82 µL, 0.66 mmol, 6 eq.) DIEA and 63.95 mg (0.12 mmol, 1.1 eq.) of TAMRA-NHS ester **33** were dissolved in a minimal amount of DMF and added to the resin-bound peptide. The reaction mixture was gently shaken overnight at ambient temperature and afterwards washed four times with each DMF and DCM. Cleavage and workup was performed as previously described. After lyophilization, 46 mg of a purple solid **11** were obtained (15.31%).

RP-HPLC, 10→80% B, t_R=15.41 min.

ESI-MS calc. for $C_{132}H_{194}N_{37}O_{25}S^+$ m/z: 911.43 meas. 911.1 $[M+3H]^{3+}$, calc. 683.83 meas. 683.60 $[M+4H]^{4+}$, 547.26 meas. 547.1 $[M+5H]^{5+}$.

TAMRA-β-alanine-heptaarginine 12 and TAMRA-β-alanine-decaarginine 13

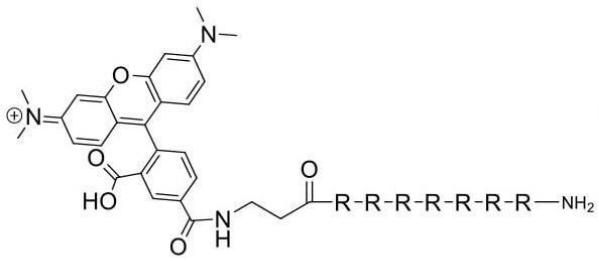

12

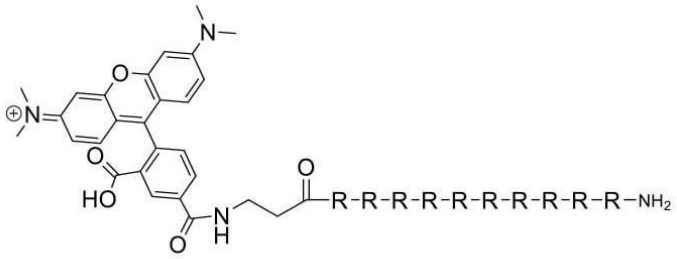

13

The synthesis was performed on 1 g preloaded *TentaGel Fmoc-Arg(Pbf)-NovaSyn TGA* resin (*Novabiochem*) with a binding capacity of 0.19 mmol/g by manual Fmoc-SPPS. After the attachment of six arginines, the resin was split and to one part additional three arginines were attached.

Afterwards, Fmoc-β-Ala was coupled to both peptides and each 0.05 mmol of the peptides were converted with TAMRA-NHS ester **33**.

To that end, 51.7 mg (69.9 µL, 0.40 mmol, 8 eq.) DIEA and 52.8 mg (0.1 mmol, 2 eq.) of TAMRA-NHS ester **33** were dissolved in a minimal amount of DMF and added to the resin-bound peptide. The reaction mixture was gently shaken overnight at room temperature and afterwards washed four times with DMF and DCM respectively. Cleavage and workup was performed as previously described. After lyophilization 19.1 mg of a purple solid **12** (24%) and 19.6 mg of purple solid **13** were obtained (19%).

RP-HPLC, 10→100% B, t_R=13.42 min for **12** and 13.12 min for **13**.

ESI-MS calc. for **12** $C_{70}H_{112}N_{32}O_{12}$ m/z: 532.29 meas. 532.57 $[M+3H]^{3+}$, 570.57 $[M+TFA+3H]^{3+}$, 608.56 $[M+2TFA+3H]^{3+}$; calc. 399.47 meas. 399.61 $[M+4H]^{4+}$, 428.13 $[M+TFA+4H]^{4+}$.

ESI-MS calc. for **13** $C_{88}H_{148}N_{44}O_{15}$ m/z: 688.49 meas. 764.71 $[M+2TFA+3H]^{3+}$, 840.79 $[M+4TFA+3H]^{3+}$, 787.76 $[M+5TFA+3H]^{3+}$, 916.78 $[M+6TFA+3H]^{3+}$; calc. 516.62 meas. 573.80 $[M+2TFA+4H]^{4+}$, 602.30 $[M+3TFA+4H]^{4+}$, 630.82 $[M+4TFA+4H]^{4+}$, 659.30 $[M+5TFA+4H]^{4+}$, 687.87 $[M+6TFA+4H]^{4+}$; calc. 413.50 meas. 459.22 $[M+2TFA+5H]^{5+}$, 482.03 $[M+3TFA+5H]^{5+}$, 504.86 $[M+4TFA+5H]^{5+}$, 527.68 $[M+5TFA+5H]^{5+}$.

Doxorubicin-GuCOSS conjugate 15

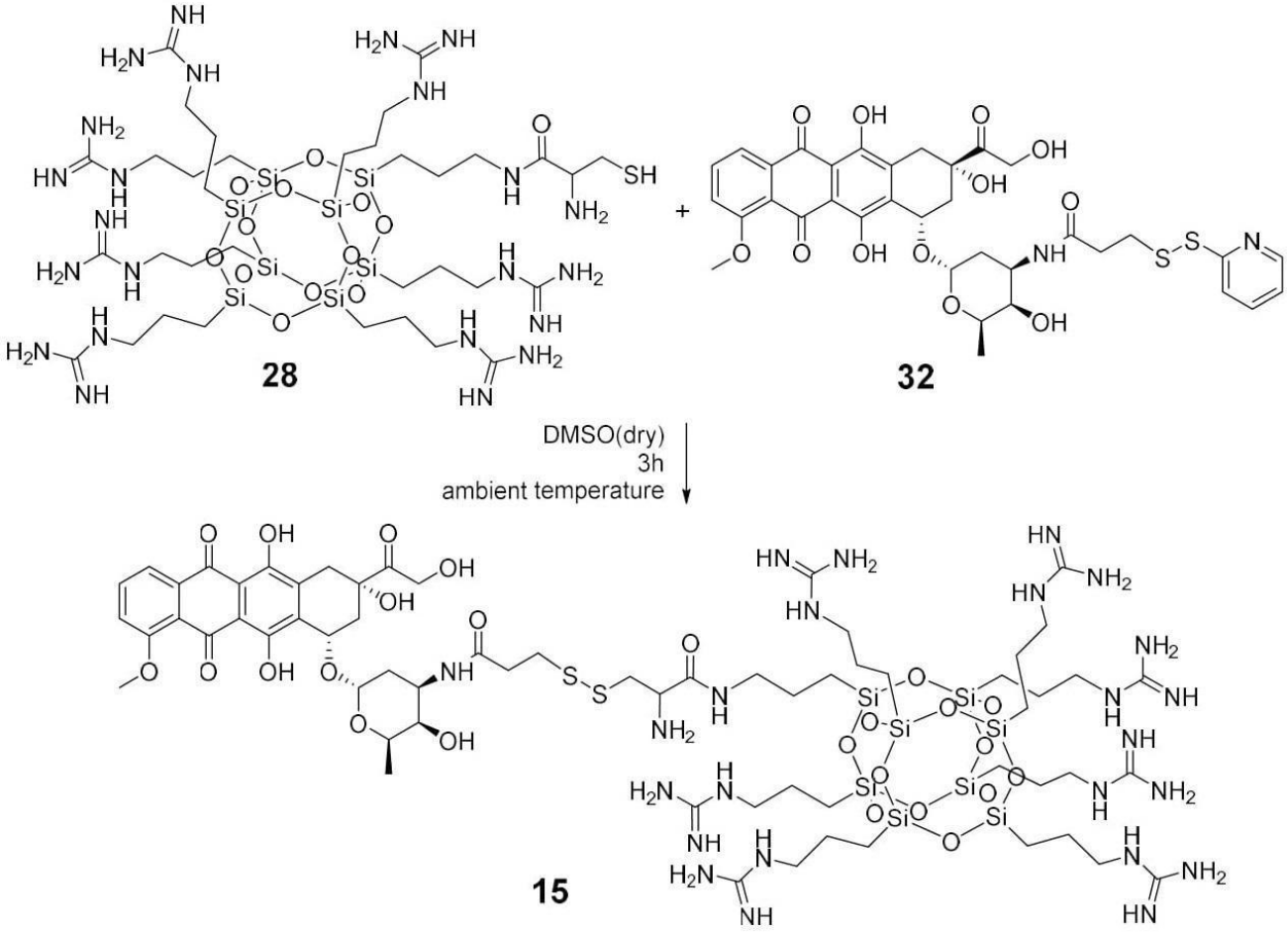

Doxorubicin-GuCOSS conjugate **15** was synthesized using 5 mg (0.0039 mmol, 1 eq.) cysteine-modified GuCOSS **28**, 3.5 mg (0.0047 mmol, 1.2 eq.) aldrithiol-activated doxorubicin **32**. **32** was dissolved in dry DMSO and **28** was added to the solution. After completion of the reaction (3 h, ambient temperature) the reaction mixture was lyophilized and purified using semi-preparative RP-HPLC with a gradient 30to100% B. After lyophilization, 1.1 mg (14.7%) of the desired product as red fluffy powder was obtained. Eluent A: 0.1% aq. acetic acid; Eluent B 90% aq. acetonitrile, 0.1% acetic acid.

RP-HPLC 0→80% B: t_R: 14.63min

HR-MS calc. for $C_{64}H_{114}N_{24}O_{25}S_2Si_8$ m/z: 477.6568 meas. 477.6562 $[M+4H]^{4+}$.

3-carboxy-*N,N,N*-trimethylpropane-1-ammonium chloride 18

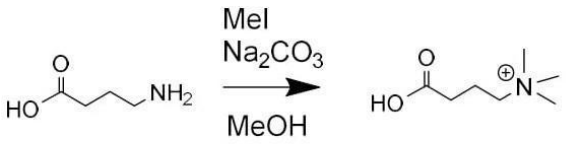

17 **18**

This synthesis was performed according to a procedure by Morano *et al.*[3] 2.2 g (21.6 mmol, 1 eq.) 4-aminobutyric acid **17** (*Alfa Aesar*) and 10 g (100 mmol, 4.6 eq.) potassium bicarbonate were combined in 250 mL of methanol under inert atmosphere. 6.9 mL (110 mmol, 5.2 eq.) methyl iodide was added and the reaction stirred for 4 days at ambient temperature. Then the solvent was removed using a rotary evaporator. The white solid was washed thrice with chloroform and dissolved in 50 mL of 6 N HCl. The solvent was removed by a rotary evaporator. The orange residue was extracted four times with acetone. The acetone was removed by using a rotary evaporator resulting in orange oil. 150 mL of ice-cold tetrahydrofuran (THF) were added and stirred for 30 min. The resulting white solid was filtered, washed twice with ice-cold THF and then dried under vacuum. 763 mg of a white precipitate **18** (19.6%) were obtained.

^{1}H NMR (500 MHz, DMSO-d6) δ: 1.81 – 1.96 (m, 2H), 2.32 (t, J = 7.1 Hz, 2H), 3.08 (s, 9H), 3.27 – 3.42 (m, 2H), 12.33 (s, 1H).

^{13}C NMR (500 MHz, DMSO-d6) δ: 17.92, 30.18, 52.26, 64.55, 173.22.

4-trimethylammoniumbutyric acid-NHS ester 19

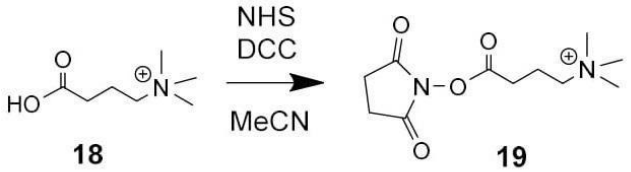

18 **19**

The synthesis was performed according to a procedure by Morano *et al.*[3] A mixture of 200 mg (1.1 mmol, 1 eq.) 3-carboxy-*N,N,N*-trimethylpropane-1-ammonium chloride **18**, 215.4 mg (1.87 mmol, 1.7 eq.) NHS and 431.6 mg (2.1 mmol, 1.9 eq.) DCC were dissolved in 8 mL dry MeCN. After complete addition at 0°C, the mixture was stirred for 16 h at ambient temperature. The reaction mixture was filtrated to remove the resulting urea derivative. The solvent was removed using a rotary evaporator. 3 mL THF were added and the solution was stirred for 5 min at 0°C. The reaction mixture was filtered and the residue was washed thrice with ice-cold THF. After solvent removal, 204.1 mg of **19** (76.2%) were obtained.

ESI-MS calc. for $C_{11}H_{19}N_2O_4^+$ m/z: 243.28, meas. 243.03 $[M+H]^+$.

N-Trt-protected β-alanine 22

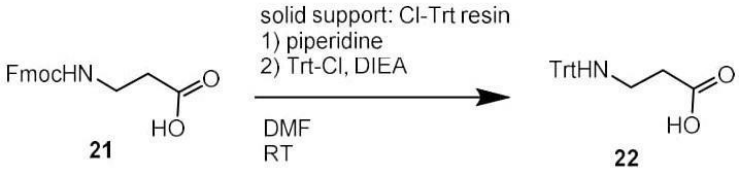

1 g 2-chlorotrityl resin (*Iris biotech GmbH*) was swollen for 1 h at ambient temperature in dry DCM. 0.995 g (3.2 mmol, 2 eq.) Fmoc-β-Ala and 0.825 mg (6.4 mmol, 4 eq., 1.112 mL) dry DIEA were added in 10 mL dry DCM and the mixture was shaken for 2 h at ambient temperature. The resin was washed 5 times with DCM and afterwards thrice using each 5 mL of a mixture of DCM, DIEA, and MeOH (17:2:1, *v*:*v*:*v*). The Fmoc protecting group was removed by double deprotection (20 vol% piperidine in DMF). The resin was washed with DCM and 1.784 g (6.4 mmol, 4 eq.) tritylchloride and 1.238 g (9.6 mmol, 6 eq., 1.674 mL) dry DIEA were added in 10 mL dry DCM and the mixture was shaken overnight at ambient temperature. The resin was washed 5 times with DCM. *N*-Trityl-protected β-alanine **22** was cleaved from the resin using 10 mL of a mixture of acetic acid, methanol, and DCM (5:1:4, *v*:*v*:*v*). The mixture was shaken for 3 h at room temperature. The solvent was removed using a rotary evaporator. 0.496 g of white solid **22** were obtained (93.5%) and used without further purification.

ESI-MS calc. for $C_{22}H_{21}NO_2$ m/z: 331.42, meas. 330.06 $[M-H]^-$.

^{1}H NMR (300 MHz, DMSO-d_6) δ: 2.20 (t, J = 6.7 Hz, 2H), 2.44 (t, J = 6.4 Hz, 2H), 2.95 (s, 1H), 7.19 (t, J = 7.3 Hz, 3H), 7.30 (t, J = 7.9 Hz, 6H), 7.41 (d, J = 7.2 Hz, 6H).

^{13}C-NMR (75 MHz, DMSO-d_6) δ: 34.75, 39.40, 70.29, 126.05, 127.67, 128.31, 145.96, 173.77.

COSS derivative 23 (monoTrt-aminoCOSS)

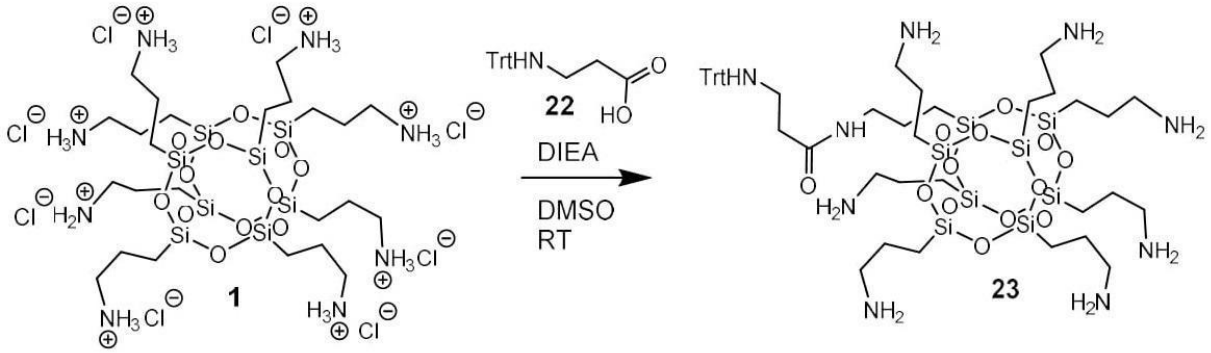

0.104 g (1.1 eq., 0.312 mmol) of β-alanine **22**, 0.148 g (1 eq., 0.284 mmol) benzotriazol-1-yl-oxytripyrrolidinophosphonium hexafluorophosphate (PyBOP) and 73.4 mg (2 eq., 0.568 mmol, 98.9 mL) dry DIEA were dissolved in 5 mL dry DMSO and shaken for 10 min at ambient temperature. After 10 min, the volume was increased to 40 mL using dry DMSO. 1 g of octaammonium COSS hydrochloride **1** was dissolved in 5 mL dry DMSO and the activated amino acid was slowly added to the vigorously stirred solution using a peristaltic pump (flow: 0.05 mL/min). The mixture was stirred for additional 2 h at room temperature and the solvent was removed by lyophilization. The oily residue was suspended in dry acetonitrile and the insoluble part was washed two times with dry acetonitrile. The precipitate was dissolved in 10 vol% aq. MeCN with 0.1 vol% AcOH and purified by semi-preparative RP-HPLC (gradient 10to100% B) with 0.1 vol% AcOH. After lyophilization 123 mg of colorless solid **23** were obtained (33%).

RP-HPLC, 10→100% B, t_R= 14.82 min.

ESI-MS calc. for $C_{46}H_{83}N_9O_{13}Si_8$ m/z: 1194.90 meas. 1194.63 $[M+H]^+$, calc. 598.45 meas. 598.26 $[M+2H]^{2+}$.

^{1}H NMR (400 MHz, DMSO-d_6) δ: 8.48 (s, 1H), 8.41 – 8.00 (m, 21H), 7.41 (s, 15H), 3.10 – 2.94 (m, 2H), 2.91 – 2.65 (m, 16H), 2.32 (s, 1H), 2.21 – 1.78 (m, 2H), 1.85 – 1.58 (m, 14H), 1.58 – 1.35 (m, 2H), 0.96 – 0.39 (m, 16H).

^{29}Si NMR (79 MHz, DMSO) δ: -65.98, -66.49, -66.52, -66.62.

3-(pyridin-2-yldisulfanyl)propanoic acid) 31

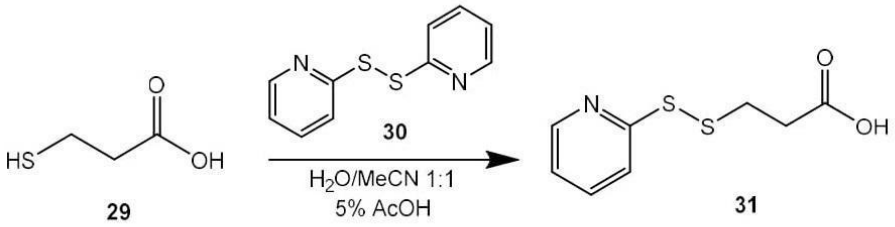

300 mg (1.3 mmol, 1 eq.) *2,2'*-dipyridyl disulfide **30** (*Aldrithiol™-2, Sigma Aldrich*) were diluted in 25.0 mL water/MeCN (1:1) with 5% acetic acid. 0.28 g (2.65 mmol, 2 eq.) 3-mercaptopropanoic acid **29** (*Sigma Aldrich*) were slowly added and the reaction mixture was stirred overnight at ambient temperature. The solvent was removed using a rotary evaporator. The precipitate was dissolved in aq. MeCN and purified by preparative RP-HPLC (gradient 10to80% B). After lyophilization, 61.9 mg of a yellow solid **31** were obtained (22.1%).

RP-HPLC, 10→100% B, t_R= 11.06min.

ESI-MS calc. for $C_8H_9NO_2S_2$ m/z: 215.29, meas. 215.94 $[M+H]^+$.

COSS derivative 27 (PG-Cys-aminoCOSS)

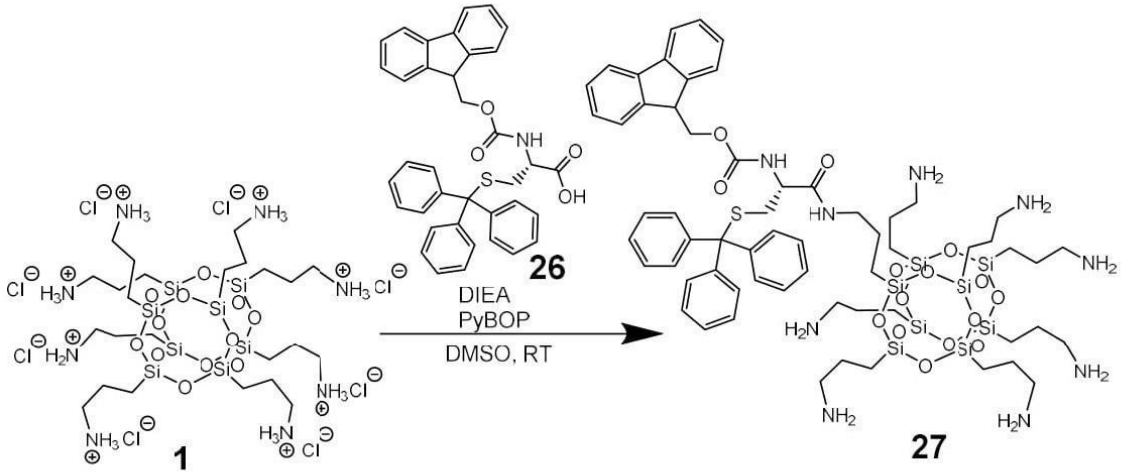

A mixture of 265.0 mg (0.45 mmol, 1 eq.) of Fmoc-Cys(Trt)-OH **26,** 1.89 mL (10.86 mmol, 24 eq.) dry DIEA and 283.0 mg (0.54 mmol, 1.2 eq.) of PyBOP was dissolved in 10 mL dry DMSO and pre-activated for 10 min. 1.06 g (0.91 mmol, 2 eq.) of octaammonium COSS hydrochloride **1** (purchased from *Hybrid Plastics* Inc., USA) were dissolved in 10.0 mL dry DMSO and vigorously stirred. The activated amino acid was added slowly using a peristaltic pump (flow: 0.05 mL/min). The mixture was stirred for additional 2 h at room temperature and the solvent was removed by lyophilization. The residue was suspended in dry acetonitrile and the insoluble part was washed twice with dry acetonitrile. The precipitate was dissolved in 10

vol% aq. MeCN with 0.1 vol% TFA and purified by semi-preparative RP-HPLC (gradient 10to50% B). After lyophilization, 145.0 mg of a white solid **27** were obtained (22.1 %).

RP-HPLC, 10→50% B, t_R= 21.5 min.

ESI-MS calc. for $C_{61}H_{93}N_9O_{15}SSi_8$ m/z: 1449.19, meas. 1449.7 $[M+H]^+$.

HR-MS calc. for $C_{61}H_{93}N_9O_{15}SSi_8$ m/z: 724.7406 measured 724.7409 $[M+2H]^{2+}$.

COSS derivative 28 (Cys-GuCOSS)

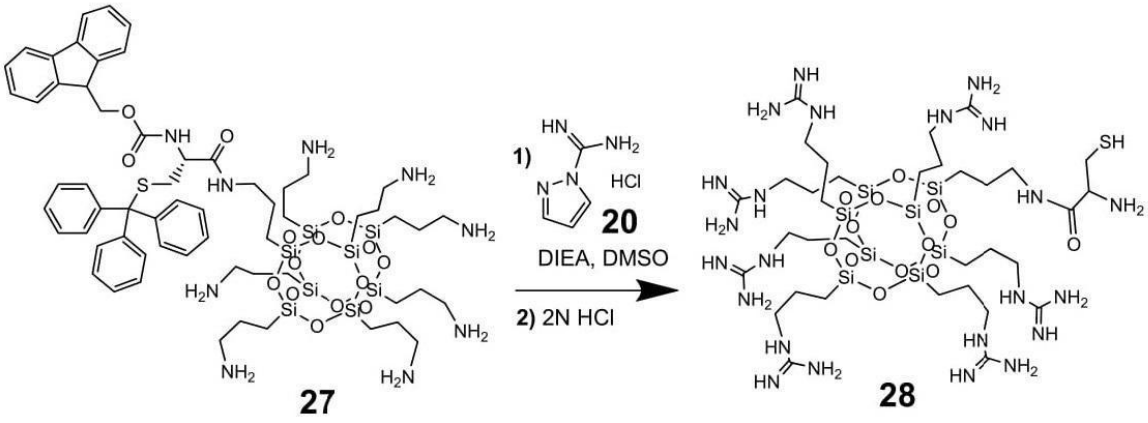

145 mg (0.12 mmol, 1 eq.) **27**, 368 mg (2.49 mmol, 21 eq.) 1*H*-pyrazole-1-carboxamidine hydrochloride **20** and 823 µL (4.73 mmol, 40 eq.) dry DIEA were mixed in 10 mL dry DMSO and the mixture was stirred for 2 days at ambient temperature (simultaneous Fmoc cleavage over the reaction course was caused by 1*H*-pyrazole formed upon guanidinylation as a by-product). Afterwards the solvent was removed by lyophilization and the oily residue was suspended in dry acetonitrile. The insoluble part was washed twice with dry acetonitrile. The precipitate was dissolved in 10 vol% aq. MeCN with 0.1 vol% TFA and purified by semi-preparative RP-HPLC (gradient 0to50% B). After lyophilization the trityl protecting group was removed by 1 mL 2 N HCl and 1 mL $CHCl_3$ and the solution was shaken for 3 h at ambient temperature. The organic phase was removed and the aqueous phase was extracted twice with each 1 mL $CHCl_3$. The combined organic phases were abolished and 9 mL deionized water was added to the aqueous phase. The solvent was removed by lyophilization. The remaining colorless solid was dissolved in 5 mL 5 vol% aq. AcOH and the solvent was removed by lyophilization. 64.0 mg of white solid **28** were obtained (42.3 %).

RP-HPLC, 0→50% B, t_R=20.12 min.

HR-MS calc. for $C_{68}H_{164}N_{46}O_{26}S_2Si_{16}$ m/z: 365.7026, meas. 365.7027 $[M+7H]^{7+}$ for the dimer.

Aldrithiol-activated doxorubicin 32

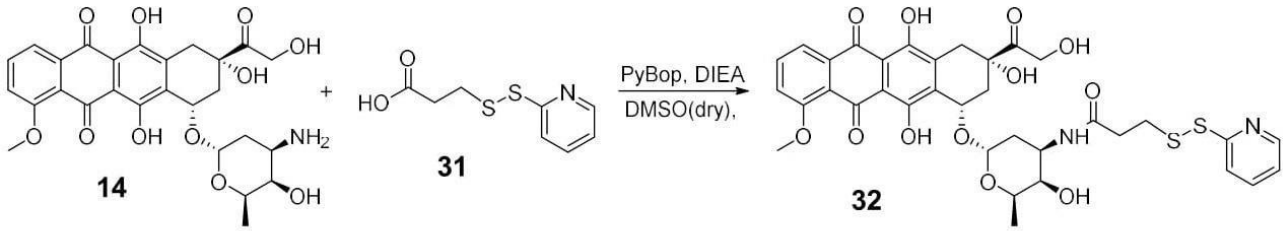

Aldrithiol-activated doxorubicin **32** was synthesized using 10 mg (0.018 mmol, 1 eq.) doxorubicin **14** (*Biomol GmbH*), 5.8 mg (0.027 mmol, 1.5 eq.) of **31**, 11.2 mg (0.22 mmol, 1.2 eq.) PyBop and 9.3 µL (0.054 mmol, 3 eq.) DIEA. After completion of the reaction (24 h, ambient temperature) the reaction mixture was lyophilized and purified using semi-preparative RP-HPLC with a gradient 40to100 %B. After lyophilization 8 mg (60%) of the desired product was obtained.

RP-HPLC 25→100 % B: t_R=11.95 min

ESI-MS calc. for $C_{35}H_{36}N_2O_{12}S_2$ m/z: 740.80, meas. 741.29 $[M+H]^+$.

5.3 Analytical data

COSS derivative 2 (TAMRA-aminoCOSS)

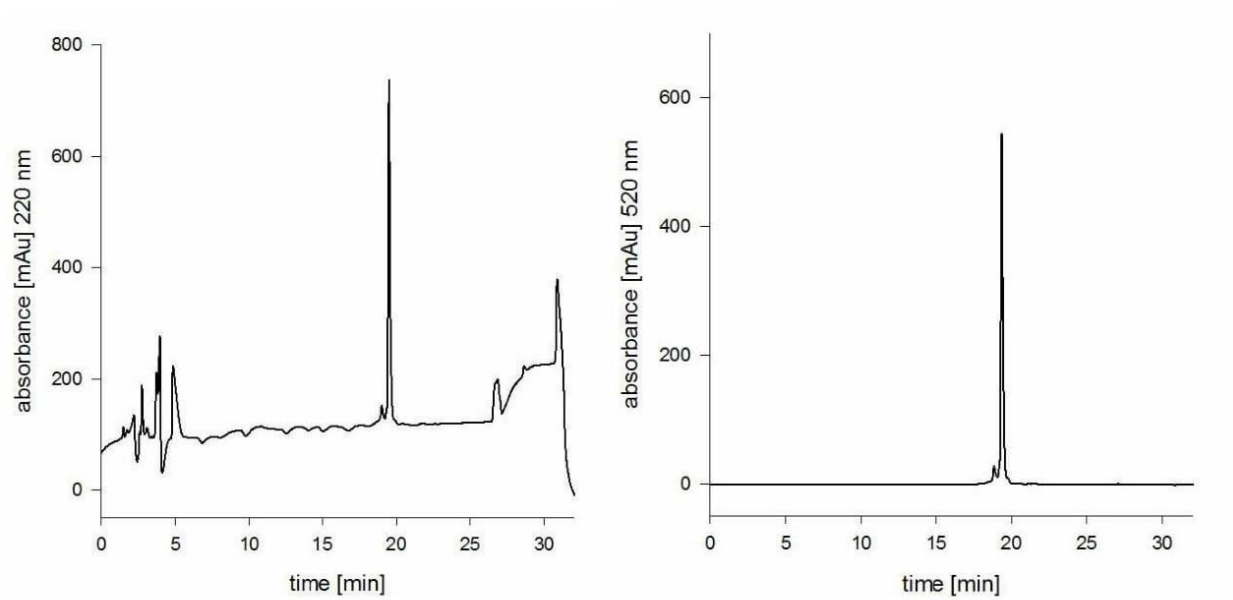

Figure S14: *Analytical HPLC diagrams of* ***2****. Left: λ=220 nm; right λ=520 nm.*

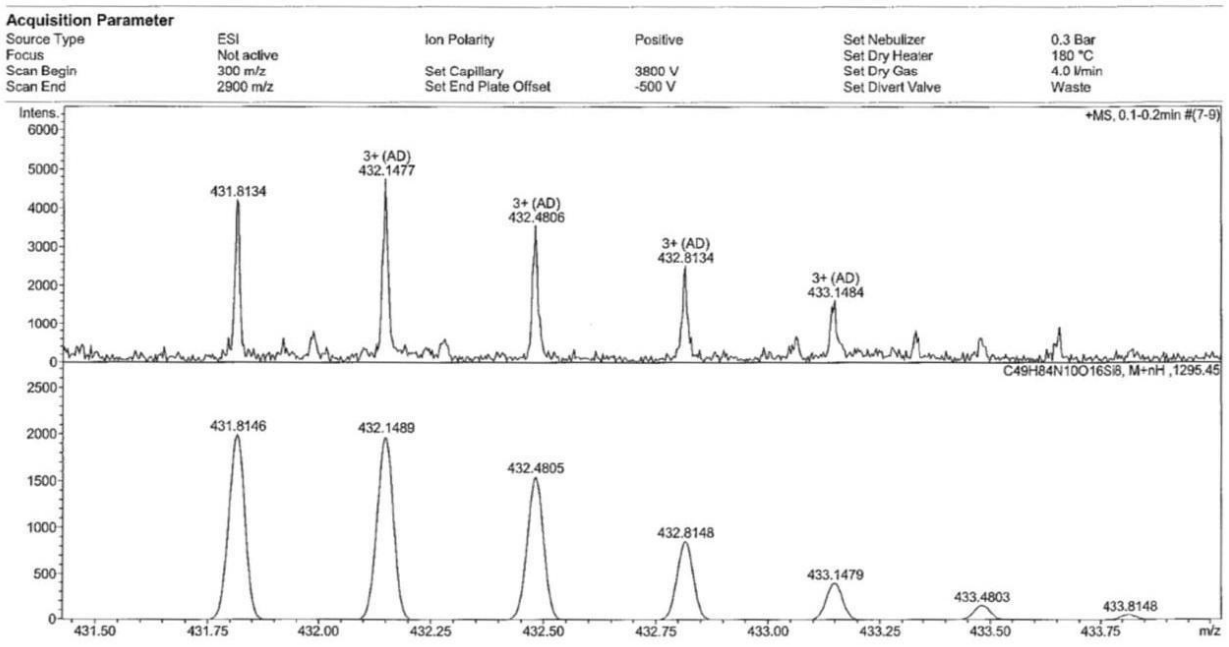

Figure S15: *HR-MS of* ***2****. m/z measured = 431.8134, m/z calculated = 431.8146* $[M+3H]^{3+}$.

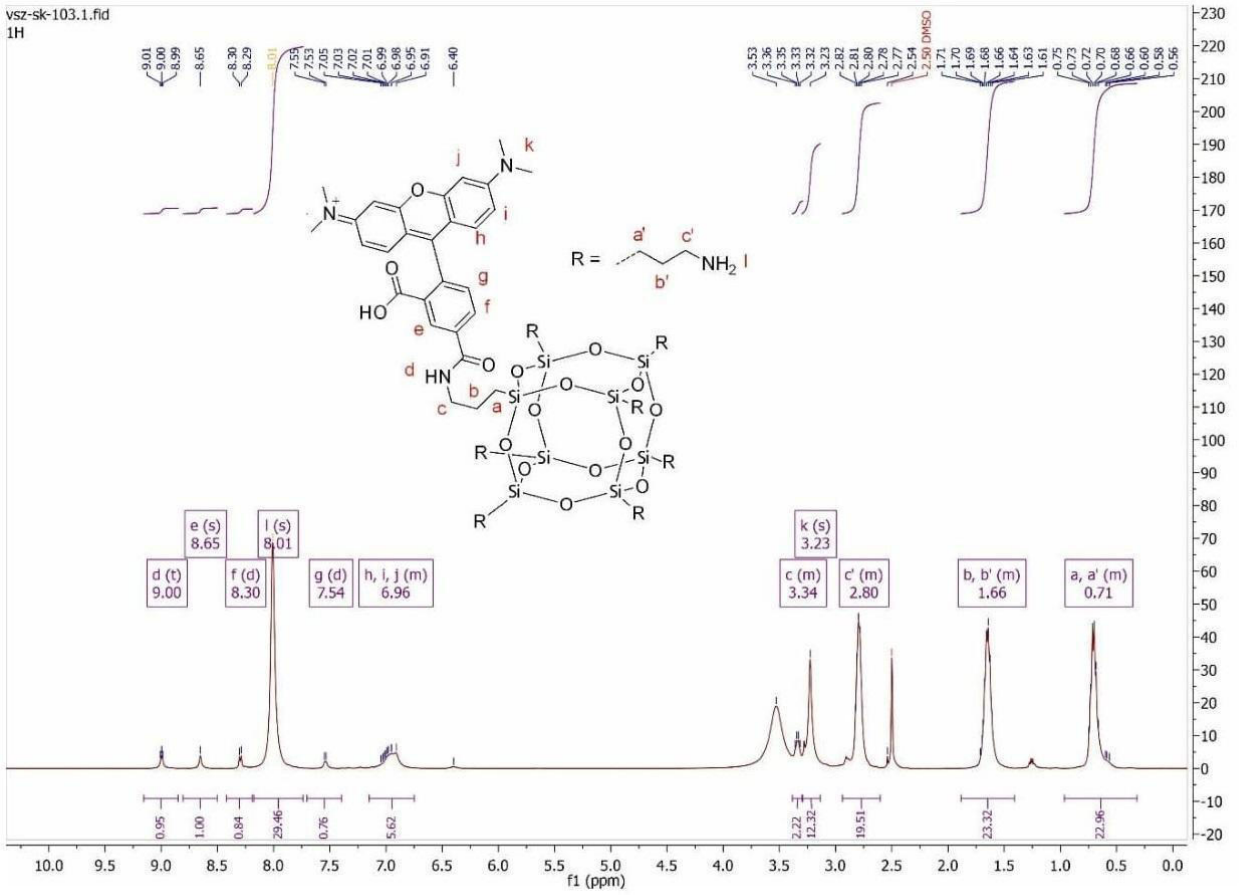

Figure S16: *^{1}H NMR of* ***2.***

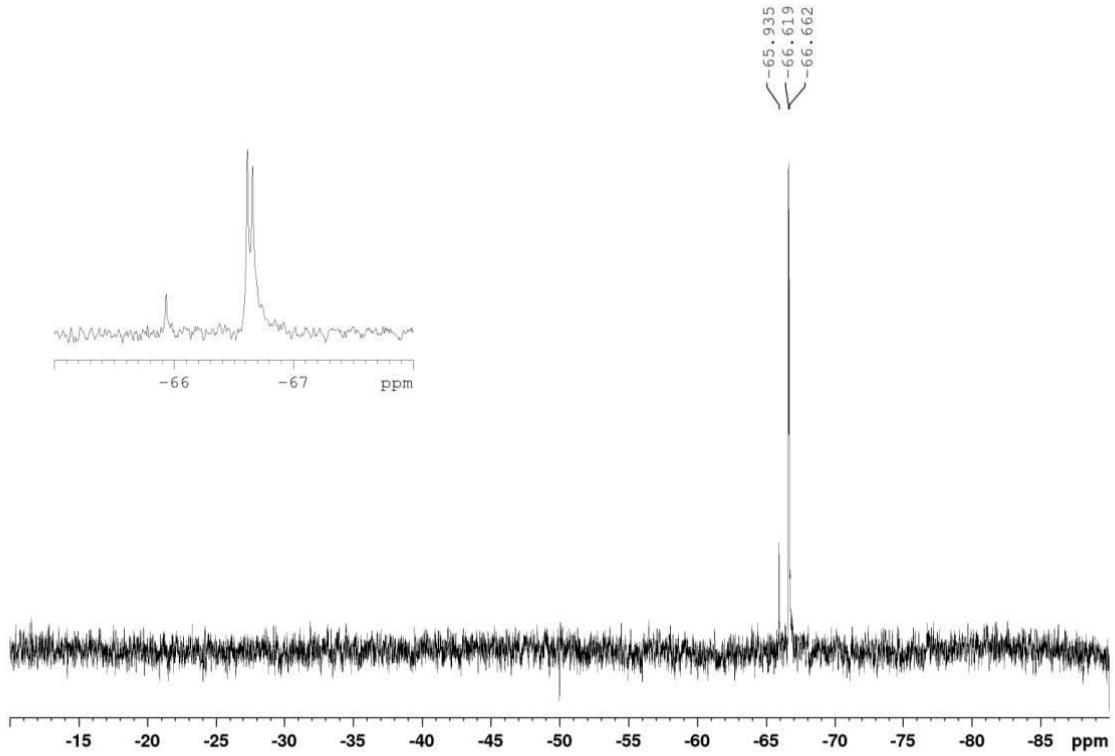

Figure S17: *^{29}Si NMR of* ***2.***

COSS derivative 3 (TAMRA-QuartCOSS)

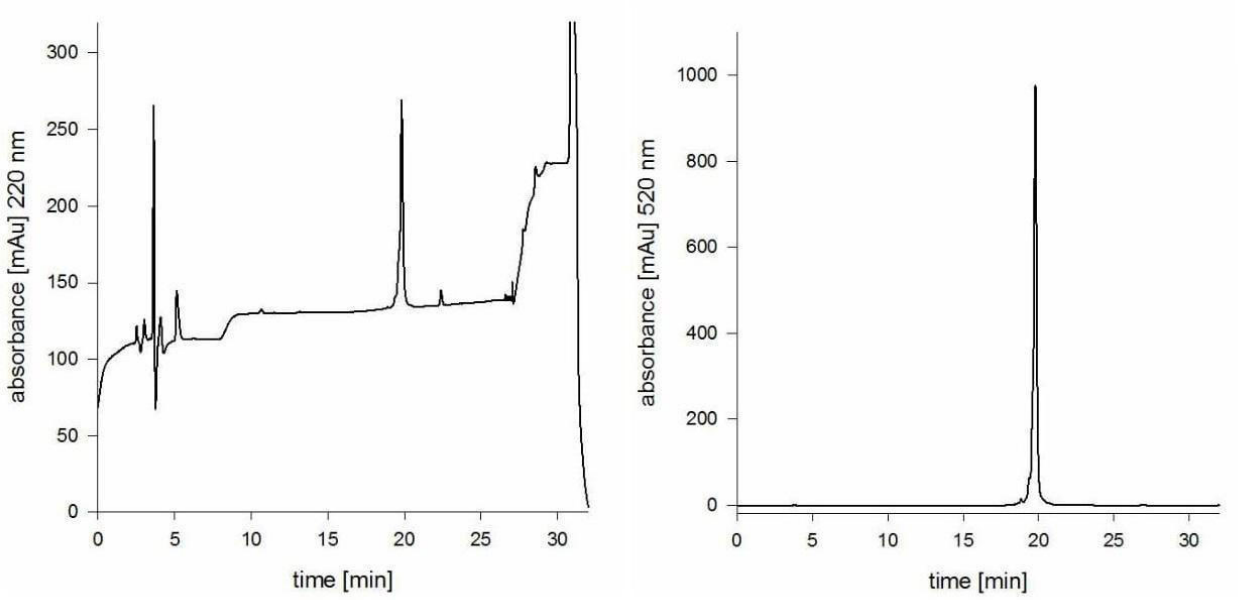

Figure S18: *Analytical HPLC diagrams of* ***3****. Left: λ=220 nm; right: λ=520 nm.*

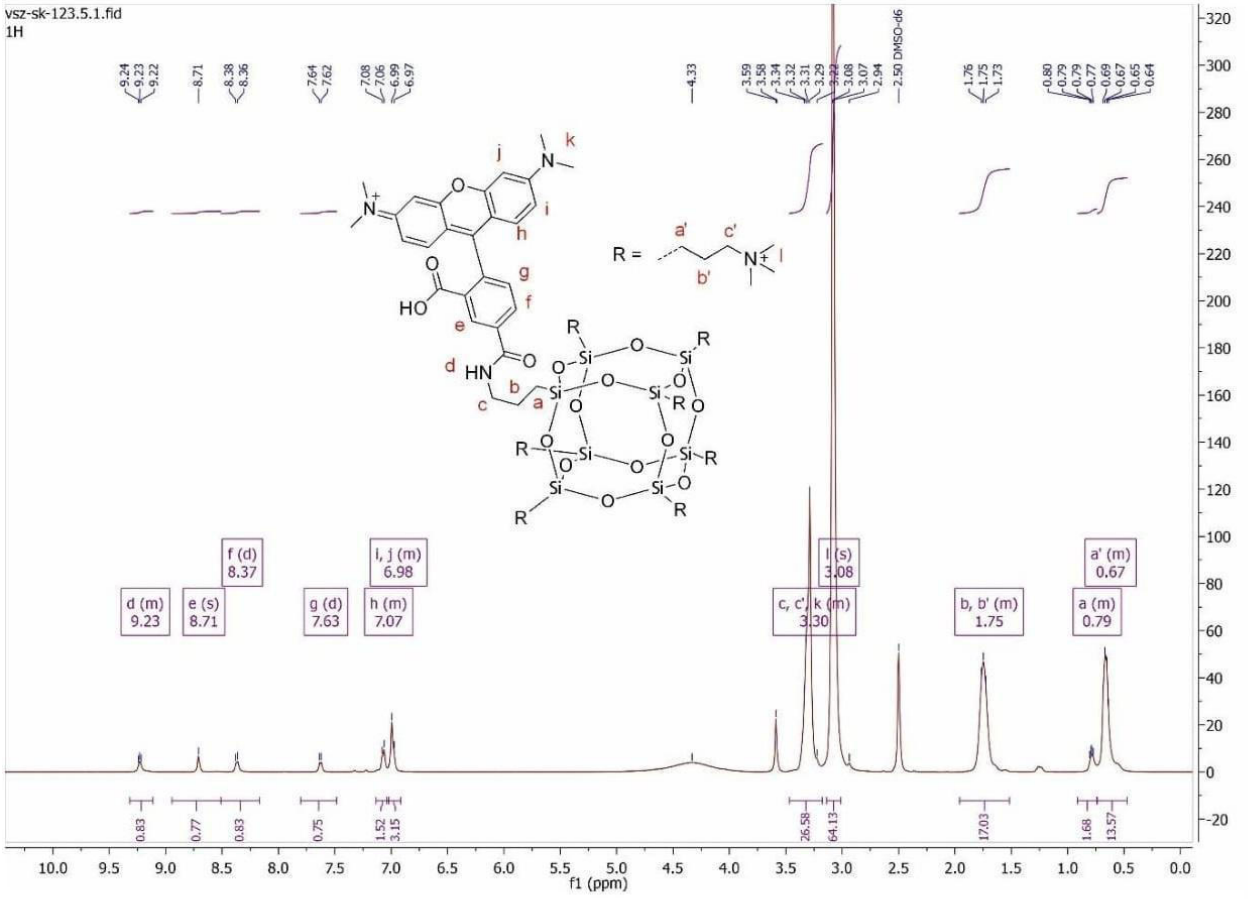

Figure S19: *^{1}H NMR of* ***3****.*

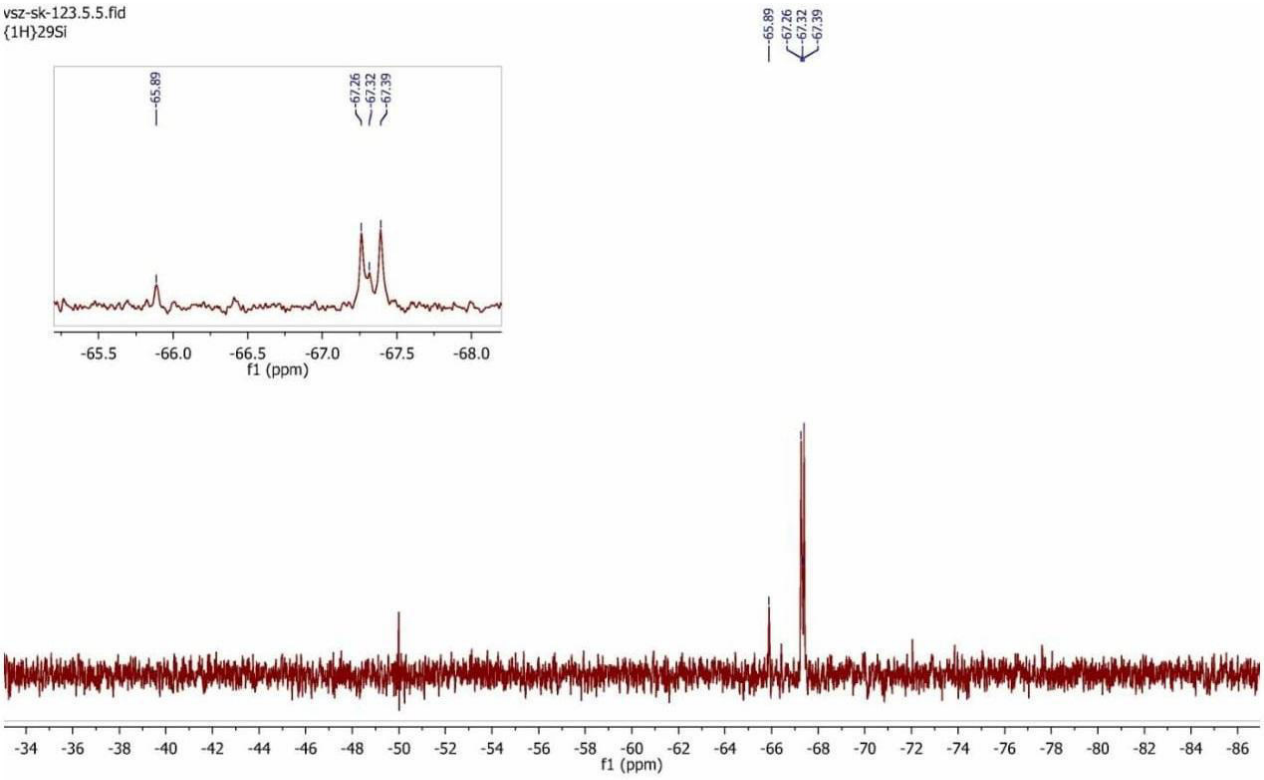

Figure S20: *^{29}Si NMR of **3**.*

COSS derivative 4 (TAMRA-GuCOSS)

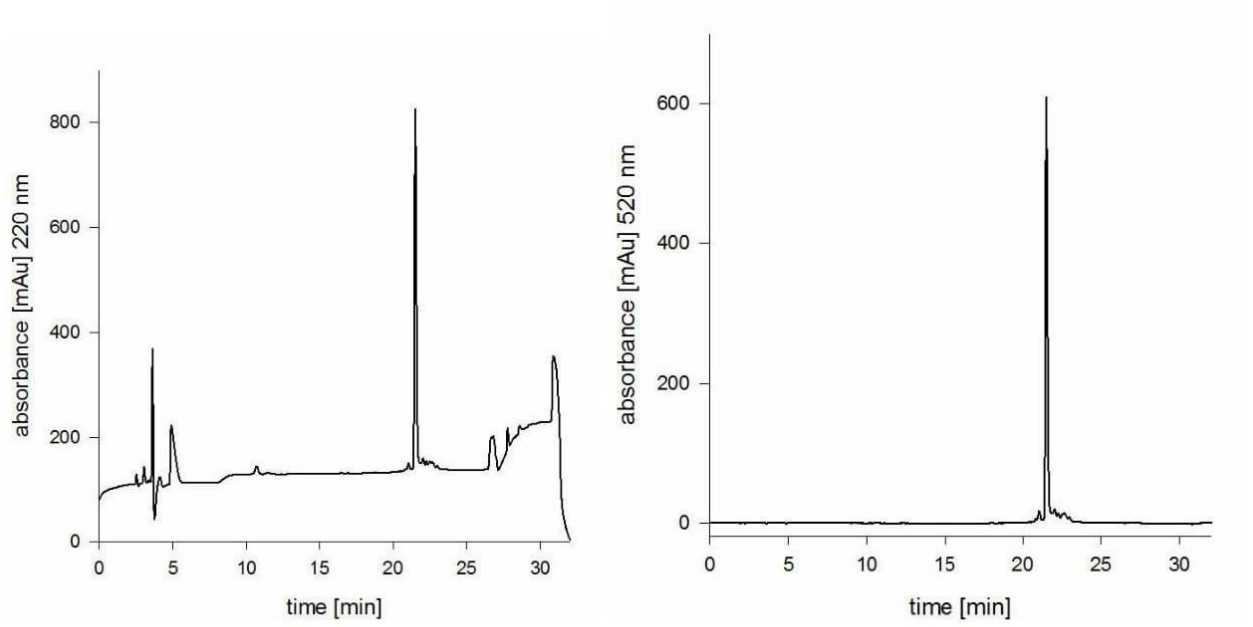

Figure S21: *Analytical HPLC diagrams of **4**. Left: λ=220 nm; right: λ=520 nm.*

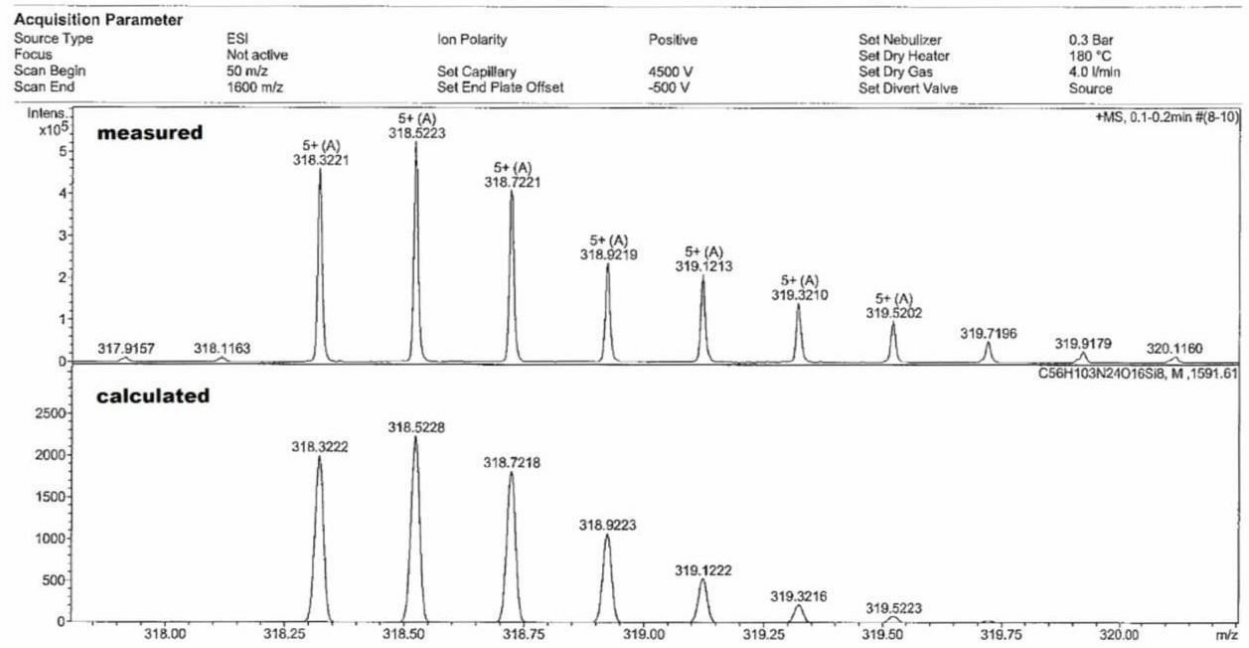

Figure S22: *HR-MS of **4**. m/z measured = 318.3221, m/z calculated = 318.3222; $[M+5H]^{5+}$.*

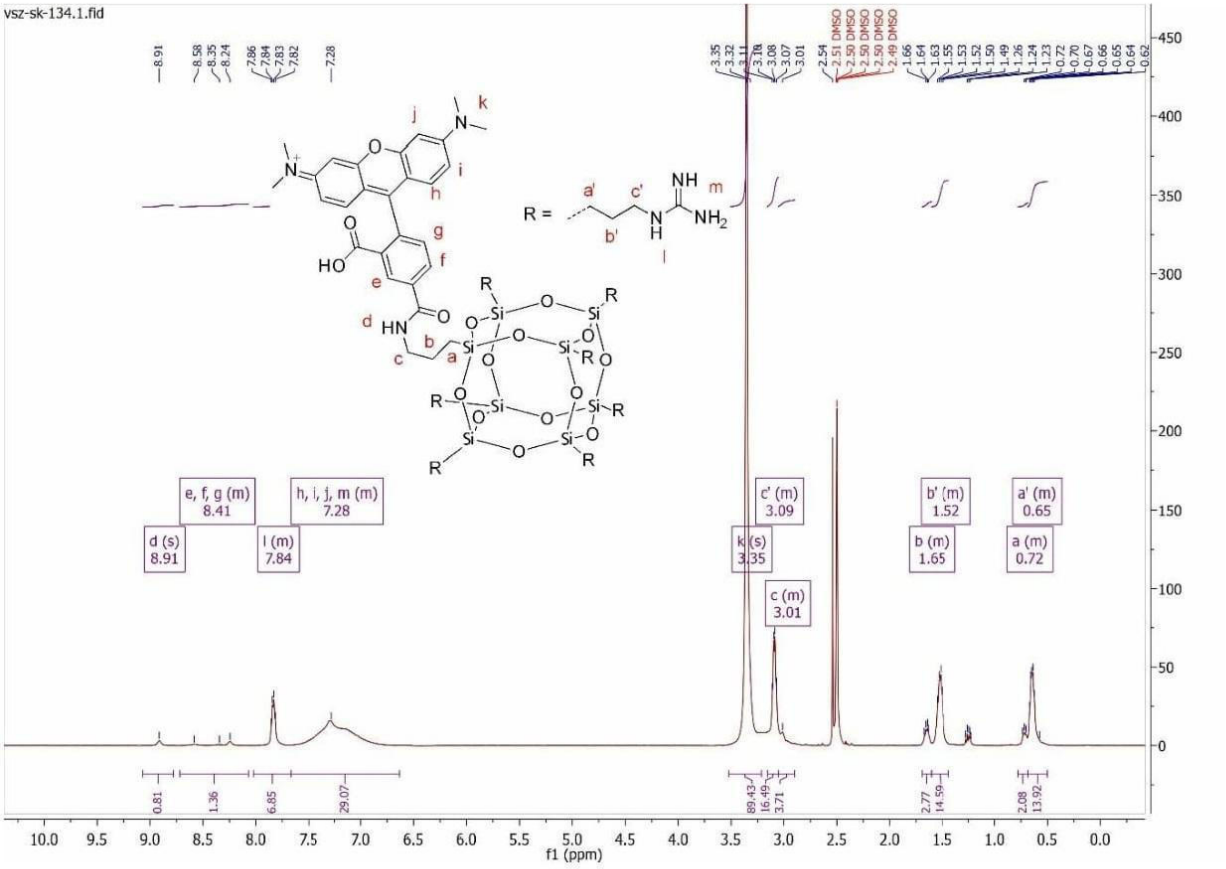

Figure S23: *^{1}H NMR of **4**.*

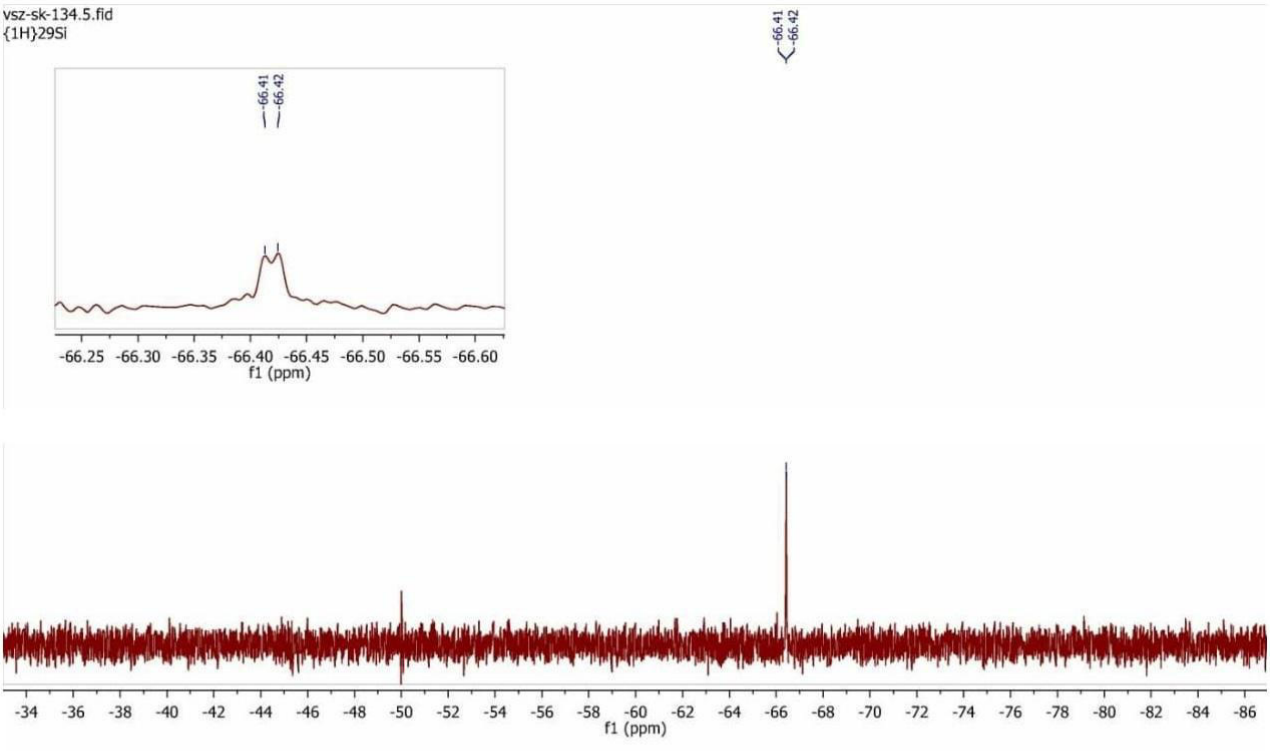

Figure S24: *^{29}Si NMR of **4**.*

COSS derivative 5 (TAMRA-aminoCOSS-L)

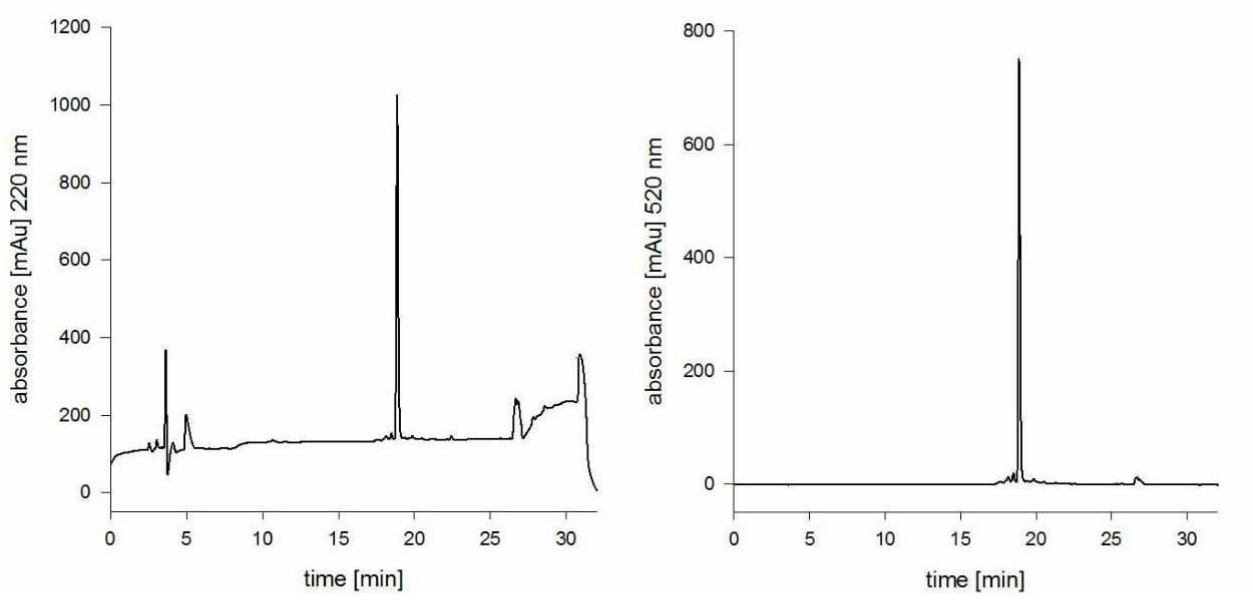

Figure S25: *Analytical HPLC diagrams of **5**. Left: λ=220 nm; right: λ=520 nm.*

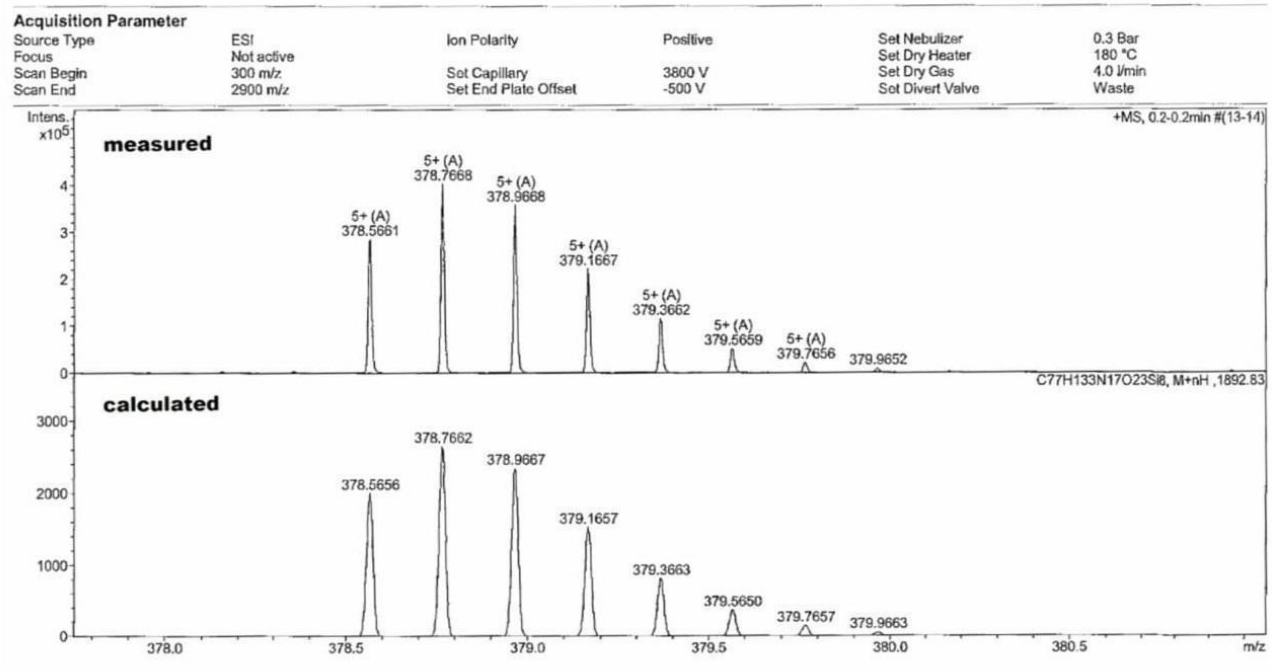

Figure S26: *HR-MS of* ***5****.Calculated for* $C_{77}H_{133}N_{17}O_{23}Si_8$ *m/z: 378.5656, measured 378.5661* $[M+5H]^{5+}$

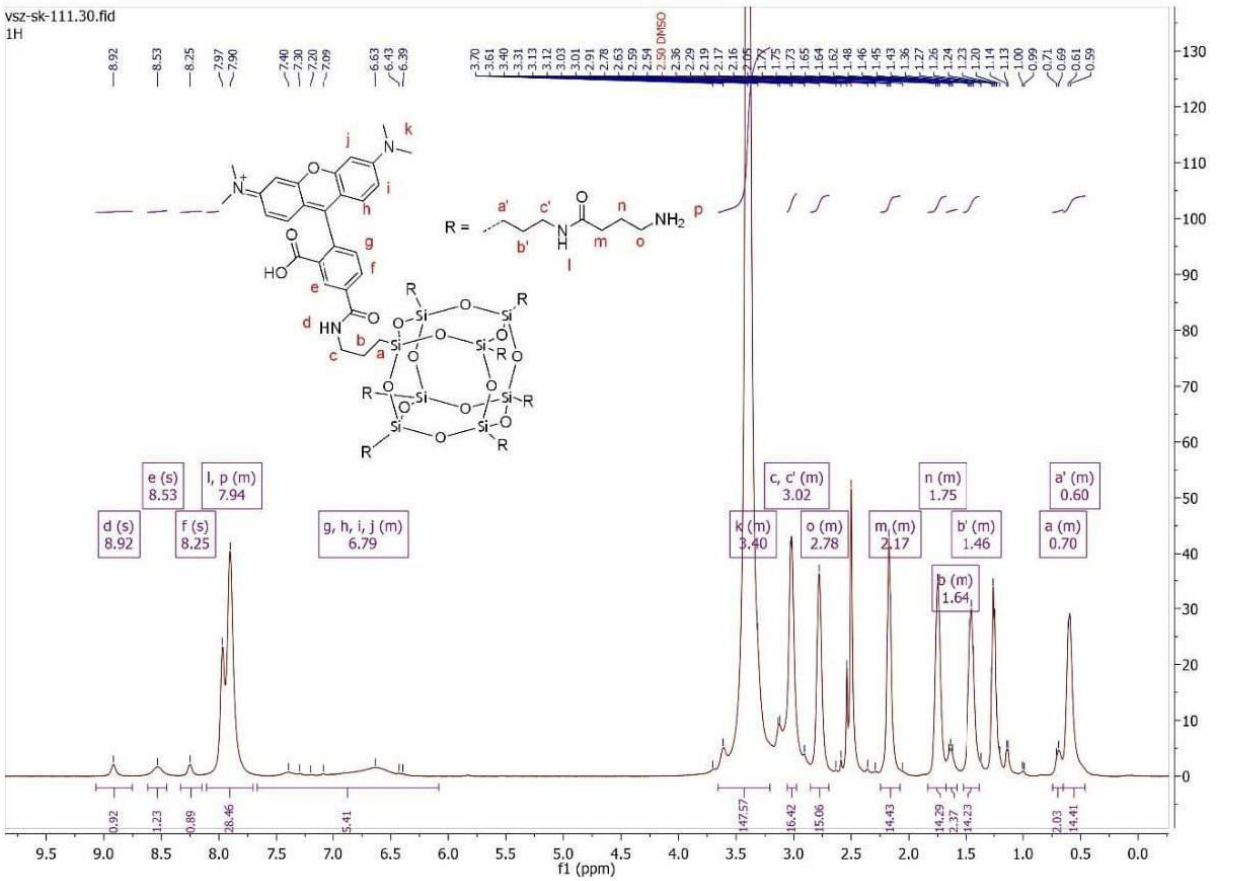

Figure S27: *^{1}H NMR of* ***5****.*

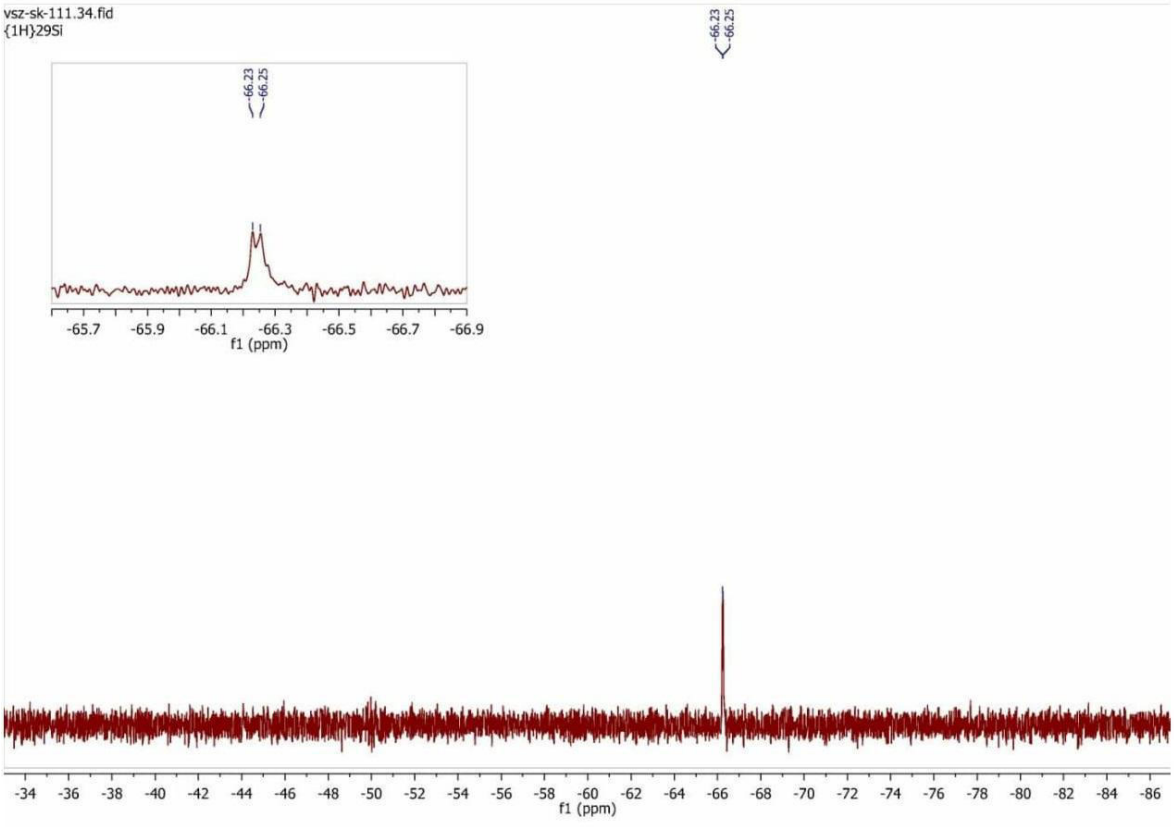

Figure S28: *^{29}Si NMR of **5**.*

COSS derivative 6 (TAMRA-quartCOSS-L)

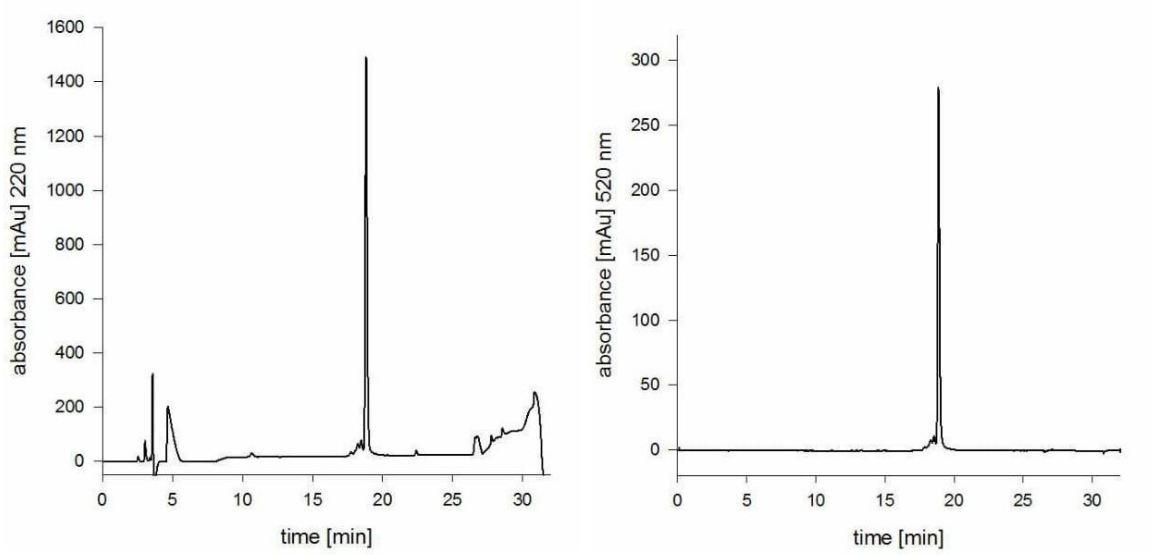

Figure S29: *Analytical HPLC diagrams of **6**. Left: λ=220 nm; right: λ=520 nm.*

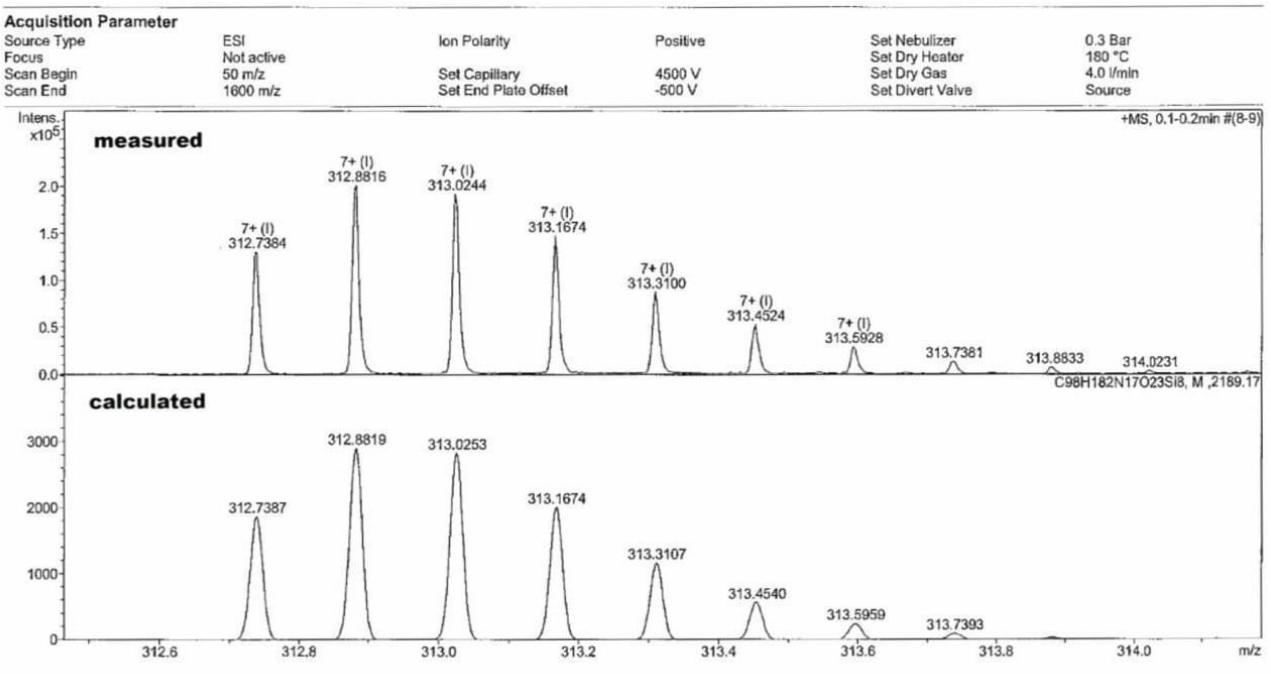

Figure S30: *HR-MS of* ***6****. Calculated for* $C_{98}H_{182}N_{17}O_{23}Si_8^{7+}$ *m/z: 312.7387, measured 312.7384* $[M]^{7+}$

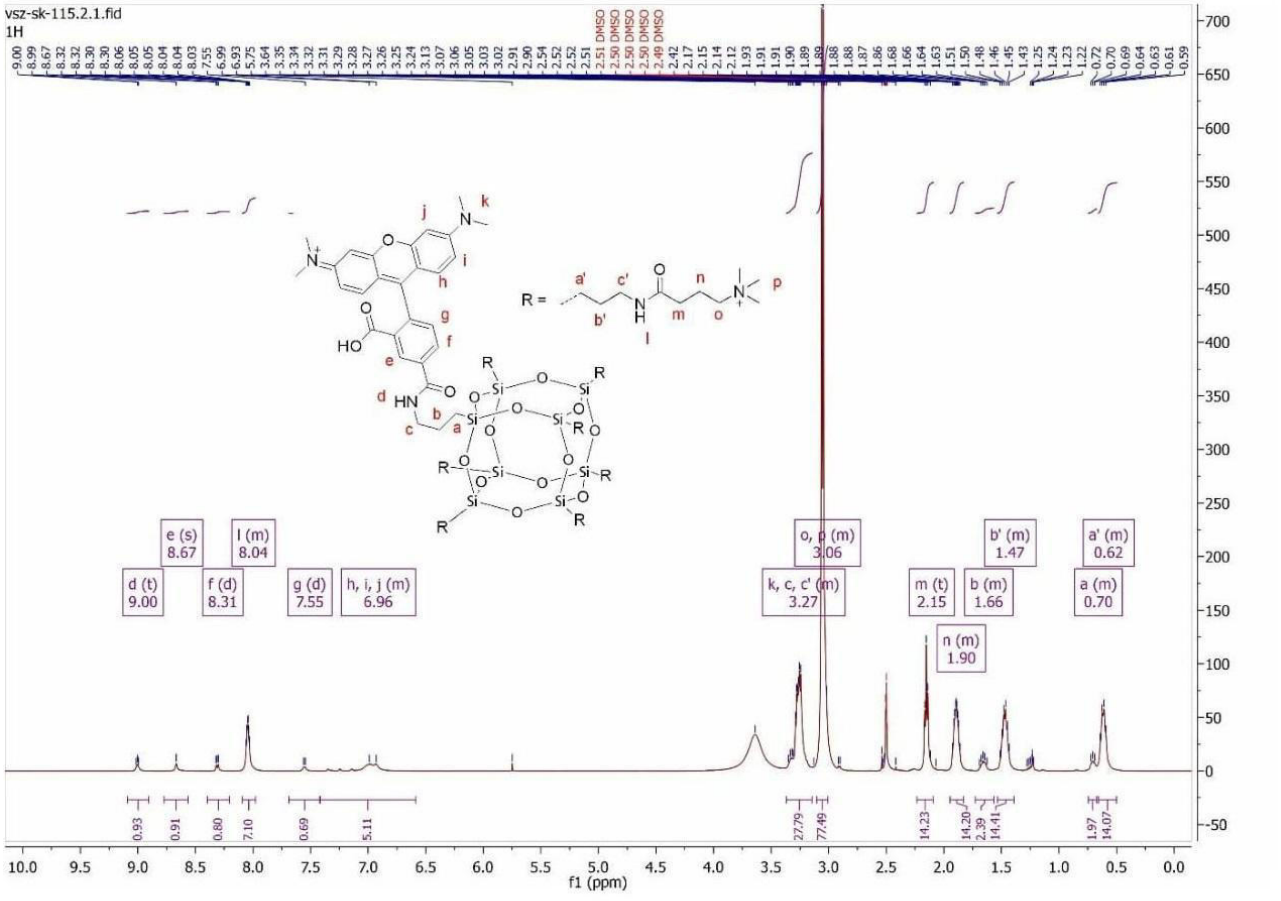

Figure S31: *^{1}H NMR of* ***6****.*

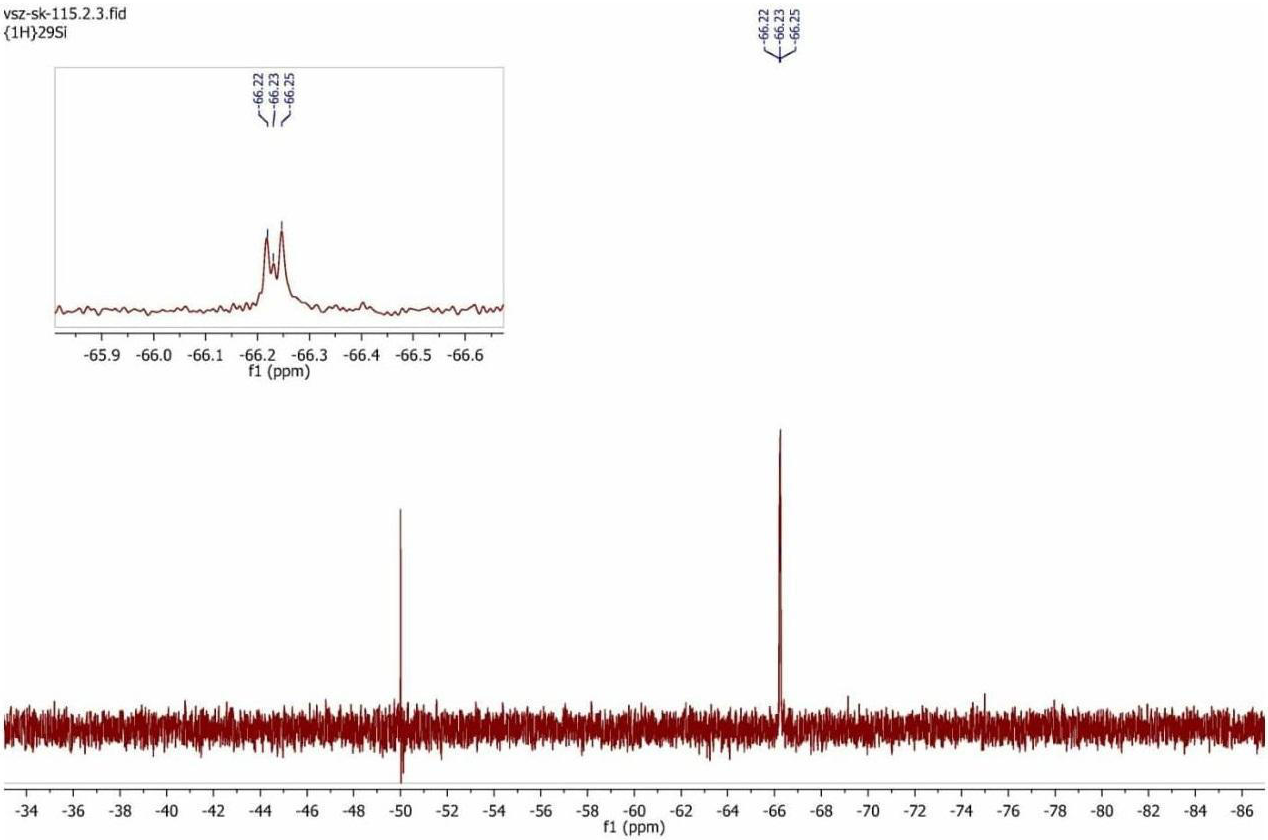

Figure S32: *^{29}Si NMR of **6**.*

COSS derivative 7 (TAMRA-GuCOSS-L)

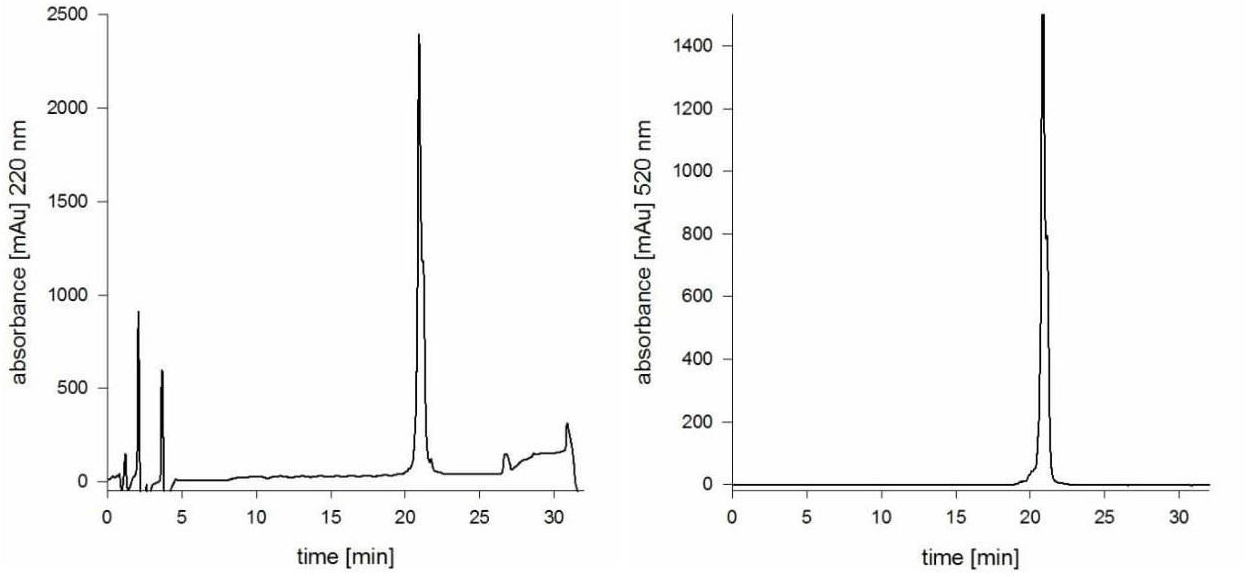

Figure S33: *Analytical HPLC diagrams of **7**. Left: λ=220 nm; right: λ=520 nm.*

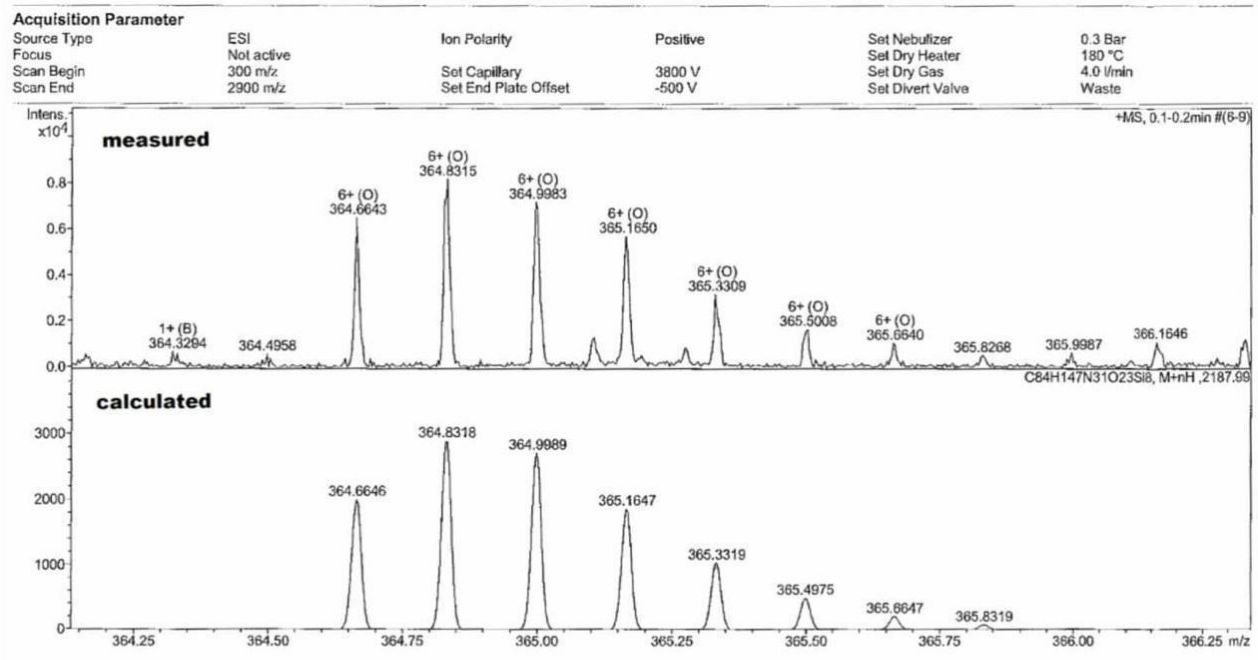

Figure S34: *HR-MS of* ***7****. Calculated for* $C_{84}H_{147}N_{31}O_{23}Si_8$ *m/z: 364.6646, measured 364.6643* $[M+6H]^{6+}$.

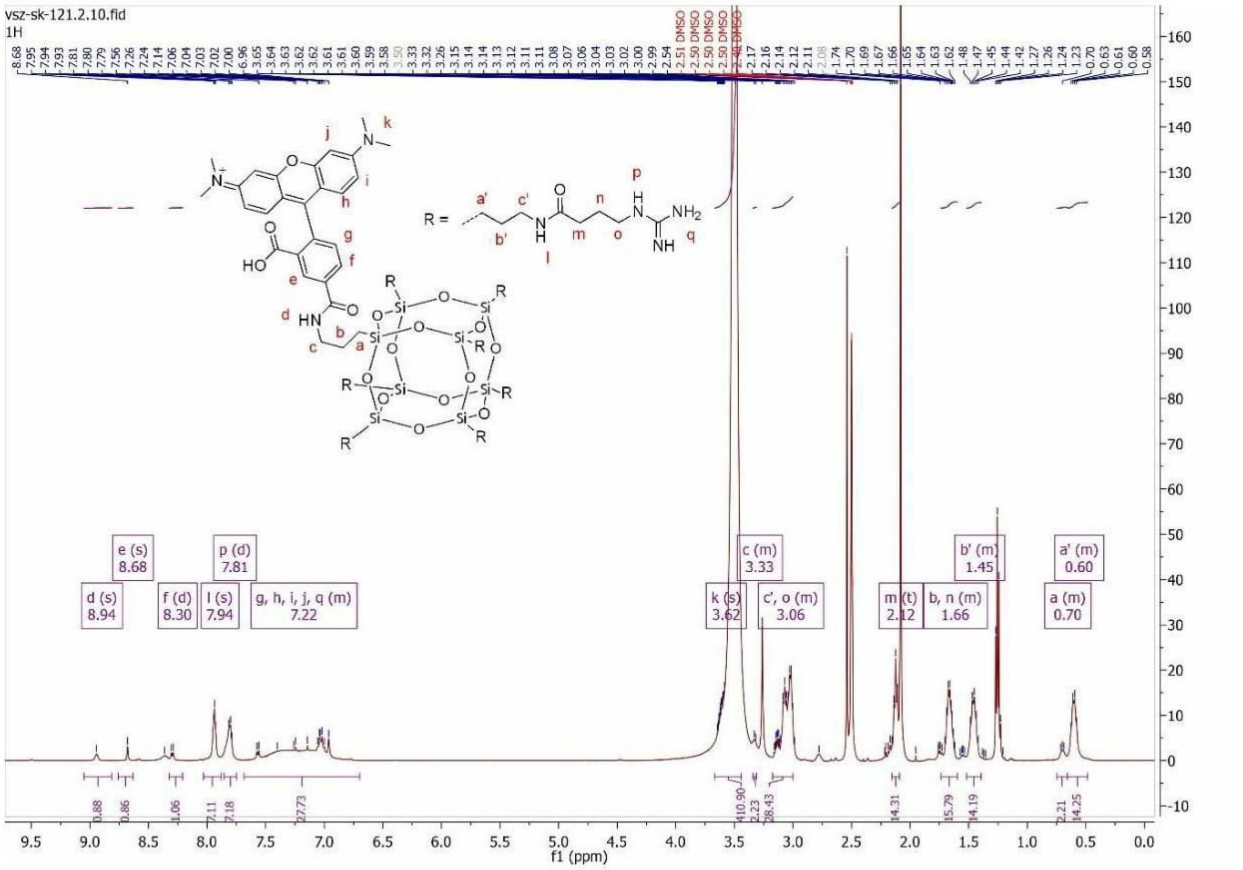

Figure S35: *^{1}H NMR of* ***7****.*

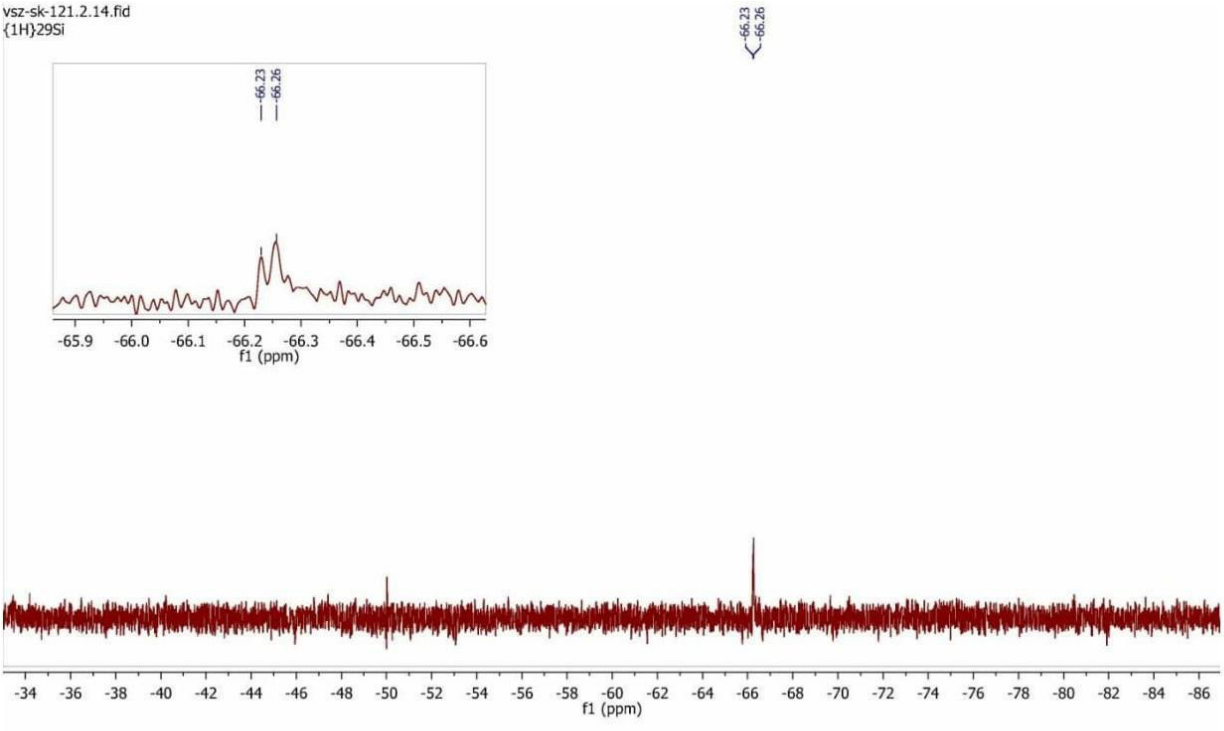

Figure S36: *^{29}Si NMR of* ***7.***

COSS derivative 8 (amino-GuCOSS)

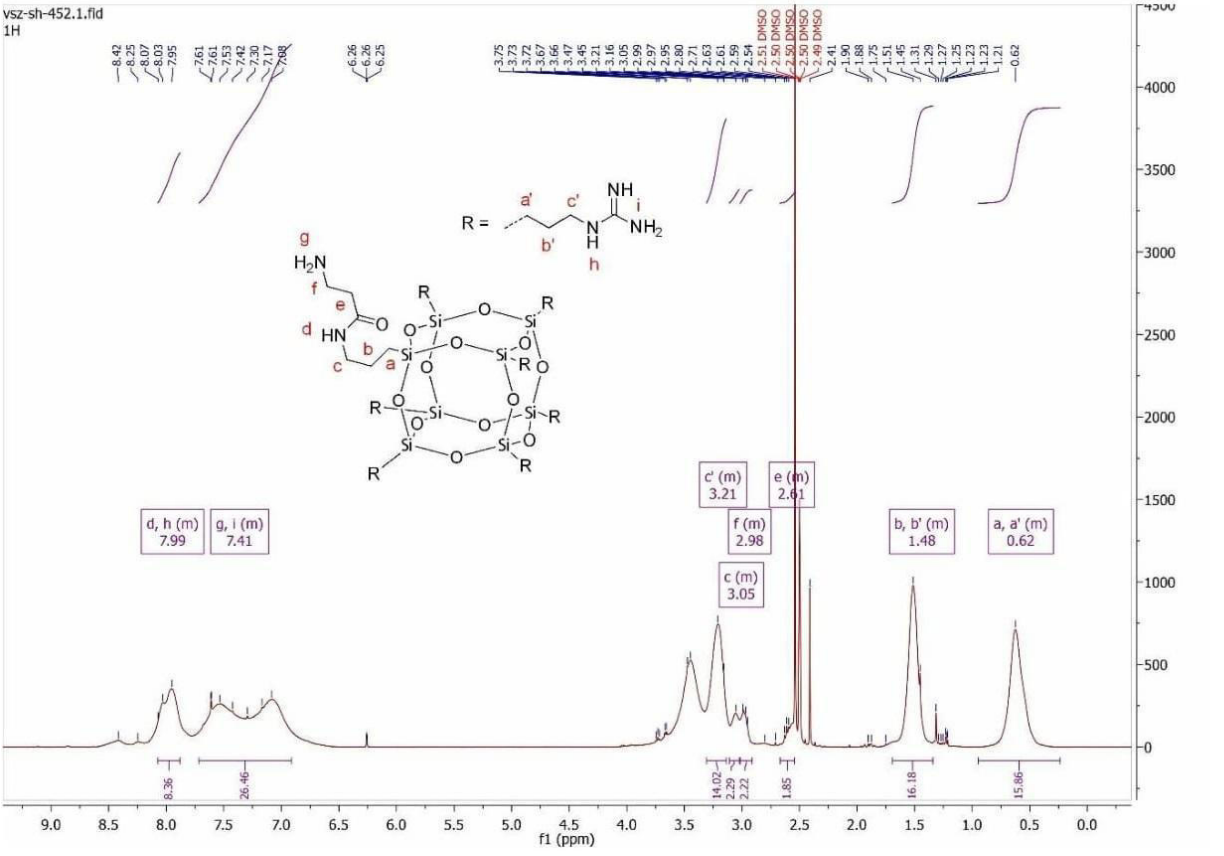

Figure S37: *^{1}H NMR of* ***8***

COSS derivative 9 (Fluorescein-TAMRA-GuCOSS)

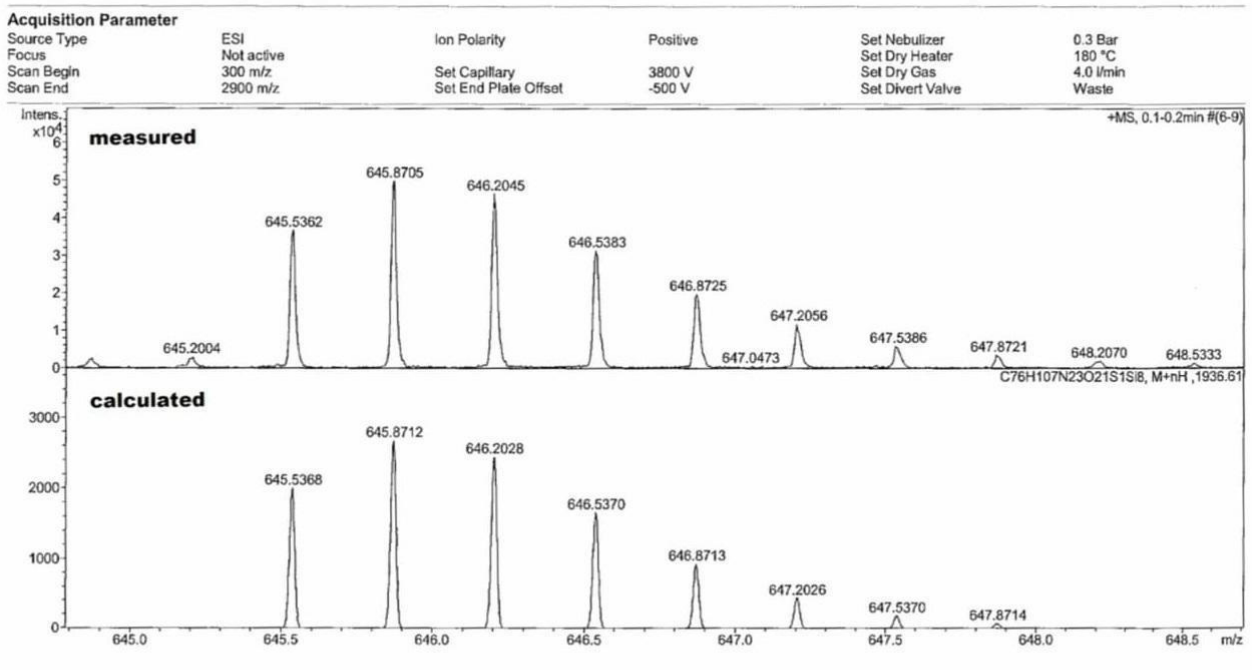

Figure S38: *HR-MS of* ***9****. Calculated for* $C_{76}H_{107}N_{23}O_{21}SSi_8$ *m/z: 645.5368, measured 645.5362* $[M+3H]^{3+}$.

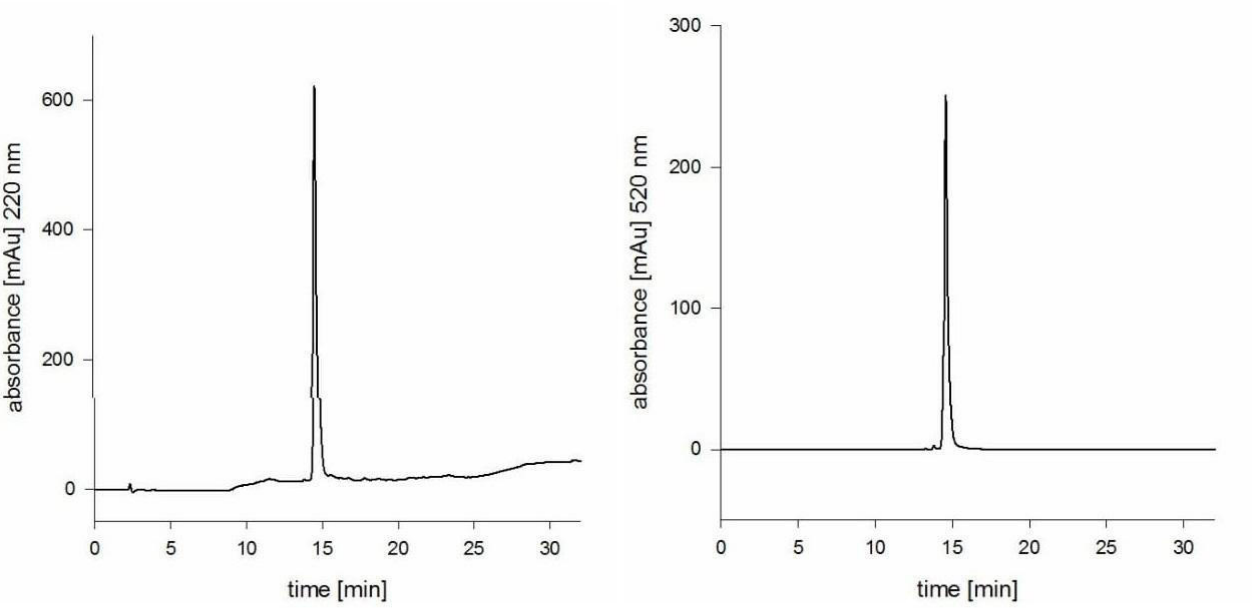

Figure S39: *Analytical HPLC diagrams of* ***9****. Left: λ=220 nm; right λ=520 nm.*

TAMRA-β-alanine-Tat peptide 10

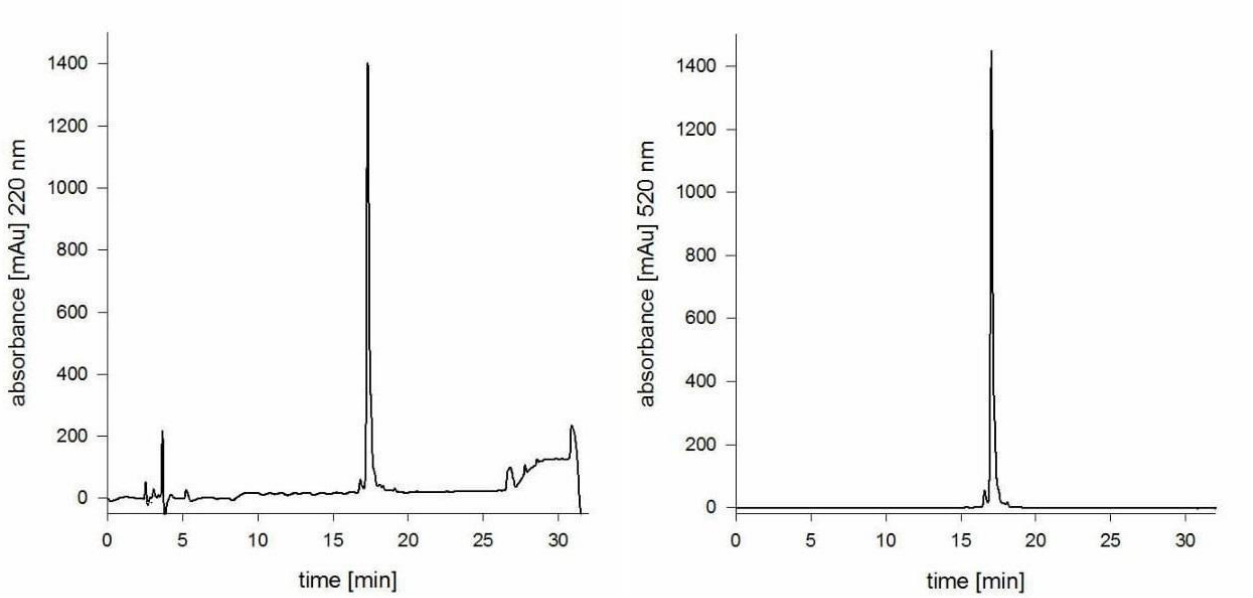

Figure S40: *Analytical HPLC diagrams of* ***10****. Left: λ=220 nm; right: λ=520 nm.*

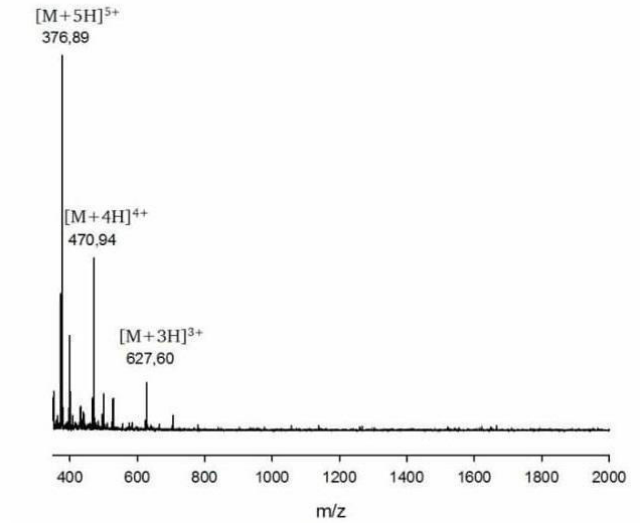

Figure S41: *ESI-MS of* ***10****. Calculated for* $C_{83}H_{135}N_{34}O_{17}^{+}$ *m/z: 628.06, measured 627.6* $[M+3H]^{3+}$*, calculated 471.30, measured 470.94* $[M+4H]^{4+}$*, calculated 377.24, measured 376.89* $[M+5H]^{5+}$*.*

TAMRA-β-alanine-Penetratin 11

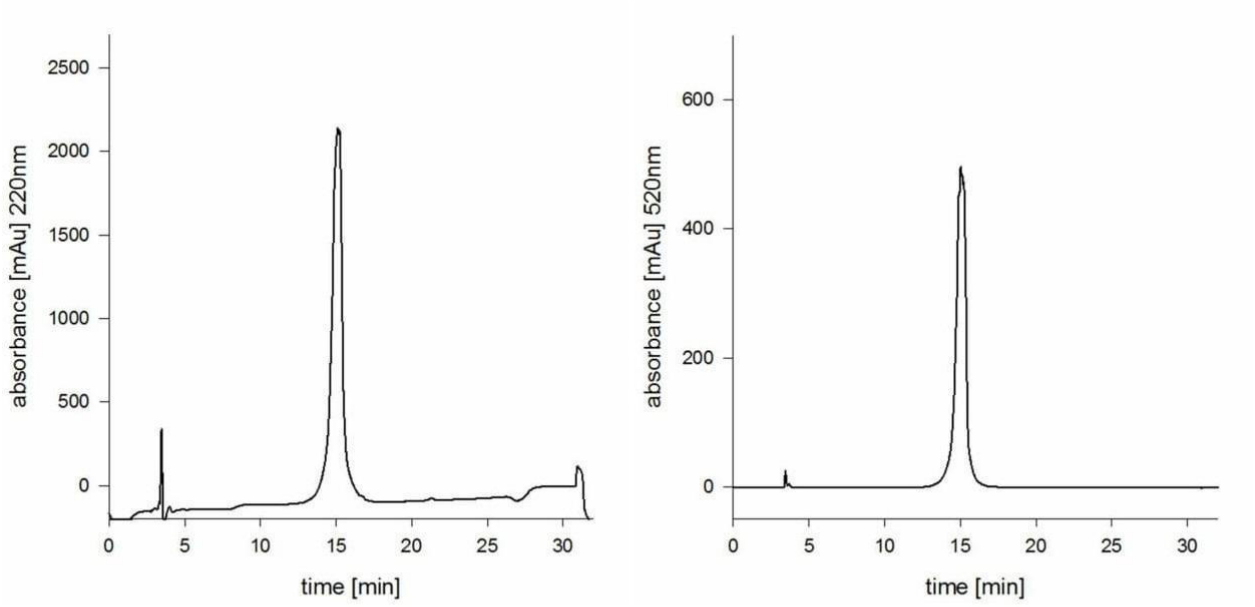

Figure S42: *Analytical HPLC diagrams of* ***11****.Left: λ=220 nm; right: λ=520 nm.*

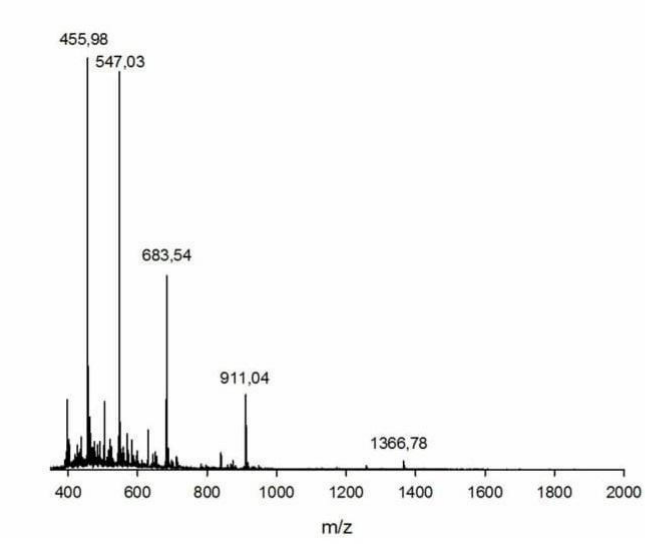

Figure S43: *ESI-MS of* ***11****. Calculated for* $C_{132}H_{194}N_{37}O_{25}S^+$ *m/z: 911.43, measured 911.1* $[M+3H]^{3+}$*, calculated 683.83, measured 683.60* $[M+4H]^{4+}$*, calculated 547.26, measured 547.1* $[M+5H]^{5+}$*.*

TAMRA-β-alanine-heptaarginine 12

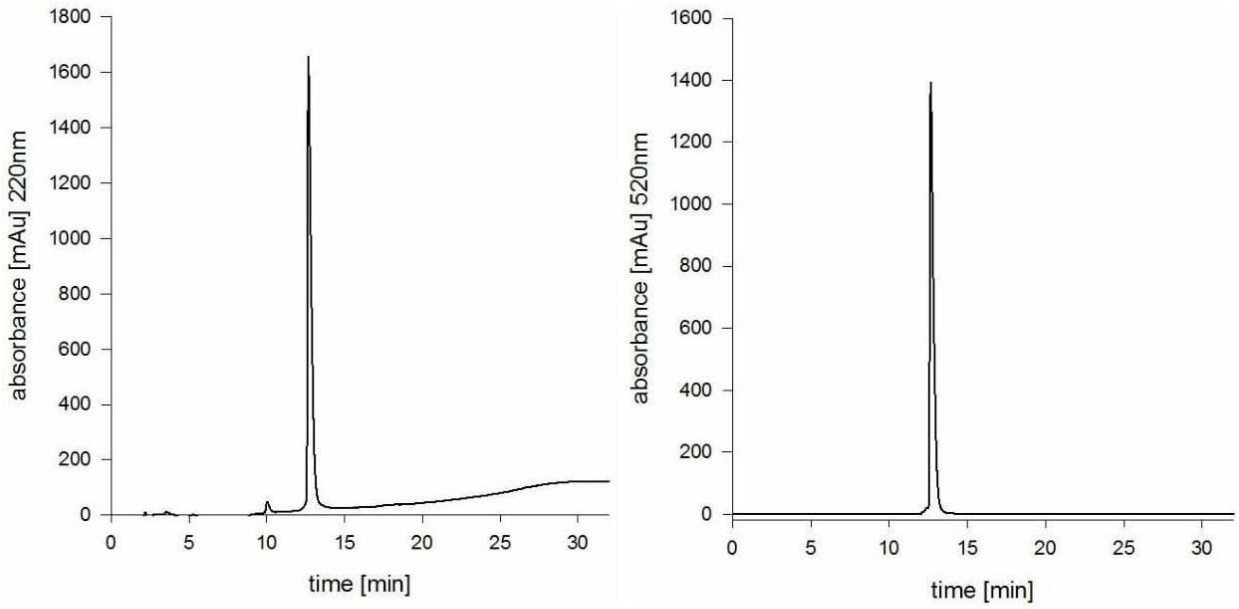

Figure S44: *Analytical HPLC diagrams* ***12****. Left: λ=220 nm; right: λ=520 nm.*

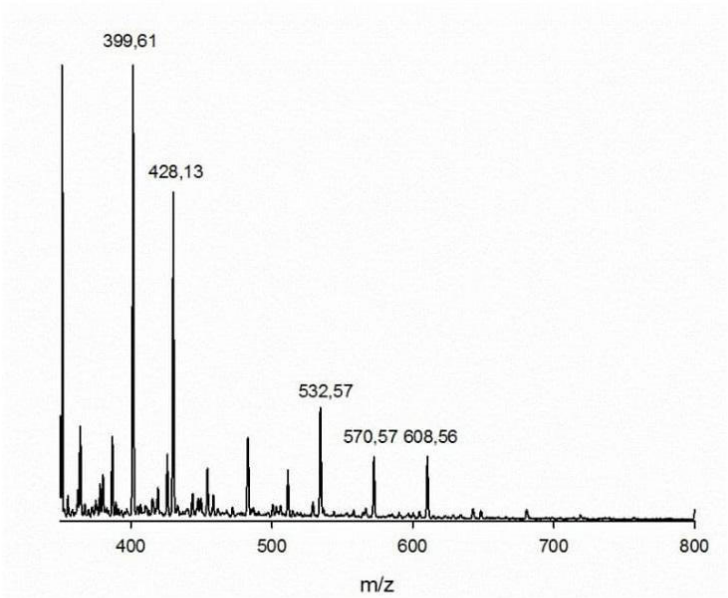

Figure S45: *ESI-MS of* ***12****. Calculated for* $C_{70}H_{112}N_{32}O_{12}$ *m/z: 532.29, measured 532.57* $[M+3H]^{3+}$, *570.57* $[M+TFA+3H]^{3+}$, *608.56* $[M+2TFA+3H]^{3+}$*; calculated 399.47, measured 399.61* $[M+4H]^{4+}$, *428.13* $[M+TFA+4H]^{4+}$.

TAMRA-β-alanine-decaarginine 13

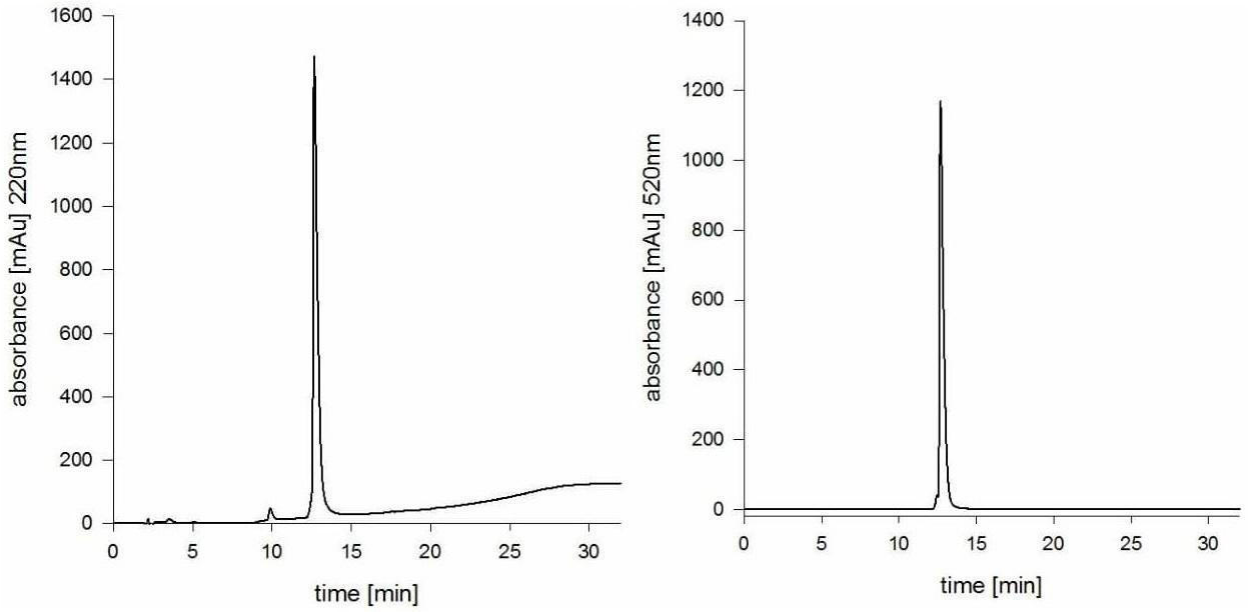

Figure S46: *Analytical HPLC diagrams of* ***13****. Left: λ=220 nm; right: λ=520 nm.*

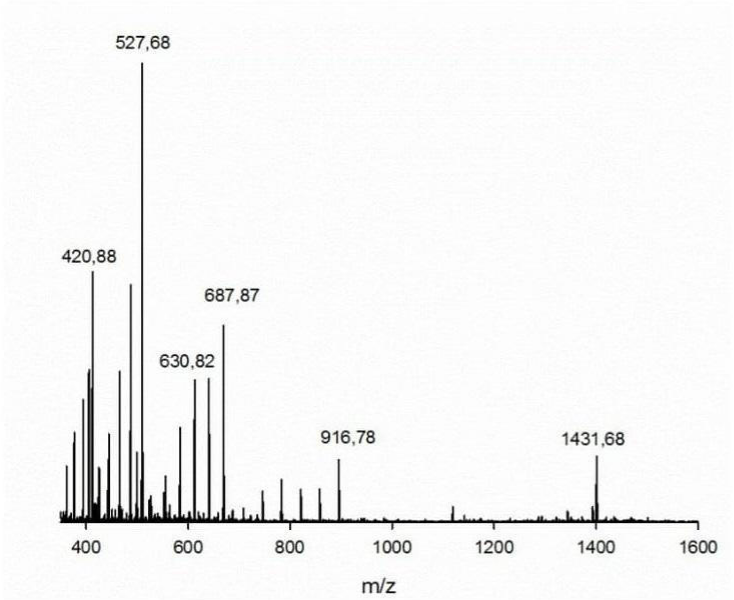

Figure S47: *ESI-MS of* ***13****. Calculated for $C_{88}H_{148}N_{44}O_{15}$ m/z: 688.49, measured 764.71 $[M+2TFA+3H]^{3+}$, 840.79 $[M+4TFA+3H]^{3+}$, 787.76 $[M+5TFA+3H]^{3+}$, 916.78 $[M+6TFA+3H]^{3+}$; calculated 516.62, measured 573.80 $[M+2TFA+4H]^{4+}$, 602.30 $[M+3TFA+4H]^{4+}$, 630.82 $[M+4TFA+4H]^{4+}$, 659.30 $[M+5TFA+4H]^{4+}$, 687.87 $[M+6TFA+4H]^{4+}$; calculated 413.50, measured 459.22 $[M+2TFA+5H]^{5+}$, 482.03 $[M+3TFA+5H]^{5+}$, 504.86 $[M+4TFA+5H]^{5+}$, 527.68 $[M+5TFA+5H]^{5+}$.*

Doxorubicin-GuCOSS derivative 15

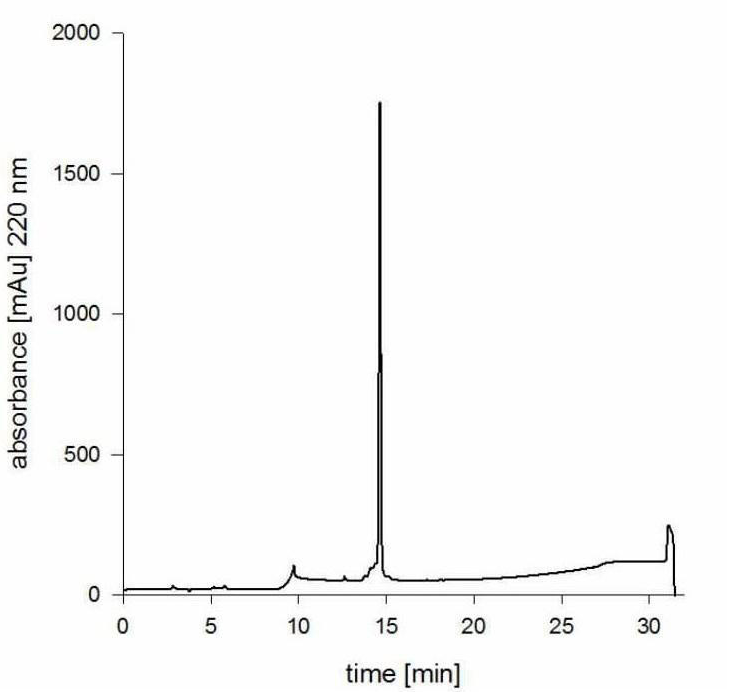

Figure S48: *Analytical HPLC diagram of* ***15****: λ=220 nm.*

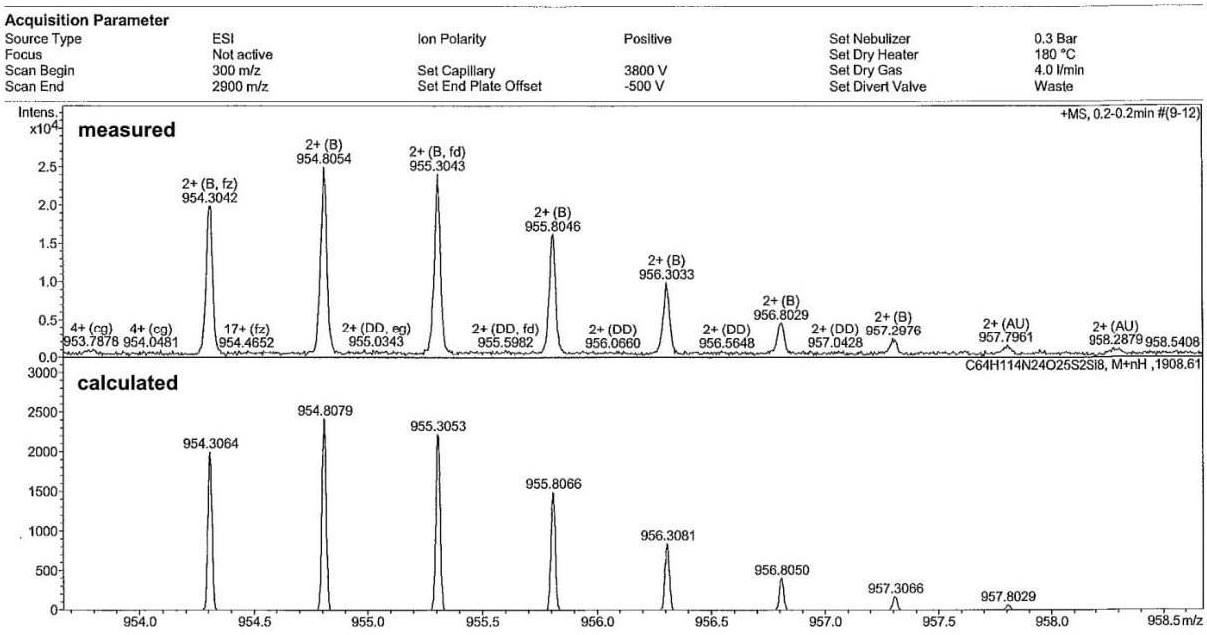

Figure S49: *HR-MS of* ***15****. Calculated for* $C_{64}H_{114}N_{24}O_{25}S_2Si_8$ *m/z: 954.3064, measured 954.3042* $[M+2H]^{2+}$.

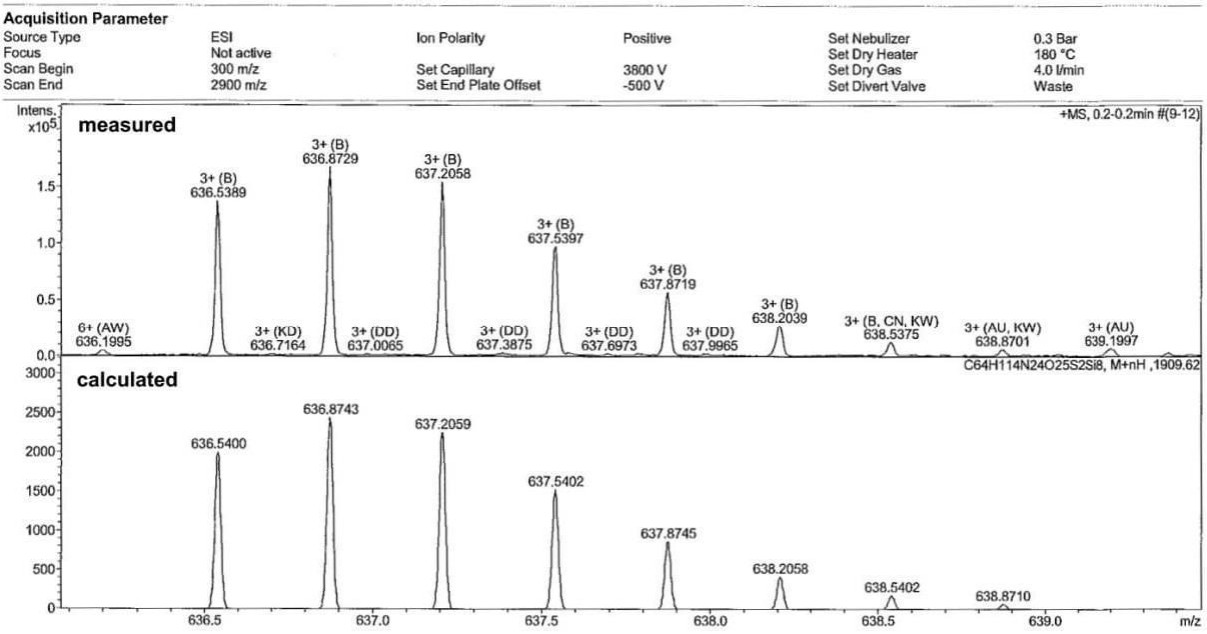

Figure S50: *HR-MS of* ***15****. Calculated for* $C_{64}H_{114}N_{24}O_{25}S_2Si_8$ *m/z: 636.5400 measured 636.5389* $[M+3H]^{3+}$.

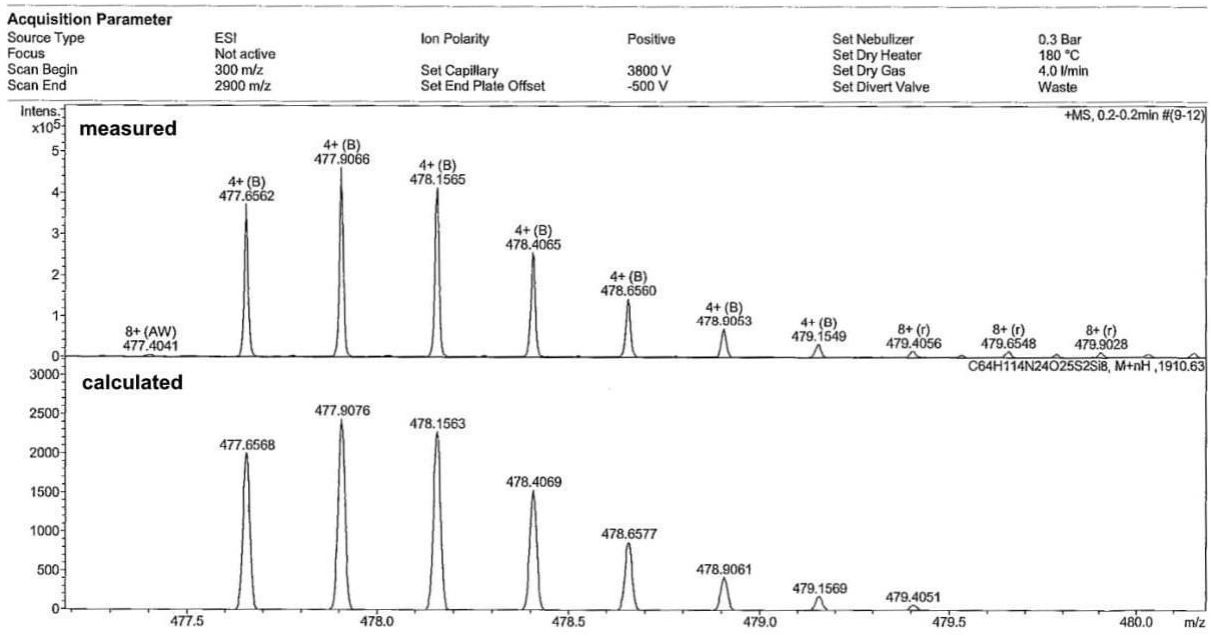

Figure S51: *HR-MS of* ***15****. Calculated for* $C_{64}H_{114}N_{24}O_{25}S_2Si_8$ *m/z: 477.6568, measured 477.6562* $[M+4H]^{4+}$.

3-carboxy-*N,N,N*-trimethylpropane-1-ammonium chloride 18

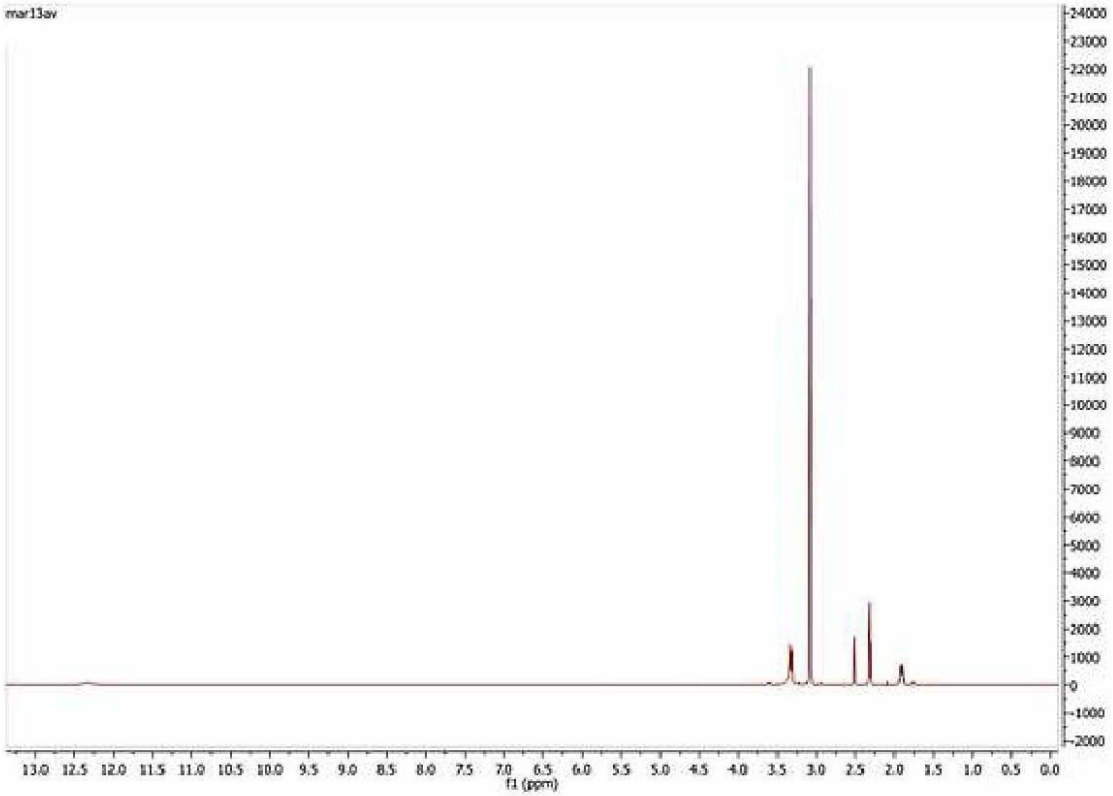

Figure S52: *^{1}H NMR of **18**.*

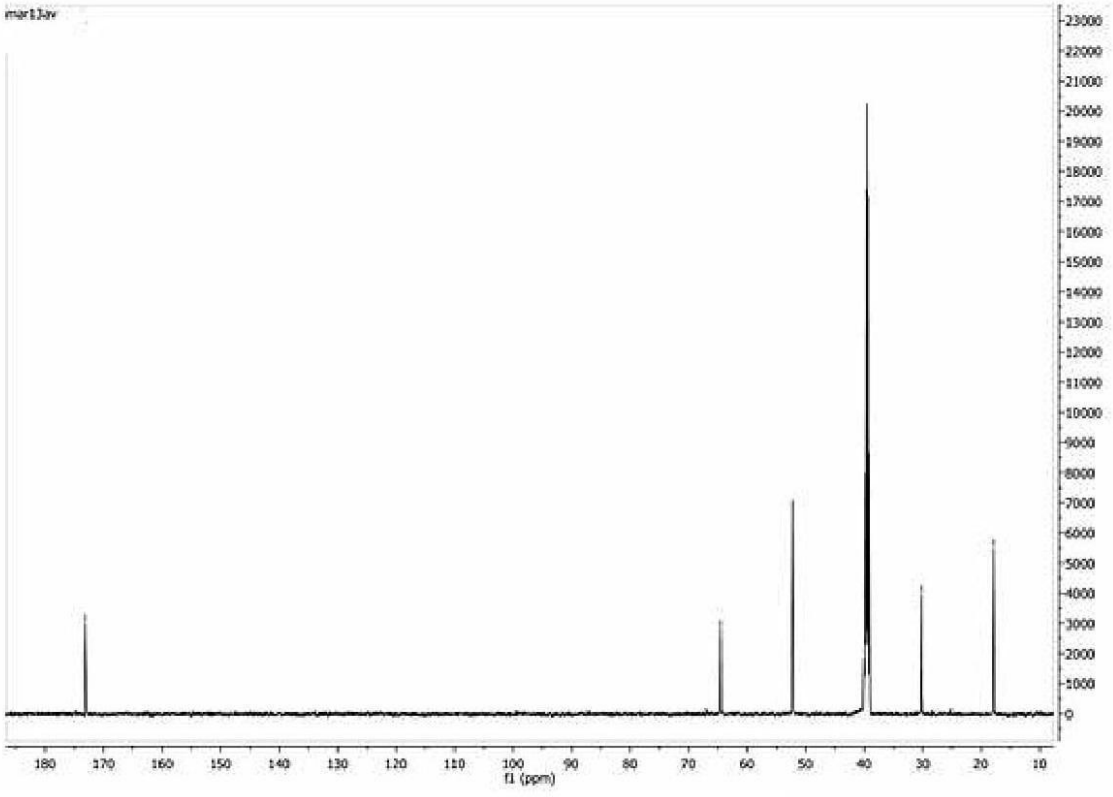

Figure S53: *^{13}C NMR of **18**.*

4-trimethylammoniumbutyric acid-NHS ester 19

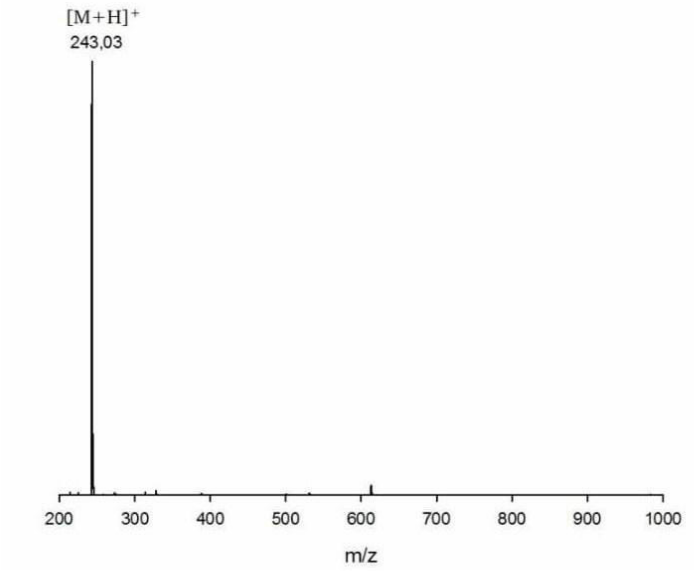

Figure S54: *ESI-MS of* ***19****. Calculated for* $C_{11}H_{19}N_2O_4^+$ *m/z: 243.28, measured 243.03* $[M+H]^+$.

N-Trt-protected β-alanine 22

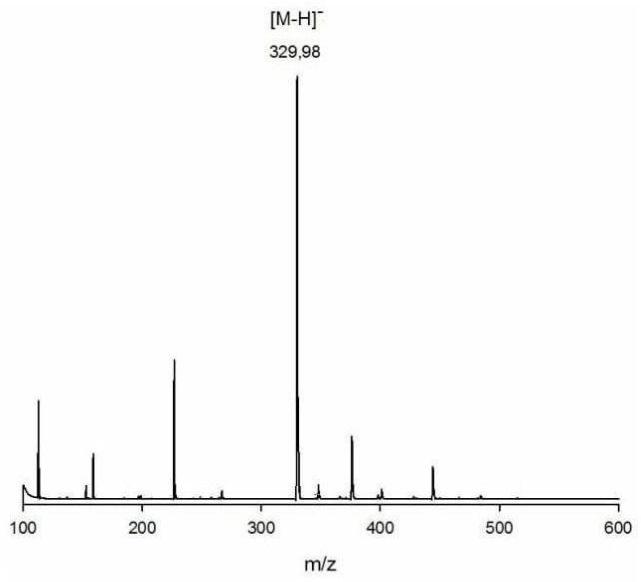

Figure S55: *ESI-MS of* ***22****. Calculated for* $C_{22}H_{21}NO_2$ *m/z: 331.42, measured 329.98* $[M-H]^-$.

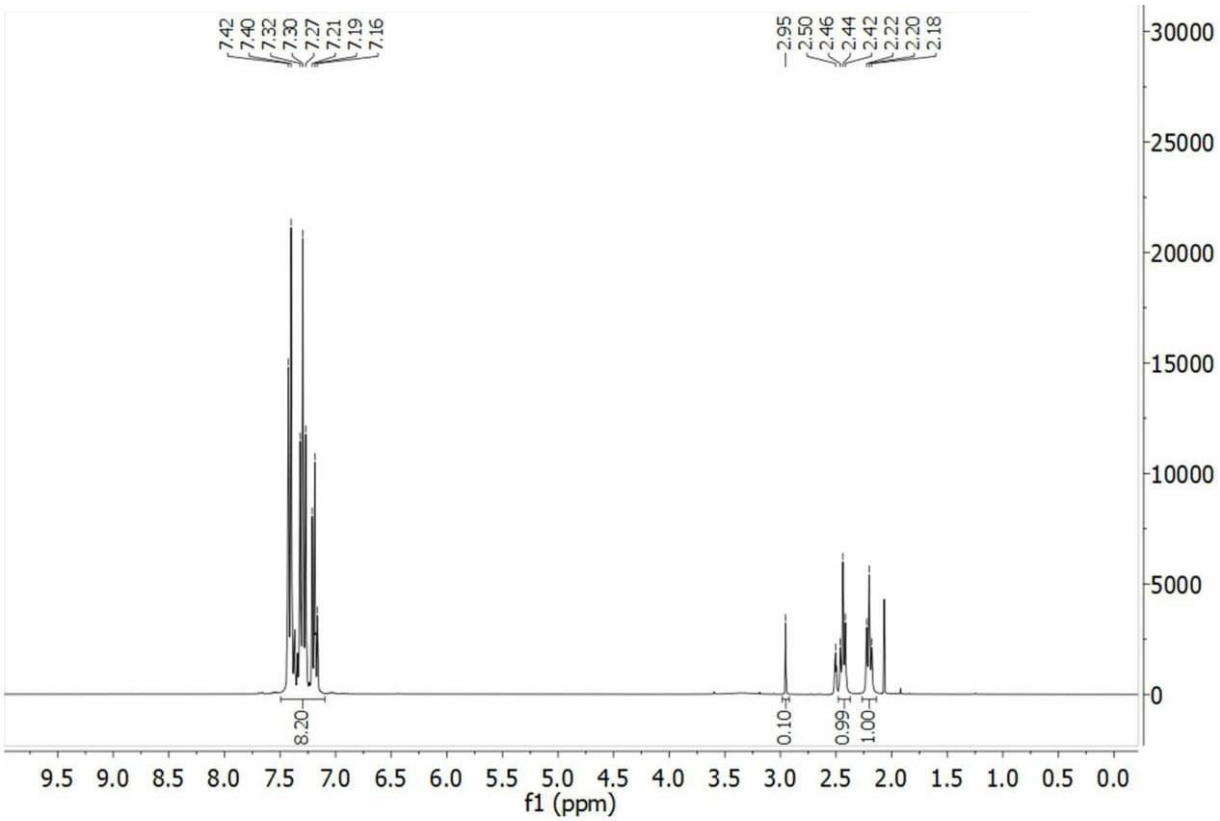

Figure S56: *^{1}H NMR of* ***22****.*

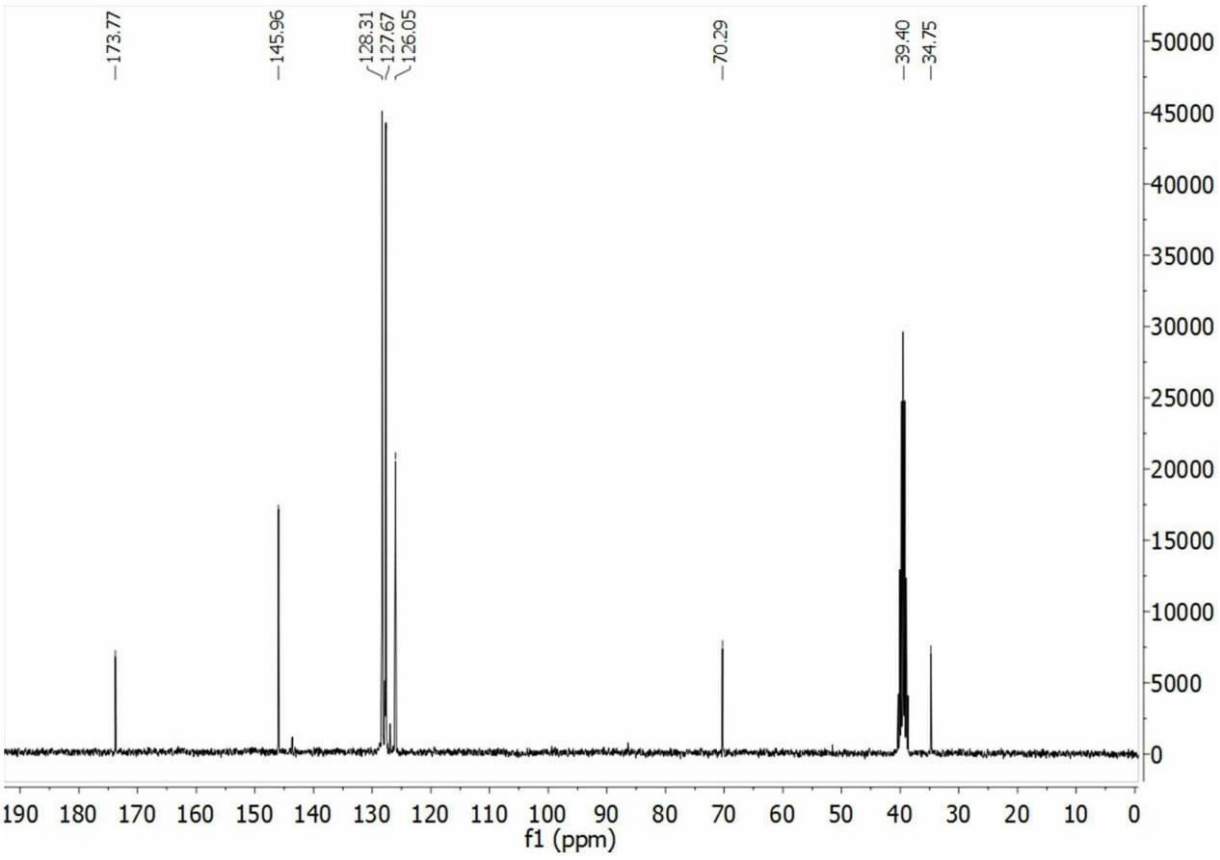

Figure S57: *^{13}C NMR of* ***22****.*

COSS derivative 23 (monoTrt-aminoCOSS)

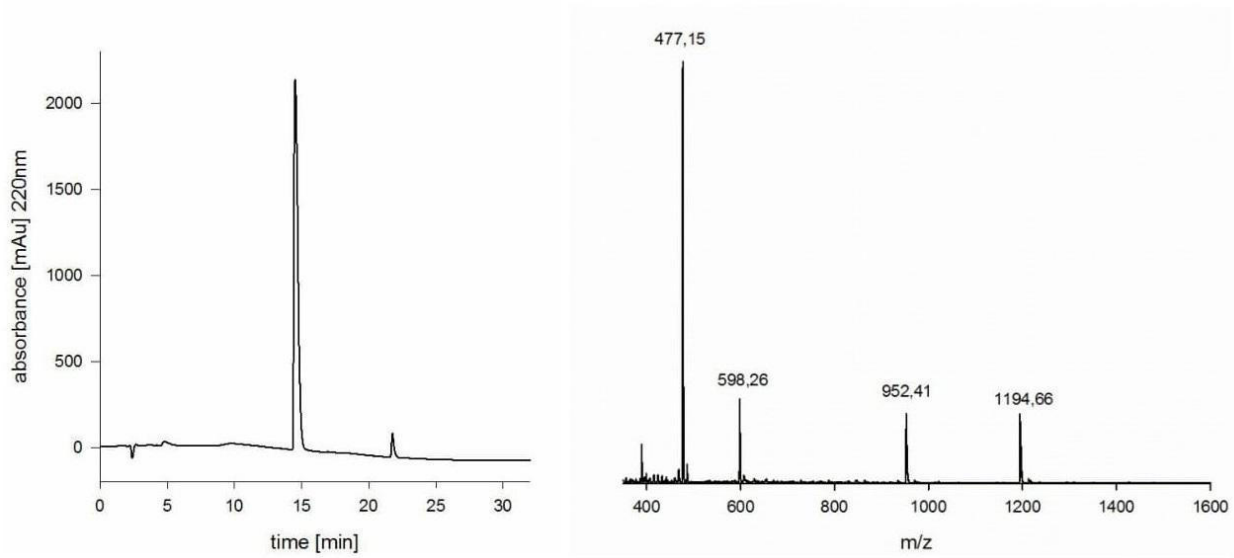

Figure S58: *Left: Analytical HPLC diagram of* ***23*** *at λ=220 nm. Right: ESI-MS spectrum of* ***23****. Calculated for* $C_{46}H_{83}N_9O_{13}Si_8$ *m/z: 1194.90, measured 1194.66* $[M+H]^+$*, calculated 598.45, measured 598.26* $[M+2H]^{2+}$.

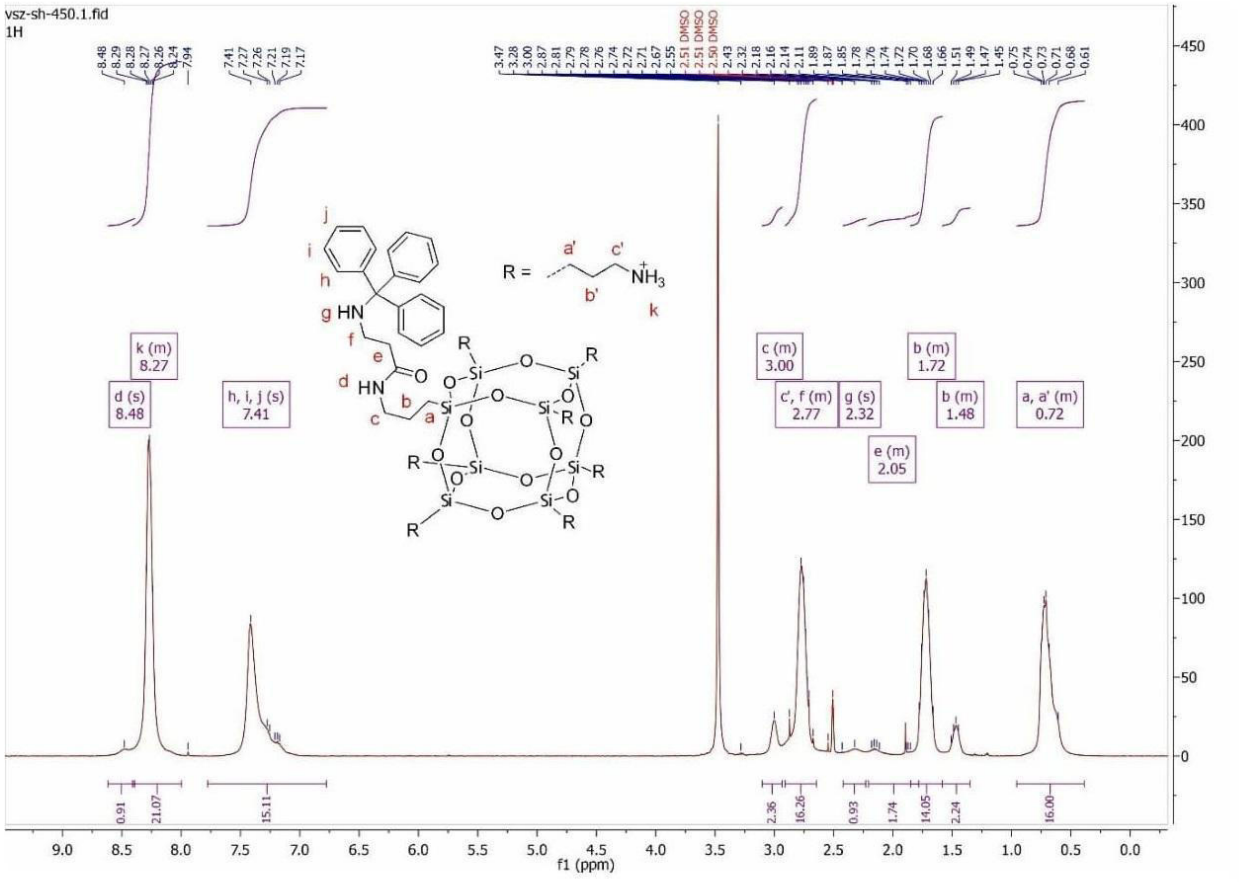

Figure S59: *^{1}H NMR spectrum of* ***23****.*

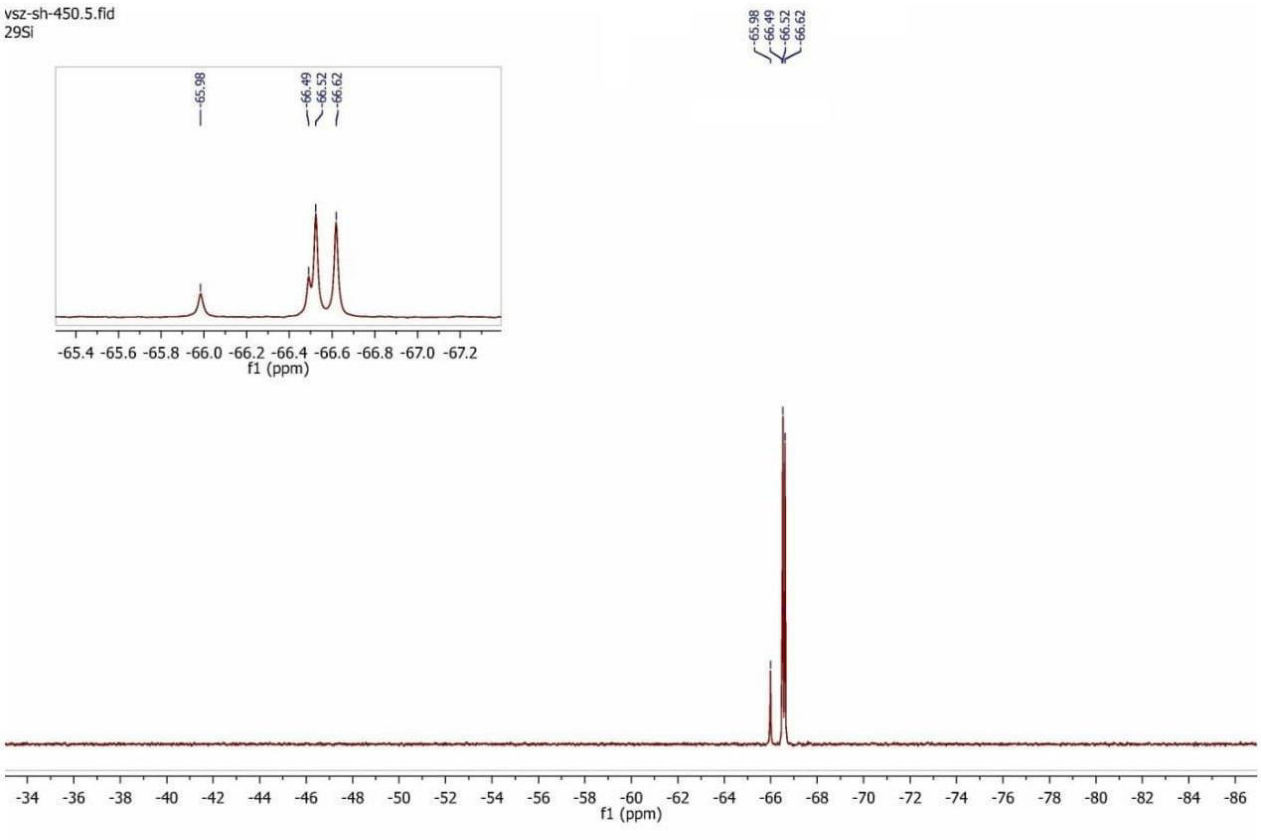

Figure S60: *^{29}Si NMR spectrum of **23**.*

COSS derivative 24 (Trt-protected GuCOSS)

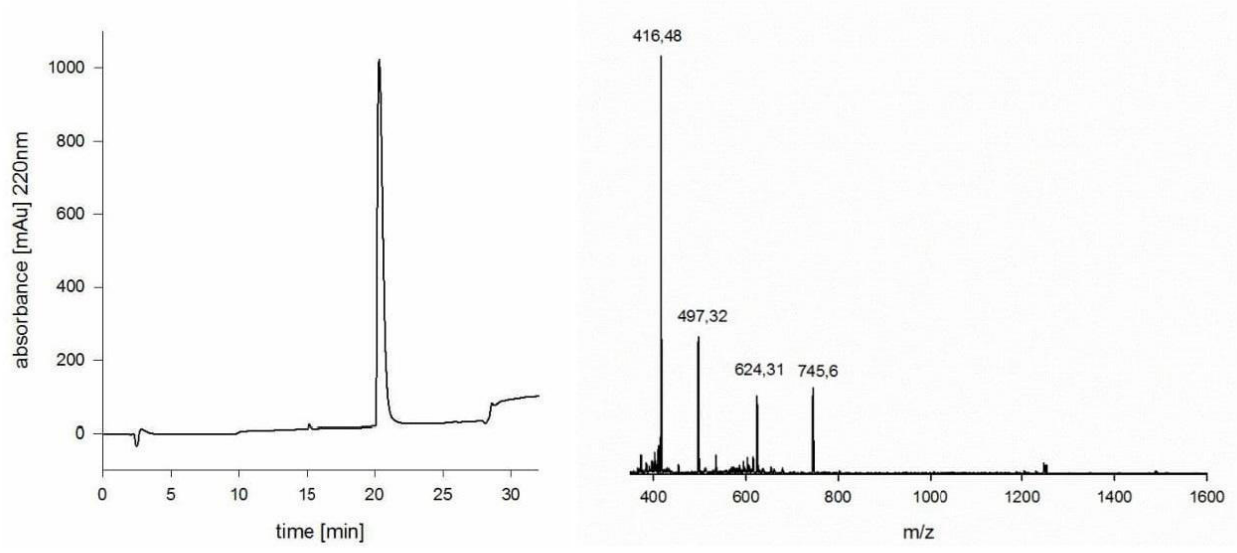

Figure S61: *Left: Analytical HPLC diagram of **24** at λ=220 nm. Right: ESI-MS of **24**. Calculated for $C_{53}H_{97}N_{23}O_{13}Si_8$ m/z: 745.58, measured 745.61 $[M+2H]^{2+}$, calculated 497.39, measured 497.32 $[M+3H]^{3+}$.*

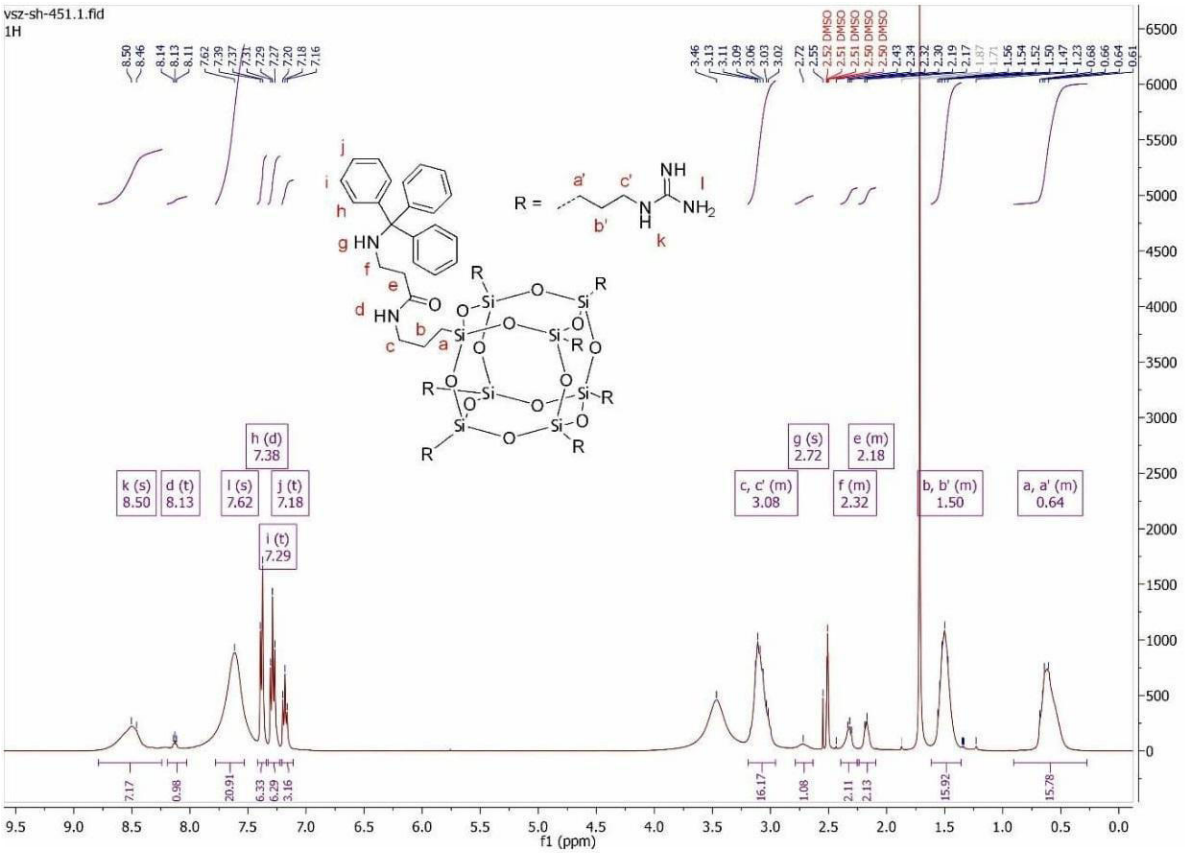

Figure S62: *^{1}H NMR spectrum of* ***24****.*

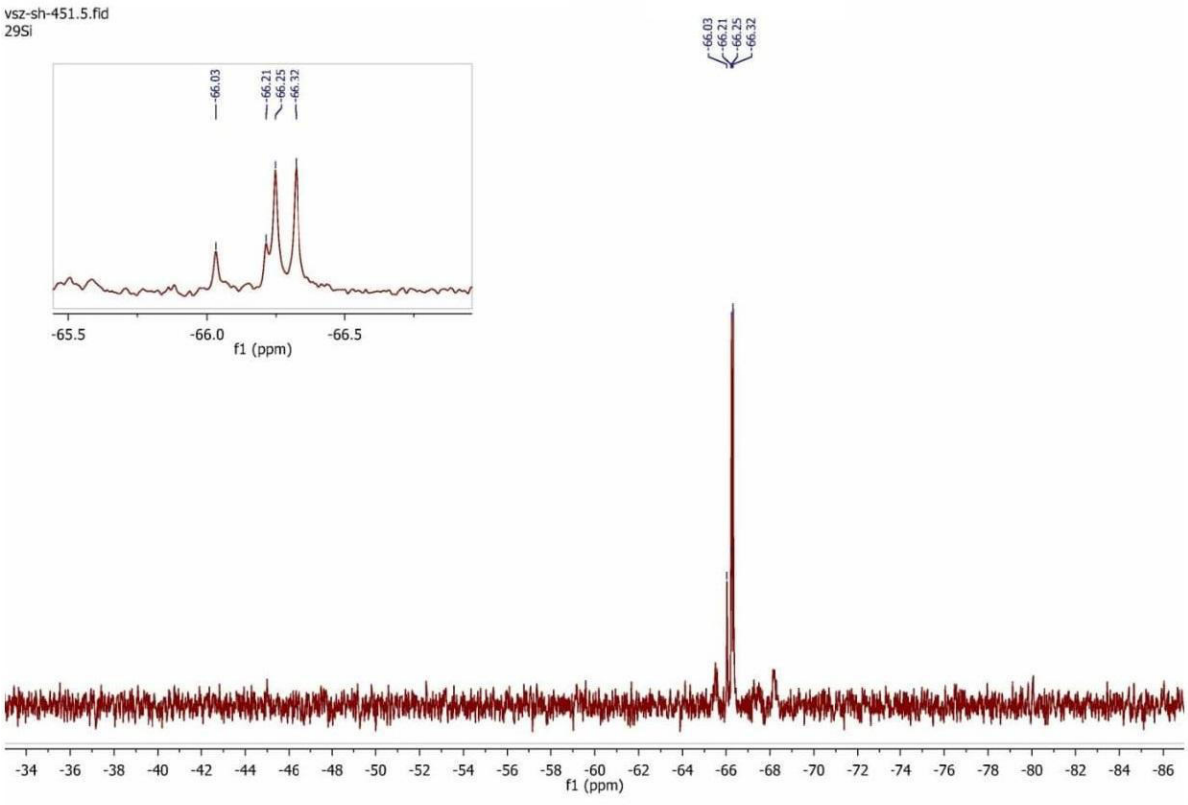

Figure S63: *^{29}Si NMR spectrum of* ***24****.*

COSS derivative 27 (PG-Cys-aminoCOSS)

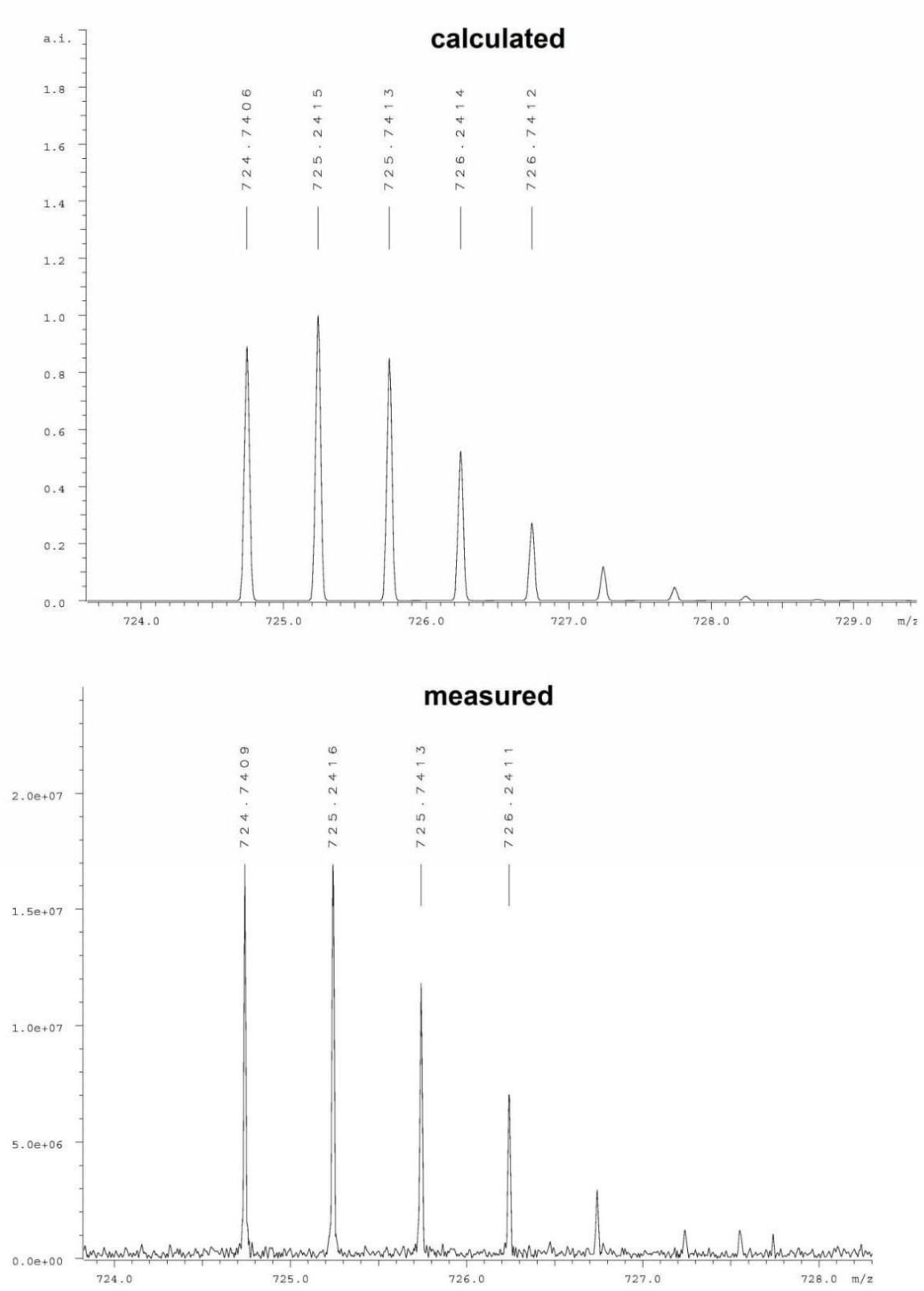

Figure S64: *HR-MS of* ***27****. Calculated for* $C_{61}H_{93}N_9O_{15}SSi_8$ *m/z: 724.7406, measured 724.7409* $[M+2H]^{2+}$.

COSS derivative 28 (Cys-GuCOSS)

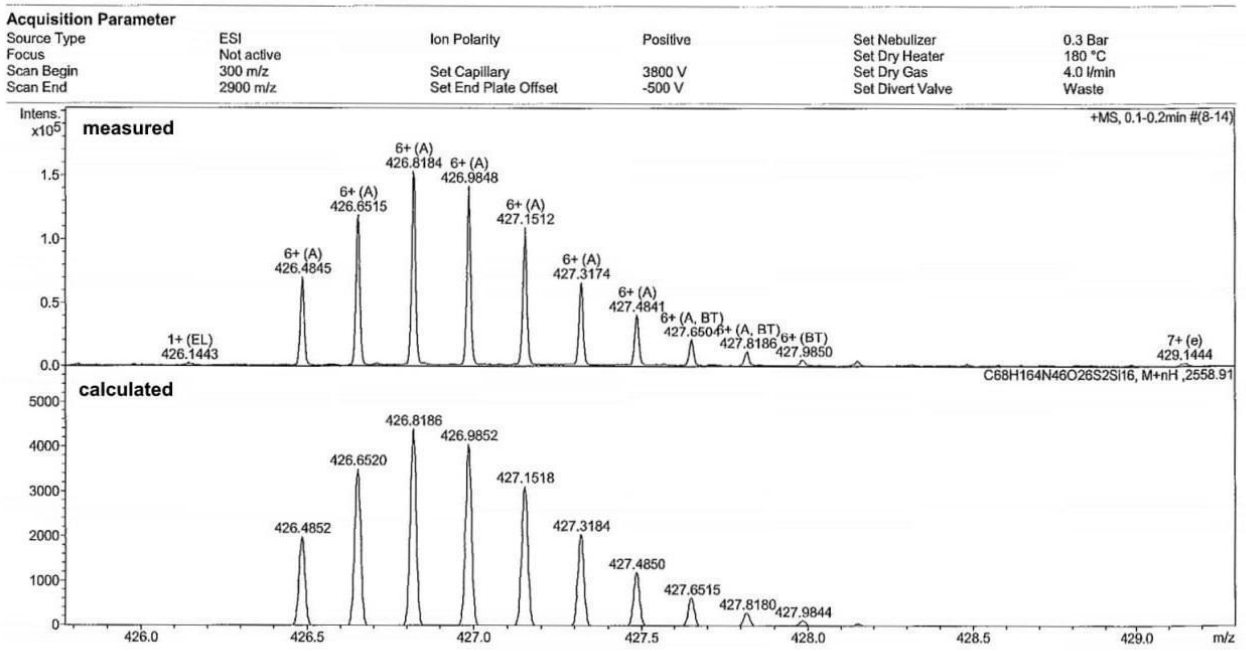

Figure S65: *HR-MS of* ***28****. Calculated for* $C_{68}H_{164}N_{46}O_{26}S_2Si_{16}$ *m/z: 426.4852, measured 426.4845* $[M+6H]^{6+}$.

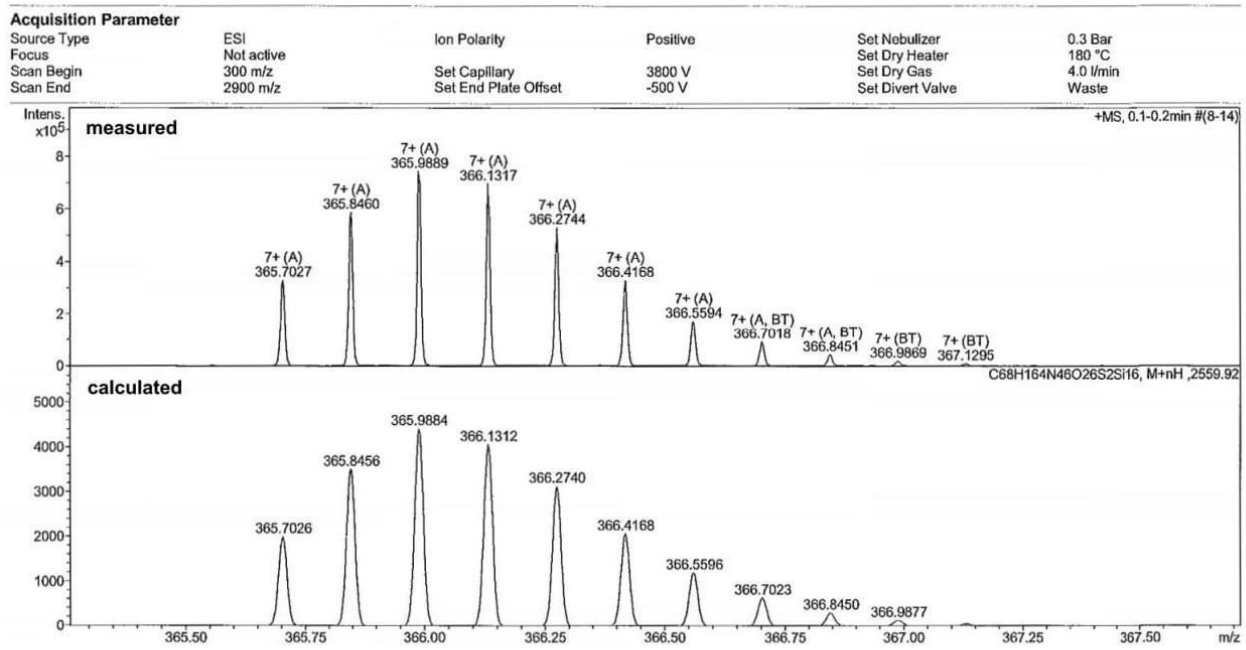

Figure S66: *HR-MS of* ***28****. Calculated for* $C_{68}H_{164}N_{46}O_{26}S_2Si_{16}$ *m/z: 365.7026, measured 365.7027* $[M+7H]^{7+}$.

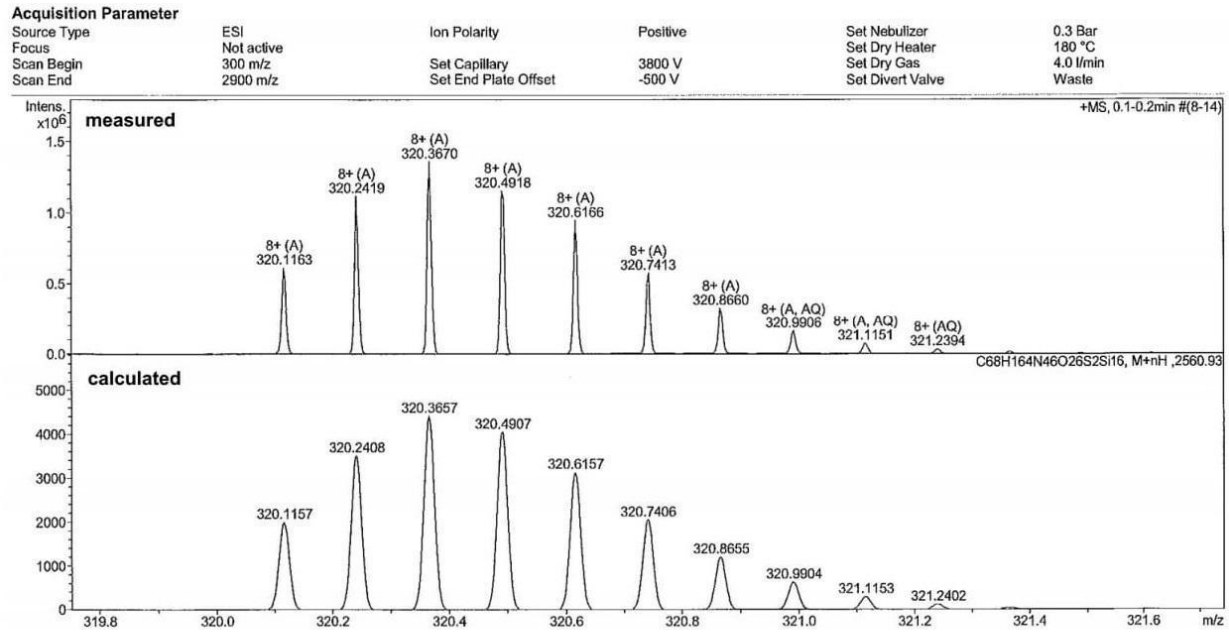

Figure S67: *HR-MS of **28**. Calculated for $C_{68}H_{164}N_{46}O_{26}S_2Si_{16}$ m/z: 320.1157, measured 320.1163 $[M+8H]^{8+}$.*

3-(pyridin-2-yldisulfanyl)propanoic acid) 31

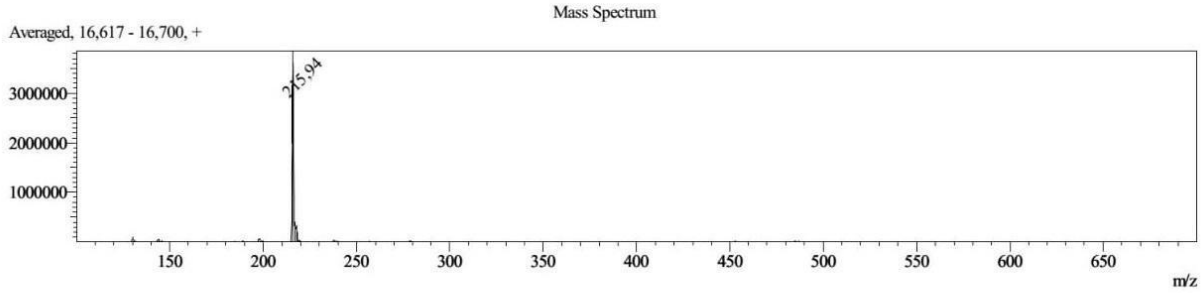

Figure S68: *ESI-MS of **31**. Calculated for $C_8H_9NO_2S_2$ m/z: 215.29, measured 215.94 $[M+H]^+$.*

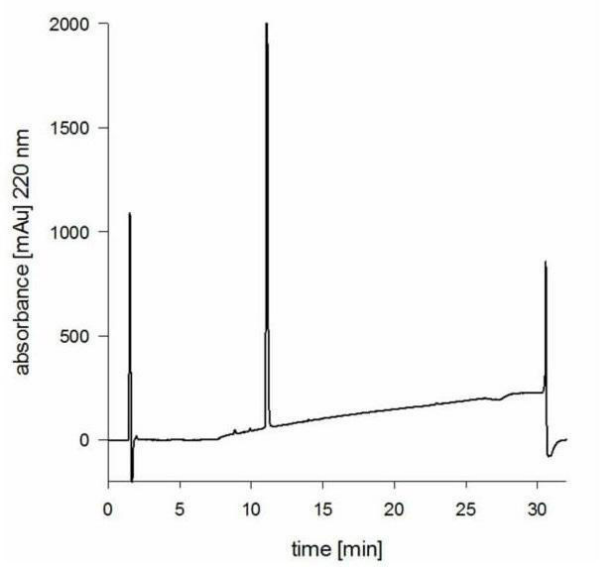

Figure S69: *Analytical HPLC diagram of **31**. λ=220 nm.*

Aldrithiol-activated doxorubicin 32

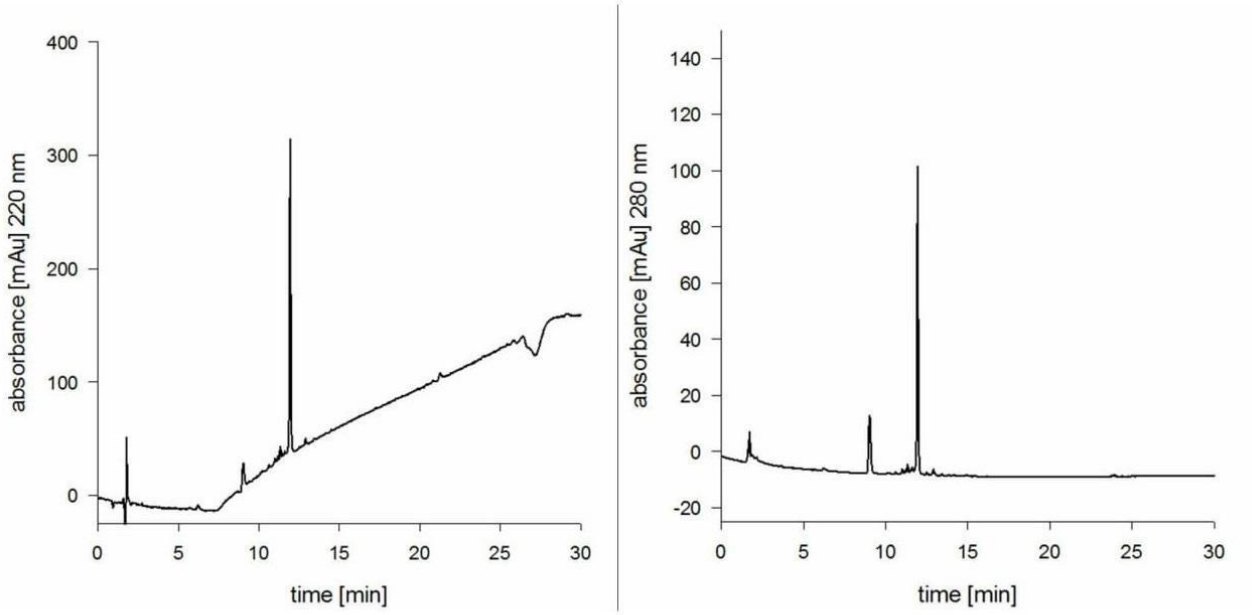

Figure S70: *Analytical HPLC diagrams of* ***32****. Left: λ=220 nm; right: λ=280 nm.*

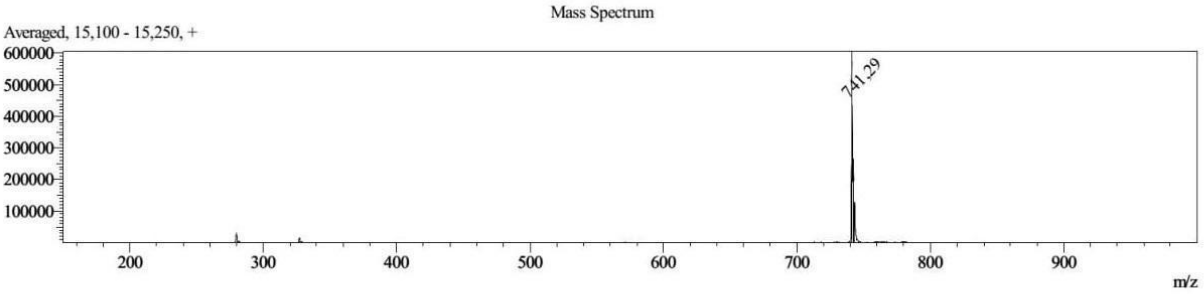

Figure S71: *ESI-MS of* ***32****. Calculated for* $C_{35}H_{36}N_2O_{12}S_2$ *m/z: 740.80, measured 741.29* $[M+H]^+$.

References

[1] a) D. W. Grogan, *J. Bacteriol.* **1989**, *171*, 6710-6719; b) T. D. Brock, K. M. Brock, R. T. Belly, W. R. L., *Arch. Mikrobiol.* **1972**, *84*, 54-68.

[2] T. Hechler, F. Pfeifer, *Molecular microbiology,* **2009**, *71*, 132-145.

[3] C. Morano, X. Zhang, L. D. Fricker, *Anal. Chem.,* **2008**, *80*, 9298-9309.

10. Abbreviations

2-CT	2-Chlorotrityl
3D	Three-dimensional
A	Alanine
AFM	Atomic force microscopy
Ala	Alanine
Arg	Arginine
Asn	Asparagine
ATR-IR	Attenuated total reflection infrared spectroscopy
Asp	Aspartic acid
Boc	*tert*-butyloxycarbonyl
BODIPY	Boron-dipyrromethene
C	Cysteine
calc.	Calculated
CD	Cyclodextrin
CHO	Chinese hamster ovary
CPP	Cell-penetrating peptide
CuAAC	Copper-catalyzed azide-alkyne cycloaddition
COSS	Cube-octameric silsesquioxane
Cys	Cysteine
D	Aspartic acid
DAR_{inv}	Diels-Alder reaction with inverse electron-demand
DCC	Dicyclohexyl carbodiimide
DCM	Dichloromethane
DHB	*2,5*-dihydroxy benzoic acid
DIC	*N,N'*-Diisopropylcarbodiimide
DIEA	*N,N'*-Diisopropylethylamine
DMEM	Dulbecco's Modified Eagle's Medium
DMF	*N,N'*-Dimethylformamide
DMSO	Dimethyl sulfoxide
DNA	Desoxyribonukleinsäure
DOTA	*1,4,7,10*-tetraazacyclododecane-*1,4,7,10*-tetraacetic acid
DTT	Dithiothreitol
E	Glutamic acid
ECM	Extracellular medium
EDTA	Ethylenediaminetetraacetic acid
Eei	Ethoxyethylidene
equiv.	Equivalent
ESI	Electronical supplemental information
ESI-MS	Electrospray ionization mass spectrometry
F	Phenylalanine
F-POSS	Flourinated polyhedral oligomeric silsesquioxane
FBS	Fetal bovine serum
FCS	Fetal calf serum
Fig.	Figure
FITC	Fluorescein isothiocyanate
Fmoc	Fluorenylmethyloxycarbonyl chloride
FRET	Förster resonance energy transfer
FT-IR	Fourier transform infrared spectroscopy
FTICR	Fourier transform ion cyclotron resonance
G	Glycine
Gd	Gadolinium

Gln	Glutamine
Glu	Glutamic acid
Gly	Glycine
GuCOSS	Cube-octameric silsesquioxan with guanidinium groups
H	Histidine
h	Hours
HATU	*1*-[Bis(dimethylamino)methylene]-*1*H-*1,2,3*-triazolo[*4,5*-b]pyridinium *3*-oxid Hexafluorophosphate
HBTU	*2*-(*1H*-benzotriazol-*1*-yl)-*1,1,3,3*-tetramethyluronium hexafluorophosphate
HEK	Human embryonic kidney
HEPES	*2*-(*4*-(*2*-Hydroxyethyl)-*1*-piperazinyl)-ethanesulfonic acid
HER2	human epidermal growth factor receptor 2
His	Histidine
HPLC	High-performance liquid chromatography
HR-MS	High-resolution mass spectrum
I	Isoleucine
ICM	Intracellular medium
Ile	Isoleucine
IR	Infrared
K	Kelvin
K	Lysine
kHz	Kilohertz
L	Leucine
LC	Liquid chromatography
LC_{50}	Lethal concentration, 50%
LC-MS	Liquid chromatography mass spectrometry
Leu	Leucine
Lys	Lysine
μm	Micrometer
μM	Micromolar
M	Methionine
M	Molar
MALDI	Matrix-assisted laser distortion/ionization
mRFP	Red fluorescent protein
mg	Milligram
meas.	Measured
Met	Methionine
MHz	Megahertz
min	Minute
mL	Milliliter
mmol	Millimol
MRI	Magnetic resonance imaging
MTBE	methyl *tert*-butyl ether
MTT	*3-(4,5*-dimethylthiazol-2yl)-*2,5*-diphenyltetrazolium bromide
N	Asparagine
NHS	*N*-Hydroxysuccinimide
nm	Nanometer
NMR	Nuclear magnetic resonance spectroscopy
O-POSS	Oligoelectrolyte polyhedral oligomeric silsesquioxanes
P	Proline
PBS	Phosphate-buffered saline
PEG	Polyethylene glycol
PEI	Polyethylenimine

Phe	Phenylalanine
Pm	Picometer
PCNA	Proliferating cell nuclear antigen
POSS	Polyhedral oligomeric silsesquioxane
Pro	Proline
PyBOP	Benzotriazol-1-yl-oxytripyrrolidinophosphonium hexafluorophosphate
Q	Glutamine
R	Arginine
RAM	Rink amide
R_f	Retardation factor
RFP	Red fluorescent protein
RP-HPLC	Reversed-phase high-performance liquid chromatography
S	Second
S	Serine
Ser	Serine
SNP	Silica nanoparticles
SPPS	Solid-phase peptide synthesis
SPAAC	Strain-promoted azide-alkyne cycloaddition
T	Threonine
TAMRA	Tetramethylrhodamine
t_R	Retention time
TFA	Trifluoro acetic acid
TEC	Thiol-ene coupling
TES	Triethylsilane
THF	Tetrahydrofuran
Thr	Threonine
TIC	Total ion current
TLC	Thin-layer chromatography
TOF	Time of flight
Trp	Tryptophane
Tyr	Tyrosine
U	Units
V	Valine
Val	Valine
W	Watt
W	Tryptophane
XTT	(*2*,*3*-Bis(*2*-methoxy-*4*-nitro-*5*-sulfophenyl)-*5*-((phenylamino)carbonyl)-*2H*-tetrazoliumhydroxid)
Y	Tyrosine

Dipl.-Ing. Sebastian Hörner
Albinistr. 1
55116 Mainz

Mainz, den 25.01.2017

Eidesstattliche Erklärung

Ich erkläre hiermit an Eides Statt, dass ich meine Dissertation selbständig und nur mit den hier angegebenen Hilfsmitteln angefertigt habe.

Dipl.-Ing. Sebastian Hörner

Dipl.-Ing. Sebastian Hörner
Albinistr. 1
55116 Mainz

Mainz, den 25.01.2017

Erklärung

Ich erkläre hiermit, noch keinen Promotionsversuch unternommen zu haben.

Dipl.-Ing. Sebastian Hörner

Lebenslauf
Dipl.-Ing. Sebastian Hörner

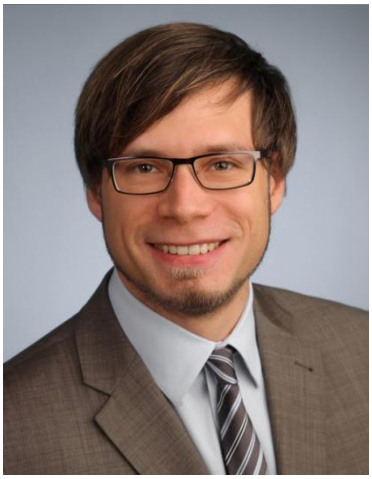

Albinistr. 1
55116 Mainz
SebastianHoerner@gmx.de

Berufserfahrung

Seit Januar 2016

Leiter der Prozessentwicklung und stellvertretender Leiter der Abteilung Wirkstoffformulierung und Drug Delivery

BioNTech RNA Pharmaceuticals GmbH, Mainz

- Prozessentwicklung für nanopartikuläre Wirkstoffformulierungen
- Prozesstransfer ins GMP-Umfeld
- Stabilisierung von Formulierungen (z. B. mittels Gefrier- oder Sprühtrocknung)
- Projektleiter des Moduls Wirkstoffformulierung IVAC® mutanome (individualized vaccines against cancer)

8/2014 – 1/2016

Wissenschaftler mit Schwerpunkt Wirkstoffformulierung

BioNTech RNA Pharmaceuticals GmbH, Mainz

- Entwicklung von Formulierungen für biotechnologisch hergestellte Wirkstoffe mit Fokus auf mRNA (parenterale, intradermale, intramuskuläre und inhalative Applikationen)
- Stabilisierung von Wirkstoffformulierungen mittels Gefriertrocknung
- Charakterisierung nanopartikulärer Formulierungen (PCS, SAXS)

Akademischer Werdegang

2/2011-12/2016

Promotion am Clemens-Schöpf-Institut für Organische Chemie und Biochemie

Technische Universität Darmstadt, Prof. Kolmar

Thema: *“Biofunctionalization of Silsesquioxan Nanoparticles”*

- Entwicklung bioabbaubarer Wirkstofftransporter
- Biofunktionalisierung von Silicium Nanopartikeln
- Assay-Entwicklung (HPLC- und massenspektrometrische Analyse Fluoreszenzmikroskopie, Durchflusszytometrie)

5/2006 - 12/2010	**Hauptstudium der Chemie** Technische Universität Darmstadt · Diplomarbeit: *“An orthogonal approach to hetero bioconjugations on cube octameric silsesquioxane scaffolds”*
9/2006 - 6/2007	**Auslandsstudium** Universidad Alcalá de Henares, Spanien
10/2003 - 4/2006	**Grundstudium der Chemie** Technische Universität Darmstadt
6/2002	**Abitur** Schulzentrum Marienhöhe, Darmstadt

Zivildienst

7/2002 - 5/2003	Kinder- und Jugendfarm, Darmstadt

Zusatzqualifikationen

Fortbildungen:

· Kalorimetrie-Training (Mettler Toledo)

· Single-Use-Disposables (Concept Heidelberg)

· GMP-Basis-Schulung (Concept Heidelberg)

· LC-MS Seminar (AB SCIEX, 2014 & 2015)

· Gesprächstechniken für Führungskräfte

· Schlüsselqualifikation interkulturelle Kompetenz

· Projektmanagement für Einsteiger/innen

· Projektmanagement und -führung in der Forschung

EDV-Kenntnisse:

· MS Office (MS Word, MS Excel, MS Power Point) (sehr gut)

· Origin (sehr gut)

· MS Visio (gut)

· MS Project (gut)

Sprachen

Englisch – fließend in Wort und Schrift
Spanisch – Grundkenntnisse

Mainz den 25. Januar 2017

Dipl.-Ing. Sebastian Hörner